

Linking Science and Technology for Global Solutions

Technical Program

Program-at-a-Glance	2
Session Listing	
Monday AM	
Monday PM	
Tuesday AM	
Tuesday PM	
Wednesday AM	
Wednesday PM	
Thursday AM	
General Posters	
Index	











M	Monday		Tues	sday	Wedn	esday	Thursday
ROOM	АМ	РМ	АМ	РМ	АМ	РМ	АМ
America's Seminar	Materials Processing under the Influence of External Fields: Session I	Materials Processing under the Influence of External Fields: Session II	Intellectual Property in Materials Science: Patents, Tech Transfer and Licensing: Patents	Intellectual Property in Materials Science: Patents, Tech Transfer and Licensing: Commercialization	Materials Processing under the Influence of External Fields: Session III	Materials Processing under the Influence of External Fields: Session IV	Materials Processing under the Influence of External Fields: Session V
Asia 1	Bulk Metallic Glasses IV: Glass Science and Technology	Bulk Metallic Glasses IV: Mechanical Properties I	Bulk Metallic Glasses IV: Alloy Development and Glass-Forming Ability	Bulk Metallic Glasses IV: Mechanical Properties II	Bulk Metallic Glasses IV: Supercooled Liquids and Crystallization	Bulk Metallic Glasses IV: Mechanical Properties III	Bulk Metallic Glasses IV: Mechanical Properties IV
Asia 2	Materials in Clean Power Systems II: Fuel Cells, Solar, and Hydrogen- Based Technologies: Plenary Session	Materials in Clean Power Systems II: Fuel Cells, Solar, and Hydrogen- Based Technologies: PEMFCs	Materials in Clean Power Systems II: Fuel Cells, Solar, and Hydrogen- Based Technologies: SOFCs I	Materials in Clean Power Systems II: Fuel Cells, Solar, and Hydrogen- Based Technologies: SOFCs II	Materials in Clean Power Systems II: Fuel Cells, Solar, and Hydrogen- Based Technologies: Materials Oxidation/ Corrosion and Protection	Materials in Clean Power Systems II: Fuel Cells, Solar, and Hydrogen- Based Technologies: Materials for Clean Coal Power Generation and Gas Separation	Materials in Clean Power Systems II: Fuel Cells, Solar, and Hydrogen- Based Technologies: Materials for Solar Cells and Photovoltaic Systems
Asia 3	Innovations in Titanium Technology Symposium: Low Cost Materials and Processing	Innovations in Titanium Technology Symposium: Novel Materials and Processes I	Innovations in Titanium Technology Symposium: Novel Materials and Processes II	Innovations in Titanium Technology Symposium: Advances in Materials Processing	Innovations in Titanium Technology Symposium: Advances in Alloy Development	Innovations in Titanium Technology Symposium: Microstructure and Properties I	Innovations in Titanium Technology Symposium: Microstructure and Properties II
Asia 4	Properties and Performance of High Temperature Alloys and Coatings: Single Crystal Alloys I	Properties and Performance of High Temperature Alloys and Coatings: Polycrystalline Alloys	Properties and Performance of High Temperature Alloys and Coatings: Single Crystal Alloys II and Oxidation	Properties and Performance of High Temperature Alloys and Coatings: Coatings and Oxidation I	Properties and Performance of High Temperature Alloys and Coatings: Coatings and Oxidation II	Properties and Performance of High Temperature Alloys and Coatings: Intermetallics and Multidiscipline	
Asia 5	SMD Symposium: Mechanical Behavior of Nanostructured Materials, in Honor of Carl Koch: Fatigue, and Strengthening Mechanisms at Small Length Scale	SMD Symposium: Mechanical Behavior of Nanostructured Materials, in Honor of Carl Koch: Processing and Characterization of Materials Subjected to Severe Plastic Deformation	SMD Symposium: Mechanical Behavior of Nanostructured Materials, in Honor of Carl Koch: Plasticity and Deformation Mechanisms at Small Length Scale I	SMD Symposium: Mechanical Behavior of Nanostructured Materials, in Honor of Carl Koch: Stability, Strain and Stress - and - Poster Sesion: Mechanical Properties of Nanostructured Materials	SMD Symposium: Mechanical Behavior of Nanostructured Materials, in Honor of Carl Koch: Plasticity and Deformation Mechanisms at Small Length Scale II	SMD Symposium: Mechanical Behavior of Nanostructured Materials, in Honor of Carl Koch: Plasticity and Deformation Mechanisms at Small Length Scale III	SMD Symposium: Mechanical Behavior of Nanostructured Materials, in Honor of Carl Koch: Microstructure and Mechanical Properties of Nanostructured Materials
Australia 2	Recycling and Waste Processing: Materials Recovery from Wastes	Recycling and Waste Processing: Batteries and Co/Ni	Recycling and Waste Processing: Automotive Recycling, Global Challenges and Opportunities	Recycling and Waste Processing: Precious Metals Recovery	Recycling and Waste Processing: Aluminum	Recycling and Waste Processing: Other Nonferrous	

LEARN • NETWORK • ADVANCE



Prog	ram-	at-a-	Gla	nce
<u> </u>	,			

Monday		Tues	sday	Wedn	esday	Thursday	ROOM
AM	РМ	АМ	РМ	AM	РМ	AM	МО
Innovations in Measurement Science to Assess the Performance of New Materials in the Real-World: Fundamental Measurement Methods	8th Global Innovations Symposium: Trends in Materials and Manufacturing Technologies for Energy Production: Plenary	Innovations in Measurement Science to Assess the Performance of New Materials in the Real-World: High Strain Rate Deformation	8th Global Innovations Symposium: Trends in Materials and Manufacturing Technologies for Energy Production: Session I	Innovations in Measurement Science to Assess the Performance of New Materials in the Real-World: Characterization of Advanced Materials	Innovations in Measurement Science to Assess the Performance of New Materials in the Real-World: Advanced Measurement Techniques		Australia 3
Advances in Microstructure- Based Modeling and Characterization of Deformation Microstructures: Characterization of Deformed Structures I	Advances in Microstructure- Based Modeling and Characterization of Deformation Microstructures: Modeling of Deformed Structures I	Advances in Microstructure- Based Modeling and Characterization of Deformation Microstructures: Characterization of Deformed Structures II	Advances in Microstructure- Based Modeling and Characterization of Deformation Microstructures: Modeling of Deformed Structures II	Advances in Microstructure- Based Modeling and Characterization of Deformation Microstructures: Modeling of Deformed Structures III	Advances in Microstructure- Based Modeling and Characterization of Deformation Microstructures: Characterization of Deformed Structures III		Europe 1
Diffusion in Advanced Materials and Processing: Atomistic and Multiscale Simulations	Diffusion in Advanced Materials and Processing: Interfaces, Surfaces and Nanostructures	Diffusion in Advanced Materials and Processing: Energy Technology	Diffusion in Advanced Materials and Processing: Materials Processing	Diffusion in Advanced Materials and Processing: Phenomenology and Experiments	Diffusion in Advanced Materials and Processing: Intermetallics and Glasses		Europe 2
Dynamic Behavior of Materials: Deformation I	Dynamic Behavior of Materials: Deformation II	Dynamic Behavior of Materials: Deformation III	Dynamic Behavior of Materials: Deformation IV	Dynamic Behavior of Materials: Mechanical Properties I	Dynamic Behavior of Materials: Mechanical Properties II	Dynamic Behavior of Materials: Fracture	Europe 3
Biological Materials Science: Bioinspired Materials	Biological Materials Science: Mechanical Behavior of Biomaterials	Biological Materials Science: Biological Materials I	Biological Materials Science: Biological Materials/ Bio-Medical - and - Poster Session	Biological Materials Science: Implant Biomaterials	Biological Materials Science: Functional Biomaterials and Devices	Biological Materials Science: Biological Materials II	Europe 4
Materials Issues for Advanced Nuclear Systems: Energy Generation and Waste Issues	Materials Issues for Advanced Nuclear Systems: Material Characterization Issues	General Abstracts: SMD: Advances in Steel I	General Abstracts: SMD: Advances in Steel II	General Abstracts: SMD: Microstructure and Properties of Materials	General Abstracts: SMD: Nickel Alloys and High Temperature Materials I		Europe 5
Refractory Metals 2007: Processing and Mechanical Deformation	Refractory Metals 2007: Oxidation and Thin Films	Fundamentals of Shape Memory and Related Transitions: Electronic Structure and Phonons	Fundamentals of Shape Memory and Related Transitions: Atomistic and Microstructural Mechanisms	Fundamentals of Shape Memory and Related Transitions: Mechanical Behavior	Fundamentals of Shape Memory and Related Transitions: Multiscale Modeling and Applications	General Abstracts: SMD: Processing and Properties of Light Metals	Europe 6
Advances in Computational Materials Science and Engineering Methods: Methods at the Atom Scale I	Advances in Computational Materials Science and Engineering Methods: Methods at the Atom Scale II	Advances in Computational Materials Science and Engineering Methods: Phase Field Methods I	Advances in Computational Materials Science and Engineering Methods: Phase Field Methods II	Advances in Computational Materials Science and Engineering Methods: Finite Element Method I	Advances in Computational Materials Science and Engineering Methods: Finite Element Method II	Advances in Computational Materials Science and Engineering Methods: Dedicated Computational Methods	Europe 7



MO	Monday		Tues	sday	Wedn	esday	Thursday
ROOM	AM	РМ	АМ	РМ	AM	РМ	AM
Europe 8	Microstructural Processes in Irradiated Materials: Dislocation - Obstacle Interactions and Radiation Induced Segregation	Microstructural Processes in Irradiated Materials: Irradiation Effects in Ceramics	Microstructural Processes in Irradiated Materials: Modeling, Microstructure and Embrittlement in Fe-Cr Alloys	Microstructural Processes in Irradiated Materials: Modeling - and - Poster Session I	Microstructural Processes in Irradiated Materials: Reactor Pressure Vessel Steels	Microstructural Processes in Irradiated Materials: He Effects, Deformation and Fracture - and - Poster Session II	Microstructural Processes in Irradiated Materials: Defect Clusters and Fundamental Radiation Effects
Europe 9	Plasticity from the Atomic Scale to Constitutive Laws: Dislocation Core Structure and Solute-Dislocation Interactions	Plasticity from the Atomic Scale to Constitutive Laws: Dislocation Solute, Precipitate and Grain Boundary Interactions	Plasticity from the Atomic Scale to Constitutive Laws: Atomistic Simulations of Dynamic Processes and Nano-Scale Plasticity	Plasticity from the Atomic Scale to Constitutive Laws: Dislocation Ensembles	Plasticity from the Atomic Scale to Constitutive Laws: Meso-Scale Plasticity	Plasticity from the Atomic Scale to Constitutive Laws: Rate Limiting Behavior and Informed Constitutive Laws	
Europe 10	Advanced Metallic Composites and Alloys for High Performance Applications: Advanced Metallics	Advanced Metallic Composites and Alloys for High Performance Applications: Fe and Ni Alloys and Composites	Advanced Metallic Composites and Alloys for High Performance Applications: Refractory Alloys and Composites	Advanced Metallic Composites and Alloys for High Performance Applications: Al Alloys and Composites	Advanced Metallic Composites and Alloys for High Performance Applications: Ti Alloys and Composites	Advanced Metallic Composites and Alloys for High Performance Applications: Metallic Composites	Computational Thermodynamics and Phase Transformations: Nanomaterials and Confined Systems II
Europe 11	Computational Thermodynamics and Phase Transformations: First Principles and Atomistic Calculations of Phase and Alloy Thermodynamics I	Computational Thermodynamics and Phase Transformations: First Principles and Atomistic Calculations of Phase and Alloy Thermodynamics II	Computational Thermodynamics and Phase Transformations: Microstructure Properties and Evolution I	Computational Thermodynamics and Phase Transformations: Microstructure Properties and Evolution II	Computational Thermodynamics and Phase Transformations: Modeling of Phase Transformations I	Computational Thermodynamics and Phase Transformations: Nanomaterials and Confined Systems I	Computational Thermodynamics and Phase Transformations: Modeling of Phase Transformations II
N. H. Foyer			General Poster Session				
Northern A1	MPMD Symposium: Mechanics and Materials Modeling and Materials Design Methodologies, in the Honor of Dr. Craig Hartley's 40 Years of Contributions to the Field of Mechanics and Materials Science: Microstructure Analysis and Representation I	MPMD Symposium: Mechanics and Materials Modeling and Materials Design Methodologies, in the Honor of Dr. Craig Hartley's 40 Years of Contributions to the Field of Mechanics and Materials Science: Homogenization/ Constitutive Behavior I	MPMD Symposium: Mechanics and Materials Modeling and Materials Design Methodologies, in the Honor of Dr. Craig Hartley's 40 Years of Contributions to the Field of Mechanics and Materials Science: Homogenization/ Constitutive Behavior II	MPMD Symposium: Mechanics and Materials Modeling and Materials Design Methodologies, in the Honor of Dr. Craig Hartley's 40 Years of Contributions to the Field of Mechanics and Materials Science: Materials Design	MPMD Symposium: Mechanics and Materials Modeling and Materials Design Methodologies, in the Honor of Dr. Craig Hartley's 40 Years of Contributions to the Field of Mechanics and Materials Science: Nanostructure, Defects and Properties	MPMD Symposium: Mechanics and Materials Modeling and Materials Design Methodologies, in the Honor of Dr. Craig Hartley's 40 Years of Contributions to the Field of Mechanics and Materials Science: Microstructure Analysis and Representation II	General Abstracts: MPMD: Structure/ Processing/ Properties Relationships
Northern A2	Materials Processing Fundamentals: Solidification and Deformation Processing	Materials Processing Fundamentals: Process Modeling	Materials Processing Fundamentals: Smelting and Refining	Materials Processing Fundamentals: Powders, Composites, Coatings and Measurements	General Abstracts: MPMD: In Situ Synthesis and Rapid Prototyping	General Abstracts: MPMD: Modeling and Simulation of Materials and Processes	General Abstracts: MPMD: Processing and Microstructural Development



Mor	nday	Tuesday Wednesday Tl		Thursday	RO		
AM	РМ	АМ	РМ	AM	РМ	АМ	ROOM
Frontiers in Solidification Science: Nucleation and Crystal Structure	Frontiers in Solidification Science: Atomic Scale - and - Poster Session	Frontiers in Solidification Science: Microstructures I	Frontiers in Solidification Science: Microstructures II	Degradation of Light Weight Alloys: Session I	Degradation of Light Weight Alloys: Session II		Northern A3
General Abstracts: MPMD: Forming of Materials and Processes	Aluminum Alloys for Transportation, Packaging, Aerospace and Other Applications: Aluminum Applications	Aluminum Alloys for Transportation, Packaging, Aerospace and Other Applications: Aluminum Products	Aluminum Alloys for Transportation, Packaging, Aerospace and Other Applications: Alloy Development	Aluminum Alloys for Transportation, Packaging, Aerospace and Other Applications: Alloy Processing	Aluminum Alloys for Transportation, Packaging, Aerospace and Other Applications: Alloy Characterization	Aluminum Alloys for Transportation, Packaging, Aerospace and Other Applications: Alloys Mechanical Behavior	Northern A4
General Abstracts: EPD: Hydrometallurgy, Wastewater Treatment	Cast Shop Technology: Cast House Operations and Melting	Cast Shop Technology: Metal Treatment	Cast Shop Technology: Quality Measurements and Grain Refining	Cast Shop Technology: Casting	Cast Shop Technology: Solidification and Microstructure	Cast Shop Technology: Cast Shop Safety	Northern E1
	Shape Casting: The 2nd International Symposium: Liquid Metal/ Solidification	Shape Casting: The 2nd International Symposium: Process Design/Analysis	Shape Casting: The 2nd International Symposium: Structure/Property	Shape Casting: The 2nd International Symposium: Modeling	Shape Casting: The 2nd International Symposium: Applications/ Novel Processes		Northern E2
General Abstracts: EPD: Pyrometallurgy, Base Metals	Friction Stir Welding and Processing IV: Session I	Friction Stir Welding and Processing IV: Session II	Friction Stir Welding and Processing IV: Session III	Friction Stir Welding and Processing IV: Session IV	Friction Stir Welding and Processing IV: Session V	Friction Stir Welding and Processing IV: Session VI	Northern E3
		Alumina and Bauxite: Alumina Refinery Safety and Integrity	Alumina and Bauxite: Alumina Refinery Design and Development	Alumina and Bauxite: Bauxite, Digestion, Red Mud, Byproducts	Alumina and Bauxite: Role of Surface Chemistry in Enhancing Refinery Performances		Northern E4
Pb-Free Electronic Solders: Alloy Design, Characterization and Service Reliability: Interfacial Effects	Pb-Free Electronic Solders: Alloy Design, Characterization and Service Reliability: Microstructure and Characterization	Pb-Free Electronic Solders: Alloy Design, Characterization and Service Reliability: Electromigration and Void Formation	Pb-Free Electronic Solders: Alloy Design, Characterization and Service Reliability: Whisker Growth, Design, and Modeling	Pb-Free Electronic Solders: Alloy Design, Characterization and Service Reliability: Processing and Reliability Issues	Pb-Free Electronic Solders: Alloy Design, Characterization and Service Reliability: Mechanical Characterization		Oceanic 1
Internet and Other Electronic Resources	Phase Stability, Phase Transformations, and Reactive Phase Formation in Electronic Materials VI: Session I	Phase Stability, Phase Transformations, and Reactive Phase Formation in Electronic Materials VI: Session II	Phase Stability, Phase Transformations, and Reactive Phase Formation in Electronic Materials VI: Session III	Phase Stability, Phase Transformations, and Reactive Phase Formation in Electronic Materials VI: Session IV	Phase Stability, Phase Transformations, and Reactive Phase Formation in Electronic Materials VI: Session V		Oceanic 2



M	Mor	nday	Tues	sday	Wednesday		Thursday
ROOM	АМ	РМ	АМ	РМ	АМ	РМ	АМ
Oceanic 3	2007 Nanomaterials: Fabrication, Properties and Applications: Session I	2007 Nanomaterials: Fabrication, Properties and Applications: Session II	2007 Nanomaterials: Fabrication, Properties and Applications: Session III	2007 Nanomaterials: Fabrication, Properties and Applications: Session IV	2007 Nanomaterials: Fabrication, Properties and Applications: Session V	2007 Nanomaterials: Fabrication, Properties and Applications: Session VI	
Oceanic 4	Wide Band-Gap Semiconductor Nanostructures: Session I	Wide Band-Gap Semiconductor Nanostructures: Session II	Wide Band-Gap Semiconductor Nanostructures: Session III	Wide Band-Gap Semiconductor Nanostructures: Session IV	Integrated Computational Materials Engineering: Lessons from Many Fields: ICME in Materials Science - and - NSF Workshop: CyberInfrastructure to CyberDiscovery for Materials Science	Integrated Computational Materials Engineering: Lessons from Many Fields: ICME in Other Fields - and - National Academies ICME Study Community Town Hall Meeting	General Abstracts: EMPMD: ZnO Thin Films and Liquid Crystals
Oceanic 5	Towards Functional Nanomaterials: Synthesis, Characterization, and Applications: Directed Nano Fabrication	Towards Functional Nanomaterials: Synthesis, Characterization, and Applications: Nano Magnetism, Ferroelectric, Mechanics, and Other Properties	Towards Functional Nanomaterials: Synthesis, Characterization, and Applications: Nanoscale Superstuctures, Metallic Nanoparticles and Plasmon	Towards Functional Nanomaterials: Synthesis, Characterization, and Applications: Nanowires and Nanotubes	Towards Functional Nanomaterials: Synthesis, Characterization, and Applications: Quantum Dots	Innovations in Electrometallurgy: Session I	Innovations in Electrometallurgy: Session II
Oceanic 6	Recent Developments in Semiconductor, Electro Optic and Radio Frequency Materials: Recent Advances in Semiconductor Technologies	Recent Developments in Semiconductor, Electro Optic and Radio Frequency Materials: Progress in Semiconductor Optoelectronics and Beyond	Metrologies for Advanced Materials and Devices: Characterization, Measurement and Testing Science: Metrology for Micro and Nano Structures	Materials in Clean Power Systems II: Fuel Cells, Solar, and Hydrogen- Based Technologies: Hydrogen Storage Materials in Conjuction with the 8th Global Innovations Symposium: Metal Powders for Energy Production and Storage Applications	8th Global Innovations Symposium: Metal Powders for Energy Production and Storage Applications: Session I in Conjuction with the Symposium on Materials for Clean Power Systems II - Hydrogen Storage	8th Global Innovations Symposium: Metal Powders for Energy Production and Storage Applications: Session II	
Oceanic 7	General Abstracts: EMPMD: GaN and Interconnects	Hume-Rothery Symposium: Scattering Studies and the Fundamental Properties of Materials: Session I	Hume-Rothery Symposium: Scattering Studies and the Fundamental Properties of Materials: Session II	Hume-Rothery Symposium: Scattering Studies and the Fundamental Properties of Materials: Session III	Hume-Rothery Symposium: Scattering Studies and the Fundamental Properties of Materials: Session IV	Hume-Rothery Symposium: Scattering Studies and the Fundamental Properties of Materials: Session V	General Abstracts: EMPMD: Magnetic and Ferroelectric Materials
Oceanic 8	Characterization of Minerals, Metals, and Materials: Characterization of Structure across Length Scales I	Characterization of Minerals, Metals, and Materials: Characterization of Structure across Length Scales II	Characterization of Minerals, Metals, and Materials: Characterization of Mechanical and Physical Properties of Materials I	Characterization of Minerals, Metals, and Materials: Characterization of Mechanical and Physical Properties of Materials II	Characterization of Minerals, Metals, and Materials: Characterization of Processing and Properties of Materials	Characterization of Minerals, Metals, and Materials: Characterization of Processing of Materials I	Characterization of Minerals, Metals, and Materials: Characterization of Processing of Materials II

LEARN • NETWORK • ADVANCE

Program-at-a-Glance



Monday		Tues	sday	Wedn	esday	Thursday	RO
АМ	РМ	АМ	РМ	АМ	РМ	АМ	ROOM
Outreach Programs in Materials Science and Engineering: Outreach Programs at Universities	Outreach Programs in Materials Science and Engineering: Outreach Programs in Industry and Government Laboratories						Pacific Hall A
General Abstracts: LMD: Session I	General Abstracts: LMD: Session II			EMPMD Symposium: Advanced Metallizations and Interconnect Technologies, in Honor of Prof. K. N. Tu's 70th Birthday: Advanced Metallizations and Interconnect Technology I	EMPMD Symposium: Advanced Metallizations and Interconnect Technologies, in Honor of Prof. K. N. Tu's 70th Birthday: Advanced Metallizations and Interconnect Technology II		Pacific Hall B
The Material Recycling Industry: Global Challenges and Opportunities: Plenary Session	General Abstracts: EPD: Hydrometallurgy, Metal Recovery	General Abstracts: EPD: High Temperature Processing	Aluminum Reduction Technology: Modelling and Design I	Aluminum Reduction Technology: Modelling II and General		Electrode Technology Symposium (formerly Carbon): Rodding and Coke Inventory	Southern 1
Aluminum Reduction Technology: Environmental and Plant Improvements	Aluminum Reduction Technology: Operational and Technology Improvements	Aluminum Reduction Technology: Slotted Anodes - Joint Session with Electrode Technology Symposium (formerly Carbon)	Aluminum Reduction Technology: Cell Fundamentals, Phenomena and Alternatives	Aluminum Reduction Technology: Anode Effects and Process Control I	Aluminum Reduction Technology: Inert Anode Operation and Low Temperature Electrolyte	Aluminum Reduction Technology: Process Control II and Bath Chemistry	Southern 2
Electrode Technology Symposium (formerly Carbon): Cathode Part I: Cathode Wear and Construction	Electrode Technology Symposium (formerly Carbon): Anode Technology and Production		Electrode Technology Symposium (formerly Carbon): Properties of Inert Anode Materials	Electrode Technology Symposium (formerly Carbon): Anode Baking Furnace Technology	Electrode Technology Symposium (formerly Carbon): Cathode Part II: Preheating and Cell Start Up	Electrode Technology Symposium (formerly Carbon): Cathode Part III: Titanium Diboride	Southern 3
Magnesium Technology 2007: Magnesium Globalization	Magnesium Technology 2007: Wrought Alloys and Forming Processes I: Deformation	Magnesium Technology 2007: Wrought Alloys and Forming Processes II: Rolling and Forming	Magnesium Technology 2007: Wrought Alloys and Forming Processes III: Extrusions	Magnesium Technology 2007: Alloy Development I	Magnesium Technology 2007: Alloy Development II	Magnesium Technology 2007: Corrosion and Coatings	Southern 4
	Magnesium Technology 2007: Automotive Applications and USAMP Programs	Magnesium Technology 2007: Casting and Solidification I	Magnesium Technology 2007: Casting and Solidification II	Magnesium Technology 2007: Primary Production, Recycling and Environmental/ Welding	Magnesium Technology 2007: Thermal Dynamics and Fundamental Research	Magnesium Technology 2007: Microstructure and Properties	Southern 5



2007 Nanomaterials: Fabrication, Properties and Applications: Session I			
2007 Nanomaterials: Fabrication, Properties and Applications: Session II	Oceanic 3	Mon PM	63
2007 Nanomaterials: Fabrication, Properties and Applications: Session III	Oceanic 3	Tue AM	117
2007 Nanomaterials: Fabrication, Properties and Applications: Session IV	Oceanic 3	Tue PM	164
2007 Nanomaterials: Fabrication, Properties and Applications: Session V	Oceanic 3	Wed AM	223
2007 Nanomaterials: Fabrication, Properties and Applications: Session VI	Oceanic 3	Wed PM	
8th Global Innovations Symposium: Metal Powders for Energy Production and Storage Applications: Session I in Conjuction with Materials for Clean Power Systems II - Hydrogen Storage	Oceanic 6	Wed AM	224
8th Global Innovations Symposium: Metal Powders for Energy Production and Storage Applications: Session II	Oceanic 6	Wed PM	276
8th Global Innovations Symposium: Trends in Materials and Manufacturing Technologies for Energy Production: Plenary	Austrailia 3	Mon PM	64
8th Global Innovations Symposium: Trends in Materials and Manufacturing Technologies for Energy Production: Session I	Austrailia 3	Tue PM	166
Advanced Metallic Composites and Alloys for High Performance Applications: Advanced Metallics	Europe 10	Mon AM	17
Advanced Metallic Composites and Alloys for High Performance Applications: Al Alloys	-		
and Composites	Europe 10	Tue PM	167
Advanced Metallic Composites and Alloys for High Performance Applications: Fe and Ni Alloys			
and Composites	-		
Advanced Metallic Composites and Alloys for High Performance Applications: Metallic Composites	Europe 10	Wed PM	
Advanced Metallic Composites and Alloys for High Performance Applications: Refractory Alloys and Composites	Europe 10	Tue AM	118
Advanced Metallic Composites and Alloys for High Performance Applications: Ti Alloys and Composites	Europe 10	Wed AM	225
Advances in Computational Materials Science and Engineering Methods: Dedicated Computational Methods	Europe 7	Thu AM	327
Advances in Computational Materials Science and Engineering Methods: Finite Element Method I	Europe 7	Wed AM	227
Advances in Computational Materials Science and Engineering Methods: Finite Element Method II	Europe 7	Wed PM	
Advances in Computational Materials Science and Engineering Methods: Methods at the Atom Scale I	Europe 7	Mon AM	18
Advances in Computational Materials Science and Engineering Methods: Methods at the Atom Scale II.	Europe 7	Mon PM	67
Advances in Computational Materials Science and Engineering Methods: Phase Field Methods I	Europe 7	Tue AM	119
Advances in Computational Materials Science and Engineering Methods: Phase Field Methods II	Europe 7	Tue PM	168
Advances in Microstructure-Based Modeling and Characterization of Deformation Microstructures: Characterization of Deformed Structures I	Europe 1	Mon AM	19
Advances in Microstructure-Based Modeling and Characterization of Deformation Microstructures: Characterization of Deformed Structures II	Europe 1	Tue AM	120
Advances in Microstructure-Based Modeling and Characterization of Deformation Microstructures: Characterization of Deformed Structures III	Europe 1	Wed PM	279
Advances in Microstructure-Based Modeling and Characterization of Deformation Microstructures: Modeling of Deformed Structures I	Europe 1	Mon PM	68
Advances in Microstructure-Based Modeling and Characterization of Deformation Microstructures: Modeling of Deformed Structures II	Europe 1	Tue PM	169
Advances in Microstructure-Based Modeling and Characterization of Deformation Microstructures: Modeling of Deformed Structures III	Europe 1	Wed AM	228
Alumina and Bauxite: Alumina Refinery Design and Development	Northern E4	Tue PM	171
Alumina and Bauxite: Alumina Refinery Safety and Integrity	Northern E4	Tue AM	122
Alumina and Bauxite: Bauxite, Digestion, Red Mud, Byproducts	Northern E4	Wed AM	229
Alumina and Bauxite: Role of Surface Chemistry in Enhancing Refinery Performance	Northern E4	Wed PM	
Aluminum Alloys for Transportation, Packaging, Aerospace and Other Applications: Alloy Characterization			
Aluminum Alloys for Transportation, Packaging, Aerospace and Other Applications:			
Alloy Development	Northern A4	Tue PM	172

LEARN • NETWORK • ADVANCE

Session Listing



Atumizent Alloy for Transportation, Packaging, Aerospace and Other Applications: Northern A4 101 AM 327 Atumizent Alloys for Transportation, Packaging, Aerospace and Other Applications: Northern A4 Mon PM 69 Atumizent Alloys for Transportation, Packaging, Aerospace and Other Applications: Northern A4 122 Atumizent Alloys for Transportation, Packaging, Aerospace and Other Applications: Northern A4 123 Atumizent Reluction Technology: Cheff Fundamentals, Phenomena and Alternatives. Southern 2 Weid AM 211 Atumizent Reluction Technology: Twommenal and Plant Improvements Southern 2 Weid AM 213 Atumizent Reluction Technology: Twommenal and Plant Improvements Southern 1 Weid AM 223 Atumizent Reluction Technology: Southern 2 Weid AM 223 Atumizent Reluction Technology: Consets Control II and Bath Chenistry Southern 2 Weid AM 223 Atumizent Reluction Technology: South Annels 1 Europe 4 Weid AM 224 Biological Materials Science: Biological Materials 1 Europe 4 Weid AM 226 Biological Materials Science: Biological Materials 1 Europe 4 Weid AM 237	Aluminum Alloys for Transportation, Packaging, Aerospace and Other Applications: Alloy Processing	Northern A4	Wed AM	230
Aluminum Aluys for Transportation, Packaging, Aerospace and Other Applications: Northern A4 The AM .09 Aluminum Neukus, for Transportation, Packaging, Aerospace and Other Applications: Northern A4 The AM .122 Aluminum Reduction Technology: Anode Elifects and Process Control I Southern 2 .Wed AM .211 Aluminum Reduction Technology: Call Fundamentals, Phenomena and Alternatives Southern 2 .Wed AM .232 Aluminum Reduction Technology: Mande Elifects and Process Control I Southern 2 .Wed PM .283 Aluminum Reduction Technology: Modelling and Design I		Northern A4	Thu AM	
Aluminum Alboys for Transportation, Packaging, Acrospace and Other Applications: Aluminum Products: Aluminum Reduction Technology: Anode Effects and Process Conrol I				
Aluminum Products Northern A4 Tite AM [122 Aluminum Reduction Technology: Cell Fundamentals, Phenomena and Alkenatives Southern 2 Wed AM 231 Aluminum Reduction Technology: Environmental and Plant Improvements Southern 2 Wed PM 213 Aluminum Reduction Technology: Environmental and Plant Improvements Southern 1 Wel PM 283 Aluminum Reduction Technology: Modelling at Design 1 Southern 1 Wel PM 274 Aluminum Reduction Technology: Coreational and Technology Improvements Southern 2 Mon PM 770 Aluminum Reduction Technology: Operational and Enh Chemistry Southern 2 Tite AM 232 Aluminum Reduction Technology: Operational and Enh Chemistry Southern 2 Tite AM 232 Aluminum Reduction Technology: Stotted Anodes - Joint Session with Electrode Technology Southern 2 Tite AM 233 Biological Materials Science: Biological Materials I Europe 4 Tite AM 330 Biological Materials Science: Biological Materials I Europe 4 Wed AM 233 Biological Materials Science: Biological Materials I Europe 4 Wed AM 233		Northern A4	Mon PM	69
Aluminum Reduction Technology: Environmental and Plant Improvements Southern 2 Tue PM		Northern A4	Tue AM	122
Aluminum Reduction Technology: Environmental and Plant Improvements	Aluminum Reduction Technology: Anode Effects and Process Control I	Southern 2	Wed AM	231
Aluminum Reduction Technology: Inert Anode Operation and Low Temperature Electrolyte	Aluminum Reduction Technology: Cell Fundamentals, Phenomena and Alternatives	Southern 2	Tue PM	173
Aluminum Reduction Technology: Modelling and Design 1	Aluminum Reduction Technology: Environmental and Plant Improvements	Southern 2	Mon AM	21
Aluminum Reduction Technology: Modelling II and General	Aluminum Reduction Technology: Inert Anode Operation and Low Temperature Electrolyte	Southern 2	Wed PM	
Aluminum Reduction Technology: Operational and Technology Improvements Southern 2 Mon PM .70 Aluminum Reduction Technology: Process Control II and Bath Chemistry Southern 2 Thu AM .329 Aluminum Reduction Technology: Sloted Anderála Europe 4 Mon AM .22 Biological Materials Science: Biological Materials I Europe 4 Tue AM .330 Biological Materials Science: Biological Materials II Europe 4 .Tue AM .330 Biological Materials Science: Biological Materials Allor-Metrical Europe 4 .Wed MA .233 Biological Materials Science: Functional Biomaterials and Devices Europe 4 .Wed PM .284 Biological Materials Science: Functional Biomaterials Europe 4 .Wed PM .284 Biological Materials Science: Functional Biomaterials Europe 4 .Wed PM .213 Biological Materials Science: Ruptant Biomaterials Europe 4 .Wed PM .214 Biological Materials Science: Ruptant Biomaterials Europe 4 .Wed PM .264 Biological Materials Science: Ruptant Biomaterials Europe 4 .Wed PM .264 Biological Materials Science: Ruptant Biomaterials and Devices Europe 4 .Wed PM	Aluminum Reduction Technology: Modelling and Design I	Southern 1	Tue PM	174
Aluminum Reduction Technology: Process Control II and Bath Chemistry	Aluminum Reduction Technology: Modelling II and General	Southern 1	Wed AM	232
Aluminum Reduction Technology: Slotted Anodes - Joint Session with Electrode Technology Tue AM 123 Biological Materials Science: Biological Materials I Europe 4 Mon AM 22 Biological Materials Science: Biological Materials I Europe 4 Tue AM 124 Biological Materials Science: Biological Materials Bio-Medical Europe 4 Tue PM 175 Biological Materials Science: Biological Materials and Devices Europe 4 Wed PM 284 Biological Materials Science: Mechanical Behavior of Biomaterials Europe 4 Mon PM .71 Biological Materials Science: Nethanical Behavior of Biomaterials Europe 4 Mon PM .71 Biological Materials Science: Nethanical Poperties I Asia 1 Tue AM 126 Bulk Metallic Glasses IV: Alloy Development and Glass-Forming Ability Asia 1 Mon PM .73 Bulk Metallic Glasses IV: Mechanical Properties I Asia 1 Mon PM .73 Bulk Metallic Glasses IV: Mechanical Properties II Asia 1 Wed PM .246 Bulk Metallic Glasses IV: Supercooled Liquids and Crystallization Asia 1 Wed AM .235 Gas Shop Technology: Cast Biops Safety Northern E1 Mon PM .74 </td <td>Aluminum Reduction Technology: Operational and Technology Improvements</td> <td>Southern 2</td> <td> Mon PM</td> <td>70</td>	Aluminum Reduction Technology: Operational and Technology Improvements	Southern 2	Mon PM	70
Biological Materials Science: Biological Materials I. Europe 4 Mon AM .22 Biological Materials Science: Biological Materials II. Europe 4 Tue AM .124 Biological Materials Science: Biological Materials II. Europe 4 Tue AM .330 Biological Materials Science: Implant Biomaterials and Devices Europe 4 Wed PM .224 Biological Materials Science: Implant Biomaterials Europe 4 Wed AM .233 Biological Materials Science: Implant Biomaterials Europe 4 Wed AM .233 Biological Materials Science: Mechanical Behavior of Biomaterials Europe 4 .10e PM .716 Biological Materials Science: Secince and Technology Asia 1 .10e AM .236 Bulk Metallic Glasses IV: Glass Science and Technology Asia 1 .10e PM .777 Bulk Metallic Glasses IV: Mechanical Properties II. Asia 1 .10e PM .777 Bulk Metallic Glasses IV: Sepercoled Liquids and Crystallization. Asia 1 .10e PM .773 Bulk Metallic Glasses IV: Sepercoled Liquids and Crystallization. Asia 1 .10e PM .744 Supercoled Liquids and Crystallization. Asia 1 .10e AM .235	Aluminum Reduction Technology: Process Control II and Bath Chemistry	Southern 2	Thu AM	329
Biological Materials Science: Biological Materials I. Europe 4 Tue AM. 124 Biological Materials Science: Biological Materials Bio-Medical Europe 4 Thu AM. 330 Biological Materials Science: Functional Biomaterials and Devices Europe 4 Tue PM. 175 Biological Materials Science: Implant Biomaterials and Devices Europe 4 Wed PM. 233 Biological Materials Science: Implant Biomaterials Europe 4 Wed PM. 71 Biological Materials Science: Poster Session Europe 4 Mon PM 71 Biological Materials Science: Instead and Glass-Forming Ability Asia 1 Tue AM. 126 Bulk Metallic Glasses IV: Altoy Development and Glass-Forming Ability Asia 1 Mon PM 73 Bulk Metallic Glasses IV: Mechanical Properties I Asia 1 Mon PM 73 Bulk Metallic Glasses IV: Mechanical Properties II Asia 1 Tue PM 177 Bulk Metallic Glasses IV: Mechanical Properties II Asia 1 Tue PM 717 Bulk Metallic Glasses IV: Mechanical Properties II Asia 1 Tue AM 331 Bulk Metallic Glasses IV: Supercooled Liquids and Crystallization Asia 1 Thu AM 331	Aluminum Reduction Technology: Slotted Anodes - Joint Session with Electrode Technology	Southern 2	Tue AM	123
Biological Materials Science: Biological Materials/Bio-Medical Europe 4 Thu AM. 330 Biological Materials Science: Functional Biomaterials and Devices Europe 4 Wed PM. 284 Biological Materials Science: Implant Biomaterials and Devices Europe 4 Wed AM 233 Biological Materials Science: Inplant Biomaterials Europe 4 Wed AM 233 Biological Materials Science: Nethanical Behavior of Biomaterials Europe 4 Mon PM .71 Bulk Metallis Classes IV: Alloy Development and Glass-Forming Ability Asia 1 Tue AM .126 Bulk Metallic Glasses IV: Mechanical Properties I Asia 1 Mon PM .73 Bulk Metallic Glasses IV: Mechanical Properties II Asia 1 Tue AM .236 Bulk Metallic Glasses IV: Mechanical Properties II Asia 1 Tue AM .236 Bulk Metallic Glasses IV: Mechanical Properties II Asia 1 Thu AM .331 Bulk Metallic Glasses IV: Processing and Mechanical Properties IV Asia 1 Thu AM .331 Bulk Metallic Glasses IV: Supercooled Liquids and Crystallization. Asia 1 Thu AM .333 Gast Shop Technology: Cast Shop Safety Northern E1 Thu AM .333 <	Biological Materials Science: Bioinspired Materials	Europe 4	Mon AM	22
Biological Materials Science: Biological Materials/Bio-Medical Europe 4 Tue PM	Biological Materials Science: Biological Materials I	Europe 4	Tue AM	124
Biological Materials Science: Functional Biomaterials and Devices Europe 4 Wed PM. .284 Biological Materials Science: Implant Biomaterials Europe 4 Wed AM .233 Biological Materials Science: Netchanical Behavior of Biomaterials Europe 4 Mon PM .71 Biological Materials Science: Poster Session Europe 4 Tue PM .176 Bulk Metallic Glasses IV: Alloy Development and Glass-Forming Ability Asia 1 Tue AM .126 Bulk Metallic Glasses IV: Mechanical Properties I Asia 1 Mon AM .23 Bulk Metallic Glasses IV: Mechanical Properties II Asia 1 Tue PM .177 Bulk Metallic Glasses IV: Mechanical Properties II Asia 1 Tue PM .177 Bulk Metallic Glasses IV: Mechanical Properties II Asia 1 Tue PM .286 Bulk Metallic Glasses IV: Processing and Mechanical Properties IV Asia 1 .104 .235 Cast Shop Technology: Cast House Operations and Melting Northern E1 Mon PM .744 Cast Shop Technology: Cast House Operations and Melting Northern E1 Tue AM .237 Cast Shop Technology: Cast Glass and Metrials: Characterization of Minerals, Metals, and Materials: Characterization of Mechanical and Physical<	Biological Materials Science: Biological Materials II	Europe 4	Thu AM	
Biological Materials Science: Implant Biomaterials Europe 4 Wed AM 233 Biological Materials Science: Mechanical Behavior of Biomaterials Europe 4 Mon PM 71 Biological Materials Science: Poster Session Europe 4 Mon PM 71 Biological Materials Science: Poster Session Europe 4 Mon PM 716 Bulk Metallic Glasses IV: Alloy Development and Glass-Forming Ability Asia 1 Tue AM 126 Bulk Metallic Glasses IV: Mechanical Properties I Asia 1 Mon AM 233 Bulk Metallic Glasses IV: Mechanical Properties II Asia 1 Mon PM 773 Bulk Metallic Glasses IV: Mechanical Properties II Asia 1 Thu AM 331 Bulk Metallic Glasses IV: Supercooled Liquids and Crystallization Asia 1 Thu AM 331 Bulk Metallic Glasses IV: Supercooled Liquids and Crystallization Asia 1 Wed AM 235 Cast Shop Technology: Cast Bhop Safety Northern E1 Mon PM 74 Cast Shop Technology: Casting Northern E1 Thu AM 333 Cast Shop Technology: Quality Messurements and Grain Refining Northern E1 Tue AM 127 Cast Shop Technology: Solidification and M	Biological Materials Science: Biological Materials/Bio-Medical	Europe 4	Tue PM	175
Biological Materials Science: Mechanical Behavior of Biomaterials Europe 4 Mon PM 71 Biological Materials Science: Poster Session Europe 4 Tue PM 176 Bulk Metallic Glasses IV: Alloy Development and Glass-Forming Ability Asia 1 Tue AM 126 Bulk Metallic Glasses IV: Glass Science and Technology Asia 1 Mon AM 23 Bulk Metallic Glasses IV: Mechanical Properties I Asia 1 Mon PM 73 Bulk Metallic Glasses IV: Mechanical Properties II Asia 1 Mon PM 73 Bulk Metallic Glasses IV: Mechanical Properties III Asia 1 Tue PM 177 Bulk Metallic Glasses IV: Mechanical Properties IV Asia 1 Thu AM 331 Bulk Metallic Glasses IV: Supercooled Liquids and Crystallization Asia 1 Wed PM 235 Cast Shop Technology: Cast House Operations and Melting Northern E1 Mon PM 74 Cast Shop Technology: Casting Northern E1 Tue AM 233 Cast Shop Technology: Casting Northern E1 Tue AM 237 Cast Shop Technology: Quality Measurements and Grain Refining Northern E1 Tue AM 127 Cast Shop Technology: Solidification and Microstruc	Biological Materials Science: Functional Biomaterials and Devices	Europe 4	Wed PM	
Biological Materials Science: Poster Session Europe 4 Tue PM 176 Bulk Metallic Glasses IV: Alloy Development and Glass-Forming Ability Asia 1 Tue AM 126 Bulk Metallic Glasses IV: Glass Science and Technology Asia 1 Mon AM 23 Bulk Metallic Glasses IV: Mechanical Properties I Asia 1 Mon AM 23 Bulk Metallic Glasses IV: Mechanical Properties II. Asia 1 Tue PM 177 Bulk Metallic Glasses IV: Mechanical Properties III. Asia 1 Wed PM 286 Bulk Metallic Glasses IV: Supercooled Liquids and Crystallization. Asia 1 Thu AM 331 Bulk Metallic Glasses IV: Supercooled Liquids and Crystallization. Asia 1 Wed AM 235 Cast Shop Technology: Cast House Operations and Melting Northern E1 Mon PM 74 Cast Shop Technology: Casting Northern E1 Tue AM 233 Cast Shop Technology: Casting Northern E1 Tue AM 237 Cast Shop Technology: Casting Northern E1 Tue AM 237 Cast Shop Technology: Metal Treatment. Northern E1 Tue AM 237 Cast Shop Technology: Quality Measurements and Grain Refining Northern	Biological Materials Science: Implant Biomaterials	Europe 4	Wed AM	233
Bulk Metallic Glasses IV: Alloy Development and Glass-Forming Ability Asia 1 Tue AM 126 Bulk Metallic Glasses IV: Glass Science and Technology Asia 1 Mon AM 23 Bulk Metallic Glasses IV: Mechanical Properties I Asia 1 Mon PM 73 Bulk Metallic Glasses IV: Mechanical Properties II Asia 1 Tue PM 177 Bulk Metallic Glasses IV: Mechanical Properties III Asia 1 Wed PM 286 Bulk Metallic Glasses IV: Supercooled Liquids and Crystallization Asia 1 Thu AM 331 Bulk Metallic Glasses IV: Supercooled Liquids and Crystallization Asia 1 Wed AM 235 Cast Shop Technology: Cast House Operations and Melting Northern E1 Mon PM 74 Cast Shop Technology: Casting Northern E1 Thu AM 333 Cast Shop Technology: Casting Northern E1 Tue AM 237 Cast Shop Technology: Quality Measurements and Grain Refining Northern E1 Tue AM 237 Cast Shop Technology: Quality Measurements and Grain Refining Oceanic 8 Tue AM 238 Characterization of Minerals, Metals, and Materials: Characterization of Mechanical and Physical Properties of Materials I Oceanic 8 Tue	Biological Materials Science: Mechanical Behavior of Biomaterials	Europe 4	Mon PM	71
Bulk Metallic Glasses IV: Glass Science and Technology Asia 1 Mon AM 23 Bulk Metallic Glasses IV: Mechanical Properties I Asia 1 Mon PM 73 Bulk Metallic Glasses IV: Mechanical Properties II Asia 1 Tue PM 177 Bulk Metallic Glasses IV: Mechanical Properties II Asia 1 Tue PM 286 Bulk Metallic Glasses IV: Mechanical Properties II Asia 1 Wed PM 286 Bulk Metallic Glasses IV: Supercooled Liquids and Crystallization Asia 1 Thu AM 331 Bulk Metallic Glasses IV: Supercooled Liquids and Crystallization Asia 1 Wed AM 235 Cast Shop Technology: Cast House Operations and Melting Northern E1 Mon PM 74 Cast Shop Technology: Casting Northern E1 Thu AM 333 Cast Shop Technology: Quality Measurements and Grain Refining Northern E1 Tue AM 127 Cast Shop Technology: Solidification and Microstructure Northern E1 Wed PM 288 Characterization of Minerals, Metals, and Materials: Characterization of Mechanical and Physical Properties of Materials I Oceanic 8 Tue AM 128 Characterization of Minerals, Metals, and Materials: Characterization of Processing and Properties	Biological Materials Science: Poster Session	Europe 4	Tue PM	176
Bulk Metallic Glasses IV: Mechanical Properties I Asia 1 Mon PM 73 Bulk Metallic Glasses IV: Mechanical Properties II Asia 1 Tue PM 177 Bulk Metallic Glasses IV: Mechanical Properties III Asia 1 Wed PM 286 Bulk Metallic Glasses IV: Processing and Mechanical Properties IV Asia 1 Hue AM 331 Bulk Metallic Glasses IV: Supercooled Liquids and Crystallization Asia 1 Wed AM 235 Cast Shop Technology: Cast House Operations and Melting Northern E1 Mon PM 74 Cast Shop Technology: Cast House Operations and Melting Northern E1 Thu AM 333 Cast Shop Technology: Cast House Operations and Grain Refining Northern E1 Tue AM 237 Cast Shop Technology: Quality Measurements and Grain Refining Northern E1 Tue AM 127 Cast Shop Technology: Solidification and Microstructure Northern E1 Wed PM 288 Characterization of Minerals, Metals, and Materials: Characterization of Mechanical and Physical Properties of Materials I Oceanic 8 Tue AM 128 Characterization of Minerals, Metals, and Materials: Characterization of Processing and Properties Oceanic 8 Wed AM 238 Charact	Bulk Metallic Glasses IV: Alloy Development and Glass-Forming Ability	Asia 1	Tue AM	126
Bulk Metallic Glasses IV: Mechanical Properties II Asia 1 Tue PM 177 Bulk Metallic Glasses IV: Mechanical Properties III Asia 1 Wed PM 286 Bulk Metallic Glasses IV: Processing and Mechanical Properties IV Asia 1 Thu AM 331 Bulk Metallic Glasses IV: Supercooled Liquids and Crystallization Asia 1 Wed AM 235 Cast Shop Technology: Cast House Operations and Melting Northern El Mon PM 74 Cast Shop Technology: Cast Shop Safety. Northern El Thu AM 333 Cast Shop Technology: Cast Grag Northern El Wed AM 237 Cast Shop Technology: Casting Northern El Thu AM 333 Cast Shop Technology: Quality Measurements and Grain Refining Northern El Tue AM 127 Cast Shop Technology: Solidification and Microstructure Northern El Wed AM 288 Characterization of Minerals, Metals, and Materials: Characterization of Mechanical and Physical Properties of Materials I Oceanic 8 Tue AM 128 Characterization of Minerals, Metals, and Materials: Characterization of Processing and Properties of Materials II Oceanic 8 Wed AM 238 Characterization of Minerals, Metals, and Materials:	Bulk Metallic Glasses IV: Glass Science and Technology	Asia 1	Mon AM	23
Bulk Metallic Glasses IV: Mechanical Properties III Asia 1 Wed PM 286 Bulk Metallic Glasses IV: Processing and Mechanical Properties IV Asia 1 Thu AM 331 Bulk Metallic Glasses IV: Supercooled Liquids and Crystallization. Asia 1 Wed AM 235 Cast Shop Technology: Cast House Operations and Melting. Northern E1 Mon PM 74 Cast Shop Technology: Cast Shop Safety Northern E1 Thu AM 333 Cast Shop Technology: Casting Northern E1 Thu AM 235 Cast Shop Technology: Casting Northern E1 Thu AM 333 Cast Shop Technology: Metal Treatment. Northern E1 Tue AM 237 Cast Shop Technology: Quality Measurements and Grain Refining Northern E1 Tue AM 127 Cast Shop Technology: Solidification and Microstructure Northern E1 Wed PM 288 Characterization of Minerals, Metals, and Materials: Characterization of Mechanical and Physical Properties of Materials I Oceanic 8 Tue AM 128 Characterization of Minerals, Metals, and Materials: Characterization of Processing and Properties Oceanic 8 Wed AM 238 Characterization of Minerals, Metals, and Materials: Characterization of Pro	Bulk Metallic Glasses IV: Mechanical Properties I	Asia 1	Mon PM	73
Bulk Metallic Glasses IV: Processing and Mechanical Properties IV. Asia 1 Thu AM.	Bulk Metallic Glasses IV: Mechanical Properties II	Asia 1	Tue PM	177
Bulk Metallic Glasses IV: Supercooled Liquids and Crystallization Asia 1 Wed AM 235 Cast Shop Technology: Cast House Operations and Melting Northern E1 Mon PM .74 Cast Shop Technology: Cast Shop Safety Northern E1 Mon PM .74 Cast Shop Technology: Cast Shop Safety Northern E1 Mu AM .333 Cast Shop Technology: Casting Northern E1 Wed AM .237 Cast Shop Technology: Metal Treatment Northern E1 Wed AM .237 Cast Shop Technology: Quality Measurements and Grain Refining Northern E1 Tue AM .127 Cast Shop Technology: Solidification and Microstructure Northern E1 Wed PM .288 Characterization of Minerals, Metals, and Materials: Characterization of Mechanical and Physical Oceanic 8 Tue AM .128 Characterization of Minerals, Metals, and Materials: Characterization of Mechanical and Physical Oceanic 8 Tue PM .179 Characterization of Minerals, Metals, and Materials: Characterization of Processing and Properties Oceanic 8 Wed AM .238 Characterization of Minerals, Metals, and Materials: Characterization of Processing of Materials I Oceanic 8 Wed AM .238 Characterization o	Bulk Metallic Glasses IV: Mechanical Properties III	Asia 1	Wed PM	
Cast Shop Technology: Cast House Operations and Melting	Bulk Metallic Glasses IV: Processing and Mechanical Properties IV	Asia 1	Thu AM	
Cast Shop Technology: Cast Shop Safety	Bulk Metallic Glasses IV: Supercooled Liquids and Crystallization	Asia 1	Wed AM	235
Cast Shop Technology: Casting	Cast Shop Technology: Cast House Operations and Melting	Northern E1	Mon PM	74
Cast Shop Technology: Metal Treatment	Cast Shop Technology: Cast Shop Safety	Northern E1	Thu AM	
Cast Shop Technology: Quality Measurements and Grain Refining	Cast Shop Technology: Casting	Northern E1	Wed AM	237
Cast Shop Technology: Solidification and Microstructure	Cast Shop Technology: Metal Treatment	Northern E1	Tue AM	127
Characterization of Minerals, Metals, and Materials: Characterization of Mechanical and Physical Properties of Materials I	Cast Shop Technology: Quality Measurements and Grain Refining	Northern E1	Tue PM	179
Properties of Materials I. Oceanic 8 Tue AM 128 Characterization of Minerals, Metals, and Materials: Characterization of Mechanical and Physical Oceanic 8 Tue PM 179 Properties of Materials II Oceanic 8 Tue PM 179 Characterization of Minerals, Metals, and Materials: Characterization of Processing and Properties Oceanic 8 Wed AM 238 Characterization of Minerals, Metals, and Materials: Characterization of Processing of Materials I. Oceanic 8 Wed AM 238 Characterization of Minerals, Metals, and Materials: Characterization of Processing of Materials I. Oceanic 8 Wed PM 289 Characterization of Minerals, Metals, and Materials: Characterization of Processing of Materials II Oceanic 8 Thu AM 334 Characterization of Minerals, Metals, and Materials: Characterization of Structure across Oceanic 8 Mon AM 25 Characterization of Minerals, Metals, and Materials: Characterization of Structure across Oceanic 8 Mon AM 25	Cast Shop Technology: Solidification and Microstructure	Northern E1	Wed PM	
Properties of Materials II Oceanic 8 Tue PM 179 Characterization of Minerals, Metals, and Materials: Characterization of Processing and Properties Oceanic 8 Wed AM 238 Characterization of Minerals, Metals, and Materials: Characterization of Processing of Materials I. Oceanic 8 Wed AM 238 Characterization of Minerals, Metals, and Materials: Characterization of Processing of Materials I. Oceanic 8 Wed PM 289 Characterization of Minerals, Metals, and Materials: Characterization of Processing of Materials II Oceanic 8 Thu AM 334 Characterization of Minerals, Metals, and Materials: Characterization of Structure across Oceanic 8 Mon AM 25 Characterization of Minerals, Metals, and Materials: Characterization of Structure across Oceanic 8 Mon AM 25		Oceanic 8	Tue AM	128
of Materials		Oceanic 8	Tue PM	179
Characterization of Minerals, Metals, and Materials: Characterization of Processing of Materials II	6 I	Oceanic 8	Wed AM	238
Characterization of Minerals, Metals, and Materials: Characterization of Structure across Length Scales I	Characterization of Minerals, Metals, and Materials: Characterization of Processing of Materials I	Oceanic 8	Wed PM	
Characterization of Minerals, Metals, and Materials: Characterization of Structure across Length Scales I	Characterization of Minerals, Metals, and Materials: Characterization of Processing of Materials II	Oceanic 8	Thu AM	
Characterization of Minerals, Metals, and Materials: Characterization of Structure across		Oceanic 8	Mon AM	25
	Characterization of Minerals, Metals, and Materials: Characterization of Structure across			



Computational Thermodynamics and Phase Transformations: First Principles and Atomistic Calculations of Phase and Alloy Thermodynamics I	Europe 11	Mon AM	
Computational Thermodynamics and Phase Transformations: First Principles and Atomistic Calculations of Phase and Alloy Thermodynamics II	Europe 11	Mon PM	77
Computational Thermodynamics and Phase Transformations: Microstructure Properties and Evolution I.	Europe 11	Tue AM	130
Computational Thermodynamics and Phase Transformations: Microstructure Properties and Evolution II	Europe 11	Tue PM	
Computational Thermodynamics and Phase Transformations: Modeling of Phase Transformations I			
Computational Thermodynamics and Phase Transformations: Modeling of Phase Transformations II	-		
Computational Thermodynamics and Phase Transformations: Nanomaterials and Confined Systems I	Europe 11	Wed PM	
Computational Thermodynamics and Phase Transformations: Nanomaterials and Confined Systems II	-		
Degradation of Light Weight Alloys: Session I	*		
Degradation of Light Weight Alloys: Session II			
Diffusion in Advanced Materials and Processing: Atomistic and Multiscale Simulations			
Diffusion in Advanced Materials and Processing: Energy Technology	-		
Diffusion in Advanced Materials and Processing: Interfaces, Surfaces and Nanostructures	-		
Diffusion in Advanced Materials and Processing: Intermetallics and Glasses	-		
Diffusion in Advanced Materials and Processing: Materials Processing	-		
Diffusion in Advanced Materials and Processing: Phenomenology and Experiments			
Dynamic Behavior of Materials: Deformation I	*		
Dynamic Behavior of Materials: Deformation II	-		
Dynamic Behavior of Materials: Deformation III	-		
Dynamic Behavior of Materials: Deformation IV	1		
Dynamic Behavior of Materials: Fracture	-		
Dynamic Behavior of Materials: Mechanical Properties I	-		
Dynamic Behavior of Materials: Mechanical Properties II	-		
Electrode Technology Symposium (formerly Carbon Technology): Anode Baking Furnace Technology .	-		
Electrode Technology Symposium (formerly Carbon Technology): Anode Technology and Production			
Electrode Technology Symposium (formerly Carbon Technology): Cathode Part I: Cathode Wear			
and Construction	Southern 3	Mon AM	30
Electrode Technology Symposium (formerly Carbon Technology): Cathode Part II: Preheating			
and Cell Start Up			
Electrode Technology Symposium (formerly Carbon Technology): Cathode Part III: Titanium Diboride			
Electrode Technology Symposium (formerly Carbon Technology): Properties of Inert Anode Materials			
Electrode Technology Symposium (formerly Carbon Technology): Rodding and Coke Inventory	Southern 1	Thu AM	
Electrode Technology Symposium (formerly Carbon Technology): Slotted Anodes - Joint Session with Aluminum Reduction Technology	Southern 2		123
Electronic, Magnetic and Photonic Materials Division Symposium: Advanced Metallizations and Interconnect Technologies, in Honor of Prof. K. N. Tu's 70th Birthday: Advanced Metallizations and Interconnect Technology I			
Electronic, Magnetic and Photonic Materials Division Symposium: Advanced Metallizations and	. Распіс пап в	wed AM	240
Interconnect Technologies, in Honor of Prof. K. N. Tu's 70th Birthday: Advanced Metallizations and Interconnect Technology II	Pacific Hall B	Wed PM	
Friction Stir Welding and Processing IV: Session I	Northern E3	Mon PM	
Friction Stir Welding and Processing IV: Session II	Northern E3	Tue AM	134
Friction Stir Welding and Processing IV: Session III	Northern E3	Tue PM	
Friction Stir Welding and Processing IV: Session IV	Northern E3	Wed AM	247
Friction Stir Welding and Processing IV: Session V	Northern E3	Wed PM	297
Friction Stir Welding and Processing IV: Session VI	Northern E3	Thu AM	341
Frontiers in Solidification Science: Atomic Scale	Northern A3	Mon PM	

Session Listing



Frontiers in Solidification Science: Microstructures I	Northern A3	Tue AM	135
Frontiers in Solidification Science: Microstructures II	Northern A3	Tue PM	
Frontiers in Solidification Science: Nucleation and Crystal Structure	Northern A3	Mon AM	31
Frontiers in Solidification Science: Poster Session	Northern A3	Mon PM	84
Fundamentals of Shape Memory and Related Transitions: Atomistic and Microstructural Mechanisms	Europe 6	Tue PM	189
Fundamentals of Shape Memory and Related Transitions: Electronic Structure and Phonons	Europe 6	Tue AM	136
Fundamentals of Shape Memory and Related Transitions: Mechanical Behavior	Europe 6	Wed AM	248
Fundamentals of Shape Memory and Related Transitions: Multiscale Modeling and Applications	Europe 6	Wed PM	299
General Abstracts: Electronic, Magnetic, and Photonic Materials Division: GaN and Interconnects	Oceanic 7	Mon AM	32
General Abstracts: Electronic, Magnetic, and Photonic Materials Division: Magnetic and Ferroelectric Materials	Oceanic 7	Thu AM	343
General Abstracts: Electronic, Magnetic, and Photonic Materials Division: ZnO Thin Films and			
Liquid Crystals			
General Abstracts: Extraction and Processing: High Temperature Processing			
General Abstracts: Extraction and Processing: Hydrometallurgy, Metal Recovery			
General Abstracts: Extraction and Processing: Hydrometallurgy, Wastewater Treatment			
General Abstracts: Extraction and Processing: Pyrometallurgy, Base Metals			
General Abstracts: Light Metals Division: Session I			
General Abstracts: Light Metals Division: Session II	Pacific Hall B	Mon PM	
General Abstracts: Materials Processing and Manufacturing Division: Forming of Materials and Processes	Northern A4	Mon AM	37
General Abstracts: Materials Processing and Manufacturing Division: In Situ Synthesis and Rapid Prototyping	Northern A2	Wed AM	249
General Abstracts: Materials Processing and Manufacturing Division: Modeling and Simulation of Materials and Processes	Northern A2	Wed PM	
General Abstracts: Materials Processing and Manufacturing Division: Processing and Microstructural Development	Northern A2	Thu AM	345
General Abstracts: Materials Processing and Manufacturing Division: Structure/Processing/Properties Relationships	Northarn A1	Thu AM	216
General Abstracts: Structural Materials Division: Advances in Steel I			
General Abstracts: Structural Materials Division: Advances in Steel I			
General Abstracts: Structural Materials Division: Advances in Steel II.			
-	-		
General Abstracts: Structural Materials Division: Nickel Alloys and High Temperature Materials I	-		
General Abstracts: Structural Materials Division: Processing and Properties of Light Metals	-		
General Poster Session	2		
Hume-Rothery Symposium: Scattering Studies and the Fundamental Properties of Materials: Session I			
Hume-Rothery Symposium: Scattering Studies and the Fundamental Properties of Materials: Session II			
Hume-Rothery Symposium: Scattering Studies and the Fundamental Properties of Materials: Session II			
Hume-Rothery Symposium: Scattering Studies and the Fundamental Properties of Materials: Session IV			
Hume-Rothery Symposium: Scattering Studies and the Fundamental Properties of Materials: Session V			
Innovations in Electrometallurgy: Session I			
Innovations in Electrometallurgy: Session II	Oceanic 5	Thu AM	
Innovations in Measurement Science to Assess the Performance of New Materials in the Real-World: Advanced Measurement Techniques	Austrailia 3	Wed PM	
Innovations in Measurement Science to Assess the Performance of New Materials in the Real-World: Characterization of Advanced Materials			252
Innovations in Measurement Science to Assess the Performance of New Materials in the Real-World:	Austrailia 3	Wed AM	255
Fundamental Measurement Methods			
Fundamental Measurement Methods Innovations in Measurement Science to Assess the Performance of New Materials in the Real-World: High Strain Rate Deformation	Austrailia 3	Mon AM	



Innovations in Titanium Technology Symposium: Advances in Alloy Development	Asia 3	Wed AM	254
Innovations in Titanium Technology Symposium: Advances in Materials Processing	Asia 3	Tue PM	
Innovations in Titanium Technology Symposium: Low Cost Materials and Processing	Asia 3	Mon AM	
Innovations in Titanium Technology Symposium: Microstructure and Properties I	Asia 3	Wed PM	
Innovations in Titanium Technology Symposium: Microstructure and Properties II	Asia 3	Thu AM	
Innovations in Titanium Technology Symposium: Novel Materials and Processes I	Asia 3	Mon PM	90
Innovations in Titanium Technology Symposium: Novel Materials and Processes II	Asia 3	Tue AM	141
Integrated Computational Materials Engineering: Lessons from Many Fields: ICME in			
Materials Science			
Integrated Computational Materials Engineering: Lessons from Many Fields: ICME in Other Fields	Oceanic 4	Wed PM	
Intellectual Property in Materials Science: Patents, Tech Transfer and Licensing: Commercialization A	America's Seminar	Tue PM	193
Intellectual Property in Materials Science: Patents, Tech Transfer and Licensing: Patents	America's Seminar	Tue AM	142
Internet and Other Electronic Resources for Materials Education: Session I	Oceanic 2	Mon AM	40
Magnesium Technology 2007: Alloy Development I	Southern 4	Wed AM	
Magnesium Technology 2007: Alloy Development II	Southern 4	Wed PM	
Magnesium Technology 2007: Automotive Applications and USAMP Programs	Southern 5	Mon PM	91
Magnesium Technology 2007: Casting and Solidification I	Southern 5	Tue AM	143
Magnesium Technology 2007: Casting and Solidification II	Southern 5	Tue PM	194
Magnesium Technology 2007: Corrosion and Coatings	Southern 4	Thu AM	
Magnesium Technology 2007: Magnesium Globalization	Southern 4-5	Mon AM	40
Magnesium Technology 2007: Microstructure and Properties	Southern 5	Thu AM	
Magnesium Technology 2007: Primary Production, Recycling and Environmental/Welding	Southern 5	Wed AM	
Magnesium Technology 2007: Thermodynamics and Fundamental Research	Southern 5	Wed PM	
Magnesium Technology 2007: Wrought Alloys and Forming Processes I: Deformation	Southern 4	Mon PM	
Magnesium Technology 2007: Wrought Alloys and Forming Processes II: Rolling and Forming	Southern 4	Tue AM	144
Magnesium Technology 2007: Wrought Alloys and Forming Processes III: Extrusions			
Materials in Clean Power Systems II: Fuel Cells, Solar, and Hydrogen-Based Technologies: Hydrogen Storage Materials in Conjuction with the 8th Global Innovations Symposium:			
Metal Powders for Energy Production and Storage Applications	Oceanic 6	Tue PM	197
Materials in Clean Power Systems II: Fuel Cells, Solar, and Hydrogen-Based Technologies: Materials for Clean Coal Power Generation and Gas Separation	Asia 2	Wed PM	
Materials in Clean Power Systems II: Fuel Cells, Solar, and Hydrogen-Based Technologies: Materials for Solar Cells and Photovoltaic Systems	Asia 2	Thu AM	353
Materials in Clean Power Systems II: Fuel Cells, Solar, and Hydrogen-Based Technologies:			
Materials in Clean Fower Systems II. Fuer Cens, Solar, and Hydrogen-Dased Technologies. Materials Oxidation/Corrosion and Protection	Asia 2	Wed AM	259
Materials in Clean Power Systems II: Fuel Cells, Solar, and Hydrogen-Based Technologies: PEMFCs	Asia 2	Mon PM	
Materials in Clean Power Systems II: Fuel Cells, Solar, and Hydrogen-Based Technologies: Plenary Session	Asia 2	Mon AM	41
Materials in Clean Power Systems II: Fuel Cells, Solar, and Hydrogen-Based Technologies: SOFCs I	Asia 2	Tue AM	145
Materials in Clean Power Systems II: Fuel Cells, Solar, and Hydrogen-Based Technologies: SOFCs II	Asia 2	Tue PM	
Materials Issues for Advanced Nuclear Systems: Energy Generation and Waste Issues	Europe 5	Mon AM	
Materials Issues for Advanced Nuclear Systems: Material Characterization Issues	Europe 5	Mon PM	
Materials Processing and Manufacturing Division Symposium: Mechanics and Materials Modeling	-		
and Materials Design Methodologies, in the Honor of Dr. Craig Hartley's 40 years of Contributions to the Field of Mechanics and Materials Science: Homogenization/Constitutive Behavior I	Northern A1	Mon PM	96
Materials Processing and Manufacturing Division Symposium: Mechanics and Materials Modeling and Materials Design Methodologies, in the Honor of Dr. Craig Hartley's 40 Years of Contributions to the Field of Mechanics and Materials Science: Homogenization/Constitutive Behavior II	Northern A1	Tue AM	146
Materials Processing and Manufacturing Division Symposium: Mechanics and Materials Modeling and Materials Design Methodologies, in the Honor of Dr. Craig Hartley's 40 Years of Contributions to the Field of Mechanics and Materials Science: Materials Design			
נט ווכיד וכום טו אוכטומוונים מום זיומנטומום סטוכווניד. זיומנטומום בטבוצוו			177

Session Listing



Materials Processing and Manufacturing Division Symposium: Mechanics and Materials Modeling and Materials Design Methodologies, in the Honor of Dr. Craig Hartley's 40 Years of Contributions to the Field of Mechanics and Materials Science: Microstructure Analysis and Representation I	Northern A1	Mon AM	44
Materials Processing and Manufacturing Division Symposium: Mechanics and Materials Modeling and Materials Design Methodologies, in the Honor of Dr. Craig Hartley's 40 Years of Contributions to the Field of Mechanics and Materials Science: Microstructure Analysis and Representation II	Northern A1	Wed PM	
Materials Processing and Manufacturing Division Symposium: Mechanics and Materials Modeling and Materials Design Methodologies, in the Honor of Dr. Craig Hartley's 40 Years of Contributions to the Field of Mechanics and Materials Science: Nanostructure, Defects and Properties			
Materials Processing Fundamentals: Powders, Composites, Coatings and Measurements			
Materials Processing Fundamentals: Process Modeling			
Materials Processing Fundamentals: Smelting and Refining			
Materials Processing Fundamentals: Solidification and Deformation Processing			
Materials Processing under the Influence of External Fields: Session I			
Materials Processing under the Influence of External Fields: Session I			
Materials Processing under the Influence of External Fields: Session III			
Materials Processing under the Influence of External Fields: Session IV			
Materials Processing under the Influence of External Fields: Session V			
Materials Processing under the influence of External Procession v	America s Seminar		
Science: Metrology for Micro and Nano Structures	Oceanic 6	Tue AM	149
Microstructural Processes in Irradiated Materials: Defect Clusters and Fundamental Radiation Effects	s Europe 8	Thu AM	355
Microstructural Processes in Irradiated Materials: Dislocation - Obstacle Interactions and Radiation Induced Segregation	Europe 8	Mon AM	48
Microstructural Processes in Irradiated Materials: He Effects, Deformation and Fracture	Europe 8	Wed PM	
Microstructural Processes in Irradiated Materials: Irradiation Effects in Ceramics	Europe 8	Mon PM	100
Microstructural Processes in Irradiated Materials: Modeling	-		
Microstructural Processes in Irradiated Materials: Modeling, Microstructure and Embrittlement in Fe-Cr Alloys	Europe 8	Tue AM	
Microstructural Processes in Irradiated Materials: Poster Session I	Europe 8	Tue PM	202
Microstructural Processes in Irradiated Materials: Poster Session II	Europe 8	Wed PM	
Microstructural Processes in Irradiated Materials: Reactor Pressure Vessel Steels	Europe 8	Wed AM	
National Academies ICME Study Community Town Hall Meeting	Oceanic 4	Wed PM	
National Science Foundation Workshop: CyberInfrastructure to CyberDiscovery for Materials Science	e Oceanic 4	Wed AM	256
Outreach Programs in Materials Science and Engineering: Outreach Programs at Universities	Pacific Hall A	Mon AM	49
Outreach Programs in Materials Science and Engineering: Outreach Programs in Industry and Government Laboratories	Pacific Hall A	Mon PM	101
Pb-Free Electronic Solders: Alloy Design, Characterization and Service Reliability: Electromigration and Void Formation	Oceanic 1	Tue AM	151
Pb-Free Electronic Solders: Alloy Design, Characterization and Service Reliability: Interfacial Effect	s Oceanic 1	Mon AM	50
Pb-Free Electronic Solders: Alloy Design, Characterization and Service Reliability: Mechanical Characterization	Oceanic 1	Wed PM	
Pb-Free Electronic Solders: Alloy Design, Characterization and Service Reliability: Microstructure and Characterization	Oceanic 1	Mon PM	
Pb-Free Electronic Solders: Alloy Design, Characterization and Service Reliability: Processing and Reliability Issues	Oceanic 1	Wed AM	
Pb-Free Electronic Solders: Alloy Design, Characterization and Service Reliability: Whisker Growth, Design, and Modeling	Oceanic 1	Tue PM	204
Phase Stability, Phase Transformations, and Reactive Phase Formation in Electronic Materials VI: Session I			
Phase Stability, Phase Transformations, and Reactive Phase Formation in Electronic Materials VI:			
Session II	Oceanic 2	Tue AM	153



Session III	ottante 2 minis		205
Phase Stability, Phase Transformations, and Reactive Phase Formation in Electronic Materials VI: Session IV	Oceanic 2	Wed AM	265
Phase Stability, Phase Transformations, and Reactive Phase Formation in Electronic Materials VI:	Occume 2		
Session V	Oceanic 2	Wed PM	
Plasticity from the Atomic Scale to Constitutive Laws: Atomistic Simulations of Dynamic Processes and Nano-Scale Plasticity	Europe 9	Tue AM	154
Plasticity from the Atomic Scale to Constitutive Laws: Dislocation Core Structure and Solute-Dislocation Interactions	Europe 9	Mon AM	51
Plasticity from the Atomic Scale to Constitutive Laws: Dislocation Ensembles	-		
Plasticity from the Atomic Scale to Constitutive Laws: Dislocation Solute, Precipitate and Grain Boundary Interactions			
Plasticity from the Atomic Scale to Constitutive Laws: Meso-Scale Plasticity	-		
Plasticity from the Atomic Scale to Constitutive Laws: Rate Limiting Behavior and Informed Constitutive Laws	-		
Properties and Performance of High Temperature Alloys and Coatings: Coatings and Oxidation I	-		
Properties and Performance of High Temperature Alloys and Coatings: Coatings and Oxidation II			
Properties and Performance of High Temperature Alloys and Coatings: Intermetallics and Multidisciple			
Properties and Performance of High Temperature Alloys and Coatings: Polycrystalline Alloys			
Properties and Performance of High Temperature Alloys and Coatings: Single Crystal Alloys I	Asia 4	Mon AM	
Properties and Performance of High Temperature Alloys and Coatings: Single Crystal Alloys II and Oxidation	Asia 4	Tue AM	
Recent Developments in Semiconductor, Electro Optic and Radio Frequency Materials: Progress in			
Semiconductor Optoelectronics and Beyond	Oceanic 6	Mon PM	108
Recent Developments in Semiconductor, Electro Optic and Radio Frequency Materials: Recent Advances in Semiconductor Technologies	Oceanic 6	Mon AM	54
Recycling and Waste Processing: Aluminum	Australia 2	Wed AM	
Recycling and Waste Processing: Automotive Recycling, Global Challenges and Opportunities	Australia 2	Tue AM	157
Recycling and Waste Processing: Batteries and Co/Ni	Australia 2	Mon PM	110
Recycling and Waste Processing: Materials Recovery from Wastes			
Recycling and Waste Processing: Other Nonferrous			
Recycling and Waste Processing: Precious Metals Recovery			
Refractory Metals 2007: Oxidation and Thin Films			
Refractory Metals 2007: Processing and Mechanical Deformation	-		
Shape Casting: The 2nd International Symposium: Applications/Novel Processes			
Shape Casting: The 2nd International Symposium: Liquid Metal/Solidification			
Shape Casting: The 2nd International Symposium: Modeling			
Shape Casting: The 2nd International Symposium: Process Design/Analysis			
Shape Casting: The 2nd International Symposium: Structure/Property	Northern E2	Tue PM	
Structural Materials Division Symposium: Mechanical Behavior of Nanostructured Materials, in Honor of Carl Koch: Fatigue, and Strengthening Mechanisms at Small Length Scale	Asia 5	Mon AM	58
Structural Materials Division Symposium: Mechanical Behavior of Nanostructured Materials, in Honor of Carl Koch: Microstructure and Mechanical Properties of Nanostructured Materials	Asia 5	Thu AM	357
Structural Materials Division Symposium: Mechanical Behavior of Nanostructured Materials, in Honor of Carl Koch: Plasticity and Deformation Mechanisms at Small Length Scale I	Asia 5	Tue AM	159
Structural Materials Division Symposium: Mechanical Behavior of Nanostructured Materials, in Honor of Carl Koch: Plasticity and Deformation Mechanisms at Small Length Scale II	Asia 5	Wed AM	271
Structural Materials Division Symposium: Mechanical Behavior of Nanostructured Materials, in Honor of Carl Koch: Plasticity and Deformation Mechanisms at Small Length Scale III			
Structural Materials Division Symposium: Mechanical Behavior of Nanostructured Materials, in Honor of Carl Koch: Poster Session: Mechanical Properties of Nanostructured Materials			

LEARN • NETWORK • ADVANCE

Session Listing



Structural Materials Division Symposium: Mechanical Behavior of Nanostructured Materials, in Honor of Carl Koch: Processing and Characterization of Materials Subjected to Severe Plastic Deformation	Asia 5	Mon PM	112
Structural Materials Division Symposium: Mechanical Behavior of Nanostructured Materials, in Honor of Carl Koch: Stability, Strain and Stress	Asia 5	Tue PM	211
The Material Recycling Industry: Global Challenges and Opportunities: Plenary Session	Southern 1	Mon AM	59
Towards Functional Nanomaterials: Synthesis, Characterization, and Applications: Directed Nano Fabrication	Oceanic 5	Mon AM	60
Towards Functional Nanomaterials: Synthesis, Characterization, and Applications: Nano Magnetism, Ferroelectric, Mechanics, and Other Properties	Oceanic 5	Mon PM	114
Towards Functional Nanomaterials: Synthesis, Characterization, and Applications: Nanoscale Superstructures, Metallic Nanoparticles and Plasmon	Oceanic 5	Tue AM	161
Towards Functional Nanomaterials: Synthesis, Characterization, and Applications: Nanowires and Nanotubes	Oceanic 5	Tue PM	220
Towards Functional Nanomaterials: Synthesis, Characterization, and Applications: Quantum Dots	Oceanic 5	Wed AM	273
Wide Band-Gap Semiconductor Nanostructures: Session I	Oceanic 4	Mon AM	62
Wide Band-Gap Semiconductor Nanostructures: Session II	Oceanic 4	Mon PM	115
Wide Band-Gap Semiconductor Nanostructures: Session III	Oceanic 4	Tue AM	162
Wide Band-Gap Semiconductor Nanostructures: Session IV	Oceanic 4	Tue PM	221

2007 Nanomaterials: Fabrication, Properties and Applications: Session I

Sponsored by: The Minerals, Metals and Materials Society, TMS Electronic, Magnetic, and Photonic Materials Division, TMS: Nanomaterials Committee *Program Organizers:* Wonbong Choi, Florida International University; Ashutosh Tiwari, University of Utah; Seung Kang, Qualcomm Inc.

Monday AM	Room: Oceanic 3
February 26, 2007	Location: Dolphin Hotel

Session Chairs: Wonbong Choi, Florida International University; Ken Teo, University of Cambridge

9:00 AM Keynote

Inorganic Nanowires: Growth and Applications: M. Meyyappan¹; ¹NASA Ames Research Center

Growth of nanowires of various inorganic materials has received much attention recently due to their potential in electronics, lasers, sensors and other applications. We have grown nanowires in various material systems: silicon, germanium, high temperature oxides(zinc oxide, tin oxide, indium oxide), antimonides of indium and gallium, and a phase change material such as germanium telluride. This talk will provide an overview of inorganic nanowire growth. We have used a vapor-liquid-solid(VLS) technique to grow the above nanowires. Catalysts other than the conventional gold have also been investigated for their effectiveness. A brief discussion on applications of these nanowires will also be provided. We have demonstrated near-infrared lasing in the telecommunication band using antimonide wires. We are pursuing memory devices using phase change nanowires. The author acknowledges contributions from Bin Yu, Jeff Sun, Alan Chin, S. Vaddiraju, M.Sunkara, Cun-zheng Ning and G. Dholakia.

9:40 AM Invited

Synthesis and Integration of Carbon Nanotubes for the Electronic Device Applications: *Wanjun Park*¹; ¹Materials and Devices Research Center, Samsung Advanced Institute of Technology

Due to one-dimensional structure of carbon nanotube (CNT) with unique electrical and chemical properties, CNTs are exciting materials for the various nano-scale applications including molecular electronics, opto-electronic devices, sensors, and so on. In particular, understanding of their electrical properties has aroused many research groups in academy and industry to explore the nano-scale electronics based on CNTs such as transistor, memory, interconnect, logic array, and so on. However many technological barriers are still remained. First of all, pure nanotubes should be separated from a mixture of single-walled, multi-walled nanotubes, and carbonaceous impurities or should be grown without impurities for reliable device performance. Another critical barrier to integrate nanotubes in devices is uncertainty and uncontrollability in positioning nanotubes on a right region. In addition, transport mechanism in CNTs should be more understood to modulate band gap of them to fabricate various device elements. In this presentation, we introduce our recent progresses to overcome the barriers focusing on the electronic device elements based on single-walled carbon nanotubes (SWNTs). Experimental and theoretical studies to control the CNT electronic structure are covered for CNT-field effect transistors. The large scale fabrication of CNT electronic elements are also given for the selective growth of CNT that is extendable to device integration. The growth and purity issues of nanotubes are demonstrated with sono-chemical route to single-walled carbon nanotube, purification method of nanotubes integrated in transistors via sulfidation, and low temperature growth (~400°C) by PECVD of SWNTs. For the positioning problems, direct photolithographic method using a mixture of catalytic precursors and conventional resists as a catalytic resist is introduced.

10:05 AM

Patterned Forest-Assembly of Single-Wall Carbon Nanotubes and Carbon Nanotube Atomic Force Microscopy Nanoprobes: Haoyan Wei¹; Sang Nyon Kim¹; Sejong Kim¹; Minhua Zhao¹; Sang-Yong Ju¹; Bryan Huey¹; Fotios Papadimitrakopoulos¹; *Harris Marcus*¹; ¹University of Connecticut, Materials Science and Engineering Program, Department of Chemical, Materials and

Biomolecular Engineering, Institute of Materials Science

This research investigated the fabrication of carbon nanotube (CNT) patterns and CNT atomic force microscopy (AFM) nanoprobes applied to nanobiosensors. Patterns of perpendicularly aligned single-wall carbon nanotube (SWNT) forests were realized on diverse substrates via Fe3+-assisted selfassembly with the aid of electron-beam writing and photolithography creating preferential nucleation sites for Fe3+ ions. A second part of this research resulted in CNT nanoprobes on conductive AFM probes fabricated using positive dielectrophoresis (DEP) involving the application of a heterogeneous electric field. Post-assembly, a novel, surfactant-assisted dissolution process was developed to further optimize the length and stiffness of these SWNT nanofibrils. The stiffness could be further tailored upon subsequent vacuum annealing. Finally, radial and longitudinal heterojunction have been demonstrated by sequential DEP assembly on the side walls and ends of previously grown nanofibrils, respectively. These CNT-AFM nanoprobes are qualified for deep structure imaging and cell membrane piercing.

10:20 AM

Surface Modification to Enhance Uniform Growth of Carbon Nano-Fibers on Larger Structural Components: *Ian Barney*¹; J.H. Su¹; R.J. Pulikollu¹; S.M. Mukhopadhyay¹; ¹Wright State University

This project focuses on the growth of Carbon nano-fibers on larger engineering structures in order to create multi-scale materials with increased surface area, where additional functionalities may be added. Nano-fibers have been fabricated using chemical vapor deposition (CVD) on substrates of silicon, graphite, foam and microfibers of graphite. Influence of pre-coating substrates with nanoscale oxide functional groups on the growth of nanotubes was investigated by comparing with growth on uncoated samples. Analyses of chemical state and structure have been preformed using x-ray photoelectron spectroscopy (XPS) and scanning and transmission electron microscopy (SEM and TEM) respectively. Results indicate that plasma-assisted silicalike coatings promote carbon nanotubes growth, showing higher growth rate and decreasing inhomogeneity. Samples were also analyzed for atomic concentration and bonding states of catalyst particles using different processing conditions and substrates. Possible growth mechanisms will be discussed as well as influence of nanoscale hair on substrate functionality.

10:35 AM Break

10:50 AM Invited

Carbon Nanotube-Based Photovoltaic Cells: Rodolfo Camacho¹; Alex Morgan¹; Trevor McLeod¹; Jack Flicker¹; Stephan Turano¹; *W. Jud Ready*¹; ¹Georgia Tech Research Institute-Electro-Optical Systems Laboratory

A 3-D aligned array of highly conductive CNT towers is grown on lithographically patterned silicon wafers. The interconnected CNT array is then coated with suitable photon absorbing bandgap materials (CdTe, CdSe, CdS) to form a p/n-junction. A conductive oxide (indium tin oxide — ITO) is deposited as the transparent top contact. In a traditional (planar) single junction solar cell, a photon of light impinges the p/n-junction at a single instance and may (or may not) create a single electron-hole pair. However, for this topographically enhanced CNT-based device, multiple impingements and scattering of the incident photon upon the p/n-junction increase the probability of absorption due to extended dwell time in the photoactive layers. This effect, whereby a single photon can interact with the p/n junction multiple times is termed "light trapping."

11:15 AM

Synthesis and Nonlinear Optical Properties of PbS Quantum Dots: Suresh Krishna Moorthy¹; Sudipta Seal¹; ¹University of Central Florida

Nanoclusters of PbS embedded in polymer matrices have recently been shown to have interesting optical properties with the capability of tuning the effective band gap over a wide spectral range. The results of a systematic investigation of the preparation and characterization of size-tuned PbS nanocrystals stabilized in the polymer nanotemplate of Nafion and their sizedependent physical properties are presented in this paper. These nanocrystals exhibit large characteristic blueshift in optical absorption from the bulk absorption onset value of 3020 nm. XRD and HRTEM measurements indicate the presence of PbS nanocrystals in the size range of 2 to 6 nm, in the regime of strong quantum confinement. Thermal and electrical properties of the polymer are found to be influenced to a great extent by the embedded PbS

Technical Program



nanocrystals. The nonlinear optical properties measured by Z-scan technique indicate potential application of PbS nanocrystals as optical limiters at low laser powers.

11:30 AM

Photoluminescence at 1.5 µm from Er in an SiO2 Layer with Ge Nanoclusters: The Local Environments of Er Atoms and Comparison with He Case of Si Nanoclusters: *Jeyanthinath Mayandi*¹; Terje Finstad¹; Chenglin Heng¹; Yanjun Li¹; Hallgeir Klette²; ¹University of Oslo; ²SINTEF

The 1.5 μ m Er+3 luminescence is of large interest due to the possible applications. We have fabricated embedded Ge nanoclusters in Er doped SiO2 films by co-sputtering and annealing. We have also prepared samples where Si - replaces Ge- clusters. We have studied the nanostructure and its dependence upon fabrication parameters by a number of techniques (HRTEM, XPS, XRD, FTIR) and correlated that with the photoluminescence intensity. We have observed that the most efficient luminescence occurs after annealing to 700°C. The film then contains a high density of amorphous Ge nanoclusters and the Er and Ge distributions are highly correlated which is unexpected and different than what is assumed for Si. The detailed shape of the luminescence peak, which is a probe for the local evoronments of Er, is different for the Si and Ge cases, in agreement that the Er and Ge nanoclusters are correlated.

11:45 AM

Interface, Defects and Intermixing in Fe Thin Films Grown on AlGaAs by MBE: *Ramasis Goswami*¹; Aubrey Hanbicki²; George Kioseoglou²; Berend Jonker²; George Spanos²; ¹Science Applications International Corporation; ²Naval Research Laboratory

Utilizing the spin degree of freedom of an electron in a semiconductor device is the basis for the emerging field of spintronics. The most successful incorporation of spins into semiconductor heterostructures results from injection from either diluted magnetic semiconductors such as ZnMnSe, or from ferromagnetic metals such as Fe or CoFe. The present investigation is centered on the overall microstructure of Fe/AlGaAs grown by molecular beam epitaxy(MBE)with an emphasis on the interface structure and intermixing at the interface. High Resolution transmission electron microscopy reveals significant amount of low angle grain boundaries in the Fe film. The measured spin polarization from these spin-LED samples increases from about 24% to 34% after annealing the room-temperature deposited film at 200°C for 10 min. Differences in the microstructural features of the as-deposited and annealed Fe films will be detailed.

12:00 PM

Growth Control of Highly Oriented Nanorods of Zinc Oxide: Jean-Claude Tedenac¹; Mezy Aude¹; Ravot Didier¹; Bretagnon Thierry¹; Lefebvre Pierre¹; Gerardin Corine¹; Tichit Didier¹; ¹Laboratoire de Physique de la Matière Condensée-UMR5617

ZnO nanowires have a great commercial stake, due to their physical and chemical properties. The wet chemical synthesis route enable the preparation of high crystal quality and proper growth orientation of ZnO nanowires. Nethertheless, control of the ZnO size, morphology, dimensionality, and self-assembly remains a very important stake, due to their tight influence on ZnO properties. Efficient control of both nanostructure dimensionality and assembly is obtained by using appropriate synthesis parameters during the seeded growth process. The synthesis of well aligned nanowires with a perpendicularly growth to the substrate and a high crystal quality is useful for the study of their physical (optical, electrical, etc) properties. Furthermore, the modification of these parameters provides us informations about the growth mechanism of the aligned nanowires. Thus, the present method provides a convenient route to obtain high quality and low cost aligned arrays of ZnO nanowires with lasing properties at room temperature.

12:15 PM

Core-Shell SiC-Al2O3 Nanowires Synthesized by a Current Heating Method: *Thanut Jintakosol*¹; Pisith Singjai¹; ¹Chiang Mai University

Synthesis of core-shell SiC-Al2O3 nanowires(NWs) by current heating of a silica-alumina-graphite rod was investigated. The rod was placed between two copper electrodes and gradually heated up to about 1400°C by passing current though it under flowing argon. The as-synthesized NWs, formed on the surface were then characterized using scanning electron microscopy, transmission electron microscopy, energy dispersive analysis of X-ray, selected area electron diffraction and X-ray diffraction and Raman spectroscopy. An increasing of a non-uniform shell thickness was observed when added alumina at higher weight ratio.

Advanced Metallic Composites and Alloys for High Performance Applications: Advanced Metallics

Sponsored by: The Minerals, Metals and Materials Society, ASM International, TMS Structural Materials Division, ASM Materials Science Critical Technology Sector, TMS/ASM: Composite Materials Committee, TMS/ASM: Mechanical Behavior of Materials Committee *Program Organizers:* Awadh Pandey, Pratt and Whitney Rocketdyne; Kevin Kendig, Air Force Research Laboratory; John Lewandowski, Case Western Reserve University

Monday AMRoom: Europe 10February 26, 2007Location: Dolphin Hotel

Session Chair: Stephen Kampe, Virginia Tech

9:00 AM Invited

The Effect of Cold Rolling on the Creep Behavior of Udimet 188 Superalloy: *Debjani Palit*¹; N. Eisinger²; Carl Boehlert¹; ¹Michigan State University; ²Special Metals Corporation

A Udimet 188 alloy was subjected to thermo-mechanical processing in attempt to understand the effects of cold-rolling deformation on the microstructure and creep behavior. Sheets were cold rolled to either 10%, 25%, or 35% deformation followed by solution treatment. This sequence was repeated four times and the grain boundary character distribution was characterized using electron backscattered diffraction. The 10% cold rolled material exhibited up to 75% of special boundaries and the 35% cold rolled samples exhibited the least amount of special boundaries (57%). The 10% and 25% cold rolled materials exhibited superior creep resistance compared to the 35% cold rolled material. In-situ creep experiments were performed inside a scanning electron microscope chamber. The material exhibited a significant extent of grain boundary cracking which increased with increasing creep strain. General high-angle grain boundaries were the most susceptible to cracking. This result has significant implications regarding grain boundary engineering of this alloy.

9:20 AM

Lightweight Truss Core Structures Formed from Expanded Metal: Brandon Bouwhuis¹; Glenn Hibbard¹; ¹University of Toronto

Periodic cellular metal (PCM) sandwich cores can be considered hybrids of the solid and gas type. These materials are competitive to conventional metallic foams in environments requiring high strength-to-weight ratios. PCM cores were constructed from work-hardened aluminum alloy 3003 expanded metal precursors using a modified bending brake method. Fabrication is limited by crack initiation at the bends, which can be related to a minimum bend radius. Annealing prior to bending expands the limit of formability by reducing the minimum bend radius, but also results in a decrease in resultant PCM mechanical performance. This study investigates a range of bending and annealing treatments during PCM fabrication as well as the resultant PCM performance to determine an optimal processing path. Metallography, microhardness profiles and mechanical testing in compression are used to correlate processing pathways to resultant microstructure and further to mechanical properties of PCMs.

9:40 AM

Application of Roll-Bonding Technique on Preparing Aluminum Foam Sandwich: *Guoyin Zu*¹; Min Zhang¹; Guangchun Yao¹; Hongbin Li¹; ¹School of Materials and Metallurgy

The technique of roll-bonding was applied to prepare the foaming compound board in order to settle the main problem that exists in the preparation of aluminum foam sandwich in this work. The result shows that the preformed core powder cake can hard integrate with the steel sheet after rolling. The tightness of rolled core powder is obviously higher than that of heat pressing compound board and the powder takes on the closely stratified structure, which creates the favorable condition for foaming. Considering integrated the factor



such as bond strength, tightness of core powder and rolling defect, the best reduction should be controlled at 60%~70%. The compound board can get the perfect foam structure under proper foaming technology: the best foaming temperature is 620~640°C; foaming time is 8~10min. Both intermetallic compound of FeAl3 and Fe/Al solid solution with about 10µm thickness occur at the interface after foaming.

10:00 AM

FeAl-Based Intermetallic Sinters Obtained by Liquid Phase Sintering: Stanislaw Józwiak¹; *Krzysztof Karczewski*¹; Zbigniew Bojar¹; ¹Military University of Technology

The results of the optimization process of liquid phase sintering of Fe and Al powders in order to fabricate FeAl intermetallic sinters were studied in this paper. The oxidation of Al particles in the sintering process is responsible for the formation of the Al2O3 films in the sintered structure that are mainly located on the interparticle boundaries, which eventually lead to the decrease of the strength of material. The exothermic reaction of the mixed Fe +Al powders (SHS) may lead to the destruction of the sinter. Control of the process parameters such as pressure, temperature and time allowed fabrication of sound FeAl sinters by eliminating such adverse effects as strong oxidation of aluminum powder, self-propagating synthesis and resulting high porosity. The proposed three-stage technological process of fabricating FeAl intermetallic alloys from pure Fe and Al elemental powders which utilizes sintering with liquid phase allows us to obtain a fine-grained material.

10:20 AM Break

10:40 AM Invited

Characterization of Particle Reinforced Metal Matrix Composite Microstructures by Three Dimensional (3D) Finite Body Tessellation: Jason Williams¹; *Nikhilesh Chawla*¹; ¹Arizona State University

The degree of clustering of particles has a significant influence on the mechanical behavior of particle reinforced metal matrix composites (MMCs). The clustered particles act as crack initiation sites and generally have a negative effect on tensile strength, ductility, toughness, and fatigue strength of the composite. Quantifying the degree of clustering in MMCs and other heterogeneous systems is a challenge. In this presentation we report on a novel, 3D finite-body tessellation scheme for quantifying the degree of clustering in SiC particle reinforced Al matrix composites. The results were compared to 2D representations and the salient differences will be highlighted. A methodology for correlating degree of clustering and mechanical properties of the composite will be discussed.

11:00 AM

Microstructure and Adhesion Strength of the Sn-9Zn-1.5Ag-1.5Bi Solder Alloy on Cu Substrate: *Chih-Yao Liu*¹; Moo-Chin Wang²; Min-Hsiung Hon¹; ¹National Cheng Kung University; ²National Kaohsiung University of Applied Sciences

The microstructure and adhesion strength between the Sn-9Zn-1.5Ag-1.5Bi and Cu substrate has been investigated. The Sn-9Zn-1.5Ag was also tested for comparison. The phase formation observed in two solders by an X-ray diffractometer (XRD), an scanning electron microscope (SEM), an energy dispersive spectrometer (EDS) and a transmission electron microscope (TEM). The adhesion strength was 8.34 ± 0.28 for Sn-9Zn-1.5Ag-1.5Bi. Fracture morphology were revealed that the fracture occurred in solder matrix by scanning electron microscopy. The intermetallic compounds Cu6Sn5 and Cu5Zn8 were observed in the Sn-9Zn-1.5Ag and Sn-9Zn-1.5Ag-1.5Bi solder alloy. After 150°C with 1000 hour aging, the adhesion strength was decreased to 3.48 ± 0.63 MPa because of the growth and decomposition intermetallic compounds.

11:20 AM

Atomic Level Characterization of the β Decomposition Products in Ti-6Al-4V Using the Local Electrode Atom Probe: Stephanie Johnson¹; David Diercks¹; Rajarshi Banerjee¹; James Cotton²; *Michael Kaufman*¹; ¹University of North Texas; ²Boeing Company

Upon cooling from above the β transus, Ti-6Al-4V undergoes a transition from BCC to HCP by a martensitic transformation at high cooling rates and by nucleation and growth at slower rates. The transition from one mechanism to the other as a function of cooling rate remains controversial as does the mechanism in which a cubic phase shears to form a higher-symmetry HCP phase. In this study, a Ti-6Al-4V sample was subjected to a modified Jominy end quench test in order to produce a range of cooling rates. Both TEM and 3-D atom probe tomography were used to analyze the sample at atomic resolution. The results will be discussed in terms of the light they shed on transformations in this class of titanium alloys. *Characterization performed using analytical facilities in the Center for Advanced Research and Technology at the University of North Texas. Partial support of The Boeing Company is appreciated.*

11:40 AM

Thermal Properties of the Diamond-Copper Interface in Hot-Pressed Metal-Matrix-Composites: *Ivica Smid*¹; Erich Neubauer²; Paul Angerer³; Kristina Cowan¹; ¹Pennsylvania State University; ²Austrian Research Centers; ³ECHEM

Copper Metal-Matrix-Composites (MMCs) based on carbon reinforcements have a high potential for application as heat sink material. Basically the thermal properties can be tailored by a simple variation of the volume fraction of the reinforcement. Another important parameter for achieving a high conductivity in the copper-carbon system is the thermal contact resistance (TCR). By a variation of the TCR the whole range between an insulating interface and a perfect heat transfer can be simulated. The experimental values of the TCR were determined by photothermal methods. The resulting bulk thermal properties have been modeled using finite element methods, allowing a prediction of the maximum achievable conductivity as a function of composition and processing. Filler particle size and shape limitations in view of bulk conductivity requirements have been determined.

12:00 PM

Processing of Nanocrystalline and Amorphous Fe-(Co)-B-Si Thin Wires for Magnetic Applications by Using in–Rotating–Liquid–Spinning: Georg Frommeyer¹; Joachim Gnauk¹; *Susanne Zeller*¹; ¹Max-Planck-Insitut für Eisenforschung

A computer controlled facility for continuous casting of metallic thin wires performing inrotating-liquid-spinning (INROLISP) was designed and installed to determine and control the near-net-shape casting process over an extended time period. In particular, the flow of the melt was experimentally investigated and theoretically described using fluid dynamic equations. The controlling process parameters, such as the velocity of the melt jet, the stable free flight length, the nozzle geometry and cooling rate were examined and optimized. Several pure metals as well as microcrystalline and amorphous alloys were cast into continuous wires of high quality. Microstructural features and mechanical properties of rapidly quenched fibres were evaluated. The production of softmagnetic amorphous and nanocrystalline FeSiB and CoFeSiB thin wires of 50 im to 120 im in diameter is an application of great potential. These microwires are used as sensor cores in highly sensitive magnetic field sensors, based on the magneto-electric Procopiu effect. The sensor properties determined by the alloy composition and the microstructure features, will be correlated with the process parameters.

Advances in Computational Materials Science and Engineering Methods: Methods at the Atom Scale I

Sponsored by: The Minerals, Metals and Materials Society, TMS Structural Materials Division, TMS: Biomaterials Committee, TMS/ASM: Computational Materials Science & Engineering *Program Organizers:* Koen Janssens, Paul Scherrer Institute; Veena Tikare, Sandia National Laboratories; Richard LeSar, Iowa State University

Monday AM	Room: Europe 7
February 26, 2007	Location: Dolphin Hotel

Session Chair: Richard LeSar, Iowa State University

9:00 AM Introductory Comments

9:05 AM Invited

Molecular Dynamics Simulations of the Structure and Properties of Confined Amorphous Films in Ceramics: Stephen Garofalini'; 'Rutgers University

The structure of thin (O(nm)) amorphous films confined between crystals or within pores significantly modifies the structure of the film and the





resultant properties of the material. Two examples include thin glassy silicate intergranular films (IGFs) between oxide or nitride crystals and water confined within nanometer size pores. In the former, the composition and structure of the IGF can significantly modify grain growth and the mechanical properties of the polycrystalline ceramic. Results of molecular dynamics (MD) simulations of silicate films in alumina and silicon nitride showing preferential segregation of species from the IGF and the effect of composition on growth of specific orientations and strength will be presented. In the second case, MD simulations of confined water using a new dissociative water potential will also be presented. The new potential matches many experimental properties of bulk water and also newly obtained data regarding the anomalous expansion of confined water.

9:40 AM Question and Answer Period

9:45 AM

Diffusion-Limited Processes Treated with Accelerated Molecular Dynamics: *Erdi Bleda*¹; Murray Daw¹; ¹Clemson University

We treat diffusion-limited processes using Accelerated Molecular Dynamics. On-the-fly kinetic Monte Carlo is combined with the Dimer Method to find the saddlepoints exiting a valley, based on energetics from the Embedded Atom Method. With this technique, we treat two cases involving diffusionlimited processes in situations with very low symmetry. First, we calculate the tracer diffusivities in ordered intermetallics as a function of composition and temperature. We investigate both a strongly ordered case (Ni3Al) and a less-strongly ordered case (Cu3Au). In the latter, we investigate especially the diffusivity near the order-disorder transition. Second, we treat the motion of an anti-phase boundary (APB) in the same intermetallics. We demonstrate how an APB can be moved perpendicular to itself perpendicular to itself via vacancy motion. We conclude that the on-the-fly kMC is useful for investigating diffusivity in intermetallics. (The author acknowledges support from NSF.)

10:10 AM Question and Answer Period

10:15 AM

Linkage between Atomistic and Continuum-Based Simulations in Nanoscale Powder Metallurgy: Amitava Moitra¹; Sungho Kim¹; Seong-Gon Kim¹; Seong Jin Park¹; *Randall German*¹; ¹Mississippi State University

The atomistic and continuum-based simulations used in this paper are concerned with the multiscale computer modeling during sintering process of nanoscale powder. Of first interest is the application and development of classical and quantum mechanical methodologies to gain insight into the fundamental characteristics of atomic movement during nanoscale powder sintering and how they influence the sintering processing and the physical properties of the material such as melting temperature decrement, sintering activation energy, and so on. These predicted material properties may play a role as bridge between two different scale simulations. This paper focuses on the material properties related to densification predicted from atomistic simulation and their possibility to use in continuum-based simulation.

10:40 AM Question and Answer Period

10:45 AM Break

11:15 AM

Multiscale Modeling of Nanoindentation: Ed McGee¹; *Steven Kenny*¹; Roger Smith¹; ¹Loughbough University

We will present a 3D multiscale model of nanoindentation that couples a molecular dynamics (MD) model with a finite element (FE) model. The MD model is used to describe the tip and the material around the tip at the atomic scale, allowing for an accurate description of plastic deformation. The FE model is used to describe the long range elastic fields in the material. We will show how this model gives contact pressures which are in better agreement with experimental results than traditional atomistic only models, illustrating that a correct description of the long range elastic field is essential. Nanoindentation of the Au (100) surface using a second nearest neighbour embedded atom potential will be used to illustrate the methodology.

11:40 AM Question and Answer Period

11:45 AM

Topological Characterization of Adsorption Phenomena Using Multi-Body Potential Expansions: Nicholas Zabaras¹; *Baskar Ganapathysubramanian*¹; ¹Cornell University

The enhancement of adsorption of (hydrogen) molecules on metallic surfaces is a key challenge for producing feasible fuel cell technologies. Along with the chemistry of the surface under consideration, the topology of the surface also plays an essential part in the adsorption phenomena. There exists a possibility to design both the material specification as well as the surface topology to further enhance the adsorption phenomena. In the present approach, long-ranged and many-body interactions are necessary to model the potential accurately. We construct many-body expansions from a large database of computed ab-initio energies which includes the interaction between the molecule and small clusters of the surface. Non-uniform surfaces are represented in terms of expanding cluster of atoms. Effects of small scale roughness and waviness of the surface on the adsorption are reported. An approach to design the topology of the surface to enhance adsorption based on optimization techniques is presented.

12:10 PM Question and Answer Period

12:15 PM

Development and Testing of MEAM Potential for Al-Mg Alloys: *Bohumir Jelinek*¹; Seong-Gon Kim¹; Jeffery Houze¹; Sungho Kim¹; Mark Horstemeyer¹; Michael Baskes²; ¹Mississippi State University; ²Los Alamos National Laboratory

A MEAM potential for Al-Mg alloys was developed based on the elastic and structural properties determined from ab-initio calculations. Transferability of the new potential was tested by comparing various bulk, surface, and point defect properties with ab-initio simulations. Volume-energy dependence of Al and Mg in fcc, hcp, bcc and simple cubic crystal structures from MEAM and ab-initio simulations was determined. Heat of formation for Al-Mg crystals in C1, C3, C9, C15, D0₃, D0₉, A12, A15, L1₂, B1, B2, and B3 was calculated using both methods. Surface formation, stacking faults, and adsorption energies were compared. For point defects calculations, a close agreement of vacancy formation energies, interstitial and substitutional point defect energies was found.

12:40 PM Question and Answer Period

Advances in Microstructure-Based Modeling and Characterization of Deformation Microstructures: Characterization of Deformed Structures I

Sponsored by: The Minerals, Metals and Materials Society, ASM-MSCTS: Texture and Anisotropy Committee, ASM-MSCTS: Texture and Anisotrophy Committee

Program Organizers: Reza Shahbazian Yassar, Center for Advanced Vehicular Systems; Sean Agnew, University of Virginia; Jiantao Liu, Alcoa Technical Center

Nonday AM	Room: Europe 1
ebruary 26, 2007	Location: Dolphin Hotel

Session Chairs: Sean Agnew, University of Virginia; Anthony Rollett, Carnegie Mellon University

9:00 AM

Ν

F

Deformation-Induced Microstructural Development of Al-Base Sheet Metals: *Stephen Banovic*¹; Mark Iadicola¹; Tim Foecke¹; ¹National Institute of Standards and Technology

Reducing automotive vehicle weight by replacing conventional steel sheet metal with lightweight materials has been initiated. However, implementation of these lightweight alloys, specifically aluminum-base materials, has been slow due to both a limited knowledge of material behavior and a lack of experience in the sheet forming process. To obtain a better understanding of the material characteristics during in-plane stretching, the underlying microstructural development of aluminum alloy sheet metals was studied. Experimental characterization consisted of light optical microscopy, electron



and x-ray diffraction techniques, and laser confocal microscopy. Evolution of the deformed microstructure will be discussed with respect to alloy composition, alloy heat treatment, and deformation parameters.

9:20 AM Invited

3DXRD Experiments and Modelling of Plastic Deformation and Recrystallization: *Dorte Juul Jensen*¹; ¹Riso National Laboratory

By the 3 dimensional x-ray diffraction (3DXRD) method it is possible to measure the crystallographic orientations in bulk samples and thus to map the microstructure non-destructively in 3D in-situ while deforming or/and annealing a sample. This method has been used to follow the rotations of bulk grains during tensile deformation. The data reveal that the initial crystallographic orientation of the grains have a major influence on their average rotations, and slip pattern analysis is used to interpret the results. During annealing both the nucleation and the growth processes strongly depend on the deformation microstructures. 3DXRD measurements have shown that nuclei may develop with orientations similar to or different from the parent orientations, and that growth typically is highly anisotropic. While no modelling of the 3DXRD nucleation observations has yet been carried out, the growth observations are compared to MD simulations of dislocation driven boundary migration and to kinetics models.

9:45 AM

Measuring Plastic Heterogeneity in Stainless Steel Using Image Correlation and Electron Backscatter Diffraction: Lai Li¹; Michael Preuss¹; Joao Quinta da Fonseca¹; M. Kamaya²; ¹University of Manchester; ²Institute of Nuclear Safety System Inc.

The characterisation of plastic heterogeneity during deformation is of great importance to relate local deformation to stress corrosion cracking and validation of plasticity modelling. In the present work two novel techniques, Digital Image Correlation (DIC) and Electronic Back Scatter Diffraction (EBSD), have been used to measure strain heterogeneity in specimens of 304H stainless steel. DIC is an optical technique, in which images of the microstructure taken during straining are compared with a reference (unstrained) image. The technique enables the measurement of strain development across the surface of the specimen on a macro and microscale. EBSD is used to measure a spread in disorientation within a grain from the mean grain orientation to yield a parameter known as the "crystal deformation". Focused Ion Beam was subsequently used to prepare Transmission Electron Microscopy samples from regions that exhibit high and low levels of deformation within a single grain.

10:05 AM

Grain Boundary Structure in Severe Plastic Deformed OFHC Cu Wires: Daudi Waryoba¹; Kalu Kalu¹; ¹Florida Agricultural and Mechanical University-Florida State University, College of Engineering and National High Magnetic Field Laboratory

In the last three decades, equal channel angular extrusion (ECAE) has received a considerable attention as one of the methods for producing ultrafine grain structures. Deformation by ECAE is achieved by extruding a billet through two intersecting channels of equal cross-section. Repeated passes result to very high strains without significant reduction in the cross-section area. Despite the difference in the deformation between ECAE and wire drawing, the two methods have shown a similar recrystallization behavior in oxygen free high conductivity (OFHC) copper. This has motivated the investigation of grain boundary structure OFHC copper after being deformed by ECAE and wire drawing.

10:25 AM Invited

Characterization of Fatigue Damage Nucleation in Aluminum Alloys: Hasso Weiland¹; ¹Alcoa Technical Center

Simulating the nucleation of fatigue damage in aluminum zinc alloys used for structural applications requires quantitative data on crack nucleation to derive rules which can be used in simulations of this process. In a series of detailed experiments, the evolution of damage in terms of particle matrix debonding, in cracking of particles and in formation of microcracks in the aluminum matrix has been studied. Selected crack nucleation sites were characterized in 3D using a FIB-based serial sectioning approach. These analyses provide insight into the mechanisms controlling nucleation of cracks in aluminum alloys during fatigue loading.

10:50 AM Break

11:05 AM Invited

Microstructure of Individual Grains in Cold-Rolled Aluminum from Orientation Inhomogeneities Resolved by EBSD: Wei He¹; Weitao Ma¹; *Wolfgang Pantleon*¹; ¹Risoe National Laboratory

A recently developed scheme for evaluation of orientation data gathered by electron back-scattering diffraction is employed on individual grains in a deformed state. The potential of the method is illustrated on cold-rolled aluminum. The orientation distribution in each grain is characterized by its anisotropy and the averaged orientation spread; the dependence of both parameters on grain size is discussed. The preferred rotation axes in each grain are determined and compared with macroscopic directions. From the disorientation angles with respect to the preferred rotation axis characteristic features of the deformation structure as alternating orientation differences or orientation gradients can be resolved. From the curvatures within the grain the components of the dislocation density tensor corresponding to the geometrically necessary dislocation content are inferred. Their spatial distribution allows determination of boundary orientations and hence a more complete description of the boundary properties by direction and orientation difference.

11:30 AM

On the In-Grain Orientation Gradient Development in Precipitation Hardening Aluminum Alloys: *Reza Shahbazian Yassar*¹; James Baird²; Mark Horstemeyer¹; Paul Wang¹; David Field³; Kyla Stolting²; John Murphy²; ¹Center for Advanced Vehicular Systems; ²Mississippi State University; ³Washington State University

Development of sound physics-based plasticity models in precipitation hardening materials requires better understanding of the interaction between the nano-scale precipitates and orientation evolution of the individual grains. This investigation is concerned with characterization of in-grain orientation gradient as a function of precipitate characteristics. Several polycrystals of 6xxx series aluminum alloys containing hardening precipitates with different morphologies and characters were subjected to tensile deformation and dislocation structure evolution was investigated using high resolution electron backscatter diffraction and transmission electron microscopy. Local misorientation and geometrically necessary dislocation content were studied for various grains as a function of precipitate characteristics. It is found that precipitate characters affect the density and distribution of geometrically necessary dislocations as well as the misorientation boundaries within the grains.

11:50 AM Invited

Phase and Crystallographic Load Distributions in a Two Phase HCP-BCC Alloy under Compression: *Song Cai*¹; Mark Daymond¹; Rick Holt¹; ¹Queen's University

Under typical processing conditions Zr-2.5Nb is 90% α -phase (hcp) and 10% β -phase (bcc); analogous to the common Ti64. Compression samples were prepared from a moderately textured plate. In a set of neutron diffraction tests, compressive load was applied along all three principle plate directions. The intergranular and interphase strains were determined in various orientations relative to the texture and load. Load sharing varies between phases as the applied load is increased with the α -phase yielding first, followed by the β -phase yield at a higher stress. The stress to initiate yield varies with orientation of load relative to texture and with heat treatment. Load partitioning also occurs between differently oriented grain families in both phases. Results have been interpreted using a multiscale modeling approach where a unit cell FE model describes the relationship between phases, and a selfconsistent polycrystal plasticity model is used to describe relationships between different crystallographic orientations.

12:15 PM

Temperature Dependence of Ductile Fracture: *Andrew Oppedal*¹; Mark Horstemeyer¹; ¹Mississippi State University

The purpose of this paper is to examine the temperature dependence of ductile fracture in various metal alloys. Ductile fracture is known to be caused by the accumulation of damage. Void nucleation, growth and coalescence are phases of damage progression, and each term has a characteristic temperature dependency that varies with the material. This effect leads to the observation that for some materials elongation to failure increases as temperature as increases,



while for other materials elongation to failure decreases as temperature increases. Some materials ductile fracture behavior is more dominated by void nucleation and others are dominated by void growth and coalescence. Our contribution is to propose a theoretical paradigm that captures this apparent discrepancy. Specific examples of magnesium, aluminum and steel alloys will be illustrated.

12:35 PM

Effect of Hot Deformation on the Ti-Al-Nb-W-B Alloys: Lan Huang¹; Peter Liaw¹; Chain Liu¹; ¹University of Tennessee

A fine grain size ($< 50 \,\mu$ m) can be obtained after HIPing and homogenization treatment, without any hot deformations or cyclic heat treatments, in the small drop-casted TiAl-based specimens, with the composition of Ti-45Al-7Nb-0.15B-0.4W. Large samples with the same composition, produced through magnetic flotation, tend to have a larger grain size ($\sim 100 \,\mu$ m) and a bigger amount of β -phase in the alloy. Heat treatments have been conducted in order to reduce the amount of β -phase. Additional deformation techniques, such as hot forging, have been chosen to refine the grain size of the alloy. The microstructual evolution of the TiAl-based alloy after hot forging and related heat treatments has been investigated. Mechanical properties of the alloy after deformation and heat treatments have been studied. The research is sponsored by the Fossil Energy Materials Program, and the National Science Foundation Combined Research-Curriculum Development Program.

Aluminum Reduction Technology: Environmental and Plant Improvements

Sponsored by: The Minerals, Metals and Materials Society, TMS Light Metals Division, TMS: Aluminum Committee

Program Organizers: Geoffrey Bearne, Rio Tinto Aluminium Ltd; Stephen Lindsay, Alcoa Inc; Morten Sorlie, Elkem Aluminium ANS

Monday AM	Room: Southern 2
February 26, 2007	Location: Dolphin Hotel

Session Chair: Jerry Marks, J. Marks and Associates

9:00 AM

Alumina Dry-Scrubbing Technology: Development of a Cascade Feeding System for Improved Capture Efficiencies: *Hugues Vendette*¹; Neal Dando²; Alain Moras³; Eric Marion¹; Weizong Xu²; ¹Solios; ²Alcoa Technical Center; ³Aluminerie de Deschambault

Aluminum smelters use alumina (ore) as an adsorbent for capturing fluoride evolved from the smelting process. A direct relationship exists between the capture efficiency of an alumina-based dry injection-type scrubber and the fluorination level of the recirculated alumina used to scrub the off-gases generated from an electrolysis potline. To take advantage of this relationship, an alternative fresh alumina distribution scheme was developed. This serial feeding system directs a maximum quantity of alumina in the first scrubber module of a series and redirects the overflow of the non-saturated alumina to the next module until the material exits the last reactor of the series. Solios and Alcoa Primary Metals have collaborated to evaluate this process at an operating smelter. Short-term test results indicate a 40-50% reduction in F emissions relative to parallel feed operation. This article will present the results observed from a subsequent long-term (several months) test of this process.

9:25 AM

Development of a System Based on Water Atomization to Decrease, Prior to Treatment, the Temperature of the Gas Emitted from Aluminium Cells: *Myriam Bonnier*¹; ¹Alcan

A common problem in Gas Treatment Centres (GTC) for primary aluminium smelters deals with gas temperatures: above a threshold, filtering media are irreversibly damaged. Traditionally, the gases are diluted with fresh air which implies over sizing –therefore higher cost for - the GTC in order not to compromise the pot suction. A system was developed without having to use dilution air. It is based on water pulverization and vaporization in ductwork prior to the GTC. This enables an accurate control of the gas temperature with total water vaporisation. First a pilot system was trialled in our R&D unit. Satisfactory results lead to the development of an industrial system based on EnviroCare equipment in our production plant in Tomago (NSW, Australia) in 2003. This patented system was then generalized to 4 GTCs in Tomago. Our experience, technical results and the economical performance of the system are discussed in the article.

Technical Program

9:50 AM

Effective Techniques to Control Fluoride Emissions: Stephen Lindsay¹; ¹Alcoa Inc

Control of fluoride emissions is an important parameter of smelting operations. This paper highlights effective means that have been used to reduce fluoride emission levels at numerous Alcoa locations. Particular attention has been paid to increases in collection efficiency and dry scrubber effectiveness. Focus areas include: fluoride evolution, draft, pot room components to emissions, dry scrubber system control and emissions monitoring systems and techniques.

10:15 AM

Research at the Albras Aluminum Company for Utilizing Mineral Clay in Place of Asbestos: *Rinaldo Braga*¹; Adinaldo Ferreira¹; ¹Albras Alumínio Brasileiro S/A

Asbestos containing gaskets have always been used to seal connections of the aluminum tapping crucibles cast iron tubes used in the pot lines at Albras. This was the most durable and cheapest material available for supporting the high temperatures and for making good seals. However, due to industrial hygiene concerns about the carcinogenic nature of asbestos, which demand special care to use and dispose of, the decision was taken at Albras to look for an alternative material to use for this and other applications. Specifically, for tapping crucibles a clay-based material has been developed with a internal metallic support which improves its resilience. An aspect of the development process was optimizing the curing time of the clay.

10:40 AM Break

10:55 AM

Development of a Wearable Gauge for Measuring Transient Peak HF Concentrations in Aluminum Smelters: *Neal Dando*¹; Weizong Xu¹; Jon Peace¹; ¹Alcoa Inc

Hydrogen fluoride is evolved from individual smelting pots during aluminum electrolysis. The vast majority of evolved HF is captured by active hooding systems and send to fume treatment centers for recovery of the gaseous fluoride and return to the pots on feed alumina. HF that escapes the active hooding systems enters the potroom and is considered as emissions, since these gases typically exit via the potroom roof vents. Potroom emissions also create the potential for workplace exposures. The current test protocol (NIOSH 7902) for testing short term exposures to HF involves pulling known volumes of room air through treated filters providing a time weighted average as opposed to a peak exposure. The International Aluminium Association funded an Alcoa proposal to develop a wearable gauge capable of measuring short term (<10 second)peak concentrations of HF in smelter potrooms. This talk will discuss the development and in-plant evaluation of this guage.

11:20 AM

Revolutionary Design of Pot Tending Machines: Nicolas Dupas¹; ¹ECL

Since the first PTM commissioned in 1962 by ECL, the designs and tasks of these cranes has evolved. For the first time in the industry, ECL has performed a total rethink of the PTM, coming up with a new patent pending concept based on: Increased performances, in terms of: commissioning time, productivity, availability rate, safety, reliability. A streamlined architecture giving significant weight and height reductions. A modular structure allowing: structural variations, optional equipment and tools, An evolutionary design taking into account future ECL developments. Consequently, the ECL New Concept PTM is lighter and more compact, and its performances can be tailored to the needs of the smelter. The New Concept PTM includes all the traditional PTM functions plus a new range of groundbreaking options that will be presented during the conference.



11:45 AM

Aluminium Smelter Hot Cavity Bath Treatment Processes: *Patrick Coulombe*¹; Alain Gaboury¹; Jean-Francois Riverin²; ¹Aluminerie Alouette Inc.; ²STR Consultants Inc.

Cavity cleaning during anode change generates a material that consists of chunks of anode cover material and frozen cryolite melt. This material is scooped and placed in bins for transport and further processing and recycling as fresh anode cover material. Handling of the cavity bath material can be labour intensive and can generate significant air emissions (particulate and gaseous fluorides). In a context of sustainable development, smelters must address this issue by ensuring that novel treatment processes are incorporated into new plant design or retrofitted to existing facilities. This article reviews typical processing methods in use in the industry and highlights a new process implemented at the Alouette Smelter where cavity bath is processed as a hot material directly from the potlines, sized, cooled and then processed in the existing cold bath treatment plant. Implementing this system in a Brownfield facility imposed constraints for space, interfaces with operations and rampup.

12:10 PM

A New Alumina Distribution and Feeding System for Aluminium Reduction Cells: *Andreas Wolf*¹; Michael Rinck¹; Peter Hilgraf¹; ¹Claudius Peters Projects GmbH

This paper describes the operation of an Alumina Distribution And Feeding System For Aluminium Reduction Cells and how Claudius Peters has applied extensive knowledge using the constructive characteristics of the horizontal distribution system, the control algorithms of the process applied for the application. In the process cycle prior to the actual production of aluminium, alumina is conveyed and distributed to the aluminium reduction cells. The general control philosophy comprise of all components from upstream interface, (secondary alumina silo), to the downstream interfaces above the pot cells. The absolute horizontal transport and intermediate distribution of alumina from the secondary alumina silo is decoupled from pot silos, by using the FLUIDCON conveying system passing alumina in axial direction by a "driving gas flow" (conveyor pipe principle). The pressure loss of the driving gas flow substitutes the inclination of the aero slides and supplies the alumina to the single pots cells without any additional feeder systems. The operating characteristic of the FLUIDCON Alumina Distribution And Feeding System results in extremely low transport velocity, energy consumption and low wear and maintenance.

Biological Materials Science: Bioinspired Materials

Sponsored by: The Minerals, Metals and Materials Society, TMS Structural Materials Division, TMS/ASM: Mechanical Behavior of Materials Committee

Program Organizers: Andrea Hodge, Lawrence Livermore National Laboratory; Chwee Lim, National University of Singapore; Eduard Artz, University of Stuttgart; Masaaki Sato, Tohoku University; Marc Meyers, University of California, San Diego

Monday AM	Room: Europe 4
February 26, 2007	Location: Dolphin Hotel

Session Chairs: Marc Meyers, University of California, San Diego; Eduard Artz, University of Stuttgart, Max Planck Institut fuer Metallforschung

9:00 AM

Bioinspired Design of Functionally Graded Dental Multilayers: *Nima Rahbar*¹; Min Huang¹; Stephen Farias¹; Onobu Akogwu¹; Winston Soboyejo¹; ¹Princeton University

This paper presents the bioinspired design of dental multilayers. Nanoindentation measurements of the dentoenamel-junction (DEJ) are shown to reveal a functionally graded transition in Young's modulus from that of enamel to that of dentin. This occurs over a distance of 10 to 100 micrometers. The graded transitions are modeled using finite element simulations that reveal a significant decrease in stress concentrations near the interface in the functionally graded structures. Bioinspired functionally graded multilayers (FGMs) are then fabricated using the powder mixing and photolithography techniques. The critical loads for cracking in these FGM are compared with those of conventional dental fracture. The FGM designs are also shown to significantly increase the critical crack lengths for fracture. The effect of loading rate are compared for the structures with and without FGM. The talk concludes with the presentation of novel bioinspired FGM design that could reduce the overall stress concentrations in dental multilayers.

9:20 AM

Mineral Bridges in Abalone Nacre: *Albert Lin*¹; Po-Yu Chen¹; Marc Meyers¹; ¹University of California, San Diego

Ocean mollusk shells are composed of aragonite/calcite crystals interleaved with layers of a viscoelastic protein, having dense, tailored structures with excellent mechanical properties. The complex nano-laminate structure is characterized and related to its mechanical properties. Abalone nacre consists of 0.5 μ m by 10 μ m aragonite bricks layered with 30 nm layers of organic matrix. Mineral bridges which perpetuate crystal growth between organic layers have been proposed in past investigations. The organic matrix separating layers of tiles is believed to provide the essential toughening mechanism. Through careful investigation a new mechanism is proposed. The mineral bridges connecting adjacent layers of tiles is shown to play a significant role in the strength of nacre. The composition and growth mechanisms of nacre are observed through close examination of laboratory-grown samples using Scanning Electron Microscopy, Atomic Force Microscopy, and Transmission Electron Microscopy. This research is funded by the National Science Foundation, grant number DMR-0510138.

9:40 AM Invited

Bio-Inspired and Biocompatible Materials with Carbon Nanorubes as Functional Elements: Hyung Gyu Park¹; Alexander Artyukhin¹; Shih-Chieh Huang¹; Yinmin Wang¹; Jason Holt¹; Michael Stadermann¹; Aleksandr Noy¹; *Olgica Bakajin*¹; ¹Lawrence Livermore National Laboratory

Carbon nanotubes are a unique system for studying bio-inspired molecular transport, as well as a potentially highly sensitive bio-sensor platform. Knowledge of the behavior of water in confined hydrophobic geometries is crucial for the comprehension of many biological processes, and for advancement of nanotechnology. We will present experimental work that has demonstrated the breakdown of classical theories when applied to the transport of gases and water through sub-2nm carbon nanotubes. We will also discuss a new hybrid nanobiomaterial that combines electronic properties of carbon nanotubes with advanced shielding properties and biocompatibility of lipid bilayers. We will demonstrate that the lipid bilayers in these structures conserve their fluidity, present electrical characterization of these structures and discuss their potential use in novel biosensing devices. This work was performed under the auspices of the US Department of Energy under contract #W-7405-Eng-48 with funding from the LDRD program.

10:10 AM Invited

Nanoengineered Bone through Electrospinning and Mineralization: Susan Liao¹; Casey Chan¹; Ramalingam Murugan¹; *Seeram Ramakrishna*¹; ¹National University of Singapore

In this study, we investigated two methods of incorporating minerals into electrospun nanofibers. Firstly, we attempt to mineralize the electrospun nanofibers by co-precipitation. Electrospun nanofibers derived from natural collagen and synthetic PLGA were used as templates for mineral formation. For collagen, nano-hydroxyapatite (nHA) crystals are formed on the surface of single nanofibers. For PLGA, pure nHA crystals are formed on the small (~100nm) and large (~320nm) diameter nanofibers. However, aggregation of the nHA was widely seen in PLGA nanofibers. This difference is the result of the abundance of Ca2+ bonding positions on collagen which allows for more distributed mineralization. In a second method, the preformed nHA/ collagen prepared by biomimetic co-precipitation was blended with collagen and then electrospun into nanofibers. The fibers diameter tends to be larger in section where there is aggregation of nHA/collagen. We speculate such nanocomposites with biomimetic nanotexture are conducive to osteoblasts adhesion, proliferation and ingrowth.

10:40 AM Break

Technical Program



10:50 AM Invited

Designing Biomimetic Model Surfaces with Enhanced Adhesion: *Eduard Artz*¹; Aranzazu del Campo²; Christian Greiner²; Emerson DeSouza²; ¹Max Planck Institut fuer Metallforschung, University of Stuttgart; ²Max Planck Institut for Metals Research, Institute for Physical Metallurgy, Universität Stuttgart

Attachment organs of insects, spiders and lizards have tought us the main ingredients of reversible adhesion systems relying on molecular surface forces: splitting up into fine contact fibers with large aspect ratios, optimized contact shape, intermediate values of Young's modulus, and hierarchical levels of the adhesion elements. Using the previously developed adhesion design maps, we have designed patterned polymer surfaces with the aim of verifying the theoretical predictions. Through a combination of photolithography, nano contact printing, and nano inking processes, well-controlled three-dimensional patterns with different contact shapes and sizes down to the micron range were produced in different polymers. Adhesion tests were performed and compared with the progress achieved in other laboratories. The results give clear evidence that patterning indeed increases the adhesion by molecular forces and that contact shape has a significant effect on the performance of the contacts. With PDMS polymers, adhesion stresses that approach the values of biological systems (e.g. in the gecko) have been obtained on a laboratory scale. In addition, the role of micro-capillarity in modulating the adhesion force has been investigated in detail; an important results is that contact splitting also enhances the attractive forces of liquid menisci, especially for intermediate wetting angles. The scope for further improvement and possible application of such surfaces will also be discussed.

11:20 AM

A Comparison of the Nanomechanical Properties of Hyaline and Repair Cartilage: Oliver Franke¹; Verena Maier¹; Kolja Gelse¹; Karsten Durst¹; Mathias Göken¹; ¹University Erlangen

In this research work transgene stimulated periost-cells were used to repair damages in the knee-joint of mini-pigs. Samples were extracted after 6 weeks and 6 months respectively and compared to healthy hyaline cartilage. Furthermore tests were carried out using a reference group with unstimulated periost cells. The mechanical properties of the different samples were determined by in vitro nano-indentation in PBS at room temperature. The positive influence of the transgene stimulation can be shown after 6 weeks as well as after 6 months. Furthermore the comparison of the results from mechanical testing with histological analysis shows a good coincidence of the two methods. For a better understanding of the hierarchical structure of cartilage and the interaction of collagen with mineral platelets, the bonecartilage interface was also investigated in-vitro.

11:40 AM

Synthetic Bone Substitutes Derived from Marine Materials: A Comprehensive Study of Microstructure, Mechanical and Biological Properties: *Xing Zhang*¹; Kenneth Vecchio¹; ¹University of California

In this investigation, dense hydroxyapatite (HAP) was created from the dense structures of seashells, *Strombus gigas* (conch) shells and *Tridacna gigas* (Giant clam) shells. Partially converted shell samples, with dense HAP layers on the surface growing inward, have an average fracture stress about 137-218MPa, which is close to the strength of compact bone. The skeletonal structures of sea urchin spines, which are composed of large single crystals of Mg-rich calcite, and form a three-dimensional fenestrated mineral network, were also studied. The spines of the echinoid *Heterocentrotus trigonarius* and *Heterocentrotus mammillatus* were converted to bioresorbable Mg-substituted calcium phosphate (β -TCMP) by the hydrothermal reaction, while maintaining the three-dimensional interconnected structures. The average compressive strength of completely converted spines is ~23MPa, which is higher than that of cancellous bone. Results from in-vivo tests in femur defects of rats will be presented to show good biocompatibility and osteoconductivity of these synthetic bone materials.

12:00 PM

Biomimetic Behavior of In Situ Formed Bioactive Composite Developed by Powder Metallurgy (PM) Processing for Load Bearing Applications: *Malobika Karanjai*¹; Sundaresan Ranganathan¹; Rama Mohan Tallapragada²; Bhagwati Kashyap²; ¹International Advanced Research Centre for Powder Metallurgy and New Materials; ²Indian Institute of Technology Bombay

A titanium based biocomposite was obtained through powder metallurgy

(PM) processing. Such composites with in situ formed calcium-phosphatic phases were bioactive in nature. The raw materials used were titanium hydride powder and powder precursors of calcium and phosphorus in the form of calcium carbonate and di ammonium hydrogen orthophosphate. The PM processing involved steps like blending and mixing, compacting and sintering. The sintered Ti-Ca-P composites had hydroxylapatite and different calcium-phosphatic phases in Ti-based matrix. When immersed in simulated body fluid, bone-like growth were observed on these composites. The biocomposites developed had adequate mechanical strength and required porosity to eventually allow the tissue growth inside. Their in vitro biomimetic behavior, fretting wear and electrochemical corrosion properties were also studied. Results are presented and discussed. To assess its suitability for use an implantable biomaterial, further in vitro cytotoxicity tests were conducted and the composites were found to be non-toxic in nature.

12:20 PM Invited

Probing Biological Control over Crystallization by In Situ Molecular Imaging and Molecular Modeling: *Roger Qiu*¹; Andrzej Wierzbicki²; John Hoyer³; George Nancollas⁴; Dan Morse⁵; Chris Orme¹; James De Yoreo¹; ¹Lawrence Livermore National Laboratory; ²University of South Alabama; ³University of Pennsylvania; ⁴University at Buffalo, SUNY; ⁵University of California-Santa Barbara

Since materials production in biological systems inherently involves nanoscale controls and structures, an understanding of the physical mechanisms by which biomolecules control crystallization can provide insights into methods of synthesizing crystalline structures for application across a wide range of technologies. For the past decade, we have utilized in situ scanning force microscopy combining with molecular modeling to probe the fundamental mechanisms by which small molecules and macromolecules control biogenic materials production. Specifically, we investigate the effect of proteins over the growth kinetics and morphology of model systems including calcium carbonate, calcium oxalate, and hydroxyapatite. Throughout all the systems investigated, we find that biological molecules control growth kinetics and modify crystal shape by selective interaction with specific steps on the existing faces of each crystal. Moreover, this specific control is directed by the stereochemical recognition between the structure of modulating molecules and the local structure of crystal steps. This work was performed under the auspices of the U.S. Department of Energy by the University of California, Lawrence Livermore National Laboratory under contract No. W-7405-Eng-48. We thank the support from the U.S. National Institutes of Health through grants DK61673 and DK33501.

Bulk Metallic Glasses IV: Glass Science and Technology

Sponsored by: The Minerals, Metals and Materials Society, TMS Structural Materials Division, TMS/ASM: Mechanical Behavior of Materials Committee *Program Organizers:* Peter Liaw, Univ of Tennessee; Raymond Buchanan, University of Tennessee; Wenhui Jiang, University of Tennessee; Guojiang Fan, University of Tennessee; Hahn Choo, University of Tennessee; Yanfei Gao, University of Tennessee

Monday AM	Room: Asia 1
February 26, 2007	Location: Dolphin Hotel

Session Chairs: Peter Liaw, University of Tennessee; W. L. Johnson, California Institute of Technology

9:00 AM Introductory Comments

9:05 AM Keynote

Potential Energy Landscapes and Amorphous Metals: William Johnson¹; ¹California Institute of Technology

The application of the Potential Energy Landscape formalism of Stillinger and Weber to the theory of metallic glasses is discussed. It is shown that the average properties of the PEL obey certain scaling laws. Specifically, the elastic properties of the frozen glass are shown to be fundamentally related to the rheological behvior of the liquid and the mechanical properties of the glassy state. A simple theoretical model is formulated and used to predict the yield



strength, ductility, and toughness of metallic glasses. The same model predicts the Newtonian and non-Newtonian flow behavior of the corresponding liquid alloys. Detailed comparison of the model with broad range of experimental data will be be presented.

9:35 AM Keynote

Fabrications and Applications of Late Transition Metal Base Bulk Glassy Alloys with Critical Diameters of Centimeter Order: Akihisa Inoue¹; ¹Tohoku University

Since the first syntheses of Mg- and La-based bulk glassy alloys with diameters above 5 mm by copper mold casting in 1989, a number of bulk glassy alloys have been formed for a variety of alloy systems by using various casting processes. The highest glass-forming ability reported up to date was obtained for Pd-Cu-Ni-P system and its critical cooling rate and maximum sample thickness reached as low as 0.02 K/s and as large as above 80 mm, respectively. In addition to the Pd-based glassy alloys, high glass-forming ability with critical diameters above one centimeter has been obtained for Zr-, Pt-, Y-, Ce-, Mg-, Fe-, Co-, Ni- and Cu-based alloy systems. This paper aims to review our recent results on the formation, workability and fundamental properties of Pd-, Pt-, Fe-, Co-, Ni- and Cu-based bulk glassy alloys with large critical diameters above 1 cm and some applications.

10:05 AM Invited

Coupled Order Parameter Nucleation Processes in Metallic Glasses: Kenneth Kelton¹; ¹Washington University and Center for Materials Innovation

Recently our synchrotron X-ray diffraction studies of electrostatically levitated samples, demonstrated that the liquids of many transition metals and their alloys develop strong icosahedral order with supercooling. In a Ti-Zr-Ni liquid this ordering couples with the nucleation of the ordered phase. The ordered regions of the liquid act as a template for the nucleation of the icosahedral phase, blurring the traditional distinction between homogeneous and heterogeneous nucleation. This is one example of a coupled nucleation process; others include a coupling between magnetic or chemical ordering and nucleation. Such coupled nucleation processes are not readily described by the commonly used classical theory of nucleation. The implications of coupled nucleation processes on glass formation and stability, nanoscale devitrification, and microalloying are discussed. Supported by the NSF under grants DMR 03-07410 and DMR-0606065, NASA under contract NNM04AA016, and AFOSR under contract 9550-05-1-0110.

10:25 AM Invited

Thermal Conductivity as a Factor Influencing Glass-Forming Ability of Bulk Glass-Forming Alloys: *Dmitri Louzguine*¹; Albertus Setyawan¹; Hidemi Kato¹; Akihisa Inoue¹; ¹Institute for Materials Research

Here we study the factors related to thermal conductivity of the molten alloy and heat transfer of the melt-mold system influencing the glass-forming ability (GFA). The initial cooling rates (for first 100 K) obtained for Cu-, Zrand Au-based bulk glass-forming alloys (bulk metallic glasses) are found to scale linearly with the thermal conductivities of the liquid base elements while Ni-based alloy shows underestimated cooling rate. Thus, one can suppose that the heat transfer at the melt-mould interface may also influences the cooling rate in case of Ni-based alloy. Biot number-based analysis is used to evaluate the cooling regimes. The results indicate that the thermal conductivity of the molten alloy and melt-mould system are important factors influencing the GFA. Moreover, as the cooling rate depends on temperature the critical cooling rate is not a suitable parameter for indicating the glass-forming ability. An exponential parameter can be used instead.

10:45 AM

Thermophysical Properties of Cu-Based Bulk-Metallic Glass-Forming Liquids: *Guojiang Fan*¹; M. Freels¹; H. Choo¹; P. K. Liaw¹; J. J. Z. Li²; W. K. Rhim²; W. L. Johnson²; W. H. Wang³; ¹University of Tennessee; ²California Institute of Technology; ³Chinese Academy of Sciences

The thermophysical properties of bulk-metallic glass-forming liquids in the molten state are important parameters, which may be closely related to their glass-forming ability, fragility, and even room-temperature mechanical properties. In this study, the thermophysical properties, including the surface tension, the viscosity, the ratio between the specific heat and the hemispherical total emissivity, the specific volume, and the density of a series of Cu-based bulk-metallic glass-forming liquids have been measured using a containerless high-temperature high-vacuum electrostatic levitation (ESL) technique. The relationship between the measured thermophysical properties in the molten liquid state and the elastic properties of the glasses at the room temperature will be compared and discussed. This work was supported by the National Science Foundation (NSF) International Materials Institutes (IMI) Program (DMR-0231320) and Integrative Graduate Education and Research Training (IGERT) Program (DGE-9987548) with Drs. C. Huber and C. J. Van Hartesveldt as the program directors, respectively.

11:00 AM

TTT Diagram for Magnesium and Zirconium-Based Bulk Amorphous Alloys: Signo Reis¹; Neal Ross¹; Richard Brow¹; ¹University of Missouri Rolla

Time-temperature-transformation (TTT) curves for magnesium and zirconium-based bulk amorphous alloys were measured using a differential thermal analysis (DTA) technique to define devitrification factors which influence the glass-forming ability. The glass transition temperature, Tg, and the liquidus temperature, TL, were obtained by heating at a rate of 0.17 Ks-1. The TTT curves were obtained using isothermal experiments to detect crystallization exotherms. For the magnesium-based glass alloy (Mg57Cu28Ag7Y11), the temperature at which the time for crystallization is minimum (the 'nose' of the TTT curve) is about 525K and the critical cooling rate is 1.27Ks-1.

11:15 AM Invited

Development and Characterization of Low Density Ca-Based Bulk Metallic Glasses: An Overview: Oleg Senkov¹; ¹UES Inc

Recent work on development of low density Ca-based bulk metallic glasses is overviewed. These glasses can be represented by a formula $Ca_A(Y,Ln)_B$ $(Mg,Sn)_C(Al,Ag,Ga,Zn)_D(Cu,Ni,Si)_E$, where Ln is a lanthanide group element; A=0.40-0.70; B=0-0.25; C=0-0.25; D=0-0.35; E=0-0.35; $B+C+D \ge 0.05$ and A+B+C+D+E=1. Good forming ability and thermal stability of these metal glasses was correlated to the specific relative atomic sizes of the alloying elements, which provide formation of efficiently packed atomic clusters. Some physical, thermodynamic and chemical properties are presented and the effect of the alloy composition on these properties is discussed.

11:35 AM Invited

Glass Forming Ability from the Local Structure Perspective: *Evan Ma*¹; ¹Johns Hopkins University

Efficient packing of space is one of the guiding principles that contribute to the relative stability of a metallic glass. Topological instability has also often been invoked to explain the composition range for glass formation. Here we discuss such structural aspects in relation to glass forming ability (GFA). We tune the atomic size ratio and correspondingly the local structure inside a glass using hydrostatic pressure. We also introduce the idea of polymorphic amorphous-to-amorphous transformation in metallic glasses. This will be discussed in light of the visitation of different energy basins in the potential energy landscape. Using the insights gained from recent structural studies, we will model the mechanical instability that could be responsible for the high GFA leading to BMGs. The high-GFA compositions that often give rise to BMG formation will be demonstrated and discussed.

11:55 AM

An Alternative Model for Structural Relaxation in Metallic Glass: Deviation from Short Range Ordering: Aiwu Zhu¹; Joseph Poon¹; Gary Shiflet¹; ¹University of Virginia

In this presentation, an alternative model of metallic glass atomic structure and its structural relaxation around the glass transition is introduced to compare with the free volume model and others. Supercooled liquids and metallic glasses are described as SRO configurations with local SRO deviation (under the quasi-chemical approximation). The chemical effect of alloys is incorporated. A simplified model using a "localized" disordering assumption is developed for analysis of structural relaxation around the glass transition which naturally leads to a "bi-molecular" mechanism for evolution of disordered regions and possibly large associated "apparent activation energy".



12:10 PM

Effect of the Frequency of Electromagnetic Vibrations on Vibrating Motion in Mg-Y-Cu Bulk Metallic Glasses: *Takuya Tamura*¹; Yuuki Maehara¹; Naoki Omura¹; Kenji Miwa¹; ¹National Institute of Advanced Industrial Science and Technology

It is known that cooling rate is an important factor. However, almost no other factors such as electric and/or magnetic fields were investigated. The present authors reported that a new method for producing Mg-Cu-Y bulk metallic glasses by using electromagnetic vibrations is effective in forming the metallic glass phase. Moreover, the present authors have reported that the glass-forming ability of Fe-Co-B-Si-Nb alloys also enhances with increasing the electromagnetic vibration force. In Fe based alloys, it was found that the amplitudes of the electromagnetic vibrations at 5kHz are of the order of micrometer, but that at high frequency are of the order of nanometer. The electromagnetic vibrating motion. Thus, this study aims to investigate effect of the frequency of the electromagnetic vibrations on the vibrating motion of the alloys in Mg-Y-Cu bulk metallic glasses.

12:25 PM

Multi-Functional Optimization Approach for Predicting Bulk Metallic Glass Systems: Sandeep Gorantla¹; Yanwen Wang¹; *Frank Miller*¹; Rajiv Mishra¹; Daniel Miracle¹; Oleg Senkov¹; ¹University of Missouri - Rolla

A multi-functional optimization approach has been developed for empirical prediction of compositions for bulk metallic glasses. In this predictive approach, Inoue's principles, atomic size-mismatch, melting temperature depression parameter and also the mole melting enthalpies parameter were included. The applicability of this predictive approach was evaluated by synthesizing several low-density Mg-based bulk metallic glass alloys. The alloys prepared based on this approach were characterized by XRD, SEM and TEM. The initial results show that inclusion of all the above principles still do not provide full predictive capability. The authors gratefully acknowledge the support of the Air Force Research Laboratory through contract no. FA8650-04-C-704 (Dr. Mary E. Kinsella, Program Manager).

12:40 PM

Primary Crystallization in Amorphous Al-Y-Fe Alloys: *Rainer Hebert*¹; John Perepezko¹; ¹University of Wisconsin

Primary Al nanocrystals develop during annealing of amorphous Al-Y-Fe alloys with solute contents between 10 and 13 at%. Following intense cold-rolling and folding, primary crystals develop at true strain levels of about -2 to -5 only for alloys such as the Al88Y5Fe7 that exhibit primary crystallization during thermal annealing while other alloys such as Al85Y10Fe5 remain amorphous even within the shear bands. At a true strain level of -13, primary crystallization develops, however, in the amorphous Al85Y10Fe5 alloy. Intense deformation thus exposes new crystallization products that reflect the non-equilibrium processing pathway. A combined HRTEM and microcalorimetry analysis of amorphous Al88Y7Fe5 alloys annealed for 10 days at 130C, i.e., 140K below the glass transition temperature shows furthermore that nanocrystals have not developed despite a decaying irreversible exothermic heat release during annealing. Within a certain time-temperature window, structural relaxation can therefore be studied separately without interfering nanocrystallization.

Characterization of Minerals, Metals, and Materials: Characterization of Structure across Length Scales I

Sponsored by: The Minerals, Metals and Materials Society, TMS Extraction and Processing Division, TMS: Materials Characterization Committee *Program Organizers:* Arun Gokhale, Georgia Institute of Technology; Jian Li, Natural Resources Canada; Toru Okabe, University of Tokyo

Monday AM	Room: Oceanic 8
February 26, 2007	Location: Dolphin Hotel

Session Chairs: Arun Gokhale, Georgia Institute of Technology; Lucille Giannuzzi, FEI Company

9:00 AM Invited

NanoCT: Visualizing of internal 3D-Structures with Submicrometer Resolution: Cornelius Wuelker¹; Dirk Neuber¹; Bill Eppich¹; *Kathleen Brockdorf*¹; ¹Phoenix/X-Ray Systems and Services GmbH

High-resolution nanoCT widely expands the spectrum of detectable internal micro-structures. The new nanotom CT system allows analysis of samples with the exceptional voxel-resolution of <0.5 microns. It is the first 160 kV nanoCT system worldwide which is tailored for highest-resolution applications in material science, geology, etc. Initial CT results demonstrate the capability to analyse the 3D-microstructure of materials with minimal sample preparation and submicrometer resolution; any internal difference in material, density or porosity can be visualized and precisely measured. For instance, it's possible to image different phases in solder joints or to analyse pore networks in rock samples. This opens a new dimension of 3D-microanalysis and will replace more destructive methods. We will discuss the influence of different environmental factors (such as X-ray focal spot size, movements and temperatures) as well as the parameters of the detection system and the reconstruction algorithm on the system design.

9:30 AM

3-D Atom Probe Tomography of Nanoscale Precipitates in Al-Si-Cu-Mg Casting Alloys: *Junyeon Hwang*¹; Rajarshi Banerjee¹; Herbert Doty²; Michael Kaufman¹; ¹University of North Texas; ²GM Powertrain, Metal Casting Technology Inc.

The 319 type Al-Si-Cu casting alloys are widely used in the automotive industry. It is well known that the θ ' precipitate plays the dominant role in strengthening these alloys. The addition of Mg to 319 aluminum alloys often enhances the strength by formation of additional precipitates. However, the structure and composition of these precipitates are not well established because of their extremely small size. In this study, three-dimensional atom probe tomography combined with high resolution transmission electron microscopy have been used to investigate the structure and composition of the precipitates at the atomic level. The results help clarify the role of Mg in the precipitation hardening of modified Type 319 aluminum alloys specifically and Al-Cu-Mg alloys in general. [Research supported by GM Powertrain. TEM and LEAP work performed using the analytical facilities in the Center for Advanced Research and Technology at the University of North Texas].

9:50 AM

Topological and Metric Considerations on Abnormal Grain Growth: Paulo Rios¹; Martin Glicksman²; ¹UFF-EEIMVR; ²University of Florida

Abnormal grain growth(AGG) is often distinguished from normal grain growth. During abnormal grain growth a few large grains, abnormal grains, dominate the grain growth process. Earlier approaches have treated AGG in purely in metrical terms by employing a "grain radius". This paper treats abnormal grain growth in terms of topological concepts such as grain boundary curvature and number of faces of the abnormal grain. Abnormal grain growth when the matrix is fully pinned and abnormal grain growth when the matrix is free to grow are examined using the new theory.

10:10 AM

Automated Shape Analysis of γ Precipitates in a Rene88-DT Super-Alloy: Jeremiah MacSleyne¹; Michael Uchic²; Marc DeGraef¹; ¹Carnegie Mellon University; ²US Air Force Research Laboratory

Depending on the heat treatment and processing conditions, g' precipitates



in super-alloys can have a wide variety of shapes, ranging from simple near spherical or cuboidal shapes to complex near-dendritic shapes. A quantitative description of such shapes is needed to allow for comparisons with numerical results from phase field computations. In this contribution, we will introduce the concept of shape or moment invariants, mathematical quantities that are invariant under translations, rotations, and linear scaling. The moment invariants of an object can be used as a multi-dimensional characterization of its shape. We will illustrate this approach by means of a serial sectioning dataset, obtained by focused ion beam milling, of a Rene88-DT super-alloy, which contains near-dendritic g' precipitates. We will analyze the precipitate shape by means of the moment invariants of second and third order, and show how these quantities can be used to classify particle shapes.

10:30 AM Break

10:45 AM Invited

An Update on FIB and DualBeam Applications and Techniques for Materials Characterization: Lucille Giannuzzi'; 'FEI Company

Focused ion beam (FIB) based instruments are no longer just expensive specimen preparation tools. DualBeam instruments (a FIB column and a scanning electron microscope (SEM) column on the same platform) can be used for unattended and automated site specific cross-sectioning or TEM specimen preparation. Incorporation of a flipstage and STEM detector in a DualBeam allows for unique FIB milling of TEM specimen preparation geometries that can be directly STEM imaged in real time with sub-nanometer resolution. In addition, the synergistic use of the FIB with the SEM allows for automated acquisition of serial slices for subsequent 3D reconstruction and tomography of microstructure (via SEM imaging), crystallography (via EBSD) and/or elemental composition (via EDS). Automated and advanced digital patterning capabilities can be used to either remove or deposit material lithography or micro- and nano-prototyping. Examples of the methods and techniques mentioned above will be presented from a variety of materials.

11:15 AM

Three-Dimensional Analysis of Damage in Incipiently Spalled Tantalum: Veronica Livescu¹; John Bingert¹; ¹Los Alamos National Laboratory

Three-dimensional microstructural reconstruction techniques were used to characterize shock-induced damage in an incipiently spalled tantalum plate. Serial sectioning was performed in steps of 4.5µm on a significant sample volume and volumetric reconstruction was performed using optical microscopy images and electron backscattered diffraction data (EBSD). The damage field was mixed-mode, with strain localization linking many of the voids. This structure differed substantially from the void cavitation dominated structure observed in a related Ta sample, tested under equivalent experimental conditions except for shorter pulse duration. Analysis of threedimensionally reconstructed void damage field provided relevant statistics such as void size, spatial distribution, and nearest-neighbor distances. Intragranular misorientation deviation maps were constructed from EBSD data and used to determine the spatial distribution of relative deformation in the microstructure. These results, incorporated with those from the shortduration sample, offer insight as to the characteristics and evolution of shock damage and the variables affecting damage features.

11:35 AM

3-D Reconstruction of Alpha Laths in Various Ti-Mo Alloys by Serial Sectioning in a Nova 600 FIB: *Robert Williams*¹; Michael Uchic²; Dennis Dimiduk²; Hamish Fraser¹; ¹Ohio State University; ²Air Force Research Laboratory/MLLMD

The development of a set of robust computational tools that permit microstructurally-based prediction of mechanical properties for commercially important titanium alloys is important to the accelerated maturation of materials. In order to facilitate accurate development of a predictive model, 3-D reconstructions of complex microstructures found in titanium alloys is vital. A custom script has been developed that allows for stage movement and realignment of the viewing area through the use of fiducial markers. Currently, the dual beam FIB has been used to section through 50 microns of material in a single run with use of the modified script. Alpha laths have been reconstructed in near alpha, alpha plus beta, and near beta Ti-Mo alloys. This talk will address the varying morphology of alpha laths and present 3-D reconstructions from various compositions and heat treatments. Sample preparation technique, both external and in-situ will be discussed, as well as analogous TEM results.

11:55 AM

A Comparison of Microstructural Quantification Using Two-Dimensional and Three-Dimensional Characterization Techniques Across a Range of Length Scales: *Peter Collins*¹; Erin Barry¹; Santhosh Koduri¹; Robert Williams¹; Gopal Viswanathan¹; Vladimir Levit¹; Hamish Fraser¹; Benjamin Peterson¹; ¹Ohio State University

The microstructural evolution of two titanium systems, namely the binary Ti-xMo system and the α/β alloy Timetal 550 (Ti-4Al-4Mo-1Zr-1Sn, wt%), have been investigated as a function of thermal history. The samples have been characterized using optical microscopy, scanning electron microscopy (SEM), orientation imaging microscopy (OM), and transmission electron microscopy (TEM). Microstructural variables that influence mechanical properties (volume fraction alpha, α -lath thickness (μ m), prior β grain factor (μ m²/ μ m³), volume fraction of colony α , and width of grain boundary α), have been quantified using a set of rigorous 2D stereological procedures. Also, novel 3D characterization techniques that span length scales (e.g., optical-Robo.Met.3D, SEM–FIB, TEM–TEM tomography) have been used to compare and contrast the same microstructural features. Finally, methods for characterization of three difficult to quantify microstructural features (athermal ω , secondary α , and β phase separation) that are nevertheless important regarding microstructural evolution and mechanical properties will be discussed.

12:15 PM

Topological and Metrical Properties of 3-D Isotropic and Non-Isotropic Polycrystals: *Martin Glicksman*¹; Paulo Rios²; ¹University of Florida; ²UFF-EEIMVR

The topological and metrical description of a polycrystal is a daunting task. A new theoretical approach is presented that uses topologically rigorous methods capable of providing exact mathematical bounds for many 3-D isotropic polycrystals properties and features. Moreover the extension of this new method to polycrystals in which the grain boundary energy is not uniform is also briefly described.

Computational Thermodynamics and Phase Transformations: First Principles and Atomistic Calculations of Phase and Alloy Thermodynamics I

Sponsored by: The Minerals, Metals and Materials Society, ASM International, TMS Electronic, Magnetic, and Photonic Materials Division, TMS Materials Processing and Manufacturing Division, ASM Materials Science Critical Technology Sector, TMS: Chemistry and Physics of Materials Committee, TMS/ASM: Computational Materials Science and Engineering Committee

Program Organizers: Corbett Battaile, Sandia National Laboratories; James Morris, Oak Ridge National Laboratory

Monday AM	Room: Europe 11
February 26, 2007	Location: Dolphin Hotel

Session Chair: Michael Gao, Carnegie Mellon University; Gus Hart, Northern Arizona University

9:00 AM Invited

Ab Initio Study of Cation-Oxygen-Vacancy Coupling in Oxygen Conducting Perovskites: *Dane Morgan*¹; Yueh-Lin Lee¹; Eric Hellstrom¹; Kuang-Sheng Hong¹; Clare Grey²; ¹University of Wisconsin; ²Stony Brook University

Fast oxygen ion conducting perovskites are important for a wide range of applications (e.g., solid oxide fuel cells). Of particular interest are perovskites with stoichiometry A2B2O5 (e.g., Ba2In2O5), where there is a high concentration of vacancies (1/6 of the oxygen sites) available to mediate transport. The vacancies interact strongly, creating significant short- and longrange-order effects (e.g., Brownmillerite ordering). A detailed understanding of the coupling between the cations and chemical ordering is still lacking. We will discuss ab initio studies of cation-oxygen-vacancy coupling in high vacancy perovskite materials. We construct an ab initio based thermodynamic model with the cluster expansion method, which makes it possible to model

LEARN • NETWORK • ADVANCE

TOZDAY AZ

Technical Program



the finite-temperature behavior of the oxygen-vacancy ordering (e.g., orderdisorder transition temperatures, oxygen site preferences, and short-rangeorder). Finally, we will discuss how these thermodynamic effects can couple to oxygen conductivity.

9:30 AM

First-Principles Calculations on Aluminum-Lanthanides and Aluminum-Actinides Phase Diagrams: *Michael Gao*¹; Anthony Rollett¹; Michael Widom¹; ¹Carnegie Mellon University

In this talk, we will present first-principles calculations on the lattice stability in 15 Al-lanthanides and 6 Al-actinides binary systems. Our goals are to (1) improve the experimentally established binary phase diagrams; (2) provide ab initio energy data of stable and hypothetical structures for compounds and elements; (3) predict the unknown phase diagrams of Al-Pm, Al-Ac, Al-Pa and Al-Np. The enthalpy at 0 K is calculated using VASP and the vibrational free energy for several systems at finite temperatures are calculated using the supercell approach within the harmonic approximation. The observed systematics and anomalies in Al-lanthanides and Al-actinides binary systems are discussed in light of current ab initio calculations. Potential revisions with the established phase diagrams are predicted; problems with current CALPHAD treatment with TCP (topologically closed packed) phases are addressed, especially the energy of the end members and the antiphase of C15 (prototype Cu2Mg, Pearson symbol cF24).

9:50 AM

Atomistic Calculation of Free Energy: Shenyang Hu¹; Michael Baskes¹; Lawrence Pratt¹; Steven Valone¹; ¹Los Alamos National Laboratory

Atomistic simulations of phase-stability require an efficient and accurate method to calculate the chemical free energy. In this study, we compared the efficiency and accuracy of two classical methods in free energy determination, Widom's inverse method and the Hamiltonian switching method. For Widom's method we employed a slab with periodic boundary conditions on the slab plane and a free surface containing steps normal to the slab plane. This geometry was chosen so that removal of an atom did not change any atomic environment. For a given configuration at a temperature T, the energy change after removing a surface atom is calculated using MD simulations. Using these energies, the excess chemical potential is calculated by Widom's method. This excess free energy is compared to that obtained using the Hamilton switching method in a bulk 3D periodic solid. Two systems were studied, pure Al and Pu-Ga alloys.

10:10 AM Invited

Formation and Stability of Ti, Y, and O-Enriched Nanoclusters in Fe: *C. L. Fu*¹; M. Miller¹; M. Kremar²; D. Hoelzer¹; C. T. Liu³; ¹Oak Ridge National Laboratory; ²Grand Valley State University; ³University of Tennessee

Stable nanoclusters (2-4 nm in diameter) in iron-based alloys have been observed at temperatures close to 1400°C. These nanoclusters appear to defy the thermal stability constraints of artificially created nanostructured materials. First-principles calculations showed that stable bonding between oxygen and vacancies is necessary to achieve high oxygen solubility in iron. Vacancies also play an indispensable role in reducing lattice strains and enhancing the oxygen binding energy in the presence of Ti and Y, resulting in the stabilization of O-enriched clusters with structures coherent with the underlying lattice. Without Y, the TiO2 phase can form, in stead of nanoclusters. However, if too much Y is present, the Y2Ti2O7 phase is likely to precipitate. These nanoclusters are in a new form of highly defective alloying state with (Ti+Y)/O atom ratio ~ 1. Research sponsored by the Division of Materials Sciences and Engineering, U.S. Department of Energy, under contract DE-AC05-00OR22725 with UT-Battelle, LLC.

10:40 AM Break

11:00 AM

Identifying Favorable H-Storage Reactions via First-Principles Thermodynamic Modeling: *Donald Siegel*¹; Christopher Wolverton¹; Jun Yang¹; Andrea Sudik¹; Vidvuds Ozolins²; ¹Ford Motor Company; ²University of California

Using density functional theory, we search for favorable H-storage reactions involving Li4BN3H10, LiBH4, and mixtures with several other hydride materials. For the new quaternary hydride Li4BN3H10, experiments have yet to definitively identify the dehydrogenation products and reaction

thermodynamics. To help clarify the reaction pathway we identify a series of four favorable dehydrogenation reactions (out of a pool of 16 candidate reactions) at experimentally-relevant temperatures. Next, we describe an approach where calculated reaction enthalpies of LiBH4 mixtures are used to guide experimental investigations of promising H-storage reactions. The predicted thermodynamics are compared with experiments, and new avenues for further study are suggested.

11:20 AM

Clustering and Short-Range Order in Fe-Cr Alloys: A Monte Carlo Study: Mikhail Lavrentiev¹; Duc Nguyen-Manh¹; Sergei Dudarev¹; Ralf Drautz²; Peter Klaver³; ¹UKAEA/EURATOM Fusion Association; ²University of Oxford; ³Queen's University Belfast

We present Monte Carlo simulations of the binary Fe-Cr alloy based on the cluster expansion approximation. At small Cr concentrations chromium atoms are well separated from each other. Clustering of Cr atoms begins at concentrations exceeding 10%. We study the size distribution of Cr clusters as a function of temperature and concentration. At low temperatures, only a few large clusters are formed with Cr-Fe interfaces parallel to the [110] planes. At higher temperatures, the number of clusters increases and their shape becomes less clear. Short-range order parameters were calculated and their negative values were confirmed near their theoretical minimum at 5% Cr. These parameters change sign at about 10.5% Cr in agreement with experiment. We find that the complex clustering and ordering processes occurring in Fe-Cr may be described using a few concentration-independent cluster expansion coefficients.

11:40 AM

Formation Mechanism of the Decomposition Morphology in Concentrated Multi-Component Alloys: Zugang Mao¹; Chantal Sudbrack¹; Kevin Yoon¹; Georges Martin¹; David Seidman¹; ¹Northwestern University

The kinetic path for nucleation and growth is commonly thought to be dictated by the initial supersaturation of solute atoms in solid-solution undergoing phase separation. We demonstrate that, in a concentrated multicomponent solid-solution, the details of the diffusion mechanism, deeply affect the early-stage morphologies of precipitation. Our arguments are based on the combined use of atomic-scale observations, employing 3-D atomprobe tomography (3-D APT) and lattice kinetic Monte Carlo simulation of a Ni(Al,Cr) alloy. By an optimized choice of thermodynamic and kinetic parameters we first reproduce experimental 3-D APT observations. We then modify the long-range vacancy-solute binding energy, without altering the thermodynamic driving force for phase separation, thereby demonstrating that the microstructural evolution changes from a coagulation-coalescence to an evaporation-condensation mechanism. The changes can only be quantitatively accounted for with non-zero values for the vacancy chemical potential and offdiagonal terms of the Onsager matrix, at variance with classical models.

12:00 PM Invited

Is There a Rational Approach to Cluster Expansion Construction? A Case Study of TiMo: Gus Hart¹; ¹Northern Arizona University

The cluster expansion (CE) has a venerable history in the study of alloys. Originally, using just a few pairwise interactions, the CE provided qualitative but useful insights into the behavior of alloys, particularly ground state searches. These days, trained by a database of first-principles data, CEs provide fast and accurate Hamiltonians for large-scale alloy simulations and ground state searches. Recently several different approaches for truncating the expansion have been advocated, including a variety of "heirarchal" systems, deriving interactions directly from CPA-based calculations, or using evolutionary approaches. Though an evolutionary approach provides the most predictive CEs, its physically dissatisfying because the interaction parameters appear as stochastic variables, devoid of physical meaning. Using the Ti-Mo binary system as a case study, we directly compare an evolutionary approach with a newly-proposed variational approach for choosing the interaction parameters, and we discuss the details of the predictions made by the CE for this system.

Diffusion in Advanced Materials and Processing: Atomistic and Multiscale Simulations

Sponsored by: The Minerals, Metals and Materials Society, TMS Structural Materials Division, ASM Materials Science Critical Technology Sector, TMS: Alloy Phases Committee, TMS: High Temperature Alloys Committee, ASM-MSCTS: Atomic Transport Committee, TMS/ASM: Nuclear Materials Committee, TMS: Solidification Committee

Program Organizers: Yong-Ho Sohn, University of Central Florida; Carelyn Campbell, National Institute of Standards and Technology; Daniel Lewis, Rensselaer Polytechnic Institute; Afina Lupulescu, Union College

Monday AM	Room: Europe 2
February 26, 2007	Location: Dolphin Hotel

Session Chairs: Yong-Ho Sohn, University of Central Florida; Zi-Kui Liu, Pennsylvania State University

9:00 AM Introductory Comments

9:10 AM Invited

Calculating Diffusion Coefficients via a First-Principles Approach: Manjeera Mantina¹; Yi Wang¹; Raymundo Arroyave²; Christopher Wolverton³; Long Qing Chen¹; *Zi-Kui Liu*¹; ¹Pennsylvania State University; ²Texas A&M University; ³Ford Motor Company

We propose a new first-principles-based procedure to determine diffusion coefficients in metals and dilute alloys. In particular, we compute the following kinetic quantities entirely from first-principles: the formation/migration enthalpies and entropies of vacancies and solute atoms. The attempt frequency for diffusion is also calculated. We illustrate the method by computing the self-diffusion coefficient of fcc Al and fcc Cu and the diffusion coefficients of Mg, Si and Cu in Al individually, through a vacancy mechanism. In the case of the dilute alloys we use the fcc-based five-frequency model to describe diffusion. We obtain results from both the local-density approximation (LDA) and the generalized-gradient approximation (GGA). The proposed method yields self-diffusion and impurity diffusion coefficients that are in good agreement with existing experimental measurements.

9:40 AM

First-Principles Computation of Transition-Metal Mobility in a Ni Matrix: *Kwai Chan*¹; Yi-Ming Pan¹; Yi-Der Lee¹; ¹Southwest Research Institute

First–principle computational methods have been utilized to compute the mobility of transition metals in binary Ni solid solutions. A local densitybased full-potential linearized augmented plane wave (FLAPW) code, named WIEN2K, was utilized to compute the electronic structure and total energy of an n-atom supercell with atom positions designed to simulate the desired diffusion processes. The computational procedure involves the calculations of the energy for vacancy formation, the energy for vacancy-solute interaction, and the energy barrier for the migration of a solute atom in the host metal. Firstprinciples computational results of the energy of formation, migration energy for self-diffusion, energy of migration barrier, and diffusion coefficient of Mo, Cr, and W solutes in Ni will be presented and compared against experimental data from the literature.

10:00 AM

Diffusion Coefficients from First Principles Using the MedeA Software Platform: *Alexander Mavromaras*¹; Walter Wolf¹; Mikael Christensen¹; Paul Saxe¹; Erich Wimmer¹; ¹Materials Design Inc

This contribution demonstrates the prediction of temperature-dependent diffusion coefficients in solids from first-principles. The methodology includes the search for transition states and the calculation of activation barriers, migration entropies and attempt frequencies as a function of temperature. These capabilities are integrated in Materials Design's software platform MedeA, which combines experimental databases and leading computational approaches with automated procedures to build models (e.g. interfaces), optimize computational parameters, and to manage and analyze large-scale computations. Examples include the interstitial diffusion of hydrogen in metals and vacancy-assisted diffusion. The present technology, together with MedeA's other state-of-the-art functionality such as the prediction of solubility

and the ability to simulate stress, offer an efficient alternative R&D approach where accurate experimental results are often difficult to obtain, in particular for materials containing grain boundaries, interfaces, and crack tips.

10:20 AM Break

10:40 AM Invited

First-Principles Prediction of Diffusion Coefficients in Non-Dilute, Multi-Component Solids: Anton Van der Ven¹; ¹University of Michigan

Alloys and complex oxides are often characterized by differing degrees of short and long-range order. This affects not only activation barriers, which vary with local order, but also leads to important correlations between successive hops of diffusing atoms. I will describe how diffusion coefficients can be calculated from first-principles in non-dilute, multi-component solids in which the role of short and long-range order is explicitly accounted for. The approach relies on the evaluation of Kubo-Green expressions, which provide the link between macroscopic diffusion coefficients and atomic trajectories sampled in kinetic Monte Carlo simulations. A first-principles description of the thermodynamics of short and long-range order in multi-component solids is achieved with the cluster expansion formalism. As examples, I will describe results from the application of this approach to alloys and oxides. For substitutional diffusion in alloys, special attention is devoted to the effect of deviations from the equilibrium vacancy concentration.

11:10 AM Invited

Multi-Scale Modelling of Interdiffusion and Stress: Marek Danielewski¹; Bartlomiej Wierzba¹; ¹AGH University of Science and Technology

The model of interdiffusion under the stress field is presented. We base on the Darken concept of the drift velocity and calorimetric equation of state. The methods necessary to obtain the numerical results at the different time and length scales will be presented. Particular emphasis will be given to the problem of the stress field and the mass diffusion time scales as well as non dimensialization of the particular problem studied. The presented coupling of the Darken method with mass, momentum and energy balances allows for quantitative, multi-scale analysis of the transport processes in non ideal solid solutions. We present the numerical simulation of the interdiffusion under the stress field in Fe-Ni-Cu alloys and compare them with experimental results. The methods based on the momentum balance and energy conservation will be compared.

11:40 AM

A Kinetic Discrete Model for Carbon Diffusion in TiC/Ti Nanometer-Scale Multilayers: B.S. Cao¹; Z.L. Wu¹; J. Gao¹; Z.P. Zhang¹; *M. Lei*¹; ¹Dalian University of Technology

The diffusion of carbon in the TiC/Ti nanometer-scale multilayers with modulation wavelengths of 5-100 nm and TiC and Ti sublayers thickness ratios of 2:3, 1:1 and 3:2 during the heating process at 800 K was calculated using a kinetic discrete model for interstitial diffusion. The kinetic discrete model has been formed based on the Martin's discrete model and the Hillert's sublattice model, in which the jump frequencies and diffusion coefficients of carbon strongly depend on the local concentration and pair interaction energy of carbon in the TiC/Ti multilayers. The diffusion process of carbon relative to the time scale was divided into three characteristic stages. The ratio of diffusion time in the stages for the TiC/Ti multilayers with same thickness ratio was found to be in square proportional to the ratio of the modulation wavelengths. The calculative diffusion of carbon in the TiC/Ti multilayers was in agreement with the experimental result.

12:00 PM

Simulation of Hydrogen-Induced Cracking in PZT Ferroelectric Ceramics Using a Phase Field Model: X. Guo¹; San-Qiang Shi²; L. Qiao³; ¹Hong Kong Polytechnic University and Beijing Institute of Technology; ²Hong Kong Polytechnic University; ³University of Science and Technology Beijing

A phase field model was developed to simulate hydrogen-induced cracking in lead zirconate ferroelectric ceramics (PZT-5). In this model, the evolution of hydrogen concentration around a crack was coupled with stress field analysis by solving both time-dependent diffusion equation and time-dependent Ginzburg-Landau strain field equation. Combined with a fracture criterion, we simulated crack initiation and propagation in PZT ceramics caused by hydrogen ingress from the environment. Numerical results showed that, as the concentration of hydrogen increased, the fracture toughness of PZT ceramics

Dynamic Behavior of Materials: Deformation I

Sponsored by: The Minerals, Metals and Materials Society, TMS Structural Materials Division, TMS/ASM: Mechanical Behavior of Materials Committee

Program Organizers: Marc Meyers, University of California; Ellen Cerreta, Los Alamos National Laboratory; George Gray, Los Alamos National Laboratory; Naresh Thadhani, Georgia Institute of Technology; Kenneth Vecchio, University of California

Monday AM	Room: Europe 3
February 26, 2007	Location: Dolphin Hotel

Session Chairs: Marc Meyers, University of California at San Diego; Eduardo Bringa, Lawrence Livermore National Laboratory

9:00 AM Invited

Atomistic Shock Simulations: From Single Crystals to Nanocrystals: *Eduardo Bringa*¹; J. Hawreliak¹; H. Lorenzana¹; ¹Lawrence Livermore National Laboratory

Atomistic simulations of shocks can explore loading times of ~0.5 ns and lengths of ~1 micron, making possible a nearly direct comparison with current laser-induced shock experiments. Some examples show that this comparison is indeed valid for shocks in fcc metals: (a) shock induced plasticity and melting of single crystals; (b) "long-time" evolution of plasticity and strength in defective single crystals; and (c) strength of shocked nanocrystals. Comparison to TEM of recovered samples and to dynamic X-ray diffraction experiments will be discussed. Work was performed under the auspices of DOE by the University of California, LLNL, under contract No.W-7405-Eng-48. References: K. Rosolankova et al., J. Phys. C., accepted, L. Koci et al., Phys. Rev. B 74, 012101 (2006), E. Bringa et al., Nature Materials, accepted, M. Shehadeh et al., Applied Phys. Lett., accepted, E. Bringa et al., Science, 309, 1838 (2005).

9:30 AM

First Principles Prediction of the Fe $\alpha - \epsilon$ Phase Transition Pathway: Donald Johnson¹; Emily Carter¹; ¹Princeton University

The pressure induced Fe α – ε phase transition is modeled with the solid state nudged-elastic-band (SSNEB) technique. The electronic structure, magnetic moments, atomic forces, and bulk cell stresses for each image are calculated with density functional theory. Spin-polarized calculations were performed using the generalized gradient approximation to the electron exchange-correlation functional. As the bulk structure deforms from body-centered-cubic to hexagonal-close-packed, the calculations predict an abrupt change from ferromagnetic to non-magnetic at the transition state. The change in magnetism accompanies large changes in the positions of Fe atoms in the bulk unit cell.

9:45 AM

Molecular Dynamics Simulation on Shock Compression of Monocrystalline Copper: Buyang Cao¹; Eduardo M. Bringa²; Marc Meyers¹; ¹University of California, San Diego; ²Lawrence Livermore National Laboratory

Molecular Dynamics simulation was used to model the effects of shock compression on [001] and [221] monocrystals. It shows that both the crystal orientation and shock pressure have a significant effect on defect substructure. The computational results are compared with experimental results. There is a discrepancy of 102-104 between the experimentally-obtained and MD calculated distance between stacking-fault packets. Two possible reasons are discussed: (a) the higher strain rate and smaller volume imparted by MD; (b) the possibility that most defects are annealed out and that observations by TEM reveal a structure completely different from the one extant during shock compression. An analysis of the nucleation of shear loops was carried out which shows that perfect dislocations are generated at the lower pressures and partial dislocations at the higher pressures. This analysis is in agreement with MD computations and with experimental observations.

Technical Program



10:00 AM

Energy Dissipation during High Rate Plastic Deformation of Zirconium: *Henry Padilla*¹; Cynthia Smith¹; John Lambros¹; Armand Beaudoin¹; Ian Robertson¹; ¹University of Illinois at Urbana/Champaign

The adiabatic compression of polycrystalline metals in the split-Hopkinson pressure bar (SHPB) is associated with a rise in temperature due to the dissipation of plastic work energy. Experiments using high speed infrared detectors and a SHPB are performed to measure the ratio of heat dissipation rate to plastic work rate in commercially pure zirconium. Deformed samples from a cross-rolled plate are examined using x-ray diffraction, electron back-scatter diffraction and TEM to provide indication of the underlying mechanisms of deformation. Analysis of the microstructure, texture and energy dissipation for orthogonal directions in the plate enable a more robust treatment of the thermomechanical coupling than stress-strain and thermal data alone.

10:15 AM Break

10:30 AM

John Rinehart Award: Marc Meyers¹; ¹University of California

The goals of the four TMS dynamic behavior of materials symposia are presented with highlights on the principal findings over the past fifteen years. The TMS symposia represent a continuation of the EXPLOMET conferences (1980-2000) that were, on their turn, initiated by the AIME symposia of 1961 and 1973. The metallurgical and materials aspects of deformation and failure have been the primary focus of these conferences. The need to recognize excellence in this field has led to the establishment of the John Rinehart Award. Previous recipients are: 1990 A. Deribas, Institute of Hydrodynamics, Russia; M. Wilkins, LLNL (ret), USA; 1995 R. Pruemmmer, Germany; A. Sawaoka, Japan; and 2000 D. Curran, SRI International (ret.), USA; D. Shockey SRI International, USA. The 2007 recipients of the John S. Rinehart Award will be announced.

10:40 AM Invited

Dislocation Mechanics for Shock-Induced Plasticity: *Ronald Armstrong*¹; Werner Arnold²; Frank Zerilli³; ¹University of Maryland; ²EADS; ³Naval Surface Warfare Center

The constitutive deformation behavior for plasticity of copper, Armco iron, and tantalum materials is described over a broad range of strain rates covering conventional compressive/tensile testing, through split-Hopkinson pressure bar (SHPB) test results, to shock-determined Hugoniot elastic limit (HEL) stresses and the follow-on shock-induced plastic strain rates. A pronounced transition occurs at the highest strain rates from plasticity being controlled by movement of the originally-resident dislocation density to the strain rate being controlled by dislocation generation at the shock front, as confirmed by connection with Swegle-Grady type shock pressure versus plastic strain rate measurements. Model description of the shock-induced plasticity results leads to prediction of a linear dependence of the effective shock stress on the logarithm of the plastic strain rate. The dependence for Armco iron and tantalum is attributed to the generation of deformation twins.

11:10 AM

Oblique Shocks and Plastic Wave Scattering Due to Interfaces in Crystalline Solids: Eric Loomis¹; Damian Swift¹; Hector Lorenzana²; James Mcnaney²; Pedro Peralta³; ¹Los Alamos National Laboratory; ²Lawrence Livermore National Laboratory; ³Arizona State University

Dynamic loading of interfaces in crystalline solids is a relatively unexplored aspect of dynamic material behavior. Differences in plastic versus hydrodynamic response to interfacial loading have important consequences such as shock front roughening in inertial confinement fusion (ICF) implosions or for high explosive applications. Laser-induced shock experiments have been performed on [100]/[111] oriented bicrystals of Nickel Aluminide with grain boundaries inclined with respect to the incoming shock front to understand plastic wave effects at the mesoscale. Line imaging velocity measurements show variations in elastic-plastic behavior from the bulk response of the [100] grain, to a transition across the grain boundary region, and finally into the bulk of the [111] grain. Continuum mechanics simulations that incorporate crystalline strength models have been performed to compare with these experimental results and with hydrodynamic calculations of oblique shocks impacting the boundary separating two materials of different shock impedance.



11:25 AM

The Influence of Stored Defects and Grain Size of the Dynamic Response of Copper in Shear: *Ellen Cerreta*¹; George Gray¹; Ian Frank¹; Carl Trujillo¹; David Korzekwa¹; Lisa Dougherty¹; ¹Los Alamos National Laboratory

Shear localization is often a dominant failure mechanism at high strain rates in ductile materials. While the constitutive behavior of copper has been established through a series of quasi-static and dynamic compression experiments over a range of temperatures, the influence of texture, microstructure, strain rate, and temperature on the development of the microstructure and substructure under high strain rate shear loading conditions remains poorly understood. The purpose of this study is to characterize the mechanical response and the deformation microstructure of as-annealed and cryogenically rolled copper under dynamic shear loading conditions and to understand the mechanisms for shear deformation with in copper as well as the role of stored defects due to cold rolling on the mechanical response.

11:40 AM

A Neutron Diffraction and Self-Consistent Modelling Study of Rate and Temperature Dependent Deformation of Textured Beryllium: *Donald Brown*¹; Bill Blumenthal¹; Bjorn Clausen¹; Carlos Tome¹; Ricardo Lebensohn¹; Sven Vogel¹; ¹Los Alamos National Laboratory

Strongly textured hot-rolled beryllium was compressed at high rates (5000/ sec) using a split-Hopkinson pressure bar and at quasi-static rates (10-3) using a conventional servo-hydraulic machine. Also, the temperature of deformation was varied from 77K to 675K. The evolution of the crystallographic texture was monitored with neutron diffraction and compared to polycrystalline plasticity models for the purpose of interpretation. A new version of the Visco-Plastic Self-Consistent (VPSC) model based on the 'affine' linearization at the grain level (instead of the 'tangent' approach of previous versions), was used in this work. The new model allows for considering the different microscopic rate-sensitivity exponents associated with slip and twinning activation. The macroscopic response of the material and the active deformation mechanisms were found to be highly dependent on the temperature and strain rate. Specifically, deformation twinning is inactive when loaded at quasi-static rates and high temperature.

11:55 AM

Dislocation Pattering and Dynamic Fracture in Shocked Ta and U-6wt%Nb: *Luke Hsiung*¹; Geoffrey Campbell¹; Gregory Archbold¹; ¹Lawrence Livermore National Laboratory

The correlation between dynamic fracture and dislocation patterning within Ta and U-6wt%Nb has been investigated. The main purpose of this study is to characterize shock-induced dislocation substructures and structural instability such as deformation twinning and phase transformations within shockrecovered fragments in order to depict the dynamic reactions and underlying mechanisms for the dynamic fracture and fragmentation of metals. The results reveal that the mechanisms of dynamic fracture are intimately related to the reactions of dislocation patterning, which in turn are governed by the mobility of dislocations under dynamic-pressure conditions. Deformation twinning phenomenon becomes significantly enhanced in metals containing highdensity or low-mobility dislocation structure. The ductility embrittlement of U-6Nb under dynamic-pressure conditions are found to mainly cause by the structural instability and the mutual collision of twin bands, which lead to the enhancement of internal cracking and cavitation.

12:10 PM

Dynamic Response of Natural and Synthetic Scheelite Single Crystals: *Zaretsky Eugene*¹; Mogilevsky Pavel²; ¹Ben-Gurion University of the Negev; ²UES Inc.

Single crystals of natural and synthetic scheelite (CaWO4) were studied in VISAR-monitored planar impact experiments up to pressure of 25 GPa. Several impact experiments with soft recovery of the shocked samples for further TEM investigation were also performed. Although the waveforms recorded in the planar impact experiments with natural and synthetic crystals differ strongly it is shown that in both cases the strength of the crystal is controlled by the dislocations of <110>{112} glide system. This is confirmed by TEM studies of soft recovered samples. Since under static compression up to 11 GPa scheelite transforms into fergusonite structure (second order transition) a special attention was paid to the presence of transition signature in the recorded velocity profiles. The striking observation of the study is the presence of such signatures in the waveforms obtained from natural crystals and the absence of those in the velocity profiles of synthetic crystals.

12:25 PM

Dynamics of Material Response to High Intensity Ultrafast Laser Ablation: *Steven Yalisove*¹; Tresa Pollock¹; Shewei Ma¹; Joel McDonald¹; ¹University of Michigan

Ultrafast pump-probe imaging is a very useful tool to study the response of a material to high intensity ultrafast laser irradiation. We will show movies with 150 femtosecond snapshots, taken every 50 picoseconds, which reveal the evolution of the ablation process. Two geometries are employed to measure the velocity of ejected materials, normal incidence (Newton's rings analysis) and parallel to the surface (to measure air shock expansion driven by ejected material). Direct measurement of ejected material velocities, along with measurements of ejected material volume, can be used to calculate the initial pressure-time distribution on the remaining material. Our studies have concentrated on Si, Si with thermally grown oxides, Ni, and Ni-based superalloys. Cross section TEM showing the dislocation injection below the irradiated zone will be presented for one of these systems and discussed in relation to the initial pressure distribution obtained from pump probe imaging results.

Electrode Technology Symposium (formerly Carbon Technology): Cathode Part I: Cathode Wear and Construction

Sponsored by: The Minerals, Metals and Materials Society, TMS Light Metals Division, TMS: Aluminum Committee *Program Organizers:* John Johnson, RUSAL Engineering and Technological Center LLC; Morten Sorlie, Elkem Aluminium ANS

Monday AM	Room: Southern 3
February 26, 2007	Location: Dolphin Hotel

Session Chair: Thomas Alcorn, Noranda Aluminum Inc

9:00 AM Introductory Comments

9:05 AM

Laboratory Test Methods for Determining the Cathode Wear Mechanism in Aluminium Cells: *Egil Skybakmoen*¹; Asbjørn Solheim¹; Sverre Rolseth¹; Henrik Gudbrandsen¹; Arne P. Ratvik¹; ¹SINTEF

The service life of aluminium Hall-Heroult cells is limited by carbon cathode wear. The true wear mechanism is still to be proven, although many laboratory attempts have been made to obtain insight into the problem. Based on different methods used in our laboratory, i.e. methods where carbon is exposed to metal or bath during electrolysis, as well as using inert anodes, our assumption is that the formation and dissolution of aluminium carbide from the cathode are central in the reaction mechanism. We have tried to verify this mechanism by measuring the cathode wear itself, by analysing carbide in the metal and the electrolyte, as well as oxidizing the dissolved carbide in the melt by using an inert anode and analyzing the gas composition. Four different laboratory test methods will be discussed, as well as reference to earlier published work on this topic.

9:30 AM

Wear of Carbon Cathodes in Cryolite-Alumina Melts: Kristin Vasshaug¹; Trygve Foosnæs¹; Geir Martin Haarberg¹; Arne Petter Ratvik²; Egil Skybakmoen²; ¹Department of Materials Science and Engineering, Norwegian University of Science and Technology; ²SINTEF Materials and Chemistry

Wear of carbon cathode blocks is one of the main factors limiting the lifetime of aluminium electrolysis cells. A laboratory test cell set-up has been designed to investigate the wear mechanism. A homogeneous graphite material was exposed to three different bath compositions (CR = 2.25, 1.80 and 1.50) with various rotation speeds of the cathode, cathodic current density and time of electrolysis. The wear was strongly influenced by bath acidity, higher wear was observed at CR = 1.8, probably due to higher carbide solubility in the bath. The wear also increased with current density at CR = 1.8, indicating an electrochemical wear mechanism. The cathode samples





have been investigated after the tests using optical microscopy and scanning electron microscope. Aluminium carbide was only found at the surface of the cathode area protected by a sintered alumina lining, while on the areas directly exposed to the electrolyte no carbide was detected.

9:55 AM

Experimental Comparison of Cathode Rodding Practices: Lucio Caruso¹; Ketil Rye²; *Morten Sorlie*²; ¹Alcoa Trasformazioni Srl; ²Elkem Aluminium ANS

Interference calculations using thermal expansion coefficients over the temperature range of interest for collector bar, cast iron and different types of bottom blocks, indicate that poor preheating prior to rodding may seriously damage blocks during cathode preheat and startup. In spite of this there are still plants using no or poor block preheating and rodding practices, e.g. section-wise casting of the bar where heat from each cast section slowly dissipates and "preheats" the neighboring section. Experimental verification of interference calculations for different bottom block rodding situations, included mechanical testing after simulated pot preheating and startup, is described and discussed.

10:20 AM

Property Change of Dry Barrier Mixes Used in a Cathode of Aluminium Reduction Cells: Alexander Proshkin¹; *Peter Polyakov*²; ¹Engineering and Technology Center, RUSAL; ²LLC Science and Technology Center "Light Metals"

Problems concerning dry barrier mix (DBM) behavior (taking into account autopsy findings) in aluminum reduction cell are discussed. Changes in properties due to attack by aggressive components are analyzed. Reaction mechanisms are proposed. Penetration depth and composition changes in industrial and bench-scale cells are presented. It is shown that DBM samples taken from a 9 months old cell have a three-layered structure. Chemical changes of the initial composition across these layers are determined. Gasphase reactions in barrier mix with formation of intermetallic compound have been established. The descriptions of possible reaction mechanisms are offered.

10:45 AM Break

11:05 AM

Anti-Corrosion Mechanism of SiC-Si3N4 Sidelining Materials in Aluminium Electrolyte: *Zhaowen Wang*¹; Xianwei Hu¹; Zhongning Shi¹; Bingliang Gao¹; Guimin Lu¹; Jianzhong Cui¹; Zhuxian Qiu¹; ¹Northeastern University

Corrosion mechanism of SiC-Si3N4 sideling materials for aluminium electrolysis in electrolytic process has been studied. The oxidation resistance of the materials at different temperatures has been obtained after tests in air, CO2 and O2 atmosphere, respectively. In environments simulating the industrial electrolysis conditions, dynamic corrosion of the materials has been performed by inletting CO2 or O2 to the electrolyte. SEM and XRD results show that the materials were significantly corroded more when oxidative gas was inlet to the electrolyte. Because SiC-Si3N4 was oxidized to SiO2 and then SiO2 dissolved to the electrolyte. It has been thought that in order to avoid sideling degradation of industrial aluminum electrolysis cell, there must be certain space between the anode and the side wall, and entire ledge on the side wall.

11:30 AM

Treatment of Spent-Potlining for Recovery of Fluoride Values: *Diego Fernandez Lisbona*¹; Karen Steel¹; ¹School of Chemical, Environmental and Mining Engineering, University of Nottingham

The leachability of NaF, CaF₂ and Na₃AlF₆ from spent pot-lining has been studied with the view to dissolve, manipulate solution equilibria, and precipitate fluoride in a form that can be recycled. Leaching results have been combined with theoretical stability constant information to understand solution equilibria and identify novel ways that it can be manipulated to produce AlF₃ and/or CaF₂, to yield a process with the criteria of minimal process reagents, number of steps, energy and waste. While AlF₃ is the preferred form for fluoride, its production in acidic media is difficult owing mainly to the unavoidably high concentrations of Na⁺. So far, we have found a chemical sequence for recovery of all fluoride as NaAlF₄. This will be presented along with other sequences being pursued. Following removal of fluoride, high degrees of separation (>95%) of the remaining refractory compounds from the graphite has proved possible using a density separation technique.

11:55 AM

Tests of Various Graphitic Cathode Blocks Materials for 300 kA Aluminum Reduction Cells: *Zhongning Shi*¹; Bijun Ren²; Junli Xu¹; Zhaowen Wang¹; Zhuxian Qiu¹; ¹Northeastern University; ²Yichuan Electric-Power and Aluminium Group

To find an excellent candidate cathode materials for decreasing the cathode voltage drops, forming good side-ledge and prolonging the cell lift time, various graphite content, such as 30%, 40%,75% and 100% graphitic cathode blocks from deferent manufacturers were tested for the 300 kA aluminum reduction cells bottom relining. The properties of cathode voltage drops, electric resistance were detected after the cell startup. The obtained data showed that the electronic resistance of cathode will increase with the decreasing of graphite content in the blocks except for the full graphitized cathode. Some semi-graphitic cathodes could attain a value of voltage drops under 300mV, which suggested that this kind of cathode blocks might be the best one for saving energy and prolong the cell lift time.

12:20 PM

Research on Crushing Character of Spent Cathode: Xiping Chen¹; Wangxing Li¹; ¹Chalco

During our industrial processing of spent potlining, crushers, especially crushing mills can not work continuously because of feed stock jam. The jam is commonly caused by sticking and sliding of spent cathode. The processing efficiency of the pilot plant is low. Generally speaking, graphite and sodium in spent cathode make spent cathode sticky, slippage and difficult to crush. The crushing character of spent cathode is studied in this paper. Influences of graphite and sodium in spent cathode on its crushing character are respectively discussed. The higher graphite or sodium content is, the more difficult to crush spent cathode. The result provides a reference for us to choose crushers for industrial scale spent potlining detoxifying plants.

Frontiers in Solidification Science: Nucleation and Crystal Structure

Sponsored by: The Minerals, Metals and Materials Society, TMS Electronic, Magnetic, and Photonic Materials Division, TMS Materials Processing and Manufacturing Division, TMS: Chemistry and Physics of Materials Committee, TMS: Solidification Committee

Program Organizers: Jeffrey Hoyt, Sandia National Laboratories; Mathis Plapp, Ecole Polytechnique; Gabriel Faivre, CNRS; Shan Liu, Iowa State University

Monday AM Room: Northern A3 February 26, 2007 Location: Dolphin Hotel

Session Chair: To Be Announced

9:00 AM Invited

Phase Field Modeling of Heterogeneous Nucleation: James Warren¹; David Saylor²; Laszlo Granasy³; Tamas Pusztai³; ¹National Institute of Standards and Technology; ²Food and Drug Administration; ³Research Institute for Solid State Physics and Optics

Heterogeneous nucleation is understood to be the dominant mechanisms initiating crystal growth of undercooled melts. Recent developments in phase field modeling of crystal growth have now provided both a new perspective on the physics of heterogeneous nucleation, as well as an extremely efficient method of implementing the phenomenon without any interface tracking or the inclusion of internal boundaries. In particular, we discuss various choices for the effective boundary condition at the liquid-heterogeneity boundary and determine the properties of the solid critical nucleus, including the free energy of formation and the contact angle as a function of undercooling. We find for particular choices of boundary conditions, we may realize an analog of the classical spherical cap model or decidely non-classical behavior. Both the mathematics of deriving the model and simulations in one, two and three dimensions will be presented and discussed.



9:30 AM Invited

Bulk Liquid Undercooling and Nucleation Kinetics Analysis: John Perepezko¹; Gerhard Wilde²; Charuayporn Santhaweesuk¹; ¹University of Wisconsin; ²University of Münster

In the examination of undercooled liquid solidification fluxing treatments with a molten glass slag are commonly used to promote deep liquid undercooling or even bulk glass formation. There have been suggestions of flux induced "nucleant removal" or "surface site deactivation", but the underlying mechanisms have remained uncertain. As a model system, the undercooling response of pure Au encased in Pyrex glass was studied systematically. Nucleation kinetics analyses of statistically significant sets of measurements reveal the presence of a new mechanism based on gas-solid interactions that triggers nucleation, through a nucleant precipitation as the first step of the interaction. A new model is proposed for a nucleant refining process, that accounts for the undercooling saturation in a self-consistent manner. The application of nucleant refining has been extended to analyze the undercooling behavior in other materials such as Cu based systems.

10:00 AM Invited

Phase Field Modeling of Polycrystalline Freezing in Two and Three Dimensions: New Developments: *Tamás Pusztai*¹; László Gránásy¹; Jack Douglas²; James Warren²; ¹Research Institute for Solid State Physics and Optics of the Hungarian Academy of Sciences; ²National Institute of Standards and Technology

Recent advances made in the application of phase field theory for crystal nucleation and polycrystalline growth is reviewed. The fact that similar polycrystalline patterns are observed in systems of different molecular nature suggests that a minimal model based on coarse-grained fields might be appropriate. In our models crystallographic orientation is represented by either a single coarse-grained orientation field in 2D, or by quaternion fields in 3D, allowing us to incorporate various nucleation modes including heterogeneous and homogeneous mechanisms for the nucleation of growth centers and for the formation of new grains at the perimeter. We address various complex polycrystalline morphologies in 2D and 3D such as polydendritic structures, particulate induced disorder in dendrites, and various spherulitic forms, and solidification in confined space. We demonstrate that a broad variety of polycrystalline structures can be recovered by changing only a few model parameters such as crystal anisotropy, branching angle, and orientational mobility.

10:30 AM

Phase-Field Simulation of Nucleation and Growth in Mg-Alloys: Janin Eiken¹; Ingo Steinbach¹; ¹RWTH-Aachen

A statistical approach to nucleation, using a temperature distribution function for nucleation on heterogeneous nucleation sites, is combined with phase field simulation of equiaxed crystal growth in a Mg alloy controlled by solute diffusion. The temperature evolution of the system is calculated from a heat balance between release of latent heat and external heat extraction. Thus the effect of inoculation by adding grain refiners, the effect of alloy composition on growth and release of latent heat and finally the effect of external cooling on the final grain density can be studied. The presentation focuses on the interrelation between nucleation density and grain morphology, that can be used to identify the leading mechanism of grain refinement.

10:50 AM Break

11:00 AM Invited

Orientation Selection in Dendritic Evolution: *Alain Karma*¹; ¹Northeastern University

This talk will present an overview of phase-field and experimental studies of orientation selection in dendritic evolution for cubic and hexagonal symmetries in the context of new knowledge of crystalline anisotropy derived from atomistic simulations in recent years. A unified theoretical picture emerges from these studies that distinguishes three different orientation selection mechanisms which lead to continuous or discontinuous variations of growth misorientations off crystal axes depending on anisotropy parameters. Kinetic effects at large growth rates are also discussed. This work was supported by the US Department of Energy.

11:30 AM Invited

Multiscale Methods and Phase Field Crystal Modeling of Microstructure: Badri Athreya¹; Pak Yuen Chan¹; Zhi Huang¹; *Jonathan Dantzig¹*; Nigel Goldenfeld¹; ¹University of Illinois

The phase field crystal (PFC) model, recently developed by Elder, Grant and co-workers, provides a means for modeling microstructure development from the atomic scale. Unlike other atomic scale techniques, the PFC model operates at diffusive time scales. This opens up for analysis a wide variety of important problems in materials science. We present a mathematical reformulation of the PFC model which enables us to solve microscale problems with atomic scale resolution, using a combination of renormalization group analysis and adaptive mesh refinement. The presentation will include several applications, including equiaxed solidification of a pure material in an undercooled melt, epitaxial growth of a strained layer, and some problems involving binary alloys.

12:00 PM Invited

Intragranular Variations of Crystallographic Orientation in Hot-Dip Al-Zn Coatings: *Alain Jacot*¹; Christoph Niederberger¹; ¹EPFL

Important variations of the crystallographic orientation within a same grain are commonly observed in certain solidification or crystal growth processes such as hot-dip galvanization of steel, thin films deposited by Epitaxial Lateral Overgrowth and directional solidification of single-crystal superalloy turbine blades. Different mechanisms have been suggested for the formation of intragranular misorientations. Thermal stresses building up during cooling as a result of differential thermal contraction could generate non-uniform plastic deformation. Microsegregation during solidification can lead to systematic solute gradients and variations of the lattice parameter. A third mechanism is plastic deformation of the dendritic network during growth owing to solidification shrinkage and capillary forces at the free surface. In an attempt to evidence the dominating mechanism, a detailed investigation has been carried out on hot-dip Al-Zn coatings. The different mechanisms are reviewed based on EBSD characterization, profilometry, chemistry analysis and phase field simulation of the dendritic morphology and solute redistribution.

General Abstracts: Electronic, Magnetic, and Photonic Materials Division: GaN and Interconnects

Sponsored by: The Minerals, Metals and Materials Society, TMS Electronic, Magnetic, and Photonic Materials Division, TMS: Alloy Phases Committee, TMS: Biomaterials Committee, TMS: Chemistry and Physics of Materials Committee, TMS: Electronic Materials Committee, TMS: Electronic Packaging and Interconnection Materials Committee, TMS: Nanomaterials Committee, TMS: Superconducting and Magnetic Materials Committee, TMS: Thin Films and Interfaces Committee

Program Organizers: Long Qing Chen, Pennsylvania State University; Sung Kang, IBM Corporation

Monday AM	Room: Oceanic 7
February 26, 2007	Location: Dolphin Hotel

Session Chair: Yu Wang, Virginia Tech

9:00 AM

Characterization of GaN Layers Grown on Metallic TiN Buffer Layers: Sangjin Lee¹; Kazuhiro Ito¹; Yu Uchida¹; Susumu Tsukimoto¹; Yuhei Ikemoto²; Koji Hirata²; Naoki Shibata²; Masanori Murakami¹; ¹Kyoto University; ²Toyoda Gosei

High density of threading dislocations was observed in the GaN layer grown on the AlN buffer layers. This believes to be a bad influence on the light emitting efficiency of the diodes. We recently reported that epitaxial, continuous, flat GaN layers were successfully grown on a metallic TiN buffer layer. In addition to the discovery, the density of threading dislocations was found to be reduced significantly in the GaN layers grown on the TiN buffer layers compared with that on the AlN buffer layers, although the GaN layer grown on the TiN buffer layers contains a few domains with opposite lattice polarity and a few horizontal dislocations was also investigated and will discuss the microstructure difference in terms of difference in the GaN growth mechanism



between on the TiN buffer layers and on the AlN buffer layers.

9:20 AM

Semi-Empirical Interatomic Potentials for Ga-N and In-N Systems: Euro Cheol Do¹; Byeong-Joo Lee¹; ¹POSTECH

New semi-empirical interatomic potentials for Ga-N and In-N systems have been developed based on the 2NN MEAM formalism, using the already developed interatomic potentials for N and In by the present authors in the present study and Ga by Baskes et al. The potential describes various physical properties (such as cohesive energy, lattice parameter, elastic constants, structural stability, etc.) of pure elements and nitrides (Zincblende and Wurtzite type of GaN and InN), in good agreement with relevant experimental and high-level calculation information. The potential can also describe reasonably well the bond length as a function of composition in the Zincblende (Ga,In)N, showing the possibility of application to the Ga-In-N ternary system. Because the potential formalism is exactly the same as other already developed MEAM potentials for bcc, fcc and hcp elements, it can be easily extended to multicomponent systems involving a wide range of elements.

9:40 AM

Epitaxial Growth of GaN Layers on Metallic TiN Buffer Layers: Kazuhiro Ito¹; Yu Uchida¹; Sangjin Lee¹; Susumu Tsukimoto¹; Yuhei Ikemoto²; Koji Hirata²; Naoki Shibata²; Masanori Murakami¹; ¹Kyoto University; ²Toyoda Gosei

GaN-based semiconductors have been used as the key elements for blue light-emitting diodes and non-conductive sapphires were extensively used as substrates for GaN layers. Until now, the best buffer layer discovered was an AlN layer to compensate for lattice mismatch of about 15% between GaN and sapphire. However, the AlN layer is an insulator, conductive buffer layers are desirable to increase the light emitting efficiency of the diodes. We recently found that epitaxial, continuous, flat GaN layers were successfully grown on a metallic TiN buffer layer. It was concluded that nitrogen enriched TiN buffer layers with the upper limit of the nitrogen content of TiN would reduce the TiN/GaN interfacial energy. Reduction of the TiN layer thickness and substrate temperature during deposition would suppress TiN grain growth during the nitrogen enrichment. These lead to increase GaN nucleation on the TiN buffer layers, and this is essential for smooth GaN growth.

10:00 AM

Formation of Controlled Copper Current Paths in Alumina Nano-Oxide Layers for GMR Spin Valves by Rapid Thermal Processing of Al-Cu Sputtered Films: Zeenath Tadisina¹; Rajeshchandra Thunuguntla¹; Subhadra Gupta¹; Robb Morris¹; Gregory Thompson¹; Jian Zhong¹; Raghvendra Pandey¹; ¹University of Alabama

A novel technique for enhancing the giant magnetoresistive (GMR) effect in perpendicular spin valves is to confine the current-carrying paths in the stack by sputter depositing an Al-Cu alloy film and then selectively oxidizing the aluminum. This forms an alumina nano-oxide layer (NOL), with the precipitates of Cu acting as the confined current paths. One of the drawbacks of this technique is that the Cu precipitates are not uniform in size or distribution, and often do not form a complete path through the oxide layer. We have used various sequences of rapid thermal anneals and quenches to control the size and distribution of the Cu precipitates in the sputtered alloy films, which were subsequently oxidized selectively to form the alumina nano-oxide layers. We will present conductive AFM and TEM studies of these Cu paths in the NOL, as well as electrical and magnetic measurements for representative devices.

10:20 AM

Properties of Ge/HfN_x as a Diffusion Barrier for Cu Metallization: Seemant Rawal¹; Lii-Cherng "Daniel" Leu¹; David Norton¹; KeeChan Kim¹; Tim Anderson¹; Lisa McElwee-White¹; ¹University of Florida

The properties of Ge/HfN_x have been investigated as a novel diffusion barrier for Cu metallization. The Ge/HfN_x bilayer was grown on p-Si(001) substrates by reactive sputtering, followed by *in-situ* deposition of Cu. Films annealed individually in Ar atmosphere at different temperatures for varying times were characterized for evidence of Cu transport through the barrier bilayer to the Si substrate. The HfN_x (7nm) layer alone failed at an anneal temperature as low as 400°C for 1 hr, while adding the Ge layer significantly improved the performance. Ge (25nm)/HfN_x (7 nm) stacks were effective for anneals at 600°C for 1 hr and 500°C for 3 hr. The annealed structures were characterized by X-ray diffraction, Atomic force microscopy, High-resolution transmission electron microscopy and Energy dispersive spectroscopy to investigate relevant diffusion barrier properties. The results indicate superior diffusion barrier properties of Ge/HfN_x for Cu metallization on Si compared to HfN_x (7nm).

Technical Program

10:40 AM Break

11:00 AM

Thermal Fatigue Characterization of Commonly-Used 63Sn37Pb Solder Joints in Electronic Assemblies: Arun Iyer¹; *Michael Oja*¹; Robert Tryon¹; ¹VEXTEC Corporation

This paper summarizes the efforts to simulate the thermal fatigue characteristics of commonly used tin lead (63Sn37Pb) solder joints in electronic assemblies. The complex topography of the solder joint was generated using energy minimization concepts. A complete geometry representative of a 63Sn37Pb soldered electronic assembly detailing the chip-to-pad interconnect was developed using the finite element software ANSYS. Microscopic measurements and material properties including the components' thermal properties were input into the FEA. The FEA-predicted stresses along with the geometry were used in VEXTEC's VPS-MICRO (probabilistic microstructural fatigue model) to predict the thermal fatigue of the interconnect joint. The influence in the electronic assembly reliability with the application of two different conformal coats was investigated. The reliability of the electronic assembly was observed to be greatly improved by the use of conformal coats. The probabilistic model was then used to predict the solder joint thermal fatigue life characteristics at varying temperatures.

11:20 AM

Characterization of Wire Bonds Subjected to Ultrasonic Welding and Thermal Cycling: Anil Saigal¹; Peterson Silva¹; *Robert Greif*¹; Michael Zimmerman¹; ¹Tufts University

LDMOS packages require greater thermal performance, excellent dimensional stability, and package flatness. For RF and microwave applications, they provide temperature stability up to 500°C and direct Cu flange assembly for greater thermal conductivity and lower junction temperatures. Ultrasonic welding is used to attach liquid crystal polymer (LCP) lids to LCP housings. This study investigates the effect of ultrasonic welding and thermal cycling on the strength and reliability of gold wire bonds inside the LDMOS package. The strength of as-welded wire bonds is between 16-20 gf. Ultrasonic welding reduces the average strength to 13 gf while increasing the spread. Thermal cycling reduces the average strength further to 11 gf. In all cases, the failure typically occurs at the wire heel on the silicon die and the bond strength still satisfies the minimum post-seal bond strength of 5.5 gf for 2 mil diameter gold wires as per Military Standard 883F.

11:40 AM

The Influence of Heat-Treatment Atmosphere on Interfacial Adhesion Strength of Cu/Cr/Polyimide Films: *Takeo Miyamura*¹; Junichi Koike¹; ¹Tohoku University

Flexibility of electronic circuit board is essential for recent miniaturized and variously-shaped electronic devices. Organic flexible films are used as substrate in flexible printed circuits (FPC) which suffers from poor interfacial adhesion strength between polymer substrate and metallic films. Previous works reported that adhesion strength decreases after heat treatment in humid atmosphere. However detailed influences of moisture and other factors on adhesion strength are not understood. We investigated the influence of heat treatment and then atmosphere on adhesion strength degradation. The samples were Cu/Cr/Polyimide multilayer films. Heat treatment was performed under moisture containing atmosphere with various levels of humidity. Adhesion strength was measured and XPS analysis was carried out. Adhesion degradation after heat treatment was induced by metal oxidation near the interface. Oxidation was enhanced by moisture diffusion in polyimide. Additionally the structural degradation of polyimide itself contributed adhesion degradation.

12:00 PM

Morphological Changes in CIGS2 upon Thickness Reduction of Absorber Layer: Parag Vasekar¹; Neelkanth Dhere¹; ¹Florida Solar Energy Center, University of Central Florida

Chalcopyrites are important contenders among thin film solar cells. Copper-Indium-Gallium Disulfide (CIGS2) is a chalcopyrite material with a near-optimum band gap of 1.5 eV. The availability and cost of indium can be



a limiting factor. The required amounts of metals can be lowered by using thinner films. There is need of a systematic matrix of experimentatiom to study the morphological changes with gradual thickness reduction of absorber. Initially small size grains are formed during the film growth. With continuing growth to large thicknesses, more favorably oriented grains coalesce to form compactly packed large-grain morphology. Solar cell performance in smaller grain chalcopyrite absorber deteriorates due to larger fraction of grain boundaries. It is essential to hasten the grain growth through coalescence to retain quality even in thinner films. This work presents an assessment of the efficacy of various techniques in improving morphology and thus the device performance at lower thicknesses.

12:20 PM

Lead and Lead Free Bulk Solder Material Characterization and High Rate Tensile Test: *Liping Zhu*¹; Wade Hezeltine¹; Todd Embree¹; Raiyo Aspandiar¹; George Hsieh¹; Rick Williams¹; ¹Intel Corporation

In this paper, two types of solder materials, Eutectic SnPb and lead free, SAC405, have been characterized and tested at different loading rates and temperatures using two types of specimen sizes, ASTM standard and miniature one. Microstructural matching analysis is first conducted to ensure that test specimens can represent real BGA solder joint in microstructure level in terms of micro hardness and grain size values. The data show that small size of specimens can be matched well in both micro hardness and grain size. As suggested, aging treatment has been used on SnPb type of specimen during their fabrications. The tensile tests are then conducted at different strain rates from 10-2 1/s to 102 1/s and two temperatures at 23C and 100C. The stress strain curves are generated for each strain rate, which can be used to develop rate dependent constitutive model for solder material including damage model.

General Abstracts: Extraction and Processing: Hydrometallurgy, Wastewater Treatment

Sponsored by: The Minerals, Metals and Materials Society, TMS Extraction and Processing Division, TMS: Aqueous Processing Committee, TMS: Materials Characterization Committee, TMS: Pyrometallurgy Committee *Program Organizers:* Boyd Davis, Kingston Process Metallurgy Inc; Michael Free, University of Utah

Monday AM	Room: Northern E1
February 26, 2007	Location: Dolphin Hotel

Session Chair: Michael Free, University of Utah

9:00 AM

Cobalt Removal from Waste Water by Use of Supported Liquid Membranes: *Kim Verbeken*¹; Marc Verhaege¹; Bruno Vanheule²; Luc Pinoy²; ¹University of Gent; ²KaHo St-Lieven

Supported liquid membranes (SLM) are an alternative technique to selectively remove metal ions from waste water. This technique has been the subject of a considerable amount of research, mainly due to several advantages compared to other techniques. The stability of the system is an important parameter when upscaling batch experiments to an installation applicable on an industrial level. In the present work, the removal of Co(II) from a synthetic CoSO4 solution is studied on lab and pilot scale. By performing batch experiments, the optimal settings, i.e. the composition of the organic phase, the pH of the feed, the type and concentration of the stripping agent were determined. SLM experiments showed a significant decrease of the mass transfer through the membrane both on lab and n pilot scale for both HCl and H2SO4 as stripping agent. The poor stability throughout the experiments proved to be a major drawback during upscaling.

9:25 AM

Separation of Ni/Fe from Industrial Waste Acid by Solvent Extraction Technique Using D2EHPA: Jae-chun Lee¹; *Manis Kumar Jha*¹; Jinki Jeong¹; Min Seuk Kim¹; Kyoungkeun Yoo¹; ¹Korea Institute of Geoscience and Minerals Resources

In order to conserve the resources and control pollution, a process has been developed for the recovery of metallic values from the industrial waste acid.

In this work two solutions obtained after the recovery of acid from waste acid by diffusion dialysis were used. The solutions analysing in g/L 23.5 Ni, 47 Fe, 0.11 Zn, 0.90 M H2SO4 (solution-I) and 12 Ni, 32.8 Fe, 0.42 Zn, 1.23 M H2SO4 (solution-II) respectively. In order to remove iron from the solutions, stoichiometric amount of H2O2 was added to oxidise ferrous ion to ferric state. The organic solvent D2EHPA was used for the selective extraction of ferric ion in multi-stage cross current steps. The McCabe Thiele diagram was also plotted to obtain the stage requirement for iron removal in continuous mode. The 99.6% and 99.85% Fe has been removed from solutions I and II respectively and pure nickel sulphate solutions obtained.

9:50 AM

Evaluation of the Elution of (Cr3+, Zn2+, Ni2+, Cu2+) from Wastewater Using Purolite C-150 and Dowex Marathon C Ion Exchange Resins: *Josiane Riani*¹; Jorge Alberto Tenório¹; Adriana Gómez¹; ¹Universidade de São Paulo

The removal of the (Cr3+, Zn2+, Ni2+, Cu2+) ion from wastewater with the purolite C-150 and dowex marathon c ion exchange resins was studied; and the performance of this resin was compared. The effect of temperature on the elution of ions metallics was investigated. The removal and elution experiments had been lead in a micron-column, in the temperatures of 25° C- 50° C. The elution of ions metallic was with 1 M H2SO4. In all the experiments the concentration of metals in solution will be determined through the technique of spectroscopy of atomic absorption (AA). Dowex marathon C shows a remarkable increase in desorption (elution) capacity for Zn (II), Ni (II) and Cu (II) if compared with the resin purolite C-150. The elution of chromium in both the cases is less fast, proving a bigger affinity of resins for chromium if compared with other ions in question.

10:15 AM

Hydrometallurgical Synthesis, Characterization and Stability of Ca-Fe-AsO4 Compounds: Levente Becze¹; George P. Demopoulos¹; ¹McGill University

The disposal of arsenic from metallurgical process liquors continues to be a subject of great importance from an environmental point of view. Currently, the most widely used method of arsenic removal from process effluents involves co-precipitation with iron(III) sulphate and simultaneous lime neutralization. Alternatively, in the case of arsenic-rich and iron-deficient solutions fixation of arsenic via scorodite precipitation may be adopted. Placement of the iron(III)-arsenate co-precipitate or scorodite solids in tailing ponds with gypsum saturated waters opens the possibility of formation of Ca-Fe-AsO4 phases the solubility of which may determine the long term viability of the current arsenic disposal practice. An extensive study of the Fe-Ca-AsO4 ternary system involving synthesis, characterization and solubility testing of solids precipitated from solutions containing various ratios of Fe(III), Ca(II) and As(V) was undertaken. Among the phases synthesized are yukonite and arseniosiderite which are found in nature as minerals.

10:40 AM Break

11:00 AM

Immobilization Mechanism of Chromium in Aqueous Solution with Ettringite: *Ji-Whan Ahn*¹; Kwang-Suk You¹; Dong Han¹; ¹Korea Institute of Geoscience

Ettringite(Ca6[Al(OH)6]2(SO4)3•26H2O), which is hydration product of calcium aluminate minerals, the greatest ability to immobilize heavy metallic ion through substitution mechanism. Aqueous solution containing calcium hydroxide, aluminum sulfate, CrCl3(trivalent chromium) was subjected to irradiate by ultrasonic under atmospheric pressure to investigate its effect on synthesis of calcium aluminate material. After collecting synthesized powders, we analyzed them with XRD, FT-IR, ICP, SEM. As a result of checked XRD peak, face(100) peak tend to shift onto the left as Cr input. We observed that Cr3+ ion in aqueous solution decreased almost 99.7%, but Al3+ ion increased. and we observed that Cr-ettringite was changed morphology by Cr input. We confirmed that Ettringite possesses the ability to behave as a host for metallic pollutants to immobilize cationic waste ions through substitution.





11:25 AM

Removal Mechanism of Orange II Azo Dye by Electrocoagulation: *Jewel Gomes*¹; David Cocke¹; Mohammad Mollah²; Hector Moreno C.¹; Eric Peterson¹; Donald Mencer³; ¹Lamar University; ²University of Dhaka; ³Wilkes University

Textile and other industrial dyes constitute an increasing environmental danger due to the large degree of aromatics present in dye molecules and their biological persistence. Conventional biological and physical methods are ineffective for their discoloration, degradation, or removal. Electrocoagulation (EC), an electrochemical technique, has been used in recent times for the most effective removal of orange II azo dye from wastewaters using iron, aluminum or their combination as electrodes. However, the mechanism of the removal process is yet to be delineated. In this paper, we propose an experimentally based removal mechanism of orange II azo dye in an electrocoagulation reactor. EC-by-products have also been investigated employing FT-IR, thermal analysis and x-ray diffraction techniques.

11:50 AM

Electrochemical Reactions for Electrocoagulation Using Aluminum Electrodes: *Hector Moreno*¹; David Cocke¹; Jewel Gomes¹; Paul Morkovsky²; Jose Parga³; Eric Peterson¹; Donald Mencer⁴; ¹Lamar University; ²Kaselco; ³Instituto Tecnologico de Saltillo; ⁴Wilkes University

Electrocoagulation as a water and wastewater treatment has been used for the removal of metals, non metals, suspended solids, organic compounds, COD and BOD. While industrial applications have primarily focused on the use of iron electrodes; aluminum works better in acidic conditions and is sometimes more effective than iron electrodes. To better understand the mechanism for EC using aluminum electrodes and their best use, we present a review of the applications of Al electrodes, followed by pH measurements at different zones around the electrodes, which illustrate the mechanism and reactions that occur at the anode and at the cathode. We find the mechanism to be congruent with solubility and Pourbaix diagrams.

General Abstracts: Extraction and Processing: Pyrometallurgy, Base Metals

Sponsored by: The Minerals, Metals and Materials Society, TMS Extraction and Processing Division, TMS: Aqueous Processing Committee, TMS: Materials Characterization Committee, TMS: Pyrometallurgy Committee *Program Organizers:* Boyd Davis, Kingston Process Metallurgy Inc; Michael Free, University of Utah

Monday AM	Room: Northern E3
February 26, 2007	Location: Dolphin Hotel

Session Chair: Melissa Trapani, BHP Billiton Olympic Dam

9:00 AM

Effect of MgO and Al2O3 on the Environmental Behavior of Chromium Based Slags: Elda García-Ramos¹; *Jose Romero-Serrano*¹; Beatriz Zeifert¹; Vanessa Ugarte-Domínguez¹; Beatriz Estrada-Mateos¹; ¹National Polytechnic Institute

The slags produced in the stainless steelmaking process contain chromium that must be stabilized to reduce the eventual polluting effects. The objective of this work is to analyze the effect of MgO and Al2O3 content and the slag basicity on the stability of the mineralogical species and the leachability of slags. The samples of the systems CaO-CaF2-SiO2-Cr2O3-MgO and CaO-CaF2-SiO2-Cr2O3-Al2O3 were prepared in an induction furnace at 1400-1500°C. The samples were analysed by X-ray diffraction and Scanning Electron Microscope to study the morphology and composition of mineral phases. The results showed that slags with MgO produced MgO•Cr2O3 spinel and calcium silicates. The slags with Al2O3 produced complex compounds, Ca2Al2SiO7, Ca4Al6CrO16 and calcium silicate crystals. Some trials were carried out to test the leachability of the slags. The results showed that owing to the stable binding of chromium in spinel or complex compounds the leachabile was decreased.

9:25 AM

Effect of Slag Composition on the Manufacture of Iron Nuggets from Carbon Composite Pellets: Alberto Nogueira¹; *Marcelo Mourao*¹; Cyro Takano¹; ¹University of Sao Paulo

Iron-carbon nuggets can be obtained by high temperature reduction of iron ore by carbonaceous material agglomerated together as a carbon composite pellet. During this process, the stable oxides contained in the materials will form a slag. This work investigates the effect of the slag composition on the formation of the iron nuggets. Pellets were prepared containing iron ore and two different carbonaceous materials, and through the addition of cement, silica and alumina the composition of the slag was varied to adjust the expected liquidus temperature to 1573 K and 2273 K. It has been shown that the formation of iron nuggets is favored for slags presenting low liquidus temperature. In order to further investigate this phenomenon, pellets containing iron powder and carbonaceous material, together with previously prepared slags, were also submitted to high temperature, and it has been shown that the carburization of the iron depends on the slag composition.

9:50 AM

The Investigation of Sponge Iron Production Parameters by Using Iron Oxide Pellets with Domestic Lignite Coals: Onuralp Yucel¹; Kemal Gecim¹; Suheyla Aydin¹; ¹ITU

The aim of the present work is to investigate the possibilities of coal-based sponge iron production for industrial applications by using different kinds of domestic (Turkish)lignite coals. Experiments were conducted in a semipilot scale rotary tube furnace. The materials used were iron oxide pellets from Divrigi Plant and Soma, and coals from Tunçbilek and Oltu domestic lignites. The effects of coal consumption ratio (Cfix/Fetot.), temperature and duration time on the metallization degree of sponge iron have been studied. From the experiments carried out at different conditions, it was found that the metallization degrees reached to an optimum range desired for industrial applications. At the temperature of 1050°C and a coal consumption ratio of 0.32, reduction process with the Soma lignite coal was completed at about 40 minutes where the pellets showed 97% average metallization degree.

10:15 AM Break

10:35 AM

Kinetics of Liquid Copper Reduction with Charcoal: *Gabriel Riveros*¹; Andrzej Warczok¹; Carlos Puga¹; ¹Universidad de Chile

Copper fire refining consists of two stages: blister copper oxidation with impurities slagging and reduction of oxidized copper. Numerous works on the kinetic of a liquid copper reduction with various reductants, such as bunker oil, propane, natural gas and ammonia, indicate two stages of reduction and factors limiting the reduction rate. Kinetic of copper reduction with charcoal has been determined by thermogravimetry combined with off-gas analysis. The results stated the basis for mathematical model of the reduction of oxidized copper in a packed bed of charcoal. Experimental simulation of the copper reduction in a packed bed of charcoal showed extremely high rate of reduction predicted from the model. Presented results allowed for development of a new process of continuous fire refining of blister copper. Pilot industrial scale tests of continuous copper refining confirmed expected rate of reduction and feasibility of a new process.

11:00 AM

Remote Cooled Element Trial in Flash Furnace Gas Space: Melissa Trapani¹; Roger Player²; Dennis Montgomerie¹; ¹BHP Billiton Olympic Dam; ²BHP Billiton Technology

The Outokumpu direct to blister flash furnace at Olympic Dam has historically experienced failure of gas space cooling elements due to wet acid corrosion. A remote cooled element is being developed to overcome acid corrosion by keeping the hot face of the element above the dew point of the corrosive species in the gas. A prototype element was installed in the Flash Furnace in November 2005. The element has exhibited hot face temperatures above 700°C. An overview of the performance of the element is presented along with heat transfer calculations for the system. Implications of the cooling element for furnace integrity and monitoring are discussed.

General Abstracts: Light Metals Division: Session I

Sponsored by: The Minerals, Metals and Materials Society, TMS Light Metals Division, TMS: Aluminum Committee, TMS: Reactive Metals Committee, TMS: Recycling Committee

Program Organizers: Neale Neelameggham, US Magnesium LLC; Anne Kvithyld, Norwegian University of Science and Technology

Monday AM	Room: Pacific Hall B
February 26, 2007	Location: Dolphin Hotel

Session Chairs: Lifeng Zhang, Norwegian University of Science and Technology; R. Vasantha Kumar, The Madras Aluminium Company (MALCO) LTD.

9:00 AM

Preparation and Application of High-Molecular-Weight Hydroxamic Acid Containing Phenyl as Flocculants for Red Mud Setting: *Chen Feng*¹; Lian-Song Wang¹; Yuan-dong Li²; ¹Northeastern University; ²Shenyang Dongwei Industrial and Mining Mechanical Fittings Company, Ltd.

Anew High-Molecular-Weight hydroxamic acid containing phenyl (HHCP) as high efficiency flocculant was synthesized. Firstly, at 15~35, Copolymerization of acrylamide and styene was carried out in a microemulsion system, in which AM aqueous solution was the continue phase and St was the dispersed phase using ST-80 as surfactants respectively. Hydroxamic functions were prepared with hydroxylamine salt at temperatures from 60° to 90°. The effect of reaction conditions on the structure was studied. The copolymer was characterized by FT-IR and UV, then the effect of copolymer on red mud setting process was tested. The clearest supernates, rapid setting velocity and high stability were observed. It suggested that the new High-Molecular-Weight hydroxamic acid containing phenyl could meet the industry demand.

9:20 AM

Preparation and Characterization of New Water Base Low Cost Coating Material for Anode Rod Stubs: *Jyoti Mukhopadhyay*¹; Upendra Singh¹; 'JNARDDC

In an aluminium smelter, molten cast iron seals both the anode block and rod assembly together. When the anode butt is returned from electrolysis cell, the spent anode butt is being cleaned up and the cast iron thimbles are removed. Presently, graphite coating is used on the stub after removing the cast iron thimbles from it. In the process, the risk of welding between the cast iron thimbles and the stub can be reduced significantly. Furthermore, the electrical conductivity of the anode assembly can also be improved to a great extent in the cell. The aim of the present investigation is two folds, (i) to prepare a water based coating material which is cheaper, and (ii) to compare the properties of the Lab developed coating materials with the coating material available commercially in the market.

9:40 AM

Reduction in Pot Turn around Time: *R. Vasantha Kumar*¹; Srinivasa Narasimhan Chakravarthy¹; Krishnaraj Thiyagarajan¹; ¹The Madras Aluminium Company (Malco) Ltd.

The time taken to bring the pot into service from the time it is shunted is termed as Pot Turn Around Time (PTT). In earlier days the average PTT in MALCO stood at 13 days, which was slowly reduced to 48hrs over a period of time. A project was under taken to reduce the PTT further, the most challenging assignment in any Aluminium industry. The team has analysed the sequence of operations and focused on the Planning and Startup aspects of the pot. The team has achieved reduction in PTT from 48hrs to 22.5 hrs and made this as Standard Operating Procedure (SOP) for repeatable sustainable execution. This paper explains in detail the steps taken by the team and the reduction in time taken to install a new pot.

10:00 AM

Experiences and Developments through 10 Years of Operation with the Abart Dry Scrubber: *Geir Wedde*¹; Parto Henriksen²; ¹Alstom; ²Alstom Norway

An advanced system for recovery of fluorides and removal of particulates and tars from aluminium reduction pot gas and anode baking furnaces, called Abart, is in operation at numerous installations world-wide. The patented Abart technology has evolved through 10 years of operation. The first Abart installation was at the Hindalco smelter in 1996. The Abart technology is installed and operates for all types of pot technologies from moderate to high amperage pots, in cold and hot climates. The Abart system is designed to handle more than three million m3/h of prebake pot gas. Continued development and improvements from customer feedback have been continuously implemented, refining the Abart technology to a highly efficient and robust dry scrubbing solution. This paper shares and reviews the experiences gained, lessons learned, and presents the latest state-of-the-art Abart technology.

10:20 AM

Recovery of Residual Metal from Spent Pot Lines for Use in Oxygen Steel Making Process: Pradeep Maitra¹; ¹M/S Dipaly Consultants

The steel produced by above stated process always contains some amount (between 400 to 1000 ppm) of oxygen,which is required to be removed from molten steel (killed). An attempt has been made in this paper to describe how the residual low purity contaminated Al is recovered from bath, collecterbars, carbon, refractories etc and granulated (-12+14 mesh) and filled in a Rollformed low carbon (0.4mm x9mm) steel tube and coiled (500 to 3000 meters length) and continuously fed the cored tube in to the liquid metal. This process of aluminium recovery is economical in one hand and environmentally acceptable solution of solid waste disposal of primary Al industries.

10:40 AM Break

10:50 AM

Characteristics of Aluminum Foam Prepared by Infiltration of Liquid Al through Ceramic Foam Bed: *Pravash Maity*¹; ¹National Institute of Foundry and Forge Tech

It was discovered that viscous sodium silicate bonded ceramic particles with controlled sodium silicate and water content when suddenly exposed to high temperature, produces ceramic foam. With this approach, ceramic foams were produced based on silica particles and sodium silicate by varying the silica particles, sodium silicate and water content. To stabilize foamy structure and to strengthen, the ceramic foams were fired at 800°C for 1 hr. The ceramic foams were crushed and graded to suitable size ranges. Liquid Al was infiltrated into the bed of ceramic foams to produce Al foams. The effects of cell size of ceramic foams and size and volume fraction of ceramic foam grains on the characteristics of the Al foams have been studied.

11:10 AM

Fundamentals of Inclusion Removal from Molten Aluminum and Silicon through Gas Bubbling: *Lifeng Zhang*¹; ¹Norwegian University of Science and Technology

This study is to investigate the fundamentals of inclusion removal from molten aluminum and silicon by attaching to the rising bubbles. A simple mathematical model for this bubble flotation process is developed. The effects of gas flow rate, bubble size and time on the inclusion removal are discussed. Based on the results of the models, it is concluded that there is an optimum bubble diameter for the inclusion removal. Finally a tentative industrial scale of bubble flotation cell is proposed, and the three dimensional fluid flow and bubble/particle motion in this cell are calculated.

11:30 AM

Structural Characterization of Liquid Al-Si Hypoeutectic Alloys: *Srirangam VenkataSuryaPrakash*¹; Sumanth Shankar¹; Matthew Kramer²; ¹LMCRC, McMaster University; ²Iowa State University

Several studies in the past decades have been devoted to characterize the solid and semi-solid structures of the commercially important Al-Si alloys. However, minimum efforts were directed to characterize the liquid structure of these alloys. Characterizing liquid structures will enable an in-depth understanding of the melt behavior and the nucleation events in the melt prior to solidification. Liquid phase diffraction experiments were carried out in two hypoeutectic alloy compositions (Al-11wt%Si & Al-11wt%Si-0.04wt%Sr) at various melt superheats ranging from 600 °C to 650 °C. Detailed experimental procedure and sample preparation techniques are presented along with quantified structure factor, pair distribution functions, and coordination numbers as a function of temperature. It is observed that there is a marked difference between the results obtained from the unmodified and Sr modified





alloys showing that addition of trace levels of Sr reduces the atom cluster size in the liquid.

11:50 AM

Structure-Functional Materials of In Situ TiB2 Particulates Reinforced A356 Composite: *Yijie Zhang*¹; ¹Yantai University

In situ TiB2 particulate reinforced A356 composite with high damping capacity and excellent strength was prepared by an exothermic reaction process via K2TiF6 and KBF4 salts. Interestingly, present experimental results indicate that both damping capacity and tensile strength are improved simultaneously. It was noted that the damping capacity of A356/TiB2 composite was much higher than that of A356 base alloy. The yield tensile strength and ultimate tensile strength of 13wt% TiB2 reinforced A356 composite are 369MPa, 389MPa. Compared to A356 base alloy, yield tensile strength and ultimate tensile strength of A356 composite are increased by 74MPa, 69MPa respectively.

General Abstracts: Materials Processing and Manufacturing Division: Forming of Materials and Processes

Sponsored by: The Minerals, Metals and Materials Society, TMS Materials Processing and Manufacturing Division, TMS/ASM: Computational Materials Science and Engineering Committee, TMS: Global Innovations Committee, TMS: Nanomechanical Materials Behavior Committee, TMS/ASM: Phase Transformations Committee, TMS: Powder Materials Committee, TMS: Process Modeling Analysis and Control Committee, TMS: Shaping and Forming Committee, TMS: Solidification Committee, TMS: Surface Engineering Committee

Program Organizers: Fernand Marquis, Naval Postgraduate School; Ralph Napolitano, Iowa State University; Neville Moody, Sandia National Laboratories

Monday AM	Room: Northern A4
February 26, 2007	Location: Dolphin Hotel

Session Chairs: Axel Specker, Institut für Integrierte Produktion; Achim Schott, IPH GmbH

9:00 AM

Approach for Flashless Precision Forging Operations for Components with Unsteady Mass Distribution: Axel Specker¹; Dominic Gruss¹; Sven Müller¹; ¹Institut für Integrierte Produktion

Precision forging is defined as a flashless forging operation which generates high quality parts concerning the surface quality and accuracy of dimensions. The present level of development allows the industrial production of axis symmetric parts like gear wheels and steering pinions by a precision forging process. Further development of flashless forging operations is necessary for realising multi-stage precision forging processes for flat long pieces. The ability to forge high-duty automotive components like crankshafts or connecting rods is expected to be a major improvement, because these components feature an extremely asymmetric mass distribution and a big specific mass. To solve the appearing technological deviances a new forging chain with three forging operations was developed. Practical testing of the process chain showed the principle feasibility of forging crankshafts with the flashless precision forging technology.

9:25 AM

Spray Forming of Al-Mg-Si-Alloy with High Volume of Mg2Si: Volker Uhlenwinkel¹; Nils Ellendt¹; Olaf Kessler²; Olaf Stelling²; ¹University Bremen; ²Foundation for Materials Science

Aluminum alloys with a high content of Mg_2 Si are superior lightweight alloys due to their low density and elevated high-temperature-strengh compared to other aluminum alloys. Alloys with more than 10 volume-% Mg_2 Si can not be casted with sufficient mechanical properties. Spray Forming is an adequate process to produce material from these alloys due to the high occurring cooling rates. Billet spray forming experiments with Aluminum alloys with three different Mg_2 Si contents of 21.8, 30 and 35 weight-% were performed. The billets were characterized regarding porosity and correlations between their average porosity and process parameters were found. First results on the extruded material will be discussed.

9:50 AM

Warm Forging of a Connecting Rod: Achim Schott¹; ¹IPH GmbH

Warm forging is an economical alternative to the conventional forging technology common for rotation-symmetric parts. It offers several advantages like reduced energy input, no scale, better surface quality and closer tolerances. The main obstacle prohibiting a transfer of the technology to the forming of long flat pieces is the increased number of forming operations and the connected problems to keep the narrow temperature tolerances. In a cooperative effort within a European consortium, forming sequences for warm forging a steering link and a connecting rod have been developed. One focus of the development of the forging process of the connecting rod was to maintain the ability of the work piece to crack after the forging and controlled cooling. Currently, the simulation results are verified during the try out of the dies and the obtainable work piece properties are investigated and documented.

10:15 AM

Improvements in Electrospark Deposition for Small Repairs through the Use of Ultrasonic Impact Treatment: *Graham Tewksbury*¹; Danial Danks¹; Sean O'Connell¹; John Kelley¹; Norma Price¹; William Wood¹; ¹Portland State University

Electrospark deposition (ESD) is a pulse capacitance welding technique traditionally used to deposit coatings for corrosion or wear resistance. Recently the technique has been examined as a potential technology for small area repair. This change from a surface coating to a micro weld repair has resulted in a substantial increase in the required properties. The application of ESD results in tensile residual stress on the repaired surface. Ultrasonic impact treatment (UIT) was used to introduce a compressive residual stress to the surface of the deposit to improve fatigue properties. The combination of ESD and UIT has the potential to minimize and in some materials eliminate the asdeposited fatigue debit of the repair. ESD + UIT deposits were characterized using optical microscopy, SEM, microhardness, and image analysis. The fatigue properties of repairs of several alloys including IN718, and 410SS were evaluated.

10:40 AM

The Kinetics of Multidimensional Infiltration: Kevin Trumble¹; ¹Purdue University

Many models are available for predicting the kinetics of liquids infiltrating porous solids in terms of the capillary pressure, applied pressure, and resistance to flow. All are restricted to unidirectional infiltration, however, as occurs in end-contact infiltration of a long cylinder. For a general shape of preform under immersion infiltration conditions, multidimensional flow must be considered. Analytical models are developed that account for the effects of convergent/divergent flow in the infiltration of discrete porous performs. The solutions can be applied to any unidirectional infiltration kinetics model, regardless of the assumptions about the capillary pressure function, wetting, etc. The results are presented in non-dimensional form to facilitate comparison of the relative infiltration times for various regular preform shapes (e.g., slab, cylinder, sphere).

11:05 AM

Optimal Blank Design for Complicated Shapes Using Modified Ideal Forming Theory: *Mohammad Parsa*¹; Samira Sokhanvaran¹; ¹University of Tehran

For deep drawing of sheet metals and converting them to specific product shapes without failure, the initial blanks should be, correctly designed. Otherwise, final products will not be sound. Using an optimum blank not only decreases consumed materials but also minimizes defects produced by metal forming operations. In the pervious work of authors by introducing some modification in the applied kinematics formulation in combination with ideal forming theory, satisfactory results have emerged for simple shapes. In the present paper, by using the modified code and considering boundary conditions, optimum blank design procedure for complicated shapes will be presented. By modifying the extremum work criterion, a method has been developed to introduce the effect of Coulomb friction. The results of prediction with and without considering boundary conditions also will be compared. The results show the capability of the new algorithm in designing the initial blank of deep drawing products.



11:30 AM

Hot Tearing Prediction during Multi-Component Alloys Solidification: Jianzheng Guo1; Jianzhong Zhu1; 1ESI US R&D

very important to understand the relationships between the alloy chemistry,

the processing, and the final properties. Such prediction is possible to a degree

by given knowledge of the microstructure, phase fractions, and defects present

in a metallic part. Hot tearing is one of the most serious defects for a casting. In

this paper a hot tearing indicator was introduced to evaluate the susceptibility

of hot tearing during casting solidification processes. The predictions are

validated by comparison with experimental measurements.

In order to predict the mechanical properties of an in-service part, it is

Innovations in Measurement Science to Assess the Performance of New Materials in the Real-World: **Fundamental Measurement Methods**

Sponsored by: The Minerals, Metals and Materials Society, TMS Materials Processing and Manufacturing Division, TMS: Shaping and Forming Committee

Program Organizers: Mark Stoudt, National Institute of Standards and Technology; Lyle Levine, National Institute of Standards and Technology; Tusit Weerasooriya, Army Research Laboratory

Monday AM	Room: Australia 3
February 26, 2007	Location: Dolphin Hotel

Session Chairs: Mark Stoudt, National Institute of Standards and Technology; Tusit Weerasooriya, Army Research Laboratory

9:00 AM Introductory Comments

9:10 AM Keynote

Mechanical Properties and Performance: Richard Fields1; 1National Institute of Standards and Technology

Mechanical properties are often used to predict the performance of materials in actual situations. Many assumptions go into the choice of mechanical properties to use to make the prediction. Successful predictions may sometimes be based on a positive correlation of the performance with the property, without a good physical connection. Failure to adequately predict performance is often followed by an attempt to improve the measurement of the mechanical property, or to define and measure new mechanical properties. Examples of all of the above cases will be presented with lessons learned. The presentation will cover the use of elastic, plastic, creep, high strain rate, fracture, and multiaxial mechanical properties to predict performance. The need for new properties will be discussed.

9:50 AM Keynote

Exploring Material-Property Space: Charts, Selection and Limits: Michael Ashby1; 1National Institute of Standards and Technology

Engineers design and make things. They make them out of materials. The attributes of the materials - their mechanical, thermal, electrical, optical and other properties - limit the design. These limits have, for centuries, stimulated attempts to develop materials that are stiffer, stronger, lighter, and better insulators or conductors than those at the time available. The attributes themselves can be though of as the axes of a multi-dimensional "materials property space" of which the image is a simple 3-D slice. Part of the space is occupied, part is empty. Much material development aims to fill out some of the empty regions, thereby enabling designs that are not at present possible. This suggests two questions. what parts of the space are most interesting? And what are its ultimate limits? The talk will introduce the ideas and the challenges they suggest.

10:30 AM Invited

Measurement of the Mechanical Properties of Lattice Materials: Norman Fleck1; 1National Institute of Standards and Technology

Abstract not available.

11:00 AM Break

11:10 AM Invited

Novel Production, Monitoring and Consolidation of Light Alloy Powders: James Foley1; 1Los Alamos National Laboratory

The drive for lighter and more fuel-efficient vehicles has spurred interest in light alloys. However, processing of advanced aluminum alloys often requires many complicated steps that are cost prohibitive for the automotive industry. Many of the costly processing steps are aimed at overcoming the effects of the Al2O3 surface film typical of commercial aluminum powder. Alternative, atomization techniques have enabled novel consolidation pathways and the ability to measure the effect of the oxide on consolidation and final mechanical properties. Advances in high temperature ultrasonic transducers have enabled in-situ monitoring of sintering. A correlation between the ultrasonic measurements and mechanical strength will be presented both for solid state and liquid phase sintering of various powders. A simplified consolidation method of Al-8Fe-4Ce will be presented along with mechanical and microstructure data obtained. In addition, the relevance of the previous results on other powders will be shown. (LA-UR-06-4573)

11:40 AM Invited

Using Atomic Force Microscopy to Reveal Slip Modes in TiAl 'Single Crystals': David Pope1; Yali Chen1; 1University of Pennsylvania

The structure of directionally solidified TiAl 'single crystals' consists of layers of tetragonal TiAl with (111) plane interfaces, the orientations of which are rotated by multiples of 120 degrees about the interface normal. This leads to (111) interfaces that consist of twins, or combinations of twins and antiphase boundaries. These interfaces totally control the nature of the deformation for all orientations of the applied stress. The details of how the interfaces accomplish this is clearly revealed in atomic force micrographs of deformed crystals. The main feature of the deformation microstructure is that the slip traces are confined to individual lamellae to the extent that the lamellae deform in a coordinated manner but the slip does not propagate from one layer to adjacent layers.

12:10 PM Invited

Application of Computed X-Ray Tomography to the Study of Damage and Ductile Fracture: David Wilkinson1; Weck Arnaud1; Akihide Hosegawa1; ¹McMaster University

Ductile fracture occurs by a process of damage accumulation in which voids are nucleated (typically at second phase particles), grow and then coalesce. Because of the stochastic nature of this process it is difficult to study experimentally. In recent years we have used computed x-ray tomography (CXT) coupled to synchrotron x-ray sources to enable 3-D visualization of damage during deformation. In this talk I will present recent results involving in situ tests on copper in which we have isolated the coalescence stage of fracture. This is accomplished by creating model samples that contain a pre-designed internal void array. The samples are fabricated by taking thin copper sheets, drilling holes using a femtosecond laser system, then stacking and diffusion bonding several sheets. These experiments give us precise measurements on void growth and coalescence for embedded voids that allow a quantitative comparison with ductile fracture models.

12:40 PM Invited

Elastic Constants and Thermal Expansion Averages of a Polycrystal: Roland Dewit1; 1Guest Scientist, National Institute of Standards and Technology

This paper derives expressions for the overall average elastic constants of a polycrystal that is statistically homogeneous and disordered. We also include Tomé's extension to the overall average thermal expansion of the polycrystal. Upper and lower bounds for the averages can easily be found by assuming a uniform strain (Voigt) or stress (Reuss). These assumptions imply a particular anisotropy of the crystallites. A self-consistent estimate for the averages can be found if it is assumed that the overall response of the polycrystal is the same as the average response of each crystallite. The polycrystal is then isotropic. The derivation method used in this paper is based on Eshelby's theory of the equivalent inclusion. The equivalent inclusion is then used to represent the crystallites. We show the derivations by Kröner and by Tomé for the selfconsistent equations. For the particular case of cubic symmetry this leads to a simple cubic equation

Technical Program



Innovations in Titanium Technology Symposium: Low Cost Materials and Processing

Sponsored by: The Minerals, Metals and Materials Society, TMS Structural Materials Division, TMS: Titanium Committee *Program Organizers:* Mehmet Gungor, Concurrent Technologies Corporation; M. Ashraf Imam, Naval Research Laboratory; F. H. (Sam) Froes, University of Idaho

Monday AM	Room: Asia 3
February 26, 2007	Location: Dolphin Hotel

Session Chairs: Mehmet Gungor, Concurrent Technologies Corporation; M. Ashraf Imam, Naval Research Laboratory

9:00 AM Keynote

Low Cost Titanium – An Update: *Francis Froes*¹; Mehmet Gungor²; M. A. Imam³; ¹University of Idaho; ²Concurrent Technologies Corporation; ³Naval Research Laboratory

Titanium is seeing ever widening uses, expanding from a concentration on aerospace applications into terrestrial transportation, consumer goods, oil and gas exploration and metal production equipment. This despite the high cost of titanium – a result of cost intensive extraction and expensive fabrication costs (a result of the low processing temperatures and frequency of conditioning necessary with titanium). To increase the use of titanium – a goal of the recent planned expansion in titanium capabilities – the high cost of titanium must be reduced. This paper will review developments in this area including extraction, melting/casting, processing/fabrication, near net shapes (castings, powder metallurgy, etc.) and set the tone for the following more specific papers.

9:30 AM Invited

Overview of Applications and Opportunities for Armstrong Low Cost Titanium: James Sears¹; ¹South Dakota School of Mines and Technology

An overview is given of the potential applications and new opportunities being developed due to the maturation of low cost titanium produced by the Armstrong Process. It has long been known that titanium would enter many new markets if production and manufacturing costs could be reduced. Since low cost titanium and titanium alloys are now becoming commercially available through the Armstrong Process many of these markets can now be exploited. The first applications will use the Armstrong Powder as melt stock source for conventional wrought titanium and as alloying additions for steel, nickel and aluminum alloys. However, the more lucrative markets will be were the Armstrong powder is used in direct conversion processes, i.e., roll forming, metal injection molding (MIM), press and sinter operations, powder forging, cold and hot Isostatic pressing (CIP and HIP), and other near-net shape manufacturing technologies.

9:50 AM Invited

Low Cost Fabrication of Titanium Alloy Components Directly from Sponge: James Withers¹; Roger Storm¹; Raouf Loutfy¹; ¹MER Corporation

The cost of a titanium alloy component is typically 10 to 30 times the cost of basic Kroll process produced sponge. In order for titanium to penetrate widespread utilization in defense, transportation and general commodity commercial application the cost of components ready for use must be dramatically reduced. Reducing the cost of primary titanium/sponge is progressing under the DARPA Initiative in Titanium. Even with low cost sponge the cost a final component via conventional processing remains too high for many applications. Alternate processing has been demonstrated to translate sponge directly into near net shape alloy components at a cost of \$4 to \$8 per pound over the cost of sponge. Low cost sponge and this alternate processing provides an avenue to produce truly low cost titanium components. The alternate one step processing will be described, produced components demonstrated and cost analysis illustrated.

10:10 AM

Development of Cost Effective Blended Elemental Powder Metallurgy Ti Alloys: Fusheng Sun¹; Kuang-O (Oscar) Yu¹; ¹RMI Titanium Company

Low cost titanium alloy compacts were produced via the powder metallurgy approach by blending elemental (BE) titanium sponge fines and master alloy. The pressed and sintered approach potentially offer relative low cost titanium hardware suitable for aerospace applications and military ground vehicle applications. Pressed and sintered Ti-6Al-4V compacts from two sources were characterized in terms of chemistry, microstructure and properties. Effects of hot rolling and deformation on the microstructure of Ti-6Al-4V compacts are reported. Processing both before and after sintering was found to have a significant impact on microstructure and properties.

10:30 AM Break

10:45 AM Invited

Investigation of Potentially Low-Cost Titanium Powders for Use in Automotive Applications: K. Scott Weil¹; Yuri Hovanski¹; Curt Lavender¹; ¹Pacific Northwest National Laboratory

A recent cost study commissioned by the Department of Energy and prepared by Camanoe Associates concluded that the use of a low-cost titanium ore as the feedstock source in a continuous reduction process could substantially drive down the cost of titanium sponge and powder, making it viable for more extensive commercial use – in particular automotive application. Pacific Northwest National Laboratory (PNNL) is currently leading a program to develop this low-cost titanium processing stream. Working with E.I. DuPont de Nemours and International Titanium Powder (ITP), PNNL has employed low-cost, ilmentite-derived titanium tetrachloride (of the type used in titanium dioxide paint pigment production) as the precursor in titanium powder synthesis. The resulting titanium powders, while containing additional impurities are being evaluated for powder metallurgy (P/M) processing. Progress on powder characterization and P/M processing will be reported.

11:10 AM

Thermomechanical Processing of "Low-Cost", Armstrong Titanium and Titanium Alloy Powders: *William Peter*¹; Craig Blue¹; John Rivard²; Clive Scorey³; Lance Jacobsen⁴; David Harper¹; Jim Kiggans¹; ¹Oak Ridge National Laboratory; ²Strategic Analysis, Inc; ³AMETEK, Inc.; ⁴International Titanium Powder, L.L.C.

Recently, considerable interest has been established in producing low cost titanium and titanium alloys. The Armstrong Process is a new method of producing titanium via reducing TiCl4 vapor in molten sodium. The process is scalable, and can be used to produce in-situ alloy powders. With potential realization of low cost Ti powder, several new processing paths are possible to produce cost reduced titanium parts. In this feasibility investigation, commercially pure (CP) Ti and Ti-6Al-4V powders produced via the Armstrong Process were used to produce plate by vacuum hot pressing, and bar stock by extrusion. After achieving wrought properties in the feasibility study, CP Ti and Ti-6Al-4V powders were consolidated to sheet via a technique of solid state cold rolling and sintering. The metallurgical, chemical, and mechanical properties of the processed titanium samples will be discussed.

11:30 AM

A Novel Process for Cost Effective Production of TiAl based Titanium Alloy Powders: Gorgees Adam¹; 'Titanox Development Limited

Titanium alloys belonging to the most advanced materials of our time because of their excellent combination of specific mechanical properties and outstanding corrosion behaviour at high temperatures. Among them, Titanium Aluminides are proven to be use in a wide range of industrial applications. However, the production of Titanium Aluminides is still cost-intensive, and their properties, especially for further alloying, are still under investigation. Titanox Development Limited-New Zealand has been successfully in creating a novel process to produce TiAl alloy powders cost effective, and with very fine particle sizes. The cost of the product powder this process will represent a very small fraction of the international prices. This technology is mainly characterised by milling, heat-treatment, mechanical separation, and chemical reduction processes. Titanium aluminides powders (TiAl and Ti3Al) with purity were achieved. These powders were used successfully for coating, near net shape forming by powder metallurgy techniques.

11:50 AM

Flowformed Ti-6Al-4V: *Mehmet Gungor*¹; Lawrence Kramer¹; Ibrahim Ucok¹; Hao Dong¹; Wm. Troy Tack¹; ¹Concurrent Technologies Corporation

Flowforming process is a cost effective means to produce tubular structures. In this paper, a development effort to produce thin-wall, large and long Ti-6Al-4V seamless tubes is described. Material efficiency of flowforming process is **MOZDAX**

A M



compared to those of competing processes such as extrusions. In addition to its cost effectiveness, flowformed material, having gone through an extreme plastic deformation, displays a very fine microstructure, which consequently, offers increased tensile and fatigue properties. This work was conducted by the Navy Metalworking Center, operated by Concurrent Technologies Corporation under Contract No. N00014-00-C-0544 to the Office of Naval Research as part of the U.S. Navy Manufacturing Technology Program.

Internet and Other Electronic Resources for Materials Education: Session I

Sponsored by: The Minerals, Metals and Materials Society, TMS: Education Committee

Program Organizer: Adam Powell, Veryst Engineering LLC

Monday AM	Room: Oceanic 2
February 26, 2007	Location: Dolphin Hotel

Session Chair: Adam Powell, Veryst Engineering LLC

9:00 AM Title Not Available: *Mark Palmer*¹; 'Kettering University Abstract not available.

9:25 AM Invited

NSF NSDL Materials Digital Library and MSE Education: Laura Bartolo¹; Sharon Glotzer²; Matthew Krane³; Adam Powell⁴; Krishna Rajan⁵; Donald Sadoway⁴; Vinod Tewary⁶; James Warren⁶; Cathy Lowe¹; ¹Kent State University; ²University of Michigan; ³Purdue University; ⁴Massachusetts Institute of Technology; ⁵Iowa State University; ⁶National Institute of Standards and Technology

The NSF National Science Digital Library is a technical and community framework for access to high quality content and tools to support innovations in education of science, technology, engineering, and mathematics. NSDL Materials Digital Library (MatDL) focuses on the materials science (MS) community of undergraduate and graduate students, educators, and researchers. MatDL is a collaborative effort with the National Institute of Standards and Technology, Kent State University, Massachusetts Institute of Technology, the University of Michigan, Purdue University, and Iowa State University. MatDL aims to bring materials science research and education closer together through innovative uses of digital libraries and the web in the MS community by providing: tools to describe, exchange, and disseminate scientific data; services and content for virtual labs in undergraduate introductory science courses; workspace for collaborative development of core undergraduate MS teaching resources; and workspace for open access development of modeling and simulation code.

9:50 AM

The Transport Phenomena Archive on the Materials Digital Library Pathway: Adam Powell¹; Matthew Krane²; Laura Bartolo³; ¹Veryst Engineering LLC; ²Purdue University; ³Kent State University

The Transport Phenomena Archive is an online space within the Materials Digital Library Pathway (www.matdl.org) for collaborative development of educational resources related to transport phenomena, with a focus on materials processing and performance. The Archive currently includes over one hundred resources, including eighty homework problems organized into 36 keywords, three courseware offerings, two extensive (25-50 page) readings, four resources on pedagogy, and nearly twenty handouts and other resources. Archive resources reside in a version control server, allowing for corrections and updates while maintaining all previous versions of each resource. A web front-end at http://lyre.mit.edu/transport/facilitates browsing and downloading of materials. A fourteen-member Editorial Board consisting of transport educators in materials and related departments reviews contributions. The Archive is open for such contributions, corrections and general comments by the materials community.

10:15 AM

Artificial Neural Network Education for Materials Scientists through Internet: *N. Reddy*¹; Ji Soo Kim¹; Chan Hee Park¹; Chong Soo Lee¹; ¹Pohang University of Science and Technology

An artificial neural network (ANN) is a massively parallel array of simple

computational units that models some of the functionality of human brain and attempts to capture some of its computational strength. ANNs exhibit learning abilities similar to that of a human brain. ANN model eliminates the limitations of the regression methods and establishes an accurate mapping between the input and output variables without any assumptions are made regarding the form of the functions relating the input and output variables. The advent of powerful computing facilities and the rapid growth in applications of ANN methods in materials science has stimulated new research initiative with the aim of bringing these two areas together. This is evident from the exponential growth in number of papers published on the subject. This paper presents comprehensive internet resources to be familiar with the ANN history, fundamentals, different algorithms, software, and implementation details in materials science.

10:40 AM

Wikipedia in Materials Education: Adam Powell¹; *Arthur Morris*²; ¹Veryst Engineering LLC; ²Thermart

Wikipedia has become a vast storehouse of human knowledge, and a first point of reference for millions of people, including many of our own students. Its characteristics of open authorship and instant publication lead to both its best strength of broad, timely coverage and also its weakness of nonuniform quality. This talk will discuss the current status and future potential of this medium as a delivery mechanism for materials education content, some experiences with its use in the classroom, and its fit with other media from textbooks to digital libraries.

11:05 AM Break

11:10 AM

Materials Technology@TMS: Education: Cathy Rohrer¹; *Todd Osman*²; ¹TMS; ²TMS Inc

TMS is launching an education component as part of Materials Technology@TMS at the TMS 2007 Annual Meeting. Digital resources that can be used in classroom lectures have been collected and catalogued on the Materials Technology@TMS Web site. The goal of this endeavor is to provide a forum for knowledge sharing, including presentations, video clips, computer animations and other digital resources. Additionally, a discussion board forum has been created to enable benchmarking best practices for materials education as well as to provide web-based networking. This presentation will highlight the use of resources on the education area of Materials Technology@TMS for material science and engineering curricula, with emphasis on "Materials 101" courses for materials engineers and students from other disciplines.

11:35 AM Panel Discussion

Open Discussion on Information Technology for Materials Education: Moderated by Adam Powell

Magnesium Technology 2007: Magnesium Globalization

Sponsored by: The Minerals, Metals and Materials Society, TMS Light Metals Division, TMS: Magnesium Committee

Program Organizers: Randy Beals, DaimlerChrysler; Neale Neelameggham, US Magnesium LLC; Mihriban Pekguleryuz, McGill University; Alan Luo, General Motors Corporation

Monday AM	Room: Southern 4/Southern 5
February 26, 2007	Location: Dolphin Hotel

Session Chairs: Randy Beals, DaimlerChrysler; Neale Neelameggham, US Magnesium LLC; Alan Luo, General Motors Corporation

9:00 AM Introductory Comments by Randy S. Beals - TMS Magnesium Committee Chair

9:05 AM

Supply and Demand Fundamentals of the Magnesium Industry: Cam Tissington¹; ¹US Magnesium LLC

The Global Supply Base of Magnesium has experienced an upheaval in the past decade with the shuttering of Western capacity and the explosion of production in China. The Global demand for magnesium, which is the



composite of a number of application segments each with its own demand drivers, has not kept pace with the explosion in production capacity. This paper examines historical and current supply-demand balances and looks at the future trends of the industry. The Global supply base of Magnesium is clearly divided between China and the balance of the world. China accounts for more than 60% of Global production and with China's expansion has come a reduction in historical capacity and technical support. Global demand continues to be fueled by a number of historical market segments including the automotive sector. Diecasting for the automotive industry is the strongest growth segment with new applications expanding magnesium's usage in the Pacific and Europe. Demand drivers suggest that the internal demand for diecast parts in China is likely to explode in the next few years.

9:35 AM

Advances in Manufacturing Processes for Magnesium Alloys: Karl Kainer¹; ¹GKSS Research Centre Geesthacht GmbH, Germany

Magnesium materials as the lightest available construction metal offer a wide range of opportunities for the usage in transportation industries. While magnesium high pressure die cast (HPDC) components have found their application the interest is now spreading to the implementation of gravity casting and advanced casting technology i.e. thixomolding or to the use of wrought materials. The reason is found in the possibility to get even more homogeneous and better properties compared to HPDC parts. Therefore alloy and manufacturing process development on the one hand for cast and on the other for extruded, forged and sheet material is a main concern to enhance the application of recently used or advanced Magnesium alloys. Castings are still form the majority of applications of magnesium alloys, although efforts to develop adequate wrought alloys have increased. In the presentation, the alloy requirements for processing of cast and wrought alloys will be discussed.

10:05 AM

Motivations Driving the Use of Magnesium in Automotive Applications: Mark Verbrugge¹; ¹General Motors Corporation

In the first portion of this talk we address the rational behind lightweighting vehicles, with an emphasis on reducing energy consumption. Insight into why new structural systems must be validated early in the vehicle development process is provided by reflecting on the value of mass de-compounding. Last, we close with a variety of promising applications for Mg in automotive systems.

10:35 AM Break

11:00 AM

Magnesium Research and Development in China: Qi'an Wang¹; Xinmin Zhang¹; *Wenfang Shi*²; ¹Chinese Ministry of Science and Technology; ²China Magnesium Center

Over the last five years, the output of China's primary magnesium and magnesium alloys has been increased from an annual production of 234,000 tons to 642,000 tons. The production scale of the magnesium industry has been increased and there are now more than 10 volume producers with a total production capacity of over 300,000 tons. The energy consumption for magnesium production has dropped 40% compared to that of year 2000. The usage of magnesium and magnesium alloys in China has also been increasing and exceeded 100,000 tons in 2005. The applied technologies have been developed for magnesium. A creep-resistant magnesium alloy has been developed, with a total creep of less than 0.1% for 100 hours a tensile strength of 120 MPa at 175°C. A pilot-scale production line for 600mm-wide and 0.5-10mm-thick magnesium sheets has been set up. Series of micro-arc oxidation equipment and process technologies for aluminum and magnesium alloys have been developed, capable of achieving one-time treatment of 4 m2 in 10 minutes. A total of 10 domestic models of magnesium die casting machines from 160 tons to 3000 tons have been developed, with over 50% of domestic market share. In the next few years, China will continue to renovate the existing silicothermic process to achieve the reduction in energy consumption by 30% and the waste-energy reuse of over 60%.

11:30 AM

Magnesium Materials Development - A Global Overview: *Mihriban Pekguleryuz*¹; ¹McGill University

The use of magnesium as a structural material has had its beginning in the post-World War II era when the physical metallurgy of magnesium was advanced through the works of scientists such as Raynor, Roberts and Busk. Current global effort in the development of magnesium as a modern and effective material for automotive, aerospace and biomedical industries benefits much from this past work. This presentation will focus on the advances in the development of magnesium-based casting and wrought alloys and their current and potential applications in transport and bio industries. It will give an overview of the international scene in magnesium materials development and the future potential of magnesium as a structural material.

Technical Program

12:00 PM

Global Magnesium Diecast Development: *Joe Petrillo*¹; ¹Meridian Technologies Inc., Canada

The demand on the Global automotive manufacturer for increased safety, passenger comfort features, and regulatory compliance is often met at the cost of increased weight and reduced fuel economy. As the lightest metal on the planet, magnesium is a key enabler to reversing the increased weight trends in the global automotive industry. Magnesium die castings enable a structure design that optimizes material usage, consolidates components, and reduces weight at competitive costs to alternative materials. Magnesium strength to weight ratio, and superior material properties combined with high pressure die casting provides a wide array of product applications for the automotive design engineer to choose from. Automotive applications around the globe utilizing magnesium today such as; cross car beams, seat frames, steering column brackets, vehicle front end structures, door closures, engine cradles and power train components are all examples of magnesium die castings providing weight reduction and performance benefits at competitive costs.

12:30 PM Panel Discussion

12:55 PM Concluding Comments by Randy S. Beals, TMS Magnesium Committee Chair

Materials in Clean Power Systems II: Fuel Cells, Solar, and Hydrogen-Based Technologies: Plenary Session

Sponsored by: The Minerals, Metals and Materials Society, ASM International, TMS Structural Materials Division, TMS/ASM: Corrosion and Environmental Effects Committee

Program Organizers: Zhenguo "Gary" Yang, Pacific Northwest National Laboratory; Michael Brady, Oak Ridge National Laboratory; K. Scott Weil, Pacific Northwest National Laboratory; Yong-Ho Sohn, University of Central Florida

Monday AM	Room: Asia 2
February 26, 2007	Location: Dolphin Hotel

Session Chair: K. Scott Weil, Pacific Northwest National Laboratory

9:00 AM Introductory Comments

9:05 AM Plenary

Progress in PEM Fuel Cell Activities: Jason Marcinkoski¹; ¹Department of Energy

The Department of Energy's (DOE's) Hydrogen, Fuel Cells, & Infrastructure Technologies Program (HFCIT) is the lead DOE organization for directing and integrating activities in hydrogen production, delivery, and storage with transportation and stationary fuel cell activities. The Program works in partnership with industry, academia, and national laboratories — and in close coordination with other DOE and federal government programs. The Program strives to overcome technical barriers, address safety concerns and develop model codes and standards, validate critical technologies, and educate key stakeholders. Polymer electrolyte membrane fuel cells (PEMFC) are the current focus for light duty vehicles because they have fast-start capability and operate at low temperatures. For transportation applications in particular, the HFCIT goal is to develop a durable fuel cell system that operates at 60% peak efficiency and costs \$30/kW for a decision to commercialize them by the year 2015.



9:50 AM Plenary

Goals and Progress of the U.S. Department of Energy's National Hydrogen Storage Project: Sunita Satyapal¹; *John Petrovic*²; Carole Read¹; George Thomas³; Grace Ordaz¹; ¹U.S. Department of Energy; ²Los Alamos National Laboratory (retired); ³Sandia National Laboratories (retired)

Storing large amounts of hydrogen on board a hydrogen-powered vehicle while meeting weight, volume, safety, cost, and other performance requirements, is a significant challenge. The U.S. Department of Energy (DOE) has set specific gravimetric, volumetric, cost, and other hydrogen storage system targets, which form the goals of the U.S. National Hydrogen Storage Project, a coordinated R&D program of competitively selected industry, university, and federal laboratory projects. The DOE has established Centers of Excellence in Metal Hydrides, Carbon-based Materials, and Chemical Hydrogen Storage, as well as independent projects on new concepts and materials, storage systems analysis, and hydrogen storage testing. Progress achieved to date will be described and the current status of hydrogen storage systems in relation to the targets will be discussed. Recent international collaborations on hydrogen storage and future plans will also be presented.

10:35 AM Break

10:50 AM Plenary

Advanced Energy Conversion Utilizing Affordable Solid Oxide Fuel Cells: Gary McVay¹; ¹Pacific Northwest National Laboratory

There have been successful high temperature fuel cells for more than fifty years. Some of them work very well and offer the hope of significantly increasing the power produced from existing fossil fuels while lowering the impact on the environment, thus creating a bridge between the hydrocarbon economy and the hydrogen economy. The greatest barrier to utilizing this wonderful energy conversion device is cost. The current cost of \$3,000 plus dollars per kilowatt is to big for most applications. The Solid-state Energy Conversion Alliance (SECA) was created to develop affordable (\$400/kW) high temperature fuel cells with performance and efficiencies suitable for a wide range of applications. This ten year program is half way through and having high degrees of success. The presentation will discuss the concept and development of SECA fuel cells, their development status, and how they fit into DOE's overall strategy for cleanly utilizing fossil fuels. The SECA program is currently the only DOE funded high temperature fuel cell development program, and is an important element to achieving the ultra high efficiency power plant of the future (FutureGen).

11:35 AM Plenary

Present Status of SOFC Development in Japan: Harumi Yokokawa¹; ¹AIST

The R&D activities on Solid Oxide Fuel Cells in Japan have been summarized on the national projects, industrial efforts and university activities. The important feature of fabrication technology in Japan is the success in establishing wet processes by several major developers. On the basis of such technology, NEDO started projects on development of Cogeneration systems ranging 10 to several ten kW(TOTO/Hitachi Manufacturer, Mitsubishi Materials/ Kansai Electric Co, Japan Acumentrics) together with a project focusing on the technological feasibility of SOFC-GT hybrid system (Mitsubishi Heavy Industry). Kyocera has developed their own stacks and cooperated with Osaka gas to test one kW cogeneration system in a real residential circumstance with a great success in a sense that obtained system efficiency(42-48%LHV) is higher than averaged grid efficiency for Fossil Fuel burning Power generators. NEDO also supports the investigations on improving durability of stack/ module, increasing performance/decreasing cost, and extending applicability of SOFCs. Other research topics on developing new electrolytes will be also reported.

Materials Issues for Advanced Nuclear Systems: Energy Generation and Waste Issues

Sponsored by: The Minerals, Metals and Materials Society, TMS Structural Materials Division, TMS/ASM: Corrosion and Environmental Effects Committee, TMS/ASM: Nuclear Materials Committee *Program Organizers:* Raul Rebak, Lawrence Livermore National Laboratory; Robert Hanrahan, Los Alamos National Laboratory; Yi-Ming Pan, Southwest Research Institute

Monday AM	Room: Europe 5
February 26, 2007	Location: Dolphin Hotel

Session Chairs: Yi-Ming Pan, Southwest Research Institute; Raul Rebak, Lawrence Livermore National Laboratory

9:00 AM Introductory Comments

9:05 AM

Novel Methods to Extend Lifetime of Structural Materials in BWR: Young Kim¹; ¹GE Global Research Center

This paper will describe the strategy developed by GE to address the corrosion issues in BWR components and provides a fundamental description of the electrochemical corrosion mechanism and describes various methods for mitigating the risk of stress corrosion cracking of reactor internals and oxide formation and deposition on the surface. These approaches are based on modifying the electrochemical nature of the metal surface, such as by the electrochemical catalysis of noble metals and/or the insulating behavior of dielectric materials to protect reactor parts that tend to degrade in the normal reactor environment and eventually to extend plant life beyond 40 years.

9:25 AM

Mechanical Property Test of Shell Longitudinal Weld after Plastic Deformation and Heat Treatment in the HTR-10 Reactor Pressure Vessel: *Rengang Zhang*¹; Maolong Zhang²; Yongkang Gu²; ¹University of Alabama; ²Shanghai Boiler Works, Ltd.

The 10 MW High Temperature Gas-cooled Test Reactor (HTR-10) is a modular pebble bed type reactor with many inherent safety features. This paper briefly introduces the structure characteristics and main designing technical parameters of the reactor pressure vessel in the HTR-10 system. The welding and rolling procedures for shell longitudinal weld are also introduced. Welding and shaping tests are carried out according to the practical shell shaping procedure. The main mechanical properties are tested for the shell longitudinal weld after plastic deformation and heat treatment. The test results are analyzed and discussed.

9:45 AM

A Zirconium Matrix Cermet for Storage and Transmutation of Transuranic Isotopes Separated from Spent Nuclear Fuel: Sean McDeavitt¹; A. R. Totemeier¹; A. Parkison¹; J. J. Wegener¹; ¹Texas A&M University

The Advance Fuel Cycle program of the U.S. Department of Energy is developing reprocessing technologies to enable sustainable nuclear energy production. The Uranium Extraction (UREX) family of processes use aqueous solvent extraction techniques to partition spent uranium from the radioactive fission products and transuranic isotopes (e.g., Np, Pu, Am and Cm). Processing methods are being developed to translate the TRU bearing solvents into mixed oxides particulates dispersed in a zirconium matrix. These processes include a hydride/dehydride method to recover nuclear grade zirconium from spent fuel cladding, TRU solvent conversion via sol-gel or direct denitration processing, and hot extrusion of the final cermet pin. The final cermet is designed to immobilize TRU isotopes for 50 to 300 years, followed by minor processing and burnup in a fast reactor. The hydride/dehidride process operates at ~500°C and the hot extrusion process operates between 600°C and 1000°C; the process development experiments will be reviewed.





10:05 AM

Mechanical Properties and Microstructure of (Zr, Ti)N Pellets as a Surrogate for (Pu,Zr)N Fuel Pellets: *Kirk Wheeler*¹; Pedro Peralta¹; Manuel Parra¹; Kenneth McClellan²; ¹Arizona State University; ²Los Alamos National Laboratories

In this work, (Zr, Ti)N was studied as a possible surrogate for (Pu, Zr)N under the Advanced Fuel Cycle Initiative program. The microstructure and mechanical properties of sintered (Zr, Ti)N pellets were examined to investigate the effects of sintering temperatures on the structural integrity and sintering kinetics as well as evaluate material segregation during sintering. The microstructure of these pellets was examined using optical and electron microscopy, orientation imaging microscopy and energy dispersive x-ray spectroscopy and compared where applicable to (Pu, Zr)N. Mechanical properties including hardness, fracture toughness and compression strength were measured at room temperature and compared to similarly prepared ZrN pellets. This work should help refine the processing parameters for manufacturing of actinide nitrides suitable for a variety of applications, including transmutation and space fuels as well as help to understand the sintering kinetics of the multi-element transmutation fuel pellets.

10:25 AM Break

10:45 AM

Coupled Multi-Electrode Investigation of Crevice Corrosion of Material Relevant to Nuclear Waste Repository: *Florent Bocher*¹; Francisco Presuel-Moreno²; John Scully¹; ¹University of Virginia; ²Florida Atlantic University

Coupled multi-electrode arrays (MEA) offer the opportunity to study electrochemical phenomenon on a spatiotemporal level. Crevice corrosion displays a wide current density distribution within the crevice due partly to ohmic potential drop. The MEA allows the fragmentation of the crevice into 250 microns diameter measurement sectors. Using such a tool, it is possible to identify the site of crevice corrosion initiation, the morphology and the influence of real conditions such as porous crevice former, proximate cathode or finite cathode. This talk will present results for stainless steel AIS 316 as well as Ni-Cr alloys such as alloy 625 and C-22.

11:05 AM

Effect of Humidity on the Oxidation Kinetics of Sub-Surface Rock Bolt Materials Using Thermogravimetry: *Anjali Talekar*¹; Raja Chellappa¹; Dhanesh Chandra¹; ¹University of Nevada

High Strength Low Alloy Steels are the sought-after materials for use as sub-surface Rock Bolt materials in the Yucca mountain repository. Oxidation studies have been carried out on various rock bolt materials like International Rollforms Split Set Friction Rock Stabilizers, Swellex, etc. and on Alloy 22 (UNS N06022) as the baseline material. Varying relative humidities [RH] from room temperature RH to 100% RH will be used as experimental conditions. The kinetics of oxidation is expected to increase with increased relative humidities and oxygen content. Rates of oxidation and the kinetic parameters like the rate constant and time exponent of rate law will be determined using thermogravimetric analyses; the proposed temperature range of interest being between 500°C to about 1000°C. Isothermal scans are carried out at 75-degree intervals. The oxide species formed will be investigated by using glancing angle X-Ray Diffraction. Microstructure analyses using SEM and EDS will be performed.

11:25 AM

Environmental Effects on Stress Corrosion Cracking of Alloy 22: *Kuang-Tsan Chiang*¹; Osvaldo Pensado¹; Pavan Shukla¹; Yi-Ming Pan¹; ¹Southwest Research Institute

Alloy 22 is the candidate material for the waste package outer container for permanent disposal of high-level radioactive waste at the potential repository in Yucca Mountain, Nevada. Slow strain rate tests revealed that bicarbonate and chloride ions, two common constituents of groundwater, act synergistically to promote transgranular stress corrosion cracking of mill-annealed Alloy 22. Chloride solutions capable of sustaining stress corrosion cracking of Alloy 22 require sufficient bicarbonate and carbonate concentrations and high corrosion potentials for transgranular crack initiation. However, high corrosion potentials can only be developed in low-pH solutions where bicarbonate and carbonate ions are not stable. Monte Carlo analyses indicate a low probability for the establishment of environmental conditions capable of sustaining stress

corrosion cracking of Alloy 22. This paper is an independent product of the CNWRA and does not necessarily reflect the view or regulatory position of the Nuclear Regulatory Commission.

11:45 AM

Evaluation of Corrosion Resistance of AKOT and Ti Grade 7 for Drip Shield in Yucca Mountain Project: *Shinji Sakashita*¹; Tomoaki Nakanishi¹; Takashi Yashiki¹; Takenori Nakayama¹; Tiangan Lian²; ¹Kobe Steel, Ltd.; ²Lawrence Livermore National Laboratory

In order to study corrosion resistance of Ti-0.4Ni-0.015Pd-0.03Ru-0.15Cr alloy (AKOT) and Ti grade 7 (Gr 7) in a Yucca Mountain high-level nuclear waste repository, the general corrosion rate, the passive behavior, and the crevice corrosion properties in a solution including Cl- and F- were evaluated by electrochemical corrosion tests. The corrosion rate of AKOT in a pH 8 solution was very small at either fluorine concentration, and it was under the measuring limit of 0.03 mm/y. The corrosion rate in the pH4 solution was very small in the region under 0.001 M [F-], but in the region over 0.001M [F-] the corrosion rate increased as the fluorine concentration increased. The electrochemical test results showed that AKOT and Gr 7 have a similar corrosion resistance under the tested conditions.

12:05 PM

Resistance of Amorphous Metal Coatings to Impact Damage: *Jeffery Haslam*¹; Joseph Farmer¹; Louis Aprigliano²; ¹Lawrence Livermore National Laboratory; ²Consultant

Amorphous metallic glass coatings deposited by thermal spray are being considered for corrosion resistant coating applications with the aim of providing a conformal, lower cost alternative to bulk, corrosion-resistant materials. The High Performance Corrosion Resistant Materials (HPCRM) program is developing some corrosion resistant amorphous metal coatings which are deposited by High Velocity Oxy-Fuel (HVOF) thermal spray techniques. While the corrosion resistance of these materials has many favorable attributes, in some applications the performance must be maintained after significant mechanical deformation of the coating and in some cases deformation of the substrate. To this end, evaluation of the mechanical and corrosion resistance of the amorphous metal coatings subsequent to localized deformation and impact loading will be performed to assess the changes in corrosion resistance following these extreme loading conditions. Deformation features of interest include shear bands which can be localized aberrations in the microstructure.

12:25 PM

Salt Fog Testing of Iron-Based Amorphous Alloys: *Raul Rebak*¹; Louis Aprigliano²; S. Day¹; Jeffery Haslam¹; Joseph Farmer¹; ¹Lawrence Livermore National Laboratory; ²Strategic Analysis Inc.

Iron-based amorphous metallic alloys have been developed to be applied as sprayed coatings on engineered structures for corrosion and wear mitigation. These materials rely on Cr, Mo and W for enhanced corrosion resistance, while B is added to promote glass formation and Y is added to lower the critical cooling rate. These alloys are known as the High-Performance Corrosion-Resistant Material – Structural Amorphous Metal (HPCRM-SAM). The amorphous alloys have in general an outstanding resistance to localized corrosion in concentrated hot chloride brines. It was of interest to determine their corrosion behavior in the salt fog test (ASTM B 117). Engineering alloys coated with amorphous metals have been exposed to several cycles of salt fog tests in parallel with witness materials such as Alloy 22 (N06022) and plain carbon steel 1018.



Materials Processing and Manufacturing Division Symposium: Mechanics and Materials Modeling and Materials Design Methodologies, in the Honor of Dr. Craig Hartley's 40 Years of Contributions to the Field of Mechanics and Materials Science: Microstructure Analysis and Representation I

Sponsored by: The Minerals, Metals and Materials Society, TMS Materials Processing and Manufacturing Division, TMS: Shaping and Forming Committee, TMS/ASM: Mechanical Behavior of Materials Committee *Program Organizers:* Brent Adams, Brigham Young University; Hamid Garmestani, Georgia Institute of Technology

Monday AM Room: Northern A1 February 26, 2007 Location: Dolphin Hotel

Session Chairs: Dennis Dimiduk, US Air Force; Gregory Rohrer, Carnegie Mellon University

9:00 AM

A Framework for Automated 3D Microstructural Analysis and Representation: *Michael Groeber*¹; Michael Uchic²; Dennis Dimiduk²; Yash Bhandari¹; Somnath Ghosh¹; ¹Ohio State University; ²Air Force Research Laboratory-MLLMD

Recently, significant advances in serial-sectioning have provided quantitative data describing the structure and crystallography of microstructures in 3D. The analysis and representation of this information can provide modeling efforts with a highly-refined and unbiased characterization of microstructure. The grain structure could be characterized and then translated directly into a 3D volume mesh for Finite Element Analysis. However, this approach requires a multitude of data sets to appropriately sample the heterogeneity observed in typical microstructures. One way to circumvent this issue is to develop computation tools that create synthetic microstructures that are statistically-equivalent. This study will discuss the development of programs that take a series of EBSD maps from a serial-sectioning experiment, and output a robust statistical analysis in 3D, as well as generate a host of synthetic structures. Importantly, the objective of this study is to provide a framework towards complete microstructure representation consistent with experimental data.

9:25 AM

Bcc Screw Dislocations: A Case Study in the Application of the Nye Tensor to Computer Simulations of Crystal Defects: *Budhika Mendis*¹; Yuri Mishin²; Craig Hartley³; Kevin Hemker¹; ¹Johns Hopkins University; ²George Mason University; ³Air Force Office of Scientific Research

The core structure of 1/2<111> screw dislocations and its effect on the mechanical properties of bcc metals has been explored extensively with computer simulations for nearly 50 years. These dislocations present a unique challenge in visualization of the core structure since the atomic displacements giving rise to non-Schmid effects are only of the order of a few picometers. J. F. Nye first introduced the Nye tensor to characterize the infinitesimal dislocation density at a given point in a crystal. Hartley and Mishin later showed how the Nye tensor could be used to visualize computer simulated defects. We apply these methods to Mo and other bcc metal screw dislocation cores and calculate the strength of the edge fractional dislocations for the first time. The technique can also be used in a number of other simulations, such as visualization of the dynamic change in dislocation core structure during glide.

9:50 AM

Microstructure and Processing Path Design Using Statistical Correlation Functions: Hamid Garmestani¹; ¹Georgia Institute of Technology

A methodology for microstructure design is developed and applied to multi-phase microstructures using statistical continuum mechanics theory linking mechanical, magnetic, and transport properties to microstructures represented by statistical correlation functions. Texture and composite volume fractions are considered as one-point functions and grain boundary character distribution and particle to particle and the effect of precipitates can be introduced using pair correlation functions and higher order statistics. In this work, homogenization techniques based on statistical continuum mechanics are used to calculate effective properties on the knowledge of the N-point Distribution Functions Two-point correlation functions are measured using both microscopy (Transmission Electron) and scattering techniques. The use of scattering techniques can provide 3-dimensional information on two-point statistics; whereas, in the case of microscopy, such information can only be obtained through the tedious task of serial sectioning. Scattering data (as opposed to imaging techniques) suffers from the basic disadvantage in that it does not provide a micrograph from the microstructure. A methodology for microstructure reconstruction has been reevaluated and optimized to provide an image from the two-point correlation functions.

10:15 AM

Computer Simulations of Realistic Microstructures of Boron Modified Titanium Alloys with Variable TiB Whisker Orientations: *Harpreet Singh*¹; Arun Gokhale¹; Arun Sreeranganathan¹; Scott Lieberman¹; Sesh Tamirisakandala²; 'Georgia Institute of Technology; ²Ohio University

A methodology for computer simulations of realistic microstructures that incorporates realistic complex particle morphologies/shapes and realistic distributions of particles has been presented earlier, where the particles were not allowed to rotate. In this contribution we study the rotation of TiB whiskers in boron modified titanium alloys. TiB whiskers can align themselves in varying directions depending upon the processing parameters such as the extent of extrusion and temperature. We present a technique via which we can simulate microstructures with different degrees of particle orientations. A relationship between particle orientations and processing parameters is established. The differences in mechanical response for these simulated microstructures are studied using FEM analysis.

10:40 AM

Examination of Lattice Rotations in Deformed Ni Microcrystals: Dennis Dimiduk¹; Michael Uchic¹; Paul Shade²; Dave Norfleet²; Michael Mills²; Amit Acharya³; ¹US Air Force; ²Ohio State University; ³Carnegie Mellon University

Strain-gradient-plasticity frequently relies on ad hoc assumptions about a "material length scale" tied to the evolution of dislocation substructure. Recently, one of the authors introduced a field theory for plasticity that escapes those ad hoc assumptions. The theory suggests that specific "microscopic ingredients" from the dislocation structure should be determined for setting levels of discretization and coarse graining. Also, some of the present authors devised a method for preparing and testing micrometer-scale single crystals. Using that method, microcrystals of pure Ni were deformed to different shear-strain levels, in Stages I and II. In order to understand the scale over which gradients evolve and to access the necessary microscopic ingredients, samples were examined in cross-section. The studies probed the specimens for development of spatially heterogeneous lattice rotations at the submicron scale via diffraction methods. The findings from these experiments will be reported within the context of the field theory for plasticity.

11:05 AM

Quantitative Characterization of Microstructural Changes Using Microstructural Anisotropy Tensor: *Ning Ma*¹; Craig Hartley²; Yunzhi Wang¹; 'Ohio State University; 'El Arroyo Enterprises LLC

In this presentation, we demonstrate that the spatial distribution of a 3D grain boundary network can be described quantitatively by the coefficients of a Microstructural Anisotropy Tensor (MAT). The developed MAT provides means of following microstructural evolution and calculating spatial distribution of strains associated with the microstructure with changes in thermo-mechanical state of materials. The 3D grain boundary data were obtained from phase field modeling technique that accounts for inclination dependent grain boundary properties. In particular, we have adopted a novel sparse data structure in the phase field simulations to avoid grain coalescence. It was shown that the measured interception density (reciprocal of mean-linear intercept length) along different directions can be well characterized by MAT for grain growth with both isotropic and anisotropic grain boundary properties.

Technical Program



11:30 AM

Techniques for Characterizing the Crystallography of Interface Planes in Polycrystals and Composites: Gregory Rohrer¹; ¹Carnegie Mellon University

Grain boundary networks within polycrystalline materials are structurally complex. Five independent parameters are required to distinguish one grain boundary from another and the different types of grain boundaries are connected in non-random configurations. While techniques for characterizing the distributions of lattice misorientations are relatively well established, techniques for measuring the distribution of grain boundary plane orientations are relatively new and still evolving. Mechanical serial sectioning, stereology, and serial sectioning in the dual beam focused ion beam SEM can all be used for this purpose. In this talk, the merits and shortcomings of these techniques will be reviewed and recent results of grain boundary plane distributions in metals and ceramics will be reviewed.

11:55 AM

Computational Modeling of Microcrack Nucleation Using a Physically Based Finite Element Crystal Plasticity Model of Experimentally Characterized Microstructures: *Thomas Bieler*¹; Martin Crimp¹; Anxian Ma²; Franz Roters²; Dierk Raabe²; ¹Michigan State University; ²Max Planck Institut fur Eisenforschung

The mechanical response of engineering materials evaluated through continuum fracture mechanics typically assumes that a crack/flaw initially exists. How such flaws originate in an otherwise flawless material, particularly at grain (or phase) boundaries is less clear. Experimentally, "good" vs. "bad" grain boundaries are often invoked as the reasons for critical damage nucleation. A fracture initiation parameter was developed for a limited ductility model material with limited slip systems. This parameter provides a new definition of grain boundary character is based upon operating slip systems (rather than an interfacial energy based definition). This provides a way to predict damage nucleation density on a physical (rather than a statistical) basis. Fracture initiation parameters have been introduced into a physically based crystal plasticity finite element user-defined subroutine that models strain gradients on the basis of evolving dislocation density, and used to simulate experimentally characterized microstructural regions that have exhibited microcracks.

Materials Processing Fundamentals: Solidification and Deformation Processing

Sponsored by: The Minerals, Metals and Materials Society, TMS Extraction and Processing Division, TMS: Process Technology and Modeling Committee, TMS: EMPMD Council, TMS: EPD Council *Program Organizer:* Princewill Anyalebechi, Grand Valley State University

Monday AM	Room: Northern A2
February 26, 2007	Location: Dolphin Hotel

Session Chair: Prince Anyalebechi, Grand Valley State University

9:00 AM

Effect of Thermomechanical Processing Parameters on Bake Hardening Ability of Hot Rolled Dual Phase (DP) Steels: Heinz Palkowski¹; Mohamed Soliman¹; *Goran Kugler*¹; ¹Technische Universität Clausthal, Institut für Metallurgie (IMET)

In recent years, the increased demand for DP steels has been mainly driven by the need of automotive industry to reduce the weight of the cars and to improve their safety. These steels are characterized by good ductility, continuous yielding, high strength and strong bake hardening effect. It is known that varying the process parameters during hot rolling has a significant influence on the properties of the steel. However, the study of the effect of those parameters on bake hardening has not been sufficiently available in the literature. Therefore, the aim of this work is to investigate the effect of hot rolling parameters on bake hardening ability of DP steels. For this purpose different thermomechanical paths have been applied to simulate the finishing steps of hot rolling process using a thermomechanical simulator. The increase in the strength due to the bake hardening has been determined for different thermomechanical schedules employed.

9:15 AM

Deformation Behavior of Hot Rolled Ferrite-Bainite Dual Phase Steels: *A. Saha Podder*¹; R. Ray¹; ¹Tata Steel

The present paper deals with the study on and correlations obtained between the microstructure, mechanical properties and deformation behavior of four hot rolled ferrite-bainite dual phase steels containing 2-6% of martensite phase. These dual phase steel contain substantial amounts of bainite (47 to 74%) and can achieve high mechanical strength coupled with adequate ductility. The deformation behavior of these ferrite-bainite steels have been studied under tensile deformation. TEM observations show a distribution of bainite plates in a high strain region exhibiting an elongated nature; a few plates are in a ruptured condition, presumably as a result of high tensile stress. The fracture of the ferrite-bainite dual phase steels mainly occurs by decohesion at phase interfaces, cracking of the second phase particles or by the formation of microvoids around inclusions and their coalescence.

9:30 AM

Comparative Analysis of Microhardness in Directional Solidified Zn-27wt%Al, Zn-27Wwt%Al + CSi and Zn-27Wwt%Al + Al2O3 Alloys and Composites: Alicia Ares¹; *Carlos Schvezov*²; ¹CONICET/FCEQyN-University of Misiones; ²FCEQyN-University of Misiones

ZA castings are competing with cast iron, bronze and aluminum because of various property and processing advantages. One particular alloy such as the ZA27 (Zn-27wt%Al) has a higher yield stress than other zinc alloys and better friction properties than brass at low velocities and dry contact between materials. The main objective of this paper is to analyze microhardness variations as a function of both sample length and sample width of Zn-27wt%Al, Zn-27wt%Al + CSi, Zn-27wt%Al + Al2O3 directionally solidified which present columnar, equiaxed and columnar to equiaxed transition structures. Also, to analyze microhardness variations as a function of type of composite produced. We noticed that the microhardness values decrease when the load increase and reach almost constant values at higher loads. The results in directionally solidified alloys and composites are compared with those in bulk alloys. We observed that bulk alloys have greater microhardness values than those directionally solidified.

9:45 AM

Undulatory Solid Shell Growth of Aluminum Alloy 3003 as a Function of the Wavelength of a Grooved Mold Surface Topography: *Princewill Anyalebechi*¹; ¹Grand Valley State University

The effects of the wavelength of a grooved mold surface topography and casting speed on the early stages of solidification of aluminum alloy 3003 have been experimentally studied. This involved the controlled production of cast shells of AA3003 alloy with an immersion tester and instrumented grooved copper molds. The grooves were 0.232 mm deep with wavelength or spacing between 1 mm and 15 mm. Castings produced with ungrooved mold surface topography and with grooves of 3 mm to 15 mm wavelength exhibited macroscopic undulatory shell growth front. The propensity for undulatory shell growth also increased with increase in casting speed. There was an apparent relationship between the macro-morphological features (depressions and humps) of the undulatory shell and subsurface microstructure. Undulatory shell growth is provisionally attributed to the irregular thermomechanical distortion of the solidifying shell engendered by spatial variations in the heat extraction profile along the mold-shell interface during solidification.

10:00 AM

Ungrooved Mold Surface Topography Effects on Cast Subsurface Microstructure: *Princewill Anyalebechi*¹; ¹Grand Valley State University

An immersion casting tester has been used to investigate the effects of different types of ungrooved copper mold surface topographies on cast subsurface microstructure of aluminum alloy 3003. The ungrooved mold surface topographies studied included smooth (untextured), spark roughened, shot-peened, and alligator. Of the four mold surface topographies investigated shells produced with the shot-peened mold surface topography exhibited the most uniform shell growth front. However, for all of the mold surface topographies, the propensity for undulatory shell growth front increased with increase in casting speed. Shot-peening of the mold surface also obviated lap formation on the as-cast ingot surface.



10:15 AM

Influence of Process Parameters on the Phase Transformation and Consequent Hardness Induced by the LENSTM Process: Liang Wang¹; Sergio Felicelli²; ¹Center for Advanced Vehicular Systems, Mississippi State University; ²Mechanical Engineering, Mississippi State University

A three-dimensional finite element model was developed to predict the temperature distribution and phase transformation in deposited stainless steel 410 (SS410) during the LENS[™] (Laser Engineered Net Shaping) rapid fabrication process. The development of the model was carried out using the SYSWELD software package. The model calculates the evolution of temperature and cooling rates in the part during the fabrication of a SS410 plate. The metallurgical transformations are taken into account using the temperature dependent material properties and the continuous cooling transformation diagram. The ferritic and martensitic transformation, as well as austenitization and tempering of martensite are considered. The final hardness is predicted from the thermal and metallurgical history of the part. The influence of process parameters like laser power, travel speed and substrate preheat on the phase transformation and the consequent hardness are analyzed and the calculated results are compared with experimental data.

10:30 AM Break

10:45 AM

Early Stages of Solidification of Aluminum Alloy 3003 and Attendant Subsurface Microstructure as a Function of Mold Material: *Princewill Anyalebechi*¹; ¹Grand Valley State University

The combined effects of mold material and casting speed on the early stages of solidification of aluminum alloy 3003 and attendant subsurface microstructure have been investigated. Instrumented pure copper, aluminum alloy 6061, and graphite molds and an immersion tester were used to make castings at different casting speeds. The surface topography of each mold was as-machined. Solidified shells produced with pure copper and aluminum alloy molds exhibited undulatory growth front and laps on the mold-casting interface. In contrast, the solid shells produced with the graphite were comparatively more uniform. However, this did not translate into freedom from subsurface segregation. Like those produced with the copper and aluminum molds, shells produced with the graphite mold contained unacceptable levels of subsurface segregation. These results suggest that the subsurface segregation on as-cast aluminum alloy ingots and slabs are caused by two different remelting-induced mechanisms.

11:00 AM

Study on Aluminum Foam with Fly Ash Increase Viscosity: Wang Yong¹; Yao Guang-chun¹; Li Bing¹; 'Northeastern University

Foam melting is to add foaming agent into melting metal, stirring and heating metal, the foaming agent decomposes at the melting temperature of aluminium, releases gas and blows up the melt. In this work, fly ash was selected as viscosity increaser in melt-foaming process. The most component are quartz and mullite was observed by XRD in the fly ash, therefore it's a kind of hardness ceramic particles. In order to improve the wetting between fly ash and aluminium, we use a small quantity of Si and Ca to debase surface tension of aluminium, to make fly ash add into molten aluminium easier. Through compression strength test, the effect of energy absorption of aluminium foam with similar aperture is in direct proportion to its density.

11:15 AM

Enhanced Hardenability Dual-Phase Steels and the Limitations Imposed by Subsequent Continuous Hot-Dip Galvanizing: *Richard Meguerian*¹; Joseph McDermid¹; ¹McMaster University

One method of increasing the hardenability and strength of advanced high strength steels (AHSS), specifically dual-phase (DP) steels, is the addition of austenite stabilizers such as Mn. However, due to the tendency of Mn to form external oxides which are seen as detrimental to subsequent reactive wetting during continuous metallic coating processes - high-Mn alloys have not found significant use in automotive applications. This study aims to examine the effect of annealing parameters (time, temperature, oxygen potential) on the wettability of several high-Mn DP steels to determine a practical limit, if any, on the Mn content of these alloys which can be continuously galvanized. The kinetics of reactive wetting will be investigated as a function of composition and annealing parameters by measuring the surface tension between the annealed substrate and galvanizing bath over time.

11:30 AM

Analysis of Defects Produced during Preparation of Pure Al Matrix Foam: Li Bing¹; Yao Guang-chun¹; Wang Yong¹; ¹Northeastern University of China

The formation causes of three kinds of defects, bubble-free layer, crack and cavity during preparation of pure Al matrix foam by foaming in melt were analyzed. Controlling the melt's viscosity and cooling from bottom were introduced to reduce the thickness of bubble-free layer, although Bubble-free layer can't be eliminated during preparation of Al foam. "Foamability" was introduced, it found that crack and cavity can be avoided by control the melt's foamability.

11:45 AM

Influence of Metallic Ca on the Viscidity of Closed-Cell Aluminum Foam: *Guojun Yang*¹; Haijun Yu¹; Guangchun Yao¹; ¹Northestern University

The mechanism of the metallic Ca to increase the viscidity of molten aluminum and the effect of different amounts of metallic Ca on the porosity of closed-cell aluminum foam were studied. It is found that there are two main intermetallic compounds (CaAl4 and CaAl2) after adding metallic Ca. The two intermetallic compounds disperse into the molten aluminum. Due to the melting point of CaAl4(697°C) is higher than the testing temperature(680°C) of preparing aluminum foam, CaAl4 existing as semi-molten, the viscidity of molten aluminum is increased. The test further approves that the effect of different amounts of metallic Ca on the porosity of closed-cell aluminum foam is obvious. The porosity of closed-cell aluminum foam is highest when the quantity of metallic Ca is about 2.5%.

12:00 PM

Study on Production of Aluminum Foam by Recycling of Scrap Aluminum: Wang Yong¹; Yao Gang-chun¹; Li Bing¹; ¹Northeastern University

In this work, we use scrap aluminium to prepare aluminium foam. By mixing up the remelting scrap aluminium foam with aluminium alloy to a certain scale, adjusting viscosity, stirring, then foaming and cooling, the aluminium foam with uniform foam structure can be obtained. Density is about 0.4g/cm3, porosity is in the range 85-90% and the cell diameter is from 4 to 7 mm. The principle of remelting scrap aluminium foam increases viscosity has been discussed. Observed by SEM, solid oxide particles in the melt and particles external aid are act on the function of viscosity increaser, allowing them to retain the remaining liquid within the cell wall and hence delay rupture. In addition, recycling of scrap aluminium foam has a certain enlighten meaning about reducing the production costs and decreasing environmental pollution.

Materials Processing under the Influence of External Fields: Session I

Sponsored by: The Minerals, Metals and Materials Society, TMS: Aluminum Committee, TMS: Magnesium Committee, TMS: Solidification Committee *Program Organizers:* Qingyou Han, Oak Ridge National Laboratory; Gerard Ludtka, Oak Ridge National Laboratory; Qijie Zhai, Shanghai University

Monday AM	Room: America's Seminar
February 26, 2007	Location: Dolphin Hotel

Session Chairs: Gerard Ludtka, Oak Ridge National Laboratory; Dmitri Molodov, Rwth Aacken University

9:00 AM Introductory Comments

9:05 AM Invited

Time-Resolved Analyses of Microstructure in Advanced Materials under High Magnetic Fields at Elevated Temperature Using Neutrons: *Gerard Ludtka*¹; Frank Klose¹; Roger Kisner¹; Jaime Fernandez-Baca¹; Gail Mackiewicz-Ludtka¹; John Wilgen¹; Roger Jaramillo¹; Louis Santodonato¹; Xun-Li Wang¹; Camden Hubbard¹; Fei Tang¹; ¹Oak Ridge National Laboratory

Fundamental science breakthroughs are being facilitated by high magnetic field studies in a broad spectrum of research disciplines. However, currently there does not exist the capability to do in-situ time-resolved quantitative analyses at high magnetic field strengths at elevated temperatures. Therefore most measurements are performed ex situ and do not capture the microstructural

LEARN • NETWORK • ADVANCE



Technical Program



evolution of the samples during high field exposure. To address this deficiency, we are developing high field magnet processing and analyses systems at the High Flux Isotope Reactor and the Spallation Neutron Source at the Oak Ridge National Laboratory which will link the analytical capabilities inherent in neutron science to the needs of magnetic processing research. Our goal is to apply advanced neutron scattering techniques to explore time-resolved characterizations of magnetically driven alloy phase transformations under transient conditions. This presentation will discuss the current status of this research endeavor with preliminary results obtained on ferrous alloys.

9:35 AM

Isothermal Phase Transformation Cycling in Steel by Application of a High Magnetic Field: Gerard Ludtka1; Roger Jaramillo1; Roger Kisner1; John Wilgen1; Gail Mackiewicz-Ludtka1; Peter Kalu2; 1Oak Ridge National Laboratory; ²Florida Agricultural and Mechanical University-Florida State University, College of Engineering and National High Magnetic Field Laboratory

A phase transformation reversal via the application and removal of a large magnetic field was investigated. Because a large magnetic field can alter the phase equilibrium between paramagnetic austenite and ferromagnetic ferrite, volume fractions for each phase constituent can be modified at constant temperature by changing the magnetic field strength. In this research elevated temperature isothermal hold experiments were performed for 5160 steel. During the isothermal hold, the magnetic field was cycled between 0 and 30 Tesla. As companion experiments, temperature cycling and isothermal holds were performed without magnetic fields. The resulting microstructures were examined using optical and SEM metallography. These microstructures indicate that a portion of the microstructure experiences isothermal transformation cycling between austenite and ferrite due to the application and removal of the 30T (Tesla) magnetic field.

10:00 AM

Influence of Strong Static Magnetic Field on the Phase Solution and Grain Growth in Cast AZ91 Magnesium Alloy during Homogenization Heat Treatment: Zhifeng Li¹; Jie Dong¹; Xiaoqing Zeng¹; Wenjiang Ding¹; ¹Shanghai Jiaotong University

5T and 10T static magnetic field was applied in the homogenization heat treatment process of AZ91 cast alloy at 420°. Quantitative optical metellurgraphy was used to investigate the influence of static magnetic on the solution rate of divorced Mg₁₇Al₁₂ eutectics at the grain boundary and the grain growth during homogenization heat treatment. It was found that the solution rate of Mg17Al12 decreased with the increasing of magnetic field strength. This effect may results from the magnetic field induced diffusion retardation. Meanwhile, grains of the AZ91 cast were found to grow with the elongation of homogenization time. With the application of the static magnetic field, the grain growth rate became smaller.

10:25 AM

Effect of Magnetic Field and Changes in Atomic Environment on the Spin Density and Energy during Diffusion: Donald Nicholson1; 1Oak Ridge National Laboratory

It is known that the activation energy for diffusion changes at the Currie temperature1 but the role played by the volume change and spin order in not understood. We have found by first principles calculation that significant changes in local magnetization occur along the vacancy diffusion path in Fe, FeCo, and FeH at low temperatures. This change together with moment changes in constrained non-collinear magnetic configurations employed to model the paramagnetic phase will be used as a basis for discussed of the change in diffusion at the Currie temperature and the effect of high magnetic fields on diffusion barriers below the Currie temperature. 1Y. Iijima, K.Kimura, and K. Hirano, Acta Metall. 36 2811 (1988). This work sponsored by DOE-OS through the Office of Basic Energy Sciences (BES) was performed at Oak Ridge National Laboratory which is managed by UT-Battelle, LLC under Contract No. De-AC05-00OR22725.

10:50 AM Break

11:00 AM Invited

Solid State Materials Processing in a High Magnetic Field: Hideyuki Ohtsuka1; 1NIMS

The effects of a high magnetic field on phase transformation temperature,

11:30 AM Invited

martensite.

Impact of Magnetic Field on Recrystallization and Grain Growth in Non-Ferromagnetic Metals: Dmitri Molodov1; 1RWTH Aachen University

The current research on texture and grain structure evolution during recrystallization and grain growth in non-magnetic metals in high magnetic fields will be reviewed. The microstructure evolution during grain growth in magnetically anisotropic materials can be affected by a magnetic field due to an additional driving force for grain boundary motion which arises from a difference in magnetic free energy density between differently oriented grains. As it is demonstrated on polycrystalline zinc, titanium and zirconium, the crystallographic texture in magnetically anisotropic non-magnetic materials can be effectively changed and controlled by means of annealing in a magnetic field. However, the magnetic effect is not only confined to magnetically anisotropic metals, but can also be observed in a material with magnetically isotropic properties. It is experimentally shown that the application of a magnetic field substantially enhances recrystallization in cold rolled commercial aluminum alloy.

12:00 PM

Application of Pulsed Magnetic Field Treatment for Residual Stress Reduction of a Welded Structure: Cai Zhipeng1; Lin Jian1; Zhao Haiyan1; Wang Mingdao2; 1Tsinghua University; 2Jing-Tai Technology Ltd. Company

Reduction of residual stress caused by pulsed magnetic field treatment is attractive since the processing is carried out at room temperature and does not produce additional deformations. Based on the effects of magnetic filed orientation and magnetic field intensity on stress relief, the residual stress reduction of a welded structure due to a particular pulsed magnetic field treatment was determined. Initially the direction of the maximum stress was investigated through change of magnetic susceptibility and the pulsed magnetic field orientation could be determined. To specify the current for the proper magnetic filed intensity, finite element method was used for the real structure. Change of residual stress was measured by hole-drilling method. By the particular treating process, reductions of residual stress of nearly 40% were obtained and this result is meaningful to apply pulsed magnetic filed treatment on other similar structures.

12:25 PM

Retained Austenite in SAE 52100 Steel Post Magnetic Processing and Heat Treatment: Nathaniel Pappas1; Thomas Watkins2; O. Burl Cavin2; Gerard Ludtka2; Roger Jaramillo2; 1Department of Energy Pre-Service Teacher Intern at Oak Ridge National Laboratory; 2Oak Ridge National Laboratory

The application of magnetic fields as a method of reducing retained austenite in steel is based on the thermodynamic argument that paramagnetic austenite is destabilized in the presence of a large magnetic field. The goal of this study was to determine the effect of applying a magnetic field on the amount of retained austenite present at room temperature after quenching. Samples of SAE 52100 steel were heat treated then subjected to a magnetic field of varying strength and time after several post-quench delay times. X-ray diffraction results will be presented detailing the amounts of retained austenite present post processing. Stronger field strengths resulted in lower percentages of retained austenite for fixed hold times. When applying a magnetic field after a post-quench delay time, the analyses indicate that decreased delay times result in less retained austenite, indicating that retained austenite becomes more stable with time after quenching.



Microstructural Processes in Irradiated Materials: Dislocation - Obstacle Interactions and Radiation Induced Segregation

Sponsored by: The Minerals, Metals and Materials Society, TMS Structural Materials Division, TMS/ASM: Nuclear Materials Committee *Program Organizers:* Charlotte Becquart, University of Lille; Gary Was, University of Michigan; Brian Wirth, University of California

Monday AM	Room: Europe 8
February 26, 2007	Location: Dolphin Hotel

Session Chairs: Roger Stoller, Oak Ridge National Laboratory; Rick Kurtz, Pacific Northwest National Laboratory

9:00 AM Invited

Dislocation Interactions with Irradiation Produced Defects: *In Situ* **TEM Deformation Study**: *I. M. Robertson*¹; M. Briceno¹; B. Clark¹; J. Fenske¹; B. Wirth²; ¹University of Illinois; ²University of California, Berkeley

Predicting the mechanical properties of materials exposed to extreme conditions depends on the underlying physical processes that form the foundation of the model. Current models capture only basic trends and fail to predict details. In the simplest cases, this shortcoming is attributable to the methods used to "average" responses to make the models tractable. Through better understanding of dislocation–obstacle interactions, physically-based models that have the potential to predict the mechanical response can be developed. In this presentation, the temperature dependence of dislocation interactions with loops, voids, helium bubbles, and precipitates as determined through dynamic in situ and static ex situ TEM studies will be described. Further insight to these interactions is obtained through molecular dynamics computer simulations for specific cases and these results will be compared to experimental observations. Lastly, we will demonstrate how this type of information can be used to formulate accurate descriptions of the constitutive laws.

9:35 AM

Atomic-Scale Plasticity in Presence of Frank Loops: David Rodney¹; Thomas Nogaret¹; Christian Robertson²; ¹GPM2-ENS de Physique Grenoble; ²SRMA-CEA Saclay

The reactions between dislocations and interstitial Frank loops are studied by Molecular Dynamics. The calculations are performed at 600K using an EAM potential describing a model FCC material with a low Stacking Fault Energy. An interaction matrix providing interaction strengths is determined. In an attempt to investigate the role of pile-ups, simulations with one or two dislocations are performed. We find that screw and edge dislocations behave differently. Edge dislocations shear Frank loops, while screw dislocations unfault Frank loops by mechanisms that involve cross-slip. After unfaulting, they are strongly pinned by the formation of helical turns. The simulations show an original unpinning effect that involves the junction of two screw dislocations around a helical turn and the transfer of a dislocation from its initial glide plane to an upper glide plane. From these observations, we propose a new scenario for clear band formation that is consistent with TEM observations.

9:55 AM

In-Situ TEM Observation of ODS EUROFER97 and Its Relation to Mechanical Properties: *Amuthan Ramar*¹; Raul Bonade¹; Phillipe Spätig¹; Robin Schäublin¹; ¹Ecole Polytechnique Fédérale de Lausanne (EPFL), Center for Research in Plasma Physics, Association Euratom-Confédération Suisse

Oxide dispersion in Ferritic/Martensitic EUROFER97 steel seems to be an efficient approach to improve strength. Oxide dispersion strengthened (ODS) steel shows good strength up to 600°C and further degrades with increase in temperature. To understand the origin in the microstructure of this drop in strength, in-situ heating experiment in TEM is performed from room temperature to 1000°C. Upon heating, neither microstructure changes nor dislocation movement is observed up to 600°C. Movement of dislocations are observed above 680°C. Phase transformation to austenite starts at 840°C. Dislocation density decreases above 900°C. Yttria particles remains unchanged up to 1000°C. Changes in mechanical properties thus does not relate to changes in yttria dispersion. It is attempted to relate these observations to the thermal activation parameters measured by the technique of repeated stress relaxations, which would allow identifying at a mesoscopic scale the microstructural mechanisms responsible for the degradation of ODS steel with temperature.

10:15 AM

Atomic-Scale Modeling of Dislocation Dynamics in Environment of Radiation Defects: Yury Osetskiy¹; David Bacon²; ¹Oak Ridge National Laboratory; ²University of Liverpool

Dynamics of dislocations in realistic environment of existing microstructure defines mechanical properties of crystalline materials. Long-range interactions between a moving dislocation and other defects can be treated within a continuum approach via interaction of their stress and strain fields. However, a vast contribution to mechanical properties depends on the direct interaction between dislocation and other defects and depends very much on the particular atomic-scale structure of the both moving dislocation core and obstacle. In this work we review recent progress in large-scale modeling of dislocation dynamics in metals at atomic level by molecular dynamics of dislocations in different lattice structures, results on temperature, strain rate and obstacle size dependences. Examples are given for bcc, fcc and hcp metals were edge and screw dislocations were interacting with vacancy (loops, voids, stacking fault tetrahedra, etc), self-interstitial clusters and secondary phase precipitates.

10:35 AM Break

10:55 AM Invited

Radiation-Induced Segregation in Advanced Reactor Structural Materials: Jeremy Busby¹; ¹Oak Ridge National Laboratory

Radiation-induced solute segregation (RIS) refers to the redistribution of elements (solute or interstitial impurities) under irradiation which can result in enrichment or depletion of that element at defect sinks such as grain boundaries. RIS has been examined for decades in structural materials for applications such as light water reactors where stainless steels experience Cr depletion, which, can impact corrosion resistance and lead to irradiation-assisted stress corrosion cracking. However, there are only very limited measurements in other structural materials such as ferritic/martensitic steels and D9 which are candidates for structural materials in several advanced reactor concepts. RIS may be important in these alloys as elemental enrichment could lead to radiation-induced precipitation which could impact mechanical properties and embrittlement. In this paper, the potential influence of RIS on structural materials for advanced reactor applications will be examined. In addition, recent advances in theoretical modeling and measurements of RIS will also be addressed.

11:30 AM

Microstructural Development and Solutes Segregation during Electro-Irradiation around Cascade Damage Introduced by Ion-Irradiation: *Heishichiro Takahashi*¹; Yuichiro Sueishi²; ¹Hokkaido University; ²Kyoto University

When the stainless steels were neutron-irradiated in fission or fusion reactors, cascade damages were introduced, and the cascade damages influence the following damage structures such as void formation, solutes segregation and so on. In order to study the effects of cascade damage on following microstructural evolution during irradiation, the irradiation experiments were carried out using ion accelerator to introduce the cascade damage and a high voltage electron microscopy for in-situ observation of structural development for the cascade damage. Following results were obtained; 1)cascade damages were introduced by Ni-ion irradiation at room temperature, 2)the cascade damages changed to SFTs due to annealing, 3)I-type dislocation loops nucleated from cascade damage and continued to grow during further electron-irradiation, 4)Ni solute segregated and Fe and Cr were depleted and the precipitates formation was often recognized around the cascade damage region.





Monte Carlo Simulation of Grain Boundary Segregation in Fe-Cr and Fe-Cr-Ni: *Je-Wook Jang*¹; Byeong-Joo Lee¹; ¹POSTECH

Segregation of constituents of binary and ternary alloys to grain boundaries may alter their structure and chemical composition, and thus significantly influence mechanical properties of the material, in particular its fracture behavior. Atomistic computer simulations offer a powerful tool for gaining insights into atomic mechanisms of grain boundary segregation. In this work, we perform a detailed study of GB segregation in Fe-Cr and Fe-Cr-Ni systems at wide ranges of temperature and GB misorientation by Monte Carlo Simulations based on 2NN MEAM potentials. The dependencies of solute segregation on the contents of solute elements and GB misorientation will be reported and interpreted energetically. The possibility of existence of grain boundary transition will also be discussed.

12:10 PM

Ab initio-Based Thermokinetics of the Ni-Cr Binary: *Julie Tucker*¹; Dane Morgan¹; Todd Allen¹; ¹University of Wisconsin

Low temperature diffusion is enhanced by the creation of point defects in irradiated materials. A fundamental understanding of the diffusion mechanisms in multi-component alloys is essential in predicting microstructural and microchemical changes such as void swelling and radiation induced segregation, which can degrade material properties, a major concern in the nuclear power industry. We combine *ab initio*, cluster expansion, Monte Carlo and kinetic Monte Carlo techniques to calculate concentration and temperature dependent diffusion coefficients where experimental data is unavailable. This methodology is applied to the face-centered cubic Fe-Ni-Cr system with a current emphasis on the Ni-Cr binary. We will present *ab initio* based thermodynamics for the Ni rich region, with an emphasis on the Ni2Cr phase and the importance of the thermodynamic factor for kinetic properties. We will also present point defect formation and migration energies for varying chemical environments to assess the impact of local environment and overall composition.

Outreach Programs in Materials Science and Engineering: Outreach Programs at Universities

Sponsored by: The Minerals, Metals and Materials Society, TMS: Public and Governmental Affairs Committee

Program Organizers: Dan Thoma, Los Alamos National Laboratory; Katherine Chen, California Polytechnic State University

Monday AM	Room: Pacific Hall A
February 26, 2007	Location: Dolphin Hotel

Session Chair: Dan Thoma, Los Alamos National Laboratory

9:00 AM Introductory Comments

9:05 AM Invited

The Materials World Modules Program and Its Impact on Secondary Science Education: Robert Chang¹; ¹Northwestern University

The Materials World Modules (MWM) program develops materials topicbased supplementary content for use in secondary science classrooms. It uses inquiry and design as the basis to stimulate discovery and creativity in students who use the modules. The program also offers teacher training, evaluation and assessment of its activities. Materials topics include: polymer, sports materials, biotechnology, nanotechnology, composites, and others. MWM provides teachers and students with printed booklets via the web and related kits for the classrooms. In this talk we will discuss how MWM is being used, and results from national-wide field tests will be presented.

9:35 AM Invited

The Summer High School Teacher (HST) Program at CMU MRSEC: *Francine Papillon*¹; Robert Wesolowski¹; Gregory Rohrer¹; ¹Carnegie Mellon University

The objective of our HST program is to create an identity for materials science and engineering among 9-12th grade students. Our experience has shown that by interacting with the teachers who develop curricula that can be used repeatedly in many classrooms, we reach far more students (7000 since 1996) in a sustained way than more direct approaches involving visits to the classroom or hosting lab tours. Each summer, three teachers spend four weeks developing a laboratory experiment and an accompanying lesson plan that illustrates the relevance of materials science to physics, chemistry, and technology. The CMU faculty serves as expert consultants in the subject matter, while the teachers apply their expertise at high school instruction to develop curricula that are archived on our web site, where they can be accessed by others. More recently, we have established an annual workshop to help more teachers adopt the curricula into their classrooms.

10:05 AM Invited

Developing and Growing Materials Engineering Outreach Activities: *Katherine Chen*¹; ¹California Polytechnic State University

An arsenal of exciting presentation slides, interactive demonstrations, and hands-on activities is used for a variety of different outreach events at Cal Poly. We have been able to tailor our Materials Engineering (MatE) outreach presentation to different age groups, and have visited kindergarten through high school classes. Demonstrations and activities have also been modified to be used in workshops of different time durations (e.g., Expanding Your Horizons, SWE, Girl Scouts, Open House). A highly successful outreach event is the "Passport to MatE-Land," where participants are on a journey and visit different stations where they can perform a quick materials-related demo or activity in order to receive a stamp in their passport. Over time, our outreach efforts have been able to grow and expand to include a summer camp, working with area schools, and partnering with a local science museum. Strategies in developing a successful outreach program will be discussed.

10:35 AM Break

10:50 AM

Scanning Electron Microscopy Education Outreach Program: Carl Boehlert¹; ¹Michigan State University

Since 2002 over 350 K-12 students and teachers have been educated through an outreach program based on scanning electron microscopy. This program involved hands-on instruction and was designed to stimulate the K-12 students' interest in learning more about Materials Science and Engineering (MSE). This successful outreach activity encouraged students to consider enrolling in university science disciplines including MSE. As this program exposed students both to the university as well as the MSE discipline, it acted as a recruitment tool. This program also satisfied the requirements for service learning as it provided a means for volunteer undergraduate students to learn and develop through thoughtfully organized service. Data was collected regarding the impact of the program on the decisions made by the K-12 students regarding their career/major choices. This presentation will highlight several aspects of this outreach program which was supported by the National Science Foundation through grant DMR-0134789.

11:20 AM

MSE Outreach Efforts at the University of Florida: *Gerhard Fuchs*¹; ¹University of Florida

Several different programs have been used at the University of Florida to help keep K-12 students interested in the sciences and then to attract undergraduate students to select a MSE major. The MSE Teach program that offers K-12 teachers lectures and laboratory experiments that can be used in the K-12 classrooms to help keep young students interested in the sciences. In addition, graduate students and faculty members have visited local K-12 school and given in-class science demonstrations that supplement existing curricula. In all cases, examples are given to link everyday activities or news events with science to help reinforce the lessons. Middle- and high-school students are also recruited to work in the laboratories during summers. Whenever possible, these students are teamed with graduate students to provide a learning experience for both the middle/high-school and graduate students. The lessons learned from these, and other, MSE outreach programs will be discussed.

11:50 AM Invited

Bringing Materials Engineering to the General Education Curriculum: *David Bahr*¹; M. Norton¹; ¹Washington State University

We have developed a course at Washington State, "Materials: the foundation of science and technology", to act as a course grounded in scientific and



technological methodologies for the general education curriculum. All students at WSU are required to take at lease one course in this broad area. This presentation will describe the course and the text which have been developed over the past five years. In particular, we will focus on the results and documentation of the course feedback, collected from over 150 students in over 30 majors from across campus. In general, the ability to interest students in aspects of (1) historical impact of materials (2) materials in specific technologies and (3) current materials issues in society has been positive. The majority of whom report a greater interest in the field and appreciation for how engineering impacts their career and society as a whole.

Pb-Free Electronic Solders: Alloy Design, Characterization and Service Reliability: Interfacial Effects

Sponsored by: The Minerals, Metals and Materials Society, TMS Electronic, Magnetic, and Photonic Materials Division, TMS: Electronic Packaging and Interconnection Materials Committee

Program Organizers: Fu Guo, Beijing University of Technology; K. Subramanian, Michigan State University; Sung Kang, IBM Corporation; Srinivas Chada, Medtronic; Laura Turbini, University of Toronto; Jin Yu, Korea Advanced Institute of Science and Technology

Monday AM	Room: Oceanic 1
February 26, 2007	Location: Dolphin Hotel

Session Chairs: Fu Guo, Beijing University of Technology; C. Robert Kao, National Taiwan University

9:00 AM Opening Remarks by Fu Guo

9:05 AM

Interfacial Reactions in Model NiTi Shape Memory Alloy Fiber Reinforced Sn Matrix Composites: James Coughlin¹; Jason Williams¹; Nikhilesh Chawla¹; ¹Arizona State University

It is well known that solder joints must retain their mechanical integrity under conditions of isothermal aging, thermal fatigue, and creep. In recent years, shape memory alloys (SMA) have received significant attention due to their ability to be deformed and return to their original dimensions, upon unloading and/or the application of heat. Recently, SMA has been used as a reinforcement phase to form "smart" composite materials. The unique properties of SMA are being exploited to design damage tolerant materials that exhibit a beneficial response under applied loading. In this paper, we report on interfacial reactions and kinetics between NiTi shape memory alloy wires in liquid Sn. It will be shown that the reaction products and kinetics are quite complex. The evolution of the microstructural constituents and the influence on deformation behavior will be discussed.

9:25 AM

Interface Reactions between Lead-Free Sn-3.5Ag Solder and Ni-W-P Metallization: *Zhong Chen*¹; Aditya Kumar¹; Jayce Lim¹; T. K. Lee²; ¹Nanyang Technological University; ²Micron Semiconductor Asia Pte Ltd

Ni-P metallization has received considerable attention for flipchip and board grid array applications in recent years. Soldering reaction between lead-free solders and Ni-P, in terms of intermetallic compound morphology and growth kinetics, and the joint strength have been extensively studied. However the interface reaction rate is still quite fast in the absolute term because of the higher Sn concentration and melting point compared with the conventional Pb-Sn solders. In the current study, a ternary alloy, Ni-W-P was formulated and its soldering reaction was compared with that the binary Ni-P. The microstructure and joint strength will be investigated.

9:45 AM

Effect of Zn Contents on Interfacial Reactions between Sn-Based Solders and Cu: *Su-Chun Yang*¹; Cheng-En Ho¹; Chien-Wei Chang¹; C. Robert Kao²; ¹National Central University; ²National Taiwan University

Sn-Ag-Cu alloys are considered the most promising lead-free alloy systems in packaging industry. However, it required the addition of minor alloy elements to improve the properties of the SnAgCu solders to pass various reliability tests and Zn is one of the candidates for the elements. The objective of this study is to investigate the effect of Zn addition on the interfacial reaction. Experimentally, different Sn-xZn solders (x = 2.0-0.5) were reacted with Cu at 250° C for 2 and 10 mins. Interestingly, the intermetallics formed at the interface were strongly dependent on the Zn content. When Zn content decreased from 2 wt.% to 0.5 wt.%, the reaction product switched from Cu5Zn8 to Cu6Sn5. This strong Zn concentration effect could be explained using the Cu–Sn–Zn phase diagram. The implication is that the type of compound forms at the interface can be controlled by adjusting the Zn concentration of the Sn-based solders.

10:05 AM

Characterization of Interfacial Reaction Layers Formed between Sn-3.5Ag Solder and Electroless Ni–P Substrate: *Han-Byul Kang*¹; Jee-Hwan Bae¹; Kyung-Hwan Kwak¹; Jae-Wook Lee¹; Min-Ho Park¹; Jeong-Won Yoon¹; Seung-Boo Jung¹; Cheol-Woong Yang¹; ¹Sungkyunkwan University

The eutectic Sn-Ag solder is one of the most promising Pb-free candidates to replace the Sn-Pb solders. In addition to solder, printed circuit boards and component surface finishes also have to be Pb-free. Electroless Ni has been widely used as a diffusion barrier layer on the Cu bond pad for flip-chip and ball-grid-array solder bumps. In this study, we investigaed the interfacial reaction between Sn-3.5Ag solder and electroless Ni-immersion gold plated Cu substrate by using various AEM techniques (STEM/EDS, CBED/NBED). Cross sectional TEM samples were prepared by ultramicrotomy. CBED/NBED technique is used for phase identification of IMCs and P-rich Ni layer. The composition redistribution was analyzed by STEM/EDS. The IMCs formed at the interface was mainly Ni3Sn4. Two distinctive layers, Ni-Sn-P and P-rich Ni layer, were found between the Ni3Sn4 and Ni–P under bump metallization. The P-rich Ni layer is composed of Ni3P and Ni rich nano crystalline phase.

10:25 AM

Au Effect on the IMC Spalling Behavior of SnAgCu Soldering on Ni/Au Finish: Don Son Jiang¹; C. Robert Kao²; C. E. Ho³; Yu-Po Wang¹; C. S. Hsiao¹; ¹Siliconware Precision Industries Company Ltd; ²National Taiwan University; ³Michigan State University

According to RoHS legislation, Pb has been banned to use from 2006 Jul and Sn3~4wt%Ag0.5wt% solder has become the main stream in industries. When current Sn3~4wt%Ag0.5wt%Cu soldering on Ni/Au pad surface, massive IMC spalling was sometimes found after reflow. Based on the previous study, the reason was attributed to the decrement in the available Cu in the solder joint. Since Au content in the solder joint is also a key factor to affect the joint quality, Au content was changed by solder volume and Au plating thickness to investigate its effect on IMC spalling behavior in current study. The result showed IMC structure became loose due to many voids in the IMC and massive spalling occurred in some worse cases as increment in Au content. Based on this result, the control of Au content in the solder joint is very important to prevent the joint from IMC spalling.

10:45 AM Break

10:55 AM

Cruciform Pattern Interfacial Reactions in the Sn-(Bi)/Te Couples: Chennan Chiu¹; Sinn-Wen Chen¹; ¹National Tsing Hua University

Sn-Bi alloys are promising Pb-free solders and Te is the primary element of bismuth telluride thermoelectric materials. The liquid/solid interfacial reactions between Sn-(Bi) and Te were examined. Very unusual cruciform patterns have been observed in the Sn/Te reaction couples reacted at 250oC. The reaction layers are porous and are composed of a Sn-SnTe two-phase mixture. Reaction layers with very uniform thickness are grown along the four sides of the rectangular Te substrate, and no reaction products are found at any of the corners. No similar cruciform patterns are observed in the Bi/Te couples. Sn-Bi/Te reaction couples with Sn-Bi alloys of various compositions are examined. The cruciform patterns of the reaction layers gradually disappear in the Sn-Bi/Te reaction couples with higher Bi amounts of the Sn-Bi alloys, and the critical composition is about Sn-50wt.%Bi.

11:15 AM

Effect of Bi on the Interfacial Reaction between Sn-3.7Ag-xBi Solders and Cu: *Min He*¹; Viola Acoff¹; ¹University of Alabama

It was reported in previous studies that the Bi addition could improve wettability and reduce the melting temperature of Sn-Ag solders. This work

A M



investigates the effect of Bi amount on the interfacial reaction between Sn-Ag-xBi solders and the Cu substrate reflowed at 250°C for different times and thermal aged at 150°C for different durations. Five types of Sn-Ag based solders, Sn-3.7Ag-xBi (x=0-4 wt%), were used in this study. The microstructure of the interfacial Cu-Sn intermetallic compound (IMC) layers between the solders and the Cu substrate has been studied. The thickness of the Cu-Sn IMCs in different solder/Cu systems has been measured. It was found that the thickness of the Cu-Sn IMC layer decreased with increasing amount of the Bi in both the reflow and thermal aging condition. The effect of Bi addition on the interfacial reaction between the solder and the Cu substrate was discussed based on the experimental results.

11:35 AM

Growth Kinetics of Intermetallic Compound Layers in Ni/Sn/Cu Ternary Diffusion Couple during Solid-State Aging: *Kyoung-Kook Hong*¹; Jea-Bong Ryu¹; Chang-Yong Park²; Joo-Youl Huh¹; ¹Korea University; ²Samsung Electronics

In ball grid array (BGA) packaging technology, the selection of appropriate surface finishes for the contact pads is the critical factors related to the BGA solder joint reliability. The organic solderability preservative (OSP) finish gives rise to a serious reliability concern related to the formation of a Cu-Ni-Sn ternary intermetallic compound (IMC) on the component side with an electrolytic Ni/Au finish, since the Ni/IMC interface is highly susceptible to brittle facture. In this study, we investigated the long range interaction between Cu and Ni across a thick Sn layer in a Ni/Sn/Cu diffusion couple during solid-state aging at 150, 175 and 200°. During the solid-state aging process, (Cu,Ni)6Sn5 IMC layer formed at the Ni/Sn interface was rapidly grown with increasing aging time, even though Ni consumption was very small. This presentation will discuss the growth relationship between ternary IMC layer at Ni/Sn interface and IMC layers at Sn/Cu interface.

11:55 AM

Phase Formation and Intermetallic Compounds of Sn-9Zn-1.5Ag-1Bi Lead-Free Solder and Cu Substrate: *Chih-Yao Liu*¹; Moo-Chin Wang²; Min-Hsiung Hon¹; ¹National Cheng Kung University; ²National Kaohsiung University of Applied Sciences

The phase formation and intermetallic compounds at interface between the Sn-9Zn-1.5Ag-1Bi on Cu substrate have been investigated. The Sn-9Zn-1.5Ag was also tested for comparison. Due to the decomposion of the intermetallic compound (IMCs), the adhesion strength increased after 1Bi wt percent addition in Sn-9Zn-1.5Ag. The phase formation observed in two solders by an X-ray diffractometer (XRD), an optical microscope (OM), an scanning electron microscope (SEM), an energy dispersive spectrometer (EDS) and a transmission electron microscope (TEM). Cu6Sn5 and Cu5Zn8 were observed in the Sn-9Zn-1.5Ag and Sn-9Zn-1.5Ag-1Bi. The adhesion strength has been investigated by pull-off test. The adhesion strength are 7.84 \pm 0.28 and 5.57 \pm 0.43 MPa for Sn-9Zn-1.5Ag-1Bi and Sn-9Zn-1.5Ag, respectively. The melting point and melting range of Sn-9Zn-1.5Ag-1Bi lead-free solder are determined as 195.8°C and 9.7°C, respectively.

12:15 PM

Metallurgical Reactions of SnAg Solder with Electroplated Ni UBM: Hsiao-Yun Chen¹; Chih Chen¹; ¹National Chiao Tung University

It is well known that Ni and its alloys possess a lower reaction rate with Sn than Cu and Cu alloys. Therefore Ni-based under bump metallization have attracted attention in recent years. In this study, the diffusion-controlled reaction between Sn-Ag between two types of Ni-based under bump metallization, electroless-Ni and electroplated-Ni, has been investigated. Morphology and growth kinetics of the formed Ni3Sn4 in both systems are study under different reflow temperatures and durations. Ni3Sn4 layer was found in the interface of the SnAg solder and the electroplated Ni layer; while three distinctive layers, Ni3Sn4, NiSnP and Ni3P, were found between Sn-Ag solders and electroless-Ni under bump metallization (UBM). Also, the growth rates and the activation energy of Ni3Sn4 IMC were estimated. The kinetic data obtained showed that the Ni3Sn4 in the SnAg/ electroless-Ni joints grows much faster than with electroplated-Ni under the same condition.

Plasticity from the Atomic Scale to Constitutive Laws: Dislocation Core Structure and Solute-Dislocation Interactions

Sponsored by: The Minerals, Metals and Materials Society, TMS Structural Materials Division, TMS/ASM: Computational Materials Science and Engineering Committee

Program Organizers: Christopher Woodward, US Air Force; Michael Mills, Ohio State University; Diana Farkas, Virginia Tech

Monday AM	Room: Europe 9
February 26, 2007	Location: Dolphin Hotel

Session Chairs: Christopher Woodward, US Air Force; William Curtin, Brown University

9:00 AM Invited

Effect of Non-Glide Stresses on Dislocation Motion and Deformation in Transition BCC Metals: *Vaclav Vitek*¹; Roman Gröger¹; John Bassani¹; ¹University of Pennsylvania

Plastic deformation of bcc metals is controlled by 1/2<111> screw dislocations that possess non-planar cores and thus a high Peierls stress. Recent molecular statics calculations revealed a complex dependence of the Peierls stress on the applied stress tensor. The Peierls barrier, which is surmounted via formation of kink pairs at finite temperatures, depends on the stress tensor in a similar way but this dependence is not found directly in 0K calculations. We first show how this information can be deduced from such calculations by requiring that the Peierls barrier reproduces correctly the effect of both shear stresses parallel and perpendicular to the slip direction at 0K. This procedure allows introduction of the effect of the full stress tensor into the model of thermally activated dislocation motion and establishing constitutive relations for the non-associated flow at finite temperatures and strain rates. Results of this development will be compared with available experiments.

9:30 AM

Ab Initio Study of the Core Structure and Mobility of Screw Dislocations in α -Fe: *Lisa Ventelon*¹; François Willaime¹; ¹Service de Recherches de Métallurgie Physique

The structure and properties of the core of screw dislocations in alpha iron are investigated by ab initio calculations performed using the SIESTA code. The results obtained for the {211} and {110} generalized stacking fault energy surfaces suggest a non-degenerate core structure, symmetrically spread across the three {110} planes, in contrast with most empirical potential results. Two different cell arrangements are compared for the calculation of the core: a periodic array of dislocation dipoles and a single dislocation within the cluster approach. As expected, the non-degenerate and degenerate easy core structures are found to be respectively stable and unstable. The very weak deviation from the purely elastic displacement field and the change in magnetic moment are analyzed. Some insight into the mobility of the dislocation and the stability of the hard core is gained from the energy landscape obtained using the drag method.

9:50 AM

Dislocation Structure and Mechanical Behavior of Co-Based B2 Intermetallics: *Oleg Kontsevoi*¹; Yuri Gornostyrev²; Arthur Freeman¹; ¹Northwestern University; ²Institute of Metal Physics

Co-based intermetallics (CoTi, CoZr, CoHf) exhibit unusual mechanical behavior that sets them apart from other B2 alloys, namely temperature yield stress anomalies and high ductility (recently found in CoZr) despite the fact that only <100> dislocations operate in plastic deformation. We investigated the structure and mobility of <100> dislocations in B2 Co-based intermetallics using our combined modified Peierls-Nabarro model approach with ab-initio generalized stacking fault (GSF) energetics. An anomalously low GSF energy was found near $1/2 <100 > \{011\}$ shear, and the splitting of the <100> $\{011\}$ dislocations structure according to the $\mathbf{b} = \mathbf{b}/2 + \mathbf{b}/2$ scheme is predicted. The dislocation mobility and hence easy plastic relaxation which will prevent brittle fracture. This unusual dislocation structure is connected with the B2



phase instability in these alloys with respect to martensitic transformation. Supported by the AFOSR (grant No. FA9550-04-1-0013).

10:10 AM Invited

Quantification of Solute Segregation at Dislocations with the Local Electrode Atom Probe: Michael Miller¹; ¹Oak Ridge National Laboratory

The mobility of a dislocation is strongly influenced by the amount and distribution of solute and precipitates along the dislocation. The interaction of dislocations with microstructural features is a key factor in defining the mechanical properties of many alloys. The wide field-of-view local electrode atom probe permits the extent and amount of solute segregation in the vicinity of dislocations to be quantified for all elements. This state-of-the-art microanalytical instrument has been applied to quantify solute segregation in several neutron irradiated pressure vessel steels and model alloys as well as mechanically alloyed, oxide dispersion strengthened ferritic steels. In addition to carbon-enriched Cottrell atmospheres, the segregation of phosphorus and several subsitutional elements including silicon, nickel and manganese to dislocations has been characterized.Research at the Oak Ridge National Laboratory SHaRE User Facility was sponsored by the Office of Basic Energy Sciences.

10:40 AM Break

11:00 AM

Influence of Solutes on the Plasticity of bcc Iron: *Youhong Li*¹; Neeraj Thirumalai¹; Peter Gordon¹; Concezione Halsey¹; Michael Luton¹; Amit Samanta²; Ju Li²; ¹ExxonMobil Research and Engineering; ²Ohio State University

It is well known that addition of solutes changes the plasticity of bcc Fe. However, the fundamental underlying mechanisms of this phenomenon remain to be understood. In this study, we have performed atomistic simulations to probe the influence of both substitutional solutes, such as Ni, and interstitial solutes, such as C, on the dislocation mobility in Fe. Embedded Atom Method (EAM) potentials for Fe-Ni system and Modified Embedded Atom Method (MEAM) potentials for Fe-C system were used in the application of molecular dynamics (MD) and molecular statics (MS) techniques to the study of the mobility of screw dislocations. The Nudged Elastic Band (NEB) method was used to estimate the activation energy barriers for double kink formation and migration wherever appropriate. The implications of these results towards understanding the influence of solutes on the plasticity of iron-based alloys are discussed.

11:20 AM Invited

Chemistry of Deformation: Solid-Solution Softening from First-Principles to Dislocation Mobility: *Dallas Trinkle*¹; ¹University of Illinois, Urbana-Champaign

Solid solution softening in bcc transition metals has traditionally been attributed to either extrinsic effects (interstitial scavenging) or intrinsic effects (direct solute-dislocation interactions). We investigate intrinsic mechanisms using first principles methods. First, the interaction energy of a transition metal solute with a single straight <111> screw dislocation in Mo and Fe is calculated using density functional theory. Next, the interaction energies and changes in resistance to dislocation mobility to predict changes in yield stress with temperature and solute concentration. Quantitatively accurate predictions require a model that accounts for clusters of solutes interacting with dislocations. Previous methods employing the solute response in bulk as an approximation to the solute response in a dislocation lead to incorrect predictions. Using solute-dislocation interactions coupled with a realistic mesoscopic model, we reproduce the strength behavior of different alloy systems despite the range of intrinsic interactions.

11:50 AM

Impurity-Point Defect Interaction in Fe-Cr Alloys: Size Effects versus Magnetic Behaviour: *Duc Nguyen-Manh*¹; M. Lavrentiev¹; S. Dudarev¹; ¹UKAEA

Interaction of impurities with point defects is an important factor influencing generation and migration behaviour of defects in irradiated FeCr ferritic-martensitic steels. Earlier attempts to calculate impurity-point defect binding energies on the basis of strain field theories had limited success and the correlation between the binding energy and the size of the impurity atom is poorly understood. In this study, microscopic aspects of solute-defect interactions are investigated by mean of density functional theory (DFT). Defect formation energies in magnetic bcc Fe-Cr alloys are calculated using binary configurations generated from DFT/Monte Carlo simulations. We find evidence that magnetism is responsible for anomalous positive binding energies between Cr and interstitial dumbbells, as well as vacancies in 6.25% Cr alloys, which is at variance with elastic theory based on strain-mediated interaction between defects and solute atoms. The origin of this behaviour is analysed by a systematic study of impurity-defect interaction involving various solute elements.

12:10 PM

Gum Metals: "Ideal" Engineering Alloys: Tianshu Li¹; J. Morris, Jr.¹; N. Nagasako²; S. Kuramoto²; *Daryl Chrzan*¹; ¹University of California; ²Toyota Central Research and Development Laboratories Inc.

A newly discovered group of alloys, called Gum Metals, approach ideal strength in bulk form, exhibit significant plastic deformation prior to failure and do not display signs of conventional dislocation activity. These observations suggest that in contrast to most engineering alloys, Gum Metals have mechanical properties determined by their ideal strengths. Two conditions must be met for a material to exhibit this "ideal" behavior: 1) the stress required to trigger dislocation plasticity in the material must exceed its ideal strength, and 2) the material must be intrinsically ductile when stressed to ideal strength. First principles electronic structure total energy calculations, when combined with anisotropic elasticity theory and a simple model of dislocation/obstacle interactions, demonstrate that Gum Metals satisfy both criteria, explaining the origins of their remarkable mechanical properties. This research is supported by Toyota Motor Corporation and, in part, by the National Science Foundation.

Properties and Performance of High Temperature Alloys and Coatings: Single Crystal Alloys I

Sponsored by: The Minerals, Metals and Materials Society, TMS Structural Materials Division, TMS: High Temperature Alloys Committee, TMS/ASM: Corrosion and Environmental Effects Committee, TMS/ASM: Mechanical Behavior of Materials Committee

Program Organizers: Qiang Feng, Beijing University of Science and Technology; Timothy Gabb, NASA Glenn Research Center; Doug Konitzer, General Electric Aviation; Roger Reed, Imperial College London; Bruce Pint, Oak Ridge National Laboratory; Sammy Tin, Illinois Institute of Technology; Shiela Woodard, Pratt and Whitney

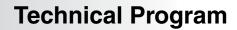
Monday AM	Room: Asia 4
February 26, 2007	Location: Dolphin Hotel

Session Chairs: Qiang Feng, Beijing University of Science and Technology; Timothy Gabb, NASA Glenn Research Center

9:00 AM Keynote

Pushing the Envelope for High Temperature Structural Materials: *Robert Schafrik*¹; ¹General Electric Company

High temperature structural materials for aero-propulsion applications must perform reliably in a high stress environment over many years. This leads to a conservative design approach— find a solution and stay with it. This is successful until the requirements drastically change. Given the relentless push for more efficient engines, extrapolations of the past can no longer deliver required performance. Fortunately, the MS&E community has continued to explore a wide range of new materials. Within the design community, materials application engineers are constantly on the look out for materials that have the potential to perform satisfactorily in advanced applications. Often, more than one candidate is identified. This gives rise to a "competition" between materials. This paper will discuss key aspects of the competitive process from an application standpoint, with the goal of identifying improvements to the material development process that could lead to faster incorporation of advanced materials in critical applications.





Single Crystal Superalloys: What Is Not Known?: Roger Reed¹; ¹Imperial College

The single crystal superalloys are about thirty years old, and some may argue that they are mature materials. But this is far from the case. In this presentation, it will be demonstrated that there are still many substantial questions which remain to be answered. For example, aspects of their creep degradation (gamma prime cutting, rafting) are still not at all understood. The physical basis for the so-called 'rhenium effect' remains to be elucidated. In the fourth generation alloys, ruthenium confers stability but the reason for this is unclear. How does the composition influence the TBC compatibility? And why are casting yields in the investment foundry still far from ideal? It will be demonstrated that much further work is required to optimise these materials, and argued that this will not be done by empiricism alone – theoretical modelling has a valuable role to play.

10:00 AM

Improved Heat Extraction, Casting Quality, and Mechanical Properties in Large Ni-Base Superalloy Casting via the Liquid-Metal Cooling (LMC) Directional Solidification Technique: *Andrew Elliott*¹; Tresa Pollock²; Ganjiang Feng¹; ¹General Electric Energy; ²University of Michigan

The conventional directional solidification (DS) process for Ni-base superalloy castings is primarily limited by radiation cooling from the mold surface producing very low thermal gradients at the solidification front when casting large industrial gas turbine parts. This results in coarse microstructural scale, increased segregation, and increased casting defect occurrence, which reduce yield and limit the performance capability of these parts. Results from René N5 and GTD-444TM castings produced by the high thermal gradient liquid-metal cooling (LMC) casting method indicate that LMC eliminates freckle-type defects and produces a 2X reduction in primary and secondary dendrite arm spacings. Additionally, LMC cast material exhibits a 1.5-2X improvement in both low-cycle fatigue and creep life. Finally, thermal modeling of both the conventional and LMC DS processes has been utilized to determine the limiting heat transfer steps of each process.

10:20 AM

Simulation of the Influence of Carbides on the Permeability of Ni-Base Superalloys: *D. Ness*¹; L. Thuinet¹; D. Bernard²; P. D. Lee¹; ¹Imperial College London; ²ICMB-CNRS

The formation of freckle chains during the directional solidification of Ni-base superalloys results from convective flow of the liquid in the mushy zone. This flow depends on the permeability and the density inversion in the interdendritic liquid. It has been hypothesized that carbide particles within the mushy zone may affect the permeability and reduce the propensity for defect formation. However, their effect has never been quantified. Experimental permeability measurements are very difficult to achieve, especially at low volume fraction solid levels, due to the changing morphology of the dendritic microstructure over time. Therefore, a numerically determined value for the permeability of directionally solidified alloys is proposed. This was achieved by first simulating solidification microstructures by means of an in-house microstructural model. The permeability was then numerically calculated using the obtained microstructures. The impact of carbides on permeability as well as the importance of accurate measurements on freckle predictions is subsequently discussed.

10:35 AM

Diffusion Braze A Ni-Based Single Crystal Alloy: Mechanical Properties and Microstructure: Zengmei Koenigsmann¹; ¹Chromalloy

More single crystal (SC) alloys have been introduced to make advanced engine components to meet the requirements of high efficiency and high operation temperature. Since it is more expensive to produce SC alloy components, it is necessary to investigate an effective repair method to extend the component service life and further reduce the cost. High temperature diffusion braze is known to be effective in repairing cracks and surface erosion of service components as it introduces less thermal stress and distortion than any welding methods. This method is especially effective in repairing stationary components. However, a common practiced diffusion braze heat treatment for Ni based alloy components significantly alters Ni based SC alloy original microstructure and results in a dramatic change in mechanical properties. This paper presents a concept of developing a diffusion braze process on Ni based SC alloys. The resulting microstructure and properties will be discussed.

10:55 AM Break

11:10 AM Invited

Local Electrode Atom Probe Characterization of Solute Enrichments and Surface Roughness of Interfaces in a CMSX-4 Superalloy: *Michael Miller*¹; Roger Reed²; ¹Oak Ridge National Laboratory; ²Imperial College

The solute distributions at the primary and secondary γ ' precipitate-matrix interfaces in crept and annealed CMSX-4 nickel base superalloy have been characterized with a local electrode atom probe. Significant enrichments of the alloying elements were observed over an ~10-20 nm distance from the interface. Differences in the solute profiles between the primary and secondary precipitates were observed. The relatively large field-of-view of the local electrode atom probe also enables the surface roughness of the interfaces to be estimated at near atomic resolution. The surface roughness of the interfaces in the crept condition was found to be significantly rougher than in the annealed condition. Research at the Oak Ridge National Laboratory SHaRE User Facility was sponsored by the Office of Basic Energy Sciences, U.S. Department of Energy, under contract DE-AC05-000R22725 with UT-Battelle, LLC.

11:35 AM

TCP Suppression in a Ruthenium-Bearing Single Crystal Nickel-Base Superalloy: *Robbie Hobbs*¹; Lijuan Zhang²; Catherine Rae²; Sammy Tin³; ¹Rolls-Royce plc; ²University of Cambridge; ³Illinois Institute of Technology

The high temperature creep strength of single crystal nickel-base superalloys has been enhanced by alloying with increasing levels of dense refractory elements. However, these additions have concurrently promoted the precipitation of topologically close-packed (TCP) phases. This depletes the important strengthening elements from the desired phases and leads to premature creep rupture at elevated temperatures. Recent initiatives to address this have involved the addition of ruthenium (Ru). Preliminary studies indicate that Ru additions directly address the microstructural stability concerns of current generation alloys. However, the mechanism(s) by which it does so remain debatable. This study attempts to isolate the underlying mechanism(s) by which a 3 wt.% Ru addition inhibits TCP precipitation in a high refractory content single crystal superalloy. Experimental results from a set of nominally identical alloys with and without Ru are presented, and the influence of Ru on the thermodynamic and kinetic factors governing TCP precipitation is discussed.

11:55 AM

Alloying Effect of Co on the Microstructural Parameters of Ni-Base Single Crystal Superalloys: *Takanobu Suzuki*¹; Tadaharu Yokokawa²; Yutaka Koizumi²; Toshiharu Kobayashi²; Hiroshi Harada²; Hachiro Imai¹; ¹Shibaura Institute of Technology; ²National Institute for Materials Science

In order to develop a Co-free Ni-base superalloy for He-gas turbine of a new type of nuclear reactor; Pebble Bed Modular Reactor (PBMR), alloying effect of Co on the microstructural parameters and mechanical properties for Re-bearing Ni-base superalloys needs to be studied. In this research, the lattice misfit between γ and γ' phases, the partitioning behaviors of alloying constituents, and the creep rupture life have been investigated. The second-generation single crystal superalloys, which contain Co in the range of 0 to 15wt% were used. Chemical composition of base alloy (0Co alloy) is Ni-4.9Cr-1.9Mo-8.7W-5.3Al-6Ta-2.4Re-0.1Hf in wt %. Base on the results of the present study, it becomes clear that the partitioning behaviors of alloying elements were enhanced with decreasing of Co content in alloys. The role in which Co plays in the lattice misfit and the creep rupture life will be mentioned in the conference.

12:10 PM

CMSX-486 (R) Single Crystal Alloy - Production Experience and Development of an Improved Version: *Jacqueline Wahl*¹; Kenneth Harris¹; ¹Cannon Muskegon Corporation

Modern turbine engine performance and life cycle requirements demand single crystal (SX) superalloy turbine airfoil and seal components. However, complex SX components, such as vane segments, can result in severe manufacturing cost challenges due to low manufacturing yield. These requirements led to the development of CMSX-486 alloy, a grain boundary strengthened SX superalloy with improved creep-rupture strength over SX CM186LC(R) alloy. CMSX-486 alloy has excellent casting yield achieved



through generous grain inspection criteria and is used as-cast, which minimizes post-cast processing costs and eliminates the risk of recrystallisation during solution heat treatment. CMSX-486 alloy has attained production status and further improvements to the alloy are under evaluation. This paper will review the unique properties which make this alloy of serious interest, with particular attention to ongoing production experience. Discussion will also include direction and results of an improved oxidation resistant version of CMSX-486 alloy which is currently under development.

12:30 PM

Phase Relationship in the Ni-Base and Rh-Base Superalloys Mixtures: *Tomonori Kitashima*¹; Hiroshi Harada¹; Kyoko Kawagishi¹; Takao Murakumo²; Akihiro Sato¹; ¹National Institute for Materials Science; ²Federal Institute for Materials Research and Testing

The Ni-base single-crystal superalloys with higher temperature capabilities can improve thermal efficiencies in aeroengines. It is obvious, however, that the temperature capability of Ni-base single-crystal superalloys can not exceed the eutectic of Ni-Al system about 1380°C. In order to develop the superalloy which can be utilized at much higher temperature about 1300°C, it is necessary to develop new superalloys with base metals of higher melting temperatures. In this research, the Ni-base and Rh-base superalloys mixtures, which is fcc-structure-base superalloy, was considered since Rh has the high melting temperature of 1903°C, and is expected to have the high oxidation resistance. The phase relationship in Rh-Nb-Ni-Al quaternary system at Nirich side was investigated.

12:50 PM

Alloying Effects and Characterization of Pt-Modified γ-Ni+γ'-Ni₃Al-Based Alloys: Andy Heidloff¹; Takeshi Izumi¹; Brian Gleeson¹; ¹Iowa State University

Novel heat-treatable γ -Ni+ γ '-Ni₃Al-based alloys having excellent resistance to both high-temperature oxidation and creep are being developed in a systematic manner using multiple alloying additions, including Pt and Ir, *i.e.*, platinum group metals (PGMs). Oxidation behavior was studied at 1000°C in both thermal cycling and isothermal conditions. PGM additions were found to reduce the detrimental effects of "strengthening" alloying additions on oxidation and to promote formation of Al₂O₃ scales. Investigation of shortterm oxidation was also conducted to determine oxide scale evolution. Microstructural characterization including elemental partitioning, volume fraction, and solvus boundaries were also examined. Lattice parameters of γ and γ' were determined at 1000°C using controlled-atmosphere HT-XRD and compared to precipitate morphologies.

Recent Developments in Semiconductor, Electro Optic and Radio Frequency Materials: Recent Advances in Semiconductor Technologies

Sponsored by: The Minerals, Metals and Materials Society, TMS Electronic, Magnetic, and Photonic Materials Division, TMS: Thin Films and Interfaces Committee

Program Organizers: Nuggehalli Ravindra, New Jersey Institute of Technology; Narsingh Singh, Northrop Grumman Corporation, ES; Aris Christou, University of Maryland; Nancy Michael, University of Texas; Bhushan Sopori, National Renewable Energy Laboratory; John Parsey, On Semiconductor

Monday AM	Room: Oceanic 6
February 26, 2007	Location: Dolphin Hotel

Session Chairs: John Parsey, On Semiconductor; Aris Christou, University of Maryland

9:00 AM Introductory Comments

9:05 AM Invited

54

Growth of Bulk and Thick Film of Oxide Materials: Narsingh Singh¹; Hong Zhang¹; David Knuteson¹; Andre Berghmans¹; David Kahler¹; Brian Wagner¹; Jack Hawkins¹; 'Northrop Grumman Corporation

Liquid phase epitaxy (LPE) is a well-developed and viable technique for

thin film growth. Since LPE growth can be performed at reduced temperatures and closer to chemical equilibrium, films with near prefect crystallinity and purity can be achieved. However, in order to grow high-quality films using the LPE growth technique, the substrate and the experimental conditions must be carefully chosen. The most important criterion is that the lattice parameters of the substrate must be commensurate with those of oxide to be grown on substrate. We will present the example of a complex oxide lanthanum gallium silicate also known as langasite. The langasite crystal belongs to the trigonal system (class 32) with lattice constants of a=8.1783Å and c=5.1014Å. One must therefore choose a substrate with appropriate symmetry and similar lattice parameters. The flux used must have no chemical interactions with, and yet is capable of dissolving the langasite compound. We present the growth condition and optimization process for achieving thin and thick film. A comparison will be made with the bulk growth of this material.

9:30 AM Invited

Engineering Routes to Nanocomposite Semiconductors for Advanced Functionality and Applications: *Nancy Michael*¹; Choong-un Kim¹; ¹University of Texas at Arlington

Semiconductor nanocrystals, with their unique optical, chemical and electrical properties, may facilitate new industrial applications. Spurred by such a possibility, various forms of such crystals have been synthesized and studied; however their use has been limited to a few cases such as fluorescence for bio-imaging. One reason behind the limited application of semiconductor nanoparticles is related to difficulty in their production. Processes which produce quality nanoparticles are not only expensive but, more importantly, work only with very few materials. Secondly, the processes often do not provide sufficient flexibility in controlling microstructure, limiting the ability to tailor nanoparticle functionality. This paper introduces new methods of producing nanoparticles having multiple embedded microstrucural features. One method highlighted is precipitation, which has proven to be effective in making nanocomposite semiconductor nanoparticles. Its working principle and effectiveness will be discussed using the example material systems like CdS, CdTe, and PbTe.

9:55 AM Invited

Germanide-Silicide Optoelectronics Technologies: Nuggehalli Ravindra¹; Martin Lepsleter²; *Anthony Fiory*¹; 'New Jersey Institute of Technology; ²BTL Fellows

New technologies for uncooled Schottky-barrier devices based on Pt-group germanide-silicide alloys for high-speed infrared detectors will be presented. Applications include imaging arrays in high performance SiGe BiCMOS circuits and optical communications links. Cut-off wavelengths are matched for specific applications through the Schottky barrier height, which is selected by semiconductor carrier doping and type, Ge concentration, and the Pt-group metal. Active regions of the devices are readily fabricated down to 10 nm. The capability of pulsed high speed operation of Schottky barrier detectors enables suppressing the dark current for compact imaging and communications systems operating at ambient temperature. Further, germanide-silicide technology exploits the inherently low parasitic series resistance of Schottky barrier contacts in optoelectronic devices. High quantum efficiency is obtained in floating-base photo transistor devices with super-beta gain, fabricated with Pt-group germanide-silicide collector contacts integrated to SiGe strainedlayer heterostructure bipolar technology.

10:20 AM Invited

Electrical Detection of Deoxyribonucleic Acid Hybridization with AlGaN/ GaN High Electron Mobility Transistors: *Byoung Sam Kang*¹; Stephen Pearton¹; Jaujiun Chen¹; Fan Ren¹; Wayne Johnson²; ¹University of Florida; ²Nitronex Corporation

Au-gated AlGaN/GaN High Electron Mobility Transistor(HEMT) structures were functionalized in the gate region with label free 3'-thiol modified oligonucleotides. This serves as a binding layer to the AlGaN surface for hybridization of matched target DNAs. X-ray photoelectron spectroscopy (XPS) shows that immobilization of thiol modified DNA covalently bonded with gold on the gated region. Hybridization between probe DNA and matched or mismatched target DNA on the Au-gated HEMT was detected by electrical measurements. The HEMT drain-source current showed a clear decrease of 115 µA as this matched target DNA was introduced to the probe DNA on the surface, showing the promise of the DNA sequence detection approach for biological sensing.





10:45 AM Break

10:55 AM

InGaAs/InAlAs Based Metal-Semiconductor-Metal Photodetector for Opto-Electronic Mixers: Soohwan Jang¹; Nuri Emanetoglu²; Travis Anderson¹; Fan Ren¹; Stephen Pearton¹; Paul Shen²; ¹University of Florida; ²US Army Research Laboratory

An InGaAs metal-semiconductor-metal (MSM) based frequency-modulated continuous wave (FM/cw) laser detection system was demonstrated. For battlefield applications, an eye-safe LADAR is required, and 1.55 μ m wavelength is preferred. Typical Schottky barrier height on InGaAs is quite low (~0.1-0.2 eV), leading to high dark current of the MSM devices and, hence, to low signal-to-noise ratio. Higher energy bandgap, lattice-matched InAlAs Schottky enhancement layers (SEL's) grown on top of the InGaAs layer were employed to improve the barrier height. Dark current and parasitic capacitance were further minimized by using "smart designs" for the MSM device by decreasing finger width and removing the semiconductor layer underneath the final metal. Photodetector using Schottky enhancement layer was shown to yield low dark current, high dc responsivity of 0.5 A/W and flat mixing responsivity with an average of 0.2A/W.

11:20 AM

Low Angle Incidence Microchannel Epitaxy of GaAs Layer on GaAs (001) Substrates: Sota Matsuoka¹; Yo Yamamoto²; Toshiyuki Kondo¹; Takahiro Maruyama¹; Shigeya Naritsuka¹; ¹Department of Materials Science and Engineering, Faculty of Science and Technology, Meijo University; ²21st CENTURY COE program "NANO FACTORY", Meijo University

Lateral growth is important for highly mismatched heteroepitaxial system, such as GaAs growth on Si because it greatly reduces dislocation density in the grown regions. If lateral growth is achieved using molecular beam epitaxy (MBE), we can get tremendous advantages, such as excellent controllability of growth for minute device structures. Low angle incidence microchannel epitaxy (LAIMCE) is one of the most promising techniques which realize lateral growth using MBE. In LAIMCE, a lateral growth is achieved by irradiating molecular beams with a low incidence angle to a substrate, on which an array of line-shaped openings are cut in a SiO2 mask. In the present work, we especially investigate the shadow effect of the edge of the SiO2 mask, which prevents the molecular beams from irradiating the GaAs layer in the openings. Finally, we found a way to eliminate the shadow effect and succeeded in an excellent lateral growth in MBE.

11:45 AM Invited

Luminescence of Long-Term Ordered Pure and Doped Gallium Phosphide: Sergei Pyshkin¹; John Ballato²; Michael Bass³; Giorgio Turri³; ¹Academy of Sciences; ²Clemson University; ³University of Central Florida

The evolution of luminescence is reported from pure, N and N:Sm doped GaP single crystals grown over 40 years ago and evaluated approximately every 15 years. These results and new Raman light scattering data indicate the long-term impurity ordering and formation of a new type of crystal lattice where periodically disposed impurities modify, improve and essentially change luminescent characteristics. At room temperature due to high perfection and low level of nonradiative recombination pure and N doped ordered GaP demonstrate bright "hot" luminescence at the photon energies more than the indirect forbidden gap. Independent of temperature the ordered GaP:N: Sm system generates with high efficiency luminescence of activators (Sm) uniformly intermixed with N recombination centers. High density exciton system bound to N impurity superlattice grown by modern technologies and GaP:N, GaP:N:Sm nanocrystals distributed in transparent fluorine-containing polymers will be used as the base elements for new generation of optoelectronic devices.

12:10 PM

Silicon Germanium Nanostructures Doped with Rare-Earth Metals: Sufian Abedrabbo¹; Dia Eddin Arafah¹; James Markham²; Anthony Fiory³; Nuggehalli Ravindra³; ¹University of Jordan; ²Advanced Fuel Research; ³New Jersey Institute of Technology

Ion Beam Mixing (IM) is utilized to form nanostructure mixtures of Silicon, Germanium and Rare-Earth metals. Light emission efficiencies of the formed structures are investigated. Various characterization techniques covering the structural, compositional, optical and electrical properties are performed.

12:35 PM

Self Assembly of Au Nanodots: Growth, Physical Properties and Challenges: *Nori Sudhakar*¹; Chunming Jin¹; Wei Wei¹; Jagdish Narayan¹; ¹North Carolina State University

Recently, self assembled metal embedded nanoparticles in wide band gap semiconductor systems have been attracting the scientific community owing to their interesting optical, electrical and mechanical properties. More often than not some of the physical properties exhibited in certain systems at nanometer length scales (<10 nm) are hard to conceptualize and quite controversial. Optical absorption properties can be modified by the size profile of the metal nanodots. We have used a pulsed laser deposition technique to grow Au nanoparticles with a concentration gradient embedded in ZnO as the matrix layers. ZnO was deposited on Si(111) substrate at 400°C followed by gold deposition and repeated this process several times. The size of the Au nanodots embedded was controlled by the thickness of the Au layer. It is envisaged that Au islands or nanodots at very low concentrations of the order of a monolayer show evidence for enhanced electrical and optical properties.

Recycling and Waste Processing: Materials Recovery from Wastes

Sponsored by: The Minerals, Metals and Materials Society, TMS Extraction and Processing Division, TMS Light Metals Division, TMS: Recycling and Environmental Technologies Committee

Program Organizers: Mark Schlesinger, University of Missouri; Robert Stephens, Teckcominco, Inc.; Donald Stewart, Alcoa Technology; Ray Peterson, Aleris International; Jan van Linden, Recycling Technology Services, Inc.; Subodh Das, SECAT; Abdel Serna-Vasquez, Aleris International; Cynthia Belt, Aleris International Inc; John Pickens, Alumitech/Aleris International; John Hryn, Praxair; Richard Kunter, Richard S. Kunter and Associates; Andreas Siegmund, Quemetco Metals Inc.; Masao Suzuki, AI Tech Associates

Monday AMRoom: Australia 2February 26, 2007Location: Dolphin Hotel

Session Chairs: Masao Suzuki, AI Tech Associates; John Hryn, Praxair

9:00 AM

Salt Cake Management at Secondary Aluminum Smelters: A Case Study of Best Practice: *John Hryn*¹; Miguel Lizaur²; ¹Argonne National Laboratory; ²Iberica de Aleaciones Ligeras, S.L. (IDALSA)

Recycling aluminum at secondary smelters usually involves the use of salt fluxes to improve aluminum recovery. Unfortunately, the use of salt fluxes results in the generation of a salt cake waste stream, containing spent salt flux, unrecovered aluminum, and non-metallic oxide residue (NMP). Attempts at developing a viable salt cake recycling technology to date have been unsuccessful, primarily due to the high energy cost of recovering a usable salt fraction from salt cake. In addition, impurities in NMP restrict its use in many market segments. From an energy and environmental perspective, the best practice today is to maximize aluminum recovery from salt cake and dispose the salt and NMP fractions in a controlled landfill. This approach to salt cake management is practiced by leading secondary aluminum companies, including IDALSA. This paper describes salt cake management at IDALSA, emphasizing the superior energy, economic, and environmental benefits of this approach.

9:25 AM

Structure of Hot Slag from Aluminum Remelt: Serguei Novichkov¹; Anatoly Zholnin; ¹Mosoblprommontazh

The ideas of dependence of the observed properties of aluminum slag (consistency of hot slag, color of cold slag, ability of hot slag to protect aluminum against oxidation, etc.) on existence of dispersed oxides of squamous or flake-like shape are well-founded. Oxide flakes, which are present in the moving liquid flux, touch each other and this results in a lesser flowability of flux. The more dispersed oxides of flake-like shape are present, the lower will be the flowability of flux. With continued increase of their concentration, the oxide flakes enter in a permanent engagement between themselves. The capillary forces of the liquid flux filling the inter-flake spaces facilitate the



engagement between oxide flakes. At a certain threshold concentration of oxide particles in the liquid flux, all flux accumulates on oxide clots. The slag loses all of its liquid properties and becomes dry and crisp. The flux, the presence of which is proved by laboratory analyses, does not protect aluminum any more against oxidation. The threshold concentration of oxides in the flux, at which the hot slag becomes crisp, depends on the geometry of oxide particles and flux surface properties.

9:50 AM

Mineralogical Study on Steel Slags Oriented to Vanadium and Titanium Recovery: Liang Yu¹; Yuanchi Dong²; *Liaosha Li*²; Yun Zhou²; Xingrong

Wu²; ¹University of Science and Technology Beijing; ²Anhui University of Technology

As some vanadium and titanium in the iron ore entered the steel slags during steelmaking, mineralogical phases of steel slags were studied oriented to the metals recovery. Samples were collected from the tailings of slag processing plants of MA Steel and BaoSteel in China. According to SEM, LOM and other studies, it was found that vanadium and titanium concentrated dominantly super cooled liquid slag with no phosphorus detected respectively. The super cooled liquid slag contains mainly calcium oxides, iron oxides, aluminum oxides, vanadium oxides and titanium oxides. It is possible to recover vanadium and titanium from it with very low phosphorus content, important for vanadium and titanium application in steel making process. Other phases found in steel slags includes: solid solution of dicalcium oxides and calcium phosphate which could be used for phosphorus recovery, dicalcium ferrite and wustite for iron, manganese and magnesium recovery.

10:15 AM

Recycling of Blast Furnace Sludge into Clayey Ceramics: *Carlos Maurício Vieira*¹; Sergio Monteiro¹; Cláudio André Dias¹; Alice Mothé¹; ¹State University of the Northern Fluminense

This work has for objective to characterize a waste generate during the steelmaking process, denoted as blast furnace sludge, and to evaluate its influence on the microstructural aspects and technological properties of a clayey ceramic, incorporated up to 20 wt.%, material. To determine the technological properties such as bulk density, linear shrinkage, water absorption and flexural strength, specimens were prepared by 18 MPa uniaxial pressure and then fired in laboratory furnace at 900°C. The microstructure of the compositions was evaluated by electron scanning microscopy and X-ray diffraction. The results showed that it is possible to recycle the blast furnace sludge into red ceramics.

10:40 AM Break

11:00 AM

Mechanical Activation of Deposited Fly Ash by Grinding: *Gabor Mucsi*¹; Barnabás Csoke¹; Csaba Sík²; ¹University of Miskolc; ²H-TPA Company Ltd.

According to laboratory experience the breaking of fly ash particles is required to increase its hydraulic potential (Opoczky, 2001). Aim of the research reported in this paper is to find relationship between the necessary effective grinding work and the hydraulic activity of fly ash. Deposited class F type fly ash from Hungary have been sampled and tested. The prepared samples were ground systematically in a laboratory Bond ball mill, while the effective grinding work was measured as well, by means of measuring the electrical power on the wiring of the mill motor. Result of this mechanical activation was tested by the following methods. The activity index was determined by the standard MSZ EN-450. Microstructure was tested by SEM, while the specific surface area was determined by the BET and Blaine devices. Relations between the parameters of the mechanical activation and the achieved hydraulic activity have been established.

11:25 AM

Characteristics of Zeolite Manufactured with Sludge Generated from Water Puriciation Plant: *Kwang-Suk You*¹; Gi-Chun Han¹; Hee-Chan Cho²; Ji-Whan Ahn¹; ¹Korea Institute of Geosicence and Mineral Resources; ²Seoul National University

The sample of sludge was obtained from water purification plant near Seoul in Korea. The chemical composition of the sludge consist of SiO2 and Al2O3, and the ratio of SiO2/ Al2O3 in sludge was about 1.4. After drying, a representative sample was controlled particle size by ball mill, that is was ground below 100 μ m. The synthesis of zeolite from sludge by-produced from water purification plant ware carried out by the alkali hydrothermal method. In 500ml of autoclave, Zeolite was synthesis at over 100°C. The reaction time was 24hr. The results indicate that the Zeolite synthesized from the sludge is mainly hydroxyl-sodality type in the solution with higher NaOH concentration. The zeolite synthesized in this method will be expected to be use for the purpose of soil improvement in large quantities.

11:50 AM

Using Weathered Granite for Ceramic Tile Production: Kalayanee Kooptarnond¹; Danupon Tonnayopas¹; ¹Prince of Songkla University

Granite is produced either in the form of block or as processed products. However the weathered granite is still has no commercial use. The investigation of using the weathered granite as alternative single raw material for making tiles was conducted. The weathered granite sample was ground to -100 and -200 mesh. These fine particles were pressed into tile form using a hydraulic press at 100 and 150 bars and fired at 1100-1250°C. The characteristics of the tiles were tested for corrosion resistance, mechanical strength, firing shrinkage and water absorption according to the Thailand Industrial Standard (TIS) for wall clay tile. Microstructure analysis of the fired products was carried out using XRD and SEM. It was found that the tile specimens fired at 1200 and 1250°C exhibited interesting water absorption properties of 0.3-4% and high mechanical strength about 50-27 MPa.

12:15 PM Invited

Generation of Hexavalent Chromium in Calcination of Chromium Containing Hydroxide and Sludge from Surface Finishing Industries: *Ryokichi Shimpo*¹; Shigeo Hoshino¹; Mitsuo Iyoda²; ¹Musashi Institute of Technology; ²Techno Industrial MFC Company, Ltd.

Waste sludge from surface finishing industries generally contains much amount of water. Though calcination seems a simple and convenient method for reducing volume and weight of the sludge, it tends to convert chromium in the sludge to the harmful hexavalent state. The aim of this study is to find out a better treatment and recycling method of the sludge, which will give less environmental loads. In order to confirm the relation between the calcining conditions and the generation of hexavalent chromium, experiments of heating artificial sludge, which was mixture of hydroxide reagents, have been compared with those of the actual sludge from a surface finishing industry. As a result, the change of the hexavalent chromium amounts leached form the calcined samples has a peak with heating temperature. It has also turned out that the heat-treated sludge can be used as the material for electric-magnetic wave absorption.

12:40 PM

How Flames/Load Interaction Affects Furnace Efficiency in Round Top Furnace Operation: *Brian Golchert*¹; Hossam Metwally¹; Ashwini Kumar¹; Cynthia Belt²; Joseph Tessandori²; ¹Fluent Inc; ²Aleris International Inc

When the burners initially fire in a roundtop furnace, the flames will impinge upon the load and will continue to impinge upon the load until the load is nearly melted. This flame impingement affects the mixing of the fuel and oxidizer and the efficiency of the furnace. Computational fluid dynamics is a powerful tool that would allow more efficacious investigation of the efficiency of the furnace under these conditions. A detailed, transient model of the furnace would be computationally expensive to perform and would result in limited additional information. Instead, a series of 'snapshots' of the furnace will be modeled. Each snapshot will be a computational model of the load at various stages of the melting process. For each snapshot, the thermal efficiency and behavior of the furnace will be quantified. This paper will present the results from this analysis along with some suggestions on how to improve furnace performance.

Technical Program



Refractory Metals 2007: Processing and Mechanical Deformation

Sponsored by: The Minerals, Metals and Materials Society, TMS Structural Materials Division, TMS: Refractory Metals Committee *Program Organizers:* Gary Rozak, HC Starck Inc; Todd Leonhardt, Rhenium Alloys Inc

Monday AM	Room: Europe 6
February 26, 2007	Location: Dolphin Hotel

Session Chairs: Todd Leonhardt, Rhenium Alloys Inc; Omer Dogan, National Energy Technology Laboratory

9:00 AM Introductory Comments in Memory of Prof. Mehmet Uz

9:05 AM

An Investigation into the Electrochemical Reduction of Zirconium Dioxide in Molten Calcium Chloride: *Derek Fray*¹; K. Mohandas¹; ¹University of Cambridge

Many metal oxides have been reduced to the metal by making the oxide the cathode in a bath of molten calcium chloride. Zirconium dioxide offers additional challenges over other metal oxides as it is highly stable, insulating and zirconium only has one valency. Other metal oxides are less stable and perhaps conducting with several sub oxides. However, by careful control of the porosity and by reducing thin pellets, it was possible to successfully reduce zirconium dioxide to the metal. The results of this work will be presented.

9:30 AM

Weldable Ductile Molybdenum Alloy Development: Brian Cockeram¹; David Alven¹; Evan Ohriner²; Lance Snead²; ¹Bechtel Bettis Inc; ²Oak Ridge National Laboratory

Molybdenum and its alloys possess many properties that make them attractive for materials of construction for high-temperature applications. These include elevated temperature strength and creep resistance, corrosion resistance to molten metals, and high thermal conductivity. One deficiency for molybdenum alloys in most applications is related to welded joints. This is due to limited ductility and relatively high ductile-to-brittle transition temperature for recrystallized material, and in particular the recrystallized heat-affected zone of welds. In earlier work it was shown that molybdenum alloyed with boron in the range of 6 to 10 ppm (by wt.) and either 1500 ppm Zr or 30 ppm Al exhibits significant room-temperature tensile elongation in gas tungsten arc (GTA) welds. Atom probe analysis showed that segregation of Zr, B, and C to grain boundaries in the heat affected zone of the weld and depletion of O at the grain boundary were associated with the improved ductility. In this study a series of arc melted molybdenum alloys containing additions of B, C, Zr, and Al are characterized with respect to tensile properties, bend properties, and impact energy. The material conditions include stress-relieved, recrystallized, and electron-beam welded samples. Microstructural behavior of these materials is also described.

9:55 AM

Room Temperature Creep and Dislocation Substructure in Electron Beam Welds in RRR Niobium: Hairong Jiang¹; Boon-Chai Ng²; *Bieler Tomas*¹; Chris Compton¹; Terry Grimm¹; ¹Michigan State University; ²Andrews University

Room temperature creep up to strains near 0.1 occurred below the yield strength in high purity niobium Electron Beam welds (EBW), but not in the polycrystalline parent material, even though they have nearly equal yield strengths. The strain-time process follows a logarithmic creep process, where exhaustion occurs, and then restarts after a stress increase or an incubation time at the same stress. To examine why, orientation imaging microscopy was used to determine the orientations of the grains and identify the most highly stressed slip systems. Selected area channeling patterns (SACPs) were used to orient the sample to optimal imaging conditions for Electron Channeling Contrast Imaging (ECCI) to identify the morphology of dislocation substructure present in the grains. The dislocation densities were high even in welds in which no measurable strain was induced, indicating that the weld solidification caused a large and apparently unstable dislocation substructure to develop.

10:20 AM Break

10:35 AM

Comparing ECAE and Rolling of Niobium: *Derek Baars*¹; Thomas Bieler¹; Ted Hartwig²; ¹Michigan State University; ²Texas A&M University

Deformation from rolling and subsequent annealing produces texture in sheet niobium. A desired {111} texture develops in middle of the sheet that improves subsequent deep drawing, however, the {100} texture that often develops at the surface is detrimental to deep drawing. Textures formed by equal channel area extrusion (ECAE), a severe deformation process that preserves sample cross-section, were investigated to determine a processing path for maximizing the desired {111} texture and minimizing the undesired {100} texture. Utilizing orientation imaging microscopy (OIM), textures produced by ECAE and rolling were compared. It was found that ECAE of a 25x25x125 mm billet, with no rotation of the square billet between passes, then rolling the billet in the longitudinal direction to reduce the thickness by a quarter-inch, then rolling in the transverse direction to final thickness, maximized the desired {111} texture compared with other ECAE processing paths and rolling.

11:00 AM

Anisotropic Deformation Characteristics of Rhenium: John Bingert¹; Paul Maudlin¹; ¹Los Alamos National Laboratory

Rhenium is an hcp, refractory transition metal with remarkable physical and mechanical properties; among these is its significant plastic anisotropy. The response of rhenium to compressive deformation over a range of temperatures was analyzed in order to investigate its anisotropic mechanical properties. Polycrystalline samples of textured plate and randomly textured hot isostatically pressed material were examined. Electron backscatter diffraction (EBSD) was used to track texture evolution and quantitatively identify and measure deformation twinning activity. The activation of the {11-21} tensile twin system was found to be a significant determinant in both the development of anisotropy and rhenium's extraordinary strain hardening response. Plastic yield surfaces were calculated using informed assumptions of relative deformation activity, and these are shown to be instructive in predicting anisotropic behavior. Material instability is also addressed through the application of bifurcation analysis incorporating plastic anisotropy.

11:25 AM

Tensile and Fracture Toughness Properties of Two Mo-Re Alloys: Mikhail Sokolov¹; 'Oak Ridge National Laboratory

Molybdenum is a refractory metal known to have a relatively low (30 MPavm) toughness even at temperatures above the ductile-to-brittle transition temperature. However, the addition of rhenium is known to improve the ductility and fabricability of molybdenum alloys. The improved ductility of Mo-41% Re and Mo-47.5% Re alloys suggests a fracture toughness of greater than 30 MPavm for these alloys. However, the actual fracture toughness values of these alloys were unknown. The objective of this testing program was to perform an initial fracture toughness characterization of these two alloys at 200, 300, and 500K. Both alloys exhibited substantial fracture toughness throughout the tested temperature range. The fracture toughness results will be discussed and compared to tensile data and other properties available in the published literature.

11:50 AM

Study on High Quality Ultra-Fine WC Powder by Turbo-Air Stream Classifying: *Liu Qingcai*¹; Zheng Yonggang¹; Yun Gui Du¹; Linyan Dong¹; ¹Chongqing University

Based on the turbo-air stream classifying principle, the quality of superfine WC powder get further improving by means of superfine pulverizing grader. Experiments show that the technology of air steam classifying has significant effect on increase of the fineness and the particle classification efficiency. By comparing different type of air stream equipment, the QYF fluid-bed superfine pulverizing grader was adopted in the experiment that was manufactured by KunShan superfine pulverizers factory as well as obtaining high quality superfine WC powder with high homogeneous.

Structural Materials Division Symposium: Mechanical Behavior of Nanostructured Materials, in Honor of Carl Koch: Fatigue, and Strengthening Mechanisms at Small Length Scale

Sponsored by: The Minerals, Metals and Materials Society, TMS Electronic, Magnetic, and Photonic Materials Division, TMS Materials Processing and Manufacturing Division, TMS Structural Materials Division, TMS: Chemistry and Physics of Materials Committee, TMS/ASM: Mechanical Behavior of Materials Committee, TMS: Nanomechanical Materials Behavior Committee

Program Organizers: Xinghang Zhang, Texas A&M University; Yuntian Zhu, Los Alamos National Laboratory; Michael Rigsbee, North Carolina State University; C. Suryanarayana, University of Central Florida; Haiyan Wang, Texas A&M University; C. T. Liu, Oak Ridge National Laboratory

Monday AMRoom: Asia 5February 26, 2007Location: Dolphin Hotel

Session Chairs: Michael Rigsbee, North Carolina State University; K. Linga Murty, North Carolina State University

9:00 AM Introductory Comments Welcome and Overview by X. Zhang

9:05 AM Keynote

Fatigue at the Nanometer and Submicrometer Scale: Anthony Escuadro¹; Kai Zhang¹; *Julia Weertman*¹; ¹Northwestern University

While a large number of studies have been carried out on the mechanical behavior of nanocrystalline and submicrometer grain-size (UFG) metals under time-independent loading or displacement conditions, comparatively little research has been done in the case of cyclic deformation. Results of fatigue behavior of such materials will be discussed. This research was sponsored by the US Department of Energy, Grant DE-FG02-02ER46002.

9:30 AM Invited

Cyclic Deformation and Fatigue at the Sub-Micron and Nano-Scale: Oliver Kraft¹; Dong Wang¹; Daniel Weygand²; Cynthia Volkert¹; ¹Forschungszentrum Karlsruhe; ²Universität Karlsruhe

We are exploring the question whether fatigue is subject to a size effect in the sub-micron and nano-regime by investigating the behavior of Cu thin films on deformable substrates during repeated cyclic loading. For the films thicker than 1 μ m, long-range dislocation structures, such as veins, are observed similar to bulk behavior. With decreasing dimension, the fatigue resistance of the films increases as larger stress amplitudes are required in order to introduce fatigue damage at a given number of cycles. Furthermore, long-range dislocation ordering does not occur. These trends are more accentuated for fatigue of films with thickness of 100 nm and below. Furthermore, we apply mesoscopic discrete dislocation dynamics simulation studying the influence of the dislocation microstructure on the deformation behavior and to predict the plastic response of small structures. The gained insights provide a basis for understanding cyclic deformation of metallic materials at various length scales.

9:50 AM

An Evaluation of the Creep Characteristics of Electrodeposited Nickel-Based Nanocomposite: Vaclav Sklenicka¹; Kveta Kucharova¹; Gabriele Vidrich²; Milan Svoboda¹; Hans Ferkel²; ¹Academy of Sciences; ²Clausthal University of Technology

Particle-reinforced nickel-based composites have extensive potential for use in structural applications at elevated temperatures. However, any use will require a detailed understanding of the creep characteristics of these composites and especially the dependence of the measured creep rates on the applied stress and the testing temperatures. This work examines these characteristics with reference to the creep behaviour of the unreinforced electrodeposited nickel. Samples of each material were tested to failure and the fracture surfaces of selected specimens were examined using scanning electron microscopy. The results show that the creep resistance of the nickel nanocomposite reinforced by nano-sized SiO2 particles at temperatures in the range from 293 to 573 K may be improved in comparison with the unreinforced nickel.

10:05 AM Invited

Optimization of Strength, Ductility and Damage Tolerance in Nanostructured Metals and Alloys: Subra Suresh¹; Ming Dao¹; ¹Massachusetts Institute of Technology

This presentation will deal with strategies for optimizing the strength, ductility and damage tolerance of engineering metals and alloys through the use of nanoscale structural features. Experimental results and transmission electron microscopy observations of deformation mechanisms will first be presented to highlight the strength, strain hardening response, strain rate sensitivity, ductility, failure mechanisms and activation volume for nanocrystalline metals relative to their microcrystalline counterparts. The effects of the introduction of nano-scale twins of different concentrations in influencing the stress-strain response of polycrystalline fcc metals in enhancing strength without severe loss of ductility will be demonstrated. A quantitative model for this effect will then be presented by recourse to detailed computational simulations of deformation processes using atomistic as well as crystal plasticity models. Attention will then be directed at the effects of grain size, down to the nanocrystalline regime, on the onset and propagation of fatigue cracks from surfaces. A particularly useful outcome of this exercise is the realization of how refinement of grain size in the nanocrystalline regime can have competing effects on fatigue crack initiation versus propagation. Experimental results for fatigue of electrodeposited nanocrystalline metals will be compared and contrasted with those of equal-channel-angular-pressed fine-grained metals. Overall strategies for enhancing resistance to fatigue through the introduction of controlled surface gradients in grain size will also be discussed.

10:25 AM

Interfacial Plasticity in Nanostructured Metals: *Ting Zhu*¹; Ju Li²; Amit Samanta²; Hyoung Gyu Kim²; Subra Suresh³; ¹Georgia Institute of Technology; ²Ohio State University; ³Massachusetts Institute of Technology

Nanocrystalline metals with grain size finer than 100 nm routinely exhibit up to five times higher strength than their coarse-grained counterparts, but suffer from greatly diminished ductility. Experiments show that introduction of coherent nano-twins in ultrafine grained copper leads to an unusual combination of high strength and high ductility, along with increased strainrate sensitivity. Here we present a mechanistic framework for rationalizing this strength versus ductility trade-off in nanostructured metals in terms of the interactions of dislocations with coherent twin boundaries (TBs). Using atomistic reaction pathway calculations, we show that TB-mediated slip transfer reactions are the rate-controlling mechanisms of plastic flow. We attribute the origin of relatively high ductility of nano-twinned copper to the hardenability of TBs as they gradually lose coherency during deformation. These results offer new avenues for tailoring material interfaces for optimized properties.

10:40 AM Break

10:50 AM Invited

Alloying Effects on the Mechanical Behavior of Nanocrystalline Metals: Ronald Scattergood¹; 'North Carolina State University

Alloying additions to nanocrystalline (nc) metals can produce solid solutions and 2nd phases. At nanoscale grain sizes the effect of these additions on the mechanical behavior will differ from that of conventional grain size metals. Grain boundary interactions and size scaling are two important considerations. The current state of knowledge on alloying effects in nc metals will be reviewed. Recent research results obtained in collaboration with Professor Koch will highlight a number of these effects. Depending on the choice of the system and the processing history, non-equilibrium solid solutions with large misfit solutes can produce hardening or softening effects. Grain boundary interactions appear to play an important role in the behavior. 2nd phase particles can also produce hardening or softening effects. The origin of these effects is related to size scaling determined by grain size vs. particle size and the relative hardness of the particles with respect to the matrix.

11:10 AM

Strength of Nanocrystalline Metals: Influence of Recovery and Recrystallization: *Tong Shen*¹; John Swadner¹; Jian Huang²; Shi Feng¹; Ming Tang¹; Evan Ma³; ¹Los Alamos National Laboratory; ²Boston College; ³Johns Hopkins University

We study the influence of recovery and recrystallization on the hardness of





nanocrystalline metals. Recovery does not decrease the hardness although 90% of the total dislocations are removed. Instead, recrystallization significantly lowers the hardness. These behaviors are opposite to what happens in work-hardened polycrystalline materials. We find that most of the dislocations stored in nanograins take the form of dislocation dipoles, which only generate short-range stress fields and contribute little to the overall strength. In fact, recovery anneal even hardens some of our nanocrystalline alloys. Our results suggest that the strength of nanocrystalline metals depends mainly on how dislocations nucleate and emit from grain boundaries. When the grain boundaries are structurally relaxed, dislocation nucleation and emission from the grain boundaries require higher stress. The latter would also be true if there is compositional segregation to the grain boundaries, which could also have consequences in reducing the ductility in some cases.

11:25 AM Invited

Effect of Solute Segregation on the Hardness of Nanocrystalline Alloys: *Ricardo Schwarz*¹; Tong Shen¹; John Swadener¹; Jian Huang²; Shi Feng¹; Ming Tang¹; ¹Los Alamos National Laboratory; ²Boston College

We used mechanical alloying to prepare single-phase nanocrystalline powders of elemental Fe, and Fe85Al4Si11, Ni90Fe1 and Ni90Fe10 alloys. We measured the structural and mechanical properties of these powders as a function of isochronal anneals at increasingly higher temperatures. As expected, increasing the annealing temperature decreases the dislocation density and increases the grain size in non-linear fashion. The hardness of the pure Fe also decreases monotonically with increasing annealing temperature. However, the hardness of the alloys first increases, reaching a rather sharp maximum (at a temperature that depends on the partial molar volume of the solute atom), and then decreases. Only after this maximum does the hardness versus grain size follow the Hall-Petch relation. These tests suggest that the often observed violations of the Hall-Petch relation in nanocrystalline materials may be caused by a redistribution of solutes at dislocations and grain boundaries.

11:45 AM

Strengthening in Nanostructured FeAI: David Morris¹; Maria Muñoz-Morris¹; ¹CENIM-CSIC

The strengthening effect of grain boundaries has been extensively studied in Fe-base alloys with grain sizes from the micron level down to the nanoscale (about 10 nm). A comparison of such hardening in nanostructured ordered FeAl and in unalloyed Fe, prepared by mechanical alloying or milling, makes it clear that the intermetallic shows much greater hardening over a wide range of grain sizes. A possible reason for such hardening may be the difficulty of nucleation of superdislocations in the intermetallic, analogous to the difficulties of nucleating pairs of Shockley partial dislocations in nanoscaled fcc materials. Evidence for the greater hardening of these intermetallics will be presented, and the origin of the hardening examined.

12:00 PM

Effect of Laser Shock Compression on Hardness of Nanostructured Metals: *Xiaojing Xu*¹; Yongkang Zhang¹; Xudong Ren¹; Jinzhong Lu¹; ¹Jiangsu University

The effect of laser shock compression on hardness of nanostructured metals was investigated. The used nanostructured metals included nanostructured CP-Ti produced by multi-step compressive deformation at liquid nitrogen temperature (LNT), nanostructured CP-Cu produced by ECAP deformation at LNT, nanostructured 2024Al produced by ECAP deformation at room temperature, and ultrafine grained Zn-22Al alloy produced by quenching into liquid nitrogen. These nanostructured metals were subjected to the laser shock compressive deformation with the strain rate as high as 1000000/second and the pressure of about 5 GPa. Microhardness tests show that the shock deformation improved the microhardness very slightly, about 11.1% for nanostructured CP-Ti, 5.2% for nanostructured CP-Cu, 4.4% for nanostructured 2024Al, and 1.7% for ultrafine grained Zn-22Al. A dislocation-based recovery model was used to understand the low hardening behaviors during the shock deformation. This theoretical analysis shows that dislocation accumulation cannot easily occur in a grain during the shock compressive deformation.

12:15 PM

Mechanical Properties of Dual-Phase Nanocrystalline Al-W and Al-Pb Alloys: *Koteswararao Rajulapati*¹; R Scattergood¹; K. Linga Murty¹; Carl Koch¹; Zenji Horita²; Terence Langdon³; ¹North Carolina State University; ²Kyushu University; ³University of Southern California

Nanocrystalline materials (grain size < 100 nm) have triggered an enormous amount of curiosity in the recent past among the scientific community because of their novel, superior and unique properties. Many researchers have demonstrated that the refinement of grain size alone can result in the multifold enhancement of mechanical strength. On the other hand, nano scaled dispersions have a positive effect on the strength of coarse grained materials. However the combined effects of nano sized dispersions and a nano scaled matrix on the mechanical strength of polycrystalline solids are yet to be established in detail. The effect of nano scaled Pb or W dispersions on the mechanical properties of nanocrystalline Al was investigated and will be presented here. This paper will cover the different processing methods used to synthesize these materials, their microstructural features, the observed mechanical properties and the governing mechanics of plasticity. This research is supported by NSF-DMR-0201474.

The Material Recycling Industry: Global Challenges and Opportunities: Plenary Session

Sponsored by: The Minerals, Metals and Materials Society, TMS Light Metals Division, TMS: Aluminum Committee Program Organizer: Subodh Das, University of Kentucky

Monday AM	Room: Southern 1
February 26, 2007	Location: Dolphin Hotel

Session Chair: Subodh Das, University of Kentucky

9:00 AM Plenary

Recycling in the Aluminum Industry: *Terrance Hogan*¹; ¹Aleris International Inc

Recycling has been practiced in the aluminum industry due to the high value of metal. Beginning in the 1970's the percentage of recycled metal as a feed source for North American industry began to grow rapidly. In 2004, recycled aluminum made up 30% of the total metal supply in North America. The rate is even higher if you look at just the United States as Primary capacity has declined. As recycling rates have increased, technology has improved to meet the increasing rates of production and to economically process lower quality scraps and by-products. Good connectivity exists between the aluminum fabricators/manufacturers and the secondary recycling industry, but less connectivity exists with the post-consumer market. In 2005 over 51 billion used beverage cans were recycled in the US, but this accounted for just 52% of the total available cans distributed to consumers. Comparisons with other countries will be made.

9:25 AM Plenary

Environmental Management of Airborne Metal Emissions in the Recycling Industry: *Karen Hagelstein*¹; John Heinze²; ¹Times Limited; ²Environmental Health Research Foundation

The paper will review current information addressing international air quality due to airborne metal emissions from recycling facilities, other human activities, and natural sources. Air quality regulations and health-based data will be consolidated to provide perspective regarding major sources of metal emissions, environmental impacts, and health risks. The ambient air metal emissions, point and non point sources, and occupational exposures in the recycling industry will be examined Research focusing on environmental management of air pollution such as material substitutions, waste management practices, worker health and safety, environmental and biological monitoring, and best available air pollution control technologies will be presented. Case studies and lessons learned from other industries such as coal fired power plants will be examined with respect to managing metal emissions, especially mercury and selenium compounds. A spreadsheet for performing a screeninglevel environmental audit for industry and/or consultant applications will also be provided.



9:50 AM Plenary

RecycleBank Pays for Recycling: Scott Lamb1; 1RecycleBank

RecycleBank is the inventor and lead implementer of Incentive Based Recycling Programs. RecycleBank rewards homeowners for the amount individual home recycles. RecycleBank provides homes with a 35, 64, or 96 gallon RecycleBank Container that has an imbedded barcode. The RecycleBank Container is equipped with wheels and a lid. Delivery and service is included. RecycleBank supports a single stream recycling system that enables households to deposit all of your recyclables (paper, cardboard, plastic, glass, tin, aluminum) in the RecycleBank Container. The amount a home recycles is translated into RecycleBank Dollars that households can use to shop at over 200 participating stores. RecycleBank was started in 2004 and is headquartered in Philadelphia. RecycleBank currently has operations in Pennsylvania, New Jersey, and Delaware with plans to launch nationally in 2007. RecycleBank partners with municipalities, waste haulers, businesses and households in a concerted effort to increase recycling rates across America.

10:15 AM Plenary

Improved UBC Melting through Advanced Processing: *Thomas Thornton*¹; Clay Hammond¹; Jan Van Linden²; Paul Campbell³; Chris Vild³; ¹Wise Alloys LLC; ²Recycling Technology Service Inc; ³Pyrotek Inc

Aluminum recycling is undergoing a global boom. In order to survive in this competitive market of high energy and raw material costs, and relatively low finished goods prices, producers must minimize conversion costs while maximizing the recoverable metal units. Wise Alloys LLC has realized significant gains in production and metal recovery while reducing energy usage after converting to a high capacity UBC continuous melting process. The essential improvements will be discussed.

10:40 AM Break

10:50 AM Plenary

Characterizing Sustainable Material Recovery Systems: A Case Study of E-Waste Materials: *Jeremy Gregory*¹; Elisa Alonso¹; Frank Field¹; Randolph Kirchain¹; ¹Massachusetts Institute of Technology

Secondary material streams have become an important component of material production and are attractive because of their economic and environmental benefits, which can significantly improve the sustainability outlook of a material system. The global economy and its implications on material flows has made decisions related to acquisition, disassembly, and material recovery from complex products increasingly difficult. This paper describes a method to characterize the pathways and attributes of eco-efficient material recovery from engineered products. The method considers material recovery effectiveness, environmental impact, and economic cost when determining eco-efficiency. Results are presented as part of a case study on materials systems associated with electronic waste (e-waste), including leaded glass. Scenarios are evaluated that vary the location of product origin, disassembly, material recovery, and end-market. The evaluation criteria are assessed at each location to determine the pathways and conditions that create the most eco-efficient solutions.

11:15 AM Plenary

Separation and Recycling Technologies of Mixed Al and Mg Scrap: *Christian Wögerer*¹; Günther Klammer²; Michael Kettner³; ¹ARC Seibersdorf Research GmbH; ²Profactor Produktionsforschungs GmbH; ³ARC Leichtmetallkompetenzzentrum Ranshofen GmbH

The increase in parts manufactured from Al and Mg has been accompanied by an increase in residues from machining and other production operations. These by-products can be contaminated with lubricants, paint, non metallic materials or other metals. This paper describes a process to separate Al and Mg chips for a separate recycling in a fast continuous process. The process chain is described from pre-treatment and removing lubricants to a new separation technology based a wet process as the key process. The challenges of the process are the composition and the kind of the wet phase of the process and parameters of the mechanical equipment like the throughput speed and the duration of stay in the reactor. The theory of the process and the first results of pilot trails are shown, advantages and disadvantages in comparison with commercial sensor based separation methods are also described.

11:40 AM Plenary

Integration between Mining and Smelting Business and Environmental Business: *Kazuaki Shimada*¹; ¹Dowa Mining Company, Ltd.

In environmental management and recycling, it is said that there are 3 factors to secure; Recovery of Valuables, Emission Control and Reduction of Residue to Landfill. From this point of view, a nonferrous metal industry has a potential to play an important role that is "The Anchor of Recycling" or "The Joint of Recycling Loop" in it. Dowa, one of Japan's leading producers of nonferrous metals has been expanding its business field to environmental management and recycling (E&R) business such as Metal Recycling, Waste Treatment and Soil Remediation and successfully by means of integration between its mining and smelting business sector and E&R business sector. It is essential for it to form the network of the plants based on the various technologies of the separation and the recovery. For further expansion of business and contribution to reducing environmental risk globally, Dowa established the plant in Suzhou, China to recover precious metals from e-wastes.

12:05 PM Question and Answer Period

Towards Functional Nanomaterials: Synthesis, Characterization, and Applications: Directed Nano Fabrication

Sponsored by: The Minerals, Metals and Materials Society, TMS Electronic, Magnetic, and Photonic Materials Division, TMS: Nanomaterials Committee *Program Organizers:* Zhiming Wang, University of Arkansas; Alexander Govorov, Ohio University; Andrey Rogach, Ludwig-Maximilians-Universität München

Monday AMRoom: Oceanic 5February 26, 2007Location: Dolphin Hotel

Session Chairs: Samuel Mao, Lawrence Berkeley National Laboratory and University of California at Berkeley; Naoki Kishimoto, National Institute for Materials Science

9:00 AM Invited

Molecular Self-Assembly on Carbon Nanotemplates: *Andrew Wee*¹; Wei Chen¹; Shi Chen¹; Xingyu Gao¹; ¹National University of Singapore

The ability to fabricate arrays of functional nanostructures with controlled size, shape and stability, is an ongoing challenge in nanotechnology. We present a study of molecular self-assembly on the carbon nanomesh on 6H-SiC(0001). The atomic structure of the carbon nanomesh has been previously determined; a carbon nanomesh arises from self-organization of excess carbon atoms forming a honeycomb arrangement atop 6H-SiC(0001) after annealing at 1100°C. The carbon nanomesh can be dynamically structured to control the periodicity and depth of the pores by annealing in vacuum. The diffusion and agglomerization behaviour of cobalt clusters on this nanomesh surface has been previously investigated using in-situ STM. It is found that Co atoms prefer to adsorb on the corner sites of this carbon nanomesh at the early stages. We will report our latest results on molecular adsorption (such as C60, CuPc) on this nanomesh template, for applications in molecular electronics and biosensors.

9:30 AM Invited

Novel Ion Beam Techniques to Control Nanoparticle Composites for Nonlinear Optical Applications: Naoki Kishimoto¹; Kenji Saito²; Jin Pan²; Haisong Wang¹; Yoshihiko Takeda¹; ¹National Institute for Materials Science; ²University of Tsukuba

Metal nanoparticles are promising for plasmonics associated with surface plasmon resonance, e.g., ultrafast nonlinear optics. Ion implantation is a promising tool to create/control nanoparticles for future optical devices. Unlike SPM-based nanofabrication, the ion implantation is a robust and efficient method to meet industrial production, having advantages of arbitrary atomic injection and good spatial controllability in depth. However, the lateral control of nanoparticles has been done limitedly with micro-beam- or masked implantation. Here, we introduce a hybrid ion implantation technique combining ion and laser irradiation, to control nanoparticles embedded in dielectrics. Photons of 2.3 eV or 3.5 eV were irradiated into SiO₂, either





sequentially or simultaneously with ion implantation of 60 keV Cu or 3 MeV Cu²⁺. Simultaneous photon irradiation of 2.3 eV selectively enhances nanoparticle precipitation in SiO₂, while sequential photon irradiation tends to dissolve pre-existent nanoparticles. Controlling laser irradiation enables us to handle nanoparticle assembly as a building block.

10:00 AM Invited

DNA-Directed Organization of Nanoparticles: *Friedrich Simmel*¹; Thomas Sobey¹; ¹Ludwig-Maximillian University-Munich

The unique molecular recognition properties of DNA in combination with powerful biochemical tools can be utilized to produce regular one- and twodimensional molecular structures. These structures may then be usedas a template for the arrangement of nanoparticles into functional geometries. As one example, we demonstrate how the biochemical procedure of rolling circle amplificiation can be used to produce one-dimensional chains of nanoparticles or other nanoscale objects. DNA's sequence-programmability allows not only to generate chains of a single type of nanoparticle, but also chains of alternating particle types or other objects. Such assemblies may be of interest in photonic or nanoelectronic applications, or for the study of protein-protein interactions.

10:30 AM

Effects of Multiplex Catalyst on the Preparation and Characteristic of Nano-Sized Alpha-Alumina: Deng Hua¹; *Xiao Jin*¹; Li Jie¹; Liu YeXiang¹; Wan Ye¹; ¹Central South University

The precursor of ammonium aluminum carbonate hydroxide was synthesized with precipitation method by using aluminum sulfate and ammonium carbonate as raw materials. Dispersant and multiplex catalyst (MC) were used to prevent agglomeration of powder particles and effects of MC on drying and sintering processes were intensively investigated. The results show that MC can effectively prevents agglomerations of precursor in drying process as well as has great potential synergistic effects on the phase transformation of alumina and reduces the phase transformation temperature of α -Al₂O₃, simultaneously maintains the powder particles in a comparatively dynamic–sintering–state and the trends of necking–formation or other rigid agglomerations are remarkably decreased, therefore the dispersion of powder particles is significantly improved. BET and ICP analysis indicate that MC is propitious to increase the specific surface area of α -Al₂O₃ and has no effect on the contents of impurities in sintered products and the content of Al₂O₃ reaches 99.97%.

10:45 AM

Synthesis and Ethanol Sensing Properties of Flower-Like ZnO Nanostructures: *Chen Yujin*¹; Zhu Chunling¹; Xiao Gang¹; ¹Harbin Engineering University

The ZnO nanostructures were prepared in a basic solution contained Zn2+ ion and ethylenediamine (EDA) under ultrasonic conditions. Through adjusting the concentration of EDA, the flower-like ZnO nanorods and nanotubes were easily obtained. Scanning electron microscopy (SEM) images showed that the nanorods contacted each other as a bundles, grown radiately and formed flower-like structures. The diameter and the length of the nanorods in bundles were less than 15 nm and ~1.3-1.8 μ m, respectively. As for ZnO nanotubes, they had a hexagonal shape and a diameter of ~250 nm. Compared with the results reported previously, the sensitivity of the flower-like nanorods is near to that of other ZnO nanostructures measured at working temperature of 300°C, however, the operating temperature sharply decreased by 160°C. Although the sensitivity of the nanotubes is lower than that of the nanorods, they also can detect ethanol at ppm level at relatively low temperature. This work was supported from the Basic Research Foundation of Harbin Engineering University (HEUFT06031).

11:00 AM Break

11:10 AM Invited

Thiol-Capped Nanocrystals: On the Way from Synthesis to Applications: Nikolai Gaponik¹; ¹TU Dresden

The colloidal synthesis of light-emitting thiol-capped semiconductor nanocrystals (NCs) is presented. The procedures of post-preparative treatment, e.g. size-selective precipitation, photochemical etching and phase transfer are shown to be powerful tools to achieve a strong luminescence quantum yield, high stability, luminescence colour purity and processability of the NCs. The various approaches to the formation of NC-based composite materials (colloidal core-shell particles, layer-by-layer assembled films, microcapsules etc.) are presented and their possible applications in photonics, optoelectronics and for bio-imaging are discussed.

11:40 AM Invited

Large-Scale Ab Initio Study of Size, Shape, and Doping Effects on Electronic Structure of Nanocrystals: Jingbo Li¹; ¹National Renewable Energy Laboratory

Semiconductor nanocrystals such as quantum dots (QDs) and quantum wires (QWs) have attracted much attention because the bandgap and optical transitions can be tailored continuously by size or shape. This feature opens up a great potential for novel device applications that require the knowledge of the size/shape-dependence of the nanocrystal's optical properties and electronic structure. Recently we have developed large-scale first-principle method to calculate the electronic structure of nanocrystals, which contain tens of thousand atoms. We find that (i)the calculated size-dependent exciton energies and absorption spectra of QDs and QWs are in good agreement with experiments; (ii)the electronic structure of a nanocrystal can be tuned not only by its size, but also by its shape; (iii)the calculated ratios of band gap increases between QWs and QDs are significantly different from 2, which are obtained from the simple particle-in-a-box effective-mass model; (iv)doping properties of QDs are significantly different from bulk semiconductors.

12:10 PM

Operation by Nanocomposite Properties by Optical Poling: *Ivan Kityk*¹; ¹J.Dlugosz University Czestochowa

Optical bicolour treatment opens a new possibility for flexible operation by principal parameters of the nanocomposites, particularly for the semiconducting nanocrystallites incorporated into the polymer matrices, metallic nanoparticles touched to the dielectric/semiconducting substraters, superconducting NC incorporated into the disordered amorphous-like background. Optical poling of such kinds of materials opens a possibility to change the linear and non-linear optical constants, transport properties like dcconductivity, thermoconductivity etc. The principal mechanisms are explained within a framework of the interaction of external bicolor coherent laser light with the surface plasmon resonances and by creation of additional grating similar to photonic crystals. Particular interest is devoted to a possibility of an achievement of giant second-order susceptibilities near the tricritical points.

12:25 PM

Biomolecule-Assisted Synthetic Route to Nanostructured Crystals: *Qing Yang*¹; ¹University of Science and Technology of China

The synthesis and assembly of nanostructures with controllable shape and size is of great interest since that both crystallographic forms and morphologies are generally responsible for the properties of the nanostructures. Recently, many strategies such as hydrothermal, solvothermal, evaporation and various template-assisted ones have been intensively employed for the synthesis of different nanostructured crystals. In the present presentation, a general biomolecule-assisted synthetic route is presented for the synthesis of several nanostructures which include CdS and PbS dendrites, bundle-like CeOHCO3 and blood-shape NdOHCO3 structures. In addition, the biomolecule-assisted synthetic route is also carried out for the fabrication of several oxide nanostructures.

12:40 PM Invited

Fabrication of Nanostructured Materials with Ultrafast Lasers: Samuel Mao¹; ¹Lawrence Berkeley National Laboratory and University of California at Berkeley

In this presentation, I will give an overview of recent progress on the fundamental understanding of ultrafast laser-material interaction and its application to the development of nanostructured materials. While laser ablation is a viable method for thin film fabrication, formation of micron-sized particulates during conventional nanosecond laser-based deposition process makes it unsuitable for growing high quality nanoscale materials. Owing to nonequilibrium non-thermal ablation mechanisms, ultrafast laser pulses characterized by their short pulse duration compared to thermal diffusion time are able to produce particulate-free precursor vapor for nanoscale material deposition. Starting with an introduction of the distinct mechanisms of non-thermal ultrafast laser ablation, I will discuss one dimensional nanomaterial



growth using femtosecond laser-based deposition approach. The applications of such nanostructures will also be discussed.

Wide Band-Gap Semiconductor Nanostructures: Session I

Sponsored by: The Minerals, Metals and Materials Society, TMS Electronic, Magnetic, and Photonic Materials Division, TMS: Electronic Materials Committee, TMS: Nanomaterials Committee, TMS: Thin Films and Interfaces Committee, TMS: Young Leaders Committee *Program Organizers:* Ashutosh Tiwari, University of Utah; Haiyan Wang, Texas A&M; Minseo Park, Auburn University

Monday AM	Room: Oceanic 4
February 26, 2007	Location: Dolphin Hotel

Session Chairs: Ashutosh Tiwari, University of Utah; Minseo Park, Auburn University

9:00 AM Introductory Comments

9:10 AM Keynote

Opportunities and Challenges in Nanostructured Materials: *Jagdish Narayan*¹; ¹North Carolina State University

This talk addresses some of the fundamental issues and critical advantages in reducing the grain size/feature size to the nanoscale regime. We find that as the grain size or feature size is reduced, there is a critical size below which the defect content can be reduced virtually to zero. This critical size for most defects in materials falls in the nanoscale regime. Thus, nanostructured materials offer a unique opportunity to realize the property of a perfect material. However, with this opportunity comes a great challenge in terms of engineering a large fraction of atoms near the surfaces/interfaces. Since the fraction of atoms near the surfaces/interfaces increases inversely with size, this fraction can get closer to unity and determine efficacy of nanostructures. We discuss briefly ways to enhance the stability and reliability by controlling the properties of interfaces. This talk summarizes recent developments in nanocrystalline structural, magnetic, electronic and photonic materials, pointing out unique and improved properties of nanostructured materials.

9:55 AM Invited

Chemical Sensing with ZnO Nanorods: *David Norton*¹; L. C. Tien¹; H. T. Wang¹; P. W. Sadik¹; B. S. Kang¹; F. Ren¹; S. J. Pearton¹; ¹University of Florida

Semiconductor nanowires are highly attractive for chemical sensing due to their high surface-to-volume ratio and the surface sensitivity to chemical absorption. Particular applications that are being investigated include chemical detection in gas in aqueous environments. In this talk, the properties of ZnO films and nanowires for gas and molecule detection will be considered. In particular, hydrogen and ozone detection, measurement of pH, detection of hydrocarbons and biomolecules will be discussed. Devices include single and multiple wire constructs. The application of noble metal nanoparticles to the nanowires was investigated as well.

10:30 AM Invited

Silicon Carbide in Harsh Environment Micro-, Nano and Sensor Systems – Applications, Challenges and Technological Trends: *F. Solzbacher*¹; ¹University of Utah

Microsystems, electronics and sensory applications will continue to see strong double digit percentage growth in the coming decades. 80% of these applications will however require the operation of these devices in harsh environments, i.e. high temperatures and aggressive gas and fluid media, such as e.g. combustion processes. The overwhelming majority of solid state materials used today cannot sustain these environments. Various polytypes of bulk and thin film silicon carbide in single crystal, poly crystalline or amorphous form have shown great promise in these applications, as sensory or electronic functional, substrate or encapsulation materials. Great potential results from merging SiC with existing MEMS technologies. The talk will present applications and market opportunities, identify some of the key technical and scientific challenges. It will present an overview of the state of the art in SiC MEMS technology and indicate technological trends. Selected examples of devices will be shown.

11:05 AM Break

11:35 AM Invited

Synthesis and Application of Wide Bandgap Semiconductor Nanowires: Han-Kyu Sung¹; *Heon-Jin Choi*¹; ¹Yonsei University

Semiconductor nanowires have great potential in the fabrication of electronic-, optoelectronic-, and sensor devices on a nano meter scale. This talk will focus on the fabrication and modulation of single crystalline semiconductor nanowires and their feasibility as building blocks for nanoscale devices. Following a brief introduction, an approach to fabricate nanowires from oxide-, nitride- and carbide semiconductor will be presented. Modulation of nanowires macroscopically, i.e., aligning and patterning of nanowires, as well as microscopocally, i.e., doping and creating heterostructures, will be presented for various nanowires. Optical, electrical and/or magnetic properties of nanowires will be discussed with emphasis on the effect of modulation. To explore the feasibility of nanowire as nanoscale building blocks, the preliminary performance of some nanowire based device structures will be discussed. Lastly, the uniqueness and potential of nanowires in electronic-, , optoelectronic-, electromagnetic-, energy conversion/storage- and bio applications will be discussed.

12:10 PM

Low Temperature Solution Based Synthesis of Exotic ZnO Nanostructures: Michael Snure¹; Ashutosh Tiwari¹; ¹University of Utah

ZnO has rapidly become a material favorite for production of nanostructures because it self assembles into a number of different structures, such as, rods, tubes, spirals, and nails. ZnO also has many desirable optical properties like a wide band gap (3.4eV) and large exciton binding energy (60meV) making it a good material for UV LEDs and lasers. Most of the production methods for making ZnO nanostructures require extreme conditions like high temperatures and vacuum making them less practical. In our lab we have developed a low temperature solution based technique for growing nano-rods, tubes and a number of other exotic nanostructures. With this solution technique we can control were and what type of structures are deposited by varying a few simple parameters.

12:35 PM

Fabrication of High Performance Schottky Rectifiers Based on Bulk GaN Substrate: Yi Zhou¹; Dake Wang¹; Claude Ahyi¹; Chin-Che Tin¹; John Williams¹; Minseo Park¹; N. Williams²; Andrew Hanser²; Edward Preble²; ¹Auburn University; ²Kyma Technologies, Inc.

Vertical Schottky rectifiers with and without implanted p-type guard ring edge termination have been fabricated on the Ga-face of a free-standing n-GaN substrate. Silicon implant has been performed on the backside of the substrate to minimize ohmic contact resistance. The device showed almost ideal forward current characteristics, with the ideality factor of ~1.1, forward turn-on voltage of ~0.85V and on-state resistance (R_{oN}) as low as 1 m Ω cm². The reverse breakdown voltage (V_B) was found to decrease with increasing schottky contact size. High reverse breakdown voltage >450 V has been achieved in rectifiers with a small contact size, producing a figure-of-merit ($V_B^{2/R}_{ON}$) > 200 MWcm⁻². The devices also showed an ultrafast reverse recovery characteristics with a reverse recovery time <20ns. The effect of reducing device structure into nanometer scale will also be discussed.

A M

Technical Program



2007 Nanomaterials: Fabrication, Properties and Applications: Session II

Sponsored by: The Minerals, Metals and Materials Society, TMS Electronic, Magnetic, and Photonic Materials Division, TMS: Nanomaterials Committee *Program Organizers:* Wonbong Choi, Florida International University; Ashutosh Tiwari, University of Utah; Seung Kang, Qualcomm Inc.

Monday PM	Room: Oceanic 3
February 26, 2007	Location: Dolphin Hotel

Session Chairs: W. Jud Ready, Georgia Tech; Otto Zhou, University of North Carolina Chapel Hill

2:00 PM Invited

Electrostatic Funneling Scheme for Wafer-Scale Fabrication of Nanoscale Devices: Seong Jin Koh¹; ¹University of Texas at Arlington

The ability to place nanoscale building blocks on the exact substrate locations is one of the key requirements for the fabrication of nanoscale devices and sensors through the bottom-up approach. In this talk, we will present a scheme called "electrostatic funneling", in which charged nanoparticles in a colloidal solution are guided by the electrostatic forces onto the targeted locations with nanoscale precision. The guiding electrostatic structures are created in combination with wet chemistry and current CMOS fabrication technology, enabling large-scale placement of nanoparticles over an entire wafer. This controlled nanoparticle placement will be demonstrated for a variety of geometries created using 200 mm and 300 mm CMOS fabrication lines. The application of the electrostatic funneling scheme to the fabrication of single electron devices and their electrical characteristics will also be presented. Supported by ONR (N00014-05-1-0030), NSF CAREER (ECS-0449958), and THECB ARP (003656-0014-2006).

2:25 PM

Maghemite Nanoparticles Obtained by Laser Pyrolysis and Their Application as Magnetic Nanofluids: *Ion Morjan*¹; Rodica Alexandrescu¹; Florian Dumitrache¹; Ion Voicu¹; Lavinia Gavrila¹; Iuliana Soare¹; Ladislau Vekas²; Doina Bica³; George Filoti⁴; Mircea Morariu⁴; Victor Kuncser⁴; ¹National Institute for Laser Plasma and Radiation Physics; ²Centre of Fundamental and Advanced Technical Research, Romanian Academy -Timisoara Division; ³University Politehnica Timisoara; ⁴National Institute of Materials Physics

Nano-sized maghemite particles (usually less than 15 nm diameter) have been directly synthesized by the laser induced pyrolysis of iron pentacarbonyl vapors. Ethylene was used as sensitizer of the induced reaction. By the controlled use of air as oxidizer, iron oxide nanoparticles in the gamma phase were obtained. The particles were characterized by X-ray diffraction, transmission electron microscopy, FTIR and Mossbauer spectroscopy. The synthesized iron-based nanoparticles were characterized by narrow size distributions. Magnetic properties are strongly dependent on the particle size and on the degree of crystallinity. For obtaining samples of magnetic nanofluids from nano maghemite, a multi-step preparation procedure was used in which through both dispersion and stabilization the breaking of inter-particle bonds and the covering with suitable surfactants of individual nanoparticles are realized. The resulted samples show relatively low saturation magnetization. They prove the viability of the applied procedure and show promising features for biological applications.

2:40 PM

Formation of Nano-Scaled Hollow Oxide Particles Using Oxidation Reaction: *Ryusuke Nakamura*¹; Daisuke Tokozakura¹; Jung Goo Lee¹; Hirotaro Mori¹; Hideo Nakajima¹; ¹Osaka University

Formation of hollow oxide nanoparticles through the oxidation of metal nanoparticles such as Cu, Zn, Al, and Pb was examined by transmission electron microscopy. After the oxidation of Cu, Zn, and Al nanoparticles in the temperature range between 295 and 423 K, solid nanoparticles turned to hollow oxides depending on the initial size of metal nanoparticles. Additionally, voids were observed at the interface between inner metal and outer oxide in the immediate stage of oxidation reaction. On the other hand, Pb nanoparticles

oxidized to PbO without nano-hole because oxygen diffusion through the oxide layer is the rate determining process in the oxidation of Pb. The comparison of the former (Cu, Zn, Al) with the latter (Pb) results indicates that nano-hole is formed as a result of clustering of vacancies which generate due to rapidly outward diffusion of metal ions through oxide layer at oxidation.

2:55 PM

A New Continuous Manufacturing Technology for Nanoparticles: Christian Wögerer¹; Georg Waldner¹; Heinz Dobesberger¹; ¹ARC Seibersdorf Research GmbH

The most important challenge is, besides development of new particles and materials based on "Nano", to create new "Production methods for a controlled mass production of Nanoparticles. Therefore ARC-sr has recently started the operation of an advanced HPMN- trial plant that enables the synthesis of various types of nanoscaled particles. The goal is establishing a proven method for the production of nanoparticles for industries. The paper shows the state of the art of various production methods with it's advantages and disadvantages and compares these technologies to the HPMN reactor. The HPMN reactor is a continuous production method for Nanoparticles with the Possibility of functionalsazion and aftertreatment in one step and he will open the door for the Industries to a cost efficient mass production of functionalized Nanoparticles and Nanoproducts. The HPMN-reactor combines the flexibility of precipitiation with the possibilities of controlling the particle characteristics and the ability of continuous processing.

3:10 PM

Environment-Friendly Synthesis of Organic-Soluble Silver Nanoparticles toward Inkjet Printing: *Kwi Jong Lee*¹; Byung Ho Jun¹; Jaewoo Joung¹; ¹Samsung Electro-Mechanics

In this study, we attempted to present an environment-friendly synthesis of narrowly dispersed silver nanoparticles in highly concentrated organic phase. The fully organic phase system contains silver salt as a silver precursor, alkanoic acid as a capping molecule, hydrocarbon solvent as a media, and transition metal salt. Even not using reducing agents such as borohydride or hydrazine, monodispersed silver nanocrystals with size of 5 nm were easily synthesized at low temperature (< 100°C). This was attributed to the difference of electrochemical reduction potential between silver and transition metal and resulted in metal-catalyzed synthesis of silver nanoparticles. Furthermore, the silver ink was printed onto plastic substrates and then metallized into electrical circuits.

3:25 PM Break

3:40 PM Invited

Intelligent Applications of Carbon Nanotubes and Their Hybrid Architectures: Swastik Kar¹; ¹Rensselaer Polytechnic Institute

We present some recent demonstrations of clever applications built from carbon nanotubes and their hybrid architectures. In the field of electronics, semiconducting carbon nanotubes can be used to fabricate field-effect transistors, and single charge transistors. Metallic nanotubes turn out to be extremely good for gigascale integration of these devices. By growing largescale aligned nanotubes on bulk metallic substrates, one can fabricate double layer capacitors (supercapacitors), VIA structures, and integrated field-emission cathodes. By a controlled infiltration of nanotubes with polymers, it is possible to have sensitive strain and pressure sensors, and achieve extremely enhanced field-emission properties. Fins of aligned multi-walled nanotube arrays have tremendous applications as heat dissipaters on hot-spots in IC circuits, due to their high thermal conductance and surface area/mass. The engineering and physics of these and other related applications will be presented, along with possible realistic, immediate applications.

4:05 PM

Synthesis and Investigation of Thermoelectric Properties of Sodium-Doped V2O5: Monika Marciniak¹; ¹University of Washington

There is a growing interest in the development of thermoelectric materials due to their potential applications such as thermoelectric power generation, small-scale refrigeration, decreasing emissions in vehicles and other. Discussed research focuses on investigating thermoelectric properties of vanadium pentaoxide (V2O5) - a material that exhibits semiconducting properties and which the properties have been enhanced by doping. Systematic synthesis of V2O5 powder with sodium chloride (NaCl) has been achieved and the



effect of doping V2O5 with sodium atoms has been investigated. A series of X-ray diffraction, X-ray Photoemission Spectroscopy tests, conductivity and Seebeck measurements have been performed. As a result, a sodium-doped V2O5 solution that exhibits potential for the high thermoelectric efficiency has been identified. The newly-developed solution is being currently utilized as n-type material in the prototype of a thermoelectric device. The device is at the stage of development and testing and its characterization should be accomplished soon.

4:20 PM

Synthesis and Study of Organic-Metallic Composite Rods Based on Ionic Liquids for Electronic Applications: Ashavani Kumar¹; *Victor Pushparaj*¹; Saravanababu Murugesan¹; Caterina Soldano¹; Jin Xie¹; George John²; Omkaram Nalamasu¹; Pulickel Ajayan¹; Robert Linhardt¹; ¹Rensselaer Polytechnic Institute; ²City College of New York

In recent years, there has been constant effort in utilizing the molecular self assembly technique to the electronic industry. We demonstrate a single step, scalable method to synthesize the conducting organic – metallic composite sub micron rods (i.e. gold nanoparticles-embedded organic molecule-based hexagonal nanostructures using a room temperature ionic liquid (RTIL)). These rods were obtained simply by dissolving gold chloride in 1-butyl, 4-methylpyridinium tetrafluoroborate(RTIL). The hexagonal shaped rods aspect ratio can be altered by changing the molar ratio of RTIL to gold chloride. XPS, NMR, FTIR, TEM and FESEM were used to characterize. These hexagonal rods were dispersed on the SiO2/Si substrate and the coplanar metal electrodes were deposited by focused ion beam technique. The current-voltage behavior obtained on our device, is similar to the organic memory cell behavior. It behaves as though the data is written once and can be read many times. (write once read many times -WORM).

4:35 PM

Asymmetric Properties of Strained SrTiO₃ Films on DyScO₃ Substrates: Susan Trolier-McKinstry¹; Michael Biegalski¹; Jeff Haeni¹; Long-Qing Chen¹; Darrell Schlom¹; Yulan Li¹; Venkat Gopalan¹; Dillon Fong²; Stephen Streiffer²; Jeff Eastman²; P. Fuoss²; Marilyn Hawley³; A.K. Tagantsev⁴; R. Uecker⁵; P. Reiche⁵; ¹Pennsylvania State University; ²Argonne National Laboratory; ³Los Alamos National Laboratory; ⁴EPFL; ⁵Institute for Crystal Growth

Using reactive MBE, strained epitaxial SrTiO₃ films were grown on DyScO₃ substrates. Films with thicknesses from 50 Å to 1000 Å were prepared to examine the films above and below the critical thickness. These films have excellent crystalline quality with rocking curve FWHM of 0.002-0.005°. These films retain excellent crystallinity above the critical thickness. One consequence of the strain is that the films experience a ferroelectric transition near room temperature, even though unstrained SrTiO₃ is an incipient ferroelectric. These films also exhibit peak dielectric constants near 20,000. The dielectric data shows frequency relaxation that was well fit by a Vogel-Fulcher equation over six orders of magnitude in frequency with a freezing temperature of 204 K. These films also exhibit clear hysteresis loops below T_{max} with an in-plane remanent polarization up to 10 μ C/cm² at 77 K. Interestingly, the in-plane electrical properties are anisotropic due to the orthorhombicity of the substrate.

4:50 PM

64

Evolution of Microstructures and Physical Properties during Annealing in Nanostructured Invar: Jeong Ho Seo¹; Jong Kweon Kim¹; *Yong Bum Park*¹; 'Sunchon National University

Fine metal masks(FMMs) are necessarily used in the process to produce organic light-emitting displays(OLEDs), and should be made of materials with low thermal expansion in order to guide evaporated luminescent materials into correct positions on glass-substrates. Invar(Fe-36%Ni alloy), whose thermal expansion coefficient(TEC) approaches zero, is the most appropriate material for the application. In the present work, FMMs of nanocrystalline Invar were fabricated by using an electroforming method. The present study has been aimed at clarifying correlation between the microstructures and physical properties which evolve during annealing in the nanostructured Invar. The TEC measured about 1.14x10-6/K in the as-deposited sample consisting of nanometer-sized grains. Grain growth took place during annealing at temperatures higher than 350°C, and the annealed specimen revealed the TEC of conventional Invar, i.e. about 2.01x10-6/K. Mechanical properties also significantly changed after annealing. Physical properties depending on the

microstructures will be discussed in terms of the crystallographic orientation dependence.

5:05 PM

Single-Step, Size-Controlled Synthesis of Colloidal Silver Nanoparticles Stabilized by Octadecylamine: *Gururaj Neelgund*¹; M.S. Dharmaprakash¹; S.A. Shivashankar¹; ¹Materials Research Centre, Indian Institute of Science

A single step process for the synthesis of size-controlled silver nanoparticles has been developed using a bifunctional molecule, octadecylamine (ODA). Octadecylamine complexes to Ag+ ions electrostatically, reduces them, and subsequently stabilizes the nanoparticles thus formed. Hence, octadecylamine simultaneously functions as both a reducing and a stabilizing agent. The amine-capped nanoparticles can be obtained in the form of dry powder, which is readily redispersible in aqueous and organic solvents. The UV-vis spectra of the nanoparticles prepared with different concentrations of ODA displayed well-defined plasmon band with the maximum absorption around 425 nm. The formation of silver metallic nanoparticles was confirmed by their XRD pattern. The binding of ODA molecule on the surface of silver has been studied by FT-IR and NMR spectroscopy. The formation of well dispersed spherical Ag nanoparticles without aggregation has been confirmed by TEM analysis. Open aperture z-scans have been performed to measure the nonlinearity of Ag nanoparticles.

5:20 PM

Synthesis and Characterization of Aluminum-Based Energetic Nanoparticles: *David Reid*¹; Sudipta Seal¹; Eric Petersen¹; ¹University of Central Florida

A wet chemical method was developed for the synthesis of core/shellstructured nanoparticles consisting of titania-encapsulated aluminum. Aluminum nanoparticles were prepared by the catalytic decomposition of a TMEDA-alane adduct in toluene. Following the precipitation of metallic aluminum, the particles were suspended in ethanol and passivated with a surfactant. The aluminum particles were monodisperse with a mean particle size of 8-10 nm by dynamic light scattering. Work is currently ongoing to produce the titania coating via a sol-gel reaction with titanium isopropoxide, allowing for the preferential growth of titania on the surface of the aluminum particles. The composition and structure of the core/shell particles will be confirmed with XPS, XRD, and TEM characterization.

8th Global Innovations Symposium: Trends in Materials and Manufacturing Technologies for Energy Production: Plenary

Sponsored by: The Minerals, Metals and Materials Society, TMS Materials Processing and Manufacturing Division, TMS: Global Innovations Committee *Program Organizers:* Joy Hines, Ford Motor Company; David Bahr, Washington State University; John Smugeresky, Sandia National Laboratories

Monday PM	Room: Australia 3
February 26, 2007	Location: Dolphin Hotel

Session Chair: Joy Hines, Ford Motor Company

2:00 PM Invited

Energy Security for the United States (and the World): *Jeffrey Wadsworth*¹; ¹Oak Ridge National Laboratory

Three closely linked challenges—energy, environment, and national security—will increasingly dominate national and international agendas, and their resolution will demand international cooperation, with science and technology playing a crucial role. First, the global need for energy is rapidly increasing, with some estimates indicating a doubling of world energy consumption by the year 2050. Second, concerns about the environmental impacts of energy production are increasing the focus on "clean" energy sources. And third, U.S. dependence on external sources of energy is increasingly recognized as a national security issue. New facilities and capabilities for designing, characterizing, and simulating the structure and function of materials are becoming available to solve these problems. After



a brief review of current and future energy demands and their impacts and implications, I will describe several areas of research that offer opportunities for materials science to provide solutions.

2:30 PM Invited

Materials for Nuclear Energy Applications: Marius Stan¹; ¹Los Alamos National Laboratory

Nuclear reactor materials are subject to a sever environment where irradiation continuously alter their thermal, mechanical, and chemical properties. It is difficult and often impossible to perform in-situ measurements to monitor the changes in fuel element materials properties. To address these issues, the concept of models and simulations as integrated experimental, theoretical, and computational methods is presented. In this approach, thermodynamic properties of actinide based alloys and ceramics are predicted using a multi-scale method. The method incorporates theory-based atomistic, meso-scale, and continuum level models into finite element simulations. At each scale, the method is illustrated with recent results such as models of free energy and phase stability, predicted defect concentrations in PuO2-x, and simulations of coupled heat transfer and oxygen diffusion in UO2+x. In the second part of the talk, a list of grand challenges in the area of materials optimization for nuclear energy applications is proposed and discussed.

3:00 PM Invited

Materials Advances for Fuel Cell Applications at the CFCI: *Héctor Abruña*¹; Francis DiSalvo¹; ¹Cornell Fuel Cell Institute, Baker Laboratory, Cornell University

This presentation will focus on the development of new materials for fuel cell applications with emphasis on ordered intermetallic phases as both bulk electrodes and nano-particles, the use of conducting non-stoichiometric oxides as supports and cathodes and novel approaches to alkaline membranes. The use of high throughput combinatorial methods and nano-structured integrated systems will also be discussed.

3:30 PM

New Low Cost Material Development Technique for Alternate Energy Applications: John Smugeresky¹; D. Gill¹; Elizabeth Holm¹; ¹Sandia National Laboratories

A new material synthesis methodology utilizing additive manufacturing techniques like LENS® is being used to develop new production quality materials for alternate energy applications, that may reduce development time and cost. Conventional alloy development requires years, consumes millions of dollars, and requires large heats of material, which are scrapped at the end of the development cycle. To reduce the time and cost to evaluate new alloys, we are using a laser based additive manufacturing technique to investigate entire alloy composition ranges with small numbers of samples in a condensed time frame wasting little material. Using iron-based alloys, we are evaluating new classes of composite materials required to meet material needs for alternate energy technologies. These consist of graded composition samples, created by mixing different constituents under precise computer control that varies the composition on a mm basis while still allowing a complete spectrum of alloy compositions. Materials analysis included various electronoptic technique evaluations for phase identity, volume fractions, and phase boundaries. An important new feature of this approach is that the resultant suitable new compositions can use the same additive manufacturing technique to make small lot production of the material either as a machining blank or as near net-shape parts. Example materials include steels that do not require heat treatment but have increased corrosion resistance, stiffness features, imbedded hollow particles in the matrix creating low density reticulated structural materials from conventional high density alloys, or hard dispersoids to control grain size and increase wear resistance. Work by Sandia is supported by the U. S. Department of Energy under contract DE-AC04-94AL85000. Sandia is a multi-program laboratory operated by Sandia Corporation, a Lockheed Martin Company, for the United States Department of Energy.

4:00 PM Invited

Development of Materials for Solar Energy: The Silicon Case: Bruno Ceccaroli¹; ¹REC Silicon AS

During the past decade, the global photovoltaic industry has grown significantly. Silicon is the dominating technology for photovoltaics (PV), covering more than 90% of all PV produced. Historically the feedstock

for PV cells has been silicon feedstock and byproducts (scrap) from the semiconductor industry. During the past decade, however, the semiconductor industry has not expanded with the same speed as the PV industry. The global PV industry will soon reach a point where it cannot be sustained by these only these raw material sources. This paper reviews the present situation and the future expectations of availability of high purity solar grade silicon and reviews the manufacturing processes of silicon starting from the natural raw materials and finishing with the solar cells. Particular emphasis is put on the chemical steps currently applied in the industry and on the possible routes to achieve a technically and economically suitable PV silicon feedstock.

Technical Program

Advanced Metallic Composites and Alloys for High Performance Applications: Fe and Ni Alloys and Composites

Sponsored by: The Minerals, Metals and Materials Society, ASM International, TMS Structural Materials Division, ASM Materials Science Critical Technology Sector, TMS/ASM: Composite Materials Committee, TMS/ASM: Mechanical Behavior of Materials Committee

Program Organizers: Awadh Pandey, Pratt and Whitney Rocketdyne; Kevin Kendig, Air Force Research Laboratory; John Lewandowski, Case Western Reserve University

Monday PM	Room: Europe 10
February 26, 2007	Location: Dolphin Hotel

Session Chair: Awadh Pandey, Pratt and Whitney Rocketdyne

2:00 PM Invited

A Cellular Transformation Involving γ (Ni-Al Solid Solution) and γ' (Ni-Al): *Marta Pozuelo*¹; Alan Ardell¹; ¹University of California

A new, previously unknown, cellular transformation was observed in a Ni-22.5% Al alloy that was arc-melted, chill cast into a water-cooled Cu crucible, homoge-nized for 74 h in a vacuum of 10⁻⁶ torr at 1125 °C and slowly cooled inside the vacuum furnace. The cellular transformation was observed in a few isolated grains, within which the transformation was complete, all the lamellae having the same orientation. There were no contiguous cellular grains; each was surrounded completely by grains of γ '. SEM and EDS confirmed that the lamellae consist of alternating plates of the γ (Ni-Al solid solution) and γ ' (Ni₃Al) phases. The interlamellar spacing was ~8 µm, with a γ and γ ' thickness ratio of 1/6. We believe that the transformation results either from heating into the $\gamma + \gamma'$ field from lower temperatures, or slow cooling into the 2-phase field, but the mechanism is not yet known.

2:20 PM

Phasefield Simulations of the Microstructural Evolution in Superalloys, during Directional Solidification and Solution Heat Treatment: *Nils Warnken*¹; Dexin Ma²; Anne Drevermann¹; Suzana Fries³; Ingo Steinbach¹; ¹Access E.V.; ²Foundry Institute of the RWTH-Aachen; ³SGF Consultancy

Directionally solidified turbines blades are exposed to highest temperatures. Made from Ni-based superalloys, the micostructure consisting of a gamma matrix with finely dispersed gamma-prime precipitates. During solidification superalloys form a heavily inhomogenous microstructure, exhibiting strong microsegregation and formation of interdendritic phases. These inhomogenities are removed by a long solution treatment at high temperatures, a lengthy and costly process. Appropriate simulations can help to improve alloys and processes. We simulate the microstructural evolution during directional solidification and solution heat treatment with the phase field method, coupled to thermodynamic and kinetic databases. The simulations cover the formation of dendritic structures and interdendritic gamma-prime as functions of process parameters. A way to identify potential microstructural instability is presented. Simulations were done with the MICRESS® software package, for a quinternary model superalloy (Ni-Al-Cr-Ta-W). The simulations show good agreement with results from directional solidification and heat treatment experiments.



2:40 PM

Post-Fabrication Strengthening of Ni-Based Thermostructural Panels: *Sara Johnson*¹; Brian Tryon¹; Fang Cao¹; Tresa Pollock¹; ¹University of Michigan

Thermostructural panels for use in emerging hypersonic flight systems require the use of advanced materials which can support substantial loads at elevated temperatures. The major challenge in this advancing technology is identifying formable structural materials that are both strong and oxidation resistant. Presently, a new processing path that begins with sheets of nickelbased alloys has been investigated where these solid-solution strengthened alloys are formed into panels and subsequently strengthened by vapor phase aluminization. Microstructure, mechanical properties, and oxidation behavior of these structural elements during processing will be discussed.

3:00 PM

Microcrystalline, Ductile in Room Temperature Ni3Al-Based Strips: Production and Properties: Pawel Jozwik¹; Zbigniew Bojar¹; ¹Military University of Technology

Results of investigation of Ni3Al-based microcrystalline intermetallic alloy with zirconium and boron addition was shown in this paper. A selection of strictly given parameters of plastic working and heat treatment allowed us to obtained a thin strips with thickness bellow 350micrometers and gamma prim grain size from 1,5 to 80 micrometers. A process proposed in the paper makes provision for strictly control of mechanical properties of Ni3Al thin strips via grain boundary strengthening. A wide set of Ni3Al strips mechanical parameters e.g.: ultimate tensile strength (UTS) from 1100MPa to 1750MPa, tensile yield strength (TYS) from 300 to 1250MPa and elongation A10 between 70 and 30% (room temperature, air atmosphere) was obtained. Such values of parameters considerably exceed a level of mechanical parameters referred in bibliography for similar strips.

3:20 PM

Electrodeposition of Ni-P Alloys from a Sulfamate Electrolyte System: Relationship between Ph Value and Structural Characteristics: *Liuwen Chang*¹; Chih-Hsiung Chen²; Honda Fang³; ¹National Sun Yat-Sen University; ²China Steel Corporation; ³MesoPhase Technologies, Inc.

This study describes the effect of pH value of the electrolyte on phosphorus content and residual stress of Ni-P deposits prepared from a sulfamate bath. In general, decreasing pH value results in a decrease of current density no matter if phosphite acid is added in the electrolyte. However, by gradually adding phosphite acid, the detrimental effect of decreasing pH value on increasing residual stress is eliminated, and finally the low pH value bring a beneficial effect on decreasing residual stress in the deposits. Lowering the pH value also results in an increase of the phosphorus content of the deposits. Possible mechanism between hydrogen evolution and phosphorus incorporation is addressed and microstructure of the resultant Ni-P deposits is also analyzed

3:40 PM

Gas Atomized Oxide Dispersion Strengthened Ferritic Stainless Steel: Joel Rieken¹; Iver Anderson²; Robert Terpstra²; Fran Laabs²; ¹Iowa State University; ²Ames Laboratory

A method has been developed to produce an as-atomized oxide dispersion strengthened ferritic stainless steel powder metal alloy that exhibits competitive mechanical properties using a highly simplified processing technique when compared to mechanically alloyed and deformation processed stainless steel powder metal alloys. This paper investigates the powder alloy, Fe-12.5Cr-1Y (wt%), that was fully consolidated through hot isostatic pressing (HIP). Scanning electron microscopy, energy dispersive spectroscopy (EDS), and x-ray diffraction was used for confirmation of different phases within the Fe matrix. A preliminary heat treatment schedule was devised in order to achieve maximum hardness and allow for further formation of yttrium dispersoids. Hardness and initial creep testing were performed, along with microstructural analysis in both as-HIP and heat treated conditions. Transmission electron microscopy with EDS capabilities verified that yttrium based particles were indeed impeding dislocation movement. Support from the DOE-FE (ARM program) through Ames Laboratory contract no. W-7405-Eng-82 is gratefully acknowledged.

4:00 PM

Interface Reactions and Their Kinetics of Al and Binary Al-Si Alloys to Mild Steel Substrates: *Werner Fragner*¹; Konrad Papis²; Roman Sonnleitner³; Peter Uggowitzer²; Jörg Löffler²; ¹ARC Leichtmetallkompetenzzentrum Ranshofen GmbH; ²Eidgenössische Technische Hochschule; ³ECHEM

To meet the requirements of weight-saving and low-cost production of components for future transport vehicles, the concept of multi-material mix is of increasing importance. In this context aluminum-iron compounds produced by means of compound casting are considered to be of particular importance, especially for the automotive industry. An essential and critical aspect of such compound castings is the formation of intermetallic phases (IMP) at the Al-Fe interface. Both the nature and the kinetics of potential IMPs are not well understood and require a systematic investigation. In this paper we document the interface formation of pure Al and binary Al-Si-alloys on a mild steel substrate in non-isothermal experiments. The different phases as well as the reaction kinetics of the IMP formation depending upon different Si content (7%, 12% and 17%) are investigated using quantitative metallography (LOM, SEM/EDX).

4:20 PM

Latest Development and Characteristics of Sandwich Structures with Sheet Metal of CrNi-Steel and Core Layer Made of Different Polymers: *Heinz Palkowski*¹; Günther Lange¹; ¹Tu Clausthal, Institut für Metallurgie, Werkstoffumformung

Metal/polymer/metal sandwich materials are finding increasing use in the automotive industry primarily as lightweight alternatives to steel and aluminium alloys. They offer functional benefits including superior sound and vibration damping, thermal insulation, crash energy absorption and corrosion resistance by alternative choice of the steel grade. In research projects (promoted by the DFG) different 3-layer sandwich materials were produced. These materials have sheet metal surface layers (austenitic high-grade steel) and a central polymer layer (also fibre reinforced). Mechanical properties had been examined and deep drawing test with different simple geometries had been done. By the combination of the qualities of different materials these sandwich materials won't replace only monolithic materials but also by requirements of development and construction open up new application fields. The latest developments at the TU Clausthal are local reinforced sandwich structures. This research work is based within the "Sonderforschungsbereich 675" which is promoted by the DFG.

4:40 PM

Nano-Particle-Strengthened Martensitic Steels by Conventional Processing: *R. Klueh*¹; N. Hashimoto²; M. Miller¹; ¹Oak Ridge National Laboratory; ²Hokkaido University

Need exists for elevated-temperature steels with higher maximum operating temperatures than the 550-620°C of present commercial martensitic steels, such as modified 9Cr-1Mo and NF616. One possibility is oxide dispersionstrengthened (ODS) steels. However, ODS steels are produced by complicated and expensive mechanical-alloying, powder-metallurgy techniques, as opposed to conventional processing (casting followed by rolling, extruding, etc.). Based on the science of precipitate strengthening (need for large numbers of small particles) and using thermodynamic modeling to explore optimum compositions, a thermomechanical treatment (TMT) was developed that increased yield stress of commercial nitrogen-containing martensitic steels 88% at 700°C. Creep-rupture tests indicated a commensurate increase in rupture life. Steels designed and produced specifically for the TMT have yield stresses at 700°C up to 200% greater than conventional steels. Characterization of the new steels indicated that precipitates were eight-times smaller at number densities over three orders of magnitude greater than in conventional steels they would replace.

5:00 PM

Enhancing the Toughness of Brazed Joints in Austenitic Steels by Microstructure Control: Noah Philips¹; Anthony Evans¹; Carlos Levi¹; ¹University of California, Santa Barbara

Brazing is used as a fabrication technology for lightweight, blast resistant sandwich panels, especially those based on austenitic stainless steels and quaternary braze alloys. When standard braze protocols are used, structurally robust nodes can only be assured by using close dimensional tolerances. This assessment examines approaches for enhancing the robustness by modifying the microstructure of the braze-affected zone. The approach includes the



Technical Program



design and analysis of a new test method for measuring the fracture toughness. Toughness was enhanced by implementing thermochemical approaches for reducing the intermetallic volumefraction, and by heat treatments that reduce the fracture pathway continuity.

5:20 PM

Low Thermal Expansion Coefficient Fe-Ni-Co Alloys - Plastic Deformation, Alloy Composition and Martensitic Transformation Relationships: *Deniz Sultan Temur*¹; Ali Arslan Kaya¹; Gurler Kaya²; Murat Kurtulus²; ¹TUBITAK MRC Materials Institute; ²Roketsan Missiles Industries Inc.

Alloy composition, heat and mechanical treatments are factors affecting linear thermal expansion coefficient in Fe-Ni-Co alloys. Although deformation lower the expansion coefficients of these alloys, an increasing deformation leads to partial transformation to martensite upon cooling and increases the thermal expansion coefficient. Thus, to obtain a low expansion coefficient, the composition of the alloy, which affects the transformation temperature, has to be controlled critically. Alloying elements generally suppresses the martensite start temperature. Carbon, present in the alloy studied, is very effective in this respect. However, it creates instability in terms of expansion behaviour and increases linear thermal expansion coefficient. A series of stabilization heat treatments hinder this instability problem allowing for controlled use of carbon in these alloys. This study focuses on the method of obtaining low expansion coefficients by applying plastic deformation in Fe-Ni-Co alloys while controlling the partial martensitic transformation as a result of composition and applied deformation.

Advances in Computational Materials Science and Engineering Methods: Methods at the Atom Scale II

Sponsored by: The Minerals, Metals and Materials Society, TMS Structural Materials Division, TMS: Biomaterials Committee, TMS/ASM: Computational Materials Science & Engineering

Program Organizers: Koen Janssens, Paul Scherrer Institute; Veena Tikare, Sandia National Laboratories; Richard LeSar, Iowa State University

Monday PM	Room: Europe 7
February 26, 2007	Location: Dolphin Hotel

Session Chair: Koen Janssens, Paul Scherrer Institute

2:00 PM Introductory Comments

2:05 PM Invited

Grain Boundary Interface Roughening and Its Effect on Grain Boundary Mobility: *David Olmsted*¹; Stephen Foiles¹; Elizabeth Holm¹; ¹Sandia National Laboratories

It is well-known that interfaces demonstrate a roughening transition, and probably obvious that grain boundary motion will be different above and below the transition. However, this issue has not often been addressed. We simulated the mobility of three flat $\Sigma 5 < 100 >$ tiltboundaries in fcc Ni as a function of temperature and driving force using molecular dynamics with an EAM potential and a synthetic driving force.¹ We find that there is an interface roughening temperature specific to each boundary, and grain boundary mobility undergoes a discontinuity at the transition temperature. This limits the temperature range over which molecular dynamics can provide an estimate of grain boundary mobility. Furthermore, because transition temperature is boundary-specific, there may be temperatures at which some grain boundaries in a microstructure are above their transition temperature (highly mobile), while others are below it (immobile). ¹KGF Janssens et al. Nature Materials 5 (2006) 124.

2:40 PM Question and Answer Period

2:45 PM

Calculations of the Vacancy Formation Energy near GP Zones and a Possible Nucleation Mechanism of Precipitates in Al-Cu Alloys: *Shenyang Hu*¹; Michael Baskes¹; Srinivasan Srivilliputhur¹; ¹Los Alamos National Laboratory

In this work, we calculated the vacancy formation energy around GPI and GPII in Al-Cu alloys using both first principles and semi-empirical calculations. The results of both sets of calculations show that compared to the vacancy

formation energy in pure Al: 1) the vacancy on the Al layer next to the GPI has a much higher formation energy; 2) the vacancy on the second nearest Al layer to the GPI has much lower formation energy; and 3) the vacancy on the middle Al layer in the GPII has the lowest formation energy. Multi-vacancy formation energies and configuration entropies are calculated and estimated. These results suggest that the vacancy concentration is enhanced around the GPI and GPII, and one possible theta-prime nucleation process could be that Cu atoms on GPI and GPII jump to the second nearest Al layer, and then order to form theta-prime nuclei.

3:10 PM Question and Answer Period

3:15 PM

A Modified Embedded Atom Method Interatomic Potential for the Fe-N System: *Byeong-Joo Lee*¹; ¹Pohang University of Science and Technology

A Modified Embedded-Atom Method (MEAM) interatomic potential for the Fe-N binary system has been developed using previously developed MEAM potentials of Fe and N. The potential parameters were determined by fitting to the dilute heat of solution and migration energy of nitrogen atoms, the vacancy-nitrogen binding energy and its configuration in bcc Fe, and to the enthalpy of formation and lattice parameter of Fe4N. The potential reproduces very well the known physical properties of nitrogen as an interstitial solute element in bcc and fcc Fe and of various nitrides. The similarity and difference between nitrogen and carbon as equally important interstitial elements in iron are also examined. The applicability of the potential to atomistic approaches for investigating interactions between nitrogen atoms and other defects such as vacancies, dislocations and grain boundaries, and also for investigating the effects of nitrogen on various deformation and mechanical behaviors of iron is demonstrated.

3:40 PM Question and Answer Period

3:45 PM Break

4:15 PM Invited

Application of Molecular Theory to Complex Fluid Interfaces: Amalie Frischknecht¹: ¹Sandia National Laboratories

Modeling complex fluid systems on the nanoscale is challenging because these systems often sit on the boundary between length scales easily handled in atomistic simulations and the larger length scales where mesoscopic models apply. One promising technique to address these systems is classical density functional theory (DFT). DFT describes fluids on the molecular level, while a parallel, 3D implementation of DFT developed at Sandia is capable of treating relatively large systems. I will introduce the theory and then describe our application of it to two problems. First, we have used DFT to study the properties of phospholipid bilayers and their interactions with alcohol and intrinsic membrane proteins. Second, I will discuss recent work modeling the properties of polymer/nanoparticle thin films. Sandia is a multiprogram laboratory operated by Sandia Corporation, a Lockheed Martin Company, for the United States Department of Energy's National Nuclear Security Administration under contract DE-AC04-94AL85000.

4:50 PM Question and Answer Period

4:55 PM

Anharmonic Lattice Statics Analysis of Defective Crystals with Many-Body Interactions: Arash Yavari¹; ¹Georgia Institute of Technology

The existing treatments of defects in crystalline solids in the lattice scale are mostly numerical and analytic and/or semi-analytic developments are missing. In this seminar we extend the anharmonic lattice statics technique developed previously by the author and coworkers to the case of defective crystals governed by many-body potentials. As examples of many-body potentials, we work with two types of potentials: (i) embedded atom potentials for alloys and (ii) bond valance potentials for ferroelectric perovskites. We show how one can do semi-analytical lattice calculations for different types of defects in this general setting. We also show how our lattice statics technique can be used as a measure of comparing different interatomic potentials in terms of the defect structure ad energetics that they predict. We also address the issue of finite temperature effects on defect structures.

5:20 PM Question and Answer Period

Advances in Microstructure-Based Modeling and Characterization of Deformation Microstructures: Modeling of Deformed Structures I

Sponsored by: The Minerals, Metals and Materials Society, ASM-MSCTS: Texture and Anisotropy Committee, ASM-MSCTS: Texture and Anisotrophy Committee

Program Organizers: Reza Shahbazian Yassar, Center for Advanced Vehicular Systems; Sean Agnew, University of Virginia; Jiantao Liu, Alcoa Technical Center

Monday PM	Room: Europe 1
February 26, 2007	Location: Dolphin Hotel

Session Chairs: Thomas Bieler, Michigan State University; Hasso Weiland, Alcoa Technical Center

2:00 PM

An Analysis of Microstructure Evolution and the Bauschinger Effect at the Micron Scale: Amine Benzerga¹; P.J. Guruprasad¹; ¹Texas A&M University

Mechanism-based discrete dislocation dynamics is used in structureproperty studies of crystal plasticity under macroscopically homogeneous deformation. Particular attention is given to the effect of microstructure evolution on the enhancement of the Bauschinger effect in single crystal specimens with dimensions in the hundreds of nanometers to tens of microns range. Constitutive rules are used which account for key short-range dislocation interactions, including junction formation and dynamic source creation. For low initial dislocation densities, the behavior is dominated by exhaustion hardening with essentially no dislocation accumulation. Within this regime, the unloading response is purely elastic but the cyclic response occasionally exhibits anasymmetry between tension and compression. By way of contrast, for high initial dislocation densities the fundamental mechanisms of athermal hardening operate effectively, thus leading to microstructure development and a strong Bauschinger effect. The magnitude of the latter is found to increase with decreasing specimen size.

2:20 PM Invited

A General Microstructural Metal Plasticity Model Applied in Testing, Processing and Forming of Aluminium Alloys: *Bjorn Holmedal*¹; Erik Nes¹; 'NTNU

In a recently completed EU Framework Program a major effort was launched with the dedicated objectives of developing comprehensive, microstructurally based, models for casting, fabrication and forming of aluminium alloys. Collaboration in this project provided an opportunity for further refinements and expansion of the original Nes-Marthinsen model. This involved the integration of work hardening and texture models. In addition important aspect such as dynamic strain aging and strain path changes during deformation was included. Computer codes have been developed which allow for implementation in FE-models. The result is a general microstructurally based metal plasticity model (the MMP-model) suitable for application in testing, processing and forming of aluminium alloys. The objective of this paper is to present an overview of the MMP-model together with a selection of relevant applications. Further, some of the basic model concepts will be discussed and contrasted in relation to alternative interpretations in the literature.

2:45 PM

Computational Modeling of Continuous Dynamic Recrystallization in Magnesium: *Kevin Boyle*¹; Elhachmi Essadiqi¹; Ravi Verma²; 'Natural Resources Canada; ²General Motors Research and Development

Magnesium components are increasingly being considered for use in vehicle structures, however, magnesium has poor room temperature ductility and is consequently processed and shaped at elevated temperatures. Dynamic recrystallization (DRX) is commonly observed during elevated temperature deformation and can profoundly influence microstructure evolution and macroscopic properties such as flow stress. A microstructural-based approach for modeling magnesium deformation which includes DRX is developed. A microstructural volume element is discretized with sub-elements and a selfconsistent crystal plasticity approach, which accounts for non-homogeneous intragranular deformation, models the sub-element deformation. A continuous DRX model, based on grain boundary-assisted nucleation of non-basal dislocations, is fully coupled to the sub-element deformation. The introduction of a length-scale, the capture distance for the boundary-emitted dislocation, determines the DRX grain size. The model is used to simulate DRX kinetics for magnesium deformed in plane strain compression. Texture, microstructure and flow stress predictions are compared to data from the literature.

3:05 PM

Coupled Simulation of Microstructure and Texture Evolution in Polycrystals: Bala Radhakrishnan¹; Gorti Sarma¹; ¹Oak Ridge National Laboratory

Thermo-mechanical processing to produce optimum grain structure and texture is key to the successful utilization of commercial aluminum alloys and steels as sheet products. Several modeling techniques have been developed in the past with a reasonably good predictive capability for bulk deformation textures. However, prediction of texture evolution during recrystallization remains very challenging because of the lack of models to fully quantify the heterogeneity at the microstructural length scale of the texture and the stored energy of deformation that largely determine the orientations and spatial distribution of nucleation sites. Uncertainties in grain boundary properties, especially grain boundary energy and mobility as a function of the boundary misorientation, make it extremely difficult to predict the recrystallization textures. We present a brief overview of the recent modeling techniques in this field, and highlight some of our recent work in thermo-mechanical processing of steel sheet by shear deformation and annealing.

3:25 PM Invited

Deformation Structures, Properties and Formability of Selected UFG Aluminium Alloys: *Hans Roven*¹; Manping Liu¹; Stephane Dumoulin¹; ¹Norwegian University of Science and Technology

Ultrafine grain (UFG)aluminium alloys can be produced by severe plastic deformation (SPD). The present work focuses on characterization of deformation structures and microstructure development occuring during Equal Channel Angular Pressing (ECAP) and High Pressure Torsion (HPT). High stacking fault materials such as aluminium, are not expected to form defomation twins. However, the present results obtained from high resolution electron microscopy on a series of alloys show numerous twin orientaion relationships in the formed nanostructure. Further, post-ECAP annealing creates improved combinations of strength, ductility and formability.

3:50 PM Break

4:05 PM

Modeling the Effects of Mechanical Twinning on the Response of a Magnesium Alloy Sheet during Strain Path Changes: Ashutosh Jain¹; Gwenaelle Proust²; Carlos Tome²; Sean Agnew¹; ¹University of Virginia; ²Los Alamos National Laboratory

Textured magnesium sheets exhibit strong tension-compression asymmetry, e.g., the yield strength in compression within the sheet plane can be as little as one half that of the yield strength in tension. This behavior has been shown to be a direct result of the interaction between the texture and mechanical twinning. Experiments involving strain path changes have shown that twinning can also cause drastic changes in the material response during strain path changes. For example, material which initially exhibits a low yield stress when strained in compression along the rolling direction can subsequently exhibit a very low yield stress when compressed along the (initially hard) sheet normal direction. The experimentally observed stress-strain response (including strain anisotropy) and crystallographic texture evolution of a magnesium alloy deformed along non-proportional strain paths are simulated using a new crystal plasticity model which accounts for a wide range of twinning, de-twinning, and secondary twinning phenomena.

4:25 PM Invited

Modeling the Effect of Microstructural Features on the Nucleation of Creep Cavities: Gorti Sarma¹; Bala Radhakrishnan¹; 'Oak Ridge National Laboratory

A crystal plasticity based finite element model has been applied to study the deformation of metals at the microstructural scale, in order to determine the effect of various microstructural features on the nucleation of creep cavities. The deformation model captures the non-uniform distributions of the equivalent plastic strain and the hydrostatic stress within the different

M





grains of the microstructure when subjected to cyclic loading conditions. These results are then coupled with a model to predict the flow of vacancies in the microstructure based on the gradients in the hydrostatic stress field. The influence of various microstructural features such as grain boundaries, triple points, and second-phase particles, on the nucleation of creep cavities is examined through the simulations. The model predictions are compared with experimental measurements on creep cavitation.

4:50 PM Invited

Modeling Recrystallization in Aluminum Using Input from Experimental Observations: *Abhijit Brahme*¹; M. Alvi¹; Anthony Rollett¹; ¹Carnegie Mellon University

A model has been constructed for the microstructural evolution that occurs during the annealing of aluminum alloys. Geometric and crystallographic observations from two orthogonal sections through polycrystalline commercial purity aluminum, using automated Electron Back-Scatter Diffraction (EBSD), were used as an input to the computer simulations to create a statistically representative three-dimensional model. The microstructure is generated using Voronoi tessellation followed by sampling on a regular grid. Assignment of orientations to the grains is controlled to ensure that both texture and nearest neighbor relationships match the observed distributions. The microstructures thus obtained are allowed to evolve using a Monte-Carlo simulation. Anisotropic grain boundary properties are used in the simulations. Nucleation is conformed to experimental observations on the likelihood of occurrences in particular neighborhoods. Current results show a good match with the experimentally observed kinetics and texture evolution but also reveal a significant lack of understanding and knowledge about grain boundary anisotropy. In this paper we will attempt to define more accurate grain boundary properties based on a survey of the currently available results of both experiments and simulations. We will also present the impact of the improved anisotropy description in relation to the effect of alloy content and temperature on the predicted microstructural evolution during recrystallization.

5:10 PM

Phase-Field Modeling of Void Evolution under Elastic-Plastic Deformation: *Shenyang Hu*¹; Yulan Li¹; Michael Baskes¹; ¹Los Alamos National Laboratory

In a deformed solid at a high temperature, atoms or vacancies may move along various paths to minimize the total energy of the system, causing the evolution of preexisting voids. The effect of elastic interactions on microstructure evolution in many important processes such as precipitation in alloys and ferroelectric transitions in films subjected to substrate elastic constraint have been extensively studied using phase-field models. As in elastic interactions, plastic deformation may also play an important role in microstructure evolution. In this work, we present a phase-field model to study vacancy diffusion and void evolution under elastic-plastic deformation. An efficient and accurate method is proposed to solve for the elastic-plastic deformation in an elastically inhomogeneous solid. Both the evolution of slip bands around voids and the effect of plastic deformation on void evolution are systematically investigated.

5:30 PM

Crystal Plasticity in Cubic Metals Using Spectral Methods: Hari Kishore Duvvuru'; Surya Kalidindi'; 'Drexel University

Over the last few decades many crystal plasticity models have been independently developed to predict the anisotropic stress-strain response and crystallographic texture evolution during deformations. These models have enjoyed reasonable success in predicting anisotropic stress-strain response of high stacking fault energy polycrystalline cubic metals together with the concurrent evolution of the underlying averaged texture. However these models are computationally intensive and hence are not widely used for various applications in industry. A new spectral framework that captures efficiently the predictions for the stresses, the lattice spins, and the strain hardening rates in individual crystals from the currently used crystal plasticity models as a function of the crystal's lattice orientation would be presented in this work. The advantages of the spectral crystal plasticity constitutive framework will be discussed in detail.

5:50 PM

Annealing Behavior of Wire Drawn and ECAE Deformed OFHC Copper: *Daudi Waryoba*¹; Peter Kalu¹; ¹Florida Agricultural and Mechanical University-Florida State University, College of Engineering and National High Magnetic Field Laboratory

Equal channel angular extrusion (ECAE) has recently received considerable attention because of its capability to introduce ultrafine grain structure, down to submicrometer range, into course grained bulk materials. One of the advantages of ECAE is its ability to produce intense and uniform deformation by simple shear while retaining the same cross-sectional area. Deformation by ECAE is achieved by extruding a billet through two intersecting channels of equal cross-section. Repeated passes impart very high strains without significant reduction in the cross-section area. The aim of this investigation is to study and compared deformation, recrystallization and growth texture in ECAE and wire drawn OFHC copper.

Aluminum Alloys for Transportation, Packaging, Aerospace and Other Applications: Aluminum Applications

Sponsored by: The Minerals, Metals and Materials Society, TMS Light Metals Division, TMS: Aluminum Committee *Program Organizer:* Subodh Das, University of Kentucky

Monday PM	Room: Northern A4
February 26, 2007	Location: Dolphin Hotel

Session Chairs: Subodh Das, University of Kentucky; Gyan Jha, ARCO Aluminum Inc

2:00 PM

Recent Trends in SCC Failures in Aluminum Beverage Cans: Shridas Ningileri¹; S.K. (Sandy) DeWeese²; ¹Secat Inc; ²Ball Corporation

Stress-corrosion cracking (SCC) in aluminum alloys have been extensively studied and documented. SCC is occasionally experienced in easy-pour aluminum ends used in beer and beverage cans typically manufactured using pre-coated 5182 – H19 aluminum sheet. SCC failures are seen in beverage cans within four days to three weeks after filling and warehousing and are experienced most frequently in summer in hotter, more humid regions of North America. This can be avoided by ensuring that the ends stay dry and minimizing the amount of residual moisture in the packages before palletizing and storage. At lower internal stresses, SCC propagates by a transgranular mode (TGSCC). As designs evolve to reduce aluminum usage in cans, intergranular SCC (IGSCC) is being seen due to higher residual manufacturing stresses and operating stresses. Higher-strength AA5182 developed for use at thinner gauges appears more susceptible to SCC. These interacting factors are presented and discussed in the paper.

2:25 PM

Investigation of "Wear" During the Processing of Aluminum Sheet Alloys: *Gyan Jha*¹; Weimin Yin²; Basil Darras³; Marwan Khraisheh³; Shridas Ningileri²; ¹ARCO Aluminum Inc; ²Secat Inc; ³University of Kentucky

The wear properties of aluminum alloys are affected by the processing techniques employed during manufacture. The addition of lubricants impacts the wear relationship between aluminum and the related tooling. The optimized interaction between aluminum sheet, tooling and the lubricant should be developed to create efficient manufacturing processes with a high finished product quality. A metallurgical investigation into factors affecting the wear behavior of aluminum sheet alloys during processing will be discussed. Results from SEM and Optical Imaging investigations will be presented.

2:50 PM

State-of-the-Art: Aleris Aluminum Recycling and Continuous Casting at Uhrichsville, Ohio: *Zhong Li*¹; Steve Kirkland¹; Dave Thompson¹; Paul Platek¹; ¹Aleris International Inc

Aleris International, Inc. is a vertically integrated major manufacturer of rolled aluminum products and a global leader in aluminum recycling and producer of specification alloys. The Company's recycling and continuous



casting plant in Uhrichsville, Ohio is a leading player in utilizing aluminum scraps and twin belt continuous caster to make aluminum alloy sheet. The combination of using various aluminum scraps, providing the molten metal to the continuous caster and making aluminum sheet has the advantages of low energy consumption, low conversion cost, high productivity and short lead time. This presentation describes aluminum recycling and continuous casting operations at the Uhrichsville, Ohio plant.

3:15 PM

M

OZDAY

P M

Characterization of Surface Defects Encountered in Twin Roll Cast Aluminum Strips: *Murat Dundar*¹; Ozgul Keles¹; ¹Assan Aluminum

Solidification mechanism in twin roll casting (TRC) technique provides various advantages for the production of aluminum alloys having narrow solidification range. High production volume in casting, reduced cost of rolling due to the gauge of initial material to be rolled and elimination of some other intermediate processes are among those. However, alloys having wide solidification range is in tendency of creating serious surface defects. They can readily deteriorate mechanical performance and results in severe complications not only in demanding applications, but also in ordinary engineering applications. If exposed to a surface treatment, they can be easily revealed by resulting in impairment of the aesthetic appearance. Present study aims microstructural characterization of surface defects created in TRC technique and their affects on some critical applications and 8000 series aluminum alloys produced for demanding applications and 8000 series alloys for packaging industry form the subject of this study.

3:40 PM Break

3:50 PM

Life Cycle Cost Analysis Methodology: A Case Study of Aluminum Applications in Passenger Cars: *Subodh Das*¹; Adrian Ungureanu²; Ibrahim Jawahir²; ¹Secat Inc; ²University of Kentucky

In light of escalating fuel prices and ongoing climate change discussions, sustainability considerations are taking a more prominent role in material selection decisions for automotive applications. This paper will present a methodology for studying the total life-cycle cost analysis employing a case study of aluminum products usage in automotive applications. This study is aimed at developing a new sustainability model to quantify the total cost encountered over the entire life cycle of a vehicle considering all the four phases of materials life: (1) pre-manufacturing, (2) manufacturing, (3) use and (4) recycling. Additionally, the environmental impact of the vehicle life time can also be quantified. A critical review of key published papers in the literature will be presented. Some preliminary data will also be presented and plan for future work will be discussed.

4:15 PM

Superplastic Deformation of Warm-Rolled 6013 Al Alloy: *Sung Soo Park*¹; Hamid Garmestani¹; D. Lee¹; Nack Kim²; Sooho Kim³; Eui Lee⁴; ¹School of Materials Science and Engineering, Georgia Institute of Technology; ²Center for Advanced Aerospace Materials, Pohang University of Science and Technology; ³General Motors Research and Development Center, Materials and Processes Laboratory; ⁴Code 4342, Naval Air Warfare Center

The 6000 series aluminum alloys have been of great interest in aerospace and automotive industry due to their low cost and balanced properties such as medium strength, good weldability, corrosion resistance and immunity to stresscorrosion cracking. In spite of these advantages, however, few 6000 series alloys have shown superplasticity as compared to other aluminum alloys such as 5000 and 7000 series alloys. Until now, various thermo-mechanical treatments have been developed to better enhance the formability of aluminum alloys using superplasticity. Nevertheless, there seems to be a necessity to come up with simpler thermo-mechanical processing which can be profitable to practical manufacturing. In this respect, it is suggested by the authors that warm rolling has a great potential to enhance the superplasticity of 6000 series alloys.

4:40 PM

70

Fabrication of Ultrahigh Strength Aluminum Alloy by the Route Consisting of Solid Solution, Large Deformation and Ageing: *Xiaojing Xu*¹; Xiaonong Cheng¹; ¹Jiangsu University

In present study, a fabrication route of the aluminum alloy with ultrahigh strength and moderate tensile ductility has been developed using 2024Al alloy as experimental materials. This fabrication route consisted of a lowtemperature Large Deformation Processing (LDP) combined with a pre-LDP solid-solution treatment plus a post-LDP low-temperature ageing treatment. The present study also found that an enhanced solid-solution treatment prior to LDP would result in an obviously higher hardness and strength, and little deterioration to tensile ductility.

5:05 PM

Fabrication of Carbon Fibers Reinforced Aluminum Foam: *Zhuokun Cao*¹; Guangchun Yao¹; Yihan Liu¹; ¹Northeastern University of China

Carbon fibers reinforced aluminum foam was prepared by adding short copper coated carbon fibers and blowing agent TiH2 in to aluminum melt. Influences of fiber content on foaming ability of the melt were discussed. Microstructure of the cell wall surface and cross section was observed by SEM to analyze the interface wetting ability and distribution of the fibers. Orientation of carbon fibers located in thin cell walls appeared to be parallel to the cell wall surface, which made reinforcement of the fibers more efficient. And suitable processing parameters, including stirring time, stirring speed and holding time were determined.

Aluminum Reduction Technology: Operational and Technology Improvements

Sponsored by: The Minerals, Metals and Materials Society, TMS Light Metals Division, TMS: Aluminum Committee *Program Organizers:* Geoffrey Bearne, Rio Tinto Aluminium Ltd; Stephen Lindsay, Alcoa Inc; Morten Sorlie, Elkem Aluminium ANS

Monday PM	Room: Southern 2
February 26, 2007	Location: Dolphin Hotel

Session Chair: Gretta Stephens, Alcoa - Point Henry

2:00 PM

The 77 Day Safe Start-Up of ALBA Line-5: Abdul Raoof Abdulla1; 1ALBA

In February 2005, Alba successfully launched its bid to set a new world record for the fastest and safest start up of an aluminium reduction line when it kicked off its ambitious 100 Days Safe Start-up challenge. At the time, Alba was hoping that, by achieving the safe start up of its newest reduction line in just 100 days, it would break the current world record by more than 80 days. The plan was to bring the largest expansion project in Bahrain's history to a glorious end by earning the Kingdom international recognition for its industrial development while firmly positioning Alba at the new world aluminium superpower. With initial plans of commissioning an average of four pots a day, the line 5 operations team soon increased to six pots a day which made a global industrial history by commissioning 336 pots in just 77 days.

2:25 PM

Technical Improvement in Inalum: Dante Sinaga¹; Harmon Yunaz¹; Syahrul Bice¹; M. Kondo¹; ¹PT INALUM

PT Indonesia Asahan Aluminium, Inalum, the only aluminum smelter in South East Asia region, is a Sumitomo's Technology smelter, started up in February 1982. Designed at 225,000 t/year,175 kA, 87.5% CE, 14,500 kWh/t-Al DC, unit productivity 450 t/pot.year and AE frequency more than 2.5 times/pot.day, today Inalum has achieved better in performance : productivity more than 250,000 t/year, 188 kA and 196 kA (21 pots pilot project with booster), 92.5% CE, around 14,000 kWh/t-Al DC,unit productivity 510 t/ pot.year, and AE frequency less than 0.8 time/pot.day by total performance improvement strategy. The basic concept is best practice approach which mainly are optimization of operation parameters and modification of computer software with minimum investment, such as higher bath acidity, lower alumina concentration, higher amperage, modified busbar arrangement, larger anode size and pot design development, lower metal pad, slot anodes, higher anode, larger anode's stub and hole, teeth blade, and improve anode quality.

2:50 PM

Operational and Control Improvements in Reduction Lines at Aluminium Delfzijl: *Marco Stam*¹; Mark Taylor²; John Chen²; Sikke van Dellen¹; ¹Aluminium Delfzijl B.V.; ²University of Auckland

Nowadays viability of smelters requires operation of cells at or beyond





known performance limits. At Aldel over the last six years the intensity of electrical energy dissipation and alumina dissolution per cubic centimetre of liquid bath have increased by 50% as production (+14%) and specific energy consumption (-5%) have improved. The cell imbalances resulting from this increased intensity must be sensed quickly and their causes corrected or removed to maintain the cells in their most efficient operating zone. This defines a new control objective for smelting relating to diagnosis of causes of abnormality in strongly interactive multivariate processes. Timely identification of these causes of variation is linked to operational practice improvement and better control decisions in reduction lines. This paper describes smelter based improvement of operational practices and control decisions using the above objective. Statistical multivariate control surfaces are presented for operating cells and identified abnormal behaviours are discussed.

3:15 PM

Henan Hongkong Longquan Aluminum Co. Ltd., China-Second Phase: Haibo She¹; Bijun Ren²; Juanzhang Zhang³; ¹SAMI; ²Henan Hongkong Longquan Aluminum Company Ltd.; ³Luoyang Longquan Tiansong Carbon Company Ltd.

Henan Hongkong Longquan Aluminum Co. Ltd. (LQAL) and Luoyang Longquan Tiansong Carbon Co.Ltd. (TSC) were put separately into operation since June 2002 and April 2003. A paper, Henan Hongkong Longquan Aluminum Co. Ltd., China-Growing Up were published about the two projects in Light Metal 2004. In October 2003, LQAL began to construct the second SY300 potline with a capacity of 200,000 tpy. In November 2003, TSC began to construct the second carbon plant with a capacity of 80,000 tpy. The second potline produced the first aluminum ingot in November 2004. The technologies of the second potline and carbon plant were still supplied by Shenyang Aluminum and Magnesium Engineering and Research (SAMI), China, which are improved by SAMI base on those being used in the first. Since putting into operation, the second potline and carbon plant show lower investment and better technological indexes than the first.

3:40 PM Break

3:55 PM

The Latest Developments of Alcan's AP36 and ALPSYS Technologies: *Oliver Martin*¹; B. Benkahla¹; T. Tomasino¹; Sylvain Fardeau¹; Claude Richard¹; Isabelle Hugron¹; ¹Alcan Inc

The Aluminium Pechiney AP36, 360 kA technology has now been on the market for one year. The economical benefits of AP36 on investment and operation cost have been a key decision factor for new smelter projects that are currently under way. To maintain its technological leadership, Alcan is going on with its AP3X HALE development program aiming at continuing the amperage increase while improving the energy performance, maintaining benchmark current efficiency and reducing anode effects. This article describes some important steps of the development cycle : cell design, industrial test, but also process control support using ALPSYS. It first gives the results achieved in the Saint-Jean-de-Maurienne AP36 booster section. It then shows the benefits of improved process control. And it finally describes the latest AP37 developments.

4:20 PM

The Results of Amperage Increase in Pre-Baked Cells OA-300 M1 from 300 to 330 KA: *Yuri Bogdanov*¹; Viatcheslav Veselkov¹; Aleksei Nadtochy²; Vladimir Skornyakov³; ¹SibVAMI; ²"Ural Aluminium Smelter" Branch JSC, "SUAL" JSC; ³"SUAL" JSC

300 KA Pre-baked cells OA-300 developed by "SibVAMI" JSC were put in operation at the test site of the Ural Aluminium smelter in April-May, 2005. During the operating period all design technical and economic indices were obtained in test cells. The measurements executed and the analysis of electrical, thermal, magnetohydrodynamic and strength properties showed the correctness of solutions taken during designing. The technology level over that period can be characterized as stable. The experience of operation and calculations executed using mathematical models showed that a cell design has a potential to amperage increase without any significant design change and it still has high technical and economic indices. According to that it was decided to increase amperage in test cells in two stages: stage one – up to 315 KA, stage two – up to 330 KA. This paper is dedicated to the test results of pilot cells to increase amperage.

4:45 PM

Experience and Pitfalls with Amperage Increase in Hydro Aluminum Potlines during the Last Ten Years: Halvor Kvande¹; *Bjørn Moxnes*¹; Havard Gikling¹; Marvin Bugge¹; ¹Hydro Aluminium AS

Hydro Aluminium has increased the primary metal production in its Norwegian smelters over the last ten years by 25% by increasing the amperage with a very low investment cost. The capacity creep program has been implemented to increase the production of primary metal, reduce the specific energy consumption, and increase the manning productivity. Both the energy and manning costs are high in Norway, so the program has been an important part to improve the international competitiveness. The capacity creep has been achieved by utilizing technical slack in the existing system and by introducing some new cell technological elements. To succeed with the future program some valuable lessons have been learned about how to avoid pitfalls. Organization of the interaction between operation and R&D and the proper use of booster cells have been and will continue to be important issues.

5:10 PM

Production Boost at Alro: Cristian Stanescu¹; Gheorghe Dobra¹; Satish Manaktala¹; ¹ALRO S A

At the end of 2002 the Alro smelter in Romania started an ambitious program to increase its smelter capacity through an amperage increase program that involved re-design of the anode and cathode configurations and substantially altering the cell heat balance. To manage the potential risks, a test section was established in order to test all the changes in preparation for industrial scale application to the potlines. Test section performance and results were presented in the TMS 2005 proceedings. Subsequently all the technical modifications perfected in the test section were implemented in the potlines that led to a 30% increase in smelter capacity at a capital cost of less than \$500/ton. This paper reports on the industrial scale implementation of the project and the achieved performance as compared to the test section. The paper further alludes to the stage 2 smelter performance enhancement program currently being evaluated on the test section.

Biological Materials Science: Mechanical Behavior of Biomaterials

Sponsored by: The Minerals, Metals and Materials Society, TMS Structural Materials Division, TMS/ASM: Mechanical Behavior of Materials Committee

Program Organizers: Andrea Hodge, Lawrence Livermore National Laboratory; Chwee Lim, National University of Singapore; Eduard Artz, University of Stuttgart; Masaaki Sato, Tohoku University; Marc Meyers, University of California, San Diego

Monday PM	Room: Europe 4
February 26, 2007	Location: Dolphin Hotel

Session Chairs: John Nychka, University of Kentucky; Jikou Zhou, Lawrence Livermore National Laboratory

2:00 PM

Structural and Mechanical Properties of Avian Materials: Sara Bodde¹; Yasuaki Seki¹; Bimal Kad¹; Marc Meyers¹; ¹University of California

The structure and mechanical properties of avian materials including beak, claw, and feather are investigated. The beak structure of selected species of Toucan and Hornbill is a sandwich composite with an exterior consisting of staggered keratin tiles and a core consisting of closed-cell foam. Edges of the closed cell foam are bony trabeculae while faces are lipid membranes. Tensile and compressive tests on keratinous exterior, foam core, and composite cross sections are performed in order to determine the influence of individual structural elements and the interaction of the two on mechanical properties of the beak. Micro- and nano-hardness testing are performed on keratinous specimens from claw, feather, and beak under different humidity conditions. Structure of specimens before mechanical testing and fracture patterns after mechanical testing are imaged using electron and optical microscopy. This research is funded by the National Science Foundation, Division of Materials Research, Ceramics Program (Grant DMR 0510138).



2:20 PM Keynote

Mechanical Behavior of Cells on Porous Tissue Engineering Scaffolds: *Lorna Gibson*¹; Brendan Harley¹; Toby Freyman²; Ioannis Yannas¹; ¹Massachusetts Institute of Technology; ²Boston Scientific

Porous scaffolds are being developed for regenerating damaged or diseased tissues such as skin, nerve, cartilage and bone in vivo. The microstructure of the scaffolds typically resembles that of a low density open-cell foam. The pore size is a critical parameter for bioactivity: the cells must be sufficiently large for cells to migrate through them but small enough to provide a sufficiently large specific surface area, and number of binding sites, for large numbers of cells to attach to the scaffold. Scaffolds can also be used in vitro, for studying cell mechanics. We have developed uniform collagen-glycosaminoglycan scaffolds to study the contractile behaviour of fibroblasts, important in understanding wound contraction associated with the formation of scar tissue. We have also used the scaffolds to study the effect of the pore size and stiffness on cell migration speed using confocal microscopy.

3:00 PM Invited

Hierarchical Deformation Mechanisms in Tendon and Bone: Peter Fratzl¹; Himadri Gupta¹; Wolfgang Wagermaier¹; Paul Roschger²; ¹Max Planck Institute of Colloids and Interfaces; ²Ludwig Boltzmann Institute of Osteology

Bone and tendon and are hierarchically structured nanocomposite materials, based on collagen type I molecules assembled to fibrils in a parallel and staggered arrangement. In the case of bone, collagen fibrils are reinforced by nanometer sized mineral particles made of carbonated hydroxyapatite. Both types of material, tendon and bone, have remarkable mechanical properties combining high stiffness and toughness. Recent experiments combining synchrotron x-ray diffraction and in-situ deformation in native (fully hydrated) tissue have shown that not only the structure but also the deformation processes are hierarchical. In particular, (mineralized) collagen fibrils stretch less than the overall tissue when tensile force is applied to bone or tendon. This shows that a very thin (visco-) plastic matrix or "glue" layer joins the elastic fibrils and transmits load between them by shear. These findings emphasize the importance of the interface layer between fibrils in the design of stiff and tough fibrous composites.

3:30 PM

Mechanical and Ultra-Structural Analysis of Permanent Attachment Systems in Plants: *Ruth Schwaiger*¹; Tina Steinbrecher²; Deane Harder²; ¹Forschungszentrum Karlsruhe; ²University of Freiburg

Permanent attachment structures of plants have already been described by Darwin. However, neither the interface structure nor the mechanics of attachments have been systematically investigated although their outstanding mechanical performance has been recognized. Clamberers attach within few hours after making contact with the substrate. The attachment structures become subsequently lignified and stay attached for many years. These natural interfaces between different materials work under extreme conditions and therefore represent appropriate model systems for new technological concepts. Individual attachment structures as well as clusters were tested under natural growth conditions. Attachment organs of climbing plants can be characterized as composite materials with special adaptations, e.g. different cell layers that partly secrete a strong cementing substance; microscopy revealed cell diversification and accumulation of biological adhesive. We will discuss the attachment strength in terms of elapsed time since attachment occurred and substrate material. Morphological changes of attached and non-attached structures will be shown.

3:50 PM Break

4:10 PM Invited

Multi-Scale Mechanical Analysis of Aortic Tissues: *Takeo Matsumoto*¹; ¹Nagoya Institute of Technology

It is well known that arteries change their dimensions and mechanical properties adaptively in response to change in their surrounding mechanical environment. Because mechanical adaptation is driven by cells in the tissue, we need to know their mechanical environment to reveal the mechanism of the adaptation. Stress and strain applied to the cells in the tissue are not equal to those applied to the tissue, because mechanical properties of cells are much different from those of extracellular matrices such as collagen and elastin, and such difference causes microscopic residual stress in unloaded tissues. To reveal their mechanical environment, we have been measuring the mechanical properties and residual strains of smooth muscle cells and other tissue components isolated from aortic tissues as well as those of whole tissues. In this talk, I would like to introduce our recent approach to estimate the mechanical environment of aortic wall at a cellular level.

4:40 PM Invited

In Vitro Bioactivity of 45S5 Bioglass as Function of Indentation Load: *John Nychka*¹; Ding Li¹; Beth Alexander¹; ¹University of Kentucky

Many fabrication routes used to process biomaterials result in residual stresses. The presence of residual stress can cause failure or even change dissolution rates of many materials, in particular biomaterials that are designed to be resorbed. Stored strain energy can add extra thermodynamic driving force for dissolution and result in varied dissolution rates depending on the sign of the stress. This work describes *in* vitro testing in simulated body fluid after indenting the surface of 45S5 bioglass discs with varying loads. The local formation and morphology of the hydroxycarbonate apatite (HCA) layer at the surface was analyzed by scanning electron microscopy to determine effects of local residual stresses on bioactivity. The feasibility to adjust residual stresses before implantation to alter formation of the HCA layer and thus affect bioactivity is discussed as a strategy for creating gradients of bioactivity on implants.

5:00 PM

Effects of Moisture on the Mechanical Behavior of a Natural Composite Fiber: Sara Walter¹; Mark Johnson¹; Brian Flinn¹; *George Mayer*¹; ¹University of Washington

The energies to fracture of sponge spicule fibers and of silica fibers that had been drawn from the melt were measured after exposure to sea-water and distilled water, and compared to those derived in ambient air environments. The mechanical properties in bending were determined using a dynamic mechanical analysis (DMA) apparatus, operating in the static mode. Energies for the work of fracture were observed to be diminished for the spicule fibers and for silica fibers in moist vs. dry environments. The mechanisms for the influence of moisture on both the natural and synthetic fibers are discussed.

5:20 PM

Time-Dependent Deformation of Prismatic Biological Materials: *Jikou Zhou*¹; Edward Matteo²; Luke Hsiung¹; ¹Lawrence Livermore National Laboratory; ²Princeton University

Recent achievements in science and engineering provide new momentum for the study of the biological materials. In particular, emerging nano technologies make it possible for the first time in the history to explore the microstructures and properties of the components of biological materials down to the nanometer. This progress enables us to update our understanding of Prismatic materials in the nature. Prismatic microstructure is frequently observed in the surface layers of many biological materials. It is a naturally optimized microstructure to bear impact loading and penetration deformation. It is generally believed to be a brittle, poorly designed hard tissue. But we found that its mechanical behavior at small scale is strongly time-dependent. Our new understanding regarding this will be presented in this talk.

5:40 PM

Elastic Modulus Variations of Dentin Bonded Interfaces: Grayson Marshall¹; Shabnam Zartoshtimanesh¹; Sally Marshall¹; ¹University of California, San Francisco

Dentin forms the bulk of teeth and is capped by harder enamel. Bonding to dentin relies on micromechanical bonding with demineralized dentin infiltrated by bonding agents to form a hybrid layer of resin and dentin matrix. Despite good initial bond strength and new bonding methods, durability remains a problem. The dentin-enamel junction (DEJ) forms a linearly varying functionally graded interface that has been evaluated using nanoindentation and a new method (dynamic stiffness mapping, DSM) to image modulus variations (Balooch et al, JBiomech, 2004). We used DSM to evaluate various methods used to make dentin-resin-composite interfaces to determine if these interfaces are similar to the DEJ. Minimum elastic modulus occurred at the bonded interface, but values (1-10 GPa) and dimensions varied widely depending on method. Current resin-dentin bonding systems do not

Technical Program



approximate the natural DEJ and improvement might result from a biomimetic approach to such interfaces. Supported by NHI/NIDCRP01DE09859 and R01DE13029.

Bulk Metallic Glasses IV: Mechanical Properties I

Sponsored by: The Minerals, Metals and Materials Society, TMS Structural Materials Division, TMS/ASM: Mechanical Behavior of Materials Committee

Program Organizers: Peter Liaw, Univ of Tennessee; Raymond Buchanan, University of Tennessee; Wenhui Jiang, University of Tennessee; Guojiang Fan, University of Tennessee; Hahn Choo, University of Tennessee; Yanfei Gao, University of Tennessee

Monday PM	Room: Asia 1
February 26, 2007	Location: Dolphin Hotel

Session Chairs: A. S. Argon, Massachusetts Institute of Technology; Brett Conner, Air Force Office of Scientific Research

2:00 PM Keynote

What Can Plasticity in Amorphous Silicon Tell Us about Plasticity in Amorphous Metals?: *Ali Argon*¹; ¹Massachusetts Institute of Technology

Amorphous metals exhibit both many desirable characteristics such as very high plastic shear resistance and a potential for limitless plastic shear flow, but also some undesirable features such as nxt to no strain hardening and a potential for severe embrittlement through structural aging. Recent computer simulations of plasticity in amorphous silicon have not only shed new light on the fundamental mechanisms of flow by repeated nucleation of thermally assisted local shear transformations and on the mechanisms of embrittlement due to structural aging or of re-juvenation to re-gain ductility through autocatalytic plastic flow, but also on the potential for shear localization. These have immediate relevance to understanding corresponding processes in amorphous metals. There are also new and exciting developments to nurture some genuine strain hardening in certain amorphous alloys with special crystalline heterogeneities, imparting resistance to macro mechanical instabilities. These developments will be presented and discussed.

2:30 PM Invited

Low-Temperature Anelastic and Viscoelastic Deformation in an Al-Rich Metallic Glass: *Michael Atzmon*¹; Amritha Rammohan¹; ¹University of Michigan

In a metallic glass subjected to low stress, the strain consists of three contributions: elastic, anelastic and viscoelastic. The anelastic strain is recoverable and time dependent, whereas the viscoelastic strain is permanent and time dependent. While viscoelastic flow is known to depend strongly on the relaxation state, it has been suggested that anelastic behavior is not sensitive to prior annealing. In order to characterize the dependence of anelastic strain on the state of a metallic glass, bend stress relaxation measurements have been performed at temperatures significantly below the glass transition. Prior to testing, combinations of cold rolling and annealing were used to modify the relaxation state. The results will be used to discuss the defects responsible for each deformation process.

2:50 PM Invited

Flow and Fracture Studies on Bulk Metallic Glasses: John Lewandowski¹; ¹Case Western Reserve University

The flow and fracture behavior of various bulk metallic glasses are being evaluated over a range of different stress states. Continuing work is investigating the effects of superimposed pressure on the flow and fracture behavior at both room temperature and elevated temperature on bulk metallic glasses with different glass transition temperatures. In addition, the effects of changes in test temperature and strain/loading rate on both the uniaxial tensile behavior and toughness are being determined. Significant effects on the flow and fracture behavior are obtained and will be reviewed in the light of other ongoing work.

3:10 PM Invited

Thermomechanical Instability Analysis of Inhomogeneous Deformation in Amorphous Alloys and Experimental Comparisons: *Yanfei Gao*¹; T. Nich¹; P. Liaw¹; ¹University of Tennessee

Recent experiments have shown that inhomogeneous deformation in amorphous alloys critically depends on the environmental temperature and the applied strain rate, and the temperature field inside the shear band can rise up to the glass transition temperature. A thermo-viscoplastic constitutive law is developed that models both stress-driven and thermally induced strain softening behavior. A linear stability analysis is carried out to examine the conditions for the unstable growth of temperature fluctuations. A deformation mechanism map is constructed to delineate the transition of inhomogeneous deformation from coarse to fine shear-band arrangements. The theoretical results agree well with a nanoindentation experiment with varying applied strain rate and environmental temperature, and with a microindentation experiment in which the shear band spacing can be observed using the bonded interface technique.

3:30 PM

Temperature Evolutions of a Zr-Based Bulk-Metallic Glass during Compression: *Wenhui Jiang*¹; Fengxiao Liu¹; Hao Hsiang Liao¹; Hahn Choo¹; Peter Liaw¹; ¹University of Tennessee

The plastic deformation of metallic glasses at low temperatures and high strain rates is known to be inhomogeneous and localized to narrow shear bands. Recent work demonstrated that a substantial temperature rise accompanies shear banding. The increase in temperature may exert a substantial impact on the structure and properties of the shear bands. Using an infrared camera, we observed in situ the plastic deformation of the Zr52.5Cu17.9Ni14.6A110 .0Ti5.0 bulk-metallic glass during compression tests at various strain rates. The specimens exhibit an inhomogeneous deformation, manifested by the serrated plastic flow and shear banding. From the thermographical images, we quantified the temperature changes of the specimens during the compression tests and analyzed the temperature rise within the shear bands. The results provide new insights into the temperature evolutions caused by shear banding. This work was supported by the US National Science Foundation.

3:45 PM

Observation of Deformation Behavior of Metallic Glasses during In Situ Straining in Transmission Electron Microscope: *H. J. Chang*¹; E. S. Park²; W. J. Moon³; Y. J. Kim³; D. H. Kim¹; ¹Yonsei University, Center for Noncrystalline Materials; ²Harvard University; ³Korea Basic Science Institute

To understand the deformation mechanism of metallic glass and to make up for its weakness, particularly brittleness, in the end, propagation of crack and shear band during in situ straining have been observed using high voltage transmission electron microscope(HVEM). The metallic glass samples investigated include Ti40Zr29Cu9Ni8Be14, Ni60Zr40 and Al87Ni7Gd6. Plastic deformation zone(PDZ) was formed ahead of the crack tip during crack propagation. Ti-based alloy which has been confirmed to exhibit high plasticity in compression mode showed inhomogeneous plastic flow in the PDZ, leading to branching of deformed zone. HREM observation revealed that no crystallization occurred inside the PDZ(or shear band) even in Al-based alloy which has low crystallization temperature. Since nanocrystallization in the shear band of Ti- and Al-based metallic glasses has already been reported, this result indicates the thermal or diffusional effects on the structure of shear band under tensile mode can be different with that under compressive mode.

4:00 PM Invited

In-Situ Observations on Fracture Process of Fe-Based Metallic Glass Ribbons: Xianghong Xu¹; Gang Wang²; Fujiu Ke¹; *Yilong Bai*³; Weihua Wang²; ¹Department of Applied Physics, Beihang University; ²Institute of Physics, Chinese Academy of Sciences; ³Institute of Mechanics, Chinese Academy of Sciences

The notched crack propagation processes of the Fe78Si9B13 and Fe73.5Cu1Nb3Si13.5B9 metallic glass ribbons are in-situ observed by a scanning electron microscopy. The Fe78Si9B13 metallic glass ribbon behaves a shear fracture along the crack plane while the Fe73.5Cu1Nb3Si13.5B9 metallic glass ribbon exhibits a flat crack surface with some dimple structure on the crack plane. Furthermore, for the Fe78Si9B13 metallic glass ribbon, the shear direction can change with crack propagating. The plastic strain zones for the crack tips are measured. The different sizes of plastic strain zones for the



Fe78Si9B13 and Fe73.5Cu1Nb3Si13.5B9 metallic glasses might be the main reason resulting in the different fracture process. A large plastic strain zone could induce the shear deformation along the crack plane and further bring out the shear direction change, while a small plastic strain zone generates the flat crack plane in microscale and the dimple structure in nanoscale.

4:20 PM Invited

Mechanical Properties of Zr-TM-Al (TM: Cu, Ni, Co) Bulk Glassy Alloys: Yoshihiko Yokoyama¹; Akihisa Inoue¹; Peter Liaw; ¹Institute of Materials Research

Ternary Zr-TM-Al (TM: Cu, Ni and Co) bulk glassy alloys were fabricated to clarify the correlations among the volume change, thermal and mechanical properties. These alloy systems show the distinct ternary eutectic point, and bulk glassy phase forms around the ternary eutectic composition. We determine the twelve standard Zr-TM-Al bulk glassy alloys in this study. In the twelve standard Zr-TM-Al bulk glassy alloys, glass transition temperature has large positive correlation coefficient with Young's modulus and Vickers hardness, and negative large correlation coefficient with Poisson's ratio. Melting temperature has also large negative correlation coefficient with Charpy impact value, fracture strain and volume change. We also tried to enhance the volume of glassy alloys by using additive elements for each ternary eutectic alloys. Only the ternary eutectic Zr50Cu40Al10 glassy alloy shows the unique feature, whose volume is significantly enhanced by addition 3 at% noble metals of Pd, Ag, Pt and Au.

4:40 PM

Characterization of Bulk Metallic Glasses under Static Indentation, Dynamic Indentation and Scratch Process: Hongwen Zhang¹; *Ghatu Subhash*¹; ¹Michigan Technological University

The current study is devoted to a systematic investigation of shearband evolution in a Zr-based amorphous alloys subjected to static indentation, dynamic indentation and rotating single-grit scratch process. Although shear bands are identified to evolve for each of the loading scenarios, it was noted that the structure of the shearband patterns developed in each of the loading processes is considerably different. Under static indentations, three sets of shear bands have been noticed where as in the dynamic indentations, two sets of semi-circular shear bands with different curvatures were evolved. A negative rate sensitivity of hardness was observed. In the scratch process, the shear bands structure is more complex and needs further in-depth study. A model based on Mohr-couloumb criterion for hardness-yield strength relationship is developed and has been shown to be applicable for metallic glasses of various compositions.

4:55 PM

Experiments on High Strain-Rate Compression of Bulk Metallic Glasses: *George Sunny*¹; Vikas Prakash¹; John Lewandowski¹; ¹Case Western Reserve University

Liquidmetal-1 (LM-1) is a Zr-based bulk metallic glass (BMG) with both desirable processing (1 K/s critical cooling rate) and mechanical properties (2 GPa quasistatic yield strength, 2% elastic strain). The Split-Hopkinson Pressure Bar (SHPB) was employed to investigate the dynamic compressive behavior of LM-1 for strain rates between 200/s and 3000/s in order to investigate the effects of L/D ratio and annealing on peak stress and strain-to-failure, and modified inserts were utilized for the SHPB in order to reduce the effects of stress concentrations on the behavior of LM-1. To examine the macroscopic fracture behavior of LM-1, an ultra high-speed camera was employed to perform in-situ video of the deformation and failure process of LM-1 at 200,000 frames/sec. In addition, scanning electron microscopy was performed to investigate effects of L/D ratio and annealing on the failure surface features. Details of SHPB experiments performed on Fe-based BMGs will also be discussed.

5:10 PM

Dynamic Compressive Deformation Behavior of Zr-Based Amorphous Alloy and Composite: Yang Gon Kim¹; Dong-Geun Lee²; Byoungchul Hwang²; Sunghak Lee¹; Nack Kim¹; ¹Pohang University of Science and Technology; ²Korea Institute of Machinery and Materials

Quasi-static and dynamic compressive deformation behavior of Zr-based amorphous alloy and composite was investigated in this study. Quasi-static compressive test results indicated that the compressive strength of the amorphous composite was similar to that of the amorphous alloy while the ductility was better than that of the amorphous alloy. Under dynamic loading, the maximum shear stress and ductility of the amorphous alloy and composite were considerably lower than those under quasi-static loading because of the decreased resistance to fracture. The deformation and fracture behaviors occurring under quasi-static and dynamic loading conditions were explained by fracture mechanisms. Deformation under dynamic loading lowered strain and compressive strength because of the reduced fracture resistance, and the composite showed more excellent compressive strength and ductility than the alloy. These findings consequently suggested that applying the evaluation criteria for mechanical properties measured under quasi-static loading could cause risks when Zr-based amorphous alloys were used under dynamic loading conditions.

5:25 PM

Formability of Zr57Nb5Al10Cu15.4Ni12.6 Bulk Metallic Glass: Y. Wang¹; S. Gorantla¹; Rajiv Mishra¹; F. Miller¹; R. Brow¹; Daniel Miracle²; ¹University of Missouri; ²US Air Force

The viscous flow of bulk metallic glasses in the supercooled liquid region is considered to have a potential application in forming of complex shapes, but the room temperature brittleness of these components limits their application. The high temperature deformation behavior of Zr57Nb5Al10Cu15.4Ni12.6 bulk metallic glass and the effect of the high temperature forming on room temperature ductility have been investigated. Compression tests were conducted at different temperatures and initial strain rates in the supercooled liquid region. Samples with different microstructures were obtained, including fully amorphous, partially devitrified, and fully crystallized. A forming map was established based on the high temperature compressive flow properties and Vogel-Fulcher-Tammann equation for viscosity. Room temperature mechanical properties of the samples with different microstructures were measured by compression and tension tests. The authors gratefully acknowledge the support of the Air Force Research Laboratory through contract no. FA8650-04-C-704 (Dr. Mary E. Kinsella, Program Manager).

Cast Shop Technology: Cast House Operations and Melting

Sponsored by: The Minerals, Metals and Materials Society, TMS Light Metals Division, TMS: Aluminum Committee Program Organizers: David DeYoung, Alcoa Inc; Rene Kieft, Corus Group; Morten Sorlie, Elkem Aluminium ANS

Monday PM	Room: Northern E1
February 26, 2007	Location: Dolphin Hotel

Session Chairs: Richard Bruski, Novelis, Inc; Pierre Bouchard, STAS, Inc.

2:00 PM Introductory Comments

2:05 PM

World Class Melting Operations: David White¹; ¹The Schaefer Group, Inc. This presentation will cover the seven basic requirements to become a

world class melting operation. It will cover measuring requirements, control requirements, metal melt loss requirements, energy usage requirements, safety requirements, energy audits and metal cleanliness requirements. This presentation will have pictures of do's and don'ts in the industry. It will cover various types of furnaces for melting and holding aluminum as well as degassing and filtration systems. A detailed discussion of energy saving myths will be presented as well as the best ROI modifications to make to exisitng equipment.

2:25 PM

Technology Trends in the Modern Aluminium Casthouse Furnaces: *Mike Unitt*¹; Andrew Haberl¹; Barry Houghton¹; ¹Solios

The ongoing quest for improvement in metal quality and quantity by the new breed smelters drives the Casthouse Equipment suppliers to higher-level technology. This is particularly the case in the supply of cast house furnaces. This paper will reflect on the latest technologies to comply with quality, production and safety demands, New advances in electrically heated furnaces,



electromagnetic stirring, new advances in Refractory materials, types of metal charging and improvements in furnace controls will be discussed. Other aspects of these technologies used by Solios Thermal should not only reflect the on the capital, maintenance and energy cost's but should also reflect on the environmental impact improvements that can be made.

2:45 PM

Optimised Oxy-Fuel Melting Process at Sapa Heat Transfer: *Henrik Gripenberg*¹; Anders Johansson²; ¹Linde Gas Division; ²Sapa Heat Transfer

Linde Gas has developed a new oxyfuel burner concept for reverbatory melting furnaces. The innovative burner design provides lower peak flame temperatures and a more uniform heat flux and temperature profile in the melting furnace. The objectives with the new technology are to improve melt rates, reduce dross formation and to reduce NOx emissions. Sapa Heat Transfer has ten years experience from oxyfuel melting in a 28 metric ton reverbatory melting furnace producing rolling mill slabs of mainly AA3003. The melting operation of the furnace was optimised during 2002 and an ABB electromagnetic stirrer was installed 2005. To further optimise the operations of this high performing furnace, the conventional oxyfuel burners were replaced for the new low temperature oxyfuel technology. The paper will present the new technology with a focus on the one-year evaluation and results from the installations at Sapa.

3:05 PM

Advances in Molten Metal Pump Technology Expand the Capability of Aluminum Reverberatory Furnace Production Rates: *Mark Bright*¹; Richard Chandler¹; Richard Henderson¹; ¹Pyrotek Inc.

Forced circulation in aluminum reverberatory furnaces by molten metal pumps can provide numerous benefits such as higher production rates, reduced melt loss, increased fuel efficiency and improved metal quality. Up to now, it was assumed to be sufficient if the entire furnace volume was circulated approximately 4-6 times per hour. However, with recent innovations in molten metal pump technology, Metaullics Systems has been able to deliver furnace circulation turns in excess of ten times per hour. Advanced design concepts in the new high capacity J-50 circulation pump now permit metal producers to achieve significantly higher melt rates than previously observed in existing reverberatory furnaces. Design features which support such reliable high-output operation will be reviewed. Laboratory and computer simulations predicting increased melt rates have been validated by melt rate measurements in aluminum production facilities, which will be described.

3:25 PM Break

3:45 PM

An Update of Twin Chamber Furnace Technology for Recycling of Aluminium Scrap: *Hans-Walter Graeb*¹; Jan de Groot¹; ¹Thermcon Overns B.V.

The paper will present an update on the latest Twin Chamber Furnace technology for the recycling of (contaminated) aluminium scrap. Based on a new furnace built in 2005 details of the design including heat transfer, elimination of hazardous fumes from the contaminants, but also flexibility in the operation of the furnace with respect to input materials will be described. Safety aspects with respect of the operation will be discussed where as the flue gas cleaning meeting the latest clean air regulations are part of the design of such recycling facility and are discussed in depth. An example of running cost will be included in the paper.

4:05 PM

Computer Simulations of Melt Flow and Particle Removal in the Cyclone: *Andrey Turchin*¹; Dmitry Eskin¹; John Courtenay²; Laurens Katgerman³; ¹NIMR; ²MQP Ltd; ³TU Delft

A large number of techniques have been used today to purify the melt in metallurgical processing operations. The existence of oxides films and other nonmetallic inclusions can dramatically affect the quality and properties of the final cast and wrought product. The objective of the present work is to study the efficiency of the novel system for removal of the particles from the melt in a real industrial application. The computer simulations of the particle motion with flow performed for a wide range of particle sizes show the high efficiency of the cyclone system, which gives an opportunity to apply it in a wide range of flow velocities typical of industrial melt transfer systems. The principal design of the cyclone with the specific dimensions taken from computer model is used to build a pilot-scale cyclone in order to validate the results of computer simulations.

4:25 PM

Energy Saving Myths in the Industry: *David White*¹; ¹The Schaefer Group, Inc.

This covers nine different "Energy Saving" concepts and what the misconceptions are about each one. It will cover ways to implement the nine different energy savings ideas cost effectively and give ROI numbers to prove them. This is a must for anyone considering recuperation, regenerative burners and or relining furnaces for energy saving purposes.

Characterization of Minerals, Metals, and Materials: Characterization of Structure across Length Scales

Sponsored by: The Minerals, Metals and Materials Society, TMS Extraction and Processing Division, TMS: Materials Characterization Committee *Program Organizers:* Arun Gokhale, Georgia Institute of Technology; Jian Li, Natural Resources Canada; Toru Okabe, University of Tokyo

Monday PM	Room: Oceanic 8
February 26, 2007	Location: Dolphin Hotel

Session Chairs: Jian Li, Natural Resources Canada; Arun Gokhale, Georgia Institute of Technology

2:00 PM Invited

Atomic-Level Characterization of Alloys Using Aberration-Corrected Scanning Transmission Electron Microscopy: David Williams¹; Masashi Watanabe¹; ¹Lehigh University

Scanning transmission electron microscopy (STEM) involving electron energy-loss spectrometry (EELS) and X-ray energy dispersive spectrometry (XEDS) is one of the best approaches to characterize materials. It is now possible to identify the nature of individual atomic configurations by STEM with recently developed aberration correctors. The STEM aberration corrector permits to refine incident probes to sub-Ångstrom levels, and hence analysis can be performed on individual atomic columns identified by high-angle annular dark-field (HAADF) imaging. In this study, an L12-ordered Ni3A1 based intermetallic compound has been characterized by using two types of aberration corrected STEMs at Lehigh. The dominant face-centered sites can be easily distinguished from the corner sites by the HAADF imaging. According to the results from the atomic-column analysis, Ti (one of alloying elements) was mainly distributed on the corner sites. Therefore, such site preferences of alloying or even impurity elements can be determined directly in the aberration-corrected STEM.

2:30 PM

The Impact of Indexing Parameters on the Speed and Accuracy of Automated Electron Backscatter Diffraction Measurements: Matthew Nowell¹; *Stuart Wright*¹; John Carpenter¹; ¹EDAX-TSL

Automated Electron backscatter diffraction (EBSD) or Orientation Imaging Microscopy (OIM) has become widely used in materials science research laboratories around the world. As the OIM technology has matured, scanning speeds have increased. Depending on the technology and/or parameters used in the indexing software, the scanning speeds may be limited by the computer processing speed or on the camera speed. The impact of various indexing and processing parameters on the speed and angular resolution of the measurements are investigated. Strategies for optimizing both speed and accuracy are explored.

2:50 PM

A New Scheme to Index Micro-Laue X-Ray Diffraction Patterns: Vipul Gupta¹; Sean Agnew¹; ¹University of Virginia

A new automatic indexing scheme for Micro-Laue diffraction patterns obtained using synchrotron X-rays is implemented as previously done for micro-beam electron diffraction pattern obtained in a Transmission Electron Microscope. Digital images of experimental Laue diffraction patterns are compared to calculated diffraction patterns or templates. Determination of



crystallographic orientation is based on the degree of matching as defined by a normalized correlation index. The technique boasts a number of advantages over traditional methods: i) no peak search analysis is required; ii) the algorithm is the same for any crystallography; iii) superimposed diffraction patterns, obtained from neighboring grain or second phase particles, can be indexed; and iv) deformed materials with poor quality and streaky Laue patterns can also be indexed. Current indexation statistics and required processor time will be presented.

3:10 PM

3DAP Study of Alloy Element Effects on the Tempering of Steel: *Chen Zhu*¹; Xiangyuan Xiong²; Alfred Cerezo¹; George Krauss³; George Smith¹; ¹University of Oxford; ²Monash University; ³Colorado School of Mines

It is well known that the addition of alloy elements increases the resistance of carbon-containing martensitic steels to softening during tempering treatments. In the case of high silicon steels, the rate-controlling process has previously been identified as being the rejection of this element during the growth and coarsening of cementite. However, the mechanisms of other alloy elements remain obscure. We are studying the tempering of, AISI/SAE4340 (Fe-1.83at%C-0.69Mn -0.83Cr -1.67Ni-0.51Si - 0.15Mo) in the temperature range 250°C-400°C. We are using 3-D atom probe techniques to map the redistribution of all major alloying elements between ferrite and carbide phases as a function of temperature and time. It is remarkable that significant retardation of softening rate is observed at tempering temperatures as low as 300°C, where substitutional solute redistribution is barely detectable, even by the most sophisticated 3DAP data analysis techniques. Possible explanations for the observed effects on tempering kinetics will be discussed.

3:30 PM

Characterization of Nano-Scale Compositional Fluctuations in Sm-Ba-Cu-O Superconductor by TEM and STEM/EELS: *Shih-Yun Chen*¹; Alexandre Gloter²; Christian Colliex²; In-Gann Chen³; Maw-Kuen Wu¹; ¹Institute of Physics, Academia Sinica; ²Laboratoire de Physique des Solides, CNRS-UMR 8502; ³Department of Materials Science and Engineering, National Cheng-Kung University

Sm-Ba-Cu-O materials doped with nano-scale RE2BaCuO5 (nmRE211, RE=Y, Sm and Nd) exhibit superior superconductivity in high magnetic fields. According to the results of transport behavior analysis and the knowledge of growth mechanism, the existence of nano-scale compositional fluctuations was suggested. To further elucidate the characteristics of the compositional fluctuation regions, in this study, microstructure of nmY211 doped SmBCO materials were investigated using transmission electron microscopy (TEM) and electron energy loss spectra (EELS). Lamella structures with width range from several to several tens nm were observed throughout the matrix. The chemical distribution, valence structure, thickness, and crystal structure in these lamella structures were compared with those found in the NEG ((Nd, Eu, Gd)-Ba-Cu-O) materials. In addition, regions with higher content of Y with a higher density of defects around were found in the matrix. The distribution of Y, lattice distortion, and the ratio of Sm/Ba in these regions were also analyzed.

3:50 PM Break

4:10 PM Invited

Microstructural Characterization of Snow Firn Using SEM/EDS/EBSP: Ian Baker¹; R. Obbard¹; D. Iliescu¹; D. Meese¹; ¹Dartmouth College

In this paper, we present results of a preliminary microstructural study of snow firn specimens taken from different depths in cores retrieved at or near the South Pole by the U.S International Trans-Antarctic Scientific Expedition. We used techniques that we previously developed to examine ice cores involving controlled sublimation in a cold-stage-equipped SEM. From grain boundary grooves we were able to see where the previously-existing snow crystals were joined, and, hence, could determine grain sizes. Through analysis of secondary electron images of the firn, the porosity and the internal surface area per unit volume of the pores were determined. Finally, we determined the microchemistry of impurities in the firn using EDS and demonstrated that the orientations of the firn crystals could be ascertained using EBSP. Supported by NSF grant OPP 0440523 and ARO contract DAAD 19-03-1-0110.

4:40 PM

Microstructural Characterization of Ti-Nb Alloys with 2% Al: Sergio Monteiro¹; Lioudmila Matlakhova¹; Anatoly Matlakhov¹; ¹State University of the Northern Rio de Janeiro

Quenched alloys from the titanium-niobium system are of considerable scientific and technological interest due to their special properties such as superconductivity, shape memory effect and high damping capacity. The addition of aluminum tends to accentuate these properties in association with microstructural changes that may occur in an extensive interval of temperatures. In the present work the structural transformations taking place in Ti based alloys with 2 wt.% of aluminum and Nb content varying from 15 to 40 wt.% were investigated by X-ray diffraction, thermoanalysis and both optical and scanning electron microscopy. The results indicate that alloy with metastable alpha' or alpha'' martensite transform to metastable beta and then to stable alpha in the 250 to 450°C range. Alloys with greater Nb content, in that the metastable beta is the initial structure, undergo phase decomposition below 200°C forming stable beta and then stable alpha at higher temperature.

5:00 PM

Texture Characterization of Cold-Rolled Ti-6Al-4V Specimens by Thermoelectric Power Measurements: *Hector Carreon*¹; ¹Universidad Michoacana de San Nicolás de Hidalgo

This paper presented experimental data that illustrates the intrinsic sensitivity of the thermoelectric contact technique based on Seebeck effect in order to detect the presence of texture induced anisotropy with different deformation degrees, 1.6mm, 3.2mm, and 6.4 mm thickness-reduction, in cold-rolled Ti-6AL-4V specimens. The results show the thermoelectric power (TEP) coefficient behaviour with respect to the anisotropy and microstructure in a highly-textured material that presents morphological and crystallographic texture. Ultrasonic measurements of shear wave velocities were also conducted in order to obtain a direct correlation between the presence of a significant anisotropy in Ti-6Al-4V specimens and the TEP measurements before and after annealing. Thermoelectric power measurements offer a means to assess the evolution of texture, which allows for a better correlation between anisotropy and the material microstructure and properties. Of course, the TEP values depend on the physical nature and degree of the imperfection to be characterized.

5:20 PM

An Electron Microscope Study of Tweed Structure in GdNi Intermetallic Alloys: Ozan Ugurlu¹; Yaroslav Mudryk²; *L. Scott Chumbley*¹; Vitalij Pecharsky²; ¹Iowa State University; ²Ames Laboratory

We describe an extensive microstructure characterization of heat-treated GdNi intermetallic alloys using various electron microscopy techniques. Previous x-ray diffraction studies of these alloys showed broader peaks then what was expected from simulations. Detailed examination of the microstructure using Transmission Electron Microscopy (TEM) revealed a tweed structure and High Resolution TEM (HRTEM) images show a highly strained lattice structure. Streaking seen in Selected Area Diffraction (SAD) patterns indicate an extremely small size scale structure. In addition to the tweed structure, staking faults have been observed during TEM studies. This paper presents these results coupled with Microprobe, Scanning TEM (STEM) and Orientation Microscopy (OIM) studies that have been conducted to reconcile the broad x-ray diffraction peaks observed with direct observation of the structure using advanced microscopy techniques.

5:40 PM

Non-Metallic Inclusions in Metals: From Nanometer to Milimeter: *Lifeng Zhang*¹; ¹Norwegian University of Science and Technology

This study aims to characterize the Non-Metallic Inclusions (NMI) in metals, such as steel, aluminum and silicon. Several approaches, such as optical microscope, SEM, X-ray, Slime test, etc, are used to detect and evaluate NMIs from nanometer to millimeter in these metals. The size distribution, morphology and composition of inclusions are investigated. A fundamental model is developed to to predict inclusion composition, quantity and size distribution evolution during metal processing, including the effects of metallurgical thermodynamics, nucleation, growth, collisions, bubble interactions, turbulent flow transport, and entrapment by the solidifying steel. By finding ways to incorporate the microscale model results into the macroscale models, new insights into the relative importance of different mechanisms will



be developed. The current research will combine the Nano- and Micro-scale Inclusion Nucleation and Growth Phenomena with the Macro-scale Flow Pattern and Inclusion Transport.

Computational Thermodynamics and Phase Transformations: First Principles and Atomistic Calculations of Phase and Alloy Thermodynamics II

Sponsored by: The Minerals, Metals and Materials Society, ASM International, TMS Electronic, Magnetic, and Photonic Materials Division, TMS Materials Processing and Manufacturing Division, ASM Materials Science Critical Technology Sector, TMS: Chemistry and Physics of Materials Committee, TMS/ASM: Computational Materials Science and Engineering Committee

Program Organizers: Corbett Battaile, Sandia National Laboratories; James Morris, Oak Ridge National Laboratory

Monday PM	Room: Europe 11
February 26, 2007	Location: Dolphin Hotel

Session Chair: Hamish Fraser, Ohio State University; Anton Van der Ven, University of Michigan

2:00 PM Invited

Kinetics of Phase Transformations from First Principles: Anton Van der Ven¹; ¹University of Michigan

While much progress has been made in the first-principles prediction of the thermodynamics of multi-component solids, predicting the kinetics of solid-state phase transformations remains a major challenge. A large class of phase transformations in multi-component solids involves a redistribution of its constituents, which requires atomic diffusion. First-order phase transformations also require the passage of interfaces separating new phases from old phases. One approach to simulate first-order diffusional phase transformations from first-principles is through parameter passing, whereby kinetic coefficients describing atomic diffusion and interface mobilities are implemented in a continuum description. In this talk, I will describe firstprinciples approaches to predict diffusion coefficients in multi-component solids and focus on a class of first-order phase transformations in intercalation compounds and metal hydrides in which the moving interface is coherent and migrates through dislocation glide.

2:30 PM Invited

Precipitation in Al-Mg-Si from First-Principles: Christopher Wolverton¹; Yi Wang²; Chinnappan Ravi³; Hui Zhang²; Tao Wang²; Long Qing Chen²; Zi-Kui Liu²; ¹Ford Motor Company; ²Pennsylvania State University; ³Indira Gandhi Centre for Atomic Research

Precipitation in Al-Mg-Si alloys has been extensively studied, since this ternary forms the basis of a wide variety of commercial alloys (e.g., 6xxx series alloys). The observed precipitation sequence is complex and involves a wide variety of metastable phases (e.g., GP zones, β ", β '). We have undertaken an extensive first-principles study of many key precipitate properties: T=0 energetics and crystal structures, vibrational entropies, interfacial structure and energies, and lattice-mismatch and coherency strain energies. By incorporating these first-principles results into CALPHAD databases, we can predict the metastable phase equilibria and phase fractions of precipitate phases in a wide variety of 6xxx alloys. Interfacial and strain energies can be used to elucidate the key factors in controlling the morphologies of precipitates in this system, and we incorporate these energetics in phase-field models and predict the resulting precipitate shapes.

3:00 PM

Stress Anisotropy Controls Pathway of Martensitic Transformation in Titanium: *Richard Hennig*¹; Dallas Trinkle²; ¹Cornell University; ²University of Illinois Urbana-Champaign

The pressure-driven martensitic phase transformation in titanium from the ductile hcp to the brittle omega phase can limit titanium's mechanical properties. Under hydrostatic stress conditions this phase transition proceeds via a sixatom pathway with an energy barrier of 9 meV/atom. Ab-initio calculations characterize how non-hydrostatic stresses affect the transformation barriers

of the two lowest-energy pathways and show under which conditions the anisotropic stresses result in a change of transformation pathway. The results indicate that the two orientation relationships observed in diamond anvil and shock experiments are caused by different stress conditions.

Technical Program

3:20 PM

On Some Aspects of Phase Transitions in Mechanically Driven Alloys: *Jong Lee*¹; ¹Michigan Technological University

An interesting feature observed in mechanical alloying is temporal oscillations in phase fractions. For example, the microstructure of a binary Ni-Zr alloy is shown to vary cyclically between a crystalline and an amorphous state. In our earlier work, such cyclical phase transitions were described in terms of a thermodynamic model which shows a time-dependent free energy function. In this work, we present non-equilibrium molecular dynamics (NEMD) results. For a model Ni-Zr alloy, both compressive and shearing deformation modes are applied to mimic a ball milling process. Atomic interactions are expressed through a many-body, tight-binding as well as a Lennard-Jones potential. Both compressive and shearing deformation modes display amorphization from the homogeneous, elastically deformed crystalline state at high strain rates. Shearing deformation, however, is shown to be much more effective for phase transitions, forming a 2-dimensional layered structure at high shear strain rates.

3:40 PM Break

4:00 PM Invited

Reliable First-Principles Prediction of Alloy Thermodynamic Characterization Data via Cluster Expansion Methods: *Duane Johnson*¹; Teck Tan¹; N. Zarkevich¹; ¹University of Illinois

Using cluster expansion (CE) techniques and a database of structural formation energies form first-principles electronic-structure calculations, we predict phase stability and structural phase transformations in multicomponent alloys. We present results from our automated thermodynamic toolkit (TTK) that controls all facets of the CE fitting and density-functional calculation and includes two methods for constructing CE basis sets: our published optimal truncation method and a genetic algorithm method that uses a niching algorithm to prevent solution stagnation, where reliability from these approaches can be estimated. We then show that there are two mean-field limits that permit rapid and accurate estimates of concentration-dependent order-disorder transformations without Monte Carlo, with the appropriate limiting choice determined a priori by the CE interactions. We exemplify these various results in a number of alloy systems, including combining defect calculations with elasticity theory to establish design maps for improving materials properties.

4:30 PM Invited

The Tensorial Cluster Expansion: Axel van de Walle¹; ¹California Institute of Technology

While the cluster expansion formalism is traditionally used to parametrize the configurational-dependence of scalar properties (such as the total energy), this talk introduces a generalization of this formalism to tensorial quantities (such as elastic constants, phase-transformation-induced strains, permanent dielectric dipoles, etc). This new method generates a suitable orthogonal basis for the space of all mappings from lattice configurations to tensors. It also provides symmetry rules to determine which terms in the Tensorial Cluster Expansion are equivalent by symmetry and must therefore share a common coefficient. The proposed framework encompasses, as special cases, a number of existing tools, including the local cluster expansion (used for modeling the properties of point defects), the "symmetrized" cluster expansions (used for predicting tensorial properties of disordered phases), and transferable force constants (used for efficient lattice dynamics calculations). This formalism also provides a simple language to describe the coupling between symmetrybreaking phase transformations and materials properties.

5:00 PM

Using Multi-Body Energy Expansions from Ab Initio Calculations for Computation of Alloy Phase Structures: Nicholas Zabaras¹; Veera Sundararaghavan¹; ¹Cornell University

Cluster expansion methods (CEM) are quite successful for modeling energies of substitutional and interstitial alloys. However, in alloys involving constituents with large size differences, structural relaxations play an important role and convergence properties of the CEM diminish. In such cases, long-ranged and many-body interactions are necessary to model the



energy accurately. We construct such many-body expansion through statistical learning over a very large database of ab-initio energies. Modern regression and cross validation techniques allow efficient handling of the continuous degrees of freedom in the expression for N-body potentials and ensure optimal selection of parameters for convergence of the expansion. This approach provides a more realistic energy functional for use in MC simulations of thermodynamic properties of alloy systems. As an improvement over the cluster expansion method, the methodology enables identification of stable phase structures that do not fall within the superstructures of FCC, HCP or BCC parent lattices.

5:20 PM

Vibrational Thermodynamics of Vanadium Alloys: *Oliver Delaire*¹; Max Kresch¹; Matthew Lucas¹; Tabitha Swan-Wood¹; Brent Fultz¹; ¹California Institute of Technology

We investigated the effects of alloying on the lattice dynamics and electronic structure of bcc vanadium. Using inelastic neutron scattering, we have measured the phonon density of states and vibrational entropy of random solid solutions of vanadium with transition metal impurities. The effect of alloying on the phonon DOS is thermodynamically significant, comparable in magnitude to the configurational entropy of mixing. A clear trend was observed for solutes across the 3d-series, and down the Ti, V and Ni columns. Using density functional theory, we calculated the geometry and electronic structure for the alloys, and computed the stiffness of certain vibrational modes. The electronic entropy of alloying was calculated and found to follow the same trend as the vibrational entropy, although it is smaller in magnitude. Experimental investigations of the phonon DOS were also conducted on concentrated V-Cr alloys and A15 V-based compounds.

Diffusion in Advanced Materials and Processing: Interfaces, Surfaces and Nanostructures

Sponsored by: The Minerals, Metals and Materials Society, TMS Structural Materials Division, ASM Materials Science Critical Technology Sector, TMS: Alloy Phases Committee, TMS: High Temperature Alloys Committee, ASM-MSCTS: Atomic Transport Committee, TMS/ASM: Nuclear Materials Committee, TMS: Solidification Committee

Program Organizers: Yong-Ho Sohn, University of Central Florida; Carelyn Campbell, National Institute of Standards and Technology; Daniel Lewis, Rensselaer Polytechnic Institute; Afina Lupulescu, Union College

Monday PM	Room: Europe 2
February 26, 2007	Location: Dolphin Hotel

Session Chairs: Graeme Murch, University of Newcastle; Yuri Mishin, George Mason University

2:00 PM Invited

Growth Kinetics on Nanoscale: Finite Diffusion Permeability of Interfaces: *Dezso Beke*¹; Zoltán Erdélyi¹; ¹University of Debrecen

Growth kinetic is either diffusion or interface reaction controlled process, characterized by parabolic or linear relationships, respectively. The well known diffusion paradox, predicting infinitely fast diffusion kinetics at short times (distances) for diffusion control will be discussed and resolved, by showing that the diffusion permeability across the interface should be finite at the very beginning of the process. Thus one can arrive at an *atomistic interpretation of the interface transfer coefficient, K*, and at *linear growth kinetics* even if there is no extra potential barrier present at the interface, usually assumed in the interpretation of interface reaction control. It is also shown that this phenomenon is a typical nanoeffect: after a certain diffusion distance (lying between 0.01 and 300 nm, depending on the composition dependence of the diffusion coefficient) the finite permeability of the interface will not restrict the growth and normal diffusion control will be observed.

2:30 PM

Diffusion Mechanisms in Nanocrystalline and Nanolaminated Au-Cu: *Alan Jankowski*¹; ¹Lawrence Livermore National Laboratory

The development of pulsed electro-deposition leads to the synthesis of Au-Cu alloys (0-20 wt.% Cu) with grain sizes less than 5 nm. However,

the nanocrystalline grain structure is thermally unstable. Anneal treatments are used to identify the temperature range of the two dominant diffusion mechanisms – bulk and grain boundary. To assess the transition between mechanisms, the low temperature range for bulk diffusion is established utilizing the decay of static concentration waves in composition-modulated nanolaminates. A transition in the dominant mechanism for grain growth from grain boundary to bulk diffusion occurs with an increase in temperature. The activation energy for bulk diffusion is found to be 1.8 eV/atom whereas that for grain growth at low temperatures is only 0.2 eV/atom. The temperature for transitioning from the dominant mechanism of grain boundary to bulk diffusion is found to be dependent on composition, generally trending at 57% the alloy melt temperature.

2:50 PM

Modeling of Oxygen Diffusion and Segregation at Interfaces in Ag-MgO Composites: Thomas Fiedler¹; Nilindu Muthubandara²; Andreas Ochsner¹; *Irina Belova*²; Graeme Murch²; ¹University of Aveiro; ²University of Newcastle

The presence of atomic oxygen at internal metal-ceramic oxide interfaces significantly affects the physical properties of the interfaces which in turn affects the bulk properties of the composite (metal+ceramic oxide) material. We address this problem for the conditions of a constant source of oxygen at the surface(s) and various periodic and random arrangements of ceramic oxide inclusions (MgO) embedded in the metal matrix Ag. With experimentally determined atomic transport quantities we simulate the concentration depth profiles and segregation of oxygen to the interfaces using independent Monte Carlo and Finite Element methods.

3:10 PM

Stability and Shrinkage by Diffusion of Hollow Nanospheres: Alexander Evteev¹; Elena Levchenko¹; Irina Belova¹; *Graeme Murch*¹; ¹University of Newcastle

Recently, hollow nanospheres of cobalt selenide and cobalt sulphide have been formed from cobalt nanocrystals in Se or S environments (Y. Yin et al. Science Vol.304 ,p711 (2004). The process of formation is believed to be driven by interdiffusion with an extreme Kirkendall effect as Co is replaced by incoming vacancies. There has been considerable interest in the stability of hollow nanospheres compared with the corresponding solid nanospheres. Using Molecular Dynamics we have analyzed single metallic systems exemplified by Pd. We found that small hollow nanospheres (up to about 10 000 atoms) collapsed quickly, but not by classical vacancy-assisted mechanisms, but by mechanisms involving Shockley partial dislocations. For larger systems, too much energy appears to be required for such mechanisms, and the collapse is mediated by the usual vacancy mechanism.

3:30 PM Break

3:50 PM Invited

Diffusion along Dislocation Cores in Metals: G. Pun¹; *Y. Mishin*¹; ¹George Mason University

Diffusion along dislocations can control the kinetics of many processes in materials, including coarsening of disperse particles, dislocation bypass, dynamic strain ageing, creep and sintering. The amount of experimental data on dislocation diffusion is very limited and theoretical understanding of the relevant atomic mechanisms is rudimental, if existent. We give a brief overview of current knowledge of dislocation diffusion and discuss possible approaches to the modeling of this process on the atomic level. Results of atomistic simulations of dislocation diffusion in Al, Ni, and Ni-Al alloys are presented. The simulations reveal the dominant atomic mechanisms and point to the nearly equal role of vacancies and interstitials. The effect of solute interaction with the dislocation core on the rates of solute and solvent diffusion is examined for edge, screw and mixed dislocations in Al. The impact of this work on understanding of diffusion kinetics in plastically deformed materials is discussed.

4:20 PM

Anomalous Diffusion along Interfaces in Crystalline Solids: Raghavan Narayanan¹; Alexander King¹; ¹Purdue University

It is often neglected that Fick's law depends on a particular set of assumptions concerning the nature of Einstein's random walk theory. We elucidate the conditions under which Fick's diffusion law can be applied to a



Technical Program

given problem. Those diffusion processes that do not obey these conditions are called anomalous diffusion processes. We outline arguments which support the possibility that grain boundary diffusion might fall under this category. We also explain the mathematical methods needed to model such processes and we present diffusion profiles corresponding to these anomalous diffusion processes for both instantaneous source and constant source experimental conditions. It is also pointed out that the formalism can be easily extended to surface diffusion, triple junction diffusion and diffusion through amorphous media. We consider the requirements for making measurements of these types of anomaly in interfacial diffusion experiments. Acknowledgment: This work is supported by the National Science Foundation, grant #0504813.

4:40 PM

Revised Mixing Models for Diffusion in Polycrystals: *Ying Chen*¹; Christopher Schuh¹; ¹Massachusetts Institute of Technology

Steady-state polycrystalline diffusion can be described by a homogeneousmedium effective diffusivity comprised of multiple diffusion paths, e.g., bulk, grain boundaries, dislocation cores and triple junctions. The classic Hart equation for the effective diffusivity is the sum of volume averaged individual diffusivities, which implicitly neglects the complex geometrical arrangement of these microstructural elements. In this talk we propose an effectivemedium diffusion model that incorporates various short-circuit diffusion contributions based on realistic topological arrangements. For example, we account for the grains being enclosed by grain boundary facets, rather than assuming that they are parallel elements. This analysis shows that the overall diffusivity of polycrystals is overestimated by the Hart equation, especially for nanocrystalline materials. On the other hand, short-circuit diffusion coefficients, inferred by comparing the Hart equation with the effective diffusivity obtained from diffusant penetration curves, are underestimated.

5:00 PM

Diffusion of Mn into Grain Boundaries and Triple Junctions in LiF Thin Films: Hakkwan Kim¹; Alexander King¹; ¹Purdue University

Diffusion is faster in polycrystalline thin films than bulk materials, and grain size distribution plays an important role. Grain boundaries and triple junctions can act as rapid diffusion paths. The mechanism of manganese diffusion in polycrystalline lithium fluoride thin films has been studied by doping LiF films with Mn via a diffusion process. Manganese was deposited onto fully-dense polycrystalline LiF films and heat-treated so as to penetrate into the LiF by diffusion. The Mn distribution was investigated using the electron energy loss image filtering technique in the TEM and the misorientations and the grain boundary planes were determined by conventional transmission electron microscopy and diffraction. It is found that by controlling the diffusion conditions, Mn can be made to diffuse only into the grain boundaries, and we are now working on restricting it to the triple junctions.

Dynamic Behavior of Materials: Deformation II

Sponsored by: The Minerals, Metals and Materials Society, TMS Structural Materials Division, TMS/ASM: Mechanical Behavior of Materials Committee

Program Organizers: Marc Meyers, University of California; Ellen Cerreta, Los Alamos National Laboratory; George Gray, Los Alamos National Laboratory; Naresh Thadhani, Georgia Institute of Technology; Kenneth Vecchio, University of California

Monday PM	Room: Europe 3
February 26, 2007	Location: Dolphin Hotel

Session Chairs: Ronald Armstrong, University of Maryland; Dennis Grady, Applied Research Associates

2:00 PM Invited

Energy Localization in Meteoritic Target Materials: Hydrodynamic Instabilities and Planar Deformation Features (PDFs) in Quartz: *Robert Graham*¹; M. Martin²; N. N. Thadhani²; B. Morosin³; ¹The Tome Group; ²Georgia Institute of Technology; ³Sandia National Laboratories

Materials at meteoritic impact-sites are complex, but there has been considerable success in first-order modeling based on the idealized conditions utilized in Hugoniot materials descriptions. The determination of Hugoniot pressure from interpretation of widely-observed planar deformation features (PDFs) in quartz is of considerable interest. Localization processes restrict second-order interpretation. Recent work on the Bee Bluff Structure of South Texas (The Uvalde Crater) has shown the importance of catastrophic paradigm modeling. The target materials are Eocene Carrizo Formation Sandstone and Eocene Indio Formation calcareous siltstone, iron-rich siltstone and shale, and loosely lithified calcareous silt. As in other sedimentary target materials, the numbers of quartz grains with PDFs is low relative to crystalline target materials. Furthermore, the orientations and numbers of PDF sets differs from crystalline materials. Evidence for hydrodynamic instability is widespread.

2:30 PM Invited

Shear Localization Resistance by Design: *Gregory Olson*¹; ¹Northwestern University

Multiscale ductile fracture simulation clarifies the importance of microvoiddriven shear localization in both fracture toughness and ballistic plugging resistance. Under the ONR D3D Digital Structure Consortium initiative, 3D simulation of multiparticle interaction at the submicron level demonstrates the mechanism of terminal shear localization, while computational quantum mechanics identifies opportunities to enhance particle interfacial bonding. Exploiting dispersed-phase transformation plasticity to retard microvoid shear localization, a martensitic steel designed for blast protection demonstrates extreme toughness, and precipitation strengthened austenitic TRIP steel designs show high potential for greatly enhanced dynamic stretch ductility. Integrating recent research results, new martensitic steel prototypes demonstrate exceptional resistance to ballistic plugging failure.

2:45 PM

Shearband Patterns under Static and Dynamic Indentations in Bulk Metallic Glasses: *Ghatu Subhash*¹; Hongwen Zhang¹; ¹Michigan Technological University

Static and dynamic Vickers indentations were performed on ZrHf-based bulk amorphous alloys. A negative rate sensitivity of indentation hardness has been observed. The slip steps of shear bands evolved beneath and surrounding the dynamic indentations have been characterized and then compared to those evolved under static indentations. For equivalent loads, dynamic indentations produced more severe deformation pattern on the loading surface than static indentations. Using bonded interface technique, the induced shearband patterns beneath the indentations were studied. In static indentations, most of the deformation was primarily accommodated by closely spaced semi-circular shearbands surrounding the indentation. In dynamic indentations two sets of widely spaced semi-circular shearbands with two different curvatures were observed. The observed shearband patterns were rationalized based on the variations in the confinement pressure and strain rate with in the indentation region during dynamic indentations.

3:00 PM

Kinetics Modeling under Shock-Loading Conditions: Steven Valone¹; ¹Los Alamos National Laboratory/MST-8

Shock loading induces complex kinetic processes leading to such macroscopic phenomena as plastic deformation, phase transformations, and spall. The associated rates are typically modeled as first-order processes. The form of any rate constant is then assumed to be of an Arrhenius form.¹ This form of rate law assumes an equilibrium distribution of velocities in the system.² Clearly, in a shock-loaded system, the velocity distribution needs to be centered on the particle-velocity, u_p.³ A revision in the Arrhenius rate model leads to u_p-dependent rate constants. At high shock loading, the rate constant naturally switches to a power-law dependence in keeping with observation. ¹D. L. Preston, D. Tonks, and D. C. Wallace, J. Appl. Phys. 93, 211 (2003). ²H. A. Kramers, Physica (Amsterdam) 7, 284 (1940). ³S. M. Valone, J. Chem. Phys. 118, 9606 (2003).

3:15 PM Break

3:30 PM Invited

Plastic Processes Leading to Damage and Failure: *T. Wright*¹; K. Ramesh²; ¹US Army Research Laboratory; ²Johns Hopkins University

Damage and failure in ductile materials are often the consequences of deformation processes that lead first to strain softening, next to material instability, and then to localization. Instability and localization produce



extremely inhomogeneous deformation over regions that are too small for direct constitutive measurement so that the state within the localized region can only partially be inferred from external measurements. In this talk it will be shown that direct physical modeling, using standard mechanics and constitutive response without resort to postulated damage parameters, can still be applied at the small scales of localization, and lead to useful quantitative predictions concerning the morphology and timing of localization. Two examples will be discussed; the formation of adiabatic shear bands and the nucleation and growth of voids at high rates.

4:00 PM

Dynamic Failure of Silicon Nitride under Combined Pressure and Shear Impact: George Sunny¹; David Nathenson¹; *Vikas Prakash*¹; ¹Case Western Reserve University

Plane shock wave experiments inducing compression and simultaneous compression and shear were performed on a AS800 grade silicon nitride ceramic. The experiments were conducted using the 82.5 mm single stage gas gun facility at CWRU. A multi-beam VALYN VISAR was used to obtain the free surface velocity time profiles. The results of these experiments were used to understand the dependence of its spall strength on shock induced compressive and shear stresses. In addition, a series of shock and reshock experiments were conducted to understand the state of damage under planar shock compression. In the talk the nature of the failure front and the observed variation in the measured spall strength of SiN will be discussed.

4:15 PM

Dynamic Response of 5083-H131 Aluminum Alloy: J. Boteler¹; D. Dandekar²; ¹NSWC -Indian Head; ²Army Research Laboratory

The material response of 5083-H131 aluminum alloy subjected to dynamic loading has been investigated. In the work reported here we examine the spall strength, Hugoniot EOS, and Hugoniot Elastic Limit (HEL) over the stress range 1.5-8.0 GPa. Measurement of these dynamic properties provide hydrocode modelers with critical information required for accurate modeling of material response to intense loading. Experiments were performed on the Army Research Laboratory 102 mm bore single-stage light gas gun. Impact conditions were uniaxial and planar to within 1 mrad of tilt. VISAR was used to record particle velocity histories with 0.5 ns temporal resolution. The shock Hugoniot for 5083-H131 is extrapolated to 50 GPa and compared to the previous high pressure results of Hauver (1973). The dynamic response including HEL and spall strength of 5083-H131 is compared to other commonly used aluminum alloys.

4:30 PM

Fragments Produced when Tungsten Penetrates Aluminum: *Stephan Bless*¹; ¹University of Texas at Austin

Tungsten rods were fired at 6061T6 aluminum targets in order to investigate the origins of behind-armor debris. Penetrators were L/D = 15 rods made from 91% W-Ni-Co alloy. Behind the target, there was a witness pack composed of five steel plates of increasing thickness. Velocities were 1.7 to 2.6 km/s. Measurements consisted of witness plate perforation patterns and radiographs of the debris field. It was found that as diameter was increased, there was little change in the number of debris particles generated, as measured by the number of perforations in the first witness plate. However, the penetrating power of the particles strongly increased with rod diameter, as shown by the increased number of holes in witness plates three through five. The number of particles increased strongly with velocity.

4:45 PM

Deformation and Fracture Behaviour of Metal Matrix Composites during Dynamic Mechanical Loading: Akindele Odeshi¹; Gbadebo Owolabi¹; Meera Singh¹; *Nabil Bassim*¹; ¹University of Manitoba Winnipeg

In order to improve their mechanical properties and enlarge their structural applications, many light metals and alloys are usually reinforced with compatible ceramic fibres or particles. Due to their unique combination of properties, metal matrix composites (MMC) are finding increasing application in modern engineering design such as high velocity forming and shaping operations as well as military applications. Thus a clear understanding of their dynamic mechanical behaviour at extreme conditions of high strain-rates is very important for an enhanced performance in such applications. In this study, alumina particle reinforced aluminium-based MMC are subjected to massive

deformation at high strain-rates. A systematic evaluation and correlation of the strain-rate sensitivities, microstructural evolution during deformation and fracture behaviour of the materials are conducted and discussed. The results show that thermo-viscoplastic instabilities of the aluminium-based matrix play a significant role in dynamic deformation and failures of the investigated materials at high strain-rates.

5:00 PM

Dislocation Dynamics Simulations of High Strain Rate Deformation of FCC Cu: *Zhiqiang Wang*¹; Irene Beyerlein¹; Richard LeSar²; ¹Los Alamos National Laboratory; ²Iowa State University

The detailed understanding of high-rate deformation of engineering materials is crucial to many applications. We apply a novel Parametric Dislocation Dynamics (PDD) method, along with the use of high performance computing, to simulate material behavior under high-rate loadings. With careful analysis of the simulations, we can provide a detailed picture of microstructural changes, exploring the connection between these changes and the macroscopic response for different rates of deformation. Simulation results are compared with experimental observations.

5:15 PM

Collective Evolution of Dislocations and Voids in the Shock Recovered Metals from Polychromatic Microdiffraction: *Rozaliya Barabash*¹; G. Ice¹; W. Liu²; J. Belak³; M. Kumar³; ¹Oak Ridge National Laboratory; ²Advanced Photon Source; ³Lawrence Livermore National Laboratory

A 3D spatially resolved X-ray diffraction method - with a sub micrometerresolution together with MD simulations, SEM and OIM analysis are applied to understand the arrangements of voids, geometrically necessary dislocations and strain gradient distributions in samples of (123) Al and (001) Cu single crystal shocked to incipient spallation fracture. Because of strong dislocationdislocation interactions and because of interaction between dislocations and the elastic waves, an initially random high density dislocation distribution becomes unstable. As a result after the shock wave has passed correlated dislocation arrangements with dislocation walls develops. Some fraction of the dislocations may remain randomly distributed, and the rest form various correlated groupings and more organised disclination arrangements. Regions with geometrically necessary dislocations form causing local lattice curvature. The orientation and density of geometrically necessary dislocations in the shock recovered Al and Cu samples are determined.

5:30 PM

Influence of Microstructure on the Spall Failure of Aluminum Materials: Jonathan Brewer¹; Douglas Dalton¹; Evan Jackson¹; *Eric Taleff*¹; Todd Ditmire¹; ¹University of Texas

Laser-shock-induced spall failure has been studied in thin aluminum targets. Annealed high-purity aluminum targets, annealed low-purity aluminum targets and aluminum-magnesium, both annealed and cold-rolled, targets with thicknesses of 200 μ m and 500 μ m were subjected to laser shock to induce spall failures. The effects of material and microstructure on failure morphology were investigated. The apparent ductility of spall fractures decreased with increasing hardness for a given shock strain rate. Spall failure character transitioned from ductile transgranular fracture to brittle intergranular failure as hardness increased, with a mixture of failure morphologies observed at intermediate hardnesses. In low-hardness material containing inclusions, the inclusions appeared to act as nuclei for failure initiation.

5:45 PM

Effects of Strain Rate and Adiabatic Heating on the Deformation Behavior of Cold Heading Steels: *Jari Rämö*¹; Veli-Tapani Kuokkala¹; Taina Vuoristo¹; ¹Tampere University of Technology

In the cold heading process of metals, strain rates in complex parts can vary quite much and reach locally very high values. Therefore, when considering the material's deformation behavior, both the transient hardening effects at high strain rates as well as softening effects due to adiabatic heating should be accounted for. In this work, a phenomenological material model based on experiments done at strain rates in the range of 0.001...1000 1/s at temperatures extending from -150° to 650° was devised and used in FE simulations of the cold heading process. The model separates yielding, including both the upper and lower yield point, from strain hardening, which typically depend on strain rate in a different way because of the adiabatic thermal softening effects at

Technical Program



higher strains. The simulation results show good agreement with high strain rate cold heading results obtained using a direct impact Hopkinson split bar technique.

Electrode Technology Symposium (formerly Carbon Technology): Anode Technology and Production

Sponsored by: The Minerals, Metals and Materials Society, TMS Light Metals Division, TMS: Aluminum Committee *Program Organizers:* John Johnson, RUSAL Engineering and Technological Center LLC; Morten Sorlie, Elkem Aluminium ANS

Monday PM Room: Southern 3 February 26, 2007 Location: Dolphin Hotel

Session Chair: David Emerson, Alcoa

2:00 PM Introductory Comments

2:05 PM

Carbon Nanofiber Additions to Electrode Binder Phase for the Aluminium Electrolysis: *Sten Yngve Larsen*¹; Shahid Akhtar¹; Geir Ausland²; Zhixin Yu¹; Harald A. Øye¹; Trygve Foosnæs¹; ¹Norges Teknisk-Naturvitenskapelige Universitet ; ²Elkem Solar AS

It is expected that carbon nanofibers and related carbon structures will become available in large volumes in the near future. One potential application of such materials is as additives in anodes and cathodes for aluminium electrolysis. Physical and chemical properties of the nanomaterials, i.e., strength, electrical and thermal conductivity may improve the overall electrode performance. In the present work a wide range of fibre types grown catalytically have been studied and added in controlled amounts to laboratory scale electrodes containing petroleum coke fines and pitch. We have studied different manufacturing variables and report detailed investigations of the microstructure of the electrodes. Both baked and graphitized electrodes were manufactured, and their thermal expansion as well as their mechanical and electrical properties were characterized.

2:30 PM

Problems of the Stub–Anode Connection: *Siegfried Wilkening*¹; Jules Côté²; ¹VAW Aluminum Technology; ²Aluminerie Alouette Inc.

The significance of the stub-anode connection in the reduction technology of aluminium is outlined. Quite a number of measurements were performed on the stub-anode voltage drop in electrolytic production cells as well as in laboratory tests. Various aspects of the stub-anode connection will be addressed, such as stub-hole design, stub dimensions, treatment of stubs and thimbles, control procedures, cast iron composition and potential improvements.

2:55 PM

Using Troubleshooting Software to Reduce Variation and Improve Anode Quality: Barry Sadler¹; Jason Govender²; Nicole Ulbricht³; Stephen Scrase³; Kevin Viviers³; Tjaart van der Walt⁴; Simon Frank⁴; Cobus van Heerden⁴; ¹Net Carbon Consulting; ²Mozal Aluminium Smelter; ³Hillside Aluminium Smelter; ⁴CSense Systems Pty Ltd

The use of modern process control and data acquisition systems in Carbon Plants makes enormous volumes of data available to Process Engineers. Often the challenge they face is to isolate the key parameters that drive plant performance. A lack of "statistical stability" in many Carbon Plants makes this more difficult as process and product measures frequently contain unpredictable variation. This paper describes how commercial troubleshooting software has been successfully applied to large quantities of such Carbon Plant data to identify the key drivers of variation in anode quality and improvement opportunities. An example will be given of how the non-linear multivariate and fuzzy logic models constructed in these troubleshooting exercises have been developed into process control applications which have delivered significant improvements in anode quality and lower costs, e.g. lowering the green anode reject rate from around 3% to below 1%.

3:20 PM

New Green Anode Plant at BALCO - Start-Up and Operation in the First Year: *Manfred Beilstein*¹; Shailender Kumar²; K.A. Chowdary²; Anand Pandey³; Rudolf Gemein¹; ¹Outokumpu Technology GmbH; ²VEDANTA Alumina Ltd.; ³BALCO-Bharat Aluminium Company Ltd.

BALCO-Bharat Aluminium Co., a division of VEDANTA Resources PLC, operated an alumina plant and a 110,000 tpy 100 kA Soederberg smelter with a thermal power plant at Korba, Chhattisgarh State, India, since 1975. In 2003, VEDANTA announced the expansion of the smelter with the installation of a high amperage prebaked anode potline of 245,000 tpy rated capacity (GAMI technology from China), an anode plant of 150,000 tpy capacity, and a captive power station of an additional 540 MW. Outokumpu Technology GmbH of Cologne, Germany, was awarded the contract by BALCO to supply Process and Basic Engineering, Detail Engineering for critical areas, site supervision and commissioning, as well as proprietary process equipment for the new Green Anode Plant, as part of the Korba Smelter Expansion Project. This paper describes the Balco Green Anode Plant, its start-up, early operation and the production results in the first year.

3:45 PM

Effect of Vacuum Vibroforming on Porosity Development during Anode Baking: *Michal Tkac*¹; Trygve Foosnæs¹; Harald Øye¹; 'Norwegian University of Science and Technology

The anode porosity and pore development depends on the raw materials and on the production process. Thus porosity of the baked anode is summed up from of the coke pores and process pores that are created during the anode production steps mixing, forming and baking. Pilot-scale work was carried out in order to determine the effects of five parameters on the resulting porosity in the baked state. Anode samples were produced from a single source petrol coke in a two level, five-factorial experimental design with variable factors pitch content, aggregate size distribution, mixing time, atmospheric pressure vibroforming, and heating rate. Vacuum vibroforming was found to be an effective method for porosity reduction. A fully automatic image analysis method (optical microscopy) was utilized in order to determine the porosity in the baked samples. Reactivity (CO2 and air) and physical anode properties were also investigated.

4:10 PM Break

4:30 PM

Alumar Coke Blending Facility Strategy: Francisco Figueiredo¹; Aluisio Nascimento¹; *Vinicius Piffer*¹; Ciro Kato¹; Helio Truci¹; ¹Consorcio de Aluminio do Maranhao (Alumar)

This paper presents an alternative to the conventional blending facilities commonly used throughout the world. The new concept was created based on previous Green Mill experiences and lean thinking philosophy and was projected and implemented by Consórcio de Alumínio do Maranhao (ALUMAR) in August 2005. The strategy maximizes the use of Green mill current assets and minimizes the impact of coke properties variations in the process. Conventional strategy used in most plants basically consists in blending the cokes *in natura* before any granulometry classification, in order to have a homogeneous material used in the production. The new strategy consists in blending the cokes after classification, choosing coke ratios in each granulometry level, therefore using the strong aspects of individual cokes to increase the blended material quality. Anodes produced with the new blending facility have been analyzed and their properties have been compared with anodes produced with traditional blending.

4:55 PM

Review of Coke and Anode Desulfurization: *Les Edwards*¹; Keith Neyrey¹; Lorentz Lossius²; ¹CII Carbon LLC; ²Hydro Aluminium AS

The average sulfur level of petroleum cokes used by the calcining industry is increasing. During calcination, petroleum coke desulfurizes depending on the nature of the sulfur and final temperature. The main quality challenges for the coke calciner are the negative effects that desulfurization has on properties such as real density, porosity, and reactivity. The increase in coke sulfur levels also creates challenges for the aluminum industry. Although the average sulfur content of cokes used by smelters has not increased significantly due to environmental limits, the difference in sulfur level of cokes used in blends is increasing. Calciners must avoid "over-calcination" of the high sulfur cokes



used in blends since it can negatively affect the physical and mechanical properties of anodes. This paper presents a review of data and results on desulfurization, along with recommendations on how to best counter the problems that can arise from use of higher sulfur cokes.

5:20 PM

Production and Application of Coal Tar Pitch in China: *Fengqin Liu*¹; ¹Zhengzhou Research Institute of Chalco

The raw materials, current situations of coal tar pitch production in China and pitch applications in Chinese aluminum industry are reviewed in this paper. The properties of coal tar pitch produced by the different Chinese manufacturers are analyzed to show the quality characteristics of Chinese pitch. The quality evaluation system of coal tar pitch in China and the influences of the production technologies on pitch quality are discussed. The development trend of Chinese coal tar pitch production is outlined.

Friction Stir Welding and Processing IV: Session I

Sponsored by: The Minerals, Metals and Materials Society, TMS Materials Processing and Manufacturing Division, TMS: Shaping and Forming Committee

Program Organizers: Rajiv Mishra, University of Missouri; Murray Mahoney, Rockwell Scientific Company; Thomas Lienert, Los Alamos National Laboratory; Kumar Jata, US Air Force

Monday PM	Room: Northern E3
February 26, 2007	Location: Dolphin Hotel

Session Chair: Rajiv Mishra, University of Missouri

2:00 PM Introductory Comments

2:05 PM Keynote

Friction Stir Welding: After a Decade of Development: *William Arbegast*¹; ¹South Dakota School of Mines and Technology

Friction Stir Welding (FSW) was invented by TWI in 1991 and transitioned to the US industries in 1995 with initial applications primarily on metallic propellant tank structures in the aerospace sector. Soon after, Friction Stir Processing (FSP) and Friction Stir Spot Welding (FSSW) of a wide variety of metallic materials was developed, followed by Friction Stir Joining (FSJ) of thermoplastics and Friction Stir Reaction Processing (FSRP)of stirred- in particles to promote thermodynamically favorable surface reactions and create new surface properties. This paper will discuss the state of development of each of these technologies and provide examples of applications currently in use.

2:30 PM

Development of FSW for Thin-Guage 5XXX Extrusions: *Kevin Colligan*¹; Mark Smitherman¹; ¹Concurrent Technologies Corporation

Industrial application of FSW in the US has not expanded as rapidly as might have been expected based on the intense R&D the process has received in the last 10 years. One reason for the slow industrialization is the high cost of the equipment required to commercially produce even very simple geometric shapes, such as integrally stiffened panels, welded from extrusions. The Navy Metalworking Center (NMC) has undertaken a program to develop very low cost friction stir welding equipment for the production of large stiffened panels. As part of this effort, the NMC is developing fixed-geometry bobbin and conventional FSW tools and procedures for welding thin gauge 5xxx aluminum extruded shapes. This paper describes the welding tool development program and the results of joint strength and microstructure characterization carried out on the NMC project.

2:45 PM

Buckling Behavior of Friction Stir Welded 7075 Compression Panels Stiffened with Single Angle Stiffeners: *Anil Patnaik*¹; William Arbegast²; Matthew Heringer¹; Karl Koch¹; ¹South Dakota School of Mines and Technology; ²Advanced Materials Processing Center, South Dakota School of Mines and Technology

Friction stir welding (FSW) of skin stiffened compression panels is being developed as a rivet replacement technology. Compression panels were fabricated by lap welding 0.062 inch thick 7075-T6511 angles to 0.080 inch

thick 7075-T7 skins. Panel lengths varied from 6 inches to 26 inches covering elastic and inelastic buckling. Structural tests were conducted to determine the compressive strength and deformation characteristics of the panels. The proposed paper will discuss the process parameter development, fixturing and tooling, weld process forces, and the fabrication of the panels. Test results will be presented along with the details of initial buckling loads, failure loads, and failure modes of the test panels. Test results will be compared with some of the theoretical predictions applicable to riveted compression panels. Static structural performance of the FSW skin stiffened panels determined from the tests was found to be better than the predicted performance.

3:00 PM

Friction Stir Welding of an Aluminum Coal Hopper Railcar: Casey Allen¹; Dana Medlin¹; Clark Oberebt¹; Haven Mercer¹; William Arbegast¹; ¹South Dakota School of Mines and Technology

The friction stir welding (FSW) process was used to fabricate a subscale section of an aluminum railcar used to ship coal. Coal comprises approximately forty percent by weight of all freight shipped by rail in the United States. The primary mode of transportation is the open-top hopper car. Traditional joining techniques for this type of vehicle include bolting, riveting and fusion welding. An analysis was performed to evaluate the cost effectiveness of FSW as a joining process. Key elements of analysis included materials selection and availability, preliminary static and fatigue properties, manufacturability and life-cycle cost benefits analysis. Results of this analysis demonstrated a potential cost savings of 20 percent while integrating with existing rolling structure and maintaining durability of the basic coal hopper design. The successful fabrication of the subscale prototype demonstrated overall feasibility of the concept and generated valuable data concerning joint and fixturing and tooling requirements.

3:15 PM

Heat Transfer Considerations for Designing FSW Sandwiched Panel Sturctures for Cryogenic Applications: *Michael Langerman*¹; ¹South Dakota School of Mines

As a result of research investigating "Integrated Thermal Structures", several cryogenic tank wall panel designs consistent with aerospace applications were analyzed for thermal efficiency under assumed cryogenic, aero-heating, and flight loading conditions. One wall considered was internally fabricated with aluminum and formed through super-plastic formed (SPF) deformation of friction stir welded (FSW) panels. These designs included both corrugated and "egg-carton-like" geometries, the cavities of which could be evacuated, filled with air, or filled with a different gas such as argon. One design objective was to minimize heat transfer through the walls including the effects of natural convection, if applicable. Results from the thermal analysis of the panel walls show that the sandwich structure appear to have advantages over other, traditional, wall designs, such as conventional wall cavity structures filled with foamed materials. Results from the analytical analysis are presented herein.

3:30 PM Break

3:45 PM

Static Structural Performance of 7075 Aluminum Friction Stir Welded Helicopter Beams: William Arbegast¹; *Anil Patnaik*²; Bernard Frankl³; ¹Advanced Materials Processing Center - South Dakota School of Mines and Technology; ²South Dakota School of Mines and Technology; ³North Carolina State University

Three friction stir welded built-up beams were manufactured for a helicopter rotorcraft airframe structure. A 0.125 inch thick 7075-T6 Alclad aluminum sheet was welded to the stems of 7075-T6511 aluminum "T" extrusions using full penetration FSW butt joints to form the I-shaped beams. Structural design, process parameters, fixturing and tooling were developed to replace the currently used riveted beams and thin walled machined beams. The overall objective of the project was to demonstrate equivalent static and fatigue performance of FSW built-up beams at a lower weight ratio and production costs. The proposed paper will discuss static structural performance of one of the FSW beams that was tested to failure. Beam analysis was done using classical theory and finite element analysis. The test results will be presented along with a comparison with the theoretical predictions. Process parameters and force data for the weld process will also be discussed.



4:00 PM

A Study on Friction Stir Welding with Heating of Aluminum Alloy A-5052: *Susumu Hioki*¹; Takehiko Takahashi¹; Yuuta Kaneko¹; Riiti Suszuki¹; ¹Akita Prefectural University

Conventional Friction Stir Welding (FSW) is that weld materials are joined at room temperature by stirring softened materials due to frictional heat of rotating tool. Therefore, high speed and high efficiency would be expected, as preheating make weld materials more softened, as well known that yield point goes lower due to heating. In this study, FSW was done to improve welding speed on friction stir welding of aluminum alloy (A5052) for high vacuum vessel for processing of electronics devices. As the result, welding speed was 2.0 time to more than 3.0 at 300 degree Celsius comparing with conventional FSW at room temperature, using improved a milling machine with heater.

4:15 PM

Study of the Effect of Artificial Aging on Microstructural Evolution of Friction Stir Welded Thin Sheet 2024-T3 Using Transmission Electron Microscopy: *Alpesh Shukla*¹; William Baeslack²; ¹Rensselaer Polytechnic Institute; ²Ohio State University

The as-welded and post-weld-heat-treated microstructures obtained in thin sheet aluminum alloys can be considerably different than those obtained in thick plate welds. As-welded and artificially aged microstructures were studied using TEM in friction stir welds produced in various conditions; and the effect of aging time on the microstructure of FS welds was studied. FS welded at low traverse speeds, the welds were characterized by a stir-zone consisting of low concentration of GPB zones, an over-aged microstructure near the TMAZ/HAZ boundary consisting of coarse S precipitates and another under-aged region further away in the HAZ consisting of either GPB II zones or fine S phase. This results into an undesirable microstructure, consisting of hard and soft regions. However, with proper selection of welding parameters, a FS weld with a uniform microstructure can be developed which on aging, results into a uniform peak-aged microstructure consisting of fine S phase.

4:30 PM

Static Strength Comparison of Discontinuous Friction Stir Welded Stiffened Panels: Joshua Merry¹; Bryan Tweedy¹; Christian Widener¹; Dwight Burford¹; ¹Wichita State University

Recent advancements in friction stir welding (FSW) technology have potential for applications in aerospace structures. Friction stir spot welds have been found in some cases to be much stronger than rivets in the same material thickness, while maintaining the discontinuous crack growth path preferred by aircraft designers. In this study, panels with discontinuous welds were prepared which were identical to previously investigated friction stir lap welded and riveted panels. The structures under study were subscale flat stiffened panels. The panels were fabricated with two hat-section stiffeners. The sheet was 0.040-in 2024-T3, and the stiffeners were 7075-T6 spaced on 8.0 inch centers, which is representative of a transport fuselage design. The 2-ft x 2-ft stiffened panels were statically tested in diagonal tension. The results are compared directly to riveted and continuous friction stir lap welded panels.

4:45 PM

Fatigue Crack Propagation Behavior of Friction Stir Welded 5083-H32 and 6061-T651 Aluminum Alloys: *Seongjin Hong*¹; Sangshik Kim¹; Chang Gil Lee²; Sung-Joon Kim²; ¹Gyeongsang National University; ²Korea Institute of Machinery and Materials

Friction stir welding (FSW) is a new solid-state joining technique, which offers high joint quality and relatively few defects. In this study, the FCP behavior of FSWed 5083-H32 and 6061-T651 alloys was examined with the fatigue crack growing either along the dynamically recrystallized zone (DXZ) at variable ΔK or across the weld zone at constant ΔK . The FCP behavior of FSWed 5083-H32 and 6061-T651 specimens is substantially influenced by the presence of FSW zone. The FCP behavior of both specimens in the DXZ appeared to be determined by the beneficial compressive residual stress and the detrimental grain refinements. The FCP behavior of FSWed 5083-H32 and 6061-T651 specimens is discussed based on residual stress measurement and fractographic observation.

5:00 PM

Development of Design Curves for Tensile Strength and Fatigue Characteristics of 7075 T73 Aluminum FSW Butt Joints: Srikanth Kandukuri¹; William Arbegast¹; Anil Patnaik¹; Casey Allen¹; ¹South Dakota School of Mines and Technology

Aluminum 7075-T73 plates of different thickness were welded with varying pseudo heat index (PHI). All welds were made under position control. Studies indicate that there exits a relationship between PHI and the weld quality for friction stir welded joints. PHI is a measure of heat input into the weld process and is dependant on processing parameters like rotation speed, travel speed and forge force. The joints were evaluated for its strength and also for fatigue life to investigate the response of weld quality in relation to PHI. Ultimate tensile strengths were plotted against PHI with statistically based lower tolerance bounds (T90 and T99) with 95% confidence intervals using the methods mentioned in Military Handbook. The study revealed that the ultimate tensile strengths of butt joints decreased with the increase in PHI. The paper describes the statistical design charts for tensile strength and fatigue characteristics of friction stir welded butt welds.

5:15 PM

Relationships between Process Variables Related to Heat Generation in Friction Stir Welding of Aluminum: Kevin Colligan¹; ¹Concurrent Technologies Corporation

Friction stir welding was invented in 1991 by The Welding Institute as a solid-state method of joining metals which was initially applied to the joining of aluminum alloys. Process improvements have extended the use of the technique to other metals, to thicker materials, to higher travel speeds, and to a variety of applications. In addition, detailed study of the process has led to a better understanding of how the process actually works in terms of material flow produced by different kinds of tools. However, no publications have comprehensively described the relationships between the different processing variables and how these variables affect key process conditions, such as temperature distribution, material conditions at the welding tool, etc. This paper seeks to describe the relationships between the independent process variables, such as travel speed, spindle speed, and anvil condition, and the dependent process outcomes, such as the spindle torque, heat generation, and workpiece temperature. A conceptual model is proposed that relates the main processing variables by showing the influence of physical effects on heat generation in the workpiece. Case studies are used to confirm and explore the relationships expressed in the conceptual model.

Frontiers in Solidification Science: Atomic Scale

Sponsored by: The Minerals, Metals and Materials Society, TMS Electronic, Magnetic, and Photonic Materials Division, TMS Materials Processing and Manufacturing Division, TMS: Chemistry and Physics of Materials Committee, TMS: Solidification Committee

Program Organizers: Jeffrey Hoyt, Sandia National Laboratories; Mathis Plapp, Ecole Polytechnique; Gabriel Faivre, CNRS; Shan Liu, Iowa State University

Monday PM	Room: Northern A3
February 26, 2007	Location: Dolphin Hotel

Session Chair: To Be Announced

2:00 PM Invited

A Quantitative Parameter-Free Prediction of Simulated Crystal-Nucleation Times: *James Morris*¹; Rachel Aga¹; Jeffrey Hoyt²; Mikhail Mendelev³; ¹Oak Ridge National Laboratory; ²Sandia National Laboratories; ³Ames Laboratory

The applicability of classical nucleation theory to crystal nucleation from the liquid remains open. We demonstrate that an accurate prediction of crystal-nucleation times obtained from molecular dynamics simulations can be made in the large undercooling limit, where transient nucleation dominates. All parameters are determined from separate simulations, so there are no fitting parameters in the comparison between theory and simulation. Transient nucleation must be included to explain the simulation results. An



effective temperature dependence of the interfacial free energy is introduced. System size dependence studies show that the occurrence of nucleation in MD simulations is limited by the system size; nucleation is typically observed only if the average expected number of critical nuclei in the simulated system is at least unity. This research is sponsored by the Division of Materials Science and Engineering, Office of Basic Energy Sciences, US Department of Energy under Contract No. DE-AC05-00OR-22725 with UT-Battelle.

2:30 PM Invited

Crystal-Melt Interfacial Free Energies from Computer Simulation: From Hard Spheres to Molecules: Brian Laird¹; ¹University of Kansas

The crystal-melt interfacial free energ is a primary controlling parameter in the morphology and kinetics of crystal growth, In this talk I will review our recent work on the calculation, via MD computer simulation, of the interfacial free energy for number of model systems ranging from single and binary hard spheres to models of molecular materials, such as succinonitrile.

3:00 PM Break

3:20 PM Invited

Atomistic-Simulation Studies of Faceted Crystal-Melt Interfaces: Dorel Buta¹; *Mark Asta*²; Jeffrey Hoyl³; ¹Northwestern University; ²University of California; ³Sandia National Laboratories

Solidification morphologies in faceted crystals are often strongly influenced by the properties of steps at the solid-liquid interface. This talk presents results of recent applications of molecular-dynamics simulations to the study of the intrinsic properties of steps at faceted crystal-melt interfaces in two model systems: the Stillinger-Weber model of elemental Si and a model immiscible alloy system. Both equilibrium and non-equilibrium simulations are employed in the study of step structure, free energies and mobilities. The simulation results highlight important differences between steps at crystal-melt interfaces, relative to those in the more widely studied case of crystal-vapor surfaces. In elemental Si the steps are predicted to be highly diffuse in their structure, and to possess relatively low step free energies and high mobilities. The consequences of these findings for the mechanisms of nanowire growth from liquid catalysts will be discussed.

3:50 PM Invited

Molecular Dynamics Simulation of Solidification and Vitrification in Al and Al-Fe Alloys: *Mikhail Mendelev*¹; Cai-Zhuang Wang¹; Kai-Ming Ho¹; James Morris²; ¹Ames Laboratory; ²Oak Ridge National Laboratory

Molecular dynamics simulations were performed to study phase transformations in supercooled liquid Al and Al-Fe alloys. We found that the Ercolessi-Adams (EA) potential provides vitrification for the cooling rates achievable in MD simulation while other Al potentials provide crystallization. The reason for this difference and the features of the vitrification in the EA Al is discussed. The simulation of supercooled Al-Fe alloys, using an Al potential where nucleation occurs on MD time scales, showed that if the Fe concentration was less than 5 % the system demonstrated crystallization, while for larger Fe concentration, a vitrification was observed. We analyze the thermodynamics of these alloys, the effect of Fe on the kinetic coefficients, and the structural units forming in the supercooled liquid. MIM and JRM acknowledge support from the Division of Materials Science and Engineering, BES Office, US DOE under Contract No. W-7405-ENG-82 with ISU and No. DE-AC05-00OR-22725 with UT-Battelle, respectively.

Frontiers in Solidification Science: Poster Session

Sponsored by: The Minerals, Metals and Materials Society, TMS Electronic, Magnetic, and Photonic Materials Division, TMS Materials Processing and Manufacturing Division, TMS: Chemistry and Physics of Materials Committee, TMS: Solidification Committee

Program Organizers: Jeffrey Hoyt, Sandia National Laboratories; Mathis Plapp, Ecole Polytechnique; Gabriel Faivre, CNRS; Shan Liu, Iowa State University

Monday, 4:20 PM	Room: Northern A3
February 26, 2007	Location: Dolphin Hotel

3D Reconstruction of Coarse Dendritic Microstructures during the Solidification of Al-Cu Alloys: *Demian Ruvalcaba*¹; Dmitry Eskin¹; Laurence Katgerman²; ¹Netherlands Institute for Metals Research; ²Delft University of Technology

Defects that develop during solidification of aluminium alloys (e.g. hot tearing) depend on the morphology evolution of the microstructure. Quenching (i.e. "freezing") of the microstructure during solidification may be used as a technique for studying the solidification of aluminium alloys, however the metallographic examination of the as-quenched structure shows an overestimation of the solid fraction as related to the temperature of quenching. In the present study, the 3D microstructure reconstruction of as-quenched samples revealed features that showed a coalescence of the finer solid phase that solidifies upon quenching, which may cause the overestimation of the solid fraction as compared to the lever rule and Scheil. The paper presents observations of the 3D microstructure development during the solidification of an Al-7 wt% Cu alloy by using the quenching technique and serial sectioning. The identification and removal of structure instabilities may help in reconstructing the microstructure that develops during solidification.

Alloy Crystal-Melt Interfacial Properties from Atomistic Simulations: *Chandler Becker*¹; David Olmsted²; Mark Asta³; Jeffrey Hoyt²; Stephen Foiles²; ¹Northwestern University; ²Sandia National Laboratories; ³University of California

Crystal-melt interfacial properties are critical in controlling growth kinetics and microstructural morphologies during dendritic solidification. We will discuss recent work on crystal-melt interfaces in model Lennard-Jones alloys to understand the relative importance of chemical interactions and size effects in controlling interfacial properties. These include the equilibrium adsorption, interface stress, and interfacial free energy. The Monte-Carlo and Molecular-Dynamics simulation methods used to create and equilibrate simulation cells will be described, along with the calculations of composition, density, and stress profiles. We will also discuss the dependence of the interfacial free energy and its crystalline anisotropy on composition as calculated with the capillary fluctuation method. The results will be discussed in the context of phase-field models of dendritic solidification.

Bubble Formation and Solid-Pore Interactions in Directional Solidification: *Ying Sun*¹; Christoph Beckermann²; ¹State University of New York-Binghamton; ²University of Iowa

Phase-field simulations are performed of bubble formation and solidpore interactions during directional solidification. Gas bubbles nucleate and grow in the supersaturated liquid ahead of the solidification front. Flows are induced by the large density contrast between the bubbles and the melt, as well as by interactions of the bubbles with the solid. A phase-field method is used to model interfaces and triple-junction motions in the present solidliquid-gas system. Flows and species transport in the gas and liquid phases are solved using a diffuse interface model for two-phase flow. Pore growth and topology changes, solid-pore interactions, and the final shape of the pores are investigated as a function of the contact angle at the triple-junction, initial gas concentration, nucleation supersaturation, nuclei density, and important solidification parameters. Interactions of pores with planar, cellular, and dendritic microstructures are examined in detail. The conditions for different bubble growth morphologies are summarized.



Technical Program

Coherence of Dendritic Sidebranching in Directional Solidification of a Dilute Alloy: *Alain Pocheau*¹; Simona Bodéa¹; Marc Georgelin¹; ¹Institut de Recherche sur les Phénomènes Hors Equilibre

Dendrites are characterized by repetitive emissions of sidebranches on a needle form. They stand as the main solidification structure of dilute alloys whose regularity monitors that of the resulting solid. A long-standing question has then referred to the level of regularity of dendritic emissions. We experimentally evidence here, in directional solidification of a succinonitrile dilute alloy, the large coherence of dendritic sidebranching within bursts of about a dozen of branches or less. In particular, correlation functions of the signal given by cuts of interface profiles reveal a burst distribution that is uncorrelated in occurrence, length and in phase of sidebranching but which contrasts with the large coherence of sidebranching inside each burst. The former feature may explain the appearance of uncorrelated sidebranching in former experiments. The latter feature reveals a puzzling self-organization of dendrites till the reset of sidebranch emissions. Both their mechanisms remain to be understood.

Columnar to Equiaxed Transition and Fragmentation in Al-Ni and Al-Si Alloys furing Directional Solidification: *Hyejin Jung*¹; Nathalie Mangelinck-Noel¹; Henri Nguyen-Thi¹; Bernard Billia¹; Adeline Buffet²; Jurgen Hartwig²; José Baruchel²; ¹L2MP,UMR 6137, University Paul Cezanne Aix-Marseille 3, Faculte de Saint Jerome; ²ESRF-Polygone Scientifique Louis Néel

The control of the columnar to equiaxed transition (CET) is critical to obtain desired final properties of industrial products. To get equiaxed microstructures in aluminium alloys, one method consists in adding particles to provoke nucleation of equiaxed grains in the melt. On the other hand, fragmentation is another mechanism responsible for the formation of an equiaxed microstructure as in castings. Our objective is to understand how the formation and the evolution of the different microstructures are influenced by the temperature gradient, pulling rate, and refiners in Al-Ni3.5wt% and Al-Si7.0wt% alloys. First, directional solidification experiments are performed in a Bridgman furnace in bulk samples where convection and 3D effects can be studied. Second, using synchrotron radiation at ESRF we characterise in situ and in real-time the solid-liquid interface during directional solidification of thin samples. This technique yields information on the dynamics of CET, the detachment of dendrites side arms and crystallography.

Dendritic Seaweed Growth and the Relationship to Spontaneous Grain Refinement: Andrew Mullis¹; ¹Leeds University

Above a critical undercooling a range of metals and alloys undergo spontaneous grain refinement, accompanied by a discontinuous break in the velocity-undercooling curve. This change in growth morphology is likely to be brought about by a transition from dendritic growth to the growth of dendritic seaweed and remelting at elevated undercooling. We have provided evidence in support of this model by the direct observation of a frozen in seaweed morphology observed in deeply undercooled Cu. Moreover, the velocity-undercooling curve for this material shows a discontinuous break coincident with the onset of seaweed growth. In this paper we will present phase-field simulations of the solidification of both pure metals and alloys that demonstrate how remelting of a dendritic seaweed structure gives rise to a realistic grain refined microstructure, such that the transition to a dendritic seaweed morphology could explain all of the commonly observed features associated with spontaneous grain refinement.

Determining the Freezing Rate during Final-Stage Solidification of the Ni-Base Superalloy IN713LC: *Magnus Lekstrom*¹; Neil D'Souza²; Hongbiao Dong³; Mahmoud Ardakani¹; Barbara Shollock¹; ¹Imperial College London; ²Rolls-Royce plc; ³University of Leicester

The evolution of fraction solid and the local freezing rate during solidification of the IN713LC superalloy were determined using an enthalpy-based method. Enthalpy curves were extracted from Differential Thermal Analysis (DTA) experiments and used to calculate the fraction liquid present during the course of solidification. Solute segregation aspects were incorporated into the analysis through selective Energy Dispersive X-ray Spectroscopy (EDS) measurements in the inter-dendritic region of the DTA samples. These measurements were taken to represent the elemental composition of the liquid during the last stages of solidification. A multi-component thermodynamic database, JMatPro[™] was used to deduce the solid and liquid enthalpies using input from the compositional measurements. The enthalpy changes were thus taking both temperature and solute composition into account. This approach was carried out on different heats with slightly varying alloy chemistries. The influence of minor variations in solute content on the freezing rate was thus examined.

Fully Implicit, Adaptive Grid Methods for Phase-Field Simulation of Solidification in Pure Metals and Alloys: Jan Rosam¹; Andrew Mullis¹; Peter Jimack¹; ¹University of Leeds

One of the most powerful techniques for modelling dendritic micro structures is the Phase Field method. The resulting governing equations are time dependent highly non linear PDEs. Solving these equations numerically is still a very challenging task. Two techniques permit theses difficulties to be surmounted, mesh adaptivity and fully implicit time integration methods. Implicit methods are more expensive per step than explicit ones because the intermediate approximations have to be solved from a system of non linear algebraic equations but alloy the use of much larger time steps due to their unconditional stability. We combined a variable time stepping method based on a second-order fully implicit time integration scheme, in which we use an non linear Multgrid solver, to demonstrate the superiority of implicit methods in respect to CPU time and accuracy. The method has been applied to Phase Field models for pure metals and binary alloy solidification.

Influence of Processing Variables on Microporosity Formation in Al-4.5% Cu Alloy: Joo Ro Kim¹; Reza Abbaschian²; ¹University of Florida; ²University

Cu Alloy: Joo Ro Kim¹; Reza Abbaschian²; ¹University of Florida; ²University of California Riverside

When liquid metal feeding is restricted to the interdendritic areas in a casting, microporosity occurs because of the solidification shrinkage and gas evolution. The total volume, size and distribution of microporosity have been found to depend strongly not only on as well as thermophysical properties of the alloys, but also on the mushy zone thickness, interdendritic channel and hydrostatic pressure. The latter are affected by processing variables such as solidification rate, thermal gradients and alloy composition. The results of recent investigation on the influence of processing variables on microporosity formation in Al-4.5 wt% Cu alloy are presented. The processing techniques employed consisted of directional solidification and Axial heat Processing. The latter technique provides for controlled thermal gradient and mushy zone thickness. In addition, reduction of convection can modify the solidification structure. A comparison of experimental and calculated results will be presented and optimum condition to minimize microporosity will be suggested.

Limits of Stability and Spacing Adjustment Mechanisms of Eutectic Growth: *Melis Serefoglu*¹; Ralph Napolitano¹; ¹Iowa State University

Stability limits of eutectic growth structures and morphological spacing adjustment mechanisms are investigated by using the succinonitrile and camphor transparent organic metal analog system. Interrupted directional growth experiments and uniform undercooling radial growth experiments are performed to probe these limits and governing mechanisms. Various 2D specimen thicknesses are used to examine the effect of dimensionality on spacing limits and adjustment dynamics. Experimental results are compared with the stability limits suggested by the analyses of Jackson and Hunt, Seetharaman and Trivedi, and Akamatsu et al.

Metastable Phase Formation of Rare-Earth Sesquioxides by Containerless Process: Atsunobu Masuno¹; Yasutomo Arai¹; Jianding Yu¹; ¹Japan Aerospace Exploration Agency

Containerless processing promotes deeper undercooling in molten materials because of suppressing inhomogeneous nucleation and often brings out a metastable phase. We systematically investigated solidification processes in undercooled rare-earth oxides and yttrium sesquioxides using an aerodynamic levitation technique because these materials are candidates for high dielectric insulators instead of SiO₂. Double recalescence indicative of two successive phase transformation was observed for all the oxides. A melting point (T_{ml}) following the first recalescence was higher than that of the second one (T_{m2}) for Y₂O₃ as well as most of the oxides. This means usual transformation from a high temperature phase to a low temperature one. For Lu₂O₃, however, T_{m1} was lower than T_{m2} , suggesting the existence of a metastable phase between the two recalescences. The duration of life of this metastable phase was tens of milliseconds.



Microstructures of Zn-Cd Dilute Alloys Directionally Solidified: Fornaro Osvaldo¹; Hugo Palacio²; ¹IFIMAT-UNICEN, CONICET; ²IFIMAT-UNICEN, CICPBA

Cellular and dendritic growth of HCP Zn-Cd alloys is strongly influenced by crystalline anisotropy, being fundamental in the fixing of the operative conditions during dendritic growth, and takes a fundamental role in the formation of cellular growth. Also, critical values of velocity and wavelength for planar to cellular transition changes slightly even for small missorientation between growth and preferential growth directions. In this work, directional solidification of HCP Zn-Cd dilute alloys were developed, for different solidification conditions, in oerder to obtain morphologies from planar to cellular and dendritic structures.

Modeling of Microstructure Evolution from Liquid State to Room Temperature in Steels: *Adrian Catalina*¹; Doru Stefanescu²; Leo Chuzhoy¹; Michael Johnson¹; ¹Caterpillar Inc.; ²Ohio State University

Modeling of solidification microstructure for alloys undergoing solid-state transformations is only a first step toward obtaining the room-temperature microstructure on which the mechanical properties are strongly dependent. Therefore, a previously developed model for microstructure evolution during solidification of multicomponent alloys was further enhanced by adding the capability of describing the solid-state transformations in steels. The proposed deterministic model describes grain nucleation, growth, and coarsening by means of a strong coupling between the thermal and solutal fields at the grain/ matrix interface. This coupling procedure allows relaxing the assumption used in previously published models that growth is controlled mainly by solute diffusion. It can also account for any number of alloying/impurity elements in the alloy chemical composition. Computed evolution of microstructures and segregation patterns from liquid state to room-temperature will be presented for steels of various chemical compositions emphasizing the influence of cooling rate and solidification microstructure on the final room-temperature microstructure.

Non-Equilibrium Solidification of Intermetallic Compounds in the Ni-Al Alloy System: Sven Reutzel¹; *Helena Hartmann*¹; Peter Galenko²; Hamid Assadi³; Dieter Herlach²; ¹Ruhr-University Bochum, Germany; ²German Aerospace Center (DLR); ³Tarbiat Modarres University, Iran

Ni-Al alloy system exhibits particular solidification behaviour due to chemical long-range order of the intermetallic compounds $Ni_3Al (L1_2)$ and NiAl (B2). Using rapid solidification technique their slow solidification kinetics leads to the entrapment of solute atoms and/or disorder, respectively. In the present work containerless processing by applying electromagnetic levitation technique is used to analyse the aspects of dendrite growth, as observed in solidification of undercooled Ni-Al melts. Sharp-interface modelling is used to illustrate the effect of chemical order on the solidification kinetics of intermetallic phases. Both experimental results and theoretical work denote the role of chemical order in solidification of Ni-Al intermetallics.

Non-Newtonian Behaviour of Liquid Metals: Zhongyun Fan¹; Vijay Vasarni¹; ¹Brunel University

A long-standing belief is that liquid metals are Newtonian liquids, implying that their viscosities are independent of shear rate. Here we show that liquid metals are non-Newtonian liquids. We found that at temperatures close to their melting temperature, the viscosity of liquid metals increases linearly with increasing shear rate, clearly showing a shear thickening behaviour. The viscosity data obtained by extrapolation to zero shear rate are in good agreement with the literature values measured at extremely low shear rate. Furthermore, we found that the slope of viscosity against shear rate is proportional to the product of liquid density and square of the atomic diameter of the metal. We believe that this discovery will have profound influence on the future research into the atomic structure of liquid metals, nucleation during solidification, glass formation and viscosity measurement. It will provide a new dynamic approach to the research in such disciplines.

Phase-Field Modeling of Solidification with Density Change and Solid Movement: *Ying Sun*¹; Christoph Beckermann²; ¹State University of New York-Binghamton; ²University of Iowa

A phase-field model has been developed to simulate solidification with density change and solid movement. Treating the solid phase as a very viscous fluid, the phase-field equation is coupled with a diffuse interface model for two-phase flows with surface tension, phase change, and density and viscosity differences between the phases. The model is validated for one-dimensional density change flow normal to a solidification front. Two-dimensional dendritic growth with flow due to a density change is then examined and the results are compared to an analytical solution. Finally, the model is used to simulate concurrent growth and settling of free equiaxed dendrites in an undercooled melt. Flows are induced by buoyancy and shrinkage upon solidification. Melt convection, settling velocity, crystal rotation, and tip operating state are investigated as a function of the shrinkage, equiaxed grain density, and relevant solidification parameters.

Phase-Field Simulations of Buoyancy-Driven Convective Effects on Dendritic Growth of Binary Alloys: Juan Ramirez¹; Sharen Cummins¹; ¹Los Alamos National Laboratory

We couple a quantitative 2D phase-field model for binary alloy solidification with a fluid flow solver to examine the effects of natural thermal and solutal convection during equiaxed dendritic growth. The phase-field model employs the anti-trapping current concept to eliminate spurious solute trapping and is coupled via a momentum drag term to a diffuse interface version of the Navier-Stokes equations. We simulate the growth of dilute succinonitrileacetone in a closed container for undercoolings of experimental relevance. Additionally, we examine the effect of initial acetone concentration in the melt. We employ an adaptive finite volume discretization for the solution of the governing equations.

Phase-Field Simulations of Rod Eutectic Growth: Andrea Parisi¹; *Mathis Plapp*¹; ¹Ecole Polytechnique

The solidification of eutectic alloys is simulated in three dimensions by means of an efficient phase-field model. In particular, the rod morphology is investigated by calculating steady state solutions for varying spacing and composition. It is found that the undercooling versus spacing curves at fixed composition are in good agreement with the Jackson-Hunt theory up to some critical spacing which depends on the composition. For intermediate to high volume fractions of the minority phase, at this critical spacing a transition from circular to elongated rods occurs. This transition is a bifurcation: for spacings larger than the critical spacing, two different steady states, elongated along different axes, exist for the same spacing and composition. In contrast, for low volume fractions, an oscillatory instability occurs at the critical spacing which leads to chaotic dynamics of the rod patterns. The consequences of these findings for pattern selection in extended systems are discussed.

The Effects of Internal Convection on Phase Selection in Undercooled Fe-Cr-Ni Alloys: Alaina Hanlon¹; Douglas Matson²; *Robert Hyers*¹; ¹University of Massachusetts; ²Tufts University

Computational fluid dynamics along with experimental results are used to explain the effect induced convection has on metastable phase lifetimes in solidifying Fe-Cr-Ni alloys. Differences are observed in the transformation time from the metastable to stable phase between electromagnetically levitated (EML) and electrostatically levitated (ESL) samples. It was hypothesized that Magnetohydrodynamic convection within EML samples causes dendritic interactions leading to early stable phase nucleation. As the metastable dendrites grow into the melt, free-stream flow causes the primary arms to deflect. Secondary arms of adjacent dendrites then collide, triggering stable phase nucleation as described by Classical Nucleation Theory. Three alloys at different undercoolings were tested. For all 5 conditions tested, quantitative agreement exists between the calculated time required for dendrite collision and the experimental metastable phase lifetimes for EML. Internal flow within EML samples is strong enough to trigger early stable phase nucleation; explaining the observed difference in metastable phase lifetimes.

Transition from Cells to Dendrites in a Directional Solidification Process: Jing Teng¹; *Shan Liu*¹; Rohit Trivedi¹; ¹Iowa State University

Detailed experimental studies have been carried out to investigate the transition from cells to dendrites in a directional solidification process of succinonitrile base transparent alloys. This transition is not sharp and is closely related with the existence of a range of primary spacings. The critical spacing (λ_{cd}) where a cell changes to a dendrite is correlated with the alloy composition C_o , temperature gradient G and growth velocity V through the relationship $\lambda_{cd}(GV)^{1/3}C_o=C$, where C is a constant depending on the properties of an alloy system. Experimental results in succinonitrile-salol and succinonitrile-

M

OZDAY

M

ZOZDA> NZ

Technical Program



camphor alloys are thoroughly analyzed in order to uncover the fundamental physics governing the cell-dendrite transition.

Solidification Behavior of Immiscible Alloy under High Magnetic Field: En-Gang Wang¹; Xiaowei Zuo¹; Lin Zhang¹; Jicheng He¹; ¹Northeastern University

The immiscible alloys in liquid-phase region are characterized by separation structure in conventional casting method, and thus they have been considered to be no technical applicability. Much effort has been made to obtain homogenous microstructure, including casting in space under microgravity condition. In the present study, solidifying behavior of immiscible alloy, e.g. Cu-Pb, Cu-Nb alloy, etc, were investigated under high magnetic fields ($0\sim12T$) or a combined electromagnetic fields with different magnetic conditions. The results show that the separation and coacervation of liquid droplets in immiscible gap has been partly restrained under magnetic field; the Cu-rich phase in the hypermonotectic Cu-Pb alloy has been changed to spherical particles under high magnetic field. Moreover; the mechanism of the special solidifying structure of immiscible alloy was analyses based on solidification and the characteristic of high magnetic field.

General Abstracts: Extraction and Processing: Hydrometallurgy, Metal Recovery

Sponsored by: The Minerals, Metals and Materials Society, TMS Extraction and Processing Division, TMS: Aqueous Processing Committee, TMS: Materials Characterization Committee, TMS: Pyrometallurgy Committee *Program Organizers:* Boyd Davis, Kingston Process Metallurgy Inc; Michael Free, University of Utah

Monday PM	Room: Southern 1
February 26, 2007	Location: Dolphin Hotel

Session Chair: Michael Free, University of Utah

2:00 PM

Review of Hydrometallurgical Options to Separate Cobalt and Manganese from Acidic Solutions: Cesar Ferron¹; ¹HydroProc Consultants

Cobalt and manganese are closely associated in nature, and their separation within acidic leach solutions can represent a challenge for the hydrometallurgist. This paper presents a review of some of the options available to the process engineers. Processes such as sulphide precipitation, hydroxide precipitation and solvent extraction will be discussed, as well as oxidative precipitation, with particular emphasis on the selective oxidative precipitation of manganese using sulphur dioxide-oxygen mixtures.

2:25 PM

Processing of Electroplating Effluent for the Recovery of Zinc and Chromium Using Ion Exchange Technique: Manis Kumar Jha¹; Vinay Kumar²; Jae-chun Lee¹; ¹Korea Institute of Geoscience and Mineral Resources; ²National Metallurgical Laboratory

In order to reduce the pollution and conserve the resources, a process has been proposed to recover zinc and chromium from the electroplating effluent following ion exchange technique. The studies for the extraction of zinc in different contact time, pH of the solution, resin dose, mechanism of adsorption etc. were made for the recovery of zinc from the solution using cationic resin, Lewatit VP OC 1026. The resin, Lewatit VP OC 1026 has been found to be selective for the extraction of zinc from the effluent leaving total chromium in the raffinate. The zinc was effectively eluted from loaded resin with dilute sulphuric acid. The mechanism of extraction of zinc was found to follow the Langmuir isotherm. The chromium was extracted from the raffinate using anionic resin, Amberlite IRA 400 Cl and loaded chromium eluted effectively with 15% NaCl / 20% NaOH.

2:50 PM

Precipitation of Aluminum from Concentrated Chloride Solutions: Vera Gella¹; George Demopoulos¹; ¹McGill University

The effect of several parameters, including temperature, aging time, degree of neutralization (OH/Al ratio) and therefore final pH, base addition rate, background electrolyte and concentration on precipitation of aluminum from chloride solutions by neutralization was investigated. Both degree of neutralization and base addition rate proved to be key parameters controlling the formation of crystalline aluminum oxyhydroxide phases. In the aluminum chloride system, several phases including pseudoboehmite, aluminum oxyhydroxide (AlOOH), and bayerite (Al(OH)3) phases were precipitated under various experimental conditions. Aging time and washing media were also found to have an effect on the degree of crystallinity of the solids produced. The greatest impact on the solids precipitated from aluminum chloride solutions was the addition of magnesium chloride to the mother solution. Preliminary testwork involving these mixed solutions are also discussed.

3:15 PM

Effects of Acidithiobacillus Ferrooxidans on the Electro-Generative Simultaneous Leaching for Sphalerite-MnO2: *Xiao Li*¹; Jianshe Liu¹; ¹Central South University

The electro-generative leaching (EGL) is a new hydrometallurgical technology. The principle for the electro-generative leaching is applied to simultaneous leaching of sphalerite-MnO2 in this paper. A galvanic system for the bio-electro-generative leaching (BEGL) has been set up. A study has been made of the effects on rate of zinc extraction from sphalerite under the conditions of presence and absence of A. ferrooxidans, respectively. The unreacted shrinking core model is used for describing the reaction-relative and diffusion-relative phenomena presented in the process of the electro-generative leaching with and without bacteria. The activation energies of the anodic reaction for leaching system in the presence and in the absence of bacteria are calculated as 11.97 and 14.39 kJ/mol, respectively, indicating that it can decrease by A. ferrooxidans. XRD and SEM were used to study the effect of A. ferrooxidans on the ores in the electro-generative simultaneous leaching.

3:40 PM Break

4:00 PM

Chlorine Leaching Technology of Precious Metals in Copper Anode Slimes: Harumasa Kurokawa¹; Satoshi Asano¹; Koji Sakamoto¹; Shinichi Heguri¹; *Takashi Hashikawa*¹; ¹Sumitomo Metal Mining Company, Ltd.

Sumitomo Metal Mining has been recovering the silver contained in the blister copper, later gold and silver from the copper anode slimes, with the conventional cupellation for about 400 years. The thorough hydrometallurgical process for precious metals refining using the chlorine leaching technology was originated and developed by Sumitomo, thereafter commercialized in 2004 at Toyo copper smelter and refinery. This new process enabled the shorter term recovery of gold and manpower saving, in addition, the elevation of occupational safety and working condition has been obtained. Superiority to the existing hydrometallurgical processes was also confirmed, example for the achievement of high purity gold and silver production without the electrorefining process and higher recovery ratio of rhodium and other PGMs.

4:25 PM

Selective Extraction of Precious Metals with Amide Compounds: *Hirokazu* Narita¹; Mikiya Tanaka¹; Kazuko Morisaku¹; Ken Tamura²; ¹National Institute of Advanced Industrial Science and Technology; ²Chiba Institute of Technology

The separation and purification of the precious metals are mainly performed by solvent extraction. Since the development of a successful solvent extraction process depends on the choice of the appropriate extractants, the present authors investigated the solvent extraction of gold, palladium and platinum in HCl solutions using amide compounds diluted with n-dodecane and 2-ethylhexanol, and found that three amide compounds have excellent extraction properties: (i) The monodentate N,N-di-n-octyllauramide (DOLA) shows a good selectivity for Au(III) under the 0.5 M DOLA - <3.0 M HCl system. (ii) The tridentate N,N'-dimethyl-N,N'-di-n-octyl-thiodiglycolamide (MOTDGA) extracts Pd(II) >50 times faster than the conventional extraction reagent with a good selectivity, and shows good acid-resistance. (iii) The tridentate N,N'-dimethyl-N,N'-di-n-octyl-diglycolamide (MODGA) displays a high selectivity for Pt(IV) over some base metals.

4:50 PM

Shape-Controlled Synthesis of Porous Fibrous Cobalt Powder: *Jing Zhan*¹; Chuanfu Zhang¹; Chengyong Dong¹; Jianhui Wu¹; ¹Central South University

The fibrous precursor can be obtained by coordination precipitation process, using oxalate, cobalt chloride and ammonia. The composition and morphology of fibrous precursor were characterized by XRD, IR, DTA/TGA



and SEM analysis. The results show that XRD pattern and composition of the precursor with fibrous morphology precipitated at pH=9.0 are different from that of β -CoC2O4•2H2O precipitated at pH=1.0. The mechanism on the thermal decomposition of fibrous precursor was addressed. The influences of various conditions in pyrolysis, including the temperature , time, atmosphere, and the morphology of the precursor, on the morphology, average size and specific surface area of the Co powders were investigated in detailed. The final product-fibrous cobalt powders with about 0.3~0.5 μ m in size and 40~60 in aspect ratio were produced by thermal decomposition at 400~500°C in the weak reducing atmosphere. The structure of pores in cobalt powders is capillary tube with open ports and the majority is mesoporous.

General Abstracts: Light Metals Division: Session II

Sponsored by: The Minerals, Metals and Materials Society, TMS Light Metals Division, TMS: Aluminum Committee, TMS: Reactive Metals Committee, TMS: Recycling Committee Program Organizers: Neale Neelameggham, US Magnesium LLC; Anne

Kvithyld, Norwegian University of Science and Technology

Monday PM	Room: Pacific Hall B
February 26, 2007	Location: Dolphin Hotel

Session Chair: Konrad Papis, ETH Zurich

2:00 PM

Mechanical Deformation of Nanostructured Magnesium Alloy and Its Modelling: *Yujie Wei*¹; Lallit Anand²; ¹Brown University; ²Massachusetts Institute of Technology

Impressive properties have recently been reported for powder-consolidated nanocrystalline Mg-based materials by Lu et al. (Rev Adv Mat Sci 2004;6:28). We have conducted TEM microscopy, performed standard tension and compression, 3-point bending, notched-bar tension experiments on this material. The strength level is 400 MPa and there is a very small tension-compression asymmetry; also, while the tensile ductility is at a respectable level of approximately 9%, the ductility in compression is substantially higher, approaching levels greater than 35% at low strain rates. Further, the material shows strain-softening in both tension and compression and exhibited pronounced strain-rate sensitivity. In order to develop a simulation capability for the engineering design of structural components made from such materials, we have formulated continuum-level constitutive equations which could faithfully model the complicated experimentally-observed pressure and strain-rate sensitive response of such a material. We will present in detail the experiments and the model in the talk.

2:20 PM

Simulation for Loss of Electromagnetic Stirring Force Due to the Penetrated Aluminum into the Furnace Lining: Koichi Takahashi¹; Makoto Maruyama¹; Nobuhito Ishikawa¹; Mitsuhiro Otaki¹; ¹Furukawa-Sky Aluminum Corporation

Electromagnetic stirrer (EMS) has been practically used in aluminum melting and/or holding furnace in order to enhance melting rate of scrap aluminum and mixing speed of molten aluminum. However, the stirring effect of EMS decreased in case of a long period manufacturing without changing the furnace lining. In this paper the electromagnetic analysis on the basis of the Maxwell equation and thermal fluid dynamics analysis taking into account aluminum ingot melting were developed. As a result of the electromagnetic field analysis, it turned out that the refractory brick penetrated by molten aluminum shielded against the alternating magnetic field. Theoretical results of magnetic density at the bottom of furnace showed a good agreement of the actual measurement. Thermal fluid dynamics analysis indicated a delay of aluminum melting due to the loss of the electromagnetic stirring force in case of the penetration of aluminum into the furnace lining.

2:40 PM

Effect of Rolling Deformation and Aging on the Texture and Tensile Behavior of AA6061: Samuel Adedokun¹; ¹FAMU-FSU College of Engineering

Works have been reported by various authors on heat treatment and rolling deformation to study the behavior of various metals and alloys at different situations. These situations may include the artificial aging time, artificial aging temperature, percentage rolling deformation, deformation rate, solution heat treatment time and solution heat treatment temperature. Grain size, texture, mechanical and other properties are thereafter studied. This research project focuses on aluminum alloy 6061 (AA6061-T651) and investigates its texture evolvement after multipass rolling deformation (70% and 80%) followed by artificial aging at 160°C and 200°C for periods between 30 and 120 minutes. The correlations between the percentage deformation, artificial aging time and artificial aging temperature are looked into. Texture evolution and tensile response in alloy are also investigated. The texture was studied using an x-ray machine with texture goniometer attached, while the tensile response was examined by the use of an ATS machine. Results indicate there are variations in the texture and tensile response of the materials with respect to aging time, percentage deformation and artificial aging time, percentage deformation and artificial aging time, percentage deformation and artificial aging time, and ATS machine.

3:00 PM

Al-Al and Al-Mg Compound Casting: *Konrad Papis*¹; Peter Uggowitzer¹; ¹Swiss Federal Institute of Technology-Zurich

'Compound casting' is a process where a melt is cast onto or around a solid metallic 'insert'. The advantages of this process are the possibility of multi-step casting (facilitated by perfect joining) and weight-saving construction (i.e., Al-Mg compound structures). Inherent difficulties when joining aluminium are the natural oxide layer and the formation of intermetallic phases (IMPs). In this project, the solid substrate used is an aluminium alloy, and the melt is either aluminium or magnesium, containing various alloying elements (Cu, Si, Zn). Compounds with flawless (oxide-, IMP-less) interfaces were produced successfully by replacing the oxide layer with a zinc layer. This was accomplished by pickling the substrate in a solution containing zincate-ions, and subsequent zinc galvanizing. Composition and mechanical properties were investigated by SEM/EDX and microhardness measurements after the 'compound casting' process and after successive heat treatments.

3:20 PM Break

3:30 PM

Adaptive Control of Database Based Low Pressure Al Die Casting Machine with Acquisition of the Dynamic Dispersion of the Metal Front within the Die: *Christian Wögerer*¹; Dedinak Andreas¹; Richard Kretz²; Peter Schuldenzucker²; ¹ARC Seibersdorf Research GmbH; ²LKR ARC Leichtmetallkompetenzzentrum Ranshofen GmbH

The quality of castings significantly depends on the constancy of optimal cast parameters for the specific die and alloy. This paper presents the modifications of an existing die casting machine guarantying a constant quality of the cast process by automatically adapting the optimal parameters even during variations of alloy compositions and temperature of the melt. Therefore the control implies a database based model of the fluidity of certain alloys and their variations. The optimal casting parameters are often identified by simulation. These simulations are hard to verify, habitually in time consuming fill-and-stop casts with partial fillings. Against, the described control system allows the acquisition of the dynamic dispersion of the metal front within the die for every cast enabling a fast analysis of actual casting parameters or a quick verification of the simulation. The required combined metal-front and temperature sensors have been developed ad hoc for this control system.

3:50 PM

Comparison of the Corrosion Behaviors of Twin-Roll Cast and DC Cast AA 6016 and AA6082 for Automotive Applications: *Aziz Dursun*¹; Beril Dilsizoglu¹; Mustafa Ürgen²; Köksal Kurt²; Gerhard Anger³; ¹Assan Aluminium; ²Istanbul Technical University; ³AMAG Automotive GmbH

Recent studies conducted on continuosly cast 6000 series alloys showed that microstructural features and mechanical performances of these materials exhibit very satisfactory results. These features have to be supported by other material characteristics, such as general corrosion behavior and corrosion of welded parts in order to be competitive against steel and even the DC casthot rolled equivalents. In the present study we aimed to study and make comparison between the corrosion behaviors of DC and TRC cast 6000 series aluminum alloys. Pitting and micro galvanic corrosion of TIG welded DC and TRC cast samples were tested and evaluated. CV experiments and salt spray tests were employed to determine their pitting and micro galvanic corrosion behaviors. The corrosion behavior is discussed by considering the surface





macro and microstructural features of the samples. The results revealed the importance of surface segregation and welding electrode selection on corrosion performance.

4:10 PM

Heat Distribution Characterization of Thermal Insulating Coatings: Christopher Wilhelm¹; *Eui Lee²*; David Piatkowski²; Omar S. Es-Said¹; Alex Chi³; ¹Loyola Marymount University; ²Naval Air Systems Command; ³Demeton Inc.

New coatings were developed for the Marine Corps AM2 6061-T6 aluminum alloy mats to produce a durable long lasting nonskid coating that could withstand the heat from the vertical exhaust. The purpose of the experiments performed in this project was to test the heat resistance of these new coatings in six different combinations with a base coat and nonskid top coat. These combinations are a mixture of NiAl, NiCr-SiC, Al2O3 and ZrO2. Each of the combinations of coatings was exposed directly to the flame of three torches for different periods of time, with a constant distance, to simulate exhaust plume from the take-off/vertical landing air craft. Tensile, conductivity, and hardness tests were conducted. Optical microscopy samples were taken to inspect coating integrity and the microstructure of each plate after exposure. The data was compiled to determine which combination of coatings had the best heat resistant qualities.

4:30 PM

Property Investigation of Ti-Al6-V4 Produced by Additive Manufacturing: *Johannes Vlcek*¹; ¹European Aeronautic Defence and Space Company

Additive manufacturing is an interesting process technology for structural repair or overhaul of engine components. In order to evaluate the technology for repair or direct component manufacturing the properties under dynamic loading and fracture toughness values are of interest. Ti-Al6-V4 material was produced in selective laser melting, selective electron beam melting and fused metal deposition by laser nozzle deposition. The materials were tested in high cycle fatigue tests in the as melted, mill annealed 850°C/2h condition and after hot isostatic pressing. Maximum ultimate tensile strength was measured to be 1100 MPa with an elongation greater than 12%. The fatigue resistance at 10^7 load cycles for the material deposited by laser nozzle and the one produced by electron beam melting + HIP can be assumed around 600 MPa. Different surface conditions – machined and condition after SLM – were evaluated. The paper discusses micro-structural features.

Hume-Rothery Symposium: Scattering Studies and the Fundamental Properties of Materials: Session I

Sponsored by: The Minerals, Metals and Materials Society, TMS Electronic, Magnetic, and Photonic Materials Division, TMS: Alloy Phases Committee *Program Organizers:* Patrice Turchi, Lawrence Livermore National Laboratory; Wolfgang Donner, University of Houston; J. Robertson, Oak Ridge National Laboratory

Monday PM	Room: Oceanic 7
February 26, 2007	Location: Dolphin Hotel

Session Chairs: David Price, Centre de Recherche sur la Matière Divisée; Didier de Fontaine, University of California Berkeley

2:00 PM Introductory Comments

2:10 PM Keynote

How Big is an Atom: Simon Moss1; 1University of Houston

While atomic size mismatch and electron/atom ratio (e/a) are determinants in phase stability, experimental, theoretical and computational methods, unavailable in Hume-Rothery's day, have made enormous progress possible. We discuss atom size in a material and its determination, along with standard crystallography, through diffuse scattering at the national synchrotron and neutron scattering facilities, and our in-house x-ray lab. The topics cover metallic alloys, semiconductor III-V films and multilayers, oxides, and glasses, where local size plays an often non-intuitive role. Studies range from the Fe-C dipole distortion in martensite, to the interfacial strain in thin III-V multilayers, to local size effects in alloys with a very small mismatch (Fe-Cr) and an appreciable mismatch (Ni-Pt vs, CuAu). We have also explored the O-vacancy-induced modulations in YBCO and the rapidly diffusing Au in Pb, all variants on the same theme of "size." *Supported by the DOE/BES, NSF/DMR, and the State of Texas.

3:00 PM Invited

Neutron Scattering Studies of Short-Range Order, Atomic Displacements, and Effective Pair Interactions in a Null Matrix 62Ni0.52Pt0.48 Crystal: *Jose Rodriguez*¹; S. C. Moss²; J. L. Robertson³; J. R. D. Copley¹; D. A. Neumann¹; J. Major⁴; ¹National Institute of Standards and Technology; ²University of Houston; ³Oak Ridge National Laboratory; ⁴Max Planck Institute fuer Metallforschung

The best known exception to the Heine-Samson and Bieber-Gautier arguments for ordering effects in transition metal alloys (similar to the Hume-Rothery rules) is a NiPt alloy. Using the Disk Chopper Spectrometer (DCS) at NIST, we have investigated a Null-Matrix Crystal 62Ni0.52Pt0.48, (62Ni has a negative scattering length, nearly equal in magnitude to Pt). Its composition has therefore been chosen whereby all effects depending on the average lattice scattering vanish. The only remaining contributions to the diffuse scattering are the Short Range Order (SRO) and Size Effect (SE) terms. Such data permit the extraction of the SRO parameters (concentration-concentration correlations) as well as the displacement parameters (concentration-displacement correlations). Using the Krivoglaz-Clapp-Moss theory, we obtained the Effective Pair Interactions (EPI). The results can be used to model the alloy in the context of electronic theory of alloy phase stability, including an evaluation of the potentially important aspect of charge transfer and ionicity.

3:30 PM Break

3:50 PM Invited

Ordered and Disordered Surface Phases of Bi on Cu (111): *Elias Vlieg*¹; ¹Radboud University Nijmegen

Bi layers on Cu(111) show a 'rich' phase diagram. At room temperature, three ordered phases are found. Going from low to high coverages, first a substitutional surface alloy is formed, followed by an overlayer structure (thus de-alloying occurs) and finally leading to a uniaxial-incommensurate phase. The atomic structure of these phases has been determined using X-ray diffraction, while their formation has been observed in real-time using low-energy electron microscopy (LEEM). The overlayer phase melts around 260°C. We have found that the 'liquid' Bi shows considerable order that depends strongly on coverage. At a coverage above 0.5 monolayer, the liquid has local ordering properties that resemble the room temperature structure. Despite the hexagonal symmetry of the substrate, we find that the liquid Bi does not show hexatic order, but has an orthorhombic orientational order that occurs in three domains.

4:20 PM Invited

First-Principles Theory of Short- and Long-Range Order in Ultrathin Surface Alloy Films of Bulk-Immiscible Metals: Tejodher Muppidi¹; Bo Yang²; Mark Asta²; *Vidvuds Ozolins*¹; ¹University of California, Los Angeles; ²University of California, Davis

Formation of two-dimensional (2D) nanoscale patterns (stripes and disks) has been observed in several surface alloy systems composed of bulkimmiscible species. These 2D structures occur due to competition between short-range chemical bonds favoring phase separation and long-range elastic forces favoring intermixing. Long-range oscillations in the short-range order parameters have also been predicted to occur above the ordering transition. We present an accurate theoretical framework that incorporates interatomic interactions obtained from first-principles electron-structure methods. The central role in this formalism belongs to a Fourier transform of long-ranged pair interactions, which include both alloying and elastic strain effects. Applications to several metallic alloy systems on isotropic Ru(0001) and anisotropic Mo(110) substrates will be shown, and implications for achieving highly ordered stripe patterns will be discussed.

Innovations in Titanium Technology Symposium: Novel Materials and Processes I

Sponsored by: The Minerals, Metals and Materials Society, TMS Structural Materials Division, TMS: Titanium Committee

Program Organizers: Mehmet Gungor, Concurrent Technologies Corporation; M. Ashraf Imam, Naval Research Laboratory; F. H. (Sam) Froes, University of Idaho

Monday PM	Room: Asia 3
February 26, 2007	Location: Dolphin Hotel

Session Chairs: Francis Froes, University of Idaho; James Sears, South Dakota School of Mines and Technology

2:00 PM Keynote

Development of the FFC Cambridge Process for the Production of Titanium and Its Alloys: *Richard Dashwood*¹; Martin Jackson¹; Kevin Dring²; Kartik Rao¹; Rohit Bhagat¹; Daniel Brett¹; Douglas Inman¹; ¹Imperial College London; ²Norsk Titanium AS

The FFC Cambridge process involves the electrodeoxidation of TiO2 in a molten CaCl2 electrolyte to yield titanium metal. This process has attracted significant interest as a potential alternative to the Kroll process for the primary production of titanium or, when a mixed oxide precursor is used, as a low-cost method for producing alloy powder. For the last five years researchers at Imperial College London have been conducting fundamental studies to ascertain the electrochemical mechanisms involved in the process as well as evaluating the potential of the process to produce titanium alloys. This paper will demonstrate how electrochemical techniques such as cyclic voltammetry and AC impedance have been used to elucidate the key thermodynamic and kinetic aspects of the process. The paper will also present the results obtained from the production of a number of alloys highlighting the capability of the process to produce novel and complex alloys.

2:30 PM Invited

Operation of Electrolysis Cells for the Direct Production of Titanium from Solid Oxide Precursors: *Kevin Dring*¹; Odd-Arne Lorentsen²; Eirik Hagen²; Christian Rosenkilde²; ¹Norsk Titanium AS; ²Norsk Hydro ASA

Norsk Titanium, in collaboration with Hydro Oil & Energy, has investigated the direct electrochemical electrolysis for the production of titanium from its oxides. While immersed in a molten CaCl₂-based electrolyte, titanium-oxygen compounds were cathodically polarized against anodes of various compositions. The use of graphitic anodes resulted in the formation of molten carbonates, carbon scum on the electrolyte surface, and carbide contamination of the cathode product, which led to significant reductions in current efficiency. Consequently, a variety of inert anode candidates have been evaluated, all of which feature the additional benefit of oxygen evolution as the anodic electrolysis product. The formation of titanium occurred in a sequential manner, with the lower oxides of titanium, in conjunction with calcium titanate species, forming at intermediate reduction times. Titanium metal was only produced during the final stages of electrolysis, and the diffusion of oxygen out of the Ti-O solid solution was rate determining.

2:50 PM

Electrochemical Reduction of Titanium Oxide from CaCl2 Melts Saturated with CaO: Joel Katz¹; ¹Los Alamos National Laboratory

Titanium oxide was electrochemically reduced to titanium in a calcium chloride melt saturated with calcium oxide. The process is repeatable and reproducible. Several samples underwent reduction for periods of up to two weeks in the melts, which were held between 930 and 950°C. Cells were maintained between 2.6 and 3.2 V, which is sufficient to allow the electrolysis of calcium oxide to occur as follows. CaO = Ca2+ + O2- The calcium ions are thought to be responsible for the actual reduction. Reduction was performed both under conditions of carbon saturation, i.e., graphite crucible and anode, and under carbon free conditions. When a graphite anode is used the overall reaction is thought to be: TiO2 + C = Ti + CO2 and for the carbon free process: TiO2 = Ti + O2 Information on impurity levels of the as reduced titanium will be discussed.

3:10 PM

Synthesis and Enrichment of Titanium Subchlorides in Molten Salts: Osamu Takeda¹; Toru Okabe¹; ¹University of Tokyo

With the purpose of establishing a new (semi-) continuous/high-speed titanium production process based on the magnesiothermic reduction of titanium subchlorides (TiCl_x, x = 2, 3) referred to as the subhalide reduction process, a novel synthetic process of TiCl_x by using molten salts as the reaction medium was investigated. Titanium tetrachloride (TiCl₄), supplied by a peristaltic pump at the rate of 0.13~0.72 g/min, was reacted with feed titanium sponge immersed in molten magnesium chloride (MgCl₂) at 1273 K under argon atmosphere. It was demonstrated that the efficiency of the formation of TiCl_x was drastically improved by using molten salts as the reaction medium as compared with that of the synthesis by employing the direct reaction of TiCl₄ gas with solid titanium. Some results regarding the enrichment of TiCl_x in molten salts will also be shown.

3:30 PM Break

3:45 PM Keynote

Thermodynamic, Kinetic, and Microstructural Aspects in the Electrochemical Reduction of Titanium Dioxide in Molten Calcium Chloride: *Carsten Schwandt*¹; Duncan Alexander²; Derek Fray¹; ¹University of Cambridge; ²Arizona State University

An investigation into the fundamentals of the electrochemical reduction of titanium dioxide to titanium metal in molten calcium chloride is presented. Partially and fully reduced samples were prepared by terminating the reduction process after different reaction times and characterised by means of X-ray diffraction analysis. Based on the observed time-dependent changes in phase composition as well as thermodynamic and kinetic considerations, the reaction path has been derived. The key result is that the reduction proceeds through several well-defined stages and involves the formation and decomposition of titanium sub-oxides and calcium-containing compounds. Some of the partially-reduced samples were examined further through light optical microscopy, scanning electron microscopy and energy dispersive X-ray analysis. This has revealed that the electrochemical conversion of titanium dioxide to titanium metal is accompanied by substantial changes in the microstructure. Implications of the results obtained on the up-scaling of the process will also be discussed.

4:10 PM

Production of Ti-Al Alloys Using Ionic Liquid Electrolytes at Low Temperatures: *Debabrata Pradhan*¹; Ramana Reddy¹; ¹University of Alabama Ionic liquids are novel low temperature salts and their application in extraction of metals was investigated. Present study is focused on the production of Ti-Al alloys from AlCl₃-1-Methyl-3-butylimidazolium chloride (BmimCl)-TiCl₄ ionic melt at low temperatures. Titanium was used as the anode. Very fine Al-Ti alloy particles were deposited on copper substrate at 2.5 V and 100°C using the above melt at a molar ratio of 2:1:0.009 (AlCl₃: BmimCl: TiCl₄). Morphology of the produced Al-Ti alloy was investigated using SEM-EDS and XRD. The Ti-Al alloys containing up to 20 wt % Ti was produced.

4:30 PM

Precipitation of Rutile Nano-Sized Particles via Forced Hydrolysis of a Titanium Tetrachloride Solution: Cecile Charbonneau¹; George P. Demopoulos¹; ¹McGill University

This study investigates the production of titanium dioxide (TiO2) nano-sized particles for advanced technological applications including solar cells. During the preliminary phase of this project, the hydrolysis of titanium tetrachloride (TiCl4) solution by heating under atmospheric pressure conditions has been examined. Monitoring of solution composition changes was accomplished by Inducted Coupled Plasma (ICP) and acid titration measurements. The precipitates were submitted to X-Ray Diffraction (XRD) analyses and Electron Microscopy observations. Agglomerates of crystalline nano-sized particles of rutile were formed. This paper will examine the influence of experimental parameters such as the temperature at which forced hydrolysis is carried out as well as the concentration of the TiCl4 solution on the kinetics of the hydrolysis reaction and the characteristics of the solid products.

LEARN • NETWORK • ADVANCE





4:50 PM

Producing Titamium by Titania Electrolysis in a 5KA Cell: *Huimin Lu*¹; Huanqing Han¹; ¹Beijing University of Aeronautics and Astronautics

In this paper, the theoretical energy consumption of TiO2 electrolysis is calculated and the real energy consumption of TiO2 electrolysis is measured in a 5kA electrolysis cell. In the experiments of TiO2 electrolysis, some important measures like the modification of cell design and ultrasonic electrolytic technology are adopted for improving the current efficiency. This process produces titanium with 0.38%O, 0.032%C, 0.0090H, 0.061N and 0.12%Fe, the current efficiency range is 70%~82%, the energy consumption is 7.984kWh/kg Ti and carbon dioxide is discharged on carbon anode. This new technique has low energy consumption, high current efficiency and less pollution for the environment. The reduction mechanism of TiO2 to Ti was also studied.

Magnesium Technology 2007: Automotive Applications and USAMP Programs

Sponsored by: The Minerals, Metals and Materials Society, TMS Light Metals Division, TMS: Magnesium Committee Program Organizers: Randy Beals, DaimlerChrysler; Neale Neelameggham, US Magnesium LLC; Mihriban Pekguleryuz, McGill University; Alan Luo, General Motors Corporation

Monday PM	Room: Southern 5
February 26, 2007	Location: Dolphin Hotel

Session Chairs: Randy Beals, DaimlerChrysler; Bob Powell, General Motors Research and Development Center

2:00 PM

Summary of "Magnesium Vision 2020: A North American Automotive Strategic Vision for Magnesium": Gerald Cole¹; ¹LightWeight Strategies LLC

This paper summarizes the monograph, "Magnesium Vision 2020. A North American Automotive Strategic Vision for Magnesium"1 prepared under the auspices of the United States Automotive Materials Partnership The objective was to understand the infrastructural and technical challenge that can increase the use of magnesium in the automotive industry. One hundred sixty three (163) Research and Technology Development Themes (RTDTs), or RTD projects were developed that addressed issues of corrosion, fastening, and processing-other-than-high pressure die casting to produce automotive magnesium parts. A major problem identified in the study is the limited ability of the current magnesium industrial infrastructure to supply RTD and implementation-ready automotive magnesium components. One solution is to create a magnesium cyber center where globally networked experts would be able to innovate in process and product development, model metalworking and non-HPDC foundry processes, and integrate theoretical predictions/models of metallurgical structure with component function.

2:20 PM

USAMP High Integrity Magnesium Automotive Components Project (HIMAC): Bruce Cox¹; *Randy Beals*¹; Larry Ouimet²; Richard Osborne²; Alan Luo²; Naiyi Li³; Jacob Zindel³; ¹Daimler Chrysler; ²General Motors Corporation; ³Ford Motor Company

The US Automotive Materials Partnership (USAMP) and the Department of Energy launched the High Integrity Magnesium Automotive Components Project (HIMAC) in 2006 to determine the feasibility of producing magnesium control arms. Vehicle weight reduction is a key enabler to meet future stringent CAFÉ requirements, and this can best be achieved by the use of more light weight materials such as magnesium. The purpose of this project is to develop (existing and new) metal casting process technologies and tools required to manufacture cost effective high integrity cast magnesium automotive chassis components and increase production of magnesium components requiring geometries and properties not possible with existing high pressure die casting (HPDC) process limitations. This project will develop existing aluminum low pressure permanent mold and squeeze casting processes for the production of magnesium structural castings. Processing costs as well as technical and manufacturing issues for each process will be developed and validated.

2:40 PM

Development of Enabling Technologies for Magnesium Automotive Body Applications: Alan Luo¹; Anil Sachdev; ¹General Motors Corporation

Magnesium is making inroads in automotive body applications for mass reduction and vehicle performance improvement; however, there are significant challenges for the lightweight magnesium alloys to meet the demanding requirements of automotive body structures, such as stiffness, crashworthiness, durability as well as noise, vibration and harshness (NVH). This talk will outline the development of enabling technologies of high-integrity casting, extrusion, sheet forming, corrosion protection, and joining and assembly. Current and future magnesium body applications will be discussed.

3:00 PM

Ultra-Large Castings for Lightweight Vehicle Structures: *Mike Maj*¹; Randy Beals²; ¹Ford Motor Company; ²DaimlerChrysler

The Ultra Large Casting (ULC) project undertaken by the U. S. Automotive Materials Partnership (USAMP) with the support of the U.S. Department of Energy will assess the manufacturing feasibility, economics and mass reduction potential of thin wall structural castings of aluminum and magnesium applied to automotive weight reduction. The ULC project will establish a rationale for using light metal castings in place of conventional stamped and welded steel automotive primary body structures to reduce vehicle weight. The ULC project will be executed in two concurrent phases: Phase I will focus on evaluating the capabilities of emerging new casting processes that show promise to improve the quality, consistency and mechanical properties of cast components vs. conventional casting processes. Phase II will focus on the design, analysis, production and testing a "real-world" vehicle application meeting the ULC Team's criteria for mass reduction, cost and performance.

3:20 PM

Thin-Wall Molding of Magnesium Alloys: Frank Czerwinski¹; ¹Husky Injection Molding Systems

The paper describes technical aspects of manufacturing thin wall components using magnesium injection molding. The conventional and novel processing routes, taking advantage of controlling the melt temperature and its flow into the mold, are analyzed along with requirements imposed on alloy properties both in the molten state and after solidification. Some directions for alloy development are defined. The processing details are accompanied by recent advances in hardware design, aimed to optimize injection parameters and alloy distribution systems (hot runners).

3:40 PM Break

4:00 PM

A Lightweight Automobile Body Concept Featuring Ultra-Large, Thin-Wall Structural Magnesium Castings: Stephen Logan¹; ¹DaimlerChrysler

This paper describes a lightweight automobile body structure concept developed at DaimlerChrysler to support a high fuel-efficiency vehicle project. This concept incorporated ultra-large thin-wall magnesium castings for most of the structure to achieve more than 40% weight reduction with a minimal cost increase over a conventional steel structure while achieving significantly improved structural performance as evaluated through CAE simulations. A business case analysis was conducted and one concept vehicle was built for the purpose of demonstrating concept feasibility. The paper also describes several large thin-wall die casting body applications that are in current production or have been used in recent production automotive applications and identifies areas where further development could improve the likelihood of a magnesium intensive body structure becoming a production reality at a later time.

4:25 PM

Casting and Testing of the USAMP Magnesium Intensive Powertrain: Joy Hines¹; Robert McCune¹; John Allison¹; *Bob Powell*²; Larry Ouimet³; William Miller³; Randy Beals⁴; Lawrence Kopka⁴; Peter Ried⁵; ¹Ford Motor Company; ²General Motors Research and Development Center; ³General Motors Powertrain; ⁴Daimler Chrysler Corporation; ⁵Ried and Associates LLC

The US Automotive Materials Partnership (USAMP) and the US Department of Energy launched the Magnesium Powertrain Cast Components Project (MPCC) in 2001 to determine the feasibility and desirability of producing a magnesium-intensive engine. The Engine consists of a V6 engine with a low pressure sand cast magnesium engine block with a thermal spray cylinder liner, die cast structural oil pan, die cast front engine cover and a thixomolded rear oil



seal carrier. These components were redesigned using extensive Finite Element Analysis (FEA) and manufactured using newly developed magnesium alloys suitable for powertrain applications. The components were then assembled in a series of engine builds. The engines were put through a number of controlled durability tests using engine dynamometers. This presentation will focus on the testing results and lessons-learned in this program.

4:50 PM

Friction Stir Welding of Dissimilar Magnesium Alloys for Automotive Applications: *Frank Hunt*¹; Harsha Badarinarayan¹; Kazutaka Okamoto¹; Diana Platt²; ¹Hitachi America, Ltd; ²University of Michigan

Friction stir welding (FSW) shows advantages for joining magnesium alloys for automotive applications. In this research, the feasibility of FSW dissimilar magnesium alloys was studied. Die cast magnesium MRI-153 and AZ31 (plate) were butt-welded using the FSW technique. Coupons were prepared under various weld conditions such as; tool rotation speed (rpm) and weld speed. The effects of weld parameters on the alloys have been quantified in terms of hardness profile across the weld as well as tensile strength. Other key characteristics of the weld were analyzed including: macrostructure, weld surface and cross section.

5:15 PM

Microstructure and Creep of Die-Cast Magnesium Alloys: *Jessica TerBush*¹; Akane Suzuki¹; Nicholas Saddock¹; J. Jones¹; Tresa Pollock¹; ¹University of Michigan

The microstructure of crept samples of die-cast AXJ530, MRI153M, and MRI230D has been examined via transmission electron microscopy. Creep properties were characterized by USAMP, as part of the Magnesium Powertrain Cast Components (MPCC) program. Samples were crept in tension at 70 or 110 MPa at temperatures of 398 and 453 K for approximately 500 hours or until rupture. At 70 MPa/398 K (low stress/low temp condition), minimum creep rates varied from ~1×10⁻¹¹ s⁻¹ for AXJ530 and MRI230D to ~1×10⁻¹⁰ s⁻¹ for MRI153M. At 110 MPa/453 K (high stress/high temp condition), minimum creep rates varied from ~3×10⁻⁸ s⁻¹ for AXJ530 and MRI230D to ~1×10⁻⁶ s⁻¹ for MRI153M. Dislocations present in the α -Mg matrix were studied in order to gain further information on mechanisms of creep deformation of these die-cast alloys. The dislocation substructures present in both the grain interiors and in the vicinity of the intermetallic-containing eutectic will be discussed.

Magnesium Technology 2007: Wrought Alloys and Forming Processes I: Deformation

Sponsored by: The Minerals, Metals and Materials Society, TMS Light Metals Division, TMS: Magnesium Committee

Program Organizers: Randy Beals, DaimlerChrysler; Neale Neelameggham, US Magnesium LLC; Mihriban Pekguleryuz, McGill University; Alan Luo, General Motors Corporation

Monday PM	Room: Southern 4
February 26, 2007	Location: Dolphin Hotel

Session Chairs: Mihriban Pekguleryuz, McGill University; Xiaoqin Zeng, Shanghai Jiao Tong University

2:00 PM

Numerical Modelling of Large Strain Deformation in Magnesium Alloy AM30: Julie Levesque¹; Kaan Inal²; Kenneth Neale¹; Alan Luo³; Raja Mishra³; Lan Jiang⁴; Stephane Godet⁵; ¹University of Sherbrooke; ²University of Waterloo; ³General Motors Research and Development Center; ⁴McGill University; ⁵Université catholique de Louvain

In this paper, a new constitutive framework based on a ratedependent crystal plasticity theory is presented to simulate large strain deformation phenomena in HCP metals such as magnesium. The new framework is incorporated into in-house codes. The simulations are performed using a crystal plasticity model in which crystallographic slip and deformation twinning are the principal deformation mechanisms. Simulations of various stress states (uniaxial tension, uniaxial compression and the ring hoop tension test) for the magnesium alloy AM30 are performed and the results are compared with experimental observations of specimens deformed at 200°C.

2:20 PM

Mechanical Behavior of Wrought AM50 at Room and Elevated Temperature: *Paul Krajewski*¹; Amir Eliezer²; ¹General Motors Corporation; ²Sumi Shumoon College of Engineering

The mechanical behavior of AM50 magnesium sheet was evaluated at both 25C and 450C. The AM50 sheet was produced by rolling both ingot cast and die cast slabs via unidirectional and bidirectional (cross rolling). The die cast material had a significantly finer grain size than the ingot cast material. Room temperature tensile testing of the AM50 showed comparable strength values between the as-cast and die cast materials, but poorer elongation in the die cast material. Similarly, elevated temperature testing of the AM50 showed that despite the finer grain size, the die cast material had significantly poorer ductility, which was attributed to the early onset of cavitation. The cavitation and fracture behavior of these materials will be discussed.

2:40 PM

Hot Deformation Mechanisms in Mg-1%Zn Alloys: *Geoff Seale*¹; Jon Carter²; Ravi Verma³; Paul Krajewski²; Elhachmi Essadiqi⁴; Faramarz Zarandi¹; Stephen Yue¹; ¹McGill University; ²General Motors Corporation; ³General Motors Research and Development Center; ⁴CANMET Materials Technology Laboratory

To investigate the hot deformation and fracture characteristics of Mg-1wt% Zn alloys containing a range of Al levels, rolled specimens were tensile tested over a range of strain rates and elevated temperatures. Strain rate versus flow stress was plotted on log-log scales to reveal the transition in deformation mechanisms as a change in the slope of these curves. The mechanism changes in going from low to high strain rates, are one with uniform elongation failure to one with necking behavior. This change in deformation mechanism is reinforced by fractography analysis. The fracture surfaces show two separate deformation mechanisms along with what appears to be a transition fracture surface combining the features of both necking and cavitation. There does not appear to be an effect of Al on this deformation transition. Mn does appear to favor the uniform elongation regime where it begins at lower strains than the alloys without Mn.

3:00 PM

Texture Evolution in AM30 Mg Alloy Deformed along Different Strain Paths: Lan Jiang¹; John Jonas¹; Raj Mishra²; Alan Luo²; Anil Sachdev²; Stéphane Godet³; ¹McGill University; ²General Motors; ³Université Catholique de Louvain

The evolution of texture in an AM30 Mg alloy was examined after deformation by uniaxial tension, uniaxial compression and ring hoop tension testing (RHTT). Temperatures from ambient to 200°C were covered at a strain rate of 0.1/s. The samples were cut from extruded AM30 Mg alloy tubes. Specimens deformed to various strain levels were examined by optical microscopy and electron backscattered diffraction (EBSD) techniques. The results indicate that the initial extrusion texture and strain path together play important roles in the formation of different types of twins, which in turn significantly influence the evolution of the deformation texture. Contraction and double twinning are the dominant twinning mechanisms in uniaxial tension, while extension textures indicate that the active twinning planes are the ones with the highest Schmid factors.

3:20 PM

Nucleation and Growth Phenomena during Recrystallization of Magnesium - Rare Earth Metal Alloys: Jeremy Senn¹; Sean Agnew¹; Ashutosh Jain¹; ¹University of Virginia

Traditional Mg sheet alloys develop a strong basal fiber texture during rolling which is not significantly altered by annealing. This texture is responsible for the anisotropy and tension-compression strength asymmetry of the alloys, which contributes to their poor sheet formability. Recent studies have shown that recrystallization of alloys containing rare earth elements can dramatically alter and/or weaken the deformation texture. A number of alloys containing Y and/or Nd are deformed in plane strain compression and then annealed. The distinct roles of nucleation and growth during recrystallization are explored. For e.g., it is of interest to know whether particle stimulated nucleation is an important contributing mechanism. The present results highlight two facts: i) texture alteration is most effective during super-solvus anneals after grain boundary pinning particles have dissolved, and ii) the weak texture component

LEARN • NETWORK • ADVANCE





MOZDAX

P M

that persists after recrystallization is typical of shear band in the deformation microstructure.

3:40 PM Break

4:00 PM

In-Situ Neutron Diffraction Study of Mechanical Twinning in a Textured Magnesium Alloy during Strain Path Changes: *Ashutosh Jain*¹; Donald Brown²; Bjorn Clausen²; Sean Agnew¹; ¹University of Virginia; ²Los Alamos National Laboratory

Experiments involving non-proportional loading have been conducted to study the role of twinning in the deformation of textured magnesium alloy sheet, plate and extruded samples loaded in tension and compression along different directions (e.g., sheet rolling, transverse, and normal directions.) Changes of strain path are imposed by uniaxial loading in one direction followed by loading along another direction, including full strain reversal. A range of twinning, de-twinning, and secondary twinning phenomena are thus explored. In-situ neutron diffraction experiments show that twinning is preceded by slip in the twinning grains. Furthermore, the diffraction data are used to determine the stress levels within the grains as they are twinning, as well as the stresses within the twins that appear. The role of twinning during non-monotonic strain paths, such as compression along RD followed by compression along ND or TD is thus investigated through mechanical behavior and evolution of texture, and internal strains.

4:20 PM

Relation between Deformation Twin and Deformation-Induced Surface Relief in AZ31 Mg Alloy Sheets: *Daisuke Ando*¹; Takeo Miyamura¹; Junichi Koike¹; ¹Department of Materials Science, Tohoku University

Deformation twins are frequently observed in Mg alloys at room temperature. Twins of the {1012} type have been known to be an important deformation mechanism. Though other types of deformation twins were reported in the past, the twin types have been in dispute and their roles on deformation mechanisms have not been well understood. In this work, we performed tensile test of rolled sheets of AZ31 Mg alloys at room temperature. A number of large surface relief were observed in a region near a fractured edge. TEM observation showed the formation of twins under the large surface relief. Crystallographic analysis indicated that the basal planes of the twins were tilted by approximately 370 with respect to the matrix. This is considered to make basal dislocations highly active within the twins. The localized deformation may lead to the formation of crack-like faults and to failure in a macroscopically brittle manner.

4:40 PM

Twinning and Ductile Failure of Mg-3Al-1Zn: *Matthew Barnett*¹; ¹Deakin University

In general, magnesium alloys display lower ductilities than other metal systems that display equivalent strength. Some authors have suggested that twinning plays a role in this phenomenon. In the present work two series of samples cut in different directions from an extruded bar are examined to test this idea. One series was cut to favour {2110}twinning, the other to suppress it. The reduction in area measured in tensile tests performed at temperatures between room temperature and 250° showed negligible difference between the two series of samples. The series in which {2110}twinning was not favoured displayed copious amounts of twinning that was assumed, based on EBSD analysis, to be on the {1110} plane. These twins were associated with flow localization and void formation and are thus likely to play an important role in ductile failure.

5:00 PM

On the Post Superplastic Forming Properties of AZ31 Magnesium Alloy: *Marwan Khraisheh*¹; Fadi Abu-Farha¹; ¹University of Kentucky

It is evident that cavitation develops during Superplastic forming of AZ31 magnesium alloy. The level of cavitation depends on different process parameters including temperature, strain and strain rate. Large amount of cavitation may have detrimental effects on the mechanical properties of the formed components. In this work, we examine the post Superplastic forming mechanical properties of AZ31 magnesium alloys under various process parameters and correlate the results with the level of cavitation achieved during Superplastic forming.

5:20 PM

Explanation on the Elongation Variation of AZ31 Alloy at the Elevated Temperature: *Yong Nam Kwon*¹; Y.-S. Lee¹; J.-H. Lee¹; ¹Korea Institute of Machinery and Materials

In the present study, the commercially rolled AZ31 alloy sheets with the grain size of ranging from 6 to 150 μ m were used for tensile tests. For all grain sizes, elongation increased with temperature increment. However, the differences in grain size did not give a larger elongation differences even at the temperature range where superplastic deformation behavior might be operating for the small grained alloy. This trend was also found in biaxial bulging test. Results indicated that different deformation mechanisms were operating with grain size variation even though elongation was recorded similarly. Microstructural observation showed that grain boundary sliding occurs in the case of smaller grained alloy while dislocation slip is operating for larger grains. However, very fast grain made dislocation slip as the operating deformation mechanism after a certain amount of strain in fine grained alloy. Also, dynamic recrystallization made an important role for ductility of AZ31 alloy.

Materials in Clean Power Systems II: Fuel Cells, Solar, and Hydrogen-Based Technologies: PEMFCs

Sponsored by: The Minerals, Metals and Materials Society, ASM International, TMS Structural Materials Division, TMS/ASM: Corrosion and Environmental Effects Committee

Program Organizers: Zhenguo "Gary" Yang, Pacific Northwest National Laboratory; Michael Brady, Oak Ridge National Laboratory; K. Scott Weil, Pacific Northwest National Laboratory; Yong-Ho Sohn, University of Central Florida

Monday PM	Room: Asia 2
February 26, 2007	Location: Dolphin Hotel

Session Chairs: Ali R-Raissi, University of Central Florida; Eve Steigerwalt, Dana Corporation

2:00 PM Invited

Membrane Degradation Mechanisms in Polymer Electrolyte Membrane Fuel Cells: *James Fenton*¹; Vishal Mittal¹; Russ Kunz²; ¹University of Central Florida; ²University of Connecticut

Membrane degradation mechanisms in PEMFCs were studied using an in-situ and nondestructive technique, which relies on the measurement of the membrane degradation rate in a fuel cell. Degradation of Nafion membranes were studied and the fluoride emission rate (FER) as measured from the fuel cell effluent water analysis was used as a quantitative indicator of the membrane degradation rate. The degradation mechanisms as proposed in the literature and the ones hypothesized from the experimental findings will be discussed.

2:35 PM Invited

Overview of Polymer Electrolyte Membrane Fuel Cell Stack Sealing: *Eve Steigerwalt*¹; Mike Anderson¹; Jacob Meyer¹; ¹Dana Corporation

An overview of the function and types of sealing manufacturing methods (including liquid injection molding, high-consistency rubber molding, curein-place gaskets, screen-printing, and others) will be presented, along with the necessary product and material parameters necessary to design a gasket profile. Finite Element Analysis (FEA) is widely used to derive the load versus deflection curve of a gasket profile. FEA examples will be presented on different types of gasket designs and parameters. Finally, the advantages and disadvantages of a new sealing solution will be presented.

3:10 PM

Modeling Platinum Loss in PEM Fuel Cell Cathodes: Edward Holby¹; *Dane Morgan*¹; Yang Shao-Horn²; ¹University of Wisconsin-Madison; ²Massachusetts Institute of Technology

Loss of electrochemically active surface area (ECASA) in the carbonsupported platinum electrocatalyst cathode is a key issue in meeting automotive cost efficiency and durability standards for polymer electrolyte membrane fuel cells (PEMFCs). Recent work has suggested that Ostwald ripening of platinum nanoparticles, dissolution and precipitation of aqueous platinum ions



off of the carbon support, and carbon corrosion are all significant mechanisms for ECASA loss. By adapting a numerical model put forth by Darling and Meyers,¹ the time evolution of particle size distributions (PSDs) and their associated ECASAs under PEMFC conditions are simulated. These results indicate that the initial Pt PSD can have an important impact on the long-term durability of PEMFCs. The effects of Pt surface diffusion and corrosion of the carbon support on ECSA are currently being integrated into the model. ¹R. M. Darling and J. P. Meyers, J. Electrochem. Soc. 150, A1523-A1527 (2003).

3:35 PM

Study on the Proton Conduction Mechanism in Proton Exchange Membranes Using AC Impedance Technique: Jinjun Shi¹; Bor Jang¹; ¹Wright State University

AC impedance technique is used to explore the proton conduction mechanism in proton exchange membranes. This study can be used to prove or invalid the two proton conduction mechanisms, Grotthuss mechanism and vehicle mechanism, which are widely adopted to explain the proton conduction in proton exchange membranes. The proton conduction mechanism will be explained at different hydration levels of the membrane. This study helps understand the proton conduction mechanism in PEM fuel cells and be used to design new proton exchange materials as well.

3:55 PM Break

4:05 PM Invited

Materials and Catalysis Aspects of Hydrogen Generation from Amine Borane Complexes – A Review: *Ali T-Raissi*¹; Nahid Mohajeri¹; Olawale Adebiyi¹; Karthikeyan Ramasamy¹; ¹University of Central Florida

Ammonia-borane complex has very high hydrogen content of 19.6 wt% and hence, is a promising material as a hydrogen carrier for proton exchange membrane fuel cells (PEMFC). Release of hydrogen in the AB complex can occur by either thermolysis or hydrolysis. In this paper, we present a review of the state-of-the-art with respect to the hydrogen generation via catalytic reactions of ammonia-borane and other amine borane complexes. In particular, we will discuss the materials aspects and role of transition metal and other catalysts in facilitating hydrogen release as well as the reaction mechanisms involved. Furthermore, we will consider the conditions under which, in addition to hydrogen, other species such as borazine, monomeric aminoborane, and diborane, etc. that have adverse effect on the PEMFC operation do evolve. The review includes our own new data obtained using in situ 11B-NMR spectroscopy and other techniques as well other researchers.

4:40 PM

A Novel Contact Element for PEM Fuel Cells: Mahmoud Abd Elhamid¹; Gayatri Vyas¹; Mark Mathias¹; Youssef Mikhail¹; ¹General Motors, Fuel Cell Activities

A novel approach has been used to reduce the contact resistance between the gas diffusion medium "GDM" and stainless steel bipolar plates in PEM fuel cells. The current approach relies on coating the GDM with a thin layer of gold. The gold was deposited on the paper using physical vapor deposition "PVD" or any other means. Through a detailed analysis, it was found that the passive oxide film on the stainless steel surface has a minimum bulk resistance and it is mainly the contact between the GDM and the passive oxide film that creates a significant contact resistance. By depositing, for example, gold, on the GDM surface, it was found that the contact resistance on the stainless steel surface with the gold coated GDM was reduced to the same values obtained when using gold coated stainless steel and a blank "uncoated" GDM.

5:05 PM

The Effects of Mechanical Forming on the Use of Clad Metals in PEM Fuel Cell Bipolar Plates: K. Scott Weil¹; Sung Tae Hong¹; Zhenguo "Gary" Yang¹; Gordon Xia¹; Jin Kim¹; ¹Pacific Northwest National Laboratory

Clad metal sheet product is currently being developed for use as bipolar plate material in polymer electrolyte membrane fuel cells (PEMFC). The concept is to incorporate a thin passivation layer, such as niobium or Ni-B, over an inexpensive mechanical support substrate, such as carbon steel, via roll bonding. The resulting material should afford the many advantages that metal interconnects have to offer, while mitigating the surface corrosion problems that typically plague many metallic bipolar plate candidate materials. In a series of out-of-stack feasibility tests, a recently developed Nb-clad steel displayed excellent promise as a potential PEMFC bipolar plate material. The next stage of development, which will be discussed in this presentation, has been to optimize the design of the material for low-cost sheet manufacture, examine the resulting formability properties as they relate to bipolar plate stamping, and investigate the subsequent corrosion properties of stamped parts under prototypic stack operating conditions.

5:30 PM

Effects of PdO Distributions over TiO2 Particles on Its Chemochromic Behaviors for Hydrogen Detection: *Nahid Mohajeri*¹; Ali T-Raissi¹; Gary Bokerman¹; Janine Captain²; Barbara Peterson³; Mary Whitten⁴; Steve Trigwell³; Cristina Berger⁴; ¹Florida Solar Energy Center; ²National Aeronautics and Space Administration; ³Arctic Slope Regional Corporation Aerospace-Kennedy Space Center; ⁴University of Central Florida

Safety is one of the major concerns associated with the use of hydrogen in industries and with a future hydrogen economy. The reasons for these concerns are that hydrogen leaks are invisible and odorless. In addition, the placing of any additives or odorants in hydrogen, such as done in natural gas, is prohibited due to stringent requirements of fuel cells for an extremely pure hydrogen source. To solve this problem, an irreversible chemochromic sensor, based on PdO/TiO2 pigments encapsulated within a silicone matrix has been developed. In this paper, the TEM studies of PdO distributions over TiO2 particles are presented and its effects on overall pigment chemochromic behavior for hydrogen leak detection will be discussed.

5:55 PM

Electrochemical Study of Cobalt Phthalocyanine/Platinum as DMFC Anodic Catalyst: Yuhao Lu¹; Ramana Reddy¹; ¹University of Alabama

A new carbon-supported Cobalt Phthalocyanine Platinum (CoPc-Pt/C) anodic catalyst for DMFC was developed by chemical deposition and heat treatment. The catalytic activity of CoPc-Pt/C for methanol oxidation reaction (MOR) was studied in the solution containing $0.5M H_2SO_4$ and 1M methanol. The polarization curves showed that CoPc-Pt/C heat-reated at higher temperatures (HT) accelerates MOR and gives a higher oxidation current than pure platinum. However, CoPc-P/C heat treated at lower temperatures exhibited negligible activity for MOR. Cyclic voltammogram results displayed a higher forward current and lower reverse current for CoPc-Pt/C (HT) than CoPt/C and Pt/C. Hence CoPc-Pt/C (HT) is more effective in oxidizing methanol to CO₂ and decreases the formation of byproduct in MOR. It can be concluded from this study that the presence of Pc and metallic Co in CoPc-Pt/C (HT) increases the electrocatalytic activity for methanol oxidation.

Materials Issues for Advanced Nuclear Systems: Material Characterization Issues

Sponsored by: The Minerals, Metals and Materials Society, TMS Structural Materials Division, TMS/ASM: Corrosion and Environmental Effects Committee, TMS/ASM: Nuclear Materials Committee *Program Organizers:* Raul Rebak, Lawrence Livermore National Laboratory; Robert Hanrahan, Los Alamos National Laboratory; Yi-Ming Pan, Southwest Research Institute

Monday PM	Room: Europe 5
February 26, 2007	Location: Dolphin Hote

Session Chairs: Robert Hanrahan, National Nuclear Security Administration; Raul Rebak, Lawrence Livermore National Laboratory

2:00 PM Introductory Comments

2:05 PM

Creep Behavior of Grain Boundary Engineered Ferritic-Martensitic Alloy T91: Gaurav Gupta¹; Gary Was¹; ¹University of Michigan

Ferritic-martensitic (F-M) alloys are expected to play a major role as structural components in Generation IV systems, where their application at high temperature is limited by loss of strength. The focus of this investigation is to understand the role of grain boundary engineering on the creep resistance of F-M alloy T91. Grain boundary engineered T91 has exhibited improved creep strength at 500-600°C in argon environment. Deterioration of creep strength is accompanied by the loss of dislocation density and coarsening of precipitates





and subgrains. Reduced coarsening of subgrains and precipitates was observed in the coincident site lattice (CSL)-enhanced condition as compared to the asreceived (AR) condition after creep tests. The role of misorientation angle of subgrain boundaries as sources and sinks for dislocations is evaluated for its effect on creep strength. The effectiveness of CSL-enhancement in creep resistance of T91 will be presented and discussed.

2:25 PM

An Analytical Model for the Amoeba Effect in UO₂Fuel Pellets: Yong Choi¹; *Jong Lee*²; ¹Sun Moon University; ²Michigan Technological University

Significant temperature gradients are present across the fuel particles when a nuclear reactor is producing power. If local temperatures are sufficiently high, nuclear fuel kernels can migrate up the thermal gradient. During this process, the barrier retaining fission product is progressively damaged. The damage in turn can lead to complete failure of the coating system. This phenomenon is called the Amoeba effect. The Amoeba effect is analyzed in terms of an interactive transport phenomenon between the solid-state diffusion of oxygen ions and the flow of CO gas molecules. For mathematical simplicity, a cylindrically-shaped kernel is assumed to treat the flow behavior of CO gas molecules through the buffer layer packed with pyrolytic carbon atoms. The results show that not only a concentration gradient in oxygen ions but also a temperature gradient with a negative heat of transport for oxygen ions can cause the Amoeba effect in UO, fuel particles.

2:45 PM

Effect of Microstructural Heterogeneity on Stress Variability in ZrN Pellets: *Manuel Parra Garcia*¹; Ajit Batwal¹; Pedro Peralta¹; ¹Arizona State University

Two-dimensional finite element models based on actual pellet microstructure can provide valuable information on effects of porosity and local density variations on mechanical behavior of actual fuels. Simplified 2-D models based on the actual microstructure of sintered ZrN pellets, surrogate for actinide nitrides, sintered at 1300C and 1600C in Argon have been fully formulated in order to determine the overall mechanical response and its variability due to microstructural heterogeneity. The 2-D models created fully account for variability in grain, pore and phase shape and size, as well as the orientation of individual grains; this makes it possible to include effects of anisotropy on the mechanical behavior of sintered nitride fuels. The variability on the stresses was studied to examine possible correlations between microstructure and local fracture. Results indicate that pore shape and size, along with crystallographic texture, can affect the overall elastic constants as a function of direction.

3:05 PM

In-Situ Neutron-Diffraction Measurements of Intergranular Strains in a Zircaloy-4 Alloy: *Elena Garlea*¹; Hahn Choo¹; Peter Liaw¹; Edward Oliver²; Javier Santisteban²; Camden Hubbard³; ¹University of Tennessee; ²ISIS, Rutherford Appleton Laboratory; ³Oak Ridge National Laboratory

The evolution of intergranular strains in a hexagonal-close-packed Zircaloy-4 was investigated in-situ, using neutron diffraction. First, a series of uniaxial tensile loads was applied to round-bar tensile specimens up to 500 MPa and the intergranular (hkl-specific) strains, parallel and perpendicular to the loading direction, were studied. The results provide a fundamental understanding of the anisotropic elastic-plastic deformation of the zirconium alloy under applied stresses at the microscopic length scale. Second, spatially-resolved internal-strain mapping was performed on a fatigue pre-cracked compacttension specimens using in-situ neutron diffraction under applied loads of 667 and 4,444 N, to determine the in-plane and through-thickness lattice-strain profiles around the crack tip. An increase in elastic lattice strains near the crack tip was observed with the increase in the applied stresses. Finally, the localized stress distribution near the crack tip in a compact-tension specimen will be discussed in the context of the elastic-plastic anisotropy.

3:25 PM

The Mechanism of Zr and Hf in Reducing Radiation-Induced Segregation in 316 Stainless Steel: Micah Hackett¹; Gary Was¹; ¹University of Michigan

The addition of oversized solutes has the potential to reduce the effects of radiation-induced segregation (RIS) in austenitic alloys. RIS has been implicated as one of several factors in enhancing stress corrosion cracking (SCC) under irradiation, so oversized solute additions could promote SCC resistance. Zr or Hf were added to 316 steels and then irradiated with 3 MeV protons at temperatures of 400 and 500°C to doses between 3 - 10 dpa. Samples were analyzed in HR-STEM to measure the grain boundary RIS for each dose and temperature. Zr additions reduced the amount of RIS at low doses, but the effect disappeared by higher doses, while Hf appeared to have only a small effect on RIS even at low dose. Resistance to RIS is believed to be due to vacancy trapping which is analyzed by kinetic rate-theory modeling.

3:45 PM Break

4:05 PM

Microstructure Evolution during Recrystallization of MoNiCr Alloy: Libor Kraus¹; Jozef Zrnik¹; ¹COMTES FHT Sro

This research provides an attempt to achieve uniform grain structure by recrystallization process from different hot and cold-working conditions followed by various annealing in NiMoCr alloy. The different structure would result in high temperature mechanical properties such as ductility, fatigue, and creep strength. The microstructural changes results from all tested programs were investigated by an optical microscope. The results showed the uniformity of the recrystallized structure strongly relating to the amount of reduction during hot working and period of annealing time. It was found that the uniformity of recrystallized structure increased with a higher amount of deformation and longer annealing time. Furthermore, the results illustrated that the recrystallized structure on the surface layer was finer than the interior of the sample. This could be due to the recrystallization occurring close to the specimen surface, which was influenced by a much higher degree of deformation and heat lost.

4:25 PM

Corrosion Behavior of Alloy 617 in Impure Helium Environment: *Deepak Kumar*¹; Gary Was¹; ¹University of Michigan

The reactive impurities, H2, H2O, CO, CO2 and CH4 in the coolant helium in the very high temperature gas reactor (VHTR) can cause oxidation, carburization and decarburization of the metallic components. A simplified helium gas chemistry with only CO and CO2 (ppm levels) was selected for corrosion experiments with alloy 617 at 900, 950 and 1000°C. Corrosion behavior was studied as a function of oxidation and carburization potentials, which are controlled by the partial pressure ratio of (CO)/(CO2). Corrosion coupons were exposed up to 1000 hrs in a helium flow system built to control the impurity levels throughout the entire exposure. Corrosion kinetics, measured by weight change, and activation energy are coupled with analysis of the structure and composition of the oxide to determine the corrosion mechanism.

4:45 PM

Strain Hardening and Plastic Instability in Structural Alloys for Advanced Nuclear Systems: Xianglin Wu¹; Xiao Pan¹; James Stubbins¹; ¹University of Illinois at Urbana-Champaign

Austenitic stainless steel has been widely used as structure materials in current light water reactors and continuing of interest in advanced nuclear systems. The flow localization process is particularly troublesome for the materials exposed in high fluence irradiation and intermediate temperature environments. Recent work shows that this process can be characterized by a critical stress: necking always occurs at the same value of true stress regardless of the level of irradiation hardening. In several FCC materials, twinning, particularly for materials with lower stacking fault energies controls the large-strain deformation processes. High work-hardening is related to the stacking fault energy (SFE) of the material and the magnitude of SFE controls the ease of cross-slip and thus, different deformation mechanisms can be activated at different stages of deformation. The competing mechanism between the mechanical twinning and dislocation-based planar slip is examined by the electron backscattered diffraction.

5:05 PM

Synchrotron X-Rays for Microstructural Investigations of Advanced Reactor Materials: *Wolfgang Hoffelner*¹; Annick Froideval¹; Manuel Pouchon¹; Jiachao Chen¹; Maria Samaras¹; ¹Paul Scherrer Institute

X-rays from synchrotron beamlines provide a powerful tool for materials analyses. Particularly under conditions where long term materials degradation under complex loading conditions (e.g. temperature, irradiation, stress) become important synchrotron X-rays can help to improve lifetime assessments. The paper summarizes recent results on materials for advanced GenIV reactors.



Oxide dispersion strengthened ferritic steels, nano-crystalline zircaloy and FeCr model alloys were taken as examples. Properties of yttria dispersoids in differently pre-treated PM2000 were studied with EXAFS. Magnetic properties of FeCr model alloys were analyzed for experimental validation of multscale modeling results. The significance of the use of magnetic interatomic potentials for different FeCr alloys is of particular interest.

5:25 PM

Stable Nanoclusters in MA/ODS Ferritic Alloys: *Michael Miller*¹; David Hoelzer¹; James Bentley¹; C. L. Fu¹; ¹Oak Ridge National Laboratory

Advanced oxide dispersion strengthened (ODS) ferritic alloys containing high number densities of nanoclusters are attractive structural materials for advanced nuclear energy concepts because of their increased creep performance and tolerance to neutron irradiation damage. Microstructural characterization with the local electrode atom probe and spectrum imaging in the transmission electron microscope together with first principle calculations have established that 2-4-nm-diameter Ti-, Y- and O-enriched nanoclusters are stable up to at least 0.9 of the melting point of the alloy. Preliminary experiments indicate that these nanoclusters appear to be stable under irradiation. These alloys are attractive for fusion reactor applications because of their potential for higher operating temperatures. The dispersed oxide particles also provide a method to trap point defects and helium. Research at the Oak Ridge National Laboratory SHaRE User Facility was sponsored by the Office of Basic Energy Sciences, U.S. Department of Energy, under contract DE-AC05-00OR22725 with UT-Battelle, LLC.

Materials Processing and Manufacturing Division Symposium: Mechanics and Materials Modeling and Materials Design Methodologies, in the Honor of Dr. Craig Hartley's 40 Years of Contributions to the Field of Mechanics and Materials Science: Homogenization/Constitutive Behavior I

Sponsored by: The Minerals, Metals and Materials Society, TMS Materials Processing and Manufacturing Division, TMS: Shaping and Forming Committee, TMS/ASM: Mechanical Behavior of Materials Committee *Program Organizers:* Brent Adams, Brigham Young University; Hamid Garmestani, Georgia Institute of Technology

Monday PM	Room: Northern A1
February 26, 2007	Location: Dolphin Hotel

Session Chairs: Anthony Rollett, Carnegie Mellon University; Nasr Ghoniem, University of California

2:00 PM

A Micromechanical Continuum Model for the Tensile Behavior of Shape Memory Metal Nanowires: Wuwei Liang¹; *Min Zhou*¹; ¹Georgia Institute of Technology

We have previously reported the discovery and characterization of a novel shape memory behavior in metal nanowires. This behavior only exists at the nanoscale and is associated with a reversible lattice reorientation. A micromechanical continuum model for the unique tensile behavior of these wires due to lattice reorientation is presented. Specifically, the lattice reorientation process is decomposed into two parts: a reversible smooth transition between phase-equilibrium states superimposed with an irreversible, dissipative twin boundary propagation process. The reversible part is modeled within the framework of strain energy functions with multiple local minima. The irreversible, dissipative nature of the twin boundary propagation is due to the ruggedness of strain energy curves associated with dislocation nucleation, gliding, and annihilation. The model captures the major characteristics of the unique behavior due to lattice reorientation and accounts for the size and temperature effects, yielding results in excellent agreement with the molecular dynamics simulation results.

2:25 PM

A Non-Linear Intermediate Viscoplastic Model for Large Deformation Behaviour and Texture Evolution in Polycrystals: Said Ahzi¹; ¹University Louis Pästeur

The aim of this work is to propose a new non linear intermediate model for large viscoplastic deformations that could predict the texture transition and stress-strain behaviour in a range that spans from the upper bound (Taylor) to the lower bound (Sachs) estimates. In this model, we introduced a single parameter as a weight function to formulate the proposed intermediate approach which combines both the lower and the upper bound estimates. For the applications, we focus on the FCC polycrystals with an initially random texture and subject to different loading conditions. The results for texture evolution show that a transition between the copper type and brass type textures can be obtained by the proposed intermediate model. The predicted stress-strain curves and textures will be shown and discussed shown in comparison to those of the viscoplastic Taylor, Sachs an self-consistent models.

2:50 PM

Crystal Plasticity Models with Multi-Time Scaling for Cyclic Deformation of Polycrystalline Metals: Somnath Ghosh¹; Sivom Manchiraju¹; ¹Ohio State University

The mechanical behavior and fatigue failure response are governed by microstructural features that include morphological and crystallographic characteristics. This paper will discuss methods of creating microstructural image-based finite element models for simulating the behavior of polycrystalline materials subjected to cyclic loading. It will present a methodology for creating a FE model of the polycrystalline microstructure, accounting for both morphology and crystallographic orientations. The microstructure simulation process involves serial sectioning together with orientation imaging microscopy. This is followed by a CAD based grain generation process to construct the 3D polycrystalline microstructure. Subsequently FEM analysis of the polycrystalline microstructure is done for cyclic loading for a large number of cycles. A multi-time scaling formulation involving a long time scale problem for describing the smooth averaged solution and an oscillatory portion will be conducted.

3:15 PM

Cyclic Behaviour of High-Density Polyethylene Used in Pipe Manufacturing: S. Sezer¹; Senol Ataoglu¹; A. Gulluoglu¹; ¹Istanbul Technical University

High-density polyethylene has become the crucial material for the piping industry, owing to its physical and chemical properties. However, though the properties of HDPE are sufficient for underground piping applications, one must still pay considerable attention to the design steps and conditions. One of the most relevant specifications of a product for underground application is its fatigue properties. This is straightforward from the fact that most of the underground piping follows the course of the streets in cities. This means that the pipes will undergo serious cyclic stresses of erratic nature. Therefore it is crucial for an engineer to understand and reproduce the conditions the pipe will be subjected to and comprehend and express the results in a mathematical fashion. This research aims to meet these requirements and provide a successful mathematical model. Thus, a square dynamic stress test, can be extended to other different types of loadings, was conducted on samples, on a cyclic loading mechanism. Then a mathematical model was derived and simulated using appropriate software. The simulation results are compared with the experimental results. The outcome is impressive in that the simulation results are mostly successful in predicting the actual behaviour of the sample under cyclic stresses.

3:40 PM

Dislocation Modeling of Localized Plasticity in Persistent Slip Bands: *Nasr Ghoniem*¹; Hael Mughrabi²; Jaafar El-Awady; ¹University of California; ²University of Erlangen

We present models of localized plastic deformation inside Persistent Slip Band channels, and for the deformation of the channel walls. First, we investigate the interaction between screw dislocations as they pass one another inside channel walls in copper. The model shows the mechanims of dislocation bowing, dipole formation and binding, and finally dipole destruction as screw dislocations pass one another. The mechanism of (dipole passing) is assessed and interpreted in terms of the fatigue saturation stress. We present results for the effects of the wall dipole structure on the dipole passing mechanism,

LEARN • NETWORK • ADVANCE



taking into consideration wall destabilization and penetration of expanding loops from one PSB cell to the next. PSB walls are generally rigid, but they maz emit dislocation loops into adjacent cells. We present studies for the conditions appropriate for the limited plasticitz of the walls themselves as they act as sources of glide dislocations.

4:05 PM

Effect of the Grain Boundary Character Distribution on Yield Strength: Bradley Fromm¹; Brent Adams¹; ¹Brigham Young University

During the past two decades new insights into the role of grain boundary character in relation to grain boundary strength have emerged. TEM studies reveal the importance of crystallographic misorientation and boundary inclination, as well as local elastic properties, in the selection of dislocation slip transmission at grain boundaries. Ex-situ studies by fine-scale Orientation Imaging Microscopy and nano-indentation have revealed complex spatial (excess and defect) patterns of lattice curvature and strength near grain boundaries at moderate levels of plastic strain. In this paper the focus is on how this recent experimental evidence can be incorporated into new models for the yield strength of single-phase polycrystals. Models that use the Grain Boundary Character Distribution, in connection with the physics supported by the experimental evidence, are introduced.

4:30 PM

Experimental Micromechanics Study of Lamellar TiAl: *Fu-pen Chiang*¹; Gunes Uzer¹; Yi Ding¹; Andrew H. Rosenberger²; ¹Stony Brook University; ²Air Force Research Laboratory Materials and Manufacturing Directorate

A unique micro-scale full field deformation measurement technique is employed to map the deformation mechanism of lamellar TiAl with grain size of about 450 μ m. We find the size effect on the determination of mechanical properties. The strain distribution inside the grain is highly heterogeneous. The grain boundary is much stiffer than the interior of the grain. We also observe several interesting phenomena of the material when a crack is present. Crack speed tends to slow down when crack approaches a grain boundary. Within a grain the slowest propagation speed is when the lamellar layers are perpendicular to the crack. Crack may jump across a grain boundary and its propagation direction can be predicted by the strain concentration congregated near the grain boundary. By mapping the deformation field surrounding the crack tip, we can evaluate the mode mixity from the speckle results at different stages of crack propagation.

4:55 PM

Exploration of the Effect of Polycrystal Microstructure on Strain Localization with a Fourier Transform Viscoplastic Model: Anthony Rollett¹; Sukbin Lee¹; Stephen Sintay¹; Ricardo Lebensohn²; ¹Carnegie Mellon University; ²Los Alamos National Laboratory

The application of a novel model of viscoplastic deformation is reported. The model discretizes the strain-strain behavior on a regular grid and employs Fourier transforms. Two examples are given. The first takes as input microstructures derived from a liquid phase sintering model that represent a metal matrix composite. The main interest is in the concentration of strain (rate) in the softer matrix phase. The second example models single-phase aerospace aluminum alloys with constituent particles. The input for this model is derived from statistically reconstructed 3D microstructures based on orthogonal EBSD cross-sections. In this case the focus is on quantifying the extent to which strain localizes at particles as a precursor to particle cracking that in turn leads to fatigue crack initiation. Such an approach permits the materials engineer to explore materials design variations and their effects on mechanical properties.

5:20 PM

Fatigue Life Variability: Modeling, Simulation, and Application: *Kwai Chan*¹; Michael Enright¹; ¹Southwest Research Institute

Variations in microstructure can lead to significant variability in fatigue life due to differences in resistance against crack initiation and growth at various levels of microstructural features. In this paper, a fatigue life-prediction methodology, developed under the AFOSR MEANS program, for predicting fatigue life variability originated from microstructural variations is summarized with illustrative examples for Ti-6Al-4V. First, a series of microstructurebased fatigue crack initiation and growth models are summarized and important random variables describing the relevant microstructural variations are highlighted. A probabilistic framework for simulating microstructural variations is presented. The predicting fatigue life scatter is then utilized in conjunction with a probabilistic code, named DARWIN®, for predicting the probability of failure of a Ti component. Finally, limitations and possible future directions for extending this methodology are discussed.

Materials Processing Fundamentals: Process Modeling

Technical Program

Sponsored by: The Minerals, Metals and Materials Society, TMS Extraction and Processing Division, TMS: Process Technology and Modeling Committee, TMS: EMPMD Council, TMS: EPD Council

Program Organizer: Princewill Anyalebechi, Grand Valley State University

Monday PM	Room: Northern A2
February 26, 2007	Location: Dolphin Hotel

Session Chair: Adam Powell, Veryst Engineering LLC

2:00 PM

CFD Modelling of Heat Transfer in Supersonic Nozzles for Magnesium Production: *Peter Witt*¹; Hasan Khan¹; Geoff Brooks²; ¹CSIRO Minerals; ²Swinburne University of Technology

An important step in developing new processes is scaling between laboratory operation, pilot scale and commercial scale plant. Scaling heat transfer is non-trivial and computational fluid dynamics allows prediction of scaling effects and aids understanding of the process. CFD modelling has been undertaken of a process being developed by CSIRO for the carbothermic reduction of magnesia. This work outlines CFD validation of heat transfer predictions between a supersonic gas stream and the nozzle wall and the impingement of the supersonic jet onto a collector plate normal to the flow. Heat transfer to the nozzle wall is well predicted by the k- ω turbulence model. Predictions of heat transfer for the impinging jet are less satisfactory with significant variation in heat flux predictions with changes in geometry, mesh resolution and turbulence model. For the later case the shear stress transport (SST) model gave the best predictions of heat flux and Nusselt number.

2:15 PM

Numerical Modeling of 3-Dimensional Thin Slab Casting Process with EMBR(Electro-Magnetic Brake): *Kee-Hyeon Cho¹*; Byung-Moon Kim²; ¹Research Institute of Industrial Science and Technology; ²GyeongBuk Regional Stragetic Agency for Innovation

The purpose of this study is to develop a coupled turbulent fluid flow and solidification model for numerical analysis of thin slab casting with Electromagnetic brake(EMBR) system. The enthalpy-porosity relation was employed to suppress the velocity within a mushy region. The electro-magnetic field was described by Maxwell equations. The application of EMBR to the mold region results in the decrease of the transfer of superheat to the narrow face, the increase of temperature in free surface region and most liquid of submold region, and the higher temperature gradient near the solidifying shell. The increasing magnetic flux density effects mainly to the surface temperature of the solidifying shell of narrow face, hardly to the one of wide face. It is shown that in case of EMBR a thicker solidifying shell is obtained at the narrow face of the thin slab.

2:30 PM

Process Design of Alloys to Achieve Desired Properties by Inverse Materials Design: *Dongsheng Li*¹; Hamid Garmestani¹; ¹Georgia Institute of Technology

Inverse materials design is used in process design on mechanical deformation of polycrystalline materials. This work studies how to predict the mechanical response and microstructure evolution of polycrystalline materials during large plastic deformation using statistical continuum mechanics. The crystal orientation distribution is presented by an n-point probability function that describes the corresponding probability functions. A Green's function was introduced to calculate the equations of equilibrium for the constitutive law in the polycrystalline materials. To find out optimized process to satisfy properties requirement, the relationship among process, microstructure and



properties are investigated in the framework of an inverse materials design. An example of application in titanium alloy is used to demonstrate how the optimized properties can be achieved by process design.

2:45 PM

Spout Formation in a Gas-Stirred Ladle – Experimental Results: *Krishnakumar Krishnapisharody*¹; Gordon Irons¹; ¹Steel Research Centre, McMaster University

Model experiments simulating the spout formation in a gas-stirred ladle were performed with and without a slag-simulating phase (oil) above the bulk liquid (water). The height and width of the spout region were obtained by means of a digital video technique over a wide range of operating conditions. A dimensional analysis of the experimental data was employed to correlate the characteristic dimensions of the spout region to the operating variables of the system and the predicted results match with the available data from other works. This analysis reveals that the ladle diameter, size and type of gas injector and physical properties of gas-liquid system do not significantly affect the spout formation. Further, the spout size information have been used to quantitatively characterize gas-liquid plumes in a companion paper.

3:00 PM

Spout Formation in a Gas-Stirred Ladle – The Key to Plume Dynamics: *Krishnakumar Krishnapisharody*¹; Gordon Irons¹; ¹Steel Research Centre, McMaster University

Experimental data on the characteristic spout dimensions and the widths of gas-liquid plumes in vessels simulating Argon-stirred Ladles have been combined to derive a macroscopic model for unconfined two-phase plumes. The model reveals that, beyond the vicinity of the gas injector, various plume parameters in different gas-liquid systems can be expressed in an unified manner using the two variables of the system viz., the gas flow rate and the axial height. Further, expressions have been obtained for the average gas fractions and the area-averaged gas and liquid velocities in the plume. These model expressions are independent of the size of the gas injector as well as the physical properties of the gas-liquid system and thus have wider applicability.

3:15 PM

Laser Surface Modification of AISI 316L Stainless Steel with WC-Si-Ni: *D. Sastikumar*¹; A. Viswanathan¹; Kumar Harish²; A.K. Nath²; ¹National Institute of Technology; ²Raja Ramanna Centre for Advanced Technology

The study deals with laser surface modification of AISI 316L stainless steel with WC-Si-Ni (40-40-20 and 80-10-10 wt. %) under different laser processing parameters. The laser irradiated specimens are characterized by Optical and SEM micrograph, Microhardness, X-ray diffraction and chemical composition analyses. The results show the formation of a thick layer (300 μ m) over the substrate with strong adhesion when the coating composition is 40-40-20 wt. % (WC-Si-Ni). For the scan speed of 2.0 m/min. and 1.5 kW laser power, a layer with uniform thickness and smooth surface morphology is observed. The hardness is in the range of 800-900 HV. When the composition is 80-10-10 wt. %, coated materials get mixed into the substrate. The microstructure exhibits flower like dendtritic growth structure. The bonding strength between the layer and the substrate is examined by the hardness study with various loads.

3:30 PM Break

3:45 PM

Evolution of the Tecnored Process – From Pilot Plant to Industrial Scale: *Jose Noldin*¹; Jose D'Abreu²; Ian Cox³; ¹Catholic University/Tecnored; ²Catholic University; ³Tecnored

The Tecnored process is a new ironmaking technology that has been developed combining empirical and theoretical fundamentals, backed by extensive tests in a dedicated pilot-plant and with close support of universities and research centers. The campaigns in the pilot-plant focused on understand, simulate and operate the furnace using different reactor sizes including a full size modular slice of the industrial furnace, which provided real-life conditions to develop the main features of the process such as internal dimensions, thermal and gaseous profiles and melting zone formation, shape and maintenance. This paper describes the different phases of the technology development with respective goals and achievements including the construction of the first full scale industrial plant.

4:00 PM

Properties of Carbonized Corn Straw as Thermal Insulating Agent of Liquid Metal: Nan Wang¹; ¹Northeastern University

The properties of carbonized corn straw were investigated for the purpose to substitute carbonized husk as thermal insulating agent of liquid metal due to the price elevation constantly in recent years. By characterizing the properties (including chemical composition, microstructure, flow property) of the obtained corn straw carbonized under different conditions, the optimal carbonation condition was determined. The carbonized corn straw has higher fixed carbon content, lager resting angel and smaller coefficient of thermal conductivity compared to carbonized husk, and thus which is considered suitable to be used as thermal insulating agent of liquid metal. The development and application of carbonized corn straw as thermal insulating agent of liquid metal not only decrease the production cost of metallurgical industries, but also develop a newly valuable way to use corn straw that was usually used as feedstuff and burning materials in village and thus the environment could be protected.

4:15 PM

Preparation of Vanadium Thin Films by Chemical Vapor Deposition: Masakazu Mukaida¹; Misaki Ishitsuka¹; Shigeki Hara¹; Hiroyuki Suda¹; Kenji Haraya¹; ¹National Institute of Advanced Industrial Science and Technology

Vanadium-base alloys are expected as hydrogen separation materials because they have higher hydrogen permeability and good workability. In the present work, vanadium thin films were prepared on porous sintered stainless steel substrates by a chemical vapor deposition (CVD) to approach the thermal expansion coefficient of films and substrates. Organometallic compounds were used as source materials. The films were deposited under controlled conditions, which were substrate temperatures, pressures of CVD chamber and flow rates of carrier gas (Ar) for source material. The morphologies of films were observed by scanning electron microscope (SEM), and the elements in the films were investigated by energy dispersive X-ray spectroscope (EDX).

Materials Processing under the Influence of External Fields: Session II

Sponsored by: The Minerals, Metals and Materials Society, TMS: Aluminum Committee, TMS: Magnesium Committee, TMS: Solidification Committee *Program Organizers:* Qingyou Han, Oak Ridge National Laboratory; Gerard Ludtka, Oak Ridge National Laboratory; Qijie Zhai, Shanghai University

Monday PM	Room: America's Seminar
February 26, 2007	Location: Dolphin Hotel

Session Chairs: Qi-Jie Zhai, Shanghai University; Ke Han, National High Magnetic Field Laboratory

2:00 PM Introductory Comments

2:05 PM Invited

Metals Solidification under the Influence of External Fields: Research Status in Shanghai University: *Qi-Jie Zhai*¹; Yu-Lai Gao¹; ¹Shanghai University

In the present study the research status of metals solidification under the influence of external fields in Shanghai University, which is one of the main academic institutions in China, was introduced. The special self-developed equipments to produce external fields were presented. At present, many kind of external fields have been developed in Shanghai University, including ultrastrong magnetostatic field, ultrasonic, electric current pulse, pulsed magnetic field, and magneto oscillation etc. Also, the research interests in the metals solidification under external fields were systematically illuminated. Besides, the application prospect of these techniques was reviewed, especially in the metallurgy industry.

2:35 PM

Study on the Pulse Magneto Oscillation Solidification Technique and Its Mechanism for Grain Refinement: Yong-Yong Gong¹; Jin-Xian Jing¹; Zan-Qi Xia¹; Yu-Lai Gao¹; Qi-Jie Zhai¹; ¹Shanghai University

In this paper, a novel pulse magnetic field that can be effectively used for grain refinement was proposed, which was defined as Pulse Magneto

Technical Program



Oscillation (PMO). The PMO physical field possesses the advantages such as non-contacting, no melt splashing and flexibility for its application. It was found that the pure Al could be distinctly refined after treated by the self-developed PMO. Based on the "crystal rain" experiments, the mechanism for grain refinement of PMO was analyzed. It was deemed that structure refinement rooted in the fall of the heterogeneous nucleus from the mould wall under the effect of PMO.

3:00 PM

Effect of Pulsed Magnetic Field on the Solidified Structure of Pure Al Melt: *Yu-Lai Gao*¹; Qiu-Shu Li¹; Hai-Bin Li¹; Qi-Jie Zhai¹; ¹Shanghai University

A comparative study was made of the effect of pulsed magnetic field on the solidification structure of pure aluminum by employing the self-developed high voltage pulsed power source at several solidification stages. It has been shown that the solidified structure was remarkably refined with applied pulsed magnetic field during or in the overall solidification process. In contrast, no significant difference in the solidification structure of aluminum was observed also with pulsed magnetic field prior to the stage of nucleation. As a result, it was convincing that the structure refinement arises from the pulsed magnetic field at the stage of nucleation and growth, yet the incubation effect was negligible.

3:25 PM

Controlling Semiconductor Growth Using Magnetic Fields and Rotation: Baskar Ganapathysubramanian¹; Nicholas Zabaras¹; ¹Cornell University

The application of a time varying magnetic field has been shown to affect the properties of the semiconductor single crystal achieved through growth from the melt. The application of a time dependent rotation of the crucible affects the flow pattern in the melt resulting in enhanced distribution of thermal effects. We will discuss a complete three dimensional simulator of the crystal growth process in the presence of a magnetic field and imposed rotation. We will investigate the three dimensional coupled effects of an externally applied magnetic field and a time varying rotation imposed on the solidifying melt. A three dimensional optimization problem will then be posed to design the temporal variation of the magnetic field and/or the rate of rotation to achieve certain goals. These goals include maximizing the pulling rate, minimizing the thermal gradient imposed, as well as controlling the shape of the melt-solid interface.

3:50 PM Break

4:00 PM Invited

High Magnetic Field Influences on Fabrication of Materials with Magnetic Phases: Ke Han¹; Bao Zhi Cui¹; ¹National High Magnetic Field Laboratory

This paper describes annealing experiment we have undertaken in a large bore high field magnet. The magnet annealing temperatures were carefully selected so that a reaction occurs at the annealing temperature and one or more components are ferro-magnetic phase at the chosen temperatures. Magnetic field has an impact on both nucleation and growth of the phases formed during the reactions. The paper reviews the effects and relevant mechanism of magnetic annealing on microstructures, crystallographic textures, exchange coupling, magnetic anisotropy, and hard magnetic properties for magnet materials. Magnetic annealing was found to promote the phase transformation and increases the nucleation sites for the formation of magnetic phases so that refinement of the microstructure is achieved. Magnetic annealing was also found to manipulate the texture of the materials. The refinement of the microstructure and the optimization of the texture result in the improvements of magnetic properties.

4:30 PM

Synthesis of Acicular Magnetite Using Coprecipitation Method under Magnetic Field: Yang XiYun¹; Chen Baizhen¹; Xu Hui¹; Shi Xichang¹; ¹Central South University

Acicular magnetite was synthesized by coprecipitation of ferrous and ferric mixed salt solution with urea in the temperature range from 90-95°C in reflux condition for 12h. The magnetite particles were characterized by X-ray powder diffraction, scanning electron microscopy and magnetization measurements. XRD showed that the mole ratio of Fe3+/Fe2+ and concentration of urea have great effects on the composition of the product. SEM showed that the type of anion and surfactant have not been able to obviously affect the shape of magnetite product. In contrary, the magnetic field has remarkable effect on the

shape of magnetite product. The particles grow along its easy-magnetization to form acicular magnetite. The acicular magnetite has a saturation magnetization of 85emu/g and a coercivity of 380 Oe.

4:55 PM

Rapid Ceramic Processing by Field-Assisted Sintering Technique: Dat Quach¹; Veaceslav Zestrea²; Vladimir Kodash¹; Gregory Toguyeni³; Joanna Groza¹; ¹University of California; ²Academy of Sciences of Moldova; ³Ecole Polytechnique de l'Universite de Nantes

The novel field-assisted sintering technique (FAST) has been successfully used to form and consolidate a number of chalcogenide spinels and tialite. For the first time the ternary magnetic sulfide compound FeCr₂S₄ was prepared from a mixture of commercially available FeS and Cr₂S₃ powders using FAST. A one-step complete reaction sintering to form FeCr₂S₄ was done at 1000°C in 10 minutes. ZnCr₂S₄ and some ternary magnetic oxide compounds (CoAl₂O₄ and Co₂AlO₄) were also prepared using the same technique. The high homogeneity of the composition of the prepared samples was confirmed by XRD analysis. In addition the hard-to-form-and-sinter tialite, Al₂TiO₅, can also be FAST-synthesized from regular Al₂O₃ and TiO₂ powders. Compared to conventional methods where the same reaction sintering step may take hours or days, current FAST-reaction sintering experiments demonstrate the ability of this novel technique to rapidly form and consolidate different ceramic compounds.

5:20 PM

Computer-Aided Processing of Advanced Dielectric Composites via Self-Assembly of Arbitrary-Shaped Ferro-Colloidal Particles in External Field: *Yu Wang*¹; ¹Virginia Tech

Ferro-colloidal processing under external field is investigated for fabrication of advanced dielectric composites by using computer modeling and simulation. Our study focuses on the self-assembly of dipolar interacting particles, its effects on composite microstructure and dielectric properties, and the underlying mechanisms. Computational model is developed based on diffuse interface field approach. It explicitly treats particle microstructure and its evolution during self-assembly and accounts for accurate long-range and short-range interaction forces among multiple particles of arbitrary shapes and sizes (the conventional point-dipole approximation is not applicable in particle self-assembly process because of non-spherical particle shapes and small interparticle distances). External field is used to tune the self-assembling forces and control particle microstructures. The model takes into account the particle size and shape polydispersities and their effects on microstructure control and property optimization. As application example, computer-aided design and processing of ceramic-filler polymer-matrix nanocomposites for high-energydensity capacitors is presented.

5:45 PM

Magnetic Alignment of Nanotubes: *Ben Wang*¹; Richard Liang¹; Chuck Zhang¹; ¹Florida A&M University-Florida State University, Engineering College

We will present two separate but related projects, both involving the use of magnetic forces to align nanotubes at Florida Advanced Center for Composite Technologies: (1) alignment of nanotubes in aqueous solution before the formation of BuckyPapers, and (2) alignment of nanotubes in epoxy resin. BuckyPapers are thin films (about 15 microns in thickness) of nanotubes held together by their own interdigitation and van der Waals forces. In the case where the application calls for individual nanotubes being "organized" in the same direction, the nanotubes are aligned in a magnetic field before the BuckyPaper is formed. With the advances of carbon fibers as composite reinforcements, the in-plane strength of composite laminates has demonstrated substantial improvement. The shear strength, however, has shown little progress. We developed a process by which nanotubes are aligned in the z direction while in epoxy resin, which is simultaneously reinforced with regular carbon fibers.

Microstructural Processes in Irradiated Materials: Irradiation Effects in Ceramics

Sponsored by: The Minerals, Metals and Materials Society, TMS Structural Materials Division, TMS/ASM: Nuclear Materials Committee *Program Organizers:* Charlotte Becquart, University of Lille; Gary Was, University of Michigan; Brian Wirth, University of California

Monday PM	Room: Europe 8
February 26, 2007	Location: Dolphin Hotel

Session Chairs: Steven Zinkle, Oak Ridge National Laboratory; Lance Snead, Oak Ridge National Laboratory

2:00 PM

Effect of Ionizing Radiation on Defect Production and Retention in Ceramics: *Steven Zinkle*¹; ¹Oak Ridge National Laboratory

Various ceramic specimens (including SiC, Al2O3, MgAl2O4, Si3N4 and AlN) were irradiated with ion beams ranging from 1 MeV H+ to 710 MeV Bi+. The specimens were subsequently examined in either plan view or crosssection using transmission electron microscopy. The oxides and Si3N4 were found to be susceptible to ionization-induced diffusion. In these materials, high fluxes of ionizing radiation produced coarsening of dislocation loops and cavities, and inhibited low-temperature amorphization. At high electronic stopping powers, displacement damage was produced in the ion tracks in the oxides and Si3N4 that could not be attributed to normal elastic collision processes. AlN and SiC showed the highest resistance to ionizing radiation, with regard to both ionization-induced diffusion and swift-heavy-ion-track displacement damage.

2:20 PM

Thermal Properties of MgO and Nd₂**Zr**₂O₇ **for Inert Matrix Fuel Applications by MD Simulation**: *Priyank Shukla*¹; Taku Watanabe¹; Juan Nino¹; Simon Phillpot¹; James Tulenko¹; ¹University of Florida

The thermal-transport properties are a key performance metric for any potential candidate of Inert Matrix Fuel (IMF) that might be an alternative to conventional UO₂. Recently, an MgO-pyrochlore cercer composite has been proposed as a potential inert matrix. We have performed molecular dynamics simulations of the thermal properties of the pyrochlore $Nd_2Zr_2O_7$ (NDZ). Our results for thermal expansion coefficient and conductivity values agree well with experiment. The thermal conductivity of NDZ is 2.09W/m-K at 1473K, compared to 2.25 W/m-K for UO₂. Similarly, simulations on MgO gave a thermal expansion of 12.2x10⁻⁶/K, which compares well with the experimental value of 13.5×10^{-6} /K. The simulated thermal conductivity of 8.2 W/m-K at 1473K is only two-thirds of the experimental value of 12W/m-K, a discrepancy whose origin we are exploring. In addition, a polycrystal of MgO has been generated, and its thermal transport properties are determined. This work was funded by DOE-NERI Award DE-FC07-05ID14649.

2:40 PM

Changes in the Mechanical Properties of Irradiated Ceramics Investigated by Nanoindentation and Computer Simulation: Asta Richter¹; *Roger Smith*²; Steven Kenny²; Bodo Wolf³; James Valdez⁴; Kurt Sickafus⁴; Ismail Gheewala²; ¹University of Applied Sciences Wildau; ²Loughborough University; ³University of Applied Sciences Lausitz; ⁴Los Alamos National Laboratory

This paper presents a nanoindentation study of both magnesia and yttrium stabilised zirconium oxide before and after Ar irradiation up to a fluence of 10^{20} Ar⁺ m⁻². The materials are compared both before and after irradiation using multi-cycling nanoindentation indicating an increase in hardness but not indentation modulus with increasing dose. The results also indicate that radiation induced defect pinning decreases the dislocation mobility to increase hardness and cause the material to become less brittle. Simulation studies confirm the experimental observation for magnesia that slip occurs in the (110) planes which can result in piling up patterns after indentation which are dependent on crystal orientation.

3:00 PM

Phase Transformation of Graphite Irradiated by High-Intensity Pulsed Ion Beams: X. Han¹; S. Miao¹; X. Zhu¹; *M. Lei*¹; ¹Dalian University of Technology

The microstructure and morphology of graphite irradiated by high-intensity pulsed ion beams (HIPIB) has been studied by varying the ion current density as 200, 350 and 1500 A/cm2 with 1-5 shots. Phase transformation from graphite to diamond-like-carbon (DLC) on HIPIB-irradiated graphite was confirmed by Raman analysis where a typical broadened asymmetric peak appeared in the range of 1100-1700 cm-1. Formation of DLC on the irradiated graphite strongly depended on the HIPIB parameters and preferably took place at 350 A/cm2 up to 5 shots. Numerical simulation of ablation process was performed to explore the transformation mechanism of DLC from graphite. The calculation showed a different temperature profile or ablation depth of graphite irradiated at 350 A/cm2, as compared to that of 200 and 1500 A/cm2. The experimental and numerical results indicate that a proper temperature and pressure front repetitively created in the top layer of ablated graphite facilitates the phase transformation.

3:20 PM

Formation and Distribution of Defect Clusters in SrTiO₃ Bi-Crystals Implanted with Xe Ions: *Minghui Song*¹; Xingjian Guo¹; Nobuo Ishikawa¹; Masaki Takeguchi¹; Kazutaka Mitsuishi¹; Miyoko Tanaka¹; Kazuo Furuya¹; ¹National Institute for Materials Science

Formation and distribution of defect clusters in SrTiO₃ bi-crystals implanted with 100 keV Xe ions, and behavior of the implanted Xe ions near the boundary of the bi-crystal were studied with transmission electron microscopy (TEM). The ion implantation was conducted in a transmission electron microscope (TEM) at 673 K. TEM observation was performed in [001] direction, which was parallel to the boundary. Bubble-like contrasts in nanometer scale were observed in the ion implanted samples. During an annealing for 10800 s. at 1073 K, the bubbles grew to about 5 nm with sphere like shapes. It was found that there were fewer bubbles in a band in width of about 10 nm near the bi-crystal boundary than in the area far away from the boundary. Detailed results on the formation and distribution of bubbles, and their relation to the bi-crystal boundary are reported and discussed.

3:40 PM Break

3:55 PM

Defect Microstructures in Silicon Carbide after Irradiation Creep Deformation at Elevated Temperatures: *Yutai Katoh*¹; Sosuke Kondo¹; Lance Snead¹; ¹Oak Ridge National Laboratory

Creep deformation and rupture are among the major failure modes of concern for high temperature structural materials. On the other hand, limited creep deformation may be favored in structural ceramics and composites, as it mitigates internal stress. In nuclear environments, irradiation-induced creep is added to thermally activated creep deformation. In many cases, irradiation creep is caused by the preferred nucleation of planar defect clusters and/or preferred absorption of supersaturated point defects at edge dislocations. Recently, irradiation creep of chemically vapor-deposited silicon carbide was studied by the authors employing the bend stress relaxation method to an inpile experiment. In this experiment, thin strip samples of silicon carbide were neutron-irradiated under elastic constraint at $450 - 1000^{\circ}$ C. This paper reports the result of microstructural examination of the crept samples.

4:15 PM

Properties of Structures, Host Atoms and Implanted Species in Ion Irradiated SiC: *Weilin Jiang*¹; Yanwen Zhang¹; Vaithiyalingam Shutthanandan¹; Mark Engelhard¹; William Weber¹; Suntharampillai Thevuthasan¹; Exarhos Gregory¹; Jie Lian²; Rodney Ewing²; ¹Pacific Northwest National Laboratory; ²University of Michigan

Single crystal 6H-SiC wafers were fully amorphized using ion irradiation. The microstructural evolution and depth profiles of the host atoms and implanted species in the amorphized SiC have been studied using a variety of experimental methods. Neither Si nor C sublattice exhibits a significant mass transport by diffusion during the ion irradiation at room temperature. Au and Ag implants in SiC are found to be immobile at high temperatures. The Si-Si bonds are not observed on the Ar⁺ sputtered SiC surface, but they exist in the bulk amorphized SiC. The absence of the Si-Si bonds is primarily due to the



preferential sputtering. In addition, thermal behavior of the implanted ¹³C in SiC also has been studied. Significant ¹³C diffusion in the amorphized SiC does not occur up to 1000 K. The results suggest that the implanted ¹³C atoms are readily trapped in the amorphized SiC.

4:35 PM

Microstructural Defects in Neutron Irradiated SiC at Very High Temperatures: Sosuke Kondo¹; Yutai Katoh¹; Lance Snead¹; ¹Oak Ridge National Laboratory

Swelling and thermo-physical property changes have been of major interest for silicon carbide (SiC) for applications in radiation services. It is well understood that the amorphous phase induced by low-temperature irradiation $(T_{irr} \sim 200^{\circ}\text{C})$ causes a significant volume expansion. In the medium temperature range of ~1000°C, saturation swelling presumably attributed to point defect / cluster accumulation has been observed. There are recent evidences that irradiation-induced void development occurs in SiC at higher temperatures, which may lead to unstable swelling as dose accumulates. However, very limited knowledge has been obtained regarding the void formation in SiC, such as temperature / fluence dependence, and influence of the initial microstructure. In this study, chemically vapor-deposited SiC samples were examined following neutron irradiation to the highest dose of ~1x10²⁶ n/m² (*E*>0.1MeV) at temperatures 600-1600°C in HFIR, Oak Ridge National Laboratory. We will report the initial result of transmission electron microscopy work, and discuss primarily void swelling.

4:55 PM

Influence of Microstructure on Thermal Defect Resistance of SiC Neutron Irradiated up to 1600°C: *Lance Snead*¹; Yutai Katoh¹; Sosuke Kondo¹; ¹Oak Ridge National Laboratory

High purity silicon carbide has been neutron irradiated from 200 to 1600°C over a range of fluences. This temperature range spans the temperature range from the critical amorphization temperature, through what is generally referred to as the point-defect swelling regime, well into the void-swelling regime. This paper will present new data on the swelling, thermal conductivity, and microstructural evolution in the void-swelling regime. Particular focus will be on the relationship between the thermal defect resistance of irradiated SiC on the as-irradiated microsctructure.

5:15 PM

The Impact of Point Defects and Clusters and on the Thermal Conductivity and Dimensional Stability of 3C-SiC: *Tjacka Bus*¹; Brian Wirth¹; Yutai Katoh²; Lance Snead²; ¹University of California, Berkeley; ²Oak Ridge National Laboratory

Silicon carbide has excellent thermal conductivity, good dimensional stability and high strength for temperatures well above 1200°C, making it a candidate structural material for advanced fission and fusion reactors. Defects introduced during manufacturing and due to radiation exposure, can significantly degrade the properties. In particular, the thermal conductivity degradation and swelling of neutron irradiated SiC are key issues which may limit its application. Recent neutron irradiation experiments suggest that the same type of defects is responsible for both swelling and loss of thermal conductivity, although the responsible defects and their evolution are not well understood. We present molecular dynamics simulations to calculate the thermal conductivity for both perfect SiC and SiC containing a variety of point defect clusters and interstitial dislocation loops by using the Green-Kubo approach. The results will be discussed in light of developing models of defect evolution under fusion relevant conditions.

Outreach Programs in Materials Science and Engineering: Outreach Programs in Industry and Government Laboratories

Sponsored by: The Minerals, Metals and Materials Society, TMS: Public and Governmental Affairs Committee

Program Organizers: Dan Thoma, Los Alamos National Laboratory; Katherine Chen, California Polytechnic State University

Monday PM	Room: Pacific Hall A
February 26, 2007	Location: Dolphin Hotel

Session Chair: Katherine Chen, California Polytechnic State University

2:00 PM Invited

Congressional Visit Days: Challenge and Opportunity for the MS&E Community: Alexander Scott¹; ¹TMS

TMS participates through the Federation of Materials Societies (FMS) in Congressional Visit Days, an advocacy program to promote federal funding for MS&E research, K-12 education and the betterment of the profession. This presentation will outline the history, purpose and practical ways for members of the MS&E Community to participate in the 2007 CVD Days. The TMS Public and Governmental Affairs Committee is the organizing group within TMS to develop our delegation, establish the message and invite the participants. A special emphasis is placed on having student members participate so they are encouraged to attend this presentation. CVD Days is a key component of TMS's advocacy program on behalf of the profession so learn how you can be a part of this vital and vibrant program.

2:30 PM Invited

Materials Camps Demonstrate Proven Success and Impact: Charles Hayes¹; Lyle Schwartz¹; ¹ASM Materials Education Foundation

ASM Materials Education Foundation created Materials Camps in 2000 to address the anticipated shortage of materials scientists, engineers and researchers. Central to the camps is the recognition that hands-on exploration of materials is a superb introduction to science, engineering and materials careers. Participants include high school students and (separately) high school science teachers. Formats are residential or non-residential. The program is provided free of charge to all participants. Explosive growth was made possible by engaging a small army of volunteers from local communities and utilizing host University lab facilities. We will describe effective recruitment strategies that resulted in 40 plus geographic locations in 2006, and that have now served thousands of students and teachers. A growing list of professional societies and corporations have joined forces in support of Materials Camps, providing expert volunteers, specialized curricular modules, hands-on learning activities, and financial support. Independent external evaluation and on-going consumer assessments will be described as they drive continuous improvement in program quality. Best Practices will be shared, including: utilizing volunteers as faculty, informal mentoring networks, strengthening local Chapters. Materials Camp has already motivated many high school students to major in materials science, enrollment data will be shared. Opportunities for individual and organizational involvement will be described. More partners, financial sponsors and volunteers are needed to broaden our reach and expand the technical scope of the program.

3:00 PM Invited

Education and Innovation Challenges: National Innovation Institutes as a New Model: *Duane Dimos*¹; Justine Johannes¹; Jeffrey Hoyt¹; Robert Hwang¹; ¹Sandia National Laboratories

Recent reports, especially from the National Academies, have articulated critical challenges for the country to remain a technical and economic leader: increasing the talent pool through improved K-12 education, strengthening the commitment to long-term research, attracting and retaining top scientists and engineers, and enhancing the innovation environment. The American Competitiveness Initiative provided a response to advance national investments in research and development, math and science education and innovation/entrepreneurship. We will discuss an important role for national laboratories as part of this effort and describe efforts at Sandia National



Laboratories to initiate a new construct, Discovery Science and Engineering Innovation Institutes. These institutes would be technology incubators and centers of learning that build off the expertise and facilities resident at the host laboratory and bring together academia, industry and government in powerful partnerships. An example, the National Institute of Nano-Engineering (NINE), will be introduced as a prototype of this idea.

3:30 PM Invited

The COSMOS Program at University of California-Davis: *Niels Jensen*¹; ¹University of California

We will briefly describe our experiences with the California State Summer School for Mathematics and Science (COSMOS), which is a 4 week program for high school students attending topical clusters in groups of about 20. One cluster, The History of Physics and Technology, is covering the historical formulation of equations of motion, electromagnetic fields, and the probing of materials and atomic structure. We expose the students to industry and National Laboratories of key interest. A core event is Los Alamos National Laboratory hosting the entire cluster for two days in New Mexico, showcasing the history and impact of the Laboratory through the Bradbury Science Museum together with contemporary research facilities and opportunities at all levels of a scientific career. It is our aim to present the students with a relationship between contemporary applied science and the world they live in; thereby emphasizing the impact a career in science can have.

4:00 PM Invited

The Los Alamos Institutes a Model for National Laboratory - University Collaborations: *Charles Farrar*¹; Gyuhae Park¹; Matthew Bement¹; Michael Todd²; ¹Los Alamos National Laboratory; ²University of California, San Diego

The newly formed Los Alamos Institutes represents a substantial Los Alamos National Laboratory investment dedicated to developing the next generation of scientists and engineers, revitalizing current LANL staff and retaining these staff. Components that are, or will be, common to all of the Institutes include: Summer schools aimed at undergraduate US-citizen student recruitment into the graduate school programs. A graduate school fellowship program through which laboratory/campus collaborative research is accomplished. Multidisciplinary curriculum development and delivery using both campus faculty and LANL staff as instructors. The degree programs are made available to both LANL staff and traditional on-campus students through distance learning infrastructure. Short courses designed to transfer new technology to industry. Annual workshops involving students, faculty, LANL staff, industry and other government lab staff that attempt to summarize the state-of-the-art and research needs in various emerging technologies.

4:30 PM Break

4:45 PM Panel Discussion

Collaboration on Outreach Programs for the Benefit of the Materials Community

Pb-Free Electronic Solders: Alloy Design, Characterization and Service Reliability: Microstructure and Characterization

Sponsored by: The Minerals, Metals and Materials Society, TMS Electronic, Magnetic, and Photonic Materials Division, TMS: Electronic Packaging and Interconnection Materials Committee

Program Organizers: Fu Guo, Beijing University of Technology; K. Subramanian, Michigan State University; Sung Kang, IBM Corporation; Srinivas Chada, Medtronic; Laura Turbini, University of Toronto; Jin Yu, Korea Advanced Institute of Science and Technology

Monday PM	Room: Oceanic 1
February 26, 2007	Location: Dolphin Hotel

Session Chairs: Laura Turbini, University of Toronto; Sinn-Wen Chen, National Tsing Hua University

2:00 PM

Asymetrical Solder Microstructure in Ni/Sn/Cu Solder Joint: Shen-njie Wang¹; *Cheng-Yi Liu*¹; ¹National Central University

Asymmetrical solder microstructure was observed in the Ni/Sn/Cu solder joint. The asymmetrical solder microstructure was resulted from the Cu concentration gradient along the Ni/Sn/Cu solder joint. The mechanical test shows that mechanical property of the Ni/Sn/Cu solder joint highly correlated with the asymmetrical solder microstructure.

2:20 PM

Extensive Electrical Measurement in Lead-Free Solder Assembly after Environmental Tests by SEM Internal Probing Technique: Toung-Yi Shih¹; Tom Hsu¹; Yung-Chi Lin¹; Jenq-Gong Duh¹; ¹National Tsing Hua University

Electrical characterization for lead-free materials in the bump technology was developed. Joint assemblies were thermally treated under various environmental tests, including highly-accelerated stress test, temperature cycling test, and high temperature storage test. Measurements of sheet resistivity and contact resistance of IMCs in solder joints were conducted under different thermal treatments. Quantitative analysis and elemental redistribution of IMCs were obtained by FE-EPMA. Various types of IMC, such as $(Cu,Ni)_6Sn_5$, $(Ni,Cu)_3Sn_4$ and $(Sn,Ag,Cu)_3Sn$ were revealed. SEM internal probing system was introduced to evaluate electric characteristics in IMC after thermal treatments. To accurately determine the resistivity performance of IMC, a novel method incorporated with SELA-EM2 and FIB was developed to prepare the joint sample. It was demonstrated that more accurate evaluation of resistivity in IMCs could be achieved by this innovative technique.

2:40 PM

Microstructure Evolution of SnAgCuEr Lead-Free Solders under High Temperature Aging: *Hu Hao*¹; Yaowu Shi¹; Zhidong Xia¹; Yongping Lei¹; Fu Guo¹; ¹Beijing University of Technology

The evolution of microstructure especially the IMC under high temperature aging process have been systematically investigated and the effects of trace amount of rare earth element Er have also been studied. The results showed that diffusion and reassemble occur in the constituent phase of solder alloy during aging process. At the same time, newly formed sphere shaped IMCs were dispersedly separated out accompanied with the dissolution of eutectic phase. Thick IMCs, which were produced at initial crystallization stage and presented a special shape, gradually became separated. ß-Sn dendrite was gradually eroded in place of eutectic phase and the composition of the constituent phases was continuously changing with the aging time.

3:00 PM

A Study of Multi-Reflowed Sn-Ag-Cu Solder Joints: Huann-Wu Chiang¹; Ting-Yu Liu¹; Yi-Shao Lai²; ¹I-Shou University; ²Advanced Semiconductor Engineering, Inc.

In this work, we studied interfacial reactions of multi-reflowed Sn-Pb and Sn-Ag-Cu ball grid array (BGA) solder joints of various Ag contents bonded on electroplated Ni/Au Cu pads. Metallurgical evolutions of the intermetallic compounds (IMCs) were scrutinized by scanning electron microscopy (SEM)

LEARN • NETWORK • ADVANCE

Technical Program



and energy dispersive X-ray spectroscopy (EDS). It was found that Ni_3Sn_4 and $(Ni,Cu)_3Sn_4$ IMC layers were developed for Sn-Pb and Sn-Ag-Cu solder alloys, respectively, on the interface between solder and pad after reflow. For Sn-Ag-Cu solder joints, the thickness of the IMC layer increases as the reflow cycle increases, and part of the layer spalls from the interface subsequently. However, for Sn-Pb solder joints, the interfacial IMC layer does not apparently change its thickness and morphology during multi-reflow. Ball shear and ball impact tests (BIT) were also performed to examine strengths of these solder joints.

3:20 PM

Kinetic and Microstructure Analysis of SAC+X Solders: Jason Walleser¹; Iver Anderson¹; Joel Harringa¹; Alfred Kracher¹; ¹Iowa State University

Joint strength and reliability concerns about lead-free solders, e.g., Sn-Ag-Cu (SAC), arise from several microstructural factors. In Sn-Pb solders, Pb effectively retards diffusion and consequent intermetallic compound (IMC) growth. However, in SAC solders, solid-state diffusion during aging can cause IMC layer growth and potential Kirkendall voids. By small substitutional addition of a fourth element in place of Cu, microstructural control during solidification and aging is possible. In prior experiments, some fourth element atoms, e.g., Zn, segregate to the IMC/Cu interface. The extent to which a fourth element segregates to the interface and how this affects relative interface motion will be investigated in solder joints with inert Mo markers, SEM, and electron microprobe measurements. Test alloys include Sn-3.5 Ag-(0.95 – y) Cu – (y) X, where X = {Zn, Ni, Co, Fe} and y = {0.05, 0.10, 0.15}, in wt%. Supported by Iowa State University Research Foundation and Nihon-Superior Co., Ltd. through Ames Lab contract no. W-7405-Eng-82.

3:40 PM Break

3:50 PM

Microstructure of Metallic Particles Reinforced Composite Solder Joints: *Peng Liu*¹; Yuan Gao¹; Jianping Liu¹; Zhidong Xia¹; Fu Guo¹; ¹Beijing University of Technology

Composite solders have attracted much attention of the "second generation" solder researchers because of the improved properties and reliability. Study on the morphology of microconstituents in composite solder offers further understanding of strengthening mechanisms. SnAg based composite solder joints with micron-sized Ni, Cu particle additions were prepared with Cu substrate. Microstructure of three different composite solders, Ni, Cu, and both Ni and Cu being reinforcement, were investigated. As a comparison, joints with eutectic SnAg and SnAgCu solder, commonly used in microelectronics, were fabricated under the same processes. Experimental results showed that the morphology of the interfacial intermetallic compounds at the interface was scalloped Cu6Sn5 in the SnAg, SnAgCu, and Cu reinforced composite solders, while composite solders with Ni particles had great difference. Detailed microstructural morphology descriptions of each composite solder and explanations of the formation mechanisms are provided in this research effort based on phase diagrams and atomic solubility theory.

4:10 PM

Processing and Material Issues Related to Lead-Free Soldering: Laura Turbini¹; ¹University of Toronto

The European requirement for lead-free electronics has resulted in higher soldering temperatures and material and process changes. While tin-lead solder melts at 183°C, the common lead-free alternatives have much higher melting temperatures. These have challenged the ingenuity of the materials and process engineers. In the lead-free era, we see changes in printed wiring board substrates designed for lower soldering temperatures being replaced by newer materials. Factors such as glass transition temperature (T_g), decomposition temperature (T_d) and coefficient of thermal expansion must be considered. Many electronic components are made for lower peak temperatures than those required by the new solders. Solder flux chemistries are changing to meet the needs of the new metal systems, and cleaning is becoming more of a challenge. Finally, there is a reliability problem – an increased potential for the growth of conductive anodic filament, an electrochemical failure mechanism that occurs in the use environment.

4:30 PM

Experimental Wettability Study of Lead-Free Solder on Cu Substrate with Varying Fluxes and Temperatures: Dongxia Xu¹; *Yongping Lei*¹; Zhidong Xia¹; Fu Guo¹; ¹Beijing University of Technology

The selection of soldering flux plays a critical role in promoting wetting and product reliability of printed circuit board assemblies. In this study, the effects of fluxes on the wetting characteristics of the Sn-3.0Ag-0.5Cu solder alloy on Cu substrate have been researched by using various flux systems at different environmental temperatures. According to the distinct characteristic of the lead-free solder—poor wettability, three kinds of fluxes (RMA flux, noclean flux with high solid content and water-soluble flux) were chosed in the wetting experiments. The wetting angle and spreadability were the evaluating indicators. The experimental observations indicated that the wettability clearly depended on soldering temperature and flux system when using the same solder. Also the corrosion potential of flux residues was measured by surface insulation resistance (SIR) testing.Samples tested with water-soluble flux had SIR readings above 10¹¹ Ω while the other two fluxes had readings averaged around 10⁸ Ω .

4:50 PM

Demonstration and Characterization of Sn3.0Ag0.5Cu/Sn57Bi1Ag Combination Solder for 3-D Multi-Stacking: *Yun Hwan Jo*¹; Joo Won Lee¹; Sun-Kyoung Seo¹; Hun Han²; Sang Won Han¹; Hyuck Mo Lee¹; ¹Korea Advanced Institute of Science and Technology; ²Samgsung Electronics Company

A combination solder of Sn-3.0Ag-0.5Cu wrapped by Sn-57Bi-1Ag was tested to apply to the 3-D multi stacking packaging. Experimental variables were chosen as follows: reflow peak temperatures (170, 185, 200 and 230°C), reflow cycles (up to 4 times) and two kinds of the mask size that control the amount of the Sn-57Bi-1Ag solder paste. We demonstrated and evaluated the combination solder structure, focusing on the micro-structural change and the shear strength.The degree of mixing in the combination solder was enhanced with an increase in the reflow temperature, but it was independent of reflow cycles. The intermetallic phase formed between the combination solder and the under bump metallurgy (UBM: Au/Ni/Cu) was (Ni,Cu)₃Sn₄.The ball shear test and lab shear test were performed. The shear strength increased with reflow temperatures, but there was little change in terms of reflow cycles.

5:10 PM

The Effects of Rare Earth Addition on Properties and Microstructure of Lead-Free Solder Balls: Yang Yu¹; *Zhidong Xia*¹; Fu Guo¹; Yaowu Shi¹; ¹Beijing University of Technology

Lead-free solder balls were prepared by using Uniform Droplet Spray (UDS) method. Minute amount of cerium-based mixed rare earth (RE) was added into solder alloy, aiming at examining the effects of different amount of RE on the physical properties, spreading property, and microstructure of the solder balls. Results showed that RE had no obvious effect on the melting temperature, but it improved the surface condition and melt property of solder balls. According to the examination on the microstructure of the solder balls, RE could affect the solidification behavior of the solder balls, which resulted in a smoother surface and better spread property.

Phase Stability, Phase Transformations, and Reactive Phase Formation in Electronic Materials VI: Session I

Sponsored by: The Minerals, Metals and Materials Society, TMS Electronic, Magnetic, and Photonic Materials Division, TMS: Alloy Phases Committee *Program Organizers:* Sinn-Wen Chen, National Tsing Hua University; Srinivas Chada, Medtronic; Chih-ming Chen, National Chung Hsing University; Young-Chang Joo, Seoul National University; A. Lindsay Greer, University of Cambridge; Hyuck Lee, Korea Advanced Institute of Science and Technology; Daniel Lewis, Rensselaer Polytechnic Institute; Katsuaki Suganuma, Osaka University

Monday PM	Room: Oceanic 2
February 26, 2007	Location: Dolphin Hotel

Session Chairs: Daniel Lewis, Rensselaer Polytechnic Institute; Young Chang Joo, Seoul National University

2:00 PM Introductory Comments

2:05 PM Invited

Thermodynamic Calculation of Phase Equilibria in the Sn-Ag-Cu-Ni-Au System: *Xing Jun Liu*¹; Cui Ping Wang¹; Feng Gao¹; Yuan Yuan Li¹; Ikuo Ohnuma²; Kiyohito Ishida²; ¹Xiamen University; ²Tohoku University

Sn-Ag-Cu base solders have been considered as the most potential solders to instead of Sn-Pb eutectic solder. Gold (Au) coatings have been used for a long time to protect conductor surface from oxidation and thereby to promote the solderability, and Nickel (Ni) often used as a diffusion barrier layer between lead-free solders and substrates to restrict the growing of intermetallic compound layers. Therefore the thermodynamic calculation of phase equilibria in the Sn-Ag-Cu-Ni-Au system, which is very important for developing lead-free solders, has been developed using the CALPHAD method. Substitutional solution model and sublattice model are respectively used to describe the solution phases and intermediate phases in this study. The calculated results are in agreement with the experimental data. Base on the present calculations, information on phase diagrams, liquidus projection, and thermodynamic properties are predicted.

2:30 PM Invited

Lead-Free Solders: Phase Relationships and Thermochemistry of Ag-Ni-Sn: *Hans Flandorfer*¹; Clemens Schmetterer¹; Usman Saeed¹; Herbert Ipser¹; ¹University of Vienna

For a comprehensive understanding of solidification behavior and interfacial reactions in solder joints a deeper insight in the phase relationships and thermochemistry of solder alloy systems is indispensable. We are currently investigating the quaternary system Ag-Cu-Ni-Sn which is a key system for lead-free soldering. Experiments are mainly focused on the constituent binary and ternary systems. The phase diagram of the system Ag-Ni-Sn was established based on XRD-, thermal analyses- and metallographic results. We present four isothermal sections, several vertical sections, a liquidus surface projection and a reaction diagram. The enthalpy of mixing of liquid alloys has been determined by means of drop calorimetry for the ternary system Ag-Ni-Sn as well as for the quaternary system Ag-Cu-Ni-Sn. The experimental integral enthalpy values have been fitted to a modified Redlich-Kister polynomial. Our results have been compared to results from well known extrapolation models e.g. the Toop model.

2:55 PM

The COST 531 Lead-Free Solders Thermodynamic Database: Andy Watson¹; *Ales Kroupa*²; Alan Dinsdale³; Adéla Zemanová²; Jirí Vízdal²; Jan Vrešť ál⁴; ¹University of Leeds; ²Academy of Sciences of the Czech Republic; ³National Physical Laboratory; ⁴Masaryk University

Owing to new legislation, lead can no longer be used in electrical and electronic equipment within Europe. COST 531 is a European action on the study of new lead-free materials for use in the electronics industry. One objective is to provide a self-consistent thermodynamic database for lead-free solder materials and substrates. With appropriate software this may be used to calculate phase equilibria and liquidus surfaces for multicomponent solders, model solidification paths and effects of impurities, and to understand the interactions between solder and substrate. The database is the result of critical assessment of experimental data produced within the action augmented by data for binary and ternary systems taken from the literature. It has been tested using MTDATA, Thermo-Calc and Pandat. The database covers the system Ag-Au-Bi-Cu-In-Ni-Pb-Pd-Sb-Sn-Zn and contains thermodynamic descriptions for 55 binary and 11 ternary systems. Its construction is on-going. This action is supported by the European Science Foundation.

3:15 PM

Thermodynamic Assessment of the Bi-Ni System and Phase Equilibria of the Sn-Bi-Ni System: *Sun-Kyoung Seo*¹; Moon Gi Cho¹; Sung Hoon Lee¹; Jong Hoon Kim²; Hyuck Mo Lee¹; ¹Korea Advanced Institute of Science and Technology; ²Hynix Semiconductor

The phase equilibria study of the Sn-Bi-Ni system is necessary to analyze the reaction of the Sn-based solders containing Bi with the Ni UBM during soldering. We reassessed the thermodynamic parameters of the Bi-Ni system with a goal to extend to the phase equilibria of the Sn-Bi-Ni system. In order to obtain the experimental data of NiBi, we synthesized the NiBi compound phase and measured the compositional range of the stable NiBi phase with temperature using an electron probe micro analyzer (EPMA). In addition, the X-ray peaks of the NiBi phase were confirmed through the powder Xray diffraction (XRD) method. In this way, we obtained the ternary Sn-Bi-Ni phase diagram using previously reported Sn-Ni and Sn-Bi systems as well as the Bi-Ni system reassessed in this work. Finally, it was compared with the previous experimental data regarding the interfacial reaction between the Sn-Bi solder and the Ni UBM.

3:35 PM Break

3:50 PM

Inhibiting the AuSn₄ Formation by Controlling the Interfacial Reaction in Solder Joints: *Li-Yin Hsiao*¹; Guh Yaw Jang¹; Jenq-Gong Duh¹; ¹National Tsing Hua University

Au is used in electronic package to protect conductor from oxidation. However, Au dissolved into solders and reacted with Sn-rich phase to form AuSn₄ during soldering. After aging, Au diffused from AuSn₄ toward solder/ metallization interface. If Ni₃Sn₄ formed at soldering interface, a layer of AuSn₄ was re-deposited on Ni₃Sn₄. In contrast, Au dissolved into Cu₆Sn₅-based IMCs to produce (Cu,Au)₆Sn₅ or (Cu,Ni,Au)₆Sn₅, as Cu₆Sn₅ or (Cu,Ni)₆Sn₅ formed at soldering interface. Gibbs energy evaluation revealed that both (Ni,Au)₃Sn₄ and (Cu,Au)₆Sn₅ were more thermodynamically stable than AuSn₄. Maximum amount of Au dissolved in Ni₃Sn₄ was 4.6at.%, while maximum dissolution of Au in Cu₆Sn₅ was 24.3at.% at 150°C. Thus, dissolution of Au in Ni₃Sn₄ was limited. Residual Au re-reacted with Sn to form layer-type AuSn₄. If Cu₆Sn₅ formed at interface, most of Au in AuSn₄ dissolved in Cu₆Sn₅. Consequently, AuSn₄ formation could be inhibited by controlling formation of Cu₆Sn₅ and Ni₃Sn₄ in solder/UBM assemblies.

4:10 PM

Interfacial Reactions in the Sn-8Zn-3Bi/Cu and Sn-8Zn-3Bi/Ni Couples: *Ching-feng Yang*¹; Sinn-wen Chen¹; ¹National Tsing-Hua University

Sn-Zn-Bi alloys are promising Pb-free solders. Interfacial reactions between the eutectic Sn-8wt%Zn-3wt%Bi alloy and the Cu and Ni substrates are examined. Two different kinds of substrates, the bulk plate and the electroplating film, are used in this study. The reactions are carried out at 250°C. Although the Zn content is only 8wt%, the Zn-Cu compounds, γ -Cu5Zn8 and e-CuZn5 phase layers, are formed at the interface of Sn-8Zn-3Bi/Cu couples. The e-CuZn5 phase is of scallop-shape morphology, and the other phase, γ -Cu5Zn8, is a planar layer. In the Sn-8Zn-3Bi/Ni couples, a Zn-Ni compound, Ni5Zn21 phase, is formed. Similar results are found in the couples where the substrates are electroplating film: the reaction phases are the same, while the growth rates are different.

4:30 PM

Effects of Minor Addition of Zn on Interfacial Reactions of Sn-Ag-Cu and Sn-Cu Solders on Various Cu Substrates during Thermal Aging: *Moon Gi Cho*¹; Hyuck Mo Lee¹; Sung K. Kang²; Da-Yuan Shih²; ¹KAIST; ²IBM T.J. Watson Research Center

The effects of Zn addition to Sn-0.7Cu and Sn-3.8Ag-0.7Cu on the interfacial reaction with Cu were investigated, focusing on the intermetallic



compound (IMC) growth, Cu consumption and void formation as functions of aging and solder compositions. Four different Cu substrates (high purity Cu, oxygen free Cu, sputtered Cu, and electroplated Cu) were prepared. Growth of IMCs (Cu_oSn_5 and Cu_3Sn) in Zn-added solders was slower than those without Zn. On the electroplated Cu, numerous voids were observed in the Cu_3Sn phase when reacted and aged with Sn-Cu and Sn-Ag-Cu solders. However, these voids were largely eliminated in the Zn-added solders. On the other three Cu voids were not found in both solders with and without Zn. Cu consumption with Zn-added solders was also lower. The beneficial effects of Zn-addition and the mechanisms in suppressing void formation and Cu consumption with an effective Zn composition have been investigated and will be discussed.

4:50 PM

Cross-Interaction between Ni and Cu across a Lead-Free Solder Joint with Different Solder Volumes: *Chien Wei Chang*¹; Su Chun Yang¹; C. Robert Kao²; ¹National Central University; ²National Taiwan University

The Ni/solder/Cu sandwich structure was one of the most common solder joint configurations in microelectronic packages. The spacing between the Ni/solder and solder/Cu interface can range from 700 microns (BGA joints) to 20 microns (Cu pillar flip-chip joints). Accordingly, the solder volume between these two interfaces can be very different. Yet, the effect of the solder volume on the cross-interaction between these two interface is still not very clear. In this study, the Ni/Sn/Cu ternary diffusion couples will be used to investigate the solder volume effect on the cross-interaction. Experimentally, a Sn layer with the thickness of 100, 200, 400 microns was electroplated over one Cu foil. A layer of pure Ni was then deposited over the as-deposited Sn. The diffusion couples were aged at 160°C, the solder joints were assembled without experiencing any high temperature process, such as reflow. The detailed reaction sequence and the mechanism will be presented.

5:10 PM

To Study the Failure Mechanism in Au-Al Ball Bonds for High Temperature Storage Test: *Liang Hung*¹; ¹Siliconware Precision Industries Company, Ltd

Since the application of thermocompression and thermosonic wire bonding, gold ball lift issue always perplexes fine pitch and higher reliability requirement and two major theories were proposed to explain the failure of Au-Al bonds. First, the formation of Kirkendall porosity in and around the ball bonds is the most widely accepted theory. Another, the corrosion of Au-Al IMC at the interface was pointed out as cause to diminish bond strength and increase electrical resistivity. The corrosion elements maybe from wafer process and EMC. Two major failure mechanisms can be accelerated with increasing temperature. It is difficult to judge which one is root cause. In this study, optimizing wire bonding parameter is controlled to reduce other factor influence (the IMC coverage > 70%). 4N gold wire without EMC is observed Kirkendall void formation during aging test. 4N gold with various EMC is discussed the corrosion behavior by FIB and SEM/EDS analysis.

5:30 PM

Ni as a Contact Material in Lead-Free Soldering: IMC Formation: *Clemens Schmetterer*¹; H. Flandorfer¹; S. Knott¹; H. Ipser¹; ¹University of Vienna

In electronics Ni is widely used as a contact material on PCB boards, most commonly as a protective layer on Cu. During the soldering process, a layer of intermetallic compounds (IMC) is formed at the interface between contact material and solder. As soldering is diffusion controlled process, the phase diagram provides the basic information for the description of interfacial reactions between solder and contact material. Several binary and ternary constituents (e.g. Ag-Ni, Ni-Sn, Ag-Ni-Sn, etc.) of the quaternary Ag-Cu-Ni-Sn system, which is the key system for the description of interactions between widespread Ag-Cu-Sn solder and a Ni containing substrate, were studied. Especially in the Ni-Sn system, which forms the basis of higher order systems, uncertainties caused by a number of not fully consistent experimental investigations from the 1930ies and 1940ies, could be clarified. In addition a suggestion for the so far not investigated phase transition in Ni3Sn2 was made. Based upon our new results a revised version of the Ni-Sn phase diagram can be presented. The system Ag-Ni-Sn will be presented in another contribution. The Ni-P-Sn system is another key-system for the description of interactions between solders and Ni-containing substrate. This system has particular relevance, as Ni-layers deposited by electroless plating always contain some

at.% Phosphorous. First results in this system can be presented. The wetting behaviour and interlayer formation of 16 Ag-Cu-Sn solder alloys on Ni was also studied. These results are compared to data using Cu as a substrate.

Plasticity from the Atomic Scale to Constitutive Laws: Dislocation Solute, Precipitate and Grain Boundary Interactions

Technical Program

Sponsored by: The Minerals, Metals and Materials Society, TMS Structural Materials Division, TMS/ASM: Computational Materials Science and Engineering Committee

Program Organizers: Christopher Woodward, US Air Force; Michael Mills, Ohio State University; Diana Farkas, Virginia Tech

Monday PM	Room: Europe 9
February 26, 2007	Location: Dolphin Hotel

Session Chairs: Dallas Trinkle, University of Illinois; Satish Rao, UES Inc.

2:00 PM Invited

Multiscale Modeling of Dynamic Strain Aging in Al-Mg Alloys: W. Curtin¹; D. Olmsted¹; ¹Brown University

Dynamic strain aging (DSA) is the phenomenon in which solute atoms diffuse around dislocations and retard dislocation motion, leading to negative strain-rate-sensitivity (nSRS) and thus to material instabilities during processing, an important issue in commercial metal alloys. Here, the atomic-scale mechanism of DSA and nSRS on experimental strain rate, temperature, and stress scales for Al-Mg is shown to be single-hop transport of solutes from the compression to the tension side of a dislocation core. An analytic expression for the strengthening versus strain rate and temperature is derived that justifies similar ad-hoc forms in the literature, and provides specific dependencies of the parameters on material properties. Kinetic Monte Carlo simulations support the mechanism and analytic model. Using literature material properties, the predicted strengthening quantitatively agrees with the experimentally-derived behavior of Al-2.5% Mg at 300K, and qualitatively agrees with the strain rate and temperature ranges of DSA and nSRS in Al-Mg alloys.

2:30 PM

First Principles Study of Dislocations in Al and Al-Mg: *Christopher Woodward*¹; Louis Hector²; Dallas Trinkle³; ¹US Air Force; ²General Motors Technical Center; ³University of Illinois, Urbana-Champaign

Details of the local dislocation strain field can strongly influence plastic deformation in fcc materials. In simple metals the lattice friction stress is strongly correlated to the splitting distance of the Shockley partials. Also, local solute-dislocation interactions have a role in producing the well known Portevin-LeChatelier effect. Previous numerical studies of dislocations in Aluminum, based on atomistics or Peierls-Nabarro methods, have produced a wide range of Shockley-partial splitting distances. Here the equilibrium dislocation strain fields for isolated ½<110> screw and edge dislocations are calculated using a first principles method with flexible boundary conditions. Using several numerical techniques the dissociation of the screw (edge) Shockley partial dislocations is found to be in the range of 5.0-7.5 Ang. (7.6-8.0 Ang.). Solute (Mg) -dislocation interactions are estimated by coupling core-volumetric distortions to the size misfit of Mg in Al. These results are compared with direct first principles calculations of the Mg-dislocation interaction energy.

2:50 PM

The Vacancy-Edge Dislocation Interaction in fcc Metals: *Emmanuel Clouet*¹; ¹SRMP, CEA Saclay

The interaction between vacancies and edge dislocations is studied in face centered cubic metals (Al, Au, Cu, Ni) at different length scales. Using empirical potentials and static relaxation, atomic simulations gives us a precise description of this interaction when the separation distance between both defects is small, whereas elasticity theory can be used for larger distances. A comparison between both approaches¹ shows that isotropic elasticity correctly predicts this interaction as long as the vacancy lies outside the dislocation core



and the stacking fault ribbon. In addition, the interaction of a vacancy with an edge dislocation that contains a jog or a super-jog is discussed. Atomic simulations show that jogs are perfect sinks and sources for vacancies even if these jogs are dissociated. ¹E. Clouet. Acta Mater., 54:3543, 2006.

3:10 PM

Point-Defect Mediated Dislocation Nucleation in Nanoidentation: *Amit Samanta*¹;

Ju Li¹; Ting Zhu²; ¹Ohio State University; ²Georgia Institute of Technology

We examine the conditions for heterogeneous nucleation of dislocations beneath an indenter in copper, aided by vacancies and interstitials near the surface. Atomistic calculations are performed to assess the stress-dependent formation and migration energies of point defects in the bulk and near the surface, which are used to predict the realistic kinetics of point-defect motion under the indenter due to the large stress gradient. The reaction pathways and activation energy barriers for dislocation nucleation near these point defects are computed using a modified nudged elastic band method, and compared with those of homogeneous nucleations. The activation volumes of pointdefect mediated dislocation nucleations are compared with homogeneous bulk and surface nucleations. Based on these data, a nucleation mechanism map is drawn as a function of temperature and indentation rate.

3:30 PM

Oxygen in Grain Boundaries: A Molecular Dynamics Study: Andreas Elsener¹; Olivier Politano²; Peter Derlet¹; Helena Van Swygenhoven¹; ¹Paul Scherrer Institute, Switzerland; ²LRRS, UMR 5613 CNRS-Université de Bourgogne, France

One of the important differences between simulation and experiments in grain boundary dominated metallic structures is the lack of impurities such as oxygen in computational samples. Molecular dynamics simulations are performed to investigate the presence of oxygen in grain boundaries on the internal stress distribution and the resulting plasticity mechanism. A modified variable charge method based on the Streitz and Mintmire (PRB 50, 11996 (1994)) approach that incorporates a local chemical potential is used to simulate oxidation in a predominantly metallic Al environment. In particular, the spatial extent of the charge transfer in the oxide region, the resulting changes in local stress distribution and how these change under an applied stress will be presented for a number of carefully selected grain boundary missorientations, and in a nanocrystalline environment. Particular emphasis will be paid to the role oxygen plays in grain boundary sliding and dislocation nucleation at the interface.

3:50 PM Break

4:10 PM Invited

Shearing Mechanisms of Gamma' Precipitates by Single (A/2) <110> Dissociated Dislocations in Ni-Based Superalloys: Brigitte Decamps¹; ¹Centre National de la Recherche Scientifique

Shearing of gamma' precipitates involving superlattice stacking faults (intrinsic (S-ISF) and/or extrinsic (S-ESF)) is one of the important deformation modes in Ni-based superalloys containing a high volume fraction of precipitates. In this work, the combination of transmission electron microscopy techniques (bright-field, weak-beam, high resolution) coupled to bright-field image matching¹ has been used to study the shearing configurations depending on several parameters such as the mechanical testing or the precipitate distribution and morphology. On this basis, elementary shearing mechanisms involving (i) the crossing of gamma/gamma' interfaces by a single (a/2) <110> dissociated matrix dislocation or a single (a/6) <112> decorrelated Shockley partial and (ii) the nucleation of a Shockley dislocation are proposed and discussed. ¹Head A.K., Humble P., Clarebrough L.M., Morton A.J. (1973) 'Computed Electron Micrographs and Defect Identification' (Amsterdam: North-Holland).

4:40 PM

Recent Development of Microscopic Phase Field Model of Dislocations: Chen Shen¹; Ju Li¹; Michael Mills¹; Yunzhi Wang¹; ¹Ohio State University

With Green's function solution of long-range elastic interactions and ab initio calculation of the generalized stacking fault (GSF) energy as model inputs, the microscopic phase field model has been shown quantitatively to be a 3D generalization of the Peierls-Nabarro model, capable of treating complex dislocation structures. The method has been applied successfully to studying dislocation core structures, structures and energies of small angle grain boundaries consisting of regular arrays of dislocations, shearing of gamma prime precipitates in Ni-base superalloys, and slip transmission across alpha/ beta interfaces in Ti alloys. In this presentation we will give a brief review of these applications and then discuss its most recent development including the extension to a discrete model based on real crystal lattice. The work is supported by AFOSR under the MEANS-2 program.

5:00 PM

Structures, Energies and Dislocation Nucleation Behaviours of $\Sigma 3$ Asymmetric Tilt Grain Boundaries: *Mark Tschopp*¹; David McDowell¹; ¹Georgia Institute of Technology

Atomistic simulations are employed to investigate the energy and structure of symmetric and asymmetric $\Sigma 3 < 110$ > tilt grain boundaries. Simulation results show that the $\Sigma 3 < 110$ > asymmetric tilt grain boundaries are composed of only structural units of the two $\Sigma 3$ symmetric tilt grain boundaries. A structural unit model for $\Sigma 3$ asymmetric tilt grain boundaries that fits all of the calculated asymmetric grain boundary structures is presented along with a partial dislocation description. The significance of these results is that both the structural unit and partial dislocation descriptions of all $\Sigma 3$ asymmetric tilt grain boundaries of the $\Sigma 3$ coherent twin and incoherent twin boundaries for both Cu and Al. Atomistic deformation simulations of dislocation nucleation for a wide range of $\Sigma 3 < 110$ > tilt boundaries are analyzed to elucidate the relationship between grain boundary structure and deformation response for this family of interfaces.

5:20 PM

The Effect of Grain Boundary Misorientation on Intragranular Slip in Zinc Bicrystals: Askar Sheikh-Ali¹; ¹Kazakh-British Technical University

Intragranular slip in zinc bicrystals with tilt boundaries of different misorientations located in the range of 48°-57° has been studied. All investigated boundaries have axis of rotation of <1010>. The amount of intragranular strain has been determined on the basis of the concept of grain boundary sliding consisting of two components dependent and independent on intragranular slip. The distribution of grain boundary sliding along the boundary has been measured using marker line technique. The result shows a strong dependence of the kinetics of intragranular slip on boundary misorientation. It is demonstrated that near coincident misorientation the slip does not obey the Schmid's law.

Properties and Performance of High Temperature Alloys and Coatings: Polycrystalline Alloys

Sponsored by: The Minerals, Metals and Materials Society, TMS Structural Materials Division, TMS: High Temperature Alloys Committee, TMS/ASM: Corrosion and Environmental Effects Committee, TMS/ASM: Mechanical Behavior of Materials Committee

Program Organizers: Qiang Feng, Beijing University of Science and Technology; Timothy Gabb, NASA Glenn Research Center; Doug Konitzer, General Electric Aviation; Roger Reed, Imperial College London; Bruce Pint, Oak Ridge National Laboratory; Sammy Tin, Illinois Institute of Technology; Shiela Woodard, Pratt and Whitney

Monday PM	Room: Asia 4
February 26, 2007	Location: Dolphin Hote

Session Chairs: James Larsen, US Air Force; Sammy Tin, Illinois Institute of Technology

2:00 PM Invited

Evaluation of 3rd Generation Powder Metallurgy Superalloys for High Temperature Gas Turbine Engine Disk Applications: *Randolph Helmink*¹; ¹Rolls-Royce/LibertyWorks

The demand for low cost gas turbine engines with improved performance and durability requires ever increasing compressor exit and turbine inlet temperatures. The primary constraint on compressor exit temperature has been the temperature capability of the materials used in the highly stressed, high pressure compressor and turbine disks. Over the past decade new, 3rd generation powder metallurgy superalloys have been developed to address these needs. These alloys have improved grain boundary structures, which, in conjunction with improved powder and component processing techniques,

Technical Program



provide greater resistance to time dependent material properties, such as creep and dwell fatigue crack growth. Rolls-Royce plc., working with Honeywell International under a cooperative arrangement, has evaluated the 3rd generation PM superalloys developed by the two companies versus some of the competitive materials. The comparison will include RR1000 developed by Rolls-Royce, Alloy 10 developed by Honeywell, LSHR developed by NASA and ME3 developed by NASA/GE/P&WA.

2:25 PM Invited

Mechanisms and Modeling of Creep in Polycrystalline Ni-Base Superalloys: Raymond Unocic¹; Peter Sarosi¹; Ju Li¹; Yunzhi Wang¹; *Michael Mills*¹; ¹Ohio State University

Polycrystalline Ni-base superalloys are used extensively in the hot section of gas turbine engines because of their inherent elevated temperature strength and creep resistance. These alloys are strengthened by varying populations of L1₂ structure γ precipitates. Materials with controlled heat treatments are being quantitatively analyzed for microstructure and chemistry using electron microscopy and 3D atom probe techniques. These characterized microstructures also provide crucial calibrating data for the phase field microstructure modeling being developed. A variety of operative deformation mechanisms have been observed after creep deformation using TEM techniques, depending upon temperature and stress. These mechanisms include include microtwinning, stacking-fault shearing of γ precipitates, Orowan looping, and dislocation climb/bypass. Developing microstructure-sensitive models for creep requires an accounting of these transitions in mechanisms. The evaluation of key activation processes, suggested from direct experimental observations of the deformation mechanisms, is being conducted using a novel combination of atomic-scale and phase field dislocation modeling.

2:50 PM

Long Term Aging of Nickel-Base Superalloys: Anita Garg¹; Timothy Gabb²; John Gayda²; ¹University of Toledo; ²NASA Glenn Research Center

The industry is demanding longer term service at high temperatures for nickel-base superalloys in gas turbine engine as well as potential space applications. However, longer term service can severely tax alloy phase stability, to the potential detriment of mechanical properties. Cast Mar-M247LC and wrought Haynes 230 superalloys were exposed and creep tested for extended times at elevated temperature. Microstructure and phase evaluations were then undertaken for comparisons.

3:10 PM

Effect of a Supersolvus Heat Treatment on the Microstructure and Mechanical Properties of a Powder Metallurgy Processed Nickel-Base Superalloy: D. Stolz¹; Gerhard Fuchs¹; ¹University of Florida

Powder Metallurgy (P/M) processed nickel-base superalloys are used as turbine disk materials in jet engines. However, the fatigue properties of P/M superalloys in the as-consolidated form have suffered because of the defect sensitivity of the as-consolidated microstructure. Expensive, thermomechanical steps are necessary to break down defects, so that the P/M parts can be considered defect-tolerant. A program was undertaken to examine the potential for utilizing an alternate heat treatment with P/M Alloy 720LI to generate a potentially defect-tolerant microstructure. This heat treatment had a soak above the γ solvus temperature followed by a controlled cool through the solvus. This produced γ grains with a regular array of large dendritic-shaped secondary γ within the grains. Mechanical testing was carried out to fully evaluate the effect of this alternate heat treatment on the mechanical properties of as-HIP Alloy 720LI.

3:30 PM

Observations on Phase Relations and Mechanical Properties of a V-Modified Alloy 718: *Michael Fahrmann*¹; Akane Suzuki²; ¹Special Metals Corporation; ²University of Michigan

One factor limiting the temperature capability of alloy 718 is its propensity for transformation of the meta-stable, strengthening γ " phase (DO22 crystal structure) to the stable δ phase (DOa crystal structure) at temperatures exceeding 1200°F. Since V forms a stable γ " Ni3V phase in the binary Ni – V system, it was speculated that partial replacement of Nb by V might enhance the thermodynamic stability of the γ " phase and, thus, inhibit its transformation to δ at elevated temperatures. To this end, a series of small 50 lbs. VIM heats was made with V substituting for Nb up to 50% on an atomic basis, the baseline being an alloy 718-type chemical composition. The results

of metallography (SEM, TEM) and tensile tests are presented for standard heat -treated as well as over-aged ($1400^{\circ}F / 350 h$) material. Phase relations and their implications for yield strength are discussed.

3:50 PM

Microstructures and Tensile Properties of New Ni-Co-Base Disk Superalloys: *Cui Chuanyong*¹; Gu Yuefeng¹; Harada Hiroshi¹; Sato Akihiro¹; Fujioka Junzo¹; ¹National Institute of Materials Science

Recently, we proposed a new concept to design disk alloys, termed as TMW alloys. This concept is based on combining the characters of gamma/ gamma prime Ni-base and gamma/gamma prime Co-base (Co-20at.% Ti) alloys. Thus, the contents of Co and Ti in these TMW alloys are higher than those in normal disk alloys. The TMW alloys were hot-rolled at 1120°C to 12 mm thick plates with 75% reduction. The microstructures were analyzed using optical microscope (OP) and scanning electron microscope (SEM). The tensile tests were performed at temperatures ranging from room temperature to 850°C. The results show that some of the TMW alloys only consist of gamma/gamma prime phases, and show better phase stability than Ni-base superalloy (U720LI). Mechanical properties tests show that the TMW alloys possess high tensile ductility and stress than the disk superalloy U720LI. The obtained results are very useful for the development of new disk alloys.

4:10 PM Break

4:25 PM Invited

Multiscale Phase Field Modeling of Phase Transformation and Plastic Deformation in Superalloys: Chen Shen¹; Ju Li¹; Michael Mills¹; *Yunzhi Wang*¹; ¹Ohio State University

The phase field method at mesoscale has become a widely used technique for modeling complex morphological patterns formed in Ni-base superalloys and their coatings. Recently, a new microscopic phase field (MPF) model of precipitate-dislocation interactions was developed by using arbitrary inelastic strain fields and generalized stacking fault (GSF) energy. In this presentation we review formulations and applications of the method in modeling microstructure evolution during precipitation, interdiffusion and plastic deformation in Nibase superalloys. Examples are chosen at both mesoscopic and microscopic length scales. At the mesoscopic level we present simulation predictions of various gamma/gamma-prime microstructures and coupled microstructural evolution of precipitates and dislocations during rafting. At the microscopic level we illustrate the ability of the MPF model in combination with the nudged elastic band method to treat shearing of gamma prime without any a priori assumptions about dislocation geometry, core structure, and formation of stacking faults.

4:50 PM Invited

A Novel Philosophy for Worst-Case Fatigue Behavior of Nickel-Base Superalloys at Elevated Temperature: James Larsen¹; Sushant Jha²; M. J. Caton¹; A. H. Rosenberger¹; R. John¹; ¹U.S. Air Force Research Laboratory; ²Universal Technology Corporation

Long-term performance and capability limits of fracture-critical hightemperature turbine engine materials are typically based largely on the expected worst-case total lifetime under fatigue. Recent studies of such lower-bound behavior in key Ni-base superalloys indicate that the life-limiting mechanisms are typically dominated the growth of damage that begins at the scale of key microstructural features, while the role of crack nucleation is minimal. This behavior provides significant insight into options for management of materials lifetime uncertainty in applications requiring damage tolerance. This presentation overviews relevant worst-case fatigue and outlines alternative approaches for improved materials reliability and utilization for facturecritical applications.

5:15 PM

Physically-Based Probabilistic Fatigue Lifetime Simulation of a Nickel-Based Superalloy: *Sushant Jha*¹; Michael Caton²; James Larsen²; ¹Universal Technology Corporation; ²U.S. Air Force

The total lifetime variability at given loading condition is suggested to be composed of at least two separate responses. These are the extreme, lifelimiting behavior, and the superimposing mean-lifetime dominating behavior. This theory was evaluated with respect to elevated temperature fatigue of a Nickel-Based Superalloy. In this material, the life-limiting (or the worst-case) vs. the mean-lifetime behavior is suggested to occur due to different degree



of heterogeneity in the competing crack initiation mechanisms. The worstcase behavior was controlled by small + long crack growth and was therefore, affected only by the crack growth response to microstructure and loading variables. The key microstructural features were simulated in a plate using 3D Poisson Point Process. Non-overlapping, virtual samples from the plate were failed according to a criterion that reflected the ranking of mechanisms in terms of the heterogeneity in distribution of the crack initiating regions. The simulated lifetimes and probabilities of fracture showed reasonable agreement with the observed fatigue variability behavior.

5:30 PM

Effect of Dwell-Loading and Grain Size on the Fatigue Variability Behavior of Nickel-Based Superalloys: *M. Caton*¹; Sushant Jha²; J. Larsen¹; ¹US Air Force Research Laboratory, Wright-Patterson Air Force Base; ²Universal Technology Corporation

The worst-case lifetimes in elevated temperature fatigue of a Nickel-Based superalloy were predominantly controlled by small + long crack growth. The dependence of crack growth, especially the small crack growth variability on microstructure and loading variables was therefore critical to understanding the life-limiting behavior. The variability in the small crack growth behavior was studied with respect to the γ grain size, both in pure-fatigue and dwell-loading condition. For a given grain size, while dwell-loading had minimal influence on the long crack growth behavior, the small crack growth rates were significantly affected. A critical crack length (that scaled with grain size) could be identified, above which the variability in growth rates was reduced to similar level as in the long crack growth. The role of small-crack growth variability in the total lifetime variability and the life-limiting behavior was determined. The findings in this study are shown to have very significant implications for damage prognosis and life-management of fracture critical components.

5:45 PM

Ultrasonic Fatigue Crack Initiation in Nickel-Base Superalloy René 88 DT at Elevated Temperature: J. Miao¹; T. M. Pollock¹; W. Jones¹; ¹University of Michigan, Ann Arbor

The fatigue behavior of nickel-base superalloy René 88 DT was examined in the lifetime range of 10^s~10^s cycles at 593°C for a load ratio of 0.05 with an ultrasonic fatigue testing apparatus operating at 20 kHz. Fractographic analyses indicated that all the fatigue cracks initiated internally. Crack initiation sites consisted of crystallographic facets formed by cracking large grain or large grain clusters. Three dimensional reconstruction of fracture surfaces showed that crack initiation facet orientations are close to the maximum shear stress plane. By using EBSD combined with 3D fracture surface reconstruction techniques, the crystallographic orientation of crack initiation facets was identified. Cyclic strain localization in favorably oriented large grains or large grain clusters is the likely mechanism of internal crack initiation at elevated temperature and under low loading stress in this alloy.

Recent Developments in Semiconductor, Electro Optic and Radio Frequency Materials: Progress in Semiconductor Optoelectronics and Beyond

Sponsored by: The Minerals, Metals and Materials Society, TMS Electronic, Magnetic, and Photonic Materials Division, TMS: Thin Films and Interfaces Committee

Program Organizers: Nuggehalli Ravindra, New Jersey Institute of Technology; Narsingh Singh, Northrop Grumman Corporation, ES; Aris Christou, University of Maryland; Nancy Michael, University of Texas; Bhushan Sopori, National Renewable Energy Laboratory; John Parsey, On Semiconductor

Monday PM	Room: Oceanic 6
February 26, 2007	Location: Dolphin Hotel

Session Chairs: Nancy Michael, University of Texas; Dia-Eddin Arafah, University of Jordan

2:00 PM Introductory Comments

2:05 PM

Improved Au Schottky Contacts on GaAs Using Cryogenic Metal Deposition: *Hung-Ta Wang*¹; Soohwan Jang¹; Travis Anderson¹; Jau-Jiun Chen¹; Byoung Sam Kang¹; Fan Ren¹; Andrew Herrero¹; Andrew Gerger¹; Brent Gila¹; Stephen Pearton¹; ¹University of Florida

The use of low temperatures (~77K) during Au Schottky contact deposition onto n-GaAs produces an increase in barrier height from 0.73 eV for room temperature diodes to 0.82 eV. There is no evidence of drift in the forward current in either type of diode and the low temperature deposited samples show smoother Au layers and more abrupt Au/GaAs interfaces as determined by X-Ray Reflectivity measurements. Both types of diodes show surface and bulk contributions to the reverse bias current. The diodes with Au deposited at cryogenic temperature did show higher ideality factors, which may result from contaminants gettered to the cold GaAs surface. The enhancement of ~0.09 eV (a 12% increase) in Schottky barrier height for Au deposited at cryogenic temperatures on n-type GaAs relative to conventional deposition at 300K(barrier height 0.73 eV) is shown to persist for annealing temperatures up to 200°C. At higher anneal temperatures, both types of diodes show a severe deterioration in rectifying behavior. The reverse breakdown voltage of low temperature deposited diodes was ~50% larger than conventional Au/ GaAs diodes. This simple process method has potential for improving output resistance and power gain and lowering gate leakage current and noise in GaAs metal-semiconductor field effect transistors (MESFETs).

2:30 PM

Formation of Ag-Si Contact in Fire-through Metallization for Solar Cells: Experimental Studies: *Vishal Mehta*¹; Bhushan Sopori¹; P. Rupnowski¹; Jesse Appel¹; Aziz Shaikh²; Nazrali Merchant²; Dave Carlson³; N. M. Ravindra⁴; ¹National Renewable Energy Laboratory; ²Ferro Electronic Materials; ³BP Solar; ⁴New Jersey Institute of Technology

Silicon solar cell metallization uses a fire-through process in which the front Ag-based, screen-printed, metallization pattern is fired through a layer of SiN:H using an RTP-like process. In this process, SiN:H also acts as an antireflection coating and helps diffuse hydrogen for passivation of impurities and defects. Furthermore, in many cases, the front and the back aluminum contact are formed simultaneously in the same firing step. Maximizing cell performance requires a thorough understanding of all the mechanisms involved in the fire-through step. We are studying fire-though contact formation using controlled temperature-time profiles to determine kinetics of SiN dissolution, metallurgy of Ag-Si interactions, and Si-Al alloy formation. Solar cells with screen-printed contacts are fired in an optical processing furnace in which the light intensity profiles are controlled and actual temperatures under the metallization pattern and in the nonmetallized regions are monitored. This paper will discuss experimental results identifying mechanisms of Si-Ag contact formation, kinetics of metallization penetration into Si, and issues pertaining to optimization of front and back contact formation and hydrogen passivation. *This work has been authored by employees of the Midwest Research Institute under Contract No. DE-AC36-99GO10337 with the U.S. Department of Energy. The United States Government retains and the publisher, by accepting the article for publication, acknowledges that the United States Government retains a non-exclusive, paid-up, irrevocable, worldwide license to publish or reproduce the published form of this work, or allow others to do so, for United States Government purposes.

2:55 PM

Microwave Performance of AlGaN/GaN High Electron Mobility Transistors on Si/SiO2/Poly-SiC Substrates: *Travis Anderson*¹; Fan Ren¹; Lance Covert¹; Jenshan Lin¹; Steve Pearton¹; Julien Thuret²; P. Bove²; H. Lahreche²; ¹University of Florida; ²Picogiga International

A key aspect for widespread applications of GaN-based HEMTs is the need for low-cost, high thermal conductivity substrates. The use of Silicon-on-Polycrystalline Silicon carbide (SopSiC) is a possible alternative by combining the low cost approach of the Silicon and poly-SiC bulk with improved thermal dissipation. This work reports the rf performance of AlGaN/GaN High Electron Mobility Transistors (HEMTs) grown on Si-on-poly-SiC (SopSiC) substrates formed by the Smart CutTM process. HEMTs with 0.3 µm gate length show cutoff frequencies (fT) of 18-27 GHz for gate-to-drain distances of 3-32 µm and maximum frequency of oscillation (f-MAX) of 43-47 GHz. The fMAX-values are slightly lower than comparable devices on conventional substrates,



Technical Program

possibly due to additional resistances or capacitances associated with the SopSiC template. While further optimization is required, this approach looks promising for applications requiring cheap large-area substrates and better thermal management than provided by pure Si substrates alone.

3:20 PM

The Performance of Cu (In,Ga)Se2 Thin Film Solar Cell Developed by Single Step Electrodposition Process: *Shyam Kumar*¹; Bhuwanehwar Prajapati¹; ¹National Institute of Foundry and Forge Technology

The CIGS solar cell is the promising candidate for converting solar energy to electricity with efficiency more than 18%. In the present work, CIGS thin film was electrodeposited on Mo substrate using AR grade CuCl2, KI, TEA, Na3C6H5O7.2H2O, SeO2, InCl3, GaCl3 and EDTA in mill molar concentration in the electrolyte. Cathodic polarization characteristics have been carried out and it is observed that at -0.70V (SCE), co deposition of all the elements takes place. The CdS film was deposited over the annealed CIGS thin film by chemical bath deposition. The stacked Mo/CIGS/CdS film was annealed in air at 4000C to form CIGS solar cell. The prominent peak of (112) plane in XRD spectra of CIGS thin film at 27.90 indicate the crystalline nature of the film. The Voc , Jsc, fill factor and efficiency are observed to be 550mV, 8 mA/cm2, 0.50 and 12% respectively.

3:45 PM Break

3:55 PM

Passivation of Silicon Solar Cells by Hydrogen-Rich Silicon Nitride Layer: Nuggehalli Ravindra¹; *Chuan Li*¹; Bhushan Sopori²; Rene Rivero²; Anthony Fiory¹; 'New Jersey Institute of Technology; ²National Renewable Energy Laboratory

Surface passivtion of silicon solar cells by hydrogen-rich silicon nitride (SiN:H) layers has been observed and exhaustively investigated for decades. However, a complete model, which can successfully explain the experimental results of the surface recombination velocity on injection level, is lacking. In this paper, a review of the model calculations of the surface recombination velocities (SRV) at the Si-SiN:H interface, by considering both the Shockley-Read-Hall(SRH) mechanism and the recombination at space charge region (scr), is presented. Bulk passivation is also important for improving the performance of photovoltaic (PV) cells, especially the cells fabricated from low-grade starting materials. The mechanism of bulk passivation is not very well known. In this paper, a semi-qualitative model for H evolution, mediated by SiN:H layer based on the theory of H transport across SiN:H medium and the theory of H trapping-detrapping mechanisms, is proposed. It is possible to achieve optimum passivation by process control.

4:20 PM Invited

Light Trapping in Solar Cells: Theory and Practical Implementation: Bhushan Sopori¹; ¹National Renewable Energy Laboratory

Light trapping is a mechanism for creating enhanced absorption in a material, beyond that of a parallel polished wafer of the same material and the same thickness. Light trapping is an important feature of all solar cells, because it allows the use of thinner cells that perform equally or better than thick cells. A thinner cell leads to lower-volume recombination of photogenerated carriers, leading to higher cell performance. Thinner wafers can also help minimize the use of semiconducting material, therefore lowering the energy cost further. Light trapping in a wafer or a solar cell requires rough or textured surface(s); hence the detailed optics of light trapping is somewhat difficult to carry out. We have developed a software package, PV Optics, which performs light-trapping calculations for solar cell applications. It determines optical absorption for a given structure and calculates photocurrent available from a given solar cell structure for many cases, such as when the cell is placed directly in the sun or encapsulated in a module. The cell can have a single- or multiple-junction configuration. This paper will review the principles of light trapping and practical approaches to incorporate effective light trapping in silicon solar cells. We will demonstrate typical use of PV Optics for the design of crystalline and amorphous silicon solar cells. *This work has been authored by employees of the Midwest Research Institute under Contract No. DE-AC36-99GO10337 with the U.S. Department of Energy. The United States Government retains and the publisher, by accepting the article for publication, acknowledges that the United States Government retains a non-exclusive, paid-up, irrevocable, worldwide license to publish or reproduce the published form of this work, or

allow others to do so, for United States Government purposes.

4:45 PM

Spintronics and Diluted Magnetic Semiconductors Based on ZnO: Shivaraman Ramachandran¹; John Prater¹; J. Narayan¹; ¹North Carolina State University

The emerging field of spintronics where the spin as well as the charge of the carriers are utilized together, promises to revolutionize microelectronics. In this talk we will address latest developments in the area of wide band gap semiconductor materials which have the potential to be synthesized as Diluted Magnetic Semiconductors(DMS) for use to fabricate spintronic devices. We will specifically focus on the present status of zinc oxide based DMS materials that have been proven to ferromagnetic at room temperature. Various aspects, including thin film growth and atomic scale characterization would be discussed. In addition, spin polarized injection into semiconductors using DMS materials will also be address.

5:10 PM Invited

Modeling of Magnetic Field Assisted Assembly of Semiconductor Devices: Nuggehalli Ravindra¹; *Sudhakar Shet*¹; Rene Rivero¹; Michael Booty¹; Anthony Fiory¹; Martin Lepselter¹; ¹New Jersey Institute of Technology

Massively parallel micro-assembly of heterogeneous devices on to the same substrate is an efficient, low-cost alternative to the conventional pick-and-place assembly of semiconductor devices. A brief explanation of the magnetic field assisted assembly (MFAA) technique is presented. A model for the magnetic forces required to efficiently place a device in a pre-determined location on the substrate for the magnetic field assisted assembly of semiconductor devices is presented. The strong close-range attractive magnetic forces that govern magnetic field assisted assembly technique are approximated using a simple geometric argument that employs relative size, distance, mass and energy considerations. The results of the model are plotted as function of various physical parameters. The predictions of the model are examined and briefly discussed with respect to magnetic field assisted assembly.

5:35 PM

Self Assembly of Au Nanodots in ZnO Matrix: Growth, Physical Properties and Challenges: *Nori Sudhakar*¹; Chunming Jin¹; Wei Wei¹; Jagdish Narayan¹; 'North Carolina State University

Recently, self assembled metal embedded nanoparticles in wide bandgap semiconductor systems have been attracting the scientific community owing to their interesting optical, electrical and mechanical properties. More often than not some of the physical properties exhibited in certain systems at nanometer length scales (<10 nm) are hard to conceptualize and quite controversial. Optical absorption properties can be modified by the size profile of the metal nanodots. We have used a pulsed laser deposition technique to grow Au nanoparticles with a concentration gradient embedded in ZnO as the matrix layers. ZnO was deposited on Si(111) substrate at 400°C followed by gold deposition and repeated this process several times. The size of the Au nanodots embedded was controlled by the thickness of the Au layer. It is envisaged that Au islands or nanodots at very low concentrations of the order of a monolayer show evidence for enhanced electrical and optical properties.



Recycling and Waste Processing: Batteries and Co/Ni

Sponsored by: The Minerals, Metals and Materials Society, TMS Extraction and Processing Division, TMS Light Metals Division, TMS: Recycling and Environmental Technologies Committee

Program Organizers: Mark Schlesinger, University of Missouri; Robert Stephens, Teckcominco, Inc.; Donald Stewart, Alcoa Technology; Ray Peterson, Aleris International; Jan van Linden, Recycling Technology Services, Inc.; Subodh Das, SECAT; Abdel Serna-Vasquez, Aleris International; Cynthia Belt, Aleris International Inc; John Pickens, Alumitech/Aleris International; John Hryn, Praxair; Richard Kunter, Richard S. Kunter and Associates; Andreas Siegmund, Quemetco Metals Inc.; Masao Suzuki, AI Tech Associates

Monday PMRoom: Australia 2February 26, 2007Location: Dolphin Hotel

Session Chair: Mark Schlesinger, University of Missouri

2:00 PM

Recycling of Cadmium from Domestic Sealed NiCd Batteries by Use of Chlorine/Air Mixtures: *Derek Fray*¹; Antony Cox¹; ¹University of Cambridge

Small domestic nickel cadmium batteries are difficult to recycle. However, by the use of a chlorinating agent and air, it is possible to chlorinate the cadmium to cadmium chlorie gas whilst negligible chlorination of the nickel occurs. Furthermore, the chlorinating agent can be obtained by controlled combustion of PVC scrap, thereby, using two waste materials to create useful products.

2:30 PM

Development of a Recycling Process for Batteries Used in Hybrid and Electric Vehicles: *Masao Miyake*¹; Yu Hosokawa¹; Hisao Kimura¹; Masafumi Maeda¹; ¹University of Tokyo

A recycling process was developed for nickel-metal hydride batteries used in hybrid and electric vehicles. By physical selection, powder containing mainly hydrogen storage alloy (Mm(Ni-Co-Mn-Al)₅; Mm: mischmetal) of negative electrode material can be recovered from the spent batteries. However, the powder is contaminated with Ni hydroxide of positive electrode material. Hydrogen reduction treatment was performed to reduce the Ni hydroxide in the recovered powder without oxidizing rare earth elements in the alloy as much as possible. The powder after the treatment was melted with argon plasma arc to separate metal and slag phases. This process produced an alloy ingot containing rare earth elements, which can be used as a raw material for negative electrodes of the batteries.

3:00 PM

Recycling Cobalt from Spent Lithium Ion Battery: *Zhidong Xia*¹; Xiaoqian Xie¹; Yaowu Shi¹; Yongping Lei¹; Fu Guo¹; ¹Beijing University of Technology

Spent lithium ion battery is a useful resource of cobalt. Based upon the analysis of the structure and composition of the battery, cobalt was recovered by wet process. X ray diffraction results showed that cobaltous oxalate and cobalt sulfate with high purity have been obtained in different process. Moreover, comparing to the cobaltous oxalate process, the cobaltous sulfate process consumes less chemical substance, therefore, is more efficient and economic.

3:30 PM Break

3:50 PM

Recovery of Nickel and Cobalt from Magnetic Steel Scrap Containing Nickel and Cobalt: Jing Zhan¹; *Chuanfu Zhang*¹; Jianhui Wu¹; Meng Bai²; ¹Central South University; ²Jiangxi Copper Guixi Smelter Xuaxin Metal Liabilities Company, Ltd

A flow sheet comprise of acidic leaching, removal of Fe by neutralization, removal of inpurity of Al, Cu, Mn and Fe, etc by p204 extraction, and p204 extracting to separate and recover nickel and cobalt from magnetic steel scrap has been prosed and tested. The results show that the purity of cobalt and nickel solution meet the demands of producing nickel and cobalt products. The recovery of cobalt amounts to 94.2% and that of nickel to 98.18%.

4:20 PM

Use of Ammonia/Ammonium Carbonate Solutions for the Recovery of Metals: Faustino Prado¹; 'Prado Technology Corporation

For more than a century, the AAC (ammonia/ammonium carbonate) process, has been applied to the recovery of non-ferrous metals. Initially the Caron process as it was called was used in the early 1940's in Cuba for the extraction of nickel from laterites. Since then it has been used for other nickel plants, including one in Greenvale, Australia. The Cuban and Australian plants have been in continuous operation since their construction. More recently, AAC solutions have been applied to the recovery of primary zinc as well as secondary zinc/copper. More specifically, two temporary recovery facilities were built in the USA for reprocessing zinc/copper residues, and a plant was built in Japan for recovery of zinc oxide from Electric Arc Furnace Dusts (EAFD). A primary zinc project is currently being planned in the Middle east and two EAFD recovery plants, one in the Middle East and another in the USA.

Refractory Metals 2007: Oxidation and Thin Films

Sponsored by: The Minerals, Metals and Materials Society, TMS Structural Materials Division, TMS: Refractory Metals Committee *Program Organizers:* Gary Rozak, HC Starck Inc; Todd Leonhardt, Rhenium Alloys Inc

Monday PM	Room: Europe 6
February 26, 2007	Location: Dolphin Hotel

Session Chairs: Gary Rozak, HC Starck Inc; Brian Cockeram, Bechtel Bettis Inc

2:00 PM

Effects of Cr and Ti Contents on the Oxidation Behavior of V-Cr-Ti Alloys:

Mehmet Uz¹; K. Natesan²; ¹Lafayette College; ²Argonne National Laboratory Oxidation studies were carried out on V and V-base alloys containing (in wt.%) 4Cr-4Ti, 5Cr-5Ti, 10Cr, 10Cr-5Ti, and 15Cr-5Ti. Experiments were performed in environments containing 760, 160, 0.1, 5 x 10-4 and 5 x 10-6 Torr oxygen at three or more temperatures ranging from about 350 to 700°C. Oxidation behavior of each alloy was modeled using the data of weight change with time. Microstructural features including grain size, and scale thickness and morphology were determined from metallographic examination of the cross-sectional area of each sample. Microhardness profiles across the sample thickness were used to determine the depth of oxygen penetration. These results will be presented, and the effects of oxygen pressure on the oxidation kinetics and microstructure of V and V-Cr-Ti alloys will be compared. Work supported by the U.S. Department of Energy, Office of Fusion Energy Research, under Contract W-31-109-Eng-38.

2:25 PM

Alloys from Nb-W-Cr System for High Temperature Applications: *Abdul Bhuiya*¹; Purushotham Kakarlapudi¹; Shailendra Varma¹; Ken Natesan²; ¹University of Texas at El Paso; ²Argonne National Laboratory

Alloys from Nb-W-Cr system have been explored for possible high temperature applications. Oxidation resistance of the alloys from this system has been tested in the range of temperature from 1000 to 1400°C in air. Weight gain per unit area as a function of oxidation time at a given temperature has been measured for a period of one week. Activation energy for oxidation will be calculated using such oxidation curves. The oxidized surfaces have been examined by EDS in SEM, XRD, AEM, XPS and optical microscopy and TEM. The effect of Y addition on the oxidation resistance has been determined. The aim of the research is to be able to explore the possibility of developing an oxidation resistant material using metal-alloy systems.

2:50 PM

Microstructure and High Temperature Oxidation Behavior of Cr-W Alloys: Omer Dogan¹; ¹National Energy Technology Laboratory

Cr alloys containing 0-30% W by weight were investigated for use in elevated temperature applications. The alloys were melted in a water-cooled, copperhearth arc furnace. Microstructure of the alloys was characterized using x-ray diffraction, scanning electron microscopy, and light microscopy. A pseudocyclic oxidation test was employed to study scale formation at 1000°C in dry



air. The scale was predominantly chromia and spalled upon cooling. Alloying with aluminum up to 8 weight percent reduced the spalling drastically. Furthermore, aluminizing the surface of the Cr-W alloys completely stopped the spalling.

3:15 PM

High Temperature Corrosion of Cr-W Alloys in Simulated Syngas: *Omer Dogan*¹; Sophie Bullard¹; Bernie Covino¹; ¹National Energy Technology Laboratory

Search for new high temperature materials for energy applications continues. This presentation will focus on degradation of Cr alloys containing 0-30%W by weight in a flowing gas mixture containing 30%CO, 8%CO2, 20%H2, 2%CH4, 0.8%H2S, 0.02%HCl, and 40%N2 by volume at temperatures up to 1000°C. A pseudo-cyclic test involving heating the specimens, holding them at temperature for varying periods, and cooling them to room temperature was employed. Mass change of the specimens was determined after each cycle. Corrosion scale on the specimens was characterized using SEM, WDX, and XRD. Various sulfides, oxides, carbides, and nitrides were determined in different layers of the scale.

3:40 PM Break

3:55 PM

Disordered Interfacial Films and Activated Sintering: Phenomenological Similarities among Ice, Ceramics and Refractory Metals: *Jian Luo*¹; Vivek Gupta¹; ¹Clemson University

Equilibrium-thickness, intergranular (and surficial) amorphous films have been widely observed in ceramics since the 1980's and recently, in a refractory metal system W-Ni (Appl. Phys. Lett. 87, 231902 (2005)). Furthermore, a series of studies revealed the stabilization of nanometer-thick, "quasiliquid," interfacial films well below the bulk solidus temperature, indicating a clear analogy to the phenomenon of ice premelting. On the other hand, solid-state activated sintering refers to the phenomenon whereby sintering rates are significantly improved because of solid-state additives. Recent studies attributed subsolidus accelerated sintering to short-circuit diffusion in disordered interfacial films for ZnO-Bi2O3 and W-Ni. Interestingly, premelting of ice was also presumed to result in the "activated sintering" of snow. This presentation critically discusses the phenomenological similarities in disordered interfacial film formation and activated sintering among ice, oxides and refractory metals. An emphasis is placed on recent results in W-Ni and an analysis of other binary refractory metals.

4:20 PM

Properties of Nickel Film Prepared by Electrochemical Deposition under Super-Gravity Condition: *Zhancheng Guo*¹; Zhangfu Yuan²; ¹Metallurgical Engineering School, University of Science and Technology of Beijing, China; ²Institute of Process Engineering, Chinese Academy of Sciences

The experimental results reveal that the nickel film prepared by electrodeposition in the super-gravity field is observed with high properties. The SEM pictures show that surface structure of nickel film deposited under the supergravity condition seems to be more uniform compared with that in normal gravity condition, and crystal grains diminish with the increase of supergravity coefficient. The XRD patterns indicate that arrangement of crystal grains of nickel film deposited under the super-gravity field is more regular and orderly. Toughness and tensile stress of nickel film are raised markedly, content of hydrogen decreases. From the polarization curves of hydrogen evolution reaction under the super-gravity field, a significant lowering of over-potential in nickel electrode was found when current density increased. The process of hydrogen evolution reaction was accelerated under the supergravity field, which was proved by the analysis of formation and outflow process of bubbles.

Shape Casting: The 2nd International Symposium: Liquid Metal/Solidification

Sponsored by: The Minerals, Metals and Materials Society, TMS Light Metals Division, TMS: Aluminum Committee, TMS: Solidification Committee

Program Organizers: Paul Crepeau, General Motors Corporation; Murat Tiryakioglu, Robert Morris Univ; John Campbell, University of Birmingham

Monday PM	Room: Northern E2
February 26, 2007	Location: Dolphin Hotel

Session Chair: Sumanth Shankar, McMaster University

2:00 PM Introductory Comments

2:10 PM

Preventative Metal Treatment through Advanced Melting System Design: *Mark Osborne*¹; Thomas Meyer²; Mike Kinosz¹; C Eckert¹; ¹Apogee Technology, Inc; ²General Motors Powertrain

Recent technology advances in aluminum melting under a U.S. Department of Energy program is changing how melt shops for foundries are designed. Metal quality has now become implicitly preventative through the use of an advanced three-stage process. First, the melting operation (Isothermal Melting) melts aluminum using high flux subsurface conduction, with a maximum metal temperature less than 22°C above the mean holding temperature. No products of combustion (i.e.: water) are produced. Second, turbulent free metal transfer occurs into integrally heated molten metal delivery ladles that are detained at the casting unit for controlled metal dispensation. These vessels functionally serve as portable holding furnaces. Finally, molten aluminum is delivered to the casting unit by a new high heat flux launder/trough system design based on conduction. Surface heating of metal does not occur and temperature can be closed loop controlled. This paper will describe the system and expected metal quality benefits.

2:35 PM

A Comparison of Methods Used to Assess Aluminium Melt Quality: Derya Dispinar¹; John Campbell²; ¹University of Istanbul; ²University of Birmingham

This study reviews and compares the techniques such as LIMCA, PoDFA, Prefil, LIAS and RPT that are used to quantify defects in liquid aluminium alloys. In general, it is found that most of the current techniques are not fully satisfactory. Only the Reduced Pressure Test (RPT) appears to give reliable results of the number and size of bifilms (and sometimes, but not infallibly, an indication of hydrogen content). The number and size are both quantifiable, and are recommended as the major quality indicators.

3:00 PM

Initial Filtration Behaviour of Liquid Aluminium Alloys: Xinjin Cao¹; ¹Institute for Aerospace Research

There has been an increasing tendency to detect liquid metal quality using the pressure filtration methods in metallurgical and manufacturing industries. Recently with the introduction of derivative methods and the classification of three flow states (i.e. initial transient, steady and terminal transient), some new insights into pressure filtration behavior of liquid aluminum alloys have been obtained. However, the initial transient stage occurring during the pressure filtration tests has not been well understood. Occasionally, the initial transient state might disappear or even last the whole period of the filtration operation. Clearly, this stage is important for the investigation of filtration behavior as a whole because it appears prior to the establishment of cake mode filtration, and thereby it has significant influences on the cake structure formed and the properties, the filtration behavior and the detection of liquid metal quality. This work discusses some fundamental aspects occurring in this stage.



3:25 PM

Radioactively Labelled Particle Tracking in Steel Castings: Youssef Beshay¹; William Griffiths¹; David Parker¹; Xianfeng Fan¹; ¹University of Birmingham

It is well established that non-metallic inclusions are detrimental to the mechanical properties of metal castings. However, the movement of such inclusions during filling and solidification of the casting is unknown. This paper describes the development of an experimental technique by which the movement of inclusions can be tracked in castings. Alumina inclusions of size 355-425 μ m were radioactively labelled using the Birmingham University cyclotron and placed at a known position in a ceramic shell mould upon a steel mesh. EN3B steel was cast into the moulds and, after the casting had solidified, the position of the radioactive particle was determined using a γ -Ray positron camera. The co-ordinates of the particle within the casting were obtained and it was successfully relocated using SEM and EDX identification. This technique is a valuable tool for any application where the presence of inclusions is critical.

3:50 PM Break

4:05 PM

The Effect of Holding Time on Double Oxide Film Defects in Al Castings: *William Griffiths*¹; Ahmed Omotunde¹; Ramin Raiszadeh²; ¹University of Birmingham; ²Shahid Bahonar University of Kerman

Once double oxide film defects have formed in liquid Al, it is anticipated that they should undergo further development due to interaction with the bulk liquid metal. This may modify their effect on the mechanical properties of a casting, and therefore requires further study. The experiments reported in this paper involved casting into ceramic investment moulds, which were then held in the liquid state for different periods of time before solidification. As a result, the interior atmosphere trapped within the double oxide film defects was allowed to interact with the surrounding melt for up to 40 minutes. Examination of the oxide films found on the fracture surfaces of tensile test bars from these castings showed changes in structure of the defect with time which can be interpreted to gain a better understanding of the effect of double oxide film defects on casting properties.

4:30 PM

How to Measure Viscosity of Liquid Aluminum Alloy: *Minhajuddin Malik*¹; Guillaume Lambotte²; Mohamed Hamed¹; Sumanth Shankar¹; ¹McMaster University; ²CRCT - Ecole Polytechnique de Montreal

Viscosity of liquid Al and Al-Si alloys are critical to better understand the solidification and porosity formation in the mushy zone towards the end of solidification of the alloy. In this paper, viscosity data from the literature for Al and Al-Si alloys are presented along with the drawbacks of the most prevalent technique used to evaluate viscosity – the oscillating vessel viscometer. Experimental techniques using an alternative rotational rheometer equipped with a cone and plate measuring geometry are presented along with results of flow characterization of molten Zn and Al-Si alloys. The results show that molten Zn exhibits Newtonian flow characteristics and molten Al-Si eutecticalloy exhibits a non-Newtonian behavior at various melt superheats and low shear rate regimes.

4:55 PM

New Approaches to Understanding Modification and Nucleation Mechanisms in Hypoeutectic Al-Si Alloys: *Kazuhiro Nogita*¹; Arne Dahle²; ¹ARC Centre of Excellence for Design in Light Metals, University of Queensland; ²University of Queensland

The demands for the performance of cast aluminium alloys continue to increase while, at least with respect to current knowledge, Al-Si alloys are already on their performance limit. Solidification of the eutectic is one of the last reactions to occur and this is where most casting defects, such as porosity and hot-tears are formed. Although it is frequently acknowledged that the solidification of the eutectic is critical for porosity formation, currently there is a lack of understanding regarding how the eutectic evolves and how it can be controlled. Recent developments in the understanding of eutectic solidification in hypoeutectic Al-Si foundry alloys will be discussed. Techniques such as EBSD/SEM, FIB/FE-TEM and micro-XRF/Synchrotron radiation have been applied. The engineering of eutectic solidification is likely to form the basis for future step improvements in the metallurgy of Al-Si foundry alloys.

5:20 PM

Unintentional Effects of Sr Additions in Al-Si Foundry Alloys: Stuart McDonald¹; Matthew Dargusch¹; *David StJohn*¹; ¹CAST Cooperative Research Centre

Strontium additions are commonly made to aluminium-silicon based foundry alloys to promote a fibrous eutectic silicon morphology. Although this structural modification is the primary goal, it has become apparent that there are several concomitant changes. This paper examines this issue, reviewing the well-known alterations in porosity distribution and eutectic grain size that accompany strontium additions and introducing new research on the effects of strontium on corrosion resistance and as-cast surface finish. It is shown that strontium additions significantly affect both surface finish and corrosion resistance, through a combination of physical and chemical mechanisms. It is concluded that despite being present at only trace levels, strontium has a powerful effect on a variety of casting properties that extends beyond a transition in the morphology of the eutectic silicon phase.

Structural Materials Division Symposium: Mechanical Behavior of Nanostructured Materials, in Honor of Carl Koch: Processing and Characterization of Materials Subjected to Severe Plastic Deformation

Sponsored by: The Minerals, Metals and Materials Society, TMS Electronic, Magnetic, and Photonic Materials Division, TMS Materials Processing and Manufacturing Division, TMS Structural Materials Division, TMS: Chemistry and Physics of Materials Committee, TMS/ASM: Mechanical Behavior of Materials Committee, TMS: Nanomechanical Materials Behavior Committee

Program Organizers: Xinghang Zhang, Texas A&M University; Yuntian Zhu, Los Alamos National Laboratory; Michael Rigsbee, North Carolina State University; C. Suryanarayana, University of Central Florida; Haiyan Wang, Texas A&M University; C. T. Liu, Oak Ridge National Laboratory

Monday PM	Room: Asia 5
February 26, 2007	Location: Dolphin Hotel

Session Chairs: Yuntian Zhu, Los Alamos National Laboratory; Tong Shen, Los Alamos National Laboratory

2:00 PM Invited

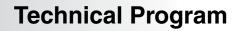
Achieving Superplastic Behavior in F.C.C. and H.C.P. Metals Processed by ECAP: Roberto Figueiredo¹; Megumi Kawasaki¹; Cheng Xu¹; *Terence Langdon*¹; ¹University of Southern California

Processing by Equal-Channel Angular Pressing (ECAP) provides the capability of producing ultrafine submicrometer grain sizes in a wide range of materials. If these grains are reasonably stable at elevated temperatures, there is an opportunity for achieving high superplastic ductilities in materials that are nominally not superplastic. This paper describes recent investigations on representative f.c.c. and h.c.p. alloys where excellent superplastic properties are attained after processing by ECAP.

2:20 PM

Development of Ultrafine Grained Structure in Low Carbon Steel by ECAP at Increased Temperatures: *Jozef Zrnik*¹; Sergey Dobatkin²; ¹COMTES FHT Sro; ²Baikov Institute of Metallurgy and Materials Science

The paper describes the refinement process of AISI 10 steel coarse grained microstructure by applying a high strain plastic deformation. The steel was subjected to ECAP in temperature range of $150 - 300^{\circ}$ C with N = 3 passes at each selected temperature. The transmission electron microscopy (TEM) was used to study the formation and stability of newly born ultrafine grain structure. The TEM of thin foils revealed that at already the lowest deformation temperature of 150°C accidentally scattered polygonized subgrains were present in deformed grained structure. As temperature of ECAP deformation was increasing the process of dynamic polygonization and recrystallization contributed to formation of submicrocrystalline grains embedded within ferrite elongated grains. Tensile test results showed that formation of advanced microcrystalline structure resulted in significant increase of yield stress and





tensile strength of steel. The strain hardening region was extended prior the softening with increasing ECAP temperature.

2:35 PM

Comparison of ECAP and Plane-Strain Machining: *Terry McNelley*¹; Srinivasan Swaminathan¹; Alexander Zhilyaev²; Srinivasan Chandrasekar³; W. Dale Compton³; Alexander King³; Kevin Trumble³; ¹Naval Postgraduate School; ²Centro Nacional de Investigaciones Metalurgicas; ³Purdue University

The shear strain during a single ECAP pass is determined mainly by the angle between die channels and is 2.0 for a 90° die with sharp corners. A billet can be subjected to repetitive ECAP and thereby experience large cumulative strains through a series of deformation stages leading to microstructure refinement down to the nano-scale. In contrast, by controlling the tool rake angle and depth of cut during plane-strain machining the resulting chip may experience shear strains varying from ~1.0 to 10 in a single stage of deformation. The mechanics, microstructure, microtexture and mechanical properties of materials processed by both ECAP and plane-strain machining are compared.

2:50 PM Invited

The Nature and Importance of Vacancy Type Defects in SPD Nanometals: *Michael Zehetbauer*¹; Daria Setman¹; Elena Korznikova²; Erhard Schafler¹; ¹University of Vienna; ²Ufa State Aviation Technical University

Recently, excessive concentrations of deformation induced vacancy type defects have been found in SPD processed nanometals but not in others which suggests them to be responsible for SPD specific properties i.e. considerable ductility, and marked shifts of phase existencies. Among the methods for vacancy analysis, that of annealing calorimetry appears advantageous because of its high speed and good reproducibility. Activation enthalpy data derived from rate-dependent peak temperature shifts inform on both the defect type and the actual diffusion mechanism, although for identification of complex vacancy defects, comparisons with XRD dislocation density measurements are indispensable. The activation enthalpy for single/double vacancy migration in SPD nanometals turns out to be about one halfth of that measured in quenched/ irradiated materials. Simultaneous systematic investigations of ductility and vacancy concentration are introduced in order to ascribe the ductility to either the load releases occurring after SPD, or to grain boundary sliding occurring during ductility testing.

3:10 PM

Characterization of Nanostructured Pure Aluminium with Different Grain Size Distributions Synthesised Using Back Pressure Equal Channel Angular Consolidation: Xiaolin Wu¹; Wei Xu¹; *Kenong Xia*¹; ¹University of Melbourne

Back pressure equal channel angular consolidation (BP-ECAC) was used to synthesise bulk materials from particles. In the present study, bulk pure aluminium was consolidated from nano particles and mixtures of nano and micro particles in varying proportions to obtain different grain size distributions. These materials were processed by equal channel angular pressing (ECAP) for 4 passes at 400°C with the application of a constant back pressure of 200 MPa. Full density was achieved in all the materials. Mechanical tests showed that hardness and strength increased significantly with increasing volume fraction of the nano particles while ductility decreased. The grain structures were characterised by XRD and TEM. Microstructures before and after deformation were examined using TEM. The effects of nano-scale and microscale structures on mechanical behaviour were analysed.

3:25 PM Break

3:35 PM Invited

Grain Boundaries Engineering of UFG Metals for Advanced Properties: Ruslan Valiev¹; ¹UFA State Aviation Technical University

Grain boundaries (GBs) engineering is concerned with tailoring different GBs (low angle and high angle ones, special and random, equilibrium and non-equilibrium) in ultrafine -grained metals by severe plastic deformation (SPD) processsing. Using various regimes and routes of SPD processing we show the ability to produce UFG materials with different grain boundaries, and this can have a dramatical effect on mechanical behaviour of the processed materials, particular, on their strength and ductility, fatigue or superplasticity. We demonstrate several examples of this approach for attaining high strength and ductility as well as enhanced superplasticity at low temperatures and high strain rates in various UFG metals and alloys. The origin of these phenomena is discussed on the basis of the results of microstructural studies and observations of deformation mechanisms.

3:55 PM

Deformation Behavior Modeling of Nanostructured CP TI: *Igor Alexandrov*¹; Roza Chembarisova¹; Vil Sitdikov¹; ¹Ufa State Aviation Technical University

Recent years investigations have convincingly demonstrated wide capabilities of the severe deformation (SPD) method applied to form nanostructured states in bulk billets of different metallic materials. It has been shown, that a small grain size, non-equilibrium grain boundary state and crystallographic texture determine the character of specific deformation behavior of SPD nanostructured billets, characterized as by high strength as well as by considerably high ductility, with the simultaneous lack of strain hardening or even with the presence of strain weakening. The current report presents the results of kinetic modeling, used to analyze features of deformation behavior of nanostructured CP Ti during tensile tests. As a result of the conducted investigations we evaluated possible contribution of different potential deformation mechanisms into formation of corresponded experimental "stress-strain" curves.

4:10 PM Invited

High Strength and Ductile Bulk Nanostructured Titanium Alloys: Jurgen Eckert¹; ¹Darmstadt University of Technology

To circumvent the ductility limitations of bulk nanostructured metals and alloys, heterogeneous materials with different type and length-scale of heterogeneities (bimodal grain size distributions, micrometer-sized second phases, phase separation etc.) have been developed to control the mechanical properties. As examples, results obtained for Ti-base bulk nanostructured alloys with heterogeneous microstructure will be presented. This type of material exhibits high strength together with pronounced work hardening and large ductility by controlling the instabilities otherwise responsible for early failure. Due to the coexistence of different phases with different intrinsic properties and length scale rather complex combinations of deformation mechanisms occur that can include dislocation slip, twinning, martensitic transformation and shear banding. We will illustrate the possibilities to manipulate such microstructures and their impact on the deformation behavior in favor of either strength and ductility, or a combination of both for a series of titanium alloys.

4:30 PM Invited

A Mechanistic Model for Shear Bands in Nanostructured Materials: Shailendra Joshi¹; *K.T. Ramesh*¹; ¹Johns Hopkins University

The impressive mechanical strengthening in nanostructured (NS) materials is juxtaposed with novel microscopic deformation mechanisms, which determine their post-yield response. An important macroscopic characteristic observed in some NS materials is the propensity to plastic instability; e.g. quasistatic compression experiments on NS-Fe^{1, 2} indicate inhomogeneous plastic flow that develops through shear banding, while CG-Fe exhibits homogeneous response. Unlike adiabatic shear bands at high rates, shear bands at quasistatic rates have been attributed to likely geometric softening due to novel mechanisms (e.g. grain rotation) triggered by grain size refinement.¹ We present a model for shear band development in NS metals at quasistatic rates. The model predicts nucleation and growth of shear bands and considers evolution of geometric softening due to grain rotation as an important mechanism. ¹Jia, D et al. (2003) Acta Mater. 51, 3495-3509. ²Carsley, JE et al. (1998) Metall. Mater. Trans. A, 29A, 2261-2271.

4:50 PM

Dynamic Mechanical Behavior of Ultrafine Grained and Nanocrystalline bcc Metals: *Qiuming Wei*¹; Kaliat Ramesh²; Evan Ma²; Brian Schuster³; Laszlo Kecskes³; Robert Dowding³; ¹University of North Carolina at Charlotte; ²Johns Hopkins University; ³US Army Research Laboratory

Recent experimental results have uncovered some novel behavior of metals with ultrafine grain (UFG, grain size d below 500 but above 100 nm) and nanocrystalline (NC, d<100 nm) microstructures. Apart from the much increased strength of UFG/NC metals, it has been observed that strain rate dependence of UFG/NC metals is a function of lattice structure. For example, in the UFG/NC regime face-centered cubic (FCC) metals have enhanced strain



rate sensitivity, while body-centered cubic (BCC) metals exhibit reduced strain rate sensitivity. Such behavior imparts strong influence on some constitutive response. We have investigated the dynamic mechanical behavior of UFG/NC BCC metals. The UFG/NC microstructures have been obtained by either topdown method (such as severe plastic deformation) or bottom-up method (such as nano-powder compaction). Uni-axial dynamic testing using compressive Kolsky bar technique of the UFG/NC BCC metals show that adiabatic shear localization is the predominant deformation mode in such metals.

5:05 PM

Scale up and Applications of Equal Channel Angular Extrusion (ECAE) for the Electronic and Aerospace Industries: *Stephane Ferrasse*¹; Frank Alford¹; Susan Strothers¹; Janine Kardokus¹; ¹Honeywell International Inc

ECAE is a promising method to produce bulk pieces of materials with submicron grain size. Two areas are critical to promote ECAE beyond the stage of a laboratory curiosity: (i) die design and scale up; (ii) understanding of the mechanical properties of submicron-grained materials. Those lines of development are pursued at Honeywell. A first case is the successful scale up and commercialization of ECAE for the production of Al and Cu alloy sputtering targets for the electronic industry. Blank dimensions are about 20 times bigger than those reported in the literature. Examples of the superior sputtering performance of ECAE targets are presented. Other reported applications include the increase in tensile strength, high cycle fatigue and toughness in medium-to-heavily alloyed Al materials used in aerospace. In alloys, reaching optimal properties requires a better understanding of the interplay between plastic deformation and precipitation mechanisms.

5:20 PM

The Effect of Geometrically-Necessary Dislocations on Grain Refinement and Mechanical Properties of an Al-7si Composite Processed by Severe Plastic Deformation: *Maria Muñoz-Morris*¹; Ivan Gutierrez¹; David Morris¹; ¹CENIM-CSIC

The effect of severe plastic deformation by equal channel angular pressing (ECAP) on microstructure refinement and changes of mechanical properties has been examined on an Al-7%Si composite and an Al-0.5%Si monolithic alloy. The coarse Si particles of the Al-7Si composite are broken into much finer equiaxed particles distributed in a banded structure at the same time as grain refinement of the Al matrix occurs, reaching sizes below 200 nm. Faster grain size refinement is observed in the composite, not only during the initial stages but also after much higher strain levels. The ECAP process leads to an increase in yield stress of almost a factor of three in the Al-7Si composite which has been described by three contributions: the undeformed/ solute strengthened matrix term, significant hardening by the high density of dislocations inside the grains, and significant hardening by the extremely fine grain sizes achieved in the composite.

Towards Functional Nanomaterials: Synthesis, Characterization, and Applications: Nano Magnetism, Ferroelectric, Mechanics, and Other Properties

Sponsored by: The Minerals, Metals and Materials Society, TMS Electronic, Magnetic, and Photonic Materials Division, TMS: Nanomaterials Committee *Program Organizers:* Zhiming Wang, University of Arkansas; Alexander Govorov, Ohio University; Andrey Rogach, Ludwig-Maximilians-Universität München

Monday PM	Room: Oceanic 5
February 26, 2007	Location: Dolphin Hotel

Session Chairs: Xiangcheng Sun, University of Western Ontario; Elena Guliants, University of Dayton Research Institute

2:00 PM Invited

Nanomagnetism by Surface Manipulation: *Xiaofeng Jin*¹; ¹Fudan University

The lattice-constant of a solid-state material is certainly a key parameter in determining its physical and chemical properties. By varying the lattice constant one can tune the electronic band structure as well as the density of states at the Fermi level, therefore change correspondingly all the physical and chemical properties. In this work, by using the "composition wedge" and "lattice-constant wedge" techniques with molecular beam epitaxy, we show that one can manipulate independently the surface chemistry and lattice constant of a single crystal substrate. Applying them to ultrathin Fe and Ni on Cu(001), two of the most important yet still controversial nanomagnetic systems, we show how to manipulate their magnetic properties including magnetic ordering and anisotropy in a well controlled way which is helpful to clarify some longstanding critical issues of the systems.

2:30 PM Invited

Tuning Properties of Functional Iron Nanoparticles in Sonochemistry: *Elena Guliants*¹; Christopher Bunker²; ¹University of Dayton Research Institute; ²Air Force Research Laboratory

Recent advances in the science of nanostructured materials have resulted in new types of nanoparticles displaying novel, unique, and potentially valuable properties. The sonochemical processes based on acoustic cavitation of a liquid medium were shown to promote ultra-fast reactions inside the bubbles formed as a result of alternating compression and rarefaction regions in the liquid. Sonication of iron pentacarbonyl Fe(CO)5, a commonly used iron precursor, resulted in essentially different reaction products depending on the use of certain solvents and coating agents to prevent agglomeration. The presence of hydrocarbon solvents during the reaction has led to the formation of zerovalent iron (Fe0) nanoparticles, whereas the water-based sonochemistry produced various iron oxide phases. Studying the effect of carboxylic acid coatings on properties of Fe0 nanoparticles allowed tuning of the thermal stability of the particles. Addition of proteins to water sonochemistry of Fe(CO)5 was observed to control magnetic phases of iron oxide.

3:00 PM

First-Principles Studies of Ferroelectric Nanodomains: *Bo-Kuai Lai*¹; Inna Ponomareva¹; Ivan Naumov¹; Igor Kornev¹; Huaxiang Fu¹; Laurent Bellaiche¹; Greg Salamo¹; ¹University of Arkansas

Ferroelectric materials have attracted considerable research interest in the past decade because of their applications in non-volatile random access memories, microactuators, and radio frequency and microwave devices. As technology is leading toward to smaller devices, our fundamental understating on ferroelectric thin films and their domain structures is extremely critical to push forward the existing technology and could lead to new applications. The motivation of this report is to use first-principles method to study the finite size effect on the formation of nanostripe domains in ferroelectric Pb(Zr0.5Ti0.5)O3 and BaTiO3 ultrathin films and how the nanostripes evolve under applied electric fields. The atomistic details of the nanostripes and their unique electric-field induced evolution sequence through the formation of nanobubbles (i.e., nanostripes -> nanobubbles -> monodomain) are revealed. The comparison between Pb(Zr0.5Ti0.5)O3 films and BaTiO3 ultrathin films is also provided.

3:15 PM

Synthesis and Characterization of Periodic Magnetic Nanostructures: Raju Ramanujan¹; Akhilesh Srivastava¹; ¹Nanyang Technological University

Magnetic nanostructures have novel applications as biosensors, plasmonic and photonic devices and as information storage media. Chemical synthesis methods were employed to prepare periodic arrays of nanowires and nanobowls in lithographically patterned, anodic aluminum oxide (AAO) and polystyrene spheres (PS) templates. Magnetic nanoparticles of cobalt and cobalt ferrite were synthesized using the reverse micelle technique in the presence of an external magnetic field, these nanoparticles were then infiltrated in the interstitials of the templates. Interconnected periodic nanobowl arrays were synthesized, the reaction conditions and annealing environment were used to alter the morphology, crystal structure and properties. Nanowires of cobalt and cobalt ferrite were also synthesized within AAO templates. The morphology and periodicity was varied by changing the template geometry and pore dimensions, the samples were annealed in order to produce nanowires with the hcp crystal structure. The effect of shape and magnetocrystalline anisotropy on properties was studied.





3:30 PM

The Application of Arrays of Nickel Nanobars: The Underlying Magnetic Properties: *Prabeer Barpanda*¹; ¹Rutgers University

Owing to its robustness and higher coercivity, nickel (Ni) nanobars are quite promising for MRAM application. An array of interacting nanobars with large shape anisotropy leads to a special domain structure known as 'inversion symmetry feature'. Upon application of exernal field, the magnetization reversal occurs by movement and breaking of this inversion symmetry. This high-energy process leads to higher coercivity. The current work studies the effect of inversion symmetry (in Ni nanobars) on the magnetisation behaviour of an array of closely-spaced nanobars. Arrays of Ni-nanobars (spaced 10 nm apart) of varying length (20~200 nm) and diameter (10~50 nm) are probed. The longitudinal magnetisation reversal revealed the formation of symmetric inversion state, which gradually formed a Neel wall at the central cross section of nanobars before switching to the other direction. This was true both for single domain and vortex state bearing Ni nanobars.

3:45 PM Break

3:55 PM Invited

Experimental Mechanics of Nanostructures - Challenges and Opportunities: *Xiaodong Li*¹; ¹University of South Carolina

Although much work has been focused on synthesis of nanostructures, the mechanical property measurements of nanostructures have been largely ignored. We have extended applications of traditional nanoindentation and atomic force microscopy (AFM) approaches to zero- and one-dimensional nanostructures for directly measuring their mechanical properties. Hardness and elastic modulus of Cu2O nanocubes, silver nanowires, gold nanowires, ZnO and ZnS nanobelts, and amorphous and crystalline boron nanobelts were measured by directing indenting them with a nanoindenter. Nanoscale deformation behavior and fracture mechanisms were studied by post insitu AFM imaging of the indents. Mechanical properties of SiO2 and GaN nanowires were obtained by directly bending individual suspended wires using an AFM tip. Calibration procedures for the AFM mechanical testing have been established. Another immediate challenge in nanotechnology is manipulation and integration of nanostructures into functional, usable structures and devices. Experimental mechanics of nanostructures are fundamental aspects for the commercialization of nanotechnology.

4:25 PM

Self-Assembly of Magnetic FePt and FePt(M) Nanoparticles: Xiangcheng Sun¹; ¹University of Western Ontario

Controlled self-assembly of magnetic nanoparticles has stimulated great interest as it may offer a convenient tool for magnetic nano- or bio-fabrication. In this study, a series of FePt and FePt(M) nanoparticles has been synthesized by chemically polyol reduction in the presence surfactants of oleic acid and oleyl amine. As-prepared particles have a chemically disordered face-centered cubic crystal with average diameter of 4 nm and are superparamagnetic. These magnetic particles were well dispersed in hydrocarbon solvents and selfassembled into particles arrays with a variety of close-packing arrangements. Larger domains of monolayer, two layers and more than five layers of particles arrays are easily fabricated. It is worthy to note that van der Waals forces, magnetic dipoles and steric repulsion among magnetic particles have been responsible for this self-assembly process. Eventually controlling preparation conditions is crucial to obtain the controlled magnetic particle arrays (or selfassembly) with uniform size and composition distributions.

4:40 PM

Interfacial Strain and Nanoferroelectric Domain of (Ba, Sr)TiO3 Films on Pt/Ti/SiO2/Si Substrate: *Jihua Zhang*¹; Chuanren Yang¹; Hongwei Chen¹; ¹University of Electronic Science and Technology of China

Stimulated by the trend of miniaturization of electronic devices, the issue of the size effect on ferroelectricity has been of high interest during the past years. Generally, interfacial strain and fine grain size have a dominant effect on ferroelectricity for thin films. In this paper, High Resolution Transmission Electron Microscope (HRTEM) was used to characterize the microstructure of Ba0.6Sr0.4TiO3 (BST) thin films prepared by radio frequency magnetron sputtering. A periodic nanoscale ferroelectric multidomain structure is observed in the BST thin film. The domains have a width of 11.11 Å (4 unit cells of the BST phase), which is much less than previous reports of critical

size (several to tens nanometers) but is close to the theory predicted. High resolution lattice fringe images show the BST/Pt interfacial strain of BST film. This is a visual representation for characterization of interfacial stress and is helpful for understanding of ferroelectricity in thin films.

4:55 PM

Optical Studies of ZnO Nanocrystals: Effect of Morphology and Surface States: Yinyan Gong¹; Tamar Andelman¹; Stephen O'Brien¹; *Igor Kuskovsky*²; ¹Columbia University; ²Queens College of CUNY

ZnO is a promising candidate for optoelectronics owing to its direct wide bandgap and large exciton binding energy. Currently, ZnO nanocrystals are being extensive studied, for device performance is often improved by the use of low-dimensional structures. Here, we present results of photoluminescence (PL) and optical absorption measurements of ZnO nanocrystals of various morphologies: nano-particles, nano-triangles, and nano-rods with differently modified surfaces. Although the PL of all nanocrystals is dominated by the UV emission, we found that the intensity of the green luminescence is strongly depends on morphology and the surface passivation. For nanocrystals of the same morphology, the green emission can be largely suppressed by modifying surfaces states, by varying the solvent.

5:10 PM

Directed Growth of Single-Wall Carbon Nanotube Bundles by Means of an "All-Laser" Processing for Nanoelectronic Device Applications: *M.A. El Khakani*¹; B. Aïssa¹; E. Champagne¹; ¹Institut National de la Recherche Scientifique, INRS-EMT

The directed growth of single wall carbon nanotubes(SWCNTs) has been achieved by means of an "all-laser" synthesis approach, which uses the same UV laser, in a first step, to deposit the catalyst nanoparticles(NPs) and, in a subsequent step, to grow the SWCNTs. The "all-laser" growth process is shown to permit the lateral bridging of adjacent patterned CoNi NPs. Indeed, random networks of SWNTs were formed on the SiO₂ or SiN coated silicon substrates. Atomic force microscopy and electron microscopy observations revealed that the SWCNTs generally self-organize into bundles with diameters of 10-20 nm which, in turn, interconnect to form random networks. On the other hand, microRaman spectra showed that the SWCNTs present a relatively narrow radial breathing mode (RBM) absorption band which corresponds to a mean nanotube diameter of 1.2 nm. The "all-laser" grown SWCNTs were directly integrated into field-effect transistor (FET) like devices and their electrical transport propertries investigated both in air and under vacuum. The "all-laser"-SWCNTs based devices are found to behave, depending of the nanodevice articheture, either as p type FETs or as ambipolar FETs with ON/OFF switching ratios in the 104-107.

Wide Band-Gap Semiconductor Nanostructures: Session II

Sponsored by: The Minerals, Metals and Materials Society, TMS Electronic, Magnetic, and Photonic Materials Division, TMS: Electronic Materials Committee, TMS: Nanomaterials Committee, TMS: Thin Films and Interfaces Committee, TMS: Young Leaders Committee *Program Organizers:* Ashutosh Tiwari, University of Utah; Haiyan Wang, Texas A&M; Minseo Park, Auburn University

Monday PMRoom: Oceanic 4February 26, 2007Location: Dolphin Hotel

Session Chair: Dhananjay Kumar, North Carolina A&T University

2:00 PM Introductory Comments D. Kumar

2:10 PM Invited

Wide Band Gap Based Semiconductor Micro- and Nanoresonators for Sensor Applications: *Oliver Ambacher*¹; K. Tonisch¹; F. Will¹; V. Cimalla¹; K. Brueckner¹; R. Stephan¹; M. Hein¹; ¹Technical University Ilmenau

Due to the combination of mechanical structures with electrically active elements for actuation and sensing, the technology of micro- and nanoelectromechanical systems bears a huge potential for sensing applications. Reported resonant frequencies up to 1 GHz and quality factors of several



10000 of ultra sensitive MEMS/NEMS are achieved at low temperatures and ultra high vacuum. For sensing applications, especially biological ones, it is necessary to work under ambient conditions or even in liquids. In this work we will demonstrate MEMS/NEMS resonators which are driven by a magnetomotive actuation under ambient conditions. We describe the fabrication of AlN and SiC micro- and nanoelectromechanical resonators of different design. We have analyzed resonators with fundamental mechanical resonant frequencies between 2 kHz and 2 MHz and quality factors in excess of 30000 in vacuum and 350 in air. Finally, results of sensitivity experiments and examples of biological and chemical sensor applications are presented.

2:45 PM Invited

Zinc Oxide Thin Films and Nanostructures: Physical Vapor Synthesis and Integration into Flexible Electronics Platforms: *Renato Camata*¹; Masashi Matsumura¹; Mevlut Bulut¹; Jonathan Williams¹; ¹University of Alabama, Birmingham

Zinc Oxide (ZnO) is a multifunctional material with a suite of desirable properties. Its wide direct bandgap and large exciton binding energy make it attractive for UV LEDs, lasers, and sensors. Nanostructures exhibiting strong piezoelectricity have great potential for applications in biosensors and nanoactuators. Biologically safe, polycrystalline films with good crystal quality, ductility, and moderate Hall mobilities, can be grown at low temperatures, making it compatible with low-cost and flexible substrates. ZnO is also a promising host for metal ions that can act as optical centers in the midinfrared. In this talk we show how we have used Nanoparticle Beam Pulsed Laser Deposition, a novel technique, to produce nanostructured ZnO films that are integrated with flexible polyimide substrates. We discuss the challenges involved in the synthesis of ZnO uniformly doped with transition metal ions in relation to other II-VI semiconductors (e.g., ZnSe) and their application in tunable mid-infrared laser sources.

3:20 PM

ZnO Based Diluted Magnetic Semiconductors and Spin Polarized Injection into ZnO: *Shivaraman Ramachandran*¹; John Prater¹; Jagdish Narayan¹; ¹North Carolina State University

Here we will discuss the various aspects of diluted magnetic semiconductor thin film growth and characterization. ZnO based DMS materials have gained attention in the last few years as the possibility of realizing room temperature ferromagnetism has been realized with consistency in Co-ZnO and Mn-ZnO. In addition, we have been able to tune the ferromagnetism in these systems as a function of carrier concentration. We have done extensive characterization on these films including magnetic, microstrucural, electronic and optical properties. From these experiments, we have been able to deduce the mechanism causing magnetic ordering in these materials. We will also discuss spin polarized injection into semiconductors using these DMS materials by making device heterostructures which would ultimately help in realizing novel functional devices like spin transistors and other spintronic devices.

3:50 PM Break

4:20 PM

Electrical and Optical Properties of Ga Doped ZnO Thin Films Grown Using PLD: *Michael Snure*¹; Minseo Park²; Ashutosh Tiwari¹; ¹University of Utah; ²Auburn University

Transparent conducting oxides (TCO) have recently gained much attention due to a number of exciting applications. ZnO has shown to be one of the most promising materials for use in TCOs because of its attractive optical and electronic properties, which are greatly enhanced when dimensions are reduced to the nanometer scale. Here, we report on a systematic study of the optical and electrical properties of Znx-1GaxO, x = 0,...,5 atomic %, thin films grown using pulse laser deposition (PLD). These films that were grown on c-plane sapphire substrates are highly transparent in the visible spectrum and show a decrease in resistance with the addition of Ga dopent. Work has also been done to see how nitrogen annealing effects the optical and electronic properties of these films.

4:45 PM

One-Dimensional ZnO Nanostructures for Dye-Sensitized Solar Cell Application: *An-Jen Cheng*¹; William Ward¹; Dake Wang¹; Curtis Shannon¹; Minseo Park¹; Yonhua Tzeng¹; Wonwoo Lee²; ¹Auburn University; ²University of Alabama, Birmingham One-dimensional (1-D) zinc oxide (ZnO) is a wide band gap semiconductor, and has been considered as an excellent semiconducting metal oxide material for dye-sensitized solar cell (DSSC) application. The nanostructures provide large surface-to-volume ratio and can also supply more efficient direct path for electrons from the dye to the conducting electrode. The ZnO samples were produced via thermal chemical vapor deposition (thermal-CVD) and a variety of ZnO nanostructures were synthesized by adjusting the processing parameters during the growth process. The ZnO samples were successfully synthesized at a relatively low growth temperature (>500°C) on an indium tin oxide (ITO) coated glass substrate. The light harvesting capability and overall efficiency can be greatly enhanced by using 1-D ZnO nanostructures (such as dendritic structures). The electrical characteristics of the DSSC is now being investigated.

5:10 PM

Effect of Annealing and Growth Conditions on Electrical, Magnetic and Magnetoresistance Properties of Manganite Thin Films: *Nori Sudhakar*¹; V. Bhosle¹; G. Trichy¹; Jagdish Narayan¹; ¹North Carolina State University

Manganites have emerged as one of the widely studied materials belonging to the important class of transitions metal oxides having perovskite structure. The physical properties of manganese oxide are highly sensitive to the growth conditions such as oxygen stoichiometry, choice of the substrate, growth temperature and growth time. Here we present a detailed study of structural, electrical transport and magnetic properties of the epitaxial thin films of cubic manganite system $La_{0.67}Ca_{0.33}MnO_3$ grown on MgO (100) single crystal substrates. Several films were grown at different oxygen partial pressures at 700°C using pulsed laser deposition technique. Temperature dependence of electrical resistivity shows a sharp metal-insulator transition (MIT) typical of manganites. For the as-deposited film the transition occurs at about 62 K and annealing the film in oxygen increased the transition temperature to 210 K. The values are compared to the bulk T_p value. The magnetic measurements corroborate and complement the transport data.

5:35 PM

Characterization of Nanostructure ZnO Thin Film Grown by Pulsed Laser Deposition: *Wonwoo Lee*¹; ¹University of Alabama at Birmingham

Zinc Oxide (ZnO) is one of promising wide bandgap semiconductor materials because of their unique and novel applications in laser, piezoelectricity, and optoelectronics. Nanostructure ZnO thin film on Si substrate was grown by pulsed laser deposition (PLD) for solar cell application. X-ray diffraction spectroscopy is used to confirm the crystalline orientation of nanostructure ZnO thin film. Optical properties are also investigated using by photoluminescence (PL). A strong PL peak located at 374 nm is attributed to the free-exciton recombination, while a broad emission peak near at 2.8 eV may be corresponded to the defect level, such as zinc vacancy, oxygen vacancy, or interstitials. Electron paramagnetic resonance spectroscopy (EPR) is used as supplementary tool to support the defects of nanostructure ZnO thin film as shown in PL measurements. The vibrational properties of the nanostructure ZnO films are investigated by Raman scattering spectroscopy.

Technical Program



General Poster Session

Sponsored by: The Minerals, Metals and Materials Society Program Organizer: James Foley, Los Alamos National Laboratory

Mon PM-Wed PMRoom:Northern Hemisphere FoyerFebruary 26-28, 2007Location:Dolphin Hotel

Al-Cu Joining: Influence of Various Surface Treatments of Al by Laser: Vamsi Balla¹; Amit Bandyopadhyay¹; ¹Washington State University

Al-Cu combination is incompatible because they have high affinity to each other at high temperatures and produce brittle, low strength and high electrical resistance intermetallics at the interface during fusion joining. This preliminary work explores the influence of various surface treatments in successfully modifying the Al surface for joining with Cu structures, using laser in Laser Engineered Net Shaping (LENSTM). Among the various surface treatments studied, heat treatment at 150°C, 1h resulted in sound interfacial bond between Al and Cu-38wt%Ni coating at 500W laser power – lowest power reported so far for Al laser processing. Other treatments such as anodising and 550°C, 1h before Ni coating revealed excessive intermetallics and large pores at the interface. Finally an attempt has been made to evaluate solderability/brazability of coated Al with Cu structures. It is concluded that by suitably modifying the surface characteristics, the metallurgical compatibility of Al and Cu can be ensured.

Deformation Behavior of 7075 Al Wrought Alloy in the Semi-Solid State: *Young-Ok Yoon*¹; Shae K. Kim¹; ¹Korea Institute of Industrial Technology

7075 Al wrought alloy with good mechanical properties has been used with tendency to obtain weight-saving in aerospace, shipbuilding and transport industries. However, it generally allows low extrusion speed and low extrudability index and also causes rather high extrusion pressure when extruded conventionally. Thixoextrusion, one of the thixoforming processes, has advantages of high productivity, reduction of the extrusion pressure, extension of the die life and cost saving due to low energy consumption compared with conventional extrusion processes. Especially, thixoextrusion process is expected to be very effective for hard-to-form materials with high strength. The aim of this study is to investigate the deformation behavior of 7075 Al wrought alloy for thixoextrusion through simple compression test in the semisolid state.

Development of Trivalent Chromium Plating Electrolyte and Plating Process for Automotive Parts: *Beomsuck Han*¹; ¹Korea Automotive Technology Institute

Every year, end of life vehicles generate between 8 and 9 million tonnes of waste in the Community. The European Commission adopted a Proposal for a Directive which aims at making vehicle dismantling and recycling more environmentally friendly, sets clear quantified targets for reuse, recycling and recovery of vehicles and their components. Hexavalent chromium is a main substance of regulated element.Trivalent chromium baths have numerous environmental and health advantages. We are developing a functional trivalent chromium plating bath using a chromium chloride(CrCl3) as a replacement for commercial hexavalent chromium plating bath. We investigate a functional chromium plating rocess using a non-toxic trivalent chromium. We compare the chromium coatings fabricated with trivalent chromium plating process with a state of art hexavalent chromium plating process.

Effects of Alumina Additions on Sintering Behavior of Ce_{0.8}Sm_{0.2}O_{1.9} Ceramics Synthesized by Pechini Method: *Joo-Sin Lee*¹; Kwang-Hoon Choi¹; Dat Quach²; Vladimir Kodash²; Joanna Groza²; ¹Kyungsung University; ²University of California

Ceria-based ceramics are difficult to be densified below 1550°C. In order to lower the sintering temperature, other methods such as the use of fine powders and the use of additives should be exploited. The preparation of ultrafine powder has been studied by many investigators. Only limited reports, however, are available on the densification of ceria-based ceramics by using sintering additives. In the present study the effects of alumina additions on the sintering behavior of Ce_{0.8}Sm_{0.2}O_{1.9} ceramics was investigated by the use of powders synthesized by Pechini method. Both sintered density and grain size increased with increasing additive content up to 1 mol% for Al₂O₃ addition.

However, they decreased with further addition of the additive. We will discuss the effects of Al_2O_3 additions on the sintering behavior of Sm_2O_3 -doped CeO₂, with particular emphasis being placed on the variation in the sintered density and microstructure.

Effects of CaO and Ca on Oxidation and Ignition Resistance of Pure Mg: *Seong-Ho Ha*¹; Jin Kyu Lee¹; Hyung-Ho Jo¹; Shae K. Kim¹; ¹Korea Institute of Industrial Technology

The applications of Mg alloys are increasing due to their good properties such as low density, good castability and high specific strength. However, molten Mg and Mg alloys are easily ignited and oxidized due to their high reactivity. Many researchers have performed studies to improve ignition and oxidation resistance of Mg through alloying to Mg alloys. It is well known that Ca, though its high cost, is used to improve ignition and oxidation resistance of Mg. However, Ca is difficult to handle due to its high reactivity. It has been attempted to improve ignition resistance of Mg alloys through CaO addition. The aim of this study is to investigate ignition and oxidation behaviors of CaO or Ca added pure Mg. Pure Mg was used instead of Mg alloys to minimize the effects of other elements.

Effects of MgO-Na₂O-P₂O₅ Doping on Flexural Properties of Beta-Tricalcium Phosphate (B-TCP) Bioceramics: *Robert Fleming*¹; Samar Kalita¹; ¹University of Central Florida

Biomedical engineering has been advanced by the discoveries of emerging biomaterials. β -TCP is an exciting material in this category. The possibility of tailoring its resorption rate, through doping shows promise of using it creating viable controlled strength-loss osteogenic bone-grafts. It has been shown that β -TCP doped with MgO-Na₂O-P₂O₅, can help control its resorption as well as enhance sintered density by 9%, hardness by 40% and compression strength by 38%. To further explore the benefits of these sintering additives, biaxial flex tests (ASTM F-394) were performed on uniaxially compacted MgO-Na₂O-P₂O₅ doped β -TCP structures. The results demonstrated as much as a 200% improvement in flexural strength over pure β -TCP. This is a surprising and fantastic improvement on the flexural strength over pure β -TCP. XRD analyses, performed on powdered sintered structures, showed no alteration in phase purity. Biodegradation and bioactivity were assessed in simulated body fluid. This presentation will present our findings.

Examination of Thiol Adsorption on Zn-Terminated and O-Terminated ZnO Substrates: Patrick Sadik¹; David Norton¹; ¹University of Florida

ZnO has been widely studied for a myriad of uses as a transparent semiconductor, as a blue/UV LED, and as a chemical sensor for both gas and liquid phase applications. The ability to grow ZnO high surface area phases including nanowires, nanorods, and nanobelts among other has greatly increased the prospects off achieving single molecule detection. For this reason the adsorption of dodecanethiol on both Zn-terminated and O-terminated ZnO substrates has been examined using RHEED and XPS measurements for temperature increments between 25°C and 500°C. We found that on both Znterminated and O-terminated ZnO substrates, dodecanethiol readily adheres to the surface at temperatures in excess of 400°C with the Zn surface having the greater thiol adsorption. On both surfaces the XPS analysis shows that the thiol (-SH) moiety seemed to be largely responsible for surface adsorption.

Fabrication and Reliability Evaluation of Au-Sn Flip Chip Solder Joint: *Jeong-Won Yoon*¹; Hyun-Suk Chun¹; Ja-Myeong Koo¹; Seung-Boo Jung¹; ¹Sungkyunkwan University

In recent years, the use of optoelectronic packages is increasing rapidly. In these packages, solder alloys are commonly employed for mounting active devices, such as laser diodes, on the substrate of the package. Solders for bonding applications in microelectronic/optoelectronic packages are classified as soft solders and hard solders. Especially, among hard solders, eutectic Au-20wt.% Sn is the preferred alloy because of its relatively low melting point, low elastic modulus, high thermal conductivity, and high strength compared with the other solders. In addition, the flip-chip technology is generally considered the ultimate first level connection because the highest density can be achieved and the path length is shortest so that optimal electrical characteristics are achieved. The objective of this research is to evaluate the interfacial reactions and mechanical reliability of the electroplated Au-Sn flip-chip solder bump. The results on the electroplating, reflowing and bump shear testing will be presented in more detail.

Linking Science and Technology for Global Solutions



Fabrication of Fe Nanoparticles by Direct Electrochemical Reduction from Fe2O3 Nanoparticles: *Won-Kyu Han*¹; Jung Ho Baik¹; So Jin Kim¹; Chung Man Choi¹; Sung Goon Kang¹; ¹Hanyang University

In this report, Fe nano particles have been prepared by direct electrochemical reduction from Fe2O3 nano particles and the reduction mechanism was investigated. To investigate the reduction mechanism, Fe2O3 has been deposited on the AISI 430 by magnetron sputtering in various Ar/O2 ratio and the cyclic voltammetry (CV) was performed in 0.5 M NaCl solution at 300 K. This result indicated that the oxygen from the Fe2O3 was ionized at -1.30 V (versus SCE) and reduced to Fe. The structure of the films were analyzed by XRD, SEM/EDS and XPS.

Laser Surface Modifications of Alumina Ceramic for Applications in Precision Grinding of Materials: *Sandip Harimkar*¹; Narendra Dahotre¹; ¹University of Tennessee

Laser Surface modification of the ceramics is a novel technique for achieving improved surface properties. The high cooling rates associated with the laser surface processing results in the formation of various novel phases and morphology. The present study deals with the tailoring the surface morphology of the alumina ceramic with a potential application in micro-scale material removal during surface grinding of materials. Thermal effects during laser surface processing are correlated with subsequent development of the microstructural features such as crystallographic and morphological textures, grain size, depth of melting etc. Also, results of the effects of microstructure development on the grinding performance are presented.

Metal Ion Doped Beta-Tricalcium Phosphate Bioceramic with Improved Properties: Alton Davenport¹; Samar Kalita¹; ¹University of Central Florida

Recent years have seen a quest for new bioresorbable biomaterials. Betatricalcium phosphate (β -TCP) with excellent biocompatibility is ideal for bone-grafting. However, β -TCP suffers from poor flexural strength, poor densification and rapid *in vivo* degradation. In our research, we improved densification and flexural strength of β -TCP by introducing small quantities of divalent metal ions coupled with material-specific sintering which also controlled its degradation rate *in vitro*. High purity metal ions, known to be prevalent in the bone mineral, were introduced into β -TCP powder via ball milling. Dense structures were prepared by uniaxial pressing with green density of 1.7 g/cc and sintered at 1250°C, in air. Results showed 5-12% increase in density, 50-120% increase in microhardness and 30-100% increase in biaxial flexural strength. XRD analysis confirmed no alteration in phase purity. Biodegradation study was performed in dynamic SBF. *In vitro* assay performed, using prostate cancer cells confirmed that these materials were non-toxic.

Microstructural Characteristics and Mechanical Properties of Thixoextruded 2024 Al Wrought Alloy: *Dong-In Jang*¹; Young-Ok Yoon¹; Shae K. Kim¹; Hyung-Ho Jo¹; ¹Korea Institute of Industrial Technology

The 2024 Al wrought alloy has been used for a wide range of applications such as automobile and aircraft. However, extrusion process for the 2024 Al wrought alloy was not easy due to its low extrudability. Thixoextrusion, one of the thixoforming processes, has advantages of high productivity, reduction of the extrusion pressure and cost saving due to low energy consumption compared with conventional extrusion processes. Especially, thixoextrusion process was expected to be very effective for hard-to-form materials with high strength. In this paper, effects of extrusion parameter, such as extrusion temperature, speed and die bearing length, on the microstructure and mechanical properties of 2024 Al wrought alloy were interested. The thixoextrusion was carried out at 607' and 631' with extrusion speeds of 10'/sec, 20'/sec and 30'/sec. The die bearing lengths were 7' and 15'. The results of thixoextrusion experiments were compared with conventional extrusion results.

Microstructural Evolution of 7075 Al Wrought Alloy for Thixoextrusion Process: Young-Ok Yoon¹; Dong-In Jang¹; Shae K. Kim¹; Hyung-Ho Jo¹; ¹Korea Institute of Industrial Technology

The study for thixoextrusion of 7075 Al wrought alloy was carried out with respect to reheating rate, isothermal holding temperature and time with an emphasis to the effect of homogenization on thixotropic microstructures during the partial remelting. The main emphasis of this study was to investigate feasibility of microstructural control in the low liquid fraction (fL<0.3) for the thixoextrusion of 7075 Al wrought alloy without additional pretreatment. The

results show that the liquid fraction and average grain size were almost uniform with respect to isothermal holding temperature and time. It is considered very useful for thixoextrusion in terms of process control such as billet temperature control and actual extrusion time. Microstructural control of 7075 Al wrought alloy both before and after homogenization could be possible and thixotropic microstructures were obtained in both specimens.

Notch Toughness of a Cu-Based Bulk Metallic Glass: *Matthew Freels*¹; Peter Liaw¹; Gongyao Wang¹; ¹University of Tennessee, Knoxville

Cu-based bulk-metallic glasses (BMGs) have received much interest of late due to their high strength and low cost compared to the widely studied Zr-based BMGs. Consequently, it is important that Cu-based BMG systems be further studied and developed. In this study, the fracture toughness of (Cu60Zr30Ti10)99Sn1 BMG was examined using the three-point bending method. Notch toughness tests were performed on an MTS servohydraulic testing machine under constant displacement rates ranging from .1mm/min. Notch radii ranged from 150 μ m to 300 μ m. Notch depth was kept constant at .45W (2.15 mm). Load versus displacement was monitored during testing. Preliminary results indicate notch toughness values calculated from the maximum load at fracture range from 35 MPa√m up to 65Mpa√m. Fracture surface characteristics, as well reasons for the large variability in the data will be explored.

On the Phase Diagram and Thermodynamics of the Al-Nd-Ni System: A Combined Approach of Experiments, CALPHAD and First-Principles Calculations: *Michael Gao*¹; Michael Widom¹; Gary Shiflet²; Marek Mihalkovic¹; 'Carnegie Mellon University; ²University of Virginia

A novel approach that combines critical experiments, CALPHAD modeling and first principles (FP) calculations is used to study the Al-Nd-Ni ternary phase diagram and the underlying thermodynamics. Two new ternary compounds are experimentally identified, i.e. Al19Nd3Ni5 and Al5NdNi2. Based on our FP calculations, they are suggested to be isostructural with Al19Gd3Ni5 (Pearson symbol oC108) and Al5CeNi2 (oI16) respectively. Other compounds that are likely stable include Al4NdNi, Al3NdNi2, Al2NdNi, AlNdNi, AlNd2Ni2 and AlNd3Ni8, whose crystal structures are suggested with FP calculations. Several compounds exhibit compositional homogeneity range via Al/Ni substitution that are measured experimentally at 773 K: Al2Nd (~3 at% Ni); Al3NdNi2 (46-52 at% Al); Al5NdNi2 (25-28 at% Al). Based on the present experimental data and FP calculations, the complete phase diagram and the thermodynamic descriptions are determined via CALPHAD modeling. Application to glass formation is discussed in light of present study.

Phase Equilibria Study and Thermodynamic Assessment of the Al-Ce-Co System Assisted by First-Principles Energy Calculations: *Michael Gao*¹; Necip Unlu²; Marek Mihalkovic¹; Michael Widom¹; Gary Shiflet²; ¹Carnegie Mellon University; ²University of Virginia

This study investigates the phase equilibria of the Al-rich Al-Ce-Co system using a range of experimental techniques including melt spinning, TEM, EPMA, XRD and DTA. The glass formation range in the Al-rich corner is determined, and a partial 773 K isotherm is constructed. Three stable ternary phases are confirmed, namely, Al8CeCo₂, Al4CeCo and AlCeCo, while a metastable phase, Al5CeCo₂, was discovered. Also confirmed are our previous results [Metall. Mater. Trans. A 2005;36A:3269.] that a polymorphous transformation of α/β Al3Ce exists in the Al-Ce binary system, and that the transformation between Al11Ce₃.oI28 and Al4Ce.tI10 can't be polymorphous. The equilibrium and metastable phases identified by the present and earlier reported experiments are further studied by first-principles calculations. Based on new experimental data and FP calculations, the thermodynamics of the Al-Co-Ce system is optimized using the CALPHAD method. Model calculated phase equilibria and phase boundaries conform with the present experimental results.

Porous Titanium Electrodes for Microbial Fuel Cell (MFC) Applications: David Beeler¹; Leroy Long¹; Emily Henderson¹; Daniel Young¹; *Raghavan Srinivasan*¹; ¹Wright State University

Microbial fuel cells (MFC) work on the principle that during metabolism certain bacteria produce electrons which can be harnessed as a source of electrical energy. This paper presents the results of a study on the production and use of porous titanium electrodes in MFC. Electrodes were produced by powder metallurgy (PM) techniques using 20 micrometer CP titanium powder,





and powders of another material as place holders. Mixtures with different titanium to place holder material ratios were cold compacted use to produce green bodies from which the place holder material was etched out. The porous compact was then sintered to produce electrodes for the MFC. Results to be presented include characterization of the titanium electrodes in terms of microstructure, specific surface area, and permeability. Results from the use of the electrodes in MFC will also be presented.

Reaction of Co Phase in the WC-Co Coatings with Molten Zinc: Byeog-Geun Seong¹; Sung-Hee Kwon²; Kyoo-Young Kim³; *Kee-Ahn Lee*²; ¹Research Institute Science and Technology; ²Andong National University; ³POSTECH

The main objective of this study is to investigate the detailed reaction mechanism of Co phase with molten zinc. Pure Co, Co-W alloys specimens were used to understand role of the phase and alloying effect. These specimens were immersion tested in Zn bath. After immersion of Co in a pure molten zinc bath at 460°C to 520°C four kinds of Co-Zn intermetallic compound layers, $\beta 1$, γ , $\gamma 1$, and $\gamma 2$ were formed on the Co matrix. Rate controlling step for this reaction was diffusion through $\beta 1$ compound layer and the activation energy was calculated to be 214.9 kJ/mole. Co-10% W alloy showed no W alloying effect on the reaction rate in a molten zinc bath but the reaction rates increased as W contents increase to 20% and 30%. $\beta 1$ layer was not formed on Co-20% W alloy and no stable Co-Zn intermetallic compound layer was found on the Co-30% alloy.

Recovery of Pd(II) and Pt(IV) Ions by Introducing SCN Soft Ligand with

Tannin Gel: Yoshio Nakano¹; Yeon Ho Kim¹; ¹Tokyo Institute of Technology We have developed a new Pd(II) and Pt(IV) recovery process from wastes such as spent catalysts or scraps, which is simple and generates little secondary waste, using tannin gel particles synthesized from condensedtannin, ubiquitous and inexpensive natural material. We have reported that in chloride solution, Pd(II) ionic species are adsorbed onto the tannin gel particles through inner-sphere redox reaction mechanism: two-electron transfer from tannin gel to chloro-palladium(II) complexes, accompanied by ligand substitution between chloro-palladium(II) complexes and hydroxyl groups of tannin gel. In the present investigation, The intermediate step (ligand substitution) plays an essential role in the Pd(II) and Pt(IV) adsorption, because the ligand substitution rate is increased by introducing a soft ligand (SCN⁻). Addition of SCN⁻ ion to chloride solution leads to the formation of chlorothiocyanocomplexes which is more favourable for the ligand substitution with tannin gel than chlorocomplexes because of the trans-effect.

Reprocessing of Silicon Carbide-Based Inert Matrix Fuels: Soraya Benitez¹; Ronald Baney¹; James Tulenko¹; ¹University of Florida

Silicon carbide (SiC) is one of the prime candidates for the fabrication of ceramic based inert matrix fuels (IMF) for the burning of plutonium and for the transmutation of long-lived actinides. However, reprocessing of SiC-based IMF to separate transuranic species for both spent and unspent nuclear fuel from the SiC matrix is not well defined. A potential reprocessing method under investigation is the use of alkali and alkali earth molten salt baths to dissolve the SiC matrix. SiC samples with and without ceria will be reprocessed using the molten salt method to determinate ease of separation, dissolution rates, and resulting compounds. Ceria is used as a surrogate for plutonium and for the transuranic species.

Stress Rupture Property of Inconel 718 Alloy: *Ji Soo Kim*¹; Chong Soo Lee¹; ¹Pohang University of Science and Technology

Stress rupture properties of base metal and weldment of Inconel 718 Alloy for aerospace applications were examined in the present study. The specimens were solution heat treated according to the specification of ASM 5596, i.e., heating to a temperature of 980°C, holding at the temperature for an hour and air cooled. Afterward, precipitation heat treatment was done by heating to 720°C for 8 hours, furnace cooled to 621°C, holding at 621°C for 8 hours and furnace cooled. The test temperatures were varied from 649°C to 760°C. With the increase of test temperature, stress rupture life was shortened at the same stress ratio. The weldement was more fragile than the base metal. Detailed microstructures and fracture surfaces after the rupture test were investigated by the optical microscope and SEM. Study of Hot Deformation Behavior of Ti-6Al-4VAlloy with Widmanstätten Microstructure by Artificial Neural Networks: N. Reddy¹; *Chan Hee Park*¹; ¹Pohang University of Science and Technology

The present work demonstrates the use of an artificial neural networks (ANN) model in generating processing maps for hot working processes for Ti-6Al-4V alloy with widmanstätten microstructure. The flow stress data for ANN model training was obtained from continuous compression tests performed on a thermo-mechanical simulator over a wide range of temperatures (700-1100°C) with the strain rates of 0.0001-100 s-1 and true strains of 0.1 to 0.6. It has been found that the flow stress values predicted by the ANN model agree closely with actual experimental values, thus indicating the possibility of using neural networks approach to tackle hot deformation problems. The specimen failures at various instances have been predicted and metallurgical explanations had been presented. The flow stress predicted at finer intervals of temperature and strain rate regions and subsequently processing maps were developed. The safe domains of hot working of alloy were identified and validated through microstructural investigations.

The Effect of Composition of Carbon Fibre on the Mechanical and Morphological Properties of PA6/Carbon Composite: *Albert Ude*¹; Husna Azhari¹; ¹National University of Malaysia Bangi

A study to investigate the mechanical property-morphology relationship of polyamide 6 reinforced carbon fibre composites has been carried out. The composites were prepared by melt mixing, in a composition of wt% PA6/wt%CF; 95/5, 90/10, 85/15, 80/20 respectively. The length of the fibre was 500µm. The mechanical properties were measured. These properties were correlated to the morphology. The mechanical properties suggest that carbon fiber has the potentials to reinforce polyamide 6; hence an increase in strength recorded, displaying that strength is a function of the volume of the reinforcement (fibre).Morphological study of the tensile fractured surface showed the mechanism of failure to be the dispersed domain pulling out of a continuous matrix, leaving voids in their alert. The size of the voids seems to correspond with the size of the fibrils, making the inference that the voids observed were space left by the pulled-out fibre distributed in different direction apparently reasonable.

X-Ray Absorption near Edge Structure Analysis of Chromium Oxynitride Thin Films: *Jun Inoue*¹; Tadachika Nakayama¹; Tsuneo Suzuki¹; Hisayuki Suematsu¹; Weihua Jiang¹; Koichi Niihara¹; ¹Nagaoka University of Technology

We have already reported the hardening in Cr(N,O) thin films by the increase in the oxygen content (x). X-ray absorption near edge structure (XANES) in the thin films was observed to clarify electronic structure change associated with the hardening. The Cr(N,O) thin films were prepared by PLD method. The beam line BL-12C of PF in High Energy Accelerator Research Organization was used for XANES measurements. It was found that the ionicity between metal and nonmetal atoms has increased by replacing nitrogen atoms in CrN by oxygen atoms, since the Cr-K edge peak shift to higher energy was observed with increasing x. Furthermore, the peak attributed to the electronic transition from 1s to band that formed by 3deg of metal atom and 2p of nonmetal atoms decreased with x increases. It can be understood the reason for this result is that the total valence electron density increased gradually with increasing x.

In-Situ Chemical Oxidation of Soil Contaminated by Benzene, Lead and Cadmium: Marcia Bragato¹; *Jorge Tenorio*¹; ¹Escola Politecnica-Universidade de Sao Paulo

Soil contamination by oil and its derivatives is found at many sites in Sao Paulo, Brazil. In this research, the chemical oxidation was used as remediation method for soil contaminated simultaneously by benzene, lead and cadmium simulating in-situ conditions. Tests were carried out under laboratory conditions. In the oxidation tests the efficiency of Fenton's reagent ($H_2O_2/$ Fe²) on the benzene oxidation was performed. Under the imposed oxidizing conditions lead in the lecheate increased in TLCP tests. Using the Fenton's reagent the increase of lead concentration in the lecheate was 4 times greater under natural conditions. On the other hand, cadmium presented the opposite behavior, *e.g.*, Cadmium concentration in the lecheate was decreased 50% for the oxidizing conditions.



Development and Validation of High Performance Thick Thermal Barrier Coating (TBC) for Application on Turbine Components: *Gabriele Rizzi*¹; A. Scrivani¹; 'Turbocoating

This paper addresses the development of thick TBC (with thickness in the range of 1.5 - 2 mm), focusing attention on the microstructure and the porosity of the Yttria Partially Stabilised Zirconia (YPSZ) coating, in relation to its resistance to thermal cycling fatigue (TCF). TBC coatings have been produced by means of a NiCoCrAIY bond coat and Yttria Partially Stabilised Zirconia top coat, both sprayed by Air Plasma Spray. The obtained samples have been characterized from the metallographic point of view in order to determine the structure and the porosity of the coating. Finally the samples have been submitted to TCF test, according to the procedure of two important OEMs. The study enabled determination of a good microstructure of the TBC coating with high TCF resistance independent of the porosity of the coating itself.

Development of CVD Overaluminising Method on Different Conicraly Bond Coats Deposited by Low Pressure Plasma Spray (LPPS), High Velocity Oxygen Fuel (HVOF) and Air Plasma Spray (APS): Gabriele Rizzi¹; A. Scrivani¹; 'Turbocoating

This paper addresses the study of Aluminium coatings deposited by CVD on CoNiCrAIY bond coats deposited by three thermal spray techniques. The different CoNiCrAIY coatings structure obtained by these three techniques (Low Pressure Plasma Spray or Vacuum Plasma Spray, High Velocity Oxygen Fuel and Air Plasma Spray) with different content of oxides and porosity could affect the deposition rate and quality of the Al coatings. The obtained samples have been characterized from the metallographic point of view (porosity, thickness and structure). Al coating thickness has been taken as parameter in order to define the Al coating deposition rate on the three different CoNiCrAIY coatings. Oxidation test has been performed in order to evaluate and compare the oxidation resistance of this three different coatings.

Self-Organized Periodic Array of Single Crystal Oxide Nano Islands: L. Zimmerman¹; Michael Rauscher¹; S. Dregia¹; J. Lee¹; S. Akbar¹; ¹Ohio State University

We have deposited a gadolinium doped ceria thin film on an yttria-stabilized zirconia substrate using RF magnetron sputtering. Subsequent spalling of the thin film and a high temperature anneal combine to create a periodic array of single crystal islands with regular size, shape, and distance from their nearest neighbors. The features can be used as a template to transfer the pattern to other materials of interest, with the high strength of the material allowing for superior durability and fidelity of pattern transfer. In its current form, the nanostructure may find use in manipulation of single proteins and single molecules of DNA, as well as in nanoscale analytics. We predict the ability to establish long-range periodicity in the alignment of the islands creating a regular 2D network of nanochannels. These structures represent a tunable, self-assembling, low-cost, non-cleanroom means of producing nanoscale features suitable for nanofluidic channel fabrication and numerous other applications. In this work, we discuss the conditions necessary to create the novel nanostructure, and highlight the influence of annealing on the structure features. We have performed preliminary characterization of the system to determine its intrinsic usefulness for a range of optical, electronic, magnetic, and biological nanofluidic applications. We also discuss early efforts to create nanofluidic devices based on the pattern.



A

Abbaschian, R85	
Abdel, E	
Abd Elhamid, M94	
Abdelrahman, M143	
Abduev, A	
Abdulla, A70	
Abe, H	
Abe, T	
Abedrabbo, S55	
Abelev, G142, 193	
Abolmaali, A249	
Abramson, A	
Abreu, A	
Abruña, H65	
Abu-Dheir, N	
Abu-Farha, F93	
Abu Al-Rub, R261	
Abu Leil, T	
AbuOmar, O	
AduOiliar, O120	
Acharya, A44, 266, 320	
Acharya, S291	
Acoff, V	
Adam, G	
Adams, B44, 96, 97, 146, 147, 199, 260, 312	
Adams, J192	
Adams, T167	
Adapa, R	
Addessio, F	
Adebiyi, O94	
Adedokun, S	
Adharapurapu, R133, 233, 243, 339	
Afanasyev, K155	
Aga, R	
Agarwal, A	
Ager, J	
Ager, J 125 Aggarwal, G 227 Aghion, E 194, 257 Agnew, S 19, 68, 75, 92, 93,	
Ager, J 125 Aggarwal, G 227 Aghion, E 194, 257 Agnew, S 19, 68, 75, 92, 93,	
Ager, J 125 Aggarwal, G 227 Aghion, E 194, 257 Agnew, S 19, 68, 75, 92, 93,	
Ager, J 125 Aggarwal, G 227 Aghion, E 194, 257 Agnew, S 19, 68, 75, 92, 93,	
Ager, J 125 Aggarwal, G 227 Aghion, E 194, 257 Agnew, S 19, 68, 75, 92, 93,	
Ager, J 125 Aggarwal, G 227 Aghion, E 194, 257 Agnew, S 19, 68, 75, 92, 93,	
Ager, J 125 Aggarwal, G 227 Aghion, E 194, 257 Agnew, S 19, 68, 75, 92, 93,	
Ager, J 125 Aggarwal, G 227 Aghion, E 194, 257 Agnew, S 19, 68, 75, 92, 93,	
Ager, J 125 Aggarwal, G 227 Aghion, E 194, 257 Agnew, S 19, 68, 75, 92, 93,	
Ager, J 125 Aggarwal, G 227 Aghion, E 194, 257 Agnew, S 19, 68, 75, 92, 93,	
Ager, J 125 Aggarwal, G 227 Aghion, E 194, 257 Agnew, S 19, 68, 75, 92, 93,	
Ager, J 125 Aggarwal, G 227 Aghion, E 194, 257 Agnew, S 19, 68, 75, 92, 93,	
Ager, J 125 Aggarwal, G 227 Aghion, E 194, 257 Agnew, S 19, 68, 75, 92, 93,	
Ager, J 125 Aggarwal, G 227 Aghion, E 194, 257 Agnew, S 19, 68, 75, 92, 93,	
Ager, J 125 Aggarwal, G 227 Aghion, E 194, 257 Agnew, S 19, 68, 75, 92, 93,	
Ager, J 125 Aggarwal, G 227 Aghion, E 194, 257 Agnew, S 19, 68, 75, 92, 93,	
Ager, J 125 Aggarwal, G 227 Aghion, E 194, 257 Agnew, S 19, 68, 75, 92, 93,	
Ager, J 125 Aggarwal, G 227 Aghion, E 194, 257 Agnew, S 19, 68, 75, 92, 93,	
Ager, J 125 Aggarwal, G 227 Aghion, E 194, 257 Agnew, S 19, 68, 75, 92, 93,	
Ager, J 125 Aggarwal, G 227 Aghion, E 194, 257 Agnew, S 19, 68, 75, 92, 93,	
Ager, J 125 Aggarwal, G 227 Aghion, E 194, 257 Agnew, S 19, 68, 75, 92, 93,	
Ager, J 125 Aggarwal, G 227 Aghion, E 194, 257 Agnew, S 19, 68, 75, 92, 93,	
Ager, J 125 Aggarwal, G 227 Aghion, E 194, 257 Agnew, S 19, 68, 75, 92, 93,	
Ager, J 125 Aggarwal, G 227 Aghion, E 194, 257 Agnew, S 19, 68, 75, 92, 93,	
Ager, J 125 Aggarwal, G 227 Aghion, E 194, 257 Agnew, S 19, 68, 75, 92, 93,	
Ager, J 125 Aggarwal, G 227 Aghion, E 194, 257 Agnew, S 19, 68, 75, 92, 93,	
Ager, J 125 Aggarwal, G 227 Aghion, E 194, 257 Agnew, S 19, 68, 75, 92, 93,	
Ager, J 125 Aggarwal, G 227 Aghion, E 194, 257 Agnew, S 19, 68, 75, 92, 93,	
Ager, J 125 Aggarwal, G 227 Aghion, E 194, 257 Agnew, S 19, 68, 75, 92, 93,	
Ager, J 125 Aggarwal, G 227 Aghion, E 194, 257 Agnew, S 19, 68, 75, 92, 93,	
Ager, J 125 Aggarwal, G 227 Aghion, E 194, 257 Agnew, S 19, 68, 75, 92, 93,	
Ager, J 125 Aggarwal, G 227 Aghion, E 194, 257 Agnew, S 19, 68, 75, 92, 93,	
Ager, J 125 Aggarwal, G 227 Aghion, E 194, 257 Agnew, S 19, 68, 75, 92, 93,	

Akogwu, O22	2
Alaradi, E123	3
Alba Baena. N	
Albers, R189	
Alcorn, T	1
Aldabergenova, S	h
Alexander, B	
Alexander, D90)
Alexandrescu, R63	3
Alexandrov, I	
Alford, F114	
Ali, A	5
Alihossieni, H279)
Allahverdi, K	
Allard, L	
Allen, C82, 83, 134, 187, 248, 298, 341, 342	2
Allen, T	
Allison, J91, 255, 288, 292, 307, 324	
Alman, D192, 193, 198	3
Almasri, A261	
Almazouzi, A	
Almer, J121	
Alonso, E60)
Alpas, A	
Altenhof, W	
Altennol, w240	J
Alven, D	7
Alvi, M69)
Alyousif, O129	
Amancherla, S169	
Ambacher, O115	5
Ambrová, M173	3
Amirthalingam, M	
An, K134, 200	
An, Q	1
Anand, L	2
	-
Andelman, T115	
Andelman, T115 Anderoglu, O211	1
Andelman, T115 Anderoglu, O211	1
Andelman, T	1
Andelman, T	1) 3
Andelman, T	1) 3 3
Andelman, T	1 3 3 3
Andelman, T	1 3 3 3
Andelman, T	1
Andelman, T. 115 Anderoglu, O. 211 Anderson, I. 66, 103, 142, 166, 264, 290 Anderson, M 93 Anderson, P. 168 Anderson, S 248 Anderson, T. 33, 55, 108, 353 Ando, D 93	1 3 3 3 3 3
Andelman, T. 115 Anderoglu, O. 211 Anderson, I. 66, 103, 142, 166, 264, 290 Anderson, M. 93 Anderson, P. 168 Anderson, S. 248 Anderson, T. 33, 55, 108, 353 Ando, D. 93 Ando, T. 250	1 3 3 3 3 3 3 3 3 3 3
Andelman, T. 115 Anderoglu, O. 211 Anderson, I. 66, 103, 142, 166, 264, 290 Anderson, M 93 Anderson, P. 168 Anderson, S 248 Anderson, T. 33, 55, 108, 353 Ando, D 93 Andor, T 250 André, J 341	1 3 3 3 3 3 3 1
Andelman, T. 115 Anderoglu, O. 211 Anderson, I. 66, 103, 142, 166, 264, 290 Anderson, M. 93 Anderson, P. 168 Anderson, S. 248 Anderson, T. 33, 55, 108, 353 Ando, D. 93 Ando, T. 250	1 3 3 3 3 3 3 1
Andelman, T. 115 Anderoglu, O. 211 Anderson, I. 66, 103, 142, 166, 264, 290 Anderson, M 93 Anderson, P. 168 Anderson, S 248 Anderson, T. 33, 55, 108, 353 Ando, D 93 Ander, J 250 André, J 341	1 0 3 3 3 3 0 1 4
Andelman, T. 115 Anderoglu, O. 211 Anderson, I. 66, 103, 142, 166, 264, 290 Anderson, M 93 Anderson, P. 168 Anderson, S 248 Anderson, T. 33, 55, 108, 353 Ando, D 93 Andor, T 250 André, J 341 Andres, D 88	1 0 3 3 3 3 3 0 1 4 3
Andelman, T. 115 Anderoglu, O. 211 Anderson, I. 66, 103, 142, 166, 264, 290 Anderson, M. 93 Anderson, P. 168 Anderson, S. 248 Anderson, T. 33, 55, 108, 353 Ando, D. 93 Ander, J. 341 Andre, S. 174 Andreas, D. 88 Andrieux, J. 182	
Andelman, T. 115 Anderoglu, O. 211 Anderson, I. 66, 103, 142, 166, 264, 290 Anderson, M 93 Anderson, P. 168 Anderson, S. 248 Anderson, S. 248 Anderson, T. 33, 55, 108, 353 Ando, D. 93 Andor, T. 250 André, J. 341 Andre, S. 174 Andreas, D. 88 Andrus, M. 197	103333014327
Andelman, T. 115 Anderoglu, O. 211 Anderson, I. 66, 103, 142, 166, 264, 290 Anderson, M 93 Anderson, P. 168 Anderson, S. 248 Anderson, T. 33, 55, 108, 353 Ando, D. 93 Andor, T. 250 André, J. 341 Andre, S. 174 Andreas, D. 88 Andrieux, J. 182 Andrieux, M. 197 Ang, J. 131, 208	10333330143273
Andelman, T. 115 Anderoglu, O. 211 Anderson, I. 66, 103, 142, 166, 264, 290 Anderson, M 93 Anderson, P. 168 Anderson, S. 248 Anderson, T. 33, 55, 108, 353 Ando, D. 93 Andor, T. 250 André, J. 341 Andre, S. 174 Andreas, D. 88 Andrieux, J. 182 Andrieux, M. 197 Ang, J. 131, 208	10333330143273
Andelman, T. 115 Anderoglu, O. 211 Anderson, I. 66, 103, 142, 166, 264, 290 Anderson, M 93 Anderson, P. 168 Anderson, S. 248 Anderson, S. 248 Anderson, T. 33, 55, 108, 353 Ando, D. 93 Andor, T. 250 André, J. 341 Andre, S. 174 Andres, D. 88 Andrus, M. 197 Ang, J. 131, 208 Anger, G. 88	10333301432733
Andelman, T. 115 Anderoglu, O. 211 Anderson, I. 66, 103, 142, 166, 264, 290 Anderson, M 93 Anderson, P. 168 Anderson, S. 248 Anderson, T. 33, 55, 108, 353 Ando, D. 93 Andor, J. 250 André, J. 341 Andre, S. 174 Andreas, D. 88 Andrieux, J. 182 Andrieux, M. 197 Ang, J. 131, 208 Angere, G. 88 Angerer, P. 18	103333014327333
Andelman, T. 115 Anderoglu, O. 211 Anderson, I. 66, 103, 142, 166, 264, 290 Anderson, M 93 Anderson, P. 168 Anderson, S. 248 Anderson, T. 33, 55, 108, 353 Ando, D. 93 Andor, T. 250 André, J. 341 Andre, S. 174 Andreas, D. 88 Andrieux, J. 182 Andrus, M. 197 Anger, G. 88 Angerer, P. 18 Aning, A. 302	1033330143273332
Andelman, T. 115 Anderoglu, O. 211 Anderson, I. 66, 103, 142, 166, 264, 290 Anderson, M 93 Anderson, P. 168 Anderson, S. 248 Anderson, T. 33, 55, 108, 353 Ando, D. 93 Andor, J. 250 André, J. 341 Andre, S. 174 Andreas, D. 88 Andrieux, J. 182 Andrieux, M. 197 Ang, J. 131, 208 Angere, G. 88 Angerer, P. 18	1033330143273332
Andelman, T. 115 Anderoglu, O. 211 Anderson, I. 66, 103, 142, 166, 264, 290 Anderson, M 93 Anderson, P. 168 Anderson, S. 248 Anderson, T. 33, 55, 108, 353 Ando, D. 93 Andor, T. 250 André, J. 341 Andre, S. 174 Andreas, D. 88 Andrieux, J. 182 Andrus, M. 197 Anger, G. 88 Angerer, P. 18 Aning, A. 302	10333301432733323
Andelman, T. 115 Anderoglu, O. 211 Anderson, I. 66, 103, 142, 166, 264, 290 Anderson, M 93 Anderson, P. 168 Anderson, S. 248 Anderson, T. 33, 55, 108, 353 Ando, D. 93 Andor, T. 250 André, J. 341 Andre, S. 174 Andreas, D. 88 Andrieux, J. 182 Andrey, M. 197 Ang, J. 131, 208 Angere, G. 88 Angerer, P. 18 Aning, A. 302 Ankem, S. 348 Annamaneni, S. 187	103333014327333237
Andelman, T. 115 Anderoglu, O. 211 Anderson, I. 66, 103, 142, 166, 264, 290 Anderson, M 93 Anderson, P. 168 Anderson, S. 248 Anderson, T. 33, 55, 108, 353 Ando, D. 93 Andre, S. 248 Andreson, T. 33, 55, 108, 353 Ando, D. 93 Andor, T. 250 André, J. 341 Andre, S. 174 Andreas, D. 88 Andriux, J. 182 Andrus, M. 197 Anger, G. 88 Angerer, P. 18 Aning, A. 302 Ankem, S. 348 Annamaneni, S. 187 Anopo, O. 350, 353	1 3 3 3 3 3 3 3 3 3 3 3 3 3
Andelman, T. 115 Anderoglu, O. 211 Anderson, I. 66, 103, 142, 166, 264, 290 Anderson, M 93 Anderson, P. 168 Anderson, S. 248 Anderson, T. 33, 55, 108, 353 Ando, D. 93 André, J. 341 André, J. 341 André, J. 88 Andréas, D. 88 Andrieux, J. 182 Andreux, M. 197 Anger, G. 88 Anger, G. 88 Anger, R. 131, 208 Anger, R. 302 Ankem, S. 348 Annamaneni, S. 187 Anopuo, O. 350, 353 Anselmi-Tamburini, U. 358	1 3 3 3 3 3 3 3 3 3 3 3 3 3 3 3 3 3 3 3
Andelman, T. 115 Anderoglu, O. 211 Anderson, I. 66, 103, 142, 166, 264, 290 Anderson, M 93 Anderson, P. 168 Anderson, S. 248 Anderson, T. 33, 55, 108, 353 Ando, D. 93 Andre, S. 248 Andreson, T. 33, 55, 108, 353 Ando, D. 93 Andor, T. 250 André, J. 341 Andre, S. 174 Andreas, D. 88 Andriux, J. 182 Andrus, M. 197 Anger, G. 88 Angerer, P. 18 Aning, A. 302 Ankem, S. 348 Annamaneni, S. 187 Anopo, O. 350, 353	1 3 3 3 3 3 3 3 3 3 3 3 3 3 3 3 3 3 3 3
Andelman, T. 115 Anderoglu, O. 211 Anderson, I. 66, 103, 142, 166, 264, 290 Anderson, M 93 Anderson, P. 168 Anderson, S. 248 Anderson, T. 33, 55, 108, 353 Ando, D. 93 Andre, J. 341 André, J. 341 Andre, S. 174 Andreas, D. 88 Andrieux, J. 182 Andrius, M. 197 Anger, G. 88 Angerer, P. 18 Aning, A. 302 Ankem, S. 348 Annamaneni, S. 187 Anopuo, O. 350, 353 Anselmi-Tamburini, U. 358 Antille, J. 283	1 3 3 3 3 3 3 3 3 1 4 3 2 7 3 3 3 3 3 3 3 3 1 4 3 2 7 3 3 3 3 3 3 1 1 4 3 3 3 3 3 3 3 3 3 3 3 3 3
Andelman, T. 115 Anderoglu, O. 211 Anderson, I. 66, 103, 142, 166, 264, 290 Anderson, M 93 Anderson, P. 168 Anderson, S. 248 Anderson, T. 33, 55, 108, 353 Ando, D. 93 Andre, J. 341 André, J. 341 Andre, S. 174 Andreas, D. 88 Andrieux, J. 182 Andrius, M. 197 Anger, G. 88 Angerer, P. 18 Aning, A. 302 Ankem, S. 348 Annamaneni, S. 187 Anopuo, O. 350, 353 Anselmi-Tamburini, U. 358 Antipov, E. 283	1 3 3 3 3 3 3 3 3 3 3 3 3 3 3 3 3 3 3 3
Andelman, T. 115 Anderoglu, O. 211 Anderson, I. 66, 103, 142, 166, 264, 290 Anderson, M 93 Anderson, P. 168 Anderson, S. 248 Anderson, S. 248 Anderson, S. 248 Anderson, T. 33, 55, 108, 353 Ando, D. 93 Andreson, T. 250 Andref, J. 341 Andre, S 174 Andreas, D 88 Andrieux, J. 182 Andrus, M. 197 Ang, J 131, 208 Anger, G. 88 Aning, A. 302 Ankem, S. 348 Annamaneni, S. 187 Anopuo, O. 350, 353 Anselmi-Tamburini, U. 358 Antille, J. 283 Antoun, B. 294	1 3 3 3 3 3 3 3 3 3 3 3 3 3
Andelman, T. 115 Anderoglu, O. 211 Anderson, I. 66, 103, 142, 166, 264, 290 Anderson, M 93 Anderson, P. 168 Anderson, S. 248 Andreson, T. 33, 55, 108, 353 Ando, D. 93 Andres, M. 93 Andres, S. 134 Andre, S. 174 Andreas, D. 88 Andrieux, J. 182 Andrus, M. 197 Ang, J. 131, 208 Anger, G. 88 Aning, A. 302 Ankem, S. 348 Aning, A. 302	1 3 3 3 3 3 3 3 3 3 3 3 3 3
Andelman, T. 115 Anderoglu, O. 211 Anderson, I. 66, 103, 142, 166, 264, 290 Anderson, M 93 Anderson, P. 168 Anderson, S. 248 Anderson, S. 248 Anderson, S. 248 Anderson, T. 33, 55, 108, 353 Ando, D. 93 Andreson, T. 250 Andref, J. 341 Andre, S 174 Andreas, D 88 Andrieux, J. 182 Andrus, M. 197 Ang, J 131, 208 Anger, G. 88 Aning, A. 302 Ankem, S. 348 Annamaneni, S. 187 Anopuo, O. 350, 353 Anselmi-Tamburini, U. 358 Antille, J. 283 Antoun, B. 294	1 3 3 3 3 3 3 3 3 3 3 3 3 3
Andelman, T. 115 Anderoglu, O. 211 Anderson, I. 66, 103, 142, 166, 264, 290 Anderson, M 93 Anderson, P. 168 Anderson, S. 248 Anderson, S. 248 Anderson, S. 248 Anderson, T. 33, 55, 108, 353 Ando, D. 93 Andreson, T. 250 Andref, J. 341 Andre, S 174 Andreas, D 88 Andrieux, J. 182 Andrus, M 197 Ang, J 131, 208 Anger, G. 88 Aning, A 302 Ankem, S. 344 Aning, A 302 Ankem, S. 348 Aning, A 302 Ankem, S. 348 Aning, A 302 Ankem, S. 348 Aning, A 302 Antelmi-Tamburini, U. 358 Antille, J. 283 Antoy, B 294 Antrekowitsch, H 138, 148	
Andelman, T. 115 Anderoglu, O. 211 Anderson, I. 66, 103, 142, 166, 264, 290 Anderson, M. 93 Anderson, P. 168 Anderson, S. 248 Anderson, S. 248 Anderson, S. 248 Anderson, T. 33, 55, 108, 353 Ando, D. 93 Andor, T. 250 André, J. 341 Andre, S. 174 Andre, S. 174 Andres, D. 88 Andrue, S. 174 Andres, D. 88 Andres, D. 88 Andrus, M. 197 Ang, J. 131, 208 Anger, G. 88 Aning, A. 302 Ankem, S. 348 Annamaneni, S. 187 Anopuo, O. 350, 353 Anselmi-Tamburini, U. 353 Antile, J. 283 Antoun, B. 294 Antrekowitsch, H 138, 148 Anyalebechi, P. 45, 46, 97, 148, 200 <td< td=""><td>1 3 3 3 3 3 3 3 3 3 3 3 3 3</td></td<>	1 3 3 3 3 3 3 3 3 3 3 3 3 3
Andelman, T. 115 Anderoglu, O. 211 Anderson, I. 66, 103, 142, 166, 264, 290 Anderson, M 93 Anderson, P. 168 Anderson, S. 248 Anderson, T. 33, 55, 108, 353 Ando, D. 93 Anderson, T. 33, 55, 108, 353 Ando, D. 93 Andor, T. 250 André, J. 341 Andre, S. 174 Andreas, D. 88 Andreas, D. 88 Andreas, D. 88 Andreas, D. 88 Anger, G. 88 Anger, G. 88 Angere, P. 18 Aning, A. 302 Ankem, S. 348 Annamaneni, S. 187 Anopuo, O. 350, 353 Anselmi-Tamburini, U 358 Antipov, E. 283 Antipov, E. 283 Antou, B. 294 Antrekowitsch, H. 138, 148 Anyalebechi, P. 45, 46, 97, 148, 200	
Andelman, T. 115 Anderoglu, O. 211 Anderson, I. 66, 103, 142, 166, 264, 290 Anderson, M 93 Anderson, P. 168 Anderson, S. 248 Anderson, S. 248 Anderson, T. 33, 55, 108, 353 Ando, D. 93 Anderson, T. 33, 55, 108, 353 Ando, D. 93 Andor, T. 250 André, J. 341 Andre, S. 174 Andre, S. 174 Andreas, D. 88 Andrue, M. 197 Ang, J. 131, 208 Anger, G. 88 Angere, P. 18 Aning, A. 302 Ankem, S. 348 Annamaneni, S. 187 Anopuo, O. 350, 353 Anselmi-Tamburini, U. 358 Antile, J. 283 Antoun, B. 294 Antrekowitsch, H 138, 148 Anyalebechi, P. 45, 46, 97, 148, 200 Aoki, Y 208	1 3 3 3 3 3 3 3 3 3 3 3 3 3
Andelman, T. 115 Anderoglu, O. 211 Anderson, I. 66, 103, 142, 166, 264, 290 Anderson, M 93 Anderson, P. 168 Anderson, S. 248 Anderson, T. 33, 55, 108, 353 Ando, D. 93 Anderson, T. 33, 55, 108, 353 Ando, D. 93 Andor, T. 250 André, J. 341 Andre, S. 174 Andreas, D. 88 Andreas, D. 88 Andreas, D. 88 Andreas, D. 88 Anger, G. 88 Anger, G. 88 Angere, P. 18 Aning, A. 302 Ankem, S. 348 Annamaneni, S. 187 Anopuo, O. 350, 353 Anselmi-Tamburini, U 358 Antipov, E. 283 Antipov, E. 283 Antou, B. 294 Antrekowitsch, H. 138, 148 Anyalebechi, P. 45, 46, 97, 148, 200	1 3 3 3 3 3 3 3 3 3 3 3 3 3
Andelman, T. 115 Anderoglu, O. 211 Anderson, I. 66, 103, 142, 166, 264, 290 Anderson, M 93 Anderson, P. 168 Anderson, S. 248 Anderson, T. 33, 55, 108, 353 Ando, D. 93 Anderson, T. 33, 55, 108, 353 Ando, D. 93 Andor, T. 250 André, J. 341 Andre, S. 174 Andreas, D. 88 Andreas, D. 88 Andreux, J. 182 Andrus, M. 197 Ang, J. 131, 208 Anger, G. 88 Angerer, P. 18 Aning, A. 302 Ankem, S. 348 Annamaneni, S. 187 Anopuo, O. 350, 353 Anselmi-Tamburini, U. 358 Antipov, E. 283 Antipov, E. 283 Antou, B. 294 Antrekowitsch, H. 138, 148 Anyalebechi, P. 45, 46, 97, 148, 200	
Andelman, T. 115 Anderoglu, O. 211 Anderson, I. 66, 103, 142, 166, 264, 290 Anderson, M 93 Anderson, P. 168 Anderson, S. 248 Anderson, T. 33, 55, 108, 353 Ando, D. 93 Anderson, T. 33, 55, 108, 353 Ando, D. 93 Andor, T. 250 André, J. 341 Andre, S. 174 Andreas, D. 88 Andrieux, J. 182 Andrus, M. 197 Ang, J. 131, 208 Anger, G. 88 Angerer, P. 18 Aning, A. 302 Ankem, S. 348 Annamaneni, S. 187 Anopuo, O. 350, 353 Anselmi-Tamburini, U. 358 Antipov, E. 283 Antou, B. 294 Antrekowitsch, H. 138, 148 Anyalebechi, P. 45, 46, 97, 148, 200 Aoki, Y. 208 Apel, M. 240	
Andelman, T. 115 Anderoglu, O. 211 Anderson, I. 66, 103, 142, 166, 264, 290 Anderson, M. 93 Anderson, P. 168 Anderson, S. 248 Anderson, T. 33, 55, 108, 353 Ando, D. 93 Anderson, T. 33, 55, 108, 353 Ando, D. 93 Ando, T. 250 André, J. 341 Andre, S. 174 Andreas, D. 88 Andreas, D. 88 Andreas, D. 88 Anger, G. 88 Anger, F. 181 Aning, A. 302 Ankem, S. 348 Annamaneni, S. 187 Anopuo, O. 350, 353 Anselmi-Tamburini, U. 358 Antille, J. 283 Antipov, E. 283 Antoun, B. 294 Antrekowitsch, H. 138, 148 Anyalebechi, P. 45, 46, 97, 148, 200 Aoki, Y. 208 Apel, M. 240	
Andelman, T. 115 Anderoglu, O. 211 Anderson, I. 66, 103, 142, 166, 264, 290 Anderson, M 93 Anderson, P. 168 Anderson, S. 248 Anderson, T. 33, 55, 108, 353 Ando, D. 93 Andor, T. 250 André, J. 341 André, S. 174 Andreas, D. 88 Andreas, D. 88 Andreux, J. 182 Andrus, M. 197 Anger, G. 88 Anger, F. 131, 208 Anger, P. 18 Aning, A. 302 Ankem, S. 344 Anamaneni, S. 187 Anopuo, O. 350, 353 Anselmi-Tamburini, U. 358 Antipov, E. 283 Antipov, E. 283 Antoun, B. 294 Antrekowitsch, H. 138, 148 Anyalebechi, P. 45, 46, 97, 148, 200 Aoki, Y. 208 Apel, M. 240 A	
Andelman, T. 115 Anderoglu, O. 211 Anderson, I. 66, 103, 142, 166, 264, 290 Anderson, M. 93 Anderson, P. 168 Anderson, S. 248 Anderson, T. 33, 55, 108, 353 Ando, D. 93 Anderson, T. 33, 55, 108, 353 Ando, D. 93 Ando, T. 250 André, J. 341 Andre, S. 174 Andreas, D. 88 Andreas, D. 88 Andreas, D. 88 Anger, G. 88 Anger, F. 181 Aning, A. 302 Ankem, S. 348 Annamaneni, S. 187 Anopuo, O. 350, 353 Anselmi-Tamburini, U. 358 Antille, J. 283 Antipov, E. 283 Antoun, B. 294 Antrekowitsch, H. 138, 148 Anyalebechi, P. 45, 46, 97, 148, 200 Aoki, Y. 208 Apel, M. 240	

Arai, Y	85
Arakawa, K	
Arbegast, W	
	.187, 248, 298, 299, 342
Archbold, G	
Ardakani, M	85
Ardell, A	
Arenholz, E	
Ares, A	45, 289
Argon, A	73
Arias, A	
Arin, M	
Arkhipov, G	
Armstrong, L	
Armstrong, R	
Arnaboldi, S	
Arnaud, W	
Arnold, W	
Arnon, A	
Arroyave, R	
Arsenault, S	
Arsenlis, T	
Artemev, A	
Artemyev, M	
Artyukhin, A	
Artz, E	
	.175, 176, 233, 284, 330
Arunkumar, S	
Asahi. R	
·	
Asano, S	
Asano, S Asay, J	
Asano, S Asay, J Ashby, M	
Asano, S Asay, J Ashby, M Asp, K	
Asano, S Asay, J Ashby, M Asp, K Aspandiar, R	
Asano, S Asay, J Ashby, M Asp, K Aspandiar, R Assadi, H	
Asano, S Asay, J Ashby, M Asp, K Aspandiar, R Assadi, H Asta, M	
Asano, S Asay, J Ashby, M Asp, K Aspandiar, R Assadi, H Asta, M Asvarov, A	
Asano, S Asay, J Ashby, M Asp, K Aspandiar, R Assadi, H Asta, M Asvarov, A Aswath, P	
Asano, S Asay, J Ashby, M Asp, K Aspandiar, R Assadi, H Asta, M Asvarov, A Aswath, P Ataoglu, S	
Asano, S Asay, J Ashby, M Asp, K Aspandiar, R Assadi, H Asta, M Asta, M Asvarov, A Aswath, P Ataoglu, S Atar, E	
Asano, S Asay, J Ashby, M Asp, K Aspandiar, R Assadi, H Asta, M Asta, M Aswath, P Ataoglu, S Atar, E Athreya, B	
Asano, S Asay, J Ashby, M Asp, K Aspandiar, R Assadi, H Asta, M Asta, M Asta, M Aswath, P Ataoglu, S Atar, E Athreya, B Atwell, D	
Asano, S Asay, J Ashby, M Asp, K Aspandiar, R Assadi, H Asta, M Asta, M Asta, M Aswath, P Ataoglu, S Atar, E Athreya, B Atwell, D Atwood, R	
Asano, S Asay, J Ashby, M Asp, K Aspandiar, R Assadi, H Asta, M Asta, M Aswarov, A Aswarov, A Aswarov, A Aswarov, A Aswarov, A Ataoglu, S Atar, E Athreya, B Athreya, B Atwell, D Atzmon, M	
Asano, S Asay, J Ashby, M Asp, K Aspandiar, R Assadi, H Asta, M Asta, M Aswarov, A Aswarov, A	
Asano, S Asay, J Ashby, M Asp, K Aspandiar, R. Assadi, H. Asta, M Asta, M Aswarov, A Aswarov, A	
Asano, S Asay, J Ashby, M Asp, K Aspandiar, R Assadi, H Asta, M Asta, M Aswarov, A Aswarov, A Aswarov, A Aswarov, A Aswarov, A Aswarov, A Aswarov, A Aswarov, A Aswarov, A Aswarov, A Ataoglu, S Ataoglu, S A	
Asano, S Asay, J Ashby, M Asp, K Aspandiar, R Assadi, H Asta, M Asta, M Aswarov, A Aswarov, A Aswarth, P Aswarth, P Ataroglu, S Atar, E Athreya, B Athreya, B Atwell, D Atwood, R Atzmon, M Ausland, G Austin, R Averback, R	
Asano, S Asay, J Ashby, M Asp, K Aspandiar, R Assadi, H Asta, M Asta, M Asta, M Aswath, P Aswath, P Ataoglu, S Ataoglu, S Atar, E Athreya, B Atwell, D Atwold, R Atzmon, M Aude, M Ausland, G Austin, R Averback, R Avila-Davila, E	
Asano, S Asay, J Ashby, M Ashby, M Aspandiar, R Aspandiar, R Assadi, H Assadi, H Asta, M. Asvarov, A. Aswath, P. Ataoglu, S. Atar, E. Athreya, B. Atwell, D Atwell, D Atwood, R. Atzmon, M. Aude, M. Ausland, G. Austin, R. Averback, R. Avila-Davila, E Avraham, S.	87
Asano, S Asay, J Ashby, M Asp, K Aspandiar, R Assadi, H Asta, M Asta, M Aswath, P Aswath, P Ataoglu, S Ataoglu, S Averback, R Avalan, S Awakura, Y	87
Asano, S Asay, J Ashby, M Asp, K Aspandiar, R Aspandiar, R Assadi, H Asta, M Asta, M Aswath, P Aswath, P Ataoglu, S Ataoglu, S Atwood, R Atwood, R Atzmon, M Ausland, G Averback, R Avila-Davila, E Avanam, S Awang, M	87 132, 243, 244 38 239 34 86 84, 89, 137 221 125, 249, 285 96 348 32 195 270 73 17 81 295 201, 207 336 257 334 298
Asano, S Asay, J Asby, M Asp, K Aspandiar, R Aspandiar, R Assadi, H Asta, M Asvarov, A. Aswath, P. Ataoglu, S. Ataoglu, S. Austin, R. Averback, R. Avraham, S. Awakura, Y. Awang, M Aydin, S.	87 132, 243, 244 38 239 34 86 84, 89, 137 221 125, 249, 285 96 348 32 195 270 73 17 81 295 201, 207 336 257 334 298 35
Asano, S Asay, J Asby, M Asp, K Aspandiar, R Aspandiar, R Assadi, H Asta, M Asvarov, A. Aswath, P. Ataoglu, S. Ataoglu, S. Ataoglu, S. Ataoglu, S. Ataoglu, S. Ataoglu, S. Ataoglu, S. Ataoglu, S. Ataoglu, S. Ataoglu, S. Atwell, D. Atwood, R. Atzmon, M. Austin, R. Averback, R. Averback, R. Avraham, S. Awakura, Y. Awang, M. Aydin, S Aydiner, C.	87 132, 243, 244 38 239 34 86 84, 89, 137 221 125, 249, 285 96 348 32 195 270 73 17 81 295 201, 207 336 257 334 298 35 121
Asano, S Asay, J Asay, J Ashby, M Aspandiar, R Aspandiar, R Assadi, H Assadi, H Assadi, H Assadi, H Assadi, P Assadi, P Astar, P Aswath, P Aswath, P Assadi, S Atar, E Atar, E Atar, E Atar, B Atar, B Averback, R Averback, R Avala, J Awang, M Aydin, S Aydiner, C Ayer, R	87
Asano, S Asay, J Asby, M Asp, K Aspandiar, R Aspandiar, R Assadi, H Asta, M Asvarov, A. Aswath, P. Ataoglu, S. Ataoglu, S. Ataoglu, S. Ataoglu, S. Ataoglu, S. Ataoglu, S. Ataoglu, S. Ataoglu, S. Ataoglu, S. Ataoglu, S. Atwell, D. Atwood, R. Atzmon, M. Austin, R. Averback, R. Averback, R. Avraham, S. Awakura, Y. Awang, M. Aydin, S Aydiner, C.	87

B

Baars, D	57
Babu, S	
Bach, F	
Backman, D	
Bacon, D	
Badarinarayan, H	
Badillo, A	
Bae, D	
Bae, G	145



Bae, J50,	
	333, 335
Bae, S	
Baek, E	
Baer, D	275
Baeslack, W	
Bagnall, S	
Bahia, H	
Bahr, D49, 64, 166,	325, 326
Bai, J	170
Bai, M	
Baik, J	
Baik, S	290
Baird, J	20
Baizhen, C	
Bakajin, O	
Baker, I	
Baker, S	160
Bakshi, S	
Balani, K	275
Balk, T	
Balla, V193, 250,	
Ballato, J	55
Balogh, L	
Balooch, G	
Bamberger, M	
Bammann, D	261
Ban. Y	284, 340
Bandar, A	170
Bandyopadhyay, A193, 250,	
Bandyopadhyay, P	
Banerjee, R18, 25, 126,	226, 234
Baney, R	
Bang, W144, 145, 149, 150,	196 205
Banovic, S	
Ballovic, S	19, 140
Bantounas, I	
Bao, Y	351
D 1 1 0	
Barabash, O	.247, 262
Barabash, R80,	191, 253
Barabash, R	191, 253 342
Barabash, R80, Barajas, A Baranov, A	191, 253 342 161
Barabash, R80, Barajas, A Baranov, A Barashev, A	191, 253 342 161 .201, 203
Barabash, R80, Barajas, A Baranov, A	191, 253 342 161 .201, 203
Barabash, R	191, 253 342 161 .201, 203 263, 264
Barabash, R	191, 253 342 161 .201, 203 263, 264 253
Barabash, R	191, 253 342 161 .201, 203 263, 264 253 332
Barabash, R	191, 253 342 161 .201, 203 263, 264 253 332 195, 353
Barabash, R	191, 253 342 161 .201, 203 263, 264 253 332 195, 353
Barabash, R	191, 253
Barabash, R	191, 253
Barabash, R	191, 253 342 161 .201, 203 263, 264 253 332 195, 353 16 164, 279 117
Barabash, R	191, 253 342 161 .201, 203 263, 264 253 332 195, 353 16 164, 279 117 179
Barabash, R	191, 253 342 161 .201, 203 263, 264 253 332 195, 353 16 164, 279 117 179 179 156, 269
Barabash, R	191, 253 342 161 .201, 203 263, 264 253 16 164, 279 17 179 179
Barabash, R	191, 253 342 161 .201, 203 263, 264 253 16 164, 279 17 179 179
Barabash, R	191, 253 342 161 .201, 203 263, 264 253 332 195, 353 16 164, 279 179 179 179 156, 269 80, 227 121, 312
Barabash, R	191, 253 342 161 .201, 203 263, 264 253 332 195, 353 16 164, 279 179 .156, 269 .180, 227 121, 312 40
Barabash, R	191, 253 342 161 .201, 203 263, 264 332 195, 353 16 164, 279 179 .156, 269 .180, 227 121, 312 40 293
Barabash, R	191, 253 342 161 .201, 203 263, 264 332 195, 353 16 164, 279 179 .156, 269 .180, 227 121, 312 40 293 85, 188
Barabash, R	191, 253 342 161 .201, 203 263, 264 253 332 195, 353 16 164, 279 179 .156, 269 .180, 227 121, 312 40 293 85, 188 299
Barabash, R	191, 253 342 161 .201, 203 263, 264 253 332 195, 353 16 164, 279 179 .156, 269 .180, 227 121, 312 40 293 85, 188 299
Barabash, R	191, 253 342 161 .201, 203 263, 264 253 332 195, 353 16 164, 279 179 .156, 269 .180, 227 121, 312 40 293 85, 188 299 316, 356
Barabash, R	191, 253 342 161 .201, 203 263, 264 253 332 195, 353 16 164, 279 179 .156, 269 179 .180, 227 121, 312 40 293 85, 188 299 316, 356 156
Barabash, R	191, 253
Barabash, R	191, 253
Barabash, R	191, 253
Barabash, R	$\begin{array}{cccccccccccccccccccccccccccccccccccc$
Barabash, R	191, 253
Barabash, R 80, Barajas, A Baranov, A Baranov, A Barashev, A Barbu, A 202, Barlat, F Barnard, B Barnett, M 93, Barney, I Barpanda, P Barrett, M 93, Barrey, I Barpanda, P Barrett, M 93, Barrey, I Barpanda, P Barrett, M 93, Barrey, I Barnett, M Barrett, C Barrett, C Barron, M Barrett, C Bartolo, L Bartsch, A Bartolo, L Basatsch, A Bassaran, B Bassatin, I Bassalto, H Bassani, I Bassani, J Bassani, I Bassani, P Bassim, N Bassler, K Battaile, C Battaile, C 26, 77, 239, 291, 327	191, 253
Barabash, R	191, 253
Barabash, R 80, Barajas, A Baranov, A Baranov, A Barashev, A Barbu, A 202, Barlat, F Barnett, M Barnett, M 93, Barney, I Barpanda, P Barresi, J Barrett, C Barrott, C Barrott, C Barrott, C Bartolo, L Barstch, A Basaran, B Baskes, M 19, 27, 67, 69, 132, 151, Basoalto, H Bassani, J Bassani, J Bassani, B Bassim, N Bassel, K Batista, E Batista, E Batista, E 26, 77,	191, 253
Barabash, R 80, Barajas, A Baranov, A Baranov, A Barashev, A Barbu, A 202, Barlat, F Barnard, B Barnett, M 93, Barney, I Barpanda, P Barrett, M 93, Barrey, I Barpanda, P Barrett, M 93, Barrey, I Barpanda, P Barrett, M 93, Barrey, I Barnett, M Barrett, C Barrett, C Barron, M Barrett, C Bartolo, L Bartsch, A Bartolo, L Basatsch, A Bassaran, B Bassatin, I Bassalto, H Bassani, I Bassani, J Bassani, I Bassani, P Bassim, N Bassler, K Battaile, C Battaile, C 26, 77, 239, 291, 327	191, 253

Baxter, J	
Baydogan, M	
Bayles, R	
Beals, R	40, 41, 91, 92, 143, 144, 194,
	.195, 257, 258, 307, 309, 350, 352
Bearne, G	
Becze, L	
Beer A	
Behrens C	
Beilstein M	
Belt, C	55, 56, 110, 157, 209, 269, 323
Bement, M	
Benkahla, B	71
,	
Berger, C	
,	
Betzwar-Kotas,	A318
Beyerlein, I	
Bhagat, R	
	K131, 298
••	D320
Bhosle, V	

Bhowmick, S234
Bhuiya, A110
Bialiauskaya, V
2
Bianhua, H
Biava, D192
Bica, D63
Bice, S70
Biegalski, M64
Bieler, T45, 57, 68, 228
Biener, J
Bigot, J
Bijun, R175, 232, 340
Bilgram, J188
Billia, B85, 188
Billinge, S139
Bilodeau, J
Bin, Z
Binci, M
Bing, L
Bingert, J26, 57
Birol, Y172
Birtcher, R
Biswas, K264
Björkas, C150
Black, W
Blanchard, P
Blandin, J257, 288, 331
Blawert, C257, 259, 350
Bleda, E19
Bless, S80
Bletchly, P122
Bley, F
Bligh, R
Blue, C
Blumenthal, B
Blumenthal, W244
Bobrovnitchii, G129, 290
Bocher, F43
Bocquet, J
Bodde, S
Bodéa, S
Boehlert, C17, 49, 226, 255, 308
Boehner, A267
Boettinger, W181
Bogdan, S
Bogdanov, Y71
Boggess, T
Bohlen, J
Boileau, J
Boin, U
Bojar, Z18, 66
Bokerman, G94
Boldsaikhan, E134, 135
Bolduc, S237
Bonade, R
Bondarenko, V
Bondarev, I
Bonnier, M21
Boom, R
Boone, S
Booty, M109
Borg, J
Borgenstam, A240
Borgenstam, A



Bouchard, P74
Bourke, M
Bourne, N
Bouville, M
Bouwhuis, B17, 254
Bove, P108
Bower, A
Boyanov, B238
Boyce, B
Boyle, K
Bradshaw, R235
Brady, M41, 93, 131, 145, 197,
Braga, C231
Braga, R
5
Bragato, M
Brahme, A69
Branagan, D358
Brandimarte, G
Brandstetter, S154
Brannon, R
Brenner, D216, 219, 357, 358
Brett, D90
Brewer, J80
Brewer, R
Briceno, M
Bright, M
Bringa, E
Brinley, E
Brinson, C248, 299
Brito, M
Brockdorf, K
Brody, H211
Brooks, C
Brooks, G97, 185
Brooks, J156
Brooks, J
Brow, R24, 74
Brow, R
Brow, R
Brown, R
Brow, R
Brow, R
Brow, R
Brow, R
Brow, R
Brow, R
Brow, R
Brow, R
Brow, R
Brow, R
Brow, R
Brow, R
Brow, R
Brow, R
Brow, R
Brow, R
Brow, R
Brow, R
Brow, R
Brow, R
Brow, R
Brow, R
Brow, R
Brow, R
Brow, R
Brow, R
Brow, R
Brow, R
Brow, R
Brow, R
Brow, R
Brow, R
Brow, R
Brow, R

С

Cabibbo, M	
Cabrera, J	
Caceres, C210, 352	
Caceres-Valencia, P	
Cady, C	
Cai, L	
Cai, M254	
Cai, S20	
Cai, W161, 344	
Cai, Z	
Calder, A	
Calin, M216	
Calinas, R275	
Camacho, Á273	
Camacho, R16	
Camata, R116, 163, 164, 176, 221, 285, 330	
Camel, D	
Campbell, C28, 78, 131, 182, 241, 293	
Campbell, G	
Campbell, J 111, 158, 159, 210, 270, 324	
Campbell, P60, 347	
Canales, A210	
Cañas, R	
Canas, R	
Cao, B28, 29	
Cao, D	
Cao, F	
Cao, G144, 310, 350	
Cao, H	
Cao, J	
Cao, W230, 281, 336	
Cao, X111, 186, 187, 238	
Cao, Z70, 129, 204, 276, 277	
Captain, J94	
Cardello, J	
Cardoso, M	
Cargill, G246	
Caris, J250, 251	
Carlberg, T179	
Carlberg, 1	
Carlson, D108	
Carlson, D	
Carlson, D 108 Carlton, C 224 Caro, A 150, 151, 154 Caro, M 150, 151 Caron, P 155, 208 Carpenter, J 75 Carreon, H 76 Carrier, J 341	
Carlson, D 108 Carlton, C 224 Caro, A 150, 151, 154 Caro, M 150, 151 Caron, P 155, 208 Carpenter, J 75 Carreon, H 76 Carrier, J 341 Carter, E 29, 268	
Carlson, D 108 Carlton, C 224 Caro, A 150, 151, 154 Caro, M 150, 151 Caron, P 155, 208 Carpenter, J 75 Carreon, H 76 Carrier, J 341 Carter, E 29, 268 Carter, J 92, 144, 258, 300	
Carlson, D 108 Carlton, C 224 Caro, A 150, 151, 154 Caro, M 150, 151 Caron, P 155, 208 Carpenter, J 75 Carreon, H 76 Carter, J 341 Carter, E 29, 268 Carter, J 92, 144, 258, 300 Caruso, L 31	
Carlson, D 108 Carlton, C 224 Caro, A 150, 151, 154 Caro, M 150, 151 Caron, P 155, 208 Carpenter, J 75 Carreon, H 76 Carter, J 341 Carter, E 29, 268 Carter, J 92, 144, 258, 300 Caruso, L 31 Casem, D 141, 304	
Carlson, D 108 Carlton, C 224 Caro, A 150, 151, 154 Caro, M 150, 151 Caron, P 155, 208 Carpenter, J 75 Carreon, H 76 Carter, J 341 Carter, E 29, 268 Carter, J 92, 144, 258, 300 Caruso, L 31	
Carlson, D 108 Carlton, C 224 Caro, A 150, 151, 154 Caro, M 150, 151 Caron, P 155, 208 Carpenter, J 75 Carreon, H 76 Carter, J 341 Carter, E 29, 268 Carter, J 31 Casem, D 141, 304 Castro-Colin, M 303	
Carlson, D 108 Carlton, C 224 Caro, A 150, 151, 154 Caro, M 150, 151 Caron, P 155, 208 Carpenter, J 75 Carreon, H 76 Carter, J 341 Carter, E 29, 268 Carter, J 31 Casem, D 141, 304 Castro-Colin, M 303 Castro-Román, M 159	
Carlson, D 108 Carlton, C 224 Caro, A 150, 151, 154 Caro, M 150, 151 Caron, P 155, 208 Carpenter, J 75 Carreon, H 76 Carrier, J 341 Carter, E 29, 268 Carter, J 92, 144, 258, 300 Carson, D 141, 304 Castro-Colin, M 303 Castro-Román, M 159 Catalina, A 86	
Carlson, D 108 Carlton, C 224 Caro, A 150, 151, 154 Caro, M 150, 151 Caron, P 155, 208 Carpenter, J 75 Carreon, H 76 Carrier, J 341 Carter, E 29, 268 Carter, J 92, 144, 258, 300 Caruso, L 31 Casem, D 141, 304 Castro-Colin, M 303 Castro-Román, M 159 Catalina, A 86 Caton, M 107, 108	
Carlson, D 108 Carlton, C 224 Caro, A 150, 151, 154 Caro, M 150, 151 Caron, P 155, 208 Carpenter, J 75 Carreon, H 76 Carrier, J 341 Carter, E 29, 268 Carter, J 92, 144, 258, 300 Causo, L 31 Castro-Colin, M 303 Castro-Román, M 159 Catalina, A 86 Cator, M 107, 108 Catoor, D 251	
Carlson, D 108 Carlton, C 224 Caro, A 150, 151, 154 Caro, M 150, 151 Caron, P 155, 208 Carpenter, J 75 Carreon, H 76 Carrier, J 341 Carter, E 29, 268 Carter, J 92, 144, 258, 300 Causo, L 31 Castro-Colin, M 303 Castro-Colin, M 159 Catalina, A 86 Cator, M 107, 108 Catoor, D 251 Caturla, M 203, 314	
Carlson, D 108 Carlton, C 224 Caro, A 150, 151, 154 Caro, M 150, 151 Caron, P 155, 208 Carpenter, J 75 Carreon, H 76 Carrier, J 341 Carter, E 29, 268 Carter, J 92, 144, 258, 300 Causo, L 31 Castro-Colin, M 303 Castro-Román, M 159 Catalina, A 86 Cator, M 107, 108 Catoor, D 251	
Carlson, D 108 Carlton, C 224 Caro, A 150, 151, 154 Caro, M 150, 151 Caron, P 155, 208 Carpenter, J 75 Carreon, H 76 Carter, J 341 Carter, E 29, 268 Carter, J 92, 144, 258, 300 Causo, L 31 Castro-Colin, M 303 Castro-Román, M 159 Catalina, A 86 Cator, D 251 Catural, M 203, 314 Cavin, O 47	
Carlson, D 108 Carlton, C 224 Caro, A 150, 151, 154 Caro, M 150, 151 Caron, P. 155, 208 Carpenter, J 75 Carreon, H. 76 Carter, J 341 Carter, E 29, 268 Carter, J 92, 144, 258, 300 Causo, L 31 Casem, D 141, 304 Castro-Román, M 159 Catalina, A 86 Caton, M 107, 108 Caton, M 203, 314 Cavin, O 47 Cazacu, O 147, 243	
Carlson, D 108 Carlton, C 224 Caro, A 150, 151, 154 Caro, M 150, 151 Caron, P. 155, 208 Carpenter, J 75 Carreon, H. 76 Carter, J 341 Carter, E 29, 268 Carter, J 92, 144, 258, 300 Causo, L 31 Casem, D 141, 304 Castro-Román, M 159 Catalina, A 86 Caton, M 107, 108 Caton, M 203, 314 Cavin, O 47 Cazacu, O 147, 243 Ceccaroli, B 65	
Carlson, D 108 Carlton, C 224 Caro, A 150, 151, 154 Caro, M 150, 151 Caron, P. 155, 208 Carpenter, J 75 Carreon, H. 76 Carter, J 341 Carter, E 29, 268 Carter, J 92, 144, 258, 300 Caruso, L 31 Casem, D 141, 304 Castro-Colin, M 303 Castro-Román, M 159 Catalina, A 86 Cator, D 251 Caturia, M 203, 314 Cavin, O 47 Cazacu, O 147, 243 Ceccaroli, B 65 Celik, O 138	
Carlson, D 108 Carlton, C 224 Caro, A 150, 151, 154 Caro, M 150, 151 Caron, P. 155, 208 Carpenter, J 75 Carreon, H. 76 Carter, J 341 Carter, E 29, 268 Carter, J 92, 144, 258, 300 Caruso, L 31 Casem, D 141, 304 Castro-Colin, M 303 Castro-Román, M 159 Catalina, A 86 Cator, D 251 Caturia, M 203, 314 Cavin, O 47 Cazacu, O 147, 243 Ceccaroli, B 65 Celik, O 138	
Carlson, D 108 Carlton, C 224 Caro, A 150, 151, 154 Caro, M 150, 151 Caron, P. 155, 208 Carpenter, J 75 Carreon, H. 76 Carter, J 341 Carter, E 29, 268 Carter, J 92, 144, 258, 300 Caruso, L 31 Casem, D 141, 304 Castro-Colin, M 303 Castro-Román, M 159 Catalina, A 86 Cator, D 251 Caturia, M 203, 314 Cavin, O 47 Cazacu, O 147, 243 Ceccaroli, B 65 Celik, O 138 Cerezo, A 76 Cerreta, E 29, 30, 79, 132, 133, 138, 183,	
Carlson, D 108 Carlton, C 224 Caro, A 150, 151, 154 Caro, M 150, 151 Caron, P. 155, 208 Carpenter, J 75 Carreon, H. 76 Carter, J 341 Carter, E 29, 268 Carter, J 92, 144, 258, 300 Caruso, L 31 Casem, D 141, 304 Castro-Colin, M 303 Castro-Román, M 159 Catalina, A 86 Cator, D 251 Caturia, M 203, 314 Cavin, O 47 Cazacu, O 147, 243 Ceccaroli, B 65 Celik, O 138	
Carlson, D 108 Carlton, C 224 Caro, A 150, 151, 154 Caro, M 150, 151 Caron, P. 155, 208 Carpenter, J 75 Carreon, H. 76 Carter, J 341 Carter, E 29, 268 Carter, J 92, 144, 258, 300 Caruso, L 31 Casem, D 141, 304 Castro-Colin, M 303 Castro-Román, M 159 Catalina, A 86 Cator, D 251 Caturia, M 203, 314 Cavin, O 47 Cazacu, O 147, 243 Ceccaroli, B 65 Celik, O 138 Cerezo, A 76 Cerreta, E 29, 30, 79, 132, 133, 138, 183,	
Carlson, D 108 Carlton, C 224 Caro, A 150, 151, 154 Caro, M 150, 151 Caro, P 155, 208 Carpenter, J 75 Carreon, H 76 Carrier, J 341 Carter, E 29, 268 Carter, J 92, 144, 258, 300 Caruso, L 31 Casem, D 141, 304 Castro-Colin, M 303 Castro-Román, M 159 Catalina, A 86 Cator, D 251 Caturla, M 203, 314 Cavin, O 47 Cazacu, O 147, 243 Cecaroli, B 65 Celik, O 138 Cerezo, A 76 Cerreta, E 29, 30, 79, 132, 133, 138, 183,	
Carlson, D 108 Carlton, C 224 Caro, A 150, 151, 154 Caro, M 150, 151 Caro, P 155, 208 Carpenter, J 75 Carreon, H 76 Carrier, J 341 Carter, E 29, 268 Carter, J 92, 144, 258, 300 Carson, D 141, 304 Castro-Colin, M 303 Castro-Román, M 159 Catalina, A 86 Cator, D 251 Caturla, M 203, 314 Cavin, O 47 Cazacu, O 147, 243 Cecaroli, B 65 Celik, O 138 Cereta, E 29, 30, 79, 132, 133, 138, 183,	
Carlson, D 108 Carlton, C 224 Caro, A 150, 151, 154 Caro, M 150, 151 Caro, P 155, 208 Carpenter, J 75 Carreon, H 76 Carrier, J 341 Carter, E 29, 268 Carter, J 92, 144, 258, 300 Caruso, L 31 Casem, D 141, 304 Castro-Colin, M 303 Castro-Román, M 159 Catalina, A 86 Cator, D 251 Caturla, M 203, 314 Cavin, O 47 Cazacu, O 147, 243 Cecaroli, B 65 Celik, O 138 Marciacu, S 125 Cetarine, B 190, 243, 250, 294, 301, 338, 348 Cetinel, S 125 Ceyhan, U 280 Cha, P 169, 287	
Carlson, D 108 Carlton, C 224 Caro, A 150, 151, 154 Caro, M 150, 151 Caro, P 155, 208 Carpenter, J 75 Carreon, H 76 Carrier, J 341 Carter, E 29, 268 Carter, J 92, 144, 258, 300 Carson, D 141, 304 Castro-Colin, M 303 Castro-Román, M 159 Catalina, A 86 Cator, D 251 Caturla, M 203, 314 Cavin, O 47 Cazacu, O 147, 243 Cecaroli, B 65 Celik, O 138 Cereta, E 29, 30, 79, 132, 133, 138, 183,	

Chada, S	
	05, 264, 265, 317, 318
Chakravarthy, S	
Chaldyshev, V	
Champagne, E	
Chan, C	
Chan, K	
Chan, L	340
Chan, P	
Chandler, R	
Chandra, D	
Chandrasekar, S	
Chang, A	
Chang, C50, 10	
Chang, E	
Chang, H	
Chang, J	
Chang, L	
Chang, R	
Chang, Y152, 196, 29	96, 310, 322, 332, 336
Chang-Chien, P	
Chan Gyung, P	
Chanturiya, V	
Chao, H	
Charbonneau, C	90
Charit, I	
Chartrand, P	
Chatterjee, U	
Chaubal, M	
Chawla, N	
Chelikowsky, J	
Chellappa, R	43
Chembarisova, R	
Chen, B	
Chen, C51, 66, 104	
	55, 296, 318, 330, 345
Chen, D	
Chen, G	
Chen, H	
Chen, I	
Chen, J54, 70, 9	
Chen, K	
Chen, L28, 32, 64, 77, 119	9, 149, 181, 198, 246
260, 290, 296, 29	97, 318, 342, 343, 344
Chen, M	
Chen, P	
Chen, Q	
Chen, R	
Chen, S	
	3, 153, 205, 232, 243
	55, 296, 297, 318, 342
Chen, T	
Chen, W60, 14	
Chen, X	
Chen, Z	
Cheney, J	
Cheng, A	
Cheng, C	
Cheng, J	
Cheng, M	
Cheng, S	
Cheng, T	
Cheng, X	
Chenggui, M	
Cheong, S	255, 290
Cheong, Y	
Cherukuri, B	
Chesonis, D	
· · · · · · · · · · · · · · · · · · ·	



Chhabildas, L
Chi, A
Chi, D
Chiang, C
Chiang, F97
Chiang, H102
Chiang, K
Chiang, L
Chiarbonello, M
Chien, W
Chimbli, S135
Chintalapati, P159
Chiu, C
Chiu, S
Cho, H56, 137, 276, 328, 334
Cho, J
Cho, K
Cho, M104
Cho, W
Cho, Y273
Choate, W276
Choi, C
Choi, H
Choi, J119, 146, 225
Choi, K
Choi, W16, 63, 117, 164, 165, 223, 274
Choi, Y
Choo, D144, 145
Choo, H23, 24, 73, 95, 126, 127, 134,
Chou, H
Chou, K
Chou, Y145
Choudhuri, D151, 153, 204
Chowdary, K81
Chowdary, K
Chrisey, D
Chrisey, D 284 Christensen, M 28 Christodoulou, J 240, 292, 307 Christou, A 54, 108 Chrzan, D 52, 207, 327 Chu, H 319 Chu, J 266, 287, 288 Chu, M 288 Chuang, H 206 Chuang, Y 152 Chuanyong, C 107 Chuikin, A 173 Chumbley, L 76, 290 Chumbley, S 290 Chumlyakov, Y 299 Chun, H 359
Chrisey, D 284 Christensen, M 28 Christodoulou, J 240, 292, 307 Christou, A 54, 108 Chrzan, D 52, 207, 327 Chu, H 319 Chu, J 266, 287, 288 Chu, M 288 Chuang, H 206 Chuang, T 305 Chuang, Y 152 Chuanyong, C 107 Chumbley, L 76, 290 Chumbley, S 290 Chumlyakov, Y 299 Chun, H 359 Chung, H 48
Chrisey, D 284 Christensen, M 28 Christodoulou, J 240, 292, 307 Christou, A 54, 108 Chrzan, D 52, 207, 327 Chu, H 319 Chu, J 266, 287, 288 Chu, M 288 Chuang, H 206 Chuang, Y 152 Chuanyong, C 107 Chuikin, A 173 Chumbley, L 76, 290 Chumbley, S 290 Chumlyakov, Y 299 Chun, H 359
Chrisey, D 284 Christensen, M 28 Christodoulou, J 240, 292, 307 Christou, A 54, 108 Chrzan, D 52, 207, 327 Chu, H 319 Chu, J 266, 287, 288 Chu, M 288 Chuang, H 206 Chuang, T 305 Chuang, Y 152 Chuanyong, C 107 Chumbley, L 76, 290 Chumbley, S 299 Chun, H 359 Chung, H 48 Chung, K 186, 247
Chrisey, D 284 Christensen, M 28 Christodoulou, J 240, 292, 307 Christou, A 54, 108 Chrzan, D 52, 207, 327 Chu, H 319 Chu, J 266, 287, 288 Chuang, H 206 Chuang, T 305 Chuang, Y 152 Chuanyong, C 107 Chubikin, A 173 Chumbley, L 76, 290 Chumylyakov, Y 299 Chung, H 359 Chung, H 48 Chung, K 186, 247 Chung, S 259
Chrisey, D 284 Christensen, M 28 Christodoulou, J 240, 292, 307 Christou, A 54, 108 Chrzan, D 52, 207, 327 Chu, H 319 Chu, J 266, 287, 288 Chuang, H 206 Chuang, T 305 Chuang, Y 152 Chuanyong, C 107 Chubikin, A 173 Chumbley, L 76, 290 Chumylyakov, Y 299 Chung, H 359 Chung, K 148 Chung, K 186, 247 Chung, S 259 Chung Ho, W 202
Chrisey, D 284 Christensen, M 28 Christodoulou, J 240, 292, 307 Christou, A 54, 108 Chrzan, D 52, 207, 327 Chu, H 319 Chu, J 266, 287, 288 Chuang, H 206 Chuang, T 305 Chuang, Y 152 Chuanyong, C 107 Chuikin, A 173 Chumbley, L 76, 290 Chumylyakov, Y 299 Chung, H 359 Chung, K 148 Chung, K 186, 247 Chung, S 259 Chung Ho, W 202 Chunling, Z 61
Chrisey, D 284 Christensen, M 28 Christodoulou, J 240, 292, 307 Christou, A 54, 108 Chrzan, D 52, 207, 327 Chu, H 319 Chu, J 266, 287, 288 Chuang, H 206 Chuang, T 305 Chuang, Y 152 Chuanyong, C 107 Chuikin, A 173 Chumbley, L 76, 290 Chumbley, S 299 Chun, H 359 Chung, K 148 Chung, K 259 Chung, S 259 Chung Ho, W 202 Chunling, Z 61
Chrisey, D 284 Christensen, M 28 Christodoulou, J 240, 292, 307 Christou, A 54, 108 Chrzan, D 52, 207, 327 Chu, H 319 Chu, J 266, 287, 288 Chuang, H 206 Chuang, H 206 Chuang, T 305 Chuang, Y 152 Chuanyong, C 107 Chuikin, A 173 Chumbley, L 76, 290 Chumbley, S 299 Chung, H 359 Chung, K 148 Chung, K 259 Chung, S 259 Chung, G 202 Chunling, Z 61 Churbaev, R 218 Churi, N 262
Chrisey, D 284 Christensen, M 28 Christodoulou, J 240, 292, 307 Christou, A 54, 108 Chrzan, D 52, 207, 327 Chu, H 319 Chu, J 266, 287, 288 Chuang, H 206 Chuang, H 206 Chuang, T 305 Chuang, Y 152 Chuanyong, C 107 Chuikin, A 173 Chumbley, L 76, 290 Chumbley, S 299 Chung, H 359 Chung, K 148 Chung, K 259 Chung, S 259 Chung, G 202 Chunling, Z 61 Churbaev, R 218 Churi, N 262
Chrisey, D 284 Christensen, M 28 Christodoulou, J 240, 292, 307 Christou, A 54, 108 Chrzan, D 52, 207, 327 Chu, H 319 Chu, J 266, 287, 288 Chu, M 286 Chuang, H 206 Chuang, T 305 Chuang, Y 152 Chuang, Q 107 Chuikin, A 173 Chumbley, L 76, 290 Chumbley, S 290 Chung, S 299 Chun, H 359 Chung, H 48 Chung, S 259 Chung, H 48 Chung, S 259 Chung, H 48 Chung, S 259 Chung, Ho, W 202 Chung, S 259 Chung, Ho, W 202 Chunling, Z 61 Churbaev, R 218 Churi, N 262 Chuzhoy, L 86
Chrisey, D 284 Christensen, M 28 Christodoulou, J 240, 292, 307 Christou, A 54, 108 Chrzan, D 52, 207, 327 Chu, H 319 Chu, J 266, 287, 288 Chu, M 286 Chuang, H 206 Chuang, T 305 Chuang, Y 152 Chuang, Q 107 Chuikin, A 173 Chumbley, L 76, 290 Chumbley, S 290 Chumbley, S 299 Chun, H 359 Chung, H 48 Chung, S 259 Chung, H 48 Chung, S 259 Chung, H 48 Chung, S 259
Chrisey, D 284 Christensen, M 28 Christodoulou, J 240, 292, 307 Christou, A 54, 108 Chrzan, D 52, 207, 327 Chu, H 319 Chu, J 266, 287, 288 Chuang, H 206 Chuang, T 305 Chuang, Y 152 Chuang, Q 107 Chukin, A 173 Chumbley, L 76, 290 Chumbley, S 290 Chung, S 299 Chun, H 359 Chung, H 48 Chung, K 148 Chung, K 206 Chung, K 209 Chung, H 48 Chung, S 259 Chung, H 148 Chung, S 259 Chung Ho, W 202 Chung Ho, W 202 Chuning, Z 61 Churaev, R 218 Churi, N 262 Chuzhoy, L 86 Chwa, E 326 Ciftja, A <td< td=""></td<>
Chrisey, D 284 Christensen, M 28 Christodoulou, J 240, 292, 307 Christou, A 54, 108 Chrzan, D 52, 207, 327 Chu, H 319 Chu, J 266, 287, 288 Chu, M 286 Chuang, H 206 Chuang, T 305 Chuang, Y 152 Chuang, Q 107 Chuikin, A 173 Chumbley, L 76, 290 Chumbley, S 290 Chumbley, S 299 Chun, H 359 Chung, H 48 Chung, S 259 Chung, H 48 Chung, S 259 Chung, H 48 Chung, S 259
Chrisey, D 284 Christensen, M 28 Christodoulou, J 240, 292, 307 Christou, A 54, 108 Chrzan, D 52, 207, 327 Chu, H 319 Chu, J 266, 287, 288 Chuang, H 206 Chuang, T 305 Chuang, Y 152 Chuang, Q 107 Chukin, A 173 Chumbley, L 76, 290 Chumbley, S 290 Chung, S 299 Chun, H 359 Chung, H 48 Chung, K 148 Chung, K 206 Chung, K 209 Chung, H 48 Chung, S 259 Chung, H 148 Chung, S 259 Chung Ho, W 202 Chung Ho, W 202 Chuning, Z 61 Churaev, R 218 Churi, N 262 Chuzhoy, L 86 Chwa, E 326 Ciftja, A <td< td=""></td<>
Chrisey, D 284 Christensen, M 28 Christodoulou, J 240, 292, 307 Christou, A 54, 108 Chrzan, D 52, 207, 327 Chu, H 319 Chu, J 266, 287, 288 Chu, M 288 Chuang, H 206 Chuang, H 206 Chuang, Y 152 Chanyong, C 107 Chuikin, A 173 Chumbley, L 76, 290 Chumbley, S 290 Chung, S 290 Chung, H 48 Chung, K 186, 247 Chung, K 186, 247 Chung, S 259 Chung, K 262 Chung, S 259 Chung, C 61 Churbaev, R 218 Churi, N 262 Churbaev, R 218 Churi, N 262 Churboy, L 86 Chorae, E 326 Cittal, A 323 Cimalla, V 115 Cimenoglu,
Chrisey, D 284 Christensen, M 28 Christodoulou, J 240, 292, 307 Christou, A 54, 108 Chrzan, D 52, 207, 327 Chu, H 319 Chu, J 266, 287, 288 Chu, M 288 Chuang, H 206 Chuang, H 206 Chuang, Y 152 Chanyong, C 107 Chuikin, A 173 Chumbley, L 76, 290 Chumbley, S 290 Chung, S 290 Chung, H 48 Chung, K 186, 247 Chung, K 186, 247 Chung, S 259 Chung, K 262 Chung, S 259 Chung, C 61 Churbaev, R 218 Churi, N 262 Chuzhoy, L 86 Chuva, E 326 Chuzhoy, L 86 Chwa, E 326 Cittal, A 323 Cimanla, V 115 Cimenoglu, H </td
Chrisey, D 284 Christensen, M 28 Christodoulou, J 240, 292, 307 Christou, A 54, 108 Chrzan, D 52, 207, 327 Chu, H 319 Chu, J 266, 287, 288 Chu, M 288 Chuang, H 206 Chuang, T 305 Chuang, Y 152 Chanyong, C 107 Chuikin, A 173 Chumbley, L 76, 290 Chumbley, S 290 Chung, S 290 Chung, H 48 Chung, K 186, 247 Chung, K 186, 247 Chung, S 259 Chung, K 262 Chung, S 259 Chung, C 61 Churbaev, R 218 Churi, N 262 Chuzhoy, L 86 Chuva, E 326 Citrija, A 323 Cimalla, V 115 Cimenoglu, H 138, 270, 348, 351 Clark, B 48
Chrisey, D 284 Christensen, M 28 Christodoulou, J 240, 292, 307 Christou, A 54, 108 Chrzan, D 52, 207, 327 Chu, H 319 Chu, J 266, 287, 288 Chu, M 288 Chuang, H 206 Chuang, T 305 Chuang, Y 152 Chuanyong, C 107 Chuikin, A 173 Chumbley, L 76, 290 Chumbley, S 290 Chung, R 209 Chung, H 48 Chung, K 299 Chung, H 48 Chung, K 259 Chung, S 259 Chung, S 259 Chung, S 259 Chung, R 218 Churi, N 262 Chuzhoy, L 86 Chwa, E 326 Chuzhoy, L 826 Chark, S 323 Cimalla, V 115 Cimenoglu, H 138, 270, 348, 351 Clark,
Chrisey, D 284 Christensen, M 28 Christodoulou, J 240, 292, 307 Christou, A 54, 108 Chrzan, D 52, 207, 327 Chu, H 319 Chu, J 266, 287, 288 Chu, M 288 Chuang, H 206 Chuang, T 305 Chuang, Y 152 Chuanyong, C 107 Chumbley, L 76, 290 Chumbley, S 290 Chumbley, S 290 Chung, H 359 Chung, H 359 Chung, K 186, 247 Chung, S 259 Chung Ho, W 202 Chunling, Z 61 Churbaev, R 218 Churi, N 262 Chuzhoy, L 86 Chwa, E 323 Cimalla, V 115 Cimenoglu, H 138, 270, 348, 351 Clark, B 48 Clark, C 345 Clarke, A 190, 249
Chrisey, D 284 Christensen, M 28 Christodoulou, J 240, 292, 307 Christou, A 54, 108 Chrzan, D 52, 207, 327 Chu, H 319 Chu, J 266, 287, 288 Chu, M 288 Chuang, H 206 Chuang, T 305 Chuang, Y 152 Chuanyong, C 107 Chuikin, A 173 Chumbley, L 76, 290 Chumbley, S 290 Chung, R 209 Chung, H 48 Chung, K 299 Chung, H 48 Chung, K 259 Chung, S 259 Chung, S 259 Chung, S 259 Chung, R 218 Churi, N 262 Chuzhoy, L 86 Chwa, E 326 Chuzhoy, L 826 Chark, S 323 Cimalla, V 115 Cimenoglu, H 138, 270, 348, 351 Clark,

Clausen, B	
Clements, B	
Clifton, R	
Clouet, E	
Cluff, D	
Cochran, J	
Cockcroft, S	
Cocke, D	
Cockeram, B	
Cohea, B	
Cole, B	
Cole, G	
Coleman, P	
Colliex, C	
Colligan, K	
Collins, P26, 121,	130, 229, 255, 306, 312
Colon, J	
Colvin, J	
Compton, C	
Compton, W	
Comstock, R	
Conner, B	
Conte, F	
Contreras, S	
Converse, G	
Conway, P	
Cooksey, M	
Coombe, V	
Cooper, R	
Copland, E	
Copley, J	
Cordero, N	
Cordill, M Corine, G	
Cortes, V	
Corwin, D	
Corwin, E	
Costanza, G	
Costello, A	
Côté, J	
Cotten, W	
Cotton, J	
Coughlin, J	
Coulombe, P	
Counter, J	
Courtenay, J Coventry, G	
Covert, L	
Covino, B	
Cowan, K	
Cowen, C	
Cox, A	
Cox, B	
Cox, I	
Craviso, G	
Crenshaw, T	
Crepeau, P	
Crimp, M Crosby, C	
Crosby, C	
Croy, J	
Csoke, B	
Cuenya, B	
•	
Cummins, S	
Currie, K	
Curtin, W	
Curtis, C	

Cutler, E	322
Czerwinski, F	91
Czyryca, E	306, 339

D

D'Abreu, J98
d'Almeida, J129, 181
D'Armas, H
D'Souza, N
Daehn, G
Dahle, A112, 179, 194, 237, 264, 265
Dahotre, N
Dai, C
Dai, K
Dai, L
Dai, S175, 232, 340
Dakshinamurthy, V
Dalmijn, W
Dalton, D80
Damm, E
Dan, X
Dandekar, D
Dando, N
Danielewski, M
Daniels, E
Danks, D
Dantzig, J
Dao, M
Dargusch, M112
Dargusen, Million 112 Darras, B
Das, A
Das, D
Das, K
Das, S
172, 209, 230, 269, 270, 282, 323, 327
Dashwood, R90, 192, 321
da Silva, A
Ua Silva, A259 Dassylva Paymond V 134
Dassylva-Raymond, V134
Dassylva-Raymond, V
Dassylva-Raymond, V 134 Datta, M 351 Datta Roy, A 165
Dassylva-Raymond, V 134 Datta, M 351 Datta Roy, A 165 Dauskardt, R 125
Dassylva-Raymond, V 134 Datta, M 351 Datta Roy, A 165 Dauskardt, R 125 Davenport, A 360
Dassylva-Raymond, V 134 Datta, M 351 Datta Roy, A 165 Dauskardt, R 125 Davenport, A 360 David, S 134, 247, 262
Dassylva-Raymond, V 134 Datta, M 351 Datta Roy, A 165 Dauskardt, R 125 Davenport, A 360 David, S 134, 247, 262 Davidson, C 237
Dassylva-Raymond, V 134 Datta, M 351 Datta Roy, A 165 Dauskardt, R 125 Davenport, A 360 David, S 134, 247, 262 Davidson, C 237 Davies, R 327, 328
Dassylva-Raymond, V 134 Datta, M 351 Datta Roy, A 165 Dauskardt, R 125 Davenport, A 360 David, S 134, 247, 262 Davidson, C 237 Davies, R 327, 328 Davis, B 34, 35, 87, 137
Dassylva-Raymond, V 134 Datta, M 351 Datta Roy, A 165 Dauskardt, R 125 Davenport, A 360 David, S 134, 247, 262 Davidson, C 237 Davies, R 327, 328 Davis, B 34, 35, 87, 137 Davis, C 247
Dassylva-Raymond, V 134 Datta, M 351 Datta Roy, A 165 Dauskardt, R 125 Davenport, A 360 David, S 134, 247, 262 Davidson, C 237 Davies, R 327, 328 Davis, B 34, 35, 87, 137 Davis, C 247 Davis, R 324, 35, 87, 137 Davis, C 247 Davisson, T 238
Dassylva-Raymond, V 134 Datta, M 351 Datta Roy, A 165 Dauskardt, R 125 Davenport, A 360 David, S 134, 247, 262 Davidson, C 237 Davies, R 327, 328 Davis, B 34, 35, 87, 137 Davis, C 247 Davison, T 238 Daw, M 19, 207, 327
Dassylva-Raymond, V
Dassylva-Raymond, V 134 Datta, M 351 Datta Roy, A 165 Dauskardt, R 125 Davenport, A 360 David, S 134, 247, 262 Davidson, C 237 Davies, R 327, 328 Davis, B 34, 35, 87, 137 Davis, C 247 Davison, T 238 Daw, M 19, 207, 327 Dawson, P 147, 199, 321 Dawson, R 349
Dassylva-Raymond, V



del Campo, A23
DeLorme, R
Delos-Reyes, M
Delzer, K
Demcnak, M
Demirkiran, H
Demkowicz, M
Demopoulos, G
Deng, J
Deng, X
Den Hond, R
Denisov, V
Dennis, K
de Nora, V283
Denton, M249
Deo, C
Deppisch, C205
Derlet, P106
DeRushie, C
Desai, T
Desai, V
Deschamps, A
Deschamps, J
Deslippe, J
DeSouza, E
Detor, A
Deuerling, J
Deutscher, R
Devincre, B
De Vries, P
DeWeese, S69
Dewit, R
De Yoreo, J23
DeYoung, D74, 127, 179, 237, 288, 333
Dezellus, O182, 226
Dezellus, O182, 226 Dharmaprakash, M64
Dezellus, O
Dezellus, O. 182, 226 Dharmaprakash, M. .64 Dhere, N. .33 Dias, C .56 Dick, R .121 Dickinson, J. .254 Didier, R .17 Didier, R. .17 Diercks, D .18, 189 Dieringa, H. .257, 352 Dieumegard, D .117 DiGiacomo, S. .340 Dilsizoglu, B .88 Dimas, P. .229 Dimiduk, D .26, 44, 130, 160, 225, 266, 320 Dimos, D .101 Ding, F .233 Ding, W. .47, 195, 196, 309, 353 Ding, Y .97 Dinh, L .214 Dinsdale, A .104
Dezellus, O
Dezellus, O
Dezellus, O
Dezellus, O
Dezellus, O. 182, 226 Dharmaprakash, M. .64 Dhere, N. .33 Dias, C .56 Dick, R .121 Dickinson, J. .254 Didier, R .17 Dider, R. .17 Didrer, S. D. .18, 189 Dieringa, H. .257, 352 Dieuwegard, D. .117 DiGiacomo, S. .340 Dilsizoglu, B. .88 Dimas, P. .229 Dimiduk, D. .26, 44, 130, 160, 225, 266, 320 Dimos, D. .01 Ding, F. .233 Ding, Y. .97 Dinh, L .214 Dinsdale, A. .104 Dinsdale, A. .104 Disbatino, M. .166 Disalvo, F. .65 Dispinar, D. .111 Ditenberg, I. .215, 218
Dezellus, O
Dezellus, O
Dezellus, O. 182, 226 Dharmaprakash, M. 64 Dhere, N. 33 Dias, C 56 Dick, R 121 Dickinson, J. 254 Didier, R 17 Didier, R. 17 Didre, S. D. 18, 189 Dieringa, H. 257, 352 Dieumegard, D. 117 DiGiacomo, S. 340 Dilsizoglu, B. 88 Dimas, P. 229 Dimiduk, D. 26, 44, 130, 160, 225, 266, 320 Dimos, D. 101 Ding, F. 233 Ding, W. 47, 195, 196, 309, 353 Ding, Y. 97 Dinh, L 214 Dinsdale, A. 104 Disabatino, M. 166 DiSalvo, F. 65 Dispinar, D. 111 Ditenberg, I. 215, 218 Ditmire, T. 80 Divakaran, P. 232 Do, E. 33
Dezellus, O
Dezellus, O. 182, 226 Dharmaprakash, M. .64 Dhere, N. .33 Dias, C .56 Dick, R .121 Dickinson, J. .254 Didier, R .17 Didrer, S. .18, 189 Dieringa, H. .257, 352 Dieumegard, D. .117 DiGiacomo, S. .340 Dilsizoglu, B. .88 Dimas, P. .229 Dimiduk, D. .26, 44, 130, 160, 225, 266, 320 Dimos, D. .101 Ding, F. .233 Ding, W. .47, 195, 196, 309, 353 Ding, Y. .97 Dinh, L .214 Dinsdale, A. .104 Dinsidale, A. .104 Disabatino, M. .166 DiSalvo, F. .65 Dispinar, D. .111 Ditenberg, I. .215, 218 Ditmire, T. .80 Divakaran, P. .232 Do, E .33 Dobatkin, S. .112
Dezellus, O. 182, 226 Dharmaprakash, M. .64 Dhere, N. .33 Dias, C .56 Dick, R .121 Dickinson, J. .254 Didier, R .17 Didier, T .17 Diercks, D .18, 189 Dieringa, H. .257, 352 Dieumegard, D. .117 DiGiacomo, S. .340 Dilsizoglu, B .88 Dimas, P. .229 Dimiduk, D .26, 44, 130, 160, 225, 266, 320 Dimos, D .101 Ding, F .233 Ding, W. .47, 195, 196, 309, 353 Ding, Y .97 Dinh, L .214 Dinsdale, A .104 Dinwiddie, R .413 Di Sabatino, M .166 DiSalvo, F .65 Dispinar, D .111 Ditenberg, I .215, 218 Ditmire, T .80 Divakaran, P .232 Do, E .33 Dobatkin, S .112 D
Dezellus, O. 182, 226 Dharmaprakash, M. .64 Dhere, N. .33 Dias, C .56 Dick, R .121 Dickinson, J. .254 Didier, R .17 Didier, T .17 Diercks, D .18, 189 Dieringa, H. .257, 352 Dieumegard, D. .117 DiGiacomo, S. .340 Dilsizoglu, B .88 Dimas, P. .229 Dimiduk, D .26, 44, 130, 160, 225, 266, 320 Dimos, D .101 Ding, F .233 Ding, W. .47, 195, 196, 309, 353 Ding, Y .97 Dinh, L .214 Dinsdale, A .04 Dinwiddie, R .413 Di Sabatino, M .166 DiSalvo, F .65 Dispinar, D .111 Ditenberg, I .215, 218 Ditmire, T .80 Divakaran, P .232 Do, E .33 Dobatkin, S .112 Do

Dogo, F	H150
Doherty	, R121, 241, 280, 282, 328
Domain	, C201, 202, 263, 315, 35
Donega	n, J220
Dong, C	8′8′
Dong, H	I
Dong, J	
Dong, L	5′
	7
	2172, 275, 28
Donner.	, W
	ie, A160
	vamy, A163, 284, 28
	R
	H
	tos, J134, 259
	tos, L
	J122, 171, 229, 280
Doucett	e, R224
	erty, L30, 133, 138
Doughe	erty, S16
	s, J32
Dowdin	ıg, R111
Downs,	Т248
Dovle, l	F16
	R2'
	S162, 362
	nann, A65, 13
	B
	Б
	, D
	nis, S330
Du, W	
Du, Y	5
	v, S27, 52, 202
Duerig,	T24
	G34
Duh, J	
Dumitra	ache, F6
Dumoul	lin, S6
Dunand	, D
	, M
	N2
	, J
Dupont	, V155, 21
Dupuic	C
Dupuis,	rd, A275
	23. 26
,	-, -
	A
	yk, J31
	c, J23
Dutton,	R138, 190, 250, 301, 34
Duval, l	H12
Duvvur	u, H69, 19
	u, O170
	, J140
DYOTAK	
	1. D
Dwived	i, D
Dwived Dye, D	1, D

Е

—
Eakins, D183, 295, 312
Earthman, J177, 249, 275, 347
Eastman, J
Easton, M
Eaton, B
Eberl, C
Ebrahimi, F
Eckert, C
Eckert, J
Edmonds, D
Edwards, B
Edwards, D
Edwards, H171
Edwards, L81
Edwards, M
Egami, T126, 235
Eggeler, G
Eick, I
Eiken, J32
Eisinger, N17
Ekenes, M
Ekpenuma, S
El-Ashry, M117, 345
El-Awady, J96
El-Azab, A
El-Bealy, M
El-Emairy, H
Elbaccouch, M
Elbarawy, K
Elboujdaini, M
Elder, K
El Ghaoui, Y
El onaoui, 1
Eliezer, A
El Kadiri, H
Elkadiri, H
El Khakani, M
Elle, J
Ellendt, N
Elliott, A53
ElMehtedi, M
Elmustafa, A135
Elsener, A106
Eltgroth, M234
Elwazri, A144
Emamian, A277, 347
Emanetoglu, N55
Embree, T34
Emerson, D81
Engberg, G228
Engelberg, D129
Engelhard, M100
Engh, A
Engler-Pinto Jr, C
Enright, M
Eppich, B
Epstein, S
Erdélyi, Z
Erdemir, A
Erdmann, R
Ergun, N
Erie, J
Ertekin, E
Es-Said, O
Escobar de Obaldia, E
Escobedo B, J159



Eskin, D	75 84 237
Esmaeili, S	
Espana, F	
Espeland, O	
Espinoza Orías, A	
Essa, M	
Essadiqi, E	
Estrada-Mateos, B	
Estrin, Y	
Eugene, Z	
Euh, K	
Evangelista, E	
Evans, A	
Evans, J	179
Evers, F	
Evteev, A	
Ewing, R	
Eylon, D	
<i>,</i> , , , , , , , , , , , , , , , , , ,	

F

Fafard, M	
Fagan, R	223
Fahrmann, M	107
Faivre, G	35, 188
Fan, C	
Fan, G23, 24, 73, 12	6.177.
Fan, X	
Fan, Y	335
Fan, Z	4, 324
Fang, H	66
Fang, J21	1, 319
Fang, X	324
Fang, Y	354
Fang, Z118, 197, 224, 22	25, 276
Fantin, D	
Fardeau, S	
Farias, E	
Farias, S	
Farid, M	
Farkas, D51, 105, 154, 15	
Farmer, J	
Farrar, C	
Faruqi, M	
Faulkner, R	
Faupel, F	
Fechner, D	
Fecht, H	
Felderman, E	
Feldman, A	119
Felicelli, S	
Fellner, P	
Feng, C	
Feng, G	
Feng, Q52, 106, 155, 156, 208, 26 Feng, S	18, 321
Feng, Y	
Feng, Z	
Fenske, G	
Fenske, J	
Fenton, J	
Fenwick, W	
Feret, F	
Ferguson, I	
Fergusson, L	
Ferkel, H	
Fernandez-Baca, J	
Fernandez Lisbona, D	31

Fernando, G	274
Ferranti, L	
Ferrasse, S	114
Ferreira, A	
Ferreira, P	.224, 275
Ferri, E	185
Ferron, C	87
Fertig, R	160
Fiedler, T	78
Field, A	
Field, D20, 149, 170,	228, 244
Field, F	60
Field, R190,	243, 249
Fielden, D	219
Fields, R	
Figueiredo, F	81
Figueiredo, R	112
Fikar, J	202
Filatov, A	
Filliben, J	140
Filoti, G	
Fine, M	.138, 282
Finel, A	
Finlayson, T	.136, 210
Finnigan, P	
Finstad, T	17
Fiory, A54, 55,	
Firrao, D	.180, 339
Fischer, J	352
Fischer, R	322
Fischer, W	123
	125
Fisher, J 342	
Fitzgerald, T	205
	200
Fitzner, K	209
Fitzpatrick, M	210
Fjær, H	
Flandorfer, H	104 105
Eland M	
Flaud, V	180
	180
Fleck, C	180 .258, 351
Fleck, C Fleck, N	180 .258, 351 38
Fleck, C Fleck, N	180 .258, 351 38
Fleck, C Fleck, N Fleming, R	180 .258, 351 38 359
Fleck, C Fleck, N Fleming, R Flicker, J	180 .258, 351 38 359 16
Fleck, C Fleck, N Fleming, R	180 .258, 351 38 359 16
Fleck, C Fleck, N Fleming, R Flicker, J Flinn, B	180 .258, 351 38 359 16 72
Fleck, C Fleck, N Fleming, R Flicker, J Flinn, B Florando, J	180 .258, 351 38 359 16 72 320
Fleck, C Fleck, N Fleming, R Flicker, J Flinn, B Florando, J Flores, K	180 .258, 351 38 359 16 72 320 187, 331
Fleck, C Fleck, N Fleming, R Flicker, J Flinn, B Florando, J Flores, K	180 .258, 351 38 359 16 72 320 187, 331
Fleck, C Fleck, N Fleming, R Flicker, J Flinn, B Florando, J Flores, K	180 .258, 351 359 16 72 320 187, 331 338
Fleck, C Fleck, N Fleming, R Flicker, J Flinn, B Florando, J Flores, K	180 .258, 351 38 359 16 72 320 187, 331 338 339
Fleck, C Fleck, N Fleming, R Flicker, J Flinn, B Florando, J Flores, K	180 .258, 351 38 359 16 72 320 187, 331 338 339
Fleck, C Fleck, N Fleming, R Flicker, J Flinn, B Florando, J Flores, K	180 .258, 351 38 359 16 72 320 187, 331 338 339 19, 140
Fleck, C Fleck, N Fleming, R Flicker, J Flinn, B Florando, J Flores, K	180 .258, 351 38 359 16 72 320 187, 331 338 339 19, 140 130, 338
Fleck, C Fleck, N Fleming, R Flicker, J Flinn, B Florando, J Flores, K	180 .258, 351 38 359 16 72 320 187, 331 338 339 19, 140 130, 338
Fleck, C Fleck, N Fleming, R Flicker, J Flinn, B Florando, J Flores, K	180 .258, 351 38 359 16 72 320 187, 331 338 339 19, 140 130, 338 38, 359
Fleck, C Fleck, N Fleming, R Flicker, J Flinn, B Florando, J Flores, K	180 .258, 351 38 359 16 72 320 187, 331 338 339 19, 140 130, 338 38, 359 130, 357
Fleck, C Fleck, N Fleming, R Flicker, J Flinn, B Florando, J Flores, K	180 .258, 351 38 359 16 72 320 187, 331 338 339 19, 140 130, 338 38, 359 130, 357
Fleck, C Fleck, N Fleming, R Flinn, B Florando, J Flores, K	180 .258, 351 38 359 16 72 320 187, 331 338 339 19, 140 130, 338 38, 359 .130, 357 .300, 346
Fleck, C Fleck, N Fleming, R Flicker, J Flinn, B. Florando, J Flores, K	180 .258, 351 38 359 16 72 320 187, 331 338 339 19, 140 130, 338 38, 359 30, 357 .300, 346 .247, 248
Fleck, C Fleck, N Fleming, R Flicker, J. Flinn, B. Florando, J. Flores, K	
Fleck, C Fleck, N Fleming, R Flicker, J. Flinn, B. Florando, J. Flores, K	
Fleck, C Fleck, N Fleming, R Flinn, B. Florando, J. Flores, K	
Fleck, C Fleck, N Fleming, R Flicker, J Flinn, B Florando, J Flores, K Flore, J Focht, E Foiles, S Follstaedt, D Foltz, J Fonda, R Fong, D Fong, J	
Fleck, C Fleck, N Fleming, R Flinn, B. Florando, J. Flores, K	
Fleck, C Fleck, N Fleming, R Flicker, J Flinn, B Florando, J Flores, K Flore, J Focht, E Foiles, S Follstaedt, D Foltz, J Fonda, R Fong, D Fong, J Foosnæs, T 30	
Fleck, C Fleck, N Fleming, R Flicker, J Flinn, B Florando, J Flores, K Flore, J Focht, E Foiles, S Follstaedt, D Foltz, J Fonda, R Fong, D Fong, J Foosnæs, T Sosmæs, T So	
Fleck, C Fleck, N Fleming, R Flicker, J Flinn, B Florando, J Flores, K Flore, J Focht, E Foiles, S Follstaedt, D Foltz, J Fonda, R Fong, D Fong, J Foosnæs, T 30	
Fleck, C. Fleck, N. Fleming, R. Flicker, J. Flinn, B. Florando, J. Flores, K. Flores, K. 126, 156, 177, Floro, J. Focht, E. Foecke, T. Foiles, S. Follstaedt, D. Foltz, J. Fonda, R. Fong, D. Fong, J. Foosmæs, T. Sorrest, D. Forrest, M.	
Fleck, C. Fleck, N. Fleming, R. Flicker, J. Flinn, B. Florando, J. Flores, K. Flores, K. 126, 156, 177, Flore, J. Focht, E. Foecke, T. Foiles, S. Follstaedt, D. Foltz, J. Fonda, R. Fong, D. Fong, J. Foosmæs, T. Sorrest, D. Forrest, M.	
Fleck, C. Fleck, N. Fleming, R. Flicker, J. Flinn, B. Florando, J. Flores, K. Flores, K. 126, 156, 177, Floro, J. Focht, E. Foecke, T. Foiles, S. Follstaedt, D. Foltz, J. Fonda, R. Fong, D. Fong, J. Foosmæs, T. Sorrest, D. Forrest, M.	
Fleck, C. Fleck, N. Fleming, R. Flicker, J. Flinn, B. Florando, J. Flores, K. Flores, K. 126, 156, 177, Floro, J. Focht, E. Foecke, T. Foiles, S. Follstaedt, D. Foltz, J. Fonda, R. Fong, D. Fong, J. Fong, J. Forest, D. Forrest, M. Forté, G. Fortin, S.	
Fleck, C. Fleck, N. Fleming, R. Flicker, J. Flinn, B. Florando, J. Flores, K. Flores, K. 126, 156, 177, Floro, J. Focht, E. Foecke, T. Foiles, S. Follstaedt, D. Foltz, J. Fonda, R. Fong, D. Fong, H. Foosnæs, T. Forrest, D. Forrest, M. Forté, G. Fortin, S. Fourment, L.	
Fleck, C. Fleck, N. Fleming, R. Flikker, J. Flinn, B. Florando, J. Flores, K. Flores, K. 126, 156, 177, Floro, J. Focht, E. Focke, T. Foiles, S. Follstaedt, D. Foltz, J. Fonda, R. Fong, D. Fong, J. Foors, S. Forest, D. Forrest, M. Forté, G. Fortin, S. Fourment, L. Fox, S.	
Fleck, C. Fleck, N. Fleming, R. Flikker, J. Flinn, B. Florando, J. Flores, K. Flores, K. 126, 156, 177, Floro, J. Focht, E. Focke, T. Foiles, S. Follstaedt, D. Foltz, J. Fonda, R. Fong, D. Fong, J. Foors, S. Forest, D. Forrest, M. Forté, G. Fortin, S. Fourment, L. Fox, S.	
Fleck, C. Fleck, N. Fleming, R. Flikker, J. Flinn, B. Florando, J. Flores, K. Flores, K. 126, 156, 177, Floro, J. Focht, E. Foecke, T. Foiles, S. Follstaedt, D. Foltz, J. Fonda, R. Fong, D. Fong, J. Foosnæs, T. Forrest, M. Forté, G. Fortin, S. Fourment, L. Fox, S. Fragner, W.	
Fleck, C. Fleck, N. Fleming, R. Fliker, J. Flinn, B. Florando, J. Flores, K. Flores, K. Focht, E. Focke, T. Foiles, S. Follstaedt, D. Foltz, J Fonda, R. Fong, D. Forng, J. Forest, D. Forrest, M. Forté, G. Fortin, S. Fort, S. Forter, R. Forter, R. Forter, S. Forter, S. Forter, S. Forter, S. Forter, S. Fourment, L. Fox, S Fragner, W. Frank, I	
Fleck, C. Fleck, N. Fleming, R. Flikker, J. Flinn, B. Florando, J. Flores, K. Flores, K. 126, 156, 177, Floro, J. Focht, E. Foecke, T. Foiles, S. Follstaedt, D. Foltz, J. Fonda, R. Fong, D. Fong, J. Foosnæs, T. Forrest, M. Forté, G. Fortin, S. Fourment, L. Fox, S. Fragner, W.	
Fleck, C. Fleck, N. Fleming, R. Flicker, J. Flinn, B. Florando, J. Flores, K. Flores, K. 126, 156, 177, Flores, K. Fort, E. Foecke, T. Foiles, S. Foilstaedt, D. Foltz, J Fonda, R. Fong, D. Fong, J. Foosnæs, T. Soosnæs, T. Sorrest, D. Forté, G. Fortin, S. Fourment, L. Fox, S. Fragner, W. Frank, I. Frank, S.	
Fleck, C. Fleck, N. Fleming, R. Flicker, J. Flinn, B. Florando, J. Flores, K. Flores, K. 126, 156, 177, Flores, K. Focht, E. Focke, T. Foiles, S. Foilstaedt, D. Follstaedt, D. Fonda, R. Fong, D. Fong, J. Foosnæs, T. Soosnæs, T. Sorrest, D. Forrest, M. Forté, G. Fortin, S. Fourment, L. Fox, S Franger, W. Frank, I. Frank, S. Franke, O.	
Fleck, C Fleck, N Fleming, R Flicker, J Flinn, B Florando, J Flores, K Flores, K Focht, E Foecke, T Foilts, S Follstaedt, D Ford, Z Fond, R Fong, D Forg, H Foosnæs, T Sorrest, D Forté, G Fortin, S Fourment, L Fox, S Fragner, W Frank, S Frank, B	
Fleck, C Fleck, N Fleming, R Flicker, J Flinn, B Florando, J Flores, K Flores, K Focht, E Foecke, T Foilts, S Follstaedt, D Ford, Z Fond, R Fong, D Forg, H Foosnæs, T Sorrest, D Forté, G Fortin, S Fourment, L Fox, S Fragner, W Frank, S Frank, B	
Fleck, C. Fleck, N. Fleming, R. Flicker, J. Flinn, B Florando, J. Flores, K. Flores, K. Focht, E. Foecke, T. Foiles, S. Foltzaedt, D. Foltzaedt, D. Forng, J. Fonda, R. Fong, D. Forng, J. Forset, D. Forrest, D. Forrest, M. Forté, G. Fortin, S. Fourment, L. Fox, S. Fragner, W. Frank, I. Frank, S. Frank, S. Frank, B. Fraser, H. 26, 77, 121, 130,	
Fleck, C Fleck, N Fleming, R Flicker, J Flinn, B Florando, J Flores, K Flores, K Focht, E Foecke, T Foilts, S Follstaedt, D Ford, Z Fond, R Fong, D Forg, H Foosnæs, T Sorrest, D Forté, G Fortin, S Fourment, L Fox, S Fragner, W Frank, S Frank, B	

Fratzl, P72, 175
Fray, D57, 90, 110
Frazer, E
Frear, D151, 317
Frederick, A
Free, M34, 35, 87, 137, 166, 303, 349
Freels, M24, 178, 360
Freeman, A51, 302
Freeney, T
Fréty, N180, 182
Frew, D
Freyman, T72
Fridy, J121
Friedman, L273
Fries, S65
Frischknecht, A67
Froes, F
Frohberg, G293
Froideval, A95
Frolov, A
Fromm, B97
Frommeyer, G
Frommeyer, G18, 306, 322 Fu, C27, 96, 190, 202, 344, 356
Frommeyer, G
Frommeyer, G 18, 306, 322 Fu, C 27, 96, 190, 202, 344, 356 Fu, E 215 Fu, H 114, 313 Fu, L 212 Fu, N 334 Fu, X 322 Fu, Y 166 Fuchs, G 49, 107, 322
Frommeyer, G 18, 306, 322 Fu, C 27, 96, 190, 202, 344, 356 Fu, E 215 Fu, H 114, 313 Fu, L 212 Fu, N 334 Fu, X 322 Fu, Y 166 Fuchs, G 49, 107, 322 Fuentes, A 125
Frommeyer, G 18, 306, 322 Fu, C 27, 96, 190, 202, 344, 356 Fu, E 215 Fu, H 114, 313 Fu, L 212 Fu, N 334 Fu, X 322 Fu, Y 166 Fuchs, G 49, 107, 322
Frommeyer, G 18, 306, 322 Fu, C 27, 96, 190, 202, 344, 356 Fu, E 215 Fu, H 114, 313 Fu, L 212 Fu, N 334 Fu, X 322 Fu, Y 166 Fuchs, G 49, 107, 322 Fuentes, A 125 Fujiwara, S 349 Fuller, C 341
Frommeyer, G 18, 306, 322 Fu, C 27, 96, 190, 202, 344, 356 Fu, E 215 Fu, H 114, 313 Fu, L 212 Fu, N 334 Fu, X 322 Fu, Y 166 Fuchs, G 49, 107, 322 Fuentes, A 125 Fujiwara, S 349 Fuller, C 341 Fuller, E 278
Frommeyer, G
Frommeyer, G
Frommeyer, G 18, 306, 322 Fu, C 27, 96, 190, 202, 344, 356 Fu, E 215 Fu, H 114, 313 Fu, L 212 Fu, N 334 Fu, X 322 Fu, Y 166 Fuchs, G 49, 107, 322 Fuentes, A 125 Fujiwara, S 349 Fuller, C 341 Fuller, E 278 Fuloria, D 228 Fultz, B 78, 303 Funato, M 162
Frommeyer, G 18, 306, 322 Fu, C 27, 96, 190, 202, 344, 356 Fu, E 215 Fu, H 114, 313 Fu, L 212 Fu, N 334 Fu, X 322 Fu, Y 166 Fuchs, G 49, 107, 322 Fuentes, A 125 Fujiwara, S 349 Fuller, C 341 Fuller, E 278 Fuloria, D 228 Fultz, B 78, 303 Funato, M 162 Funkhouser, C 168
Frommeyer, G 18, 306, 322 Fu, C 27, 96, 190, 202, 344, 356 Fu, E 215 Fu, H 114, 313 Fu, L 212 Fu, N 334 Fu, X 322 Fu, Y 166 Fuchs, G 49, 107, 322 Fuentes, A 125 Fujiwara, S 349 Fuller, C 341 Fuller, E 278 Fuloria, D 228 Funto, M 162 Funkhouser, C 168 Fuoss, P 64
Frommeyer, G 18, 306, 322 Fu, C 27, 96, 190, 202, 344, 356 Fu, E 215 Fu, H 114, 313 Fu, L 212 Fu, N 334 Fu, X 322 Fu, Y 166 Fuchs, G 49, 107, 322 Fuentes, A 125 Fujiwara, S 349 Fuller, C 341 Fuller, B 278 Fuloria, D 228 Fultz, B 78, 303 Funkhouser, C 168 Fuoss, P 64 Fugiang, A 224
Frommeyer, G 18, 306, 322 Fu, C 27, 96, 190, 202, 344, 356 Fu, E 215 Fu, H 114, 313 Fu, L 212 Fu, N 334 Fu, X 322 Fu, Y 166 Fuchs, G 49, 107, 322 Fuentes, A 125 Fujiwara, S 349 Fuller, C 341 Fuller, E 278 Fuloria, D 228 Funto, M 162 Funkhouser, C 168 Fuoss, P 64

G

Gabb, T52, 106, 107, 155, 156, 208, 268, 321
Gabbitas, B255
Gaboury, A22
Gadalla, M
Gadd, D124
Gagne, J
Gaies, J240
Gajbhiye, N164, 222
Galarraga, R122
Galenko, P86
Gall, K160, 161, 299
Gallardo, E148
Gallino, I236
Gallon, J
Galuszka-Muga, B197
Galvani, C144
Gamweger, K128
Gan, J151
Gan, W247, 248
Ganapathysubramanian, B19, 99
Gandy, D247, 262
Gang, X61
Gang, Z186
Gang-chun, Y46
Gangopadhyay, A235





Gannon, P198
Gansemer, T179
Gao. B
Gao, D
Gao, F104, 152, 314, 316
Gao, H159
Gao, J
Gao, M26, 27, 227, 354, 360
Gao, P
Gao, W
Gao, X60, 311
Gao, Y23, 73, 98, 99, 103, 126, 177, 197, 207,
235, 251, 264, 286, 288, 313, 331, 337
Gaponik, N
García-García, O
García-Ramos, E
Garg, A107, 189
Garimella, N131, 242, 260
Garkida, A137
Garlea, E95
Garlick, R
Garmestani, H
Garofalini, S18
Garvin, J
Garza, K176
Gascoin, F
Gaustad, G
Gauthier, C
Gavrila, L63
Gawde, P131
Gay, H
Gayda, J
Gayden, X
Gayle, F140
Gebelin, J
Gebhardt, U252
Gecim, K
Gell, M
Gella, V87
Gelse, K23
Gemein, R81
Genau, A
Genc. A
Gendre, M
Gengwei, J
George, Y
Georgelin, M85, 136
Gerberich, W154, 160, 207, 325
Gerdemann, S192, 193, 254
Gerger, A
Gerken, J
German, R19, 142
Gerosa, R180
Gertsberg, G194
Gesing, A158
Ghali, E
,
Gharghouri, M
Gheewala, I
Gheorghe, I172
Ghicov, A220
Ghidini, A180
Ghoniem, N
Ghosh, A
Ghosh, D
Ghosh, K
Ghosh, S44, 96, 130, 170, 199
Giannuzzi, L25, 26
Gianola, D
Gibson, L
01050II, E

Gikling, H	
Gila, B	
Gill, A	
Gill, D Gilman, J	
Gimazov, A	
Glade, S	
Glavicic, M	
Gleeson, B54	
Glicksman, M	
Glosli, J	
Gloter, A	
Glotzer, S	
Gnaeupel-Herold, T	
Gnauk, J Goddard, W	
Godet, S	
Goede, F	
Goeken, M	
Goesele, U	
Goettert, J	
Göken, M	
Gokhale, A	
Golchert, B Goldenfeld, N	
Goller, G	
Golmakani, H	
Golovashchenko, S	
Golovin, I	
Golubov, S	
Gomes, J	
Gómez, A	
Gomez, G	
Gomez, J Gómez-Briceño, D	
Goncalves, C	137
Goncalves, C Gong, Y	
Goncalves, C	
Goncalves, C Gong, Y Gonzalez, A Gonzalez, G Gonzalez, J	
Goncalves, C Gong, Y Gonzalez, A Gonzalez, G Gonzalez, J Gooch, W	
Goncalves, C Gong, Y Gonzalez, A Gonzalez, G Gonzalez, J Gooch, W Goodwin, P	
Goncalves, C Gong, Y Gonzalez, A Gonzalez, G Gonzalez, J Gooch, W Goodwin, P Goorsky, M	
Goncalves, C Gong, Y Gonzalez, A Gonzalez, G Gonzalez, J Gooch, W Goodwin, P Goorsky, M Gopalan, V	
Goncalves, C Gong, Y Gonzalez, A Gonzalez, G Gonzalez, J Gooch, W Goodwin, P Goorsky, M Gopalan, V Goranson, G	
Goncalves, C Gong, Y Gonzalez, A Gonzalez, G Gonzalez, J Gooch, W Goodwin, P Goorsky, M Gopalan, V Goranson, G Gorantla, M.	
Goncalves, C Gong, Y Gonzalez, A Gonzalez, G Gonzalez, J Gooch, W Goodwin, P Goorsky, M Gopalan, V Goranson, G	
Goncalves, C Gong, Y Gonzalez, A Gonzalez, G Gonzalez, J. Gooch, W. Goodwin, P. Goorsky, M. Gopalan, V. Goranson, G. Gorantla, M. Gorantla, S. Gordon, B. Gordon, P.	$\begin{array}{c}$
Goncalves, C Gong, Y Gonzalez, A Gonzalez, G Gonzalez, J Gooch, W Goodwin, P Goorsky, M Gopalan, V Goranson, G Gorantla, M. Gorantla, S. Gordon, B. Gordon, P. Goren, T	$\begin{array}{c}$
Goncalves, C Gong, Y Gonzalez, A Gonzalez, G Gonzalez, J Gooch, W Goodwin, P Goorsky, M Goranson, G Gorantla, N Gorantla, M Gorantla, S. Gordon, B. Gordon, P. Gornostyrev, Y	$\begin{array}{c}$
Goncalves, C Gong, Y Gonzalez, A Gonzalez, G Gonzalez, J Gooch, W Goodwin, P Goorsky, M Goranson, G Goranson, G Gorantla, M Gorantla, S Gordon, B Gordon, P Goren, T Gornostyrev, Y Gorny, A	$\begin{array}{c}$
Goncalves, C Gong, Y Gonzalez, A Gonzalez, G Gonzalez, J Gooch, W Goodwin, P Goorsky, M Goranson, G Goranson, G Gorantla, M Gorantla, S Gordon, B Gordon, P Goren, T Gornostyrev, Y Gorny, A Gorokhovsky, V	$\begin{array}{c}$
Goncalves, C Gong, Y Gonzalez, A Gonzalez, G Gonzalez, J Gooch, W Goodwin, P Goorsky, M Goranson, G Goranson, G Gorantla, M Gorantla, S Gordon, B Gordon, P Gorno, T Gornostyrev, Y Gorny, A Gorokhovsky, V Gösele, U	$\begin{array}{c}$
Goncalves, C Gong, Y Gonzalez, A Gonzalez, G Gonzalez, J Gooch, W. Goodwin, P. Goorsky, M. Gopalan, V. Goranson, G. Gorantla, N. Gorantla, S. Gordon, B. Gordon, B. Gordon, P. Goren, T. Gornostyrev, Y. Gorny, A. Gorskhovsky, V. Gösele, U. Goswami, R.	$\begin{array}{c}$
Goncalves, C Gong, Y Gonzalez, A Gonzalez, G Gonzalez, J Gooch, W Goodwin, P Goorsky, M Goranson, G Goranson, G Gorantla, M Gorantla, S Gordon, B Gordon, P Gorno, T Gornostyrev, Y Gorny, A Gorokhovsky, V Gösele, U	$\begin{array}{c}$
Goncalves, C Gong, Y Gonzalez, A Gonzalez, G Gonzalez, J Gooch, W. Goodwin, P. Goorsky, M. Gopalan, V. Gorantson, G. Gorantla, N. Gorantla, S. Gordon, B. Gordon, B. Gordon, P. Goren, T. Gornostyrev, Y. Gorny, A. Gorokhovsky, V. Gösele, U. Goswami, R. Goto, M.	$\begin{array}{c}$
Goncalves, C Gong, Y Gonzalez, A Gonzalez, G Gonzalez, J Gooch, W. Goodwin, P. Goorsky, M. Gopalan, V. Goranson, G. Gorantla, N. Gorantla, S. Gordon, B. Gordon, B. Gordon, P. Gornostyrev, Y. Gorny, A. Goroskhovsky, V. Gösele, U. Goswami, R. Goto, M. Gouda, K. Gough, N Gourlay, C.	$\begin{array}{c}$
Goncalves, C Gong, Y Gonzalez, A Gonzalez, G Gonzalez, J Gooch, W Goodwin, P Goorsky, M Goorsky, M Goranson, G. Gorantla, N. Gorantla, M. Gorantla, S. Gordon, B. Gordon, B. Gordon, P. Goren, T. Gornostyrev, Y. Gorny, A. Gorokhovsky, V. Gösele, U Goswami, R Goto, M. Gouda, K. Gough, N. Gouttebroze, S.	$\begin{array}{c} 137\\98, 115\\200\\180\\174, 227\\196\\244\\194\\$
Goncalves, C Gong, Y Gonzalez, A Gonzalez, G Gonzalez, J Gooch, W Goodwin, P Goorsky, M Goranson, G. Gorantla, N. Gorantla, M. Gorantla, S. Gordon, B. Gordon, B. Gordon, P. Goren, T. Gornostyrev, Y. Gorny, A. Gorokhovsky, V. Gösele, U Goswami, R Goto, M. Gouda, K. Gouda, K. Gourlay, C. Gouttebroze, S Govender, J.	$\begin{array}{c} 137\\$
Goncalves, C Gong, Y Gonzalez, A Gonzalez, G Gonzalez, J Gooch, W Gooch, W Goodwin, P Goorsky, M Goranson, G. Gorantla, N. Gorantla, S. Gordon, B. Gordon, B. Gordon, P. Goren, T. Gornostyrev, Y. Gorny, A. Gorokhovsky, V. Gösele, U. Goswami, R. Goto, M. Gouda, K. Gough, N. Gourlay, C. Gouttebroze, S. Govender, J. Govier, B.	$\begin{array}{c} 137\\$
Goncalves, C Gong, Y Gonzalez, A Gonzalez, G Gonzalez, J Gooch, W Goodwin, P Goorsky, M Goranta, V Goranson, G Gorantla, N Gorantla, S Gordon, B Gordon, B Gordon, P Gornostyrev, Y Gornostyrev, Y Gornostyrev, Y Gornokhovsky, V. Gösele, U Goswami, R Goto, M Gouda, K Gough, N Gourlay, C Govender, J Govier, B Govorov, A60, 114	$\begin{array}{c} 137\\98, 115\\200\\180\\174, 227\\196\\244\\154\\$
Goncalves, C Gong, Y Gonzalez, A Gonzalez, G Gonzalez, J Gooch, W Goodwin, P Goorsky, M Goranson, G Gorantla, N Gorantla, S Gordon, B Gordon, B Gordon, P Gornostyrev, Y Gornostyrev, Y Gornostyrev, Y Gornokhovsky, V. Gösele, U Goswami, R Goto, M Gouda, K Gough, N Gourlay, C. Goutebroze, S Govender, J. Govorov, A60, 114 Goyal, D	$\begin{array}{c}$
Goncalves, C Gong, Y Gonzalez, A Gonzalez, G Gonzalez, J Gooch, W Goodwin, P Goorsky, M Goorsky, M Goranson, G Goranson, G Gorantla, N Gorantla, S Gordon, B Gordon, P Gornostyrev, Y Gorno, T Gornostyrev, Y Gorny, A Gorokhovsky, V Gösele, U Goswami, R Goto, M Gouda, K Gough, N Gourlay, C Goutebroze, S Govier, B Govorov, A	$\begin{array}{c} 137\\$
Goncalves, C Gong, Y Gonzalez, A Gonzalez, G Gonzalez, J Gooch, W Goodwin, P Goorsky, M Goranson, G Gorantla, N Gorantla, S Gordon, B Gordon, B Gordon, P Gornostyrev, Y Gornostyrev, Y Gornostyrev, Y Gornokhovsky, V. Gösele, U Goswami, R Goto, M Gouda, K Gough, N Gourlay, C. Goutebroze, S Govender, J. Govorov, A60, 114 Goyal, D	$\begin{array}{c} 137\\$
Goncalves, C Gong, Y Gonzalez, A Gonzalez, G Gonzalez, J Gooch, W Goodwin, P Goorsky, M Goorsky, M Goranson, G Goranson, G Gorantla, N Gorantla, S. Gordon, B. Gordon, B. Gordon, P. Goren, T. Gornostyrev, Y. Gorny, A Gorokhovsky, V. Gösele, U Goswami, R. Goto, M. Gouda, K. Gouda, K. Gough, N Goutlebroze, S Govender, J Govier, B. Govorov, A	$\begin{array}{c} 137\\$
Goncalves, C Gong, Y Gonzalez, A Gonzalez, G Gonzalez, J Gooch, W Goodwin, P Goorsky, M Gooranta, N Goranta, N Goranta, S. Gordon, B. Gordon, B. Gordon, P. Goren, T Gornostyrev, Y Gornostyrev, Y Gornostyrev, Y Gorkhovsky, V. Gösele, U Goswami, R. Goto, M Gouda, K. Gouda, K. Gough, N Gourlay, C Goutebroze, S Govender, J. Govier, B Govan, J. Govan, J. Gorats, J Grazyk, D Grady, D	$\begin{array}{c} 137\\$

Graham, W	183
Granasy, L	
Gránásy, L	
Grant, B	
Grant, G187, 298, 327, 328,	342
Gravier, S	288
Gray, G29, 30, 79, 132, 133,	183,
Green, N	
Greenfield, S	340
Greer, A104, 153, 177, 205, 265,	
Greer, J161,	
Gregori, F	
Gregory, E	
Gregory, J	
Greif, R	
Greiner, C	
Grey, C	
Griesche, A	
Griffin, J	
Griffin, R	
Griffiths, J	
Griffiths, W112,	
Grimes, R	
Grimm, T	
Gripenberg, H	
Gritsko, V	
Groeber, M44,	
Groebner, J	
Groening, O	
Gröger, R	
Grong, Ø	
Gross, S99, 182, 251,	
Groza, J	
Grundy, A	336
Grunschel, S	
Grunspan, J	
Gruss, D	
Gschneidner, K	
Gu, G	
Gu, S171,	280
Gu, Y	42
Guan, Y	
Guang-Chun, Y	
Guang-chun, Y46,	
Guangchun, Y119, 275,	
Guangfeng, L	
Guanghui, L	
Gudbrandsen, H	30
Guduru, R	
Guenther, B	
Guerdoux, S	
Guerin, M	187
Guillot, J	
Guimazov, A	
Guliants, E	
Gul Karaguler, N	
Gulluoglu, A	
Gun'ko, Y	
Gunderov, D	
Gungor, M	
Gungormus, M	
Gunnarson, A	
Gunyuz, M	
Guo, D	
Guo, F50, 102, 103, 131, 151, 204, 264,	
Guo, J	
Guo, X	
200, 12	110



Guo, Y258	
Guo, Z111, 145, 172, 194, 205, 231, 288	
Guorong, H311	
Gupta, A163	
Gupta, G94	
Gupta, H72	
Gupta, N168	
Gupta, S33, 163, 217, 345	
Gupta, V75, 111	
Gupta, Y	
Gurov, A213	
Guruprasad, P68, 267	
Guruswamy, S166, 276	
Gusberti, V124, 174	
Gusev, A185, 329	
Gustafsson, M174	
Guthrie, R288	
Gutierrez, I114	
Gutierrez-Mendez, M336	

Н

Ha, S258, 319, 359
Haarberg, G
Haataja, M131
Haberl, A
Habermeier, H
Habingreither, R
Hackenberg, R
Hackett, M95
Haeni, J64
Hafez Haghighat, S202
Hafok, M218
Hagelstein, K
Hagen, E90
Hagen, M245
Hagie, S187
Hagiwara, R
Haigang, D142
Haiyan, Y
Haiyan, Z47
Hajra, J
Halley, J
Hallstrom, S
Halsey, C
Hamed, M112, 300
Hamer, S127, 237
Hamilton, C173
Hammerberg, J244
Hammond, C60
Hamza, A
Han, B218, 272, 359
Han, C
Han, D
Han, E
Han, G
Han, H91, 103, 154, 186, 233
Han, K
Han, L
Han, Q46, 98, 143, 261, 262, 307, 313, 354
Han, S103, 252, 275
Han, W
Han. X
Hanbicki, A
Hanlon, A
Hanrahan, R
Hansen, E
Hansen, N
Hanser, A
Hansel, A
пао, п102

Hao, Y	206
Hao, I	
Hara, S	
Harada, H	208
Haraya, K	
Harder, D	72
Hardie, G	
Hardy, J	
Hariharan, S	
Hariharaputran, R	120
Harimkar, S	
Harish, K	98
Harjunmaa, A	355
Harley, B Haro Rodriguez, S	228
Harber, D	528
Harrell, G	
Harrell, J	
Harringa, J103	. 264
Harrington, W	122
Harris, K	53
Harris, S	
Harry, P	341
Hart, G2	
Hart, J	
Hartley, C	44
Hartmann, H	
Hartwig, J Härtwig, J	85
Hartwig, T	.188
Hashikawa, T	
Hashimoto, N	
Haslam, J	
Hassan, A	
Hathcock, D	292
Haupt, T	256
Hawkins, J	
Hawley, M	64
Hawreliak, J	
Hayes, C	
Haynes, A Hazel, B	
Нагег, Б	
Не, Ј	
Не, К	
He, M	
He, S	332
He, W	20
Hebert, R	, 278
Hecht, U	
Hector, Jr., L	
Hector, L	
Heguri, S	
Heidloff, A	
Heilmaier, M Hein, M	
Heinisch, H	
Heinze, J	
Hellmig, R	
Hellstrom, E	
Helmick, D	
Helmink, R	
Hemker, K44, 208, 211, 243	, 312
Hemptenmacher, J	
Henderson, E	
Henderson, R	
Hendricks, T	
Heng, C Hennessy, K	
•	
Hennet, L	

Hennig, R
Henriksen, B
Henriksen, P
Heong Ryeal, Y
Her, E
Herbert, E
Herlach, D
Herling, D
Hermans, M
Hernández-Mayoral, M203, 263
Herrera-Trejo, M159
Herrero, A
Heyrman, M
Hezeltine, W34
Hibbard, G17, 254, 348
Hickman, Z
Higashi, K
Higuchi, K
Hilgraf, P
Hin, C
Hioki, S
Hirai, M
Hiralal, I171
Hirano, S
Hirasawa, S
Hirata, K
Hiroshi, H107
Hisatsune, K229
Hiskey, J
Hitchcock, M
Hixson, R
Ho, C
Ho, K
Но, Т
Ho, T



Horstemeyer, M19, 20, 121, 169,
Hort, N257, 259, 350, 352, 353
Horton, J247
Hosegawa, A
Ho Seop, S
Hoshino, S
Höskuldsson, G231
Hosokawa, Y110
Hotaling, N
Hou, B
Hou, G135
Hou, M165, 202
Houghton, B74
Houng, B
House, J
Houston, D
Houze, J
Hovanec, C121, 241, 328
Hovanski, Y
Howard, S187, 248, 299, 302
Hoyer, J
Hoyt, J31, 83, 84, 101, 135, 188, 337
Hryn, J55, 110, 157, 209, 269, 284, 323
Hsia, K159, 208, 268
Hsiao, C50, 265
Hsiao, H206
Hsiao, L104
Hsieh, G
Hsieh, H
Hsieh, K153
Hsiung, L30, 72
Hsu, C153, 297
Hsu, E144, 323
Hsu, F159
Hsu, T102
Hsu, Y152
Hu, G
Ни, Н
Hu, J
Hu, S
Hu, X
Hu, Z
Hua, D61 Hua, F
,-
Hua, L
Huang, B
Huang, C206, 221, 324, 354 Huang, E180, 189
Huang, F
Huang, H
Huang, J
Huang, K
Huang, L
Huang, M
Huang, P
Huang, S
Huang, T
Huang, X121, 137, 138, 211, 355
Huang, Y153, 257, 290, 353
Huang, Z
Hubbard, C46, 95, 134, 200
Hubbard, F
Hubbard, J
Hudanski, L117
Hudson, L238
Huey, B16
Hufnagel, T
Hugron, I71
Huh, J51

Hui, X	
Hulbert, D	
Hults, W	
Hung, F	
Hung, L	
Hunt, F	
Huo, Y	
Husseini, N	
Hutchins, C	
Hutchinson, J	
Hvidsten, R	
Hvistendal, J	
Hwan Cha, Y	
Hwang, B	
Hwang, D	
Hwang, J	
	.289, 290, 328, 334, 355
Hwang, R	
Hyers, R	
Hyland, M	

Ι

Iadicola, M
Ibrahiem, M
Ibrahim, I250
Ice, G80, 192, 229, 253
Idzerda, Y146, 198
Ienco, M
Iffert, M231
Ikeda, M255
Ikemoto, Y
Iliescu, D76
Imai, H53, 157
Imam, M
Inal, K
Inman, D
Inoue, A
Inoue, J
Inoue, K
Inzunza, E
Ipser, H104, 105, 318
Irons, G
Irving, D
Isac, M
Isheim, D
Ishida, H
Ishida, K104, 204, 265
Ishikawa, N
Ishitsuka, M98
Islam, Z139
Islamgaliev, R218
Ismail, A250
Itapu, S
Ito, K
Itoh, Y
Ivanisenko, J
Ivanov, K213
Ivanov, M
Ivanov, V
Iyer, A
Iyoda, M56
Izumi, T
· , ·····
J

Jablonski, P	145, 198, 335
Jackman, J	144
Jackson, E	80
Jackson, J	
Jackson, M	

Jacobsen, L	39 141
Jacot, A	32
Jagadish, C	
Jahazi, M	187
Jain, A	
Jain, M	172
Jain, P	
Jakobsen, B	
Jallu, K	300
James, A	
James, M	216
Jana, S	
Janardhan, G	
Janes, J	177
,	
Jang, B	94
Jang, D	
Jang, G	104 250
Jang, J	49
Jang, S55	108 216 210
Jang, Y	252
Jankowski, A	78 205
Janssens, K18, 67, 119, 168	, 221, 278, 327
Janz, A	300
Jao, C	
Jaques, A	132
Jaradeh, M	179
Jaramillo, D	101
Jaramillo, R	46, 47, 262
Jarmakani, H	357
Jarvis, D	158
Jasak, H	307
Jasthi, B	248, 299
Jata, K82, 134, 186	247 207 341
Jawahir, I	70
Jayaraman, T	166 276
	201
Jee, K	204
Jee, K Jeedigunta, H.	
Jeedigunta, H	
Jeedigunta, H Jelinek, B	274 19
Jeedigunta, H Jelinek, B	274 19
Jeedigunta, H Jelinek, B Jenkins, M	
Jeedigunta, H Jelinek, B Jenkins, M Jensen, M	274 19 151, 202 173
Jeedigunta, H Jelinek, B Jenkins, M Jensen, M	274 19 151, 202 173
Jeedigunta, H Jelinek, B Jenkins, M Jensen, M Jensen, N	
Jeedigunta, H Jelinek, B Jenkins, M Jensen, M Jensen, N	
Jeedigunta, H Jelinek, B Jenkins, M Jensen, M Jensen, N	
Jeedigunta, H Jelinek, B Jenkins, M Jensen, M Jensen, N Jeon, Y Jeong, C	
Jeedigunta, H Jelinek, B Jenkins, M Jensen, M Jensen, N Jeon, Y Jeong, C Jeong, J	
Jeedigunta, H Jelinek, B Jenkins, M Jensen, M Jensen, N Jeon, Y Jeong, C Jeong, J	
Jeedigunta, H Jelinek, B Jenkins, M Jensen, M Jensen, N Jeon, Y Jeong, C Jeong, J Jeong, S	
Jeedigunta, H Jelinek, B Jenkins, M Jensen, M Jensen, N Jeon, Y Jeong, C Jeong, J Jeong, S Jeong Hoon, K	
Jeedigunta, H Jelinek, B Jenkins, M Jensen, M Jensen, N Jeon, Y Jeong, C Jeong, J Jeong, S Jeong Hoon, K	
Jeedigunta, H Jelinek, B Jenkins, M Jensen, M Jensen, N Jeong, Y Jeong, C Jeong, J Jeong, S Jeong Hoon, K Jha, G	
Jeedigunta, H Jelinek, B Jenkins, M Jensen, M Jensen, N Jeon, Y Jeong, C Jeong, J Jeong, S Jeong Hoon, K	
Jeedigunta, H Jelinek, B Jenkins, M Jensen, M Jensen, N Jeong, Y Jeong, C Jeong, J Jeong, S Jeong Hoon, K Jha, G Jha, M.	
Jeedigunta, H Jelinek, B Jenkins, M Jensen, M Jensen, N Jeong, Y Jeong, C Jeong, J Jeong, S Jeong Hoon, K Jha, G Jha, M Jha, S.	
Jeedigunta, H Jelinek, B Jenkins, M Jensen, M. Jensen, N. Jeon, Y. Jeong, C Jeong, C Jeong, S. Jeong Hoon, K. Jha, G. Jha, M. Jha, S. Ji, C.	
Jeedigunta, H Jelinek, B Jenkins, M Jensen, M. Jensen, N. Jeon, Y. Jeong, C Jeong, C Jeong, S. Jeong Hoon, K. Jha, G. Jha, M. Jha, S. Ji, C.	
Jeedigunta, H Jelinek, B Jenkins, M Jensen, M. Jensen, N. Jeon, Y. Jeong, C Jeong, S. Jeong, S. Jeong Hoon, K. Jha, G. Jha, M. Jha, S. Ji, C. Ji, H.	
Jeedigunta, H Jelinek, B Jenkins, M Jensen, M. Jensen, N. Jeon, Y. Jeong, C Jeong, C Jeong, S. Jeong Hoon, K. Jha, G. Jha, M. Jha, S. Ji, C.	
Jeedigunta, H Jelinek, B Jenkins, M Jensen, M. Jensen, N. Jeon, Y. Jeong, C Jeong, J. Jeong, J. Jeong, S. Jeong Hoon, K. Jha, G. Jha, M. Jha, S. Ji, C. Ji, H. Ji, L.	
Jeedigunta, H Jelinek, B Jenkins, M Jensen, M. Jensen, N. Jeong, Y. Jeong, C. Jeong, J. Jeong, S. Jeong Hoon, K. Jha, G. Jha, M. Jha, S. Ji, C. Ji, H. Ji, L. Ji, S.	
Jeedigunta, H Jelinek, B Jenkins, M Jensen, M. Jensen, N. Jeon, Y. Jeong, C Jeong, J. Jeong, J. Jeong, S. Jeong Hoon, K. Jha, G. Jha, M. Jha, S. Ji, C. Ji, H. Ji, L.	
Jeedigunta, H Jelinek, B Jenkins, M Jensen, M. Jensen, N. Jeong, Y. Jeong, C. Jeong, J. Jeong, S. Jeong Hoon, K. Jha, G. Jha, M. Jha, S. Ji, C. Ji, H. Ji, L. Ji, S. Jia, N.	
Jeedigunta, H Jelinek, B Jenkins, M Jensen, M. Jensen, N. Jeong, Y. Jeong, C. Jeong, J. Jeong, S. Jeong Hoon, K. Jha, G. Jha, M. Jha, S. Ji, C. Ji, H. Ji, L. Ji, S. Jia, N. Jia, Z.	
Jeedigunta, H Jelinek, B Jenkins, M Jensen, M Jeong, N Jeong, C Jeong, J Jeong, S Jeong Hoon, K Jha, G Jha, M Jha, S Ji, C Ji, H. Ji, L. Ji, S. Jia, N. Jia, Z. Jian, L.	
Jeedigunta, H Jelinek, B Jenkins, M Jensen, M Jeong, N Jeong, C Jeong, J Jeong, S Jeong Hoon, K Jha, G Jha, M Jha, S Ji, C Ji, H. Ji, L. Ji, S. Jia, N. Jia, Z. Jian, L.	
Jeedigunta, H Jelinek, B Jenkins, M Jensen, M Jensen, N Jeong, Y. Jeong, C. Jeong, J. Jeong, S. Jeong Hoon, K. Jha, G. Jha, M. Jha, S. Ji, C. Ji, H. Ji, L. Ji, S. Jia, N. Jia, Z. Jian, L. Jiang, D. 50	
Jeedigunta, H Jelinek, B Jenkins, M Jensen, M Jensen, N Jeong, Y. Jeong, C. Jeong, J. Jeong, S. Jeong Hoon, K. Jha, G. Jha, M. Jha, S. Ji, C. Ji, H. Ji, L. Ji, S. Jia, N. Jia, Z. Jian, L. Jiang, D. S0 Jian, 243	
Jeedigunta, H Jelinek, B Jenkins, M Jensen, M Jensen, N Jeong, Y. Jeong, C. Jeong, J. Jeong, S. Jeong Hoon, K. Jha, G. Jha, M. Jha, S. Ji, C. Ji, H. Ji, L. Ji, S. Jia, N. Jia, Z. Jian, L. Jiang, D. S0 Jian, 243	
Jeedigunta, H Jelinek, B Jenkins, M Jensen, M Jensen, N Jeong, Y. Jeong, C. Jeong, J. Jeong, S. Jeong Hoon, K. Jha, G. Jha, M. Jha, S. Ji, C. Ji, H. Ji, L. Ji, S. Jia, N. Jia, Z. Jian, L. Jiang, D. Souther for the second	
Jeedigunta, H Jelinek, B Jenkins, M Jensen, M Jeong, N Jeong, C Jeong, J. Jeong, S. Jeong Hoon, K. Jha, G Jha, M Jha, S Ji, C Ji, H Ji, L Ji, S Jia, N Jia, Z Jian, L Jiang, D	
Jeedigunta, H Jelinek, B Jenkins, M Jensen, M Jensen, N Jeong, Y. Jeong, C. Jeong, J. Jeong, S. Jeong Hoon, K. Jha, G. Jha, M. Jha, S. Ji, C. Ji, H. Ji, L. Ji, S. Jia, N. Jia, Z. Jian, L. Jiang, D. Souther for the second	
Jeedigunta, H Jelinek, B Jenkins, M Jensen, M. Jensen, N. Jeon, Y. Jeong, C. Jeong, C. Jeong, S. Jeong Hoon, K. Ja, G. Jha, G. Jha, M. Jha, S. Ji, C. Ji, H. Ji, L. Ji, S. Jia, N. Jia, Z. Jian, L. Jiang, D. Jiang, H. Jiang, L. Jiang, W. Jiang, T. Jiang, W. Jiang, T. Jiang, W. Jiang, T. Jiang, W. Jiang, T. Jiang, M. Jiang, M. Jiang	$\begin{array}{c}$
Jeedigunta, H Jelinek, B Jenkins, M Jensen, M. Jensen, N. Jeon, Y. Jeong, C. Jeong, C. Jeong, S. Jeong Hoon, K. Jha, G. Jha, M. Jha, S. Ji, C. Ji, H. Ji, L. Ji, S. Jian, N. Jian, Z. Jian, L. Jiang, D. Jiang, H. Jiang, L. Jiang, W. Jian, S. Jiang, W. Jiang, C. Jiang, W. Jiang, C. Jiang, M. Jiang, L. Jiang, C. Jiang, W. Jiang, C. Jiang, W. Jiang, C. Jiang, M. Jiang, L. Jiang, C. Jiang, W. Jiang, C. Jiang, W. Jiang, C. Jiang, W. Jiang, C. Jiang, M. Jiang, M. Jiang	$\begin{array}{cccccccccccccccccccccccccccccccccccc$
Jeedigunta, H Jelinek, B Jenkins, M Jensen, M. Jensen, N. Jeon, Y. Jeong, C. Jeong, C. Jeong, S. Jeong Hoon, K. Ja, G. Jha, G. Jha, M. Jha, S. Ji, C. Ji, H. Ji, L. Ji, S. Jia, N. Jia, Z. Jian, L. Jiang, D. Jiang, H. Jiang, L. Jiang, W. Jiang, T. Jiang, W. Jiang, T. Jiang, W. Jiang, T. Jiang, W. Jiang, T. Jiang, M. Jiang, M. Jiang	$\begin{array}{cccccccccccccccccccccccccccccccccccc$
Jeedigunta, H Jelinek, B Jenkins, M Jensen, M. Jensen, N. Jeong, C. Jeong, C. Jeong, J. Jeong, S. Jeong Hoon, K. Jha, G. Jha, M. Jha, S. Ji, C. Ji, H. Ji, L. Ji, S. Jia, N. Jia, Z. Jian, L. Jiang, D. Jiang, F. Jiang, H. Jiang, L. Jiang, W. Jiang, Y. Jiang, Y. Jiang Y.	
Jeedigunta, H Jelinek, B Jenkins, M Jensen, M. Jensen, N. Jeon, Y Jeong, C Jeong, C Jeong, J. Jeong, S. Jeong Hoon, K. Jha, G Jha, M Jha, S Ji, C Ji, H Ji, L Ji, S Jia, N Jia, Z Jian, L Jiang, D Jiang, F Jiang, H Jiang, L Jiang, V Jiang, V Jianguo, W	
Jeedigunta, H Jelinek, B Jenkins, M Jensen, M. Jensen, N. Jeong, C. Jeong, C. Jeong, J. Jeong, S. Jeong Hoon, K. Jha, G. Jha, M. Jha, S. Ji, C. Ji, H. Ji, L. Ji, S. Jia, N. Jia, Z. Jian, L. Jiang, D. Jiang, F. Jiang, H. Jiang, L. Jiang, W. Jiang, Y. Jiang, Y. Jiang Y.	
Jeedigunta, H Jelinek, B Jenkins, M Jensen, M. Jensen, N. Jeong, C. Jeong, C. Jeong, J. Jeong, S. Jeong Hoon, K. Jha, G Jha, M Jha, S Ji, C Ji, H Ji, L Ji, S Jia, N Jia, Z Jian, L Jiang, D. Jiang, F. Jiang, H. Jiang, H. Jiang, W. Jiang, Y. Jianguo, W. Jiang, P. Jiang, P.	
Jeedigunta, H Jelinek, B Jenkins, M Jensen, M. Jensen, N. Jeong, C. Jeong, C. Jeong, J. Jeong, S. Jeong Hoon, K. Jha, G Jha, M Jha, S Ji, C Ji, H Ji, L Ji, S Jia, N Jia, Z Jian, L Jiang, D. Jiang, F. Jiang, H. Jiang, H. Jiang, Y. Jiang, Y. Jiang, Y. Jiang, P. Jiang, C.	$\begin{array}{c}$
Jeedigunta, H Jelinek, B Jenkins, M Jensen, M. Jensen, N. Jeong, Y. Jeong, C. Jeong, J. Jeong, S. Jeong Hoon, K. Jha, G Jha, M Jha, S Jia, C Ji, C Ji, H Ji, C Ji, R Jia, N Jia, Z Jian, L Jiang, D Jiang, F Jiang, H Jiang, H Jiang, H Jiang, H Jiang, C Jiang, Y Jianguo, W Jiang, C Jiang, P Jianguo, C Jiang, C Jiang, P Jianguo, C Jiang, P Jianguo, C Jiang, C Jiang, P Jianguo, C Jiang, C Jiang, C Jiang, Y Jianguo, C Jiang, C Jiang, P Jianguo, W Jianging, C Jiang, C Jiang, C Jiang, C Jiang, Y Jianguo, C Jiang, C Jiang, C Jiang, C Jiang, C Jiang, C Jiang, Y Jianguo, W Jianguo, C Jiano, Z	
Jeedigunta, H Jelinek, B Jenkins, M Jensen, M. Jensen, N. Jeong, Y. Jeong, C. Jeong, J. Jeong, S. Jeong Hoon, K. Jha, G Jha, M Jha, S Jia, C Ji, C Ji, H Ji, C Ji, R Jia, N Jia, Z Jian, L Jiang, D Jiang, F Jiang, H Jiang, H Jiang, H Jiang, H Jiang, C Jiang, Y Jianguo, W Jiang, C Jiang, P Jianguo, C Jiang, C Jiang, P Jianguo, C Jiang, P Jianguo, C Jiang, C Jiang, P Jianguo, C Jiang, C Jiang, C Jiang, Y Jianguo, C Jiang, C Jiang, P Jianguo, W Jianging, C Jiang, C Jiang, C Jiang, C Jiang, Y Jianguo, C Jiang, C Jiang, C Jiang, C Jiang, C Jiang, C Jiang, Y Jianguo, W Jianguo, C Jiano, Z	
Jeedigunta, H Jelinek, B Jenkins, M Jensen, M. Jensen, N. Jeong, Y. Jeong, C. Jeong, J. Jeong, S. Jeong Hoon, K. Jha, G Jha, M Jha, S Ji, C Ji, H Ji, L Ji, S Jia, N Jia, Z Jian, L Jiang, D. Jiang, F. Jiang, H. Jiang, H. Jiang, H. Jiang, Y. Jianguo, W. Jianguo, C. Jiang, P. Jianguo, C. Jiang, P. Jiang, J. Jiang, J. Jiang J. Jiang, J. Jiang, J. Jiang J. Jiang, J. Jiang, J.	$\begin{array}{c}$
Jeedigunta, H Jelinek, B Jenkins, M Jensen, M. Jensen, N. Jeong, Y. Jeong, C. Jeong, J. Jeong, S. Jeong Hoon, K. Jha, G Jha, M Jha, S Jia, C Ji, C Ji, H Ji, C Ji, R Jia, N Jia, Z Jian, L Jiang, D Jiang, F Jiang, H Jiang, H Jiang, H Jiang, H Jiang, C Jiang, Y Jianguo, W Jiang, C Jiang, P Jianguo, C Jiang, C Jiang, P Jianguo, C Jiang, P Jianguo, C Jiang, C Jiang, P Jianguo, C Jiang, C Jiang, C Jiang, Y Jianguo, C Jiang, C Jiang, P Jianguo, W Jianging, C Jiang, C Jiang, C Jiang, C Jiang, Y Jianguo, C Jiang, C Jiang, C Jiang, C Jiang, C Jiang, C Jiang, Y Jianguo, W Jianguo, C Jiano, Z	$\begin{array}{c}$
Jeedigunta, H Jelinek, B Jenkins, M Jensen, M. Jensen, N. Jeong, Y. Jeong, C. Jeong, J. Jeong, S. Jeong Hoon, K. Jha, G Jha, M Jha, S Ji, C Ji, H Ji, L Ji, S Jia, N Jia, Z Jian, L Jiang, D. Jiang, F. Jiang, H. Jiang, H. Jiang, H. Jiang, Y. Jianguo, W. Jianguo, C. Jiang, P. Jianguo, C. Jiang, P. Jiang, J. Jiang, J. Jiang J. Jiang, J. Jiang, J. Jiang J. Jiang, J. Jiang, J.	$\begin{array}{c}$



Jin, C	
Jin, H	
Jin, L	
Jin, M	
Jin, N	
Jin, X	
Jin, Y	
Jing, J	
Jing, P	
Jing, Y	
	, L
	sol, T17
,	
Joannop	ooulos, J
Jodoin,	B358
	es, J
	esson, B210
	on, A75
John, R	
Johnson	n, C198, 260, 333
	, D29, 77, 192
	, J
	n, M72, 86
	n, S18, 66
	n, W23, 24, 54
	I159, 270, 278
Joly, L	
Jones, F	I247
	N
	ı, B191
	B17
Jordan,	E223
Jozef, J	
	a, S18
Jozwik,	P66
Ju, S	
Juarez,	J180
Juhas, N	<i>A</i>
Jun, B	
Jun, H	
Jung, C	
Jung, G	
Jung, H	
Jung, I	
Jung, S	50, 265, 266, 318, 319, 359
Junxia,	D230
Junzo, I	F107
	, M
2	, F231
	i, J173
	N150
Juul Jen	isen, D20

K

Kacprzak, D	
Kad, B	
Kadkhodabeigi, M	175

Kahler, D
Kai, W
Kainer, K41, 145, 195, 257, 258, 259, 350, 352
Kainuma, R204, 265
Kakarlapudi, P110
Kakkar, B
Kalagara, S
Kalay, E
Kalay, E
Kalgraf, K
Kalidindi, S69, 121, 199, 200, 280, 328
Kalisvaart, P197
Kalita, S124, 176, 346, 359, 360
Kalu, K20
Kalu, P47, 69
Kalya, P135
Kamaya, M20
Kamikawa, N
Kammer, D
Kampe, S17, 168, 277, 278, 302
Kan, H
Kandukuri, S
Kane, R
Kaneko, Y83
Kang, B54, 62, 108
Kang, C
Kang, D145
Kang, H
Kang, J
Kang, J
Kang, M
Kang, S16, 32, 50, 63, 102, 104, 117,
Kao, C50, 105, 152, 204, 246, 296, 297
Ruo, C
Kaoumi, D
Kaoumi, D356
Kaoumi, D

Kawakita, H209
Kawasaki, M112
Kaya, A67, 176, 350
Kaya, G67
Kaya, R
Kayal, S
Kayan, E
Kazakov, S
Kazuo, F
Kazykhanov, V218
Ke, F73
Kecskes, L113, 243
Keiser, D
Keles, O
Kelley, J
Kelly, K
Kelsall, G
Kelson, I154
Kelton, K24, 235
Kendig, K17, 65, 118, 167, 225, 226, 277
Kenik, E
Kennedy, M
Kenny, S
Keppens, v
Kessler, M
Kessler, O
Kettner, M60
Khachaturyan, A189
Khan, H97
Khomami, B
Khraisheh, M
Khurana, S
Kieft, R74, 127, 179, 237, 288, 333
Kiggans, J
Kilmametov, A
Kim, B97, 204, 272, 273
Kim, C54, 149, 150, 186, 199, 205, 247, 252
Kim, D73, 145, 148, 177,
Kim, H58, 79, 126, 176, 272,
273, 285, 330, 335, 344
Kim, I144, 145
Kim, J40, 64, 85, 94, 104, 128,
146, 148, 154, 169, 180,
Kim, K
Kim, M
Kim, N70, 74, 145, 191 Kim, S16, 19, 70, 83, 138, 186,
Kim, T
Kim, W145, 177, 188, 202, 257, 307, 353
Kim, Y42, 73, 74, 132, 143, 178, 180,
213, 225, 266, 276, 287, 290, 292, 361
Kimura, A
Kimura, H
King, B
King, D
Kioseoglou, G17
Kirchain, R60, 270
Kirchheim, R
Kirishima, A
Kirk, M
Kirkland, S69



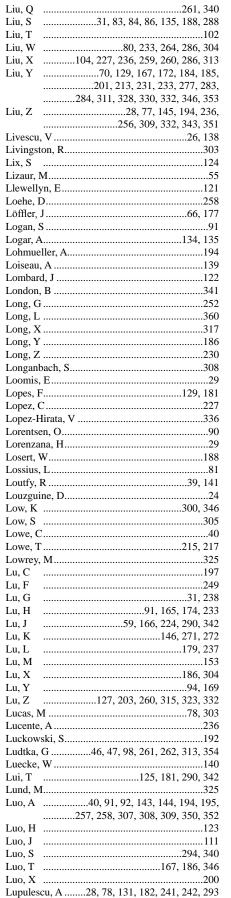
Kishimoto, H
Kishimoto, N
Kisner, R46, 47, 262 Kiss, L134, 237, 283
Kiss, L
Kitamura, T
Kitashima, T
Kityk, I61
Kjar, A122
Klammer, G
Klarstrom, D
Klatvel, 1
Klette, H
Klimenkov, M
Klingensmith, D264, 316
Klinger, L
Klinov, D
Kluse, P
Klug, K
Knap, J155
Knapp, J357
Knepper, R
Knezevic, M
Knipping, K
Knott, S
Knuteson, D54
Ko, S
Ko, Y
Kobayashi, T53, 208, 243 Koch, C59, 272, 358
Koch, K
Kocharian, A
Kockar, B
Kodash, V99, 182, 251, 359
Koduri, S26, 121, 130, 229, 312
Koenigsmann, Z53 Koeplin, H221
Koeppel, B
Koh, S
Koike, J33, 93
Koike, M
Koizumi, Y
Kokawa, H
Kolesinkova, A
Kolobov, Y
Kon Bae, L
Kondo, M70
Kondo, S100, 101
Kondo, T
Kondon, K
Kong, M
Konitzer, D52, 106, 155, 208, 268, 321
Kontsevoi, O51, 302
Koo, J
Kooptarnond, K
Корка, Е
Kordesch, M
Korinko, P167
Kornev, I
Korshunov, A
Korzekwa, D30, 243 Korznikova, E113, 213
Korzinkova, E
Kostorz, G

Kathari D	221
Kovarik, L	
Krachler, R	
Kraft, O	
Krajewski, P	92, 229, 282, 309
Kramer L	
Krasnochtchekov, P	
Krauss, G	
Krishnan V	
Kroupa, A	
Kuoler G	
,	
·	224, 232, 274, 296, 344
Kumar, C	
,	
,	
	55, 110, 157, 209, 269, 323
Kuokkala, V	80
Kuramoto, S	
Kurmanaeva, L	

67
71

L

Laabs, F	
LaCombe, J	
Laé, E	
Lahreche, H	
Lai, B	
Lai, L	
Lai, Y102,	152, 204, 233, 284
Laik, A	
Laird, B	
Lalonde, K	
Lamb, J	
Lamb, S	60
Lambotte, G	
Lambros, J	
Lan, H	
Lan, J	
Lan, K	
Landgraf, F	
Landry, P	171
Langdon, T	
Lange, G	
Langelier, B	
Langerman, M	
Largerman, M	
Larsen, S	81
	20.4
Larson, B	
Larsson, H	
Larsson, H Lashley, J	
Larsson, H Lashley, J Lasseigne, A	
Larsson, H Lashley, J Lasseigne, A Lassila, D	
Larsson, H Lashley, J Lasseigne, A Lassila, D Latysh, V	
Larsson, H Lashley, J Lasseigne, A Lassila, D Latysh, V Laube, B	
Larsson, H Lashley, J Lasseigne, A Lassila, D Latysh, V Laube, B Laughlin, J	
Larsson, H Lashley, J Lasseigne, A Lassila, D Latysh, V Laube, B Laughlin, J Launey, M	
Larsson, H Lashley, J Lasseigne, A Lassila, D Latysh, V Laube, B Laughlin, J	
Larsson, H Lashley, J Lasseigne, A Lassila, D Latysh, V Laube, B Laughlin, J Launey, M Lavender, C Lavernia, E	
Larsson, H Lashley, J Lasseigne, A Lassila, D Latysh, V Laube, B Laughlin, J Launey, M Lavender, C Lavernia, E	
Larsson, H Lashley, J Lasseigne, A Lassila, D Latysh, V Laube, B Laughlin, J Launey, M Lavender, C	
Larsson, H Lashley, J Lasseigne, A Lassila, D Latysh, V Laube, B Laughlin, J Launey, M Lavender, C Lavernia, E Lavery, N Lavigne, O	
Larsson, H Lashley, J Lasseigne, A Lassila, D Latysh, V Laube, B Laughlin, J Launey, M Lavender, C Lavernia, E Lavigne, O Lavigne, O Laventiev, M	
Larsson, H Lashley, J Lasseigne, A Lassila, D Latysh, V Laube, B Laughlin, J Launey, M Lavender, C Lavernia, E Lavery, N Lavigne, O	
Larsson, H Lashley, J Lasseigne, A Lassila, D Latysh, V Laube, B. Laughlin, J. Launey, M. Lavender, C. Lavernia, E. Lavery, N Lavigne, O. Lavrentiev, M. Lawn, B. Leach, A.	
Larsson, H Lashley, J Lasseigne, A Lassila, D Latysh, V Laube, B Laughlin, J Launey, M Lavender, C Lavernia, E Lavernia, E Laverniev, M Laventiev, M Lawn, B Leach, A Lebensohn, R	
Larsson, H Lashley, J Lasseigne, A Lassila, D Latysh, V Laube, B. Laughlin, J. Launey, M. Lavender, C. Lavernia, E. Lavernia, E. Lavery, N. Lavigne, O. Lavrentiev, M. Lawn, B. Leach, A. Lebensohn, R. 30 LeBlanc, M.	
Larsson, H Lashley, J Lasseigne, A Lasseigne, A Lassila, D Latysh, V Laube, B Laughlin, J. Launey, M. Lavender, C. Lavernia, E. Lavernia, E. Lavery, N. Lavigne, O. Lavrentiev, M. Lawn, B. Leach, A. Lebensohn, R. 30 LeBlanc, M. Leboeuf, S.	
Larsson, H Lashley, J Lasseigne, A Lassila, D Latysh, V Laube, B Laughlin, J. Launey, M. Lavender, C. Lavender, C. Lavernia, E. Lavery, N Lavigne, O. Lavrentiev, M. Lawn, B. Leach, A. Lebensohn, R. 30 LeBlanc, M. Lebouf, S. Le Bouar, Y.	
Larsson, H Lashley, J Lasseigne, A Lassila, D Latysh, V Laube, B Laughlin, J. Launey, M. Lavender, C. Lavernia, E. Laverria, E. Lavery, N. Lavigne, O. Lavrentiev, M. Lawn, B. Leach, A. Lebensohn, R	
Larsson, H Lashley, J Lasseigne, A Lasseigne, A Lassila, D Latysh, V Laube, B Laughlin, J. Launey, M. Lavender, C. Lavernia, E. Lavernia, E. Lavery, N. Lavigne, O. Lavrentiev, M. Lawing, B. Leach, A. Lebensohn, R	
Larsson, H Lashley, J Lasseigne, A Lasseigne, A Lassila, D Latysh, V Laube, B Laughlin, J Launey, M. Lavender, C. Lavernia, E. Laverria, E. Lavery, N. Lavigne, O. Lavrentiev, M. Lawin, B. Leaven, A. Lebensohn, R Lebensohn, R. Lebouf, S. Le Bouar, Y. Le Brun, P. Leckie, R. Lederich, R.	
Larsson, H Lashley, J Lasseigne, A Lasseigne, A Lassila, D Latysh, V Laube, B Laughlin, J. Launey, M. Lavender, C. Lavernia, E. Lavernia, E. Lavery, N. Lavigne, O. Lavrentiev, M. Lawing, B. Leach, A. Lebensohn, R	



Li, T	
Li, W	
Li, X	
Li, Y	
Li, Z	
Lian, J	
Lian, T	
0.	
,	
Liao, J	
Liao, S	
Liao, S	
Liaw, P	
, _	
Liberati,	M146
Lieberm	an, S44, 254, 277
Lienau,	C273, 274
Lienert,	T
Lienert,	U267, 358
	en, E160
Lim, C	
Lim, H	
Lim, J	
Lima, J	
1 5	mnong, S
Lin, A	
Lin, C	2 0.4 2 44
Lin, D	
Lin, H	
Lin, H Lin, J	
Lin, H Lin, J Lin, K	
Lin, H Lin, J Lin, K Lin, S	
Lin, H Lin, J Lin, K Lin, S Lin, W	
Lin, H Lin, J Lin, K Lin, S Lin, W Lin, Y	
Lin, H Lin, J Lin, K Lin, S Lin, W Lin, Y Lindau,	
Lin, H Lin, J Lin, K Lin, K Lin, S Lin, W Lin, Y Lindau, Lindley,	
Lin, H Lin, J Lin, K Lin, K Lin, S Lin, W Lin, Y Lindau, Lindley,	
Lin, H Lin, J Lin, K Lin, K Lin, S Lin, W Lin, Y Lindau, Lindley, Lindsay,	
Lin, H Lin, J Lin, K Lin, K Lin, S Lin, W Lin, Y Lindau, I Lindley, Lindsay,	
Lin, H Lin, J Lin, K Lin, K Lin, S Lin, W Lin, Y Lindau, I Lindley, Lindsay, Ling, Y Linhardt	
Lin, H Lin, J Lin, K Lin, K Lin, S Lin, W Lin, Y Lindau, Lindley, Lindsay, Ling, Y Linhardt Link, R	
Lin, H Lin, J Lin, K Lin, S Lin, W Lin, Y Lindau, Lindley, Lindsay	
Lin, H Lin, J Lin, K Lin, S Lin, W Lin, Y Lindau, Lindley, Lindsay	
Lin, H Lin, J Lin, K Lin, S Lin, W Lin, Y Lindau, Lindley, Lindsay	
Lin, H Lin, J Lin, K Lin, S Lin, W Lin, Y Lindau, Lindley, Lindsay	
Lin, H Lin, J Lin, K Lin, S Lin, W Lin, Y Lindau, Lindley, Lindsay, Lindsay, Ling, Y Linhardt Link, R Liou, W Lipin, V Lipko, S Litton, D	
Lin, H Lin, J Lin, K Lin, S Lin, W Lin, Y Lindau, Lindley, Lindsay, Lindsay, Ling, Y Linhardt Link, R Liou, W Lipin, V Lipko, S Litton, E	$\begin{array}{c} & 196 \\ & 355 \\ & 108 \\ & 265 \\ & 264, 297 \\ & 154 \\ & 102, 152, 154, 204, 266, 272, 319, 331 \\ \mathbf{R} & 315 \\ \mathbf{T} & 349 \\ \mathbf{S} & 21, 70, 123, 124, 173, \\ & 174, 231, 232, 283, 329 \\ & 336 \\ \mathbf{R} & 64 \\ & 140 \\ & 153 \\ & 171 \\ & 276 \\ \mathbf{O} & 208 \\ & 288, 324 \\ & 18, 21, 27, 51, 58, 102, 112, 127, \\ & 152, 159, 206, 211, 213, 251, 260, \\ \end{array}$
Lin, H Lin, J Lin, K Lin, S Lin, W Lin, Y Lindau, Lindley, Lindsay, Lindsay, Ling, Y Linhardt Link, R Liou, W Lipin, V Lipko, S Litton, E	$\begin{array}{c} & & 196 \\ & & 355 \\ & & & 108 \\ & & & 265 \\ & & & 264, 297 \\ & & & & 154 \\ & & & & 102, 152, 154, 204, 266, 272, 319, 331 \\ \mathbf{R} & & & 315 \\ \mathbf{T} & & & & 349 \\ \mathbf{S} & & & & 21, 70, 123, 124, 173, \\ & & & & & & 174, 231, 232, 283, 329 \\ & & & & & & & & 336 \\ \mathbf{R} & & & & & & & & & & & & & & & & & & &$
Lin, H Lin, J Lin, K Lin, S Lin, W Lin, Y Lindau, Lindley, Lindley, Lindsay, Ling, Y Linhardt Link, R Liou, W Lipin, V Lipko, S Litton, E Liu, B Liu, F	$\begin{array}{c} & 196 \\ & 355 \\ & 108 \\ & 265 \\ & 264, 297 \\ & 154 \\ & 102, 152, 154, 204, 266, 272, 319, 331 \\ \mathbf{R} & 315 \\ \mathbf{T} & 349 \\ \mathbf{S} & 21, 70, 123, 124, 173, \\ & 174, 231, 232, 283, 329 \\ & 336 \\ \mathbf{R} & 64 \\ & 140 \\ & 153 \\ & 171 \\ & 276 \\ \mathbf{O} & 208 \\ & 288, 324 \\ & 18, 21, 27, 51, 58, 102, 112, 127, \\ & 152, 159, 206, 211, 213, 251, 260, \\ & 266, 271, 318, 319, 323, 325, 357 \\ & 73, 82, 180, 288 \\ \end{array}$
Lin, H Lin, J Lin, K Lin, S Lin, W Lin, Y Lindau, J Lindley, Lindley, Lindsay, Ling, Y Linhardt Link, R Liou, W Lipin, V Lipko, S Litton, B Liu, C Liu, F Liu, G	$\begin{array}{c} & & 196 \\ & & & 355 \\ & & & & 108 \\ & & & & 265 \\ & & & & 264, 297 \\ & & & & & 154 \\ & & & & & 102, 152, 154, 204, 266, 272, 319, 331 \\ \mathbf{R} & & & & & 315 \\ \mathbf{T} & & & & & 349 \\ \mathbf{S} & & & & & & 21, 70, 123, 124, 173, \\ & & & & & & & & & 349 \\ \mathbf{S} & & & & & & & & & & & & & & \\ & & & & $
Lin, H Lin, J Lin, K Lin, S Lin, W Lin, Y Lindau, J Lindley, Lindley, Lindsay, Ling, Y Linhardt Link, R Liou, W Lipin, V Lipko, S Litton, B Liu, C Liu, F Liu, G Liu, H	
Lin, H Lin, J Lin, K Lin, S Lin, W Lin, Y Lindau, J Lindley, Lindley, Lindsay, Ling, Y Linhardt Link, R Liou, W Lipin, V Lipko, S Litton, B Liu, C Liu, F Liu, G	$\begin{array}{c} & 196 \\ & 355 \\ & 108 \\ & 265 \\ & 264, 297 \\ & 154 \\ & 102, 152, 154, 204, 266, 272, 319, 331 \\ R & 315 \\ T & 349 \\ S & 21, 70, 123, 124, 173, \\ & 174, 231, 232, 283, 329 \\ & 336 \\ R & 64 \\ & 140 \\ & 153 \\ & 171 \\ & 276 \\ O & 208 \\ & 288, 324 \\ & 18, 21, 27, 51, 58, 102, 112, 127, \\ & 288, 324 \\ & 18, 21, 27, 51, 58, 102, 112, 127, \\ & 288, 324 \\ & 18, 21, 27, 51, 58, 102, 112, 127, \\ & 288, 324 \\ & 18, 21, 27, 51, 58, 102, 112, 127, \\ & 288, 324 \\ & 288, 324 \\ & 288, 324 \\ & 276 \\ & 288, 324 \\ & 277, 51, 58, 102, 112, 127, \\ & 276 \\ & 288, 324 \\ & 276 \\ & 271, 318, 319, 323, 325, 357 \\ & 73, 82, 180, 288 \\ & 258 \\ & 195, 271, 314, 324 \\ & 258 \\ & 19, 68, 87, 103, 120, 121, \\ \end{array}$
Lin, H Lin, J Lin, K Lin, S Lin, W Lin, Y Lindau, J Lindley, Lindley, Lindsay, Ling, Y Linhardt Link, R Liou, W Lipko, S Litton, E Liu, B Liu, F Liu, G Liu, H Liu, J	$\begin{array}{c} & & 196 \\ & & & 355 \\ & & & & 108 \\ & & & & 265 \\ & & & & 264, 297 \\ & & & & & 154 \\ & & & & & 102, 152, 154, 204, 266, 272, 319, 331 \\ \mathbf{R} & & & & & 154 \\ & & & & & & & 154 \\ & & & & & & & & & 154 \\ & & & & & & & & & & & & 154 \\ & & & & & & & & & & & & & & & & \\ & & & & & & & & & & & & & & & \\ & & & & & & & & & & & & & & & \\ & & & & & & & & & & & & & & & \\ & & & & & & & & & & & & & & & \\ & & & & & & & & & & & & & & & \\ & & & & & & & & & & & & & & & \\ & & & & & & & & & & & & & & & \\ & & & & & & & & & & & & & & & \\ & & & & & & & & & & & & & & \\ & & & & & & & & & & & & & & \\ & & & & & & & & & & & & & \\ & & & & & & & & & & & & & \\ & & & & & & & & & & & & & \\ & & & & & & & & & & & & & \\ & & & & & & & & & & & & & \\ & & & & & & & & & & & & & \\ & & & & & & & & & & & & & \\ & & & & & & & & & & & & \\ & & & & & & & & & & & & \\ & & & & & & & & & & & & & \\ & & & & & & & & & & & & \\ & & & & & & & & & & & & \\ & & & & & & & & & & & \\ & & & & & & & & & & & \\ & & & & & & & & & & & \\ & & & & & & & & & & & \\ & & & & & & & & & & & \\ & & & & & & & & & & & \\ & & & & & & & & & & & \\ & & & & & & & & & & & \\ & & & & & & & & & & & \\ & & & & & & & & & & & \\ & & & & & & & & & & \\ & & & & & & & & & & \\ & & & & & & & & & & \\ & & & & & & & & & \\ & & & & & & & & & & \\ & & & & & & & & & & \\ & & & & & & & & & & \\ & & & & & & & & & & \\ & & & & & & & & & & \\ & & & & & & & & & & & \\ & & & & & & & & & & & \\ & & & & & & & & & & & \\ & & & & & & & & & & & \\ & & & & & & & & & & & \\ & & & & & & & & & & & \\ & & & & & & & & & & \\ & & & & & & & & & & & \\ & & & & & & & & & & & \\ & & & & & & & & & & & \\ & & & & & & & & & & \\ & & & & & & & & & & \\ & & & & & & & & & & \\ & & & & & & & & & & \\ & & & & & & & & & & \\ & & & & & & & & & \\ & & & & & & & & & \\ & & & & & & & & & \\ & & & & & & & & & \\ & & & & & & & & & & \\ & & & & & & & & & & \\ & & & & & & & & & & \\ & & & & & & & & & & \\ & & & & & & & & & & \\ & & & & & & & & & & & \\ & & & & & & & & & & & \\ & & & & & & & & & & & \\ & & & & & & & & & & & & \\ & & & & & & & & & & & & \\ & & & & & & & & & & & \\ & & & & $
Lin, H Lin, J Lin, K Lin, S Lin, W Lin, Y Lindau, J Linday, L Linday, Y Lindsay, Lin	$\begin{array}{c} & 196 \\ & 355 \\ & 108 \\ & 265 \\ & 264, 297 \\ & 154 \\ & 102, 152, 154, 204, 266, 272, 319, 331 \\ R & 315 \\ T & 349 \\ S & 21, 70, 123, 124, 173, \\ & 174, 231, 232, 283, 329 \\ & 336 \\ R & 64 \\ & 140 \\ & 153 \\ & 171 \\ & 276 \\ \hline \\ 0 & 208 \\ & 288, 324 \\ & 18, 21, 27, 51, 58, 102, 112, 127, \\ & 276 \\ \hline \\ 0 & 208 \\ & 288, 324 \\ & 18, 21, 27, 51, 58, 102, 112, 127, \\ & 276 \\ \hline \\ 0 & 208 \\ & 288, 324 \\ & 18, 21, 27, 51, 58, 102, 112, 127, \\ & 276 \\ \hline \\ 0 & 208 \\ & 288, 324 \\ & 18, 21, 27, 51, 58, 102, 112, 127, \\ & 276 \\ \hline \\ 0 & 208 \\ & 288, 324 \\ & 175 \\ & 276 \\ \hline \\ 0 & 208 \\ & 276 \\ & 271 \\ & 314, 314, 324 \\ & 258 \\ & 195, 271, 314, 324 \\ & 258 \\ & 196, 212, 228, 264, 279, 281, 343 \\ & 133, 209 \\ \end{array}$
Lin, H Lin, J Lin, K Lin, S Lin, W Lin, Y Lindau, J Lindley, Lindley, Lindsay, Ling, Y Linhardt Link, R Liou, W Lipko, S Litton, E Liu, B Liu, F Liu, G Liu, H Liu, J	$\begin{array}{c} & & 196 \\ & & & 355 \\ & & & & 108 \\ & & & & 265 \\ & & & & 264, 297 \\ & & & & & 154 \\ & & & & & 102, 152, 154, 204, 266, 272, 319, 331 \\ \mathbf{R} & & & & & 154 \\ & & & & & & & 154 \\ & & & & & & & & & 154 \\ & & & & & & & & & & & & 154 \\ & & & & & & & & & & & & & & & & \\ & & & & & & & & & & & & & & & \\ & & & & & & & & & & & & & & & \\ & & & & & & & & & & & & & & & \\ & & & & & & & & & & & & & & & \\ & & & & & & & & & & & & & & & \\ & & & & & & & & & & & & & & & \\ & & & & & & & & & & & & & & & \\ & & & & & & & & & & & & & & & \\ & & & & & & & & & & & & & & \\ & & & & & & & & & & & & & & \\ & & & & & & & & & & & & & \\ & & & & & & & & & & & & & \\ & & & & & & & & & & & & & \\ & & & & & & & & & & & & & \\ & & & & & & & & & & & & & \\ & & & & & & & & & & & & & \\ & & & & & & & & & & & & & \\ & & & & & & & & & & & & \\ & & & & & & & & & & & & \\ & & & & & & & & & & & & & \\ & & & & & & & & & & & & \\ & & & & & & & & & & & & \\ & & & & & & & & & & & \\ & & & & & & & & & & & \\ & & & & & & & & & & & \\ & & & & & & & & & & & \\ & & & & & & & & & & & \\ & & & & & & & & & & & \\ & & & & & & & & & & & \\ & & & & & & & & & & & \\ & & & & & & & & & & & \\ & & & & & & & & & & & \\ & & & & & & & & & & \\ & & & & & & & & & & \\ & & & & & & & & & & \\ & & & & & & & & & \\ & & & & & & & & & & \\ & & & & & & & & & & \\ & & & & & & & & & & \\ & & & & & & & & & & \\ & & & & & & & & & & \\ & & & & & & & & & & & \\ & & & & & & & & & & & \\ & & & & & & & & & & & \\ & & & & & & & & & & & \\ & & & & & & & & & & & \\ & & & & & & & & & & & \\ & & & & & & & & & & \\ & & & & & & & & & & & \\ & & & & & & & & & & & \\ & & & & & & & & & & & \\ & & & & & & & & & & \\ & & & & & & & & & & \\ & & & & & & & & & & \\ & & & & & & & & & & \\ & & & & & & & & & & \\ & & & & & & & & & \\ & & & & & & & & & \\ & & & & & & & & & \\ & & & & & & & & & \\ & & & & & & & & & & \\ & & & & & & & & & & \\ & & & & & & & & & & \\ & & & & & & & & & & \\ & & & & & & & & & & \\ & & & & & & & & & & & \\ & & & & & & & & & & & \\ & & & & & & & & & & & \\ & & & & & & & & & & & & \\ & & & & & & & & & & & & \\ & & & & & & & & & & & \\ & & & & $

136th	Annual Meeting & Exhibition
	10 00 100 150 106 100
Lee, C	40, 83, 139, 153, 186, 190, 214, 218, 266, 319, 327, 361
Lee, D	
Lee, E	
Lee, G	
Lee, H	
Lee, I	203, 205, 216, 223, 265, 318
Lee, I Lee, J	
200, 5	
Lee, K	
Lee, M Lee, N	
Lee, N Lee, P	
Lee, S	
,	191, 204, 213, 220, 266, 275, 294, 309
Lee, T	
Lee, W	
Lee, Y	26, 28, 93, 117, 139, 223, 257, 282, 345
Legagne Lei, M	eux, P
Lei, M Lei, Y	
	ied, G118
	erg, W244
	S
	n, M85
	n, J
Leonnar	dt, T57, 110 , J177, 286
	r, M
	r, M54
Lerch, B	
Le Roy,	G128
LeSar, R	8
	D
Levasho	v, V
Levendi	s, Y137
-	e, J92
Levine,	L
	V120, 121, 130, 217, 233, 300, 312
Lewand	owski, J17, 65, 73, 74, 118,
Lewis, I	D
LED	
Li, B	
Li, C	
Li, D	
Li, G	
Li, H	
Li, J	
	118, 128, 140, 161, 178, 179, 189, 206, 233, 238, 246, 284, 287, 289,
Li, K	
Li, L	
Li, M	
Li, N	
Li. O	

ʹͲͶϹϿϢϤϷ

LEARN • NETWORK • ADVANCE

Li, R



Lussier, A	
Luton, M	
Luyten, J	
Lynn, K	
Lyssenko, T	
5	

\mathbf{M}

Ma, A	45
Ma, D6	
Ma, E24, 58, 113, 155, 21	6, 243, 357
Ma, H	
Ma, L	
Ma, N4	4, 168, 239
Ma, S	
Ma, W	
Ma, X	223, 271
Ma, Y	· · ·
Macak, J	
Macht, M	
Mackiewicz-Ludtka, G	
MacSleyne, J	
Madan, A	
Maeda, M11	
Maehara, Y	
Magalhaes, R	
Mahajan, V	
Mahieu, P	
Mahmood, M	
Mahmoudi, M	
Mahoney, M	7, 297, 341
Maier, H	
Maier, P	
Maier, V	
Maiti, S	
Maitra, P	
Maity, P	
Maiwald, D	
Maj, M	
Major, J	
Majumdar, B	
Makhlouf, M	
Maximour, MI	
Makino K	,
Makino, K	
Makov, G	265 154
Makov, G Maldonado, S	
Makov, G Maldonado, S Malerba, L150, 20	
Makov, G Maldonado, S Malerba, L150, 20 Malik, M	
Makov, G Maldonado, S Malerba, L150, 20 Malik, M Mall, S	
Makov, G Maldonado, S Malerba, L	
Makov, G Maldonado, S Malerba, L	
Makov, G Maldonado, S Malerba, L	265 154 328 2, 203, 263 226 298, 351 244 232
Makov, G Maldonado, S Malerba, L	265
Makov, G Maldonado, S Malerba, L	265 154
Makov, G Maldonado, S Malerba, L	265
Makov, G Maldonado, S Malerba, L	265
Makov, G Maldonado, S Malerba, L	265 154 328 2, 203, 263 298, 351 298, 351 244 232 1, 316, 356 71 71 96
Makov, G Maldonado, S Malerba, L	
Makov, G Maldonado, S Malerba, L	$\begin{array}{c}$
Makov, G Maldonado, S Malerba, L	$\begin{array}{c} 265 \\ 154 \\ 328 \\ 2, 203, 263 \\ 112 \\ 226 \\ 298, 351 \\ 244 \\ 232 \\ 1, 316, 356 \\ 127 \\ 135 \\ 347 \\85, 188 \\335 \\183, 290 \\ 249 \\ 9, 248, 299 \\ \end{array}$
Makov, G Maldonado, S Malerba, L	$\begin{array}{c} 265 \\ 154 \\ 328 \\ 2, 203, 263 \\ 112 \\ 226 \\ 298, 351 \\ 244 \\ 232 \\ 1, 316, 356 \\ 127 \\ 135 \\ 347 \\ 347 \\ 347 \\ 335 \\ 183, 290 \\ 249 \\ 9, 248, 299 \\ 352 \\ \end{array}$
Makov, G Maldonado, S Malerba, L	$\begin{array}{c} 265 \\ 154 \\ 328 \\ 2, 203, 263 \\ 112 \\ 226 \\ 298, 351 \\ 244 \\ 232 \\ 1, 316, 356 \\ 127 \\ 135 \\ 347 \\ 347 \\ 347 \\ 335 \\ 183 \\ 249 \\ 9, 248, 299 \\ 352 \\ 117 \\ \end{array}$
Makov, G Maldonado, S Malerba, L	$\begin{array}{c} 265 \\ 154 \\ 328 \\ 2, 203, 263 \\ 112 \\ 226 \\ 298, 351 \\ 244 \\ 232 \\ 1, 316, 356 \\ 127 \\ 135 \\ 347 \\ 347 \\ 85, 188 \\ 335 \\ 183, 290 \\ 249 \\ 9, 248, 299 \\ 352 \\ 117 \\ 178 \\ \end{array}$
Makov, G Maldonado, S Malerba, L	$\begin{array}{c} 265 \\ 154 \\ 328 \\ 2, 203, 263 \\ 112 \\ 226 \\ 298, 351 \\ 244 \\ 232 \\ 1, 316, 356 \\ 127 \\ 135 \\ 347 \\ 135 \\ 347 \\ 335 \\ 183, 290 \\ 249 \\ 9, 248, 299 \\ 352 \\ 117 \\ 178 \\ 129, 225 \\ \end{array}$
Makov, G Maldonado, S Malerba, L	$\begin{array}{c} 265 \\ 154 \\ 328 \\ 2, 203, 263 \\ 112 \\ 226 \\ 298, 351 \\ 244 \\ 232 \\ 1, 316, 356 \\ 127 \\ 135 \\ 347 \\ 335 \\ 183, 290 \\ 249 \\ 9, 248, 299 \\ 352 \\ 117 \\ 178 \\ 129, 225 \\ 137 \\ \end{array}$
Makov, G Maldonado, S Malerba, L	$\begin{array}{c} 265 \\ 154 \\ 328 \\ 2, 203, 263 \\ 112 \\ 226 \\ 228, 351 \\ 244 \\ 232 \\ 1, 316, 356 \\ 127 \\ 232 \\ 1, 316, 356 \\ 127 \\ 71 \\ 96 \\ 135 \\ 347 \\ 85, 188 \\ 335 \\ 183, 290 \\ 249 \\ 9, 248, 299 \\ 352 \\ 117 \\ 178 \\ 129, 225 \\ 137 \\ 28 \end{array}$
Makov, G Maldonado, S Malerba, L	$\begin{array}{c}$

Mao, Y	254
Mao, Z	
Mara, N	
Marceau, D	
Marcheselli, C	278
Marciniak, M	
Marcinkoski, J	
Marcolongo, P	179
Marcus, H	16
Mariage, J	
Marian, J	154, 155
Marino, K	
Marion, E	21
Markham, J	
Markmaitree, T	197
Marks, J	
Marquis, F	
Marrow, T	
Marsen, B	354
Marsh, S	
Marshall, G	
Marshall, S	
Marte, J	277
Marthandam, V	
,	
Martin, G	
Martin, M79	9, 218, 243
Martin, O	
Martin, P	
Martin, R	356
Martin, S	231
Martinez, E	
Maruyama, M	
Maruyama, T	55
Masamoral, R	
Mashl, S	
Mason-Flucke, J	156
	150
Mastorakos, I	
Mastorakos, I Masuda C	170
Masuda, C	170 167, 226
Masuda, C Masuno, A	170 167, 226 85
Masuda, C Masuno, A Mataya, M	170 167, 226 85 190, 295
Masuda, C Masuno, A Mataya, M	170 167, 226 85 190, 295
Masuda, C Masuno, A Mataya, M Materna-Morris, E	
Masuda, C Masuno, A Mataya, M Materna-Morris, E Mates, S	
Masuda, C Masuno, A Mataya, M Materna-Morris, E Mates, S Mathias, M	
Masuda, C Masuno, A Mataya, M Materna-Morris, E Mates, S Mathias, M Mathiau, N	
Masuda, C Masuno, A Mataya, M Materna-Morris, E Mates, S Mathias, M Mathiau, N	
Masuda, C Masuno, A Mataya, M Materna-Morris, E Mates, S Mathias, M Mathias, M Mathieu, N Mathison, L	
Masuda, C Masuno, A Mataya, M Materna-Morris, E Mates, S Mathias, M Mathieu, N Mathison, L Matlakhov, A	
Masuda, C Masuno, A Mataya, M Materna-Morris, E Mates, S Mathias, M Mathieu, N Mathison, L Matlakhov, A Matlakhova, L	
Masuda, C Masuno, A Mataya, M Materna-Morris, E Mates, S Mathias, M Mathieu, N Mathison, L Matlakhov, A Matlakhova, L Matlock, D	
Masuda, C Masuno, A Mataya, M Materna-Morris, E Mates, S Mathias, M Mathieu, N Mathison, L Matlakhov, A Matlakhova, L Matlock, D	
Masuda, C Masuno, A Mataya, M Materna-Morris, E Mathias, M Mathias, M Mathias, M Mathison, L Matlakhov, A Matlakhova, L Matlakhova, D Matson, D	
Masuda, C Masuno, A Mataya, M Materna-Morris, E Mates, S . Mathias, M Mathias, M Mathison, L Matlakhov, A Matlakhov, A Matlakhova, L Matlock, D Matsukawa, Y	
Masuda, C Masuno, A Mataya, M Materna-Morris, E Mates, S . Mathias, M Mathias, M Mathison, L Matlakhov, A Matlakhov, A Matlakhova, L Matlakhova, L Matlock, D Matsunoto, K	
Masuda, C Masuno, A Mataya, M Materna-Morris, E Mates, S . Mathias, M Mathias, M Mathison, L Matlakhov, A Matlakhov, A Matlakhova, L Matlock, D Matsukawa, Y	
Masuda, C Masuno, A Mataya, M Materna-Morris, E Mates, S . Mathias, M Mathias, M Mathison, L Matlakhov, A Matlakhov, A Matlakhova, L Matlock, D Matson, D Matsunoto, K Matsumoto, T	
Masuda, C Masuno, A Mataya, M Materna-Morris, E Mates, S Mathias, M Mathias, M Mathison, L Matlakhova, L Matlakhova, L Matlakhova, L Matlock, D Matsun, D Matsumoto, K Matsumoto, K Matsumoto, T Matsumura, M	
Masuda, C Masuno, A Mataya, M Materna-Morris, E Mates, S Mathias, M Mathias, M Mathias, M Mathias, M Mathias, M Mathias, M Mathias, M Matlakhov, A Matlakhova, L Matlakhova, L Matlakhova, L Matlakhova, D Matsun, D Matsumoto, K Matsumoto, T Matsumota, T Matsunaga, T	$\begin{array}{c}$
Masuda, C Masuno, A Mataya, M Materna-Morris, E Mates, S Mathias, M Mathias, M Mathias, M Mathias, M Mathias, M Mathias, M Mathias, M Matlakhova, L Matlakhova, L Matlakhova, L Matlakhova, L Matlakhova, D Matsukawa, Y Matsumoto, K Matsumoto, T Matsumoto, T Matsumura, M Matsunaga, T Matsuoka, S	$\begin{array}{c}$
Masuda, C Masuno, A Mataya, M Materna-Morris, E Mates, S Mathias, M Mathias, M Mathias, M Mathias, M Mathias, M Mathias, M Mathias, M Matlakhov, A Matlakhova, L Matlakhova, L Matlakhova, L Matlakhova, D Matsun, D Matsumoto, K Matsumoto, T Matsumota, T Matsunaga, T	$\begin{array}{c}$
Masuda, C Masuno, A Mataya, M Materna-Morris, E Mates, S Mathias, M Mathias, M Mathias, M Mathias, M Mathias, M Mathias, M Mathias, M Mathias, M Mathias, M Matlakhova, L Matlakhova, L Matlakhova, L Matlakhova, L Matsuck, D Matsukawa, Y Matsumoto, K Matsumoto, T Matsumota, S Matsuoka, S Matsuyama, A	$\begin{array}{c}$
Masuda, C Masuno, A Mataya, M Materna-Morris, E Mates, S Mathias, M Mathias, M Mathison, L Mathison, L Matlakhov, A Matlakhov, A Matlakhov, A Matlakhov, D Matsuck, D Matsukawa, Y Matsumoto, K Matsumoto, K Matsumoto, T Matsumoto, T Matsumaga, T Matsuoka, S Matsuyama, A Matsupelli, S	$\begin{array}{c}$
Masuda, C Masuno, A Mataya, M Materna-Morris, E Mathias, M Mathias, M Matsun, D Matsunas, T Matsunas, T Matsunas, S Matsuyama, A Mattapelli, S Matteis, P	$\begin{array}{c}$
Masuda, C Masuno, A Mataya, M Materna-Morris, E Mates, S Mathias, M Mathias, M Matsun, C Matsunas, T Matsunas, T Matsunas, S Matsunas, S Matsuyama, A Mattapelli, S Matteo, E	$\begin{array}{c}$
Masuda, C Masuno, A Mataya, M Materna-Morris, E Mathias, M Mathias, M Matsun, D Matsunas, T Matsunas, T Matsunas, S Matsuyama, A Mattapelli, S Matteis, P	$\begin{array}{c}$
Masuda, C Masuno, A Mataya, M Materna-Morris, E Mates, S Mathias, M Mathias, M Matsun, D Matsun, D Matsunas, T Matsunas, T Matsunas, T Matsunas, S Matsunas, S Matsuyama, A Mattapelli, S Matteo, E Matz, L	$\begin{array}{c}$
Masuda, C Masuno, A Mataya, M Materna-Morris, E Mates, S Mathias, M Mathias, M Matson, L Matlakhova, L Matlakhova, L Matson, D Matson, D Matsuawa, Y Matsumoto, K Matsumoto, K Matsumura, M Matsunaga, T Matsunaga, T Matsuyama, A Mattayapelli, S Matteo, E Matz, L Maudlin, P	$\begin{array}{c}$
Masuda, C Masuno, A Mataya, M Materna-Morris, E Mates, S Mathias, M Mathias, M Matson, L Matson, L Matlakhova, L Matlakhova, L Matson, D Matson, D Matsuawa, Y Matsumoto, K Matsumoto, K Matsunaga, T Matsunaga, T Matsunaga, T Matsuyama, A Matsuyama, A Matteo, E Matteo, E Matteo, E Matu, L Maudlin, P Mavromaras, A	$\begin{array}{c}$
Masuda, C Masuno, A Mataya, M Materna-Morris, E Mates, S . Mathias, M Mathias, M Mathias, M Mathias, M Mathias, M Mathias, M Mathias, M Mathias, M Mathias, M Mathias, M Matlakhov, A Matlakhov, A Matlakhov, A Matlakhov, C Matson, D Matsunkawa, Y Matsunawa, Y Matsunawa, Y Matsunoto, K Matsunoto, K Matsunoto, T Matsunawa, T Matsunawa, T Matsunawa, S Matsuoka, S Matsuoka, S Matsuoka, S Mattapelli, S Matteo, E Matteo, E Maudlin, P Maxey, E	$\begin{array}{c}$
Masuda, C Masuno, A Mataya, M Materna-Morris, E Mates, S . Mathias, M Mathias, M Mathias, M Mathias, M Mathias, M Mathias, M Mathias, M Mathias, M Mathias, M Mathias, M Matlakhov, A Matlakhov, A Matlakhov, A Matlakhov, C Matson, D Matsunkawa, Y Matsunawa, Y Matsunawa, Y Matsunoto, K Matsunoto, K Matsunoto, T Matsunawa, T Matsunawa, T Matsunawa, S Matsuoka, S Matsuoka, S Matsuoka, S Mattapelli, S Matteo, E Matteo, E Maudlin, P Maxey, E	$\begin{array}{c}$
Masuda, C Masuno, A Mataya, M Materna-Morris, E Mates, S . Mathias, M Mathias, M Matlakhov, A Matlakhov, A Matlakhov, A Matlakhov, A Matlakhov, C Matson, D Matson, D Matsunoto, K Matsumoto, K Matsumoto, K Matsumoto, T Matsunoto, T Matsunota, S Matsunaga, T Matsuoka, S Matsuyama, A Mattapelli, S Matteo, E Matteo, E Maudlin, P Mayandi, J	$\begin{array}{c}$
Masuda, C Masuno, A Mataya, M Materna-Morris, E Mates, S . Mathias, M Mathias, M Mathias, M Mathias, M Mathias, M Mathias, M Mathias, M Mathias, M Mathias, M Mathias, M Matlakhov, A Matlakhov, A Matlakhov, A Matlakhov, A Matlakhov, C Matsunoto, L Matsunoto, C Matsunoto, K Matsumoto, K Matsumoto, T Matsunoto, T Matsunoto, T Matsunota, S Matsunota, S Matsuoka, S Matsuoka, S Mattapelli, S Matteo, E Matteo, E Maudlin, P Mayandi, J Mayer, G	$\begin{array}{c}$
Masuda, C Masuno, A Mataya, M Materna-Morris, E Mates, S Mathias, M Mathias, M Mathias, M Mathias, M Mathias, M Mathias, M Mathias, M Mathias, N Mathias, N Matsumoto, K Matsumoto, K Matsumoto, K Matsumoto, T Matsumoto, K Matsunaga, T Matsunaga, T Matsunaga, T Matsunaga, T Matsunaga, A Mattapelli, S Matteo, E Matteo, E Maudlin, P Mavromaras, A Maxey, E Mayer, G Mayer, J	$\begin{array}{c}$
Masuda, C Masuno, A Mataya, M Materna-Morris, E Mates, S Mathias, M Mathias, M Mathias, M Mathias, M Mathias, M Mathias, M Mathias, M Mathias, N Mathias, N Matsumoto, K Matsumoto, K Matsumoto, K Matsumoto, K Matsumoto, T Matsumoto, T Matsumoto, T Matsunaga, T Matsunaga, T Matsunaga, T Matsunaga, T Matsunaga, A Matteo, S Matteo, E Maudlin, P Mavromaras, A Maxey, E Mayer, G Mayeur, J Mayeur, J	$\begin{array}{c}$
Masuda, C Masuno, A Mataya, M Materna-Morris, E Mates, S Mathias, M Mathias, M Mathias, M Mathias, M Mathias, M Mathias, M Mathias, M Mathias, N Mathias, N Matsumoto, K Matsumoto, K Matsumoto, K Matsumoto, T Matsumoto, K Matsunaga, T Matsunaga, T Matsunaga, T Matsunaga, T Matsunaga, A Mattapelli, S Matteo, E Matteo, E Maudlin, P Mavromaras, A Maxey, E Mayer, G Mayer, J	$\begin{array}{c}$
Masuda, C Masuno, A Mataya, M Materna-Morris, E Mates, S Mathias, M Mathias, N Mathias, N Mathias, N Mathias, N Mathias, D Mathias, D Mathias, D Mathias, D Mathias, D Mathias, D Mathias, M Mathias, M Mathias, M Mathias, M Mathias, M Mathias, M Mathias, M Mathias, M Mathias, S Mathias, S May and J Mayeur, J Maziasz, P	$\begin{array}{c}$
Masuda, C Masuno, A Mataya, M Materna-Morris, E Mates, S Mathias, M Mathias, N Mathias, N Mathias, N Mathias, N Mathias, D Mathias, D Mathias, D Mathias, D Mathias, D Mathias, D Mathias, M Mathias, M Mathias, M Mathias, M Mathias, M Mathias, M Mathias, M Mathias, M Mathias, S Mathias, S Mayer, G Mayer, J Maziasz, P Mazur, Y	$\begin{array}{c}$
Masuda, C Masuno, A Mataya, M Materna-Morris, E Mates, S Mathias, M Mathias, N Mathias, N Mathias, N Mathias, N Mathias, D Mathias, D Mathias, D Mathias, D Mathias, D Mathias, D Mathias, M Mathias, M Mathias, M Mathias, M Mathias, M Mathias, M Mathias, M Mathias, M Mathias, S Mathias, S May and J Mayeur, J Maziasz, P	$\begin{array}{c}$

McCabe, R	243
McCallum, R	
McCauley, J	338
McClellan, K	
McClintock, D	
McCluskey, M	163
McColskey, D	140
McCowan, C	
McCune, R91, 35	0,351
McDaniels, R	
McDeavitt, S	
McDermid, J	46
McDonald, J	30
McDonald, S11	
McDowell, D106, 155, 199, 256, 26	51,295
McElwee-White, L	33
Mceuen, S	
McGee, E	19
McGregor, K	304
McIntosh, P122, 171, 22	
McLeod, T	16
McMurray, S	
McNaney, J	
Mcnaney, J	
McNelley, T113, 21	6.341
McPherson, R	
McVay, G	42
Medlin, D	5.299
Meek, T	
Meese, D	
Meghlaoui, A	231
Meguerian, R	
Meguerian, K	
Mehrer, H	
Mehta, V10	8,150
Meier, M12	3.245
Moldrum U	125
Meldrum, H	
Melo-Maximo, V	336
	336
Melo-Maximo, V Mena, M	336 118
Melo-Maximo, V Mena, M Mencer, D	336 118 35
Melo-Maximo, V Mena, M Mencer, D Mendelev, M	336 118 35 .83, 84
Melo-Maximo, V Mena, M Mencer, D Mendelev, M Mendis, B	336 118 35 .83, 84 4, 208
Melo-Maximo, V Mena, M Mencer, D Mendelev, M Mendis, B	336 118 35 .83, 84 4, 208
Melo-Maximo, V Mena, M Mencer, D Mendelev, M Mendis, B Meneghini, A	336 118 35 .83, 84 4, 208 271
Melo-Maximo, V Mena, M Mencer, D Mendelev, M Mendis, B Meneghini, A Menezes, G	336 118 35 .83, 84 .4, 208 271 129
Melo-Maximo, V Mena, M Mencer, D Mendelev, M Mendis, B Meneghini, A Menezes, G Meng, D	336 118 35 .83, 84 .4, 208 271 129 149
Melo-Maximo, V Mena, M Mencer, D Mendelev, M Mendis, B Meneghini, A Menezes, G	336 118 35 .83, 84 .4, 208 271 129 149
Melo-Maximo, V Mena, M Mencer, D Mendelev, M Mendis, B Meneghini, A Menezes, G Meng, D Menon, S	336 118 35 83, 84 4, 208 271 129 149 181
Melo-Maximo, V Mena, M Mencer, D Mendelev, M Mendis, B Meneghini, A Menezes, G Meng, D Menon, S Mente, P	336 118 35 83, 84 4, 208 271 129 149 181 285
Melo-Maximo, V Mena, M Mencer, D Mendelev, M Mendis, B Meneghini, A Menezes, G Meng, D Menon, S Mente, P Mercer, H	336 118 35 .83, 84 .4, 208 271 129 149 149 181 285 82
Melo-Maximo, V Mena, M Mencer, D Mendelev, M Mendis, B Meneghini, A Menezes, G Meng, D Menon, S Mente, P	336 118 35 .83, 84 .4, 208 271 129 149 149 181 285 82
Melo-Maximo, V Mena, M Mencer, D Mendelev, M Mendis, B Meneghini, A Menezes, G Meng, D Menon, S Mente, P Mercer, H Merchant, N	336 118 35 83, 84 4, 208 271 129 149 181 285 82 82 108
Melo-Maximo, V Mena, M Mencer, D Mendelev, M Mendis, B Meneghini, A Menezes, G Meno, S Menon, S Mente, P Mercer, H Merchant, N Merkle, J	336 118 35 .83, 84 .4, 208 271 129 149 181 285 82 82 108 190
Melo-Maximo, V Mena, M Mencer, D Mendelev, M Mendis, B Meneghini, A Menezes, G Meng, D Menon, S Mente, P Mercer, H Merchant, N Merkle, J Merriman, C	336 118 35 .83, 84 .4, 208 271 129 149 149 181 82 108 190 170
Melo-Maximo, V Mena, M Mencer, D Mendelev, M Mendis, B Meneghini, A Menezes, G Meno, S Menon, S Mente, P Mercer, H Merchant, N Merkle, J	336 118 35 .83, 84 .4, 208 271 129 149 149 181 82 108 190 170
Melo-Maximo, V Mena, M Mencer, D Mendelev, M Mendis, B	336 118 35 .83, 84 .4, 208 271 129 149 181 285 82 108 100 170 83
Melo-Maximo, V Mena, M Mencer, D Mendelev, M Mendis, B Meneghini, A Menezes, G Meng, D Menon, S Mente, P Mercer, H Mercer, H Merchant, N Merkle, J Merriman, C Merry, J Meskers, C	336 118 35 .83, 84 .4, 208 271 129 149 181 285 82 108 190 170 83 259
Melo-Maximo, V Mena, M Mencer, D Mendelev, M Mendis, B Meneghini, A Menezes, G Meng, D Menon, S Mente, P Mercer, H Merchant, N Merkle, J Merriman, C Merry, J Meskers, C Meslin, E	336 118 35 .83, 84 .4, 208 271 129 149 181 285 82 108 190 170 83 259 .3, 264
Melo-Maximo, V Mena, M Mencer, D Mendelev, M Mendis, B Meneghini, A Menezes, G Meno, S Mente, P Mercer, H Merchant, N Merkle, J Merriman, C Merry, J Meskers, C Meslin, E	336 118 35 .83, 84 .4, 208 271 129 149 181 285 82 108 190 170 83 259 .3, 264 56
Melo-Maximo, V Mena, M Mencer, D Mendelev, M Mendis, B Meneghini, A Menezes, G Meno, S Mente, P Mercer, H Merchant, N Merkle, J Merriman, C Merry, J Meskers, C Meslin, E	336 118 35 .83, 84 .4, 208 271 129 149 181 285 82 108 190 170 83 259 .3, 264 56
Melo-Maximo, V Mena, M Mencer, D Mendelev, M Mendis, B Meneghini, A Menezes, G Meno, S Mente, P Mercer, H Merchant, N Merkle, J Merriman, C Merriman, C Merskers, C Meskiers, C Meskin, E	336 118 35 83, 84 4, 208 271 129 149 181 285 82 108 170 83 259 3, 264 56 270
Melo-Maximo, V Mena, M Mencer, D Mendelev, M Mendis, B Meneghini, A Menezes, G Menon, S Mente, P Mercer, H Merchant, N Merkle, J Merriman, C Merry, J Meskers, C Meskin, E	336 118 35 83, 84 4, 208 271 129 149 181 285 82 108 190 170 83 259 3, 264 56 270 293
Melo-Maximo, V Mena, M Mencer, D Mendelev, M Mendis, B Meneghini, A Meneghini, A Menezes, G Menon, S Mente, P Mercer, H Merchant, N Merkle, J Merriman, C Merry, J Meskers, C Meslin, E Mesylanoglu, O Meyer, A Meyer, J	336 118 35 83, 84 4, 208 271 129 149 181 285 82 108 190 70 73 3., 264 56 270 293 93
Melo-Maximo, V Mena, M Mencer, D Mendelev, M Mendis, B Meneghini, A Meneghini, A Menezes, G Menon, S Menon, S Merte, P Mercer, H Merchant, N Merkle, J Merriman, C Merry, J Meskers, C Meskers, C Mestin, E	336 118 35 83, 84 4, 208 271 129 149 181 285 82 108 190 70 70 259 270 293 93 93 93
Melo-Maximo, V Mena, M Mencer, D Mendelev, M Mendis, B Meneghini, A Meneghini, A Menezes, G Menon, S Mente, P Mercer, H Merchant, N Merkle, J Merriman, C Merry, J Meskers, C Meslin, E Mesylanoglu, O Meyer, A Meyer, J	336 118 35 83, 84 4, 208 271 129 149 181 285 82 108 190 70 70 259 270 293 93 93 93
Melo-Maximo, V Mena, M Mencer, D Mendelev, M Mendis, B Meneghini, A Meneghini, A Menegh, D Menon, S Mente, P Mercer, H Merchant, N Merkle, J Merriman, C Meskers, C Mesyll, H Meydanoglu, O Meyer, A Meyer, J Meyer, M Meyers, M 22, 29, 71, 79, 124, 132	336 118 35 83, 84 4, 208 271 129 149 181 285 82 108 190 70 70 259 3, 264 270 293 93 93 111 2, 175, 175,
Melo-Maximo, V Mena, M Mencer, D Mendelev, M Mendis, B Meneghini, A Meneghini, A Menezes, G Menon, S Menon, S Merte, P Mercer, H Merchant, N Merkle, J Merriman, C Merriman, C Meskers, C Meslin, E	336 118 35 83, 84 4, 208 271 129 129 149 181 285 82 108 190 70 259 259 270 293 93 93 93 93 111 2, 175, 3, 243,
Melo-Maximo, V Mena, M Mencer, D Mendelev, M Mendis, B Meneghini, A Meneghini, A Menezes, G Menezes, G Menon, S Mente, P Mercer, H Merchant, N Merkle, J Merriman, C Merriman, C Meskers, C Meskers, C Meslin, E	336 118 35 83, 84 4, 208 271 129 129 149 181 285 82 108 190 70 259 .3, 264 270 293 93 93 111 2, 175, 3, 243, 8, 357
Melo-Maximo, V Mena, M Mencer, D Mendelev, M Mendis, B Meneghini, A Meneghini, A Merele, B Merele, H Merele, H Merele, J Merriman, C Merry, J Meskers, C Meslini, E Meslini, E Meslini, E Meslini, E Meyer, A Meyer, A Meyer, T Meyers, M Meyer, T Meyers, M Meyer, 330, 333 Meyyappan, M	336 118 35 .83, 84 .4, 208 271 129 129 181 285 82 108 190 170 83 259 i3, 264 56 270 93 111 2, 175, 3, 243, 357 16
Melo-Maximo, V Mena, M Mencer, D Mendelev, M Mendis, B Meneghini, A Meneghini, A Menezes, G Menezes, G Menon, S Mente, P Mercer, H Merchant, N Merkle, J Merriman, C Merriman, C Meskers, C Meskers, C Meslin, E	336 118 35 .83, 84 .4, 208 271 129 129 181 285 82 108 190 170 83 259 i3, 264 56 270 93 111 2, 175, 3, 243, 357 16
Melo-Maximo, V Mena, M Mencer, D Mendelev, M Mendis, B Meneghini, A Menezes, G Meng, D Menon, S Mene, P Mercer, H Mercr, H Merchant, N Merkle, J Merriman, C Merry, J Meskers, C Meslin, E Meskers, C Meslin, E Meyer, A Meyer, A Meyer, T Meyer, M Meyer, M	336 118 35 .83, 84 .4, 208 271 129 149 181 285 282 108 190 170 83 259 .3, 264 270 293 93 111 2, 175, 3, 243, 38, 357 16 258
Melo-Maximo, V Mena, M Mencer, D Mendelev, M Mendis, B Meneghini, A Meneghini, A Meneghini, A Meneres, G Menno, S Mente, P Mercer, H Merriman, C Merry, J Meskers, C Meskin, E Metwally, H Meyer, A Meyer, T 22, 29, 71, 79, 124, 132 271, 284, 294, 295, 330, 33 Meyappan, M Meza García, E	336 118 35 .83, 84 .4, 208 271 129 149 181 285 82 108 190 170 83 259 .3, 264 270 293 93 111 2, 175, 3, 243, 357 16 258 108
Melo-Maximo, V Mena, M Mencer, D Mendelev, M Mendis, B Meneghini, A Meneghini, A Menezes, G Meng, D Mener, P Mercer, H Merchant, N Merkle, J Merriman, C Meskers, C Mesklin, E Meydanoglu, O Meyer, A Meyer, T Meyers, M	336 118 35 .83, 84 .4, 208 271 129 129 129 285 225 259 259 259 270 293 293 93 111 2, 175, 3, 243,16 258 108 100
Melo-Maximo, V Mena, M Mencer, D Mendelev, M Mendis, B Meneghini, A Meneghini, A Meneghini, A Meneres, G Menno, S Mente, P Mercer, H Merriman, C Merry, J Meskers, C Meskin, E Metwally, H Meyer, A Meyer, T 22, 29, 71, 79, 124, 132 271, 284, 294, 295, 330, 33 Meyappan, M Meza García, E	336 118 35 .83, 84 .4, 208 271 129 129 129 285 225 259 259 259 270 293 293 93 111 2, 175, 3, 243,16 258 108 100
Melo-Maximo, V Mena, M Mencer, D Mendelev, M Mendis, B Meneghini, A Meneghini, A Menezes, G Meng, D Mener, P Mercer, H Merchant, N Merkle, J Merriman, C Meskers, C Mesklin, E Meydanoglu, O Meyer, A Meyer, T Meyers, M	336 118 35 .83, 84 .4, 208 271 129 129 129 129 285 282 108 190 170 83 259 293 93 111 2, 175, 3, 243, 16 258 108 100 336
Melo-Maximo, V Mena, M Mencer, D Mendelev, M Mendis, B Meneghini, A Meneghini, A Menezes, G Menno, S Mente, P Mercer, H Merchant, N Merkle, J Merriman, C Mery, J Meskers, C Mesklin, E Meydanoglu, O Meyer, T Meyers, M	336 118 35 .83, 84 .4, 208 271 129 129 129 129 108 100 336 93 93 93 93 93 93 93 93 93 93 93 108 93 94 93
Melo-Maximo, V Mena, M Mencer, D Mendelev, M Mendis, B Meneghini, A Meneghini, A Menezes, G Menno, S Mente, P Mercer, H Merchant, N Merkle, J Mertiman, C Mery, J Meskers, C Mesklin, E Meydanoglu, O Meyer, T Meyers, M	336 118 35 .83, 84 .4, 208 271 129 129 129 129 108 100 336 259 93 93 93 111 2, 175, 3, 243, 357 108 108 100 336 310 336 310 336 310 336 310 336 310 336 336 310 336
Melo-Maximo, V Mena, M Mencer, D Mendelev, M Mendis, B Meneghini, A Meneghini, A Menezes, G Menno, S Mente, P Mercer, H Merchant, N Merkle, J Merriman, C Mery, J Meskers, C Mesklin, E Meydanoglu, O Meyer, T Meyers, M	336 118 35 .83, 84 .4, 208 271 129 129 149 181 285 108 108 259 .3, 264 270 293 111 2, 175, 3 2, 243, 357 108 258 108 258 108 336 336 108 336 108 336 108



Mihalkovic, M	360
Mikhail, Y	94
Mikula, A	
Miles, M1	34 247
Miller, D	160
Miller, E	354
Miller, F	25. 74
Miller, J1	42, 349
Miller, M27, 52, 53, 66,	06 120
	316. 321
Miller, W	
Millett, J2	94 295
Mills, M44, 51, 105, 106, 107, 1	54, 156,
	12 220
Millwater, H	350
Milne, W	
Minakshi, M	311
Mindivan, H2	270. 348
Mingdao, W	
Minguett, J	
Minich, R	133
Minor, A	
Minoux, E	117
Miodownik, M	
Miodownik, P	205
Miotto, P	245
Miracle, D25, 74, 226, 235, 236, 2	55 332
Willacle, D	.55, 552
Mirkovic, D	309
Mishin, Y44,	
Mishra, A	218
Mishra, B1	67 225
Mishra, C	230
Mishra, R25, 74, 82	82 02
	28, 235,
	941, 342
Migro A 121 211 215 2	26 356
Misra, A121, 211, 215, 3	20, 350
Misra, D2	276, 285
Misra, D2	276, 285
Misra, D	276, 285 233, 354
Misra, D	276, 285 233, 354 171
Misra, D	276, 285 233, 354 171
Misra, D	276, 285 233, 354 171 180
Misra, D	276, 285 233, 354 171 180 300
Misra, D	276, 285 233, 354 171 180 300
Misra, D	276, 285 233, 354 171 180 300 311
Misra, D	276, 285 233, 354 171 180 300 311 100
Misra, D	276, 285 233, 354 171 180 300 311 100
Misra, D	276, 285 233, 354 171 180 300 311 100 93
Misra, D	276, 285 233, 354 171 180 300 311 100 93
Misra, D	276, 285 233, 354 171 180 300 311 100 93 229
Misra, D 2 Misra, M 125, 2 Missalla, M 125, 2 Missori, S 125, 2 Mistretta, M 125, 2 Mistretta, K 125, 2 Mistretta, M 125, 2 Mistretta, K 125, 2 Mistretta, M 125, 2 Mistretta, M 125, 2 Mistretta, M 125, 2 Mittal, N 125, 2 Miura-Fujiwara, E 12 Miwa, K 12	276, 285 233, 354 171 180 300 311 100 93 229 .25, 143
Misra, D 2 Misra, M 125, 2 Missalla, M 125, 2 Missori, S 125, 2 Mistretta, M 125, 2 Mistretta, K 125, 2 Mistretta, M 125, 2 Mistretta, K 125, 2 Mistretta, M 125, 2 Mistretta, M 125, 2 Mistretta, M 125, 2 Mittal, N 125, 2 Miura-Fujiwara, E 12 Miwa, K 12	276, 285 233, 354 171 180 300 311 100 93 229 .25, 143
Misra, D 2 Misra, M 125, 2 Missalla, M 125, 2 Missori, S 125, 2 Mistretta, M 125, 2 Mitchell, D 12 Mittal, V 12 Miura-Fujiwara, E 12 Miwa, K 12 Miyabe, Y 12	276, 285 233, 354 171 180 300 311 100 93 229 .25, 143 204
Misra, D 2 Misra, M 125, 2 Missalla, M 125, 2 Missori, S 125, 2 Mistretta, M 125, 2 Mistretta, M 10 Mitchell, D 10, 210, 2	276, 285 233, 354
Misra, D 2 Misra, M 125, 2 Missalla, M 125, 2 Missori, S 125, 2 Mistretta, M 125, 2 Mistretta, M 10 Mitchell, D 10, 210, 2	276, 285 233, 354
Misra, D 2 Misra, M 125, 2 Missalla, M 125, 2 Missori, S 125, 2 Mistretta, M 125, 2 Mistretta, M 10 Mitchell, D 10, 210, 2 Miyamura, T 110, 210, 2	276, 285 233, 354
Misra, D2Misra, M125, 2Missalla, M125, 2Missori, SMistretta, MMitchell, DMitsuishi, KMittal, VMitra-Fujiwara, EMiwa, KMiwa, KMiyabe, Y110, 210, 2Miyamura, TMizutani, U	276, 285 233, 354
Misra, D 2 Misra, M 125, 2 Missalla, M 125, 2 Missori, S 125, 2 Mistretta, M 125, 2 Mistretta, M 10 Mitchell, D 10, 210, 2 Miyamura, T 10 Mizutani, U 10	276, 285 233, 354
Misra, D 2 Misra, M 125, 2 Missalla, M 125, 2 Missori, S 125, 2 Mistretta, M Missori, S Mitrichell, D 10 Mitrua-Fujiwara, E 110, 210, 2 Miyake, M 110, 210, 2 Mizutani, U Mo, A	276, 285 233, 354
Misra, D 2 Misra, M 125, 2 Missalla, M 125, 2 Missori, S Mistretta, M Mitchell, D Mitsuishi, K Mittal, V Mitra-Fujiwara, E Miwa, K Miyabe, Y Miyake, M 110, 210, 2 Mizutani, U Mo, A Moat, R Moat, R	276, 285 233, 354
Misra, D 2 Misra, M 125, 2 Missalla, M 125, 2 Missori, S Mistretta, M Mitchell, D Mitsuishi, K Mittal, V Mitra-Fujiwara, E Miwa, K Miyabe, Y Miyake, M 110, 210, 2 Mizutani, U Mo, A Moat, R Moat, R	276, 285 233, 354
Misra, D2Misra, M125, 2Missalla, M125, 2Missori, SMistretta, MMitchell, DMitsuishi, KMitral, VMiura-Fujiwara, EMiwa, KMiyabe, YMiyabe, YMiyake, MMiyake, M110, 210, 2Mizutani, UMo, AMoat, RMoehwald, K	276, 285 233, 354
Misra, D2Misra, M125, 2Missalla, M125, 2Missori, SMistretta, MMitchell, DMitsuishi, KMittal, VMitra-Fujiwara, EMiwa, KMiyabe, YMiyabe, YMiyake, MMiyake, M110, 210, 2Mizutani, UMo, AMoat, R10	276, 285 233, 354
Misra, D2Misra, M125, 2Missalla, M125, 2Missori, SMistretta, MMitchell, DMitsuishi, KMittal, VMitra-Fujiwara, EMiwa, KMiyabe, YMiyabe, YMiyabe, YMiyake, M110, 210, 2Miyamura, TMizutani, UMoa, AMoat, RMoehwald, KMohajeri, N	276, 285 233, 354
Misra, D 2 Misra, M 125, 2 Missalla, M 125, 2 Missori, S 125, 2 Mistretta, M Mistretta, M Mitchell, D 10 Mitsuishi, K 110, 210, 2 Miyabe, Y 110, 210, 2 Miyaura, T Mizutani, U Moa, A Moat, R Moahageri, N 214, 2	276, 285 233, 354
Misra, D2Misra, M125, 2Missalla, M125, 2Missori, SMistretta, MMitchell, DMitsuishi, KMittal, VMitra-Fujiwara, EMiwa, KMiyabe, YMiyabe, YMiyabe, YMiyake, M110, 210, 2Miyamura, TMizutani, UMoa, AMoat, RMoehwald, KMohajeri, N	276, 285 233, 354
Misra, D 2 Misra, M 125, 2 Missalla, M 125, 2 Missori, S 125, 2 Mistretta, M Mistretta, M Mitchell, D 10 Mitsuishi, K 110, 210, 2 Miyabe, Y 110, 210, 2 Miyaura, T Mizutani, U Moat, R Moehwald, K Mohajeri, N 214, 2 Mohammed, A 214, 2	276, 285 233, 354
Misra, D 2 Misra, M 125, 2 Missalla, M 125, 2 Missori, S 125, 2 Mistretta, M Mistretta, M Mitchell, D 10 Mitsuishi, K 110, 210, 2 Miyabe, Y 110, 210, 2 Miyawara, T Mizutani, U Mo, A Moat, R Mohajeri, N 214, 2 Mohammed, A Mohan, P	276, 285 233, 354
Misra, D 2 Misra, M 125, 2 Missalla, M 125, 2 Missori, S 125, 2 Mistretta, M Mistretta, M Mitchell, D 10 Mitsuishi, K 110, 210, 2 Miyabe, Y 110, 210, 2 Miyaura, T Mizutani, U Moat, R Moehwald, K Mohajeri, N 214, 2 Mohammed, A 214, 2	276, 285 233, 354
Misra, D 2 Misra, M 125, 2 Missalla, M 125, 2 Missori, S 125, 2 Mistretta, M Mistretta, M Mitchell, D 10 Mitsuishi, K 110, 210, 2 Miyabe, Y 110, 210, 2 Miyaura, T Mizutani, U Moat, R Moat, R Mohajeri, N 214, 2 Mohammed, A 10 Mohandas, K 10	276, 285 233, 354
Misra, D2Misra, M125, 2Missalla, M125, 2Missori, SMistretta, MMitchell, DMitsuishi, KMitura-Fujiwara, EMiwa, KMiyabe, YMiyabe, YMiyake, M110, 210, 2Miyamura, TMizutani, UMoat, RMoat, RMohamed, F214, 2Mohammed, AMohanta, KMohanta, RMohanta, R	276, 285 233, 354
Misra, D 2 Misra, M 125, 2 Missalla, M 125, 2 Missori, S 125, 2 Missori, S Mistretta, M Mitchell, D 10 Mitsuishi, K 110, 210, 2 Miyabe, Y 110, 210, 2 Miyawara, T Miyaura, T Mizutani, U Moat, R Mohamed, K Mohamed, K Mohammed, A Mohanty, R Mohanty, R Mohanty, R	276, 285 233, 354
Misra, D 2 Misra, M 125, 2 Missalla, M 125, 2 Missori, S 125, 2 Missori, S Mistretta, M Mitchell, D 10 Mitsuishi, K 110, 210, 2 Miyabe, Y 110, 210, 2 Miyawara, T Miyaura, T Mizutani, U Moat, R Mohamed, K Mohamed, K Mohammed, A Mohanty, R Mohanty, R Mohanty, R	276, 285 233, 354
Misra, D 2 Misra, M 125, 2 Missalla, M 125, 2 Missori, S 125, 2 Missori, S Mistretta, M Mitretta, M Mitchell, D Mitsuishi, K Mittal, V Mitra-Fujiwara, E Miwa, K Miyabe, Y Miyabe, Y Miyake, M 110, 210, 2 Miyaura, T Mizutani, U Moat, R Moehwald, K Mohamed, F 214, 2 Mohanmed, A Mohanty, R Mohanty, R Mohanty, S	276, 285 233, 354
Misra, D 2 Misra, M 125, 2 Missalla, M 125, 2 Missori, S 125, 2 Missori, S Mistretta, M Mitchell, D 10 Mitsuishi, K 110, 210, 2 Miyabe, Y 110, 210, 2 Miyawara, T Miyaura, T Mizutani, U Moat, R Mohamed, K Mohamed, K Mohammed, A Mohanty, R Mohanty, R Mohanty, R	276, 285 233, 354
Misra, D2Misra, M125, 2Missalla, M125, 2Missori, SMistretta, MMitsvishi, SMittal, NMittal, VMittal, VMittal, VMittal, VMiwa, KMiyabe, YMiyabe, YMiyabe, YMiyake, M110, 210, 2Miyamura, TMizutani, UMo, AMoat, RMoehwald, KMohajeri, NMohamed, F214, 2Mohammed, AMohandas, KMohanty, RMoitra, AMokkapati, SMoldovan, P	276, 285 233, 354
Misra, D2Misra, M125, 2Missalla, M125, 2Missori, SMistretta, MMitchell, DMitsuishi, KMitura-Fujiwara, EMiwa, KMivabe, YMiyabe, YMiyabe, Y110, 210, 2Miyamura, TMizutani, UMo, AMoat, RMohamed, F214, 2Mohammed, AMohamed, AMohandas, KMohanty, RMoitar, AMokapati, SMolah, MMolah, M	$\begin{array}{c} 276, 285\\ 233, 354\\ \dots 171\\ \dots 180\\ \dots 300\\ \dots 311\\ \dots 100\\ \dots 93\\ 229\\ 225, 143\\ \dots 204\\ 289, 334\\ \dots 252\\ \dots 172\\ \dots 322\\ \dots 166\\ \dots 94\\ 271, 275\\ \dots 268\\ \dots 242\\ \dots 19\\ \dots 273\\ \dots 238\\ \dots 35\\ \end{array}$
Misra, D2Misra, M125, 2Missalla, M125, 2Missori, SMistretta, MMitsvishi, SMitsuishi, KMittal, VMitsuishi, KMittal, VMitra-Fujiwara, EMiwa, KMiyabe, YMiyabe, YMiyake, MMiyake, M110, 210, 2Miyamura, TMizutani, UMo, AMoat, RMoehwald, KMohamed, FMohamed, F214, 2Mohammed, AMohanty, RMohanty, RMoitra, AMoldovan, PMollah, MMoldov, DMolodov, D	$\begin{array}{c} 276, 285\\ 233, 354\\ \dots 171\\ \dots 180\\ \dots 300\\ \dots 311\\ \dots 100\\ \dots 93\\ \dots 229\\ 225, 143\\ \dots 204\\ 289, 334\\ \dots 252\\ \dots 172\\ \dots 322\\ \dots 166\\ \dots 94\\ 271, 275\\ \dots 296\\ \dots 268\\ \dots 57\\ \dots 242\\ \dots 19\\ \dots 273\\ \dots 238\\ \dots 35\\ \dots 46, 47\\ \end{array}$
Misra, D2Misra, M125, 2Missalla, M125, 2Missori, SMistretta, MMitsvishi, SMitsuishi, KMittal, VMitsuishi, KMittal, VMitra-Fujiwara, EMiwa, KMiyabe, YMiyabe, YMiyake, MMiyake, M110, 210, 2Miyamura, TMizutani, UMo, AMoat, RMoehwald, KMohamed, FMohamed, F214, 2Mohammed, AMohanty, RMohanty, RMoitra, AMoldovan, PMollah, MMoldov, DMolodov, D	$\begin{array}{c} 276, 285\\ 233, 354\\ \dots 171\\ \dots 180\\ \dots 300\\ \dots 311\\ \dots 100\\ \dots 93\\ \dots 229\\ 225, 143\\ \dots 204\\ 289, 334\\ \dots 252\\ \dots 172\\ \dots 322\\ \dots 166\\ \dots 94\\ 271, 275\\ \dots 296\\ \dots 268\\ \dots 57\\ \dots 242\\ \dots 19\\ \dots 273\\ \dots 238\\ \dots 35\\ \dots 46, 47\\ \end{array}$
Misra, D2Misra, M125, 2Missalla, M125, 2Missori, SMistretta, MMitsvishi, SMitsuishi, KMittal, VMitra-Fujiwara, EMiwa, KMiyabe, YMiyabe, YMiyabe, YMiyake, M110, 210, 2Miyamura, TMizutani, UMo, AMoat, RMohamed, F214, 2Mohammed, AMohandas, KMohanty, RMohanty, RMoldovan, PMollah, MMolodov, DMoloney, M	$\begin{array}{c} 276, 285\\ 233, 354\\ \dots 171\\ \dots 180\\ \dots 300\\ \dots 311\\ \dots 100\\ \dots 93\\ \dots 229\\ 225, 143\\ \dots 229\\ 225, 143\\ \dots 229\\ 225, 143\\ \dots 229\\ \dots 252\\ \dots 172\\ \dots 322\\ \dots 166\\ \dots 94\\ 171, 275\\ \dots 296\\ \dots 268\\ \dots 57\\ \dots 242\\ \dots 19\\ \dots 273\\ \dots 238\\ \dots 35\\ \dots 46, 47\\ \dots 307\\ \end{array}$
Misra, D2Misra, M125, 2Missalla, M125, 2Missori, SMistretta, MMitsvishi, SMitsuishi, KMittal, VMitsuishi, KMittal, VMitra-Fujiwara, EMiwa, KMiyabe, YMiyabe, YMiyake, MMiyake, M110, 210, 2Miyamura, TMizutani, UMo, AMoat, RMoehwald, KMohamed, FMohamed, F214, 2Mohammed, AMohanty, RMohanty, RMoitra, AMoldovan, PMollah, MMoldov, DMolodov, D	$\begin{array}{c} 276, 285\\ 233, 354\\ \dots 171\\ \dots 180\\ \dots 300\\ \dots 311\\ \dots 100\\ \dots 93\\ \dots 229\\ 225, 143\\ \dots 229\\ 225, 143\\ \dots 229\\ 225, 143\\ \dots 229\\ \dots 252\\ \dots 172\\ \dots 322\\ \dots 166\\ \dots 94\\ 171, 275\\ \dots 296\\ \dots 268\\ \dots 57\\ \dots 242\\ \dots 19\\ \dots 273\\ \dots 238\\ \dots 35\\ \dots 46, 47\\ \dots 307\\ \end{array}$
Misra, D2Misra, M125, 2Missalla, M125, 2Missori, SMistretta, MMitsretta, MMitchell, DMitsuishi, KMitral, VMiura-Fujiwara, EMiwa, KMiyabe, YMiyabe, YMiyake, M110, 210, 2Miyamura, TMizutani, UMo, AMoat, RMohamed, F214, 2Mohammed, AMohanda, KMohanty, RMohanty, RMoldovan, PMollah, MMoldov, DMoloney, MMonk, J1	$\begin{array}{c} 276, 285\\ 233, 354\\ \dots 171\\ \dots 180\\ \dots 300\\ \dots 311\\ \dots 100\\ \dots 93\\ \dots 229\\ 225, 143\\ \dots 229\\ 225, 143\\ \dots 204\\ 289, 334\\ \dots 33, 93\\ \dots 252\\ \dots 172\\ \dots 322\\ \dots 166\\ \dots 94\\ 711, 275\\ \dots 296\\ \dots 268\\ \dots 57\\ \dots 242\\ \dots 19\\ \dots 273\\ \dots 238\\ \dots 35\\ \dots 46, 47\\ \dots 307\\ 55, 337\\ \end{array}$
Misra, D2Misra, M125, 2Missalla, M125, 2Missori, SMistretta, MMitchell, DMitsuishi, KMitral, VMitra-Fujiwara, EMiwa, KMiyabe, YMiyabe, YMiyabe, YMiyake, M110, 210, 2Miyawara, TMizutani, UMo, AMoat, RMohamed, F214, 2Mohammed, AMohan, PMohanty, RMohanty, RMoldovan, PMoldovan, PMoldovan, PMoldovan, PMolah, MMoldovan, DMolantari, R1	$\begin{array}{c} 276, 285\\ 233, 354\\ \dots 171\\ \dots 180\\ \dots 300\\ \dots 311\\ \dots 100\\ \dots 93\\ \dots 229\\ 225, 143\\ \dots 204\\ 189, 334\\ \dots 33, 93\\ \dots 252\\ \dots 172\\ \dots 322\\ \dots 166\\ \dots 94\\ 171, 275\\ \dots 296\\ \dots 242\\ \dots 19\\ \dots 273\\ \dots 238\\ \dots 35\\ \dots 46, 47\\ \dots 307\\ 55, 337\\ 80, 339\\ \end{array}$
Misra, D2Misra, M125, 2Missalla, M125, 2Missori, SMistretta, MMitchell, DMitsuishi, KMitura-Fujiwara, EMiwa, KMiyabe, YMiyabe, YMiyake, M110, 210, 2Miyake, M110, 210, 2Miyahe, TMiyamura, TMizutani, UMo, AMoat, R214, 2Mohamed, F214, 2Mohammed, AMohan, PMohanty, RMohanty, RMoldovan, PMoldovan, PMollah, MMoldov, DMontanari, R1Monteiro, S56, 76, 129, 1	$\begin{array}{c} 276, 285\\ 233, 354\\ \dots 171\\ \dots 180\\ \dots 300\\ \dots 311\\ \dots 100\\ \dots 93\\ \dots 229\\ 225, 143\\ \dots 204\\ 189, 334\\ \dots 33, 93\\ \dots 252\\ \dots 172\\ \dots 322\\ \dots 166\\ \dots 94\\ 171, 275\\ \dots 296\\ \dots 242\\ \dots 19\\ \dots 273\\ \dots 238\\ \dots 35\\ \dots 46, 47\\ \dots 307\\ 55, 337\\ 80, 339\\ 79, 180, \end{array}$
Misra, D2Misra, M125, 2Missalla, M125, 2Missori, SMistretta, MMitchell, DMitsuishi, KMitral, VMitra-Fujiwara, EMiwa, KMiyabe, YMiyabe, YMiyabe, YMiyake, M110, 210, 2Miyawara, TMizutani, UMo, AMoat, RMohamed, F214, 2Mohammed, AMohan, PMohanty, RMohanty, RMoldovan, PMoldovan, PMoldovan, PMoldovan, PMolah, MMoldovan, DMolantari, R1	$\begin{array}{c} 276, 285\\ 233, 354\\ \dots 171\\ \dots 180\\ \dots 300\\ \dots 311\\ \dots 100\\ \dots 93\\ \dots 229\\ 225, 143\\ \dots 204\\ 189, 334\\ \dots 33, 93\\ \dots 252\\ \dots 172\\ \dots 322\\ \dots 166\\ \dots 94\\ 171, 275\\ \dots 296\\ \dots 242\\ \dots 19\\ \dots 273\\ \dots 238\\ \dots 35\\ \dots 46, 47\\ \dots 307\\ 55, 337\\ 80, 339\\ 79, 180, \end{array}$
Misra, D 2 Misra, M 125, 2 Missalla, M 125, 2 Missori, S Mistretta, M Mitsvishi, K Mitchell, D Mitra, V Mitra, Fujiwara, E Miwa, K Miyabe, Y Miyabe, Y Miyawara, T Miyake, M 110, 210, 2 Miyawara, T Miyamura, T Miyahe, M 110, 210, 2 Miyahe, Y Miyamura, T Miyahe, M 110, 210, 2 Mohan, K Mohand, R Mohamed, A Mohan, 2 Mohan, P 214, 2 Mohandas, K Mohand, R Mohanty, R Mohand, M Moldovan, P Mohand, M Molodov, D Mohand, M	$\begin{array}{c} 276, 285\\ 233, 354\\ \dots 171\\ \dots 180\\ \dots 300\\ \dots 311\\ \dots 100\\ \dots 93\\ \dots 229\\ 225, 143\\ \dots 229\\ 225, 143\\ \dots 204\\ 189, 334\\ \dots 33, 93\\ \dots 252\\ \dots 172\\ \dots 322\\ \dots 166\\ \dots 94\\ 271, 275\\ \dots 268\\ \dots 57\\ \dots 242\\ \dots 19\\ \dots 273\\ \dots 238\\ \dots 35\\ \dots 46, 47\\ \dots 307\\ 55, 337\\ 80, 339\\ 79, 180, 334, 335\\ \end{array}$
Misra, D2Misra, M125, 2Missalla, M125, 2Missori, SMistretta, MMitchell, DMitsuishi, KMitura-Fujiwara, EMiwa, KMiyabe, YMiyabe, YMiyake, M110, 210, 2Miyake, M110, 210, 2Miyahe, TMiyamura, TMizutani, UMo, AMoat, R214, 2Mohamed, F214, 2Mohamed, KMohanty, RMohanty, RMohanty, RMoldovan, PMoldovan, PMollah, MMoldov, DMontanari, R1Monteiro, S56, 76, 129, 1	$\begin{array}{c} 276, 285\\ 233, 354\\ \dots 171\\ \dots 180\\ \dots 300\\ \dots 311\\ \dots 100\\ \dots 93\\ \dots 229\\ 225, 143\\ \dots 229\\ 225, 143\\ \dots 204\\ 189, 334\\ \dots 33, 93\\ \dots 252\\ \dots 172\\ \dots 322\\ \dots 166\\ \dots 94\\ 271, 275\\ \dots 268\\ \dots 57\\ \dots 242\\ \dots 19\\ \dots 273\\ \dots 238\\ \dots 35\\ \dots 46, 47\\ \dots 307\\ 55, 337\\ 80, 339\\ 79, 180, 334, 335\\ \end{array}$

Moody, N37, 160, 249, 300	
Mook, W	
Moon, D	
Moon, J	
Moon, W Moore, E	
Moore, E Moran, J	
Morariu, M	
Moras, A	
Mordehai, D	
Mordike, B	
Moreno, H	
Moreno C., H	
Morgan, A	
Morgan, D	
Morgan, T	
Mori, G	
Mori, H	
Morisaku, K Morishige, T	
Morishita, M	
Morita, K	
Moriyama, M	
Morjan, I	
Morkovsky, P	
Morosin, B	
Morozov, A	
Morphett, A	
Morral, J	
Morris, A	
Morris, D	
Morris, J26, 7	
Morris, Jr., J	
Morris, R	
Morse, D	
Morse, D Morsi, K	
Morse, D Morsi, K Mortarino, G	
Morse, D Morsi, K Mortarino, G Mortensen, D	
Morse, D Morsi, K Mortarino, G Mortansen, D Mosher, D	
Morse, D Morsi, K Mortarino, G Mortensen, D Mosher, D Mosher, N	23 149 180 237 224 305
Morse, D Morsi, K Mortarino, G Mortensen, D Mosher, D Mosher, D Moskovich, N Moskovitch, N	23 149 180 237 224 309 194, 257
Morse, D Morsi, K Mortarino, G Mortensen, D Mosher, D Moskovich, N Moskovich, N Moskovitch, N	23 149 180 237 224 309
Morse, D Morsi, K Mortarino, G Mortensen, D Mosher, D Moskovich, N Moskovich, N Moskovitch, N Möslang, A Moss, S	23 149 180 237 224 309 194, 257 315
Morse, D Morsi, K Mortarino, G Mortensen, D Mosher, D Moskovich, N Moskovich, N Moskovitch, N Mossovitch, N Mossovitch, N Mossang, A Moss, S	23 149 180 237 224 309
Morse, D Morsi, K Mortarino, G Mortensen, D Mosher, D Moskovich, N Moskovich, N Moskovitch, N Mosso, S Mostafa, S Mothé, A	23 149 180 237 224 309
Morse, D Morsi, K Mortarino, G Mortensen, D Mosher, D Moskovich, N Moskovich, N Moskovitch, N Möslang, A Moss, S	23 149 180 237 224 309
Morse, D Morsi, K Mortarino, G Mortensen, D Mosher, D Moskovich, N Moskovich, N Moskovitch, N Moss, S Mostafa, S Motafa, S Mothé, A Motta, A Moura, R	23 149 180 237 224 309
Morse, D Morsi, K Mortarino, G Mortensen, D Mosher, D Moskovich, N Moskovitch, N Moskang, A Mostafa, S Mothé, A Motta, A Moura, R Mourao, M	22 149 180 237 224 309 194, 257 315 315 311 56 356 124 35
Morse, D Morsi, K Mortarino, G Mortensen, D Mosher, D Moskovich, N Moskovitch, N Möslang, A Möslang, A Mostafa, S Mothé, A Motta, A Motta, A Moura, R Mourao, M Mourer, D Moxnes, B	22 149 180 237 224 309 194, 257 315
Morse, D Morsi, K Mortarino, G Mortensen, D Mosher, D Moskovich, N Moskovitch, N Moskovitch, N Mostafa, S Mottafa, S Motta, A Moura, R Moura, M Mourao, M Mourer, D Moxnes, B Moxson, V	$\begin{array}{c} 22\\ 149\\ 180\\ 237\\ 224\\ 309\\ 194, 257\\ 315\\ 315\\ 316\\ 356\\ 124\\ 35\\ 229, 320\\ 71\\ 192\\ 229, 320\\ 71\\ 192\\ 229, 320\\ 71\\ 192\\ 35\\ 229, 320\\ 71\\ 192\\ 35\\ 229, 320\\ 71\\ 192\\ 35\\ 229, 320\\ 71\\ 192\\ 35\\ 35\\ 35\\ 35\\ 35\\ 35\\ 35\\ 35\\ 35\\ 35$
Morse, D Morsi, K Mortarino, G Mortensen, D Mosher, D Moskovich, N Moskovitch, N Moskovitch, N Mostafa, S Mostafa, S Mothé, A Motta, A Moura, R Mourao, M Mourao, M Mourae, B Moxson, V Moy, P	$\begin{array}{c} & & & & & & & & & & & & & & & & & & &$
Morse, D Morsi, K Mortarino, G Mortensen, D Mosher, D Moskovich, N Moskovitch, N Moskovitch, N Mostafa, S Mostafa, S Motta, A Moura, R Mourao, M Mourao, M Mourer, D Mouraes, B Moxson, V Moy, P Mubarok, Z	$\begin{array}{c} 22\\ 149\\ 180\\ 237\\ 224\\ 309\\ 194, 257\\ 315\\ 319\\ 356\\ 356\\ 124\\ 35\\ 229, 320\\ 71\\ 192\\ 229, 320\\ 71\\ 192\\ 140, 141, 254\\ 148\\ 35\\ 356\\ 356\\ 356\\ 356\\ 356\\ 356\\ 356\\$
Morse, D Morsi, K Mortarino, G Mortensen, D Mosher, D Moskovich, N Moskovitch, N Moskovitch, N Mostaga, A Mostafa, S Mothé, A Motta, A Moura, R Moura, R Mourao, M Mourao, M Mourer, D Moures, B Moxson, V Moy, P Mubarok, Z Muci Kuchler, K	$\begin{array}{c} 22\\ 149\\ 180\\ 237\\ 224\\ 309\\ 194, 257\\ 315\\ 39, 140, 303\\ 311\\ 566\\ 356\\ 124\\ 35\\ 229, 320\\ 71\\ 192\\ 140, 141, 254\\ 148\\ 187, 298\end{array}$
Morse, D Morsi, K Mortarino, G Mortensen, D Mosher, D Moskovich, N Moskovich, N Moskovitch, N Moskovitch, N Moskovitch, N Moskovitch, N Moskovitch, N Mostafa, S Mostafa, S Mostafa, S Mothé, A Motta, A Moura, R Moura, R Mourao, M Mourer, D Moxnes, B Moxson, V Moy, P Mubarok, Z Muci Kuchler, K	$\begin{array}{c} 22\\ 149\\ 180\\ 237\\ 224\\ 309\\ 194, 257\\ 315\\ 39, 140, 303\\ 311\\ 56\\ 356\\ 124\\ 35\\ 229, 320\\ 192\\ 140, 141, 254\\ 148\\ 187, 298\\ 298\\ 298\end{array}$
Morse, D Morsi, K Mortarino, G Mortensen, D Mosher, D Moskovich, N Moskovich, N Moskovitch, N Moskovitch, N Moskovitch, N Moskovitch, N Moskovitch, N Mostafa, S Mostafa, S Mostafa, S Mothé, A Motta, A Moura, R Moura, R Mourao, M Mourer, D Moxnes, B Moxson, V Moy, P Mubarok, Z Muci Kuchler, K Mucino, V Mucsi, G	$\begin{array}{c} 22\\ 149\\ 180\\ 237\\ 224\\ 309\\ 194, 257\\ 315\\ 39, 140, 303\\ 311\\ 56\\ 356\\ 124\\ 35\\ 229, 320\\ 192\\ 110\\ 192\\ 110\\ 192\\ 140, 141, 254\\ 148\\ 187, 298\\ 298\\ 56\\ 56\\ 56\\ 56\\ 56\\ 56\\ 56\\ 56\\ 56\\ 56$
Morse, D Morsi, K Mortarino, G Mortensen, D Mosher, D Moskovich, N Moskovich, N Moskovitch, N Moskovitch, N Moskovitch, N Moskovitch, N Moskovitch, N Moskov, S Mostafa, S Mostafa, S Mothé, A Motta, A Mouta, A Moura, R Moura, R Moura, B Moxnes, B Moxson, V Moy, P Mubarok, Z Muci Kuchler, K Mucino, V Mucsi, G Mudryk, Y	$\begin{array}{c} 22\\ 149\\ 180\\ 237\\ 224\\ 309\\ 194, 257\\ 315\\ 39, 140, 303\\ 311\\ 56\\ 356\\ 124\\ 32\\ 229, 320\\ 71\\ 192\\ 140, 141, 254\\ 187, 298\\ 298\\ 298\\ 56\\ 56\\ 76\\ 76\\ 76\\ 76\\ 76\\ 76\\ 76\\ 76\\ 76\\ 7$
Morse, D Morsi, K Mortarino, G Mortensen, D Mosher, D Moskovich, N Moskovich, N Moskovitch, N Moskovitch, N Moskovitch, N Moskovitch, N Moskovitch, N Moskov, S Mostafa, S Mostafa, S Motta, A Motta, A Moura, R Moura, R Moura, R Moura, M Mourer, D Mourer, D Moxnes, B Moxson, V Moy, P Mubarok, Z Muci Kuchler, K Mucino, V Mucis, G Mudryk, Y Mueller, W	$\begin{array}{c} 22\\ 149\\ 180\\ 237\\ 224\\ 309\\ 194, 257\\ 315\\ 89, 140, 303\\ 311\\ 56\\ 356\\ 124\\ 32\\ 229, 320\\ 140, 141, 254\\ 187\\ 298\\ 229, 320\\ 71\\ 192\\ 140, 141, 254\\ 187\\ 298\\ 298\\ 56\\ 76\\ 351\\ 351\\ 351\\ 351\\ 351\\ 351\\ 351\\ 351$
Morse, D Morsi, K Mortarino, G Mortensen, D Mosher, D Moskovich, N Moskovich, N Moskovitch, N Moskovitch, N Moskovitch, N Moskovitch, N Moskovitch, N Moss, S Mostafa, S Mostafa, S Motta, A Motta, A Mouta, A Moura, R Moura, R Moura, M Moura, B Moxnes, B Moxson, V Moy, P Mubarok, Z Muci Kuchler, K Mucino, V Mucsi, G Mudryk, Y Muga, L	$\begin{array}{c} 22\\ 149\\ 180\\ 237\\ 224\\ 309\\ 194, 257\\ 315\\ 39, 140, 303\\ 311\\ 56\\ 356\\ 124\\ 32\\ 229, 320\\ 140, 141, 254\\ 140\\ 141, 254\\ 140, 141, 254\\ 148\\ 187, 298\\ 298\\ 56\\ 56\\ 76\\ 351\\ 197\\ \end{array}$
Morse, D Morsi, K Mortarino, G Mortensen, D Mosher, D Moskovich, N Moskovich, N Moskovitch, N Mostafa, S Mostafa, S Motta, A Moura, R Moura, R Moura, R Moura, R Moura, B Mourer, D Moxnes, B Moxson, V Moy, P Musarok, Z Muci Kuchler, K Mucino, V Mucsi, G Mudryk, Y Muga, L Mughrabi, H	$\begin{array}{c} 22\\ 149\\ 149\\ 180\\ 237\\ 224\\ 309\\ 194\\ 257\\ 315\\ 319\\ 311\\ 56\\ 356\\ 124\\ 32\\ 229, 320\\ 71\\ 192\\ 229, 320\\ 71\\ 192\\ 140, 141, 254\\ 148\\ 187, 298\\ 298\\ 56\\ 76\\ 351\\ 197\\ 96\end{array}$
Morse, D Morsi, K Mortarino, G Mortarino, G Mortensen, D Mosher, D Mosher, D Moskovich, N Moskovich, N Moskovitch, N Moskovitch, N Moskovitch, A Mostafa, S Mostafa, S Mostafa, S Mostafa, S Mostafa, S Mostafa, S Motta, A Moura, R Moura, R Moura, R Moura, R Moura, R Moura, R Moura, R Moura, B Moura, B Moxson, V Moure, D Moxnes, B Moxson, V Moy, P Mubarok, Z Muci Kuchler, K Mucino, V Mucsi, G Mudryk, Y Mueller, W Muga, L Mughrabi, H Muhktar, A	$\begin{array}{c} 22\\ 149\\ 149\\ 149\\ 237\\ 224\\ 309\\ 194\\ 257\\ 319\\ 257\\ 319\\ 311\\ 56\\ 356\\ 124\\ 32\\ 229, 320\\ 71\\ 192\\ 140, 141, 254\\ 148\\ 187, 298\\ 298\\ 566\\ 76\\ 351\\ 197\\ 96\\ 272\\ 298\\ 298\\ 566\\ 76\\ 351\\ 197\\ 96\\ 272\\ 298\\ 298\\ 566\\ 76\\ 351\\ 197\\ 96\\ 272\\ 272\\ 272\\ 272\\ 272\\ 272\\ 272\\ 27$
Morse, D Morsi, K Mortarino, G Mortensen, D Mosher, D Moskovich, N Moskovich, N Moskovitch, N Moskovitch, S Mostafa, S Mothé, A Motta, A Moura, R Moura, R Moura, O M Moura, R Moura, B Moura, M Mourer, D Mourer, D Mourer, D Mourer, D Mouras, B Moxson, V Moy, P Mubarok, Z Mubarok, Z Muci Kuchler, K Mucino, V Muci, G Mudryk, Y Mueller, W Muga, L Muhktar, A Mukai, T	$\begin{array}{c} 22\\ 149\\ 149\\ 149\\ 237\\ 224\\ 309\\ 194\\ 257\\ 315\\ 319\\ 257\\ 315\\ 319\\ 257\\ 315\\ 319\\ 257\\ 315\\ 315\\ 315\\ 315\\ 315\\ 315\\ 315\\ 315$
Morse, D Morsi, K Mortarino, G Mortarino, G Mortensen, D Mosher, D Mosher, D Moskovich, N Moskovich, N Moskovitch, N Moskovitch, N Moskovitch, A Mostafa, S Mostafa, S Mostafa, S Mostafa, S Mostafa, S Mostafa, S Motta, A Moura, R Moura, R Moura, R Moura, R Moura, R Moura, R Moura, R Moura, B Moura, B Moxson, V Moure, D Moxnes, B Moxson, V Moy, P Mubarok, Z Muci Kuchler, K Mucino, V Mucsi, G Mudryk, Y Mueller, W Muga, L Mughrabi, H Muhktar, A	$\begin{array}{c} 22\\ 149\\ 149\\ 149\\ 237\\ 224\\ 309\\ 224\\ 309\\ 194, 257\\ 315\\ 319\\ 257\\ 315\\ 319\\ 257\\ 315\\ 319\\ 311\\ 56\\ 356\\ 124\\ 35\\ 229, 320\\ 124\\ 35\\ 229, 320\\ 124\\ 35\\ 229, 320\\ 124\\ 35\\ 229, 320\\ 124\\ 35\\ 229, 320\\ 124\\ 35\\ 356\\ 356\\ 356\\ 351\\ 197\\ 96\\ 272\\ 2, 184, 196, 308, 352\\ 98\\ 352\\ 98\\ 352\\ 98\\ 352\\ 98\\ 352\\ 98\\ 352\\ 98\\ 352\\ 98\\ 352\\ 98\\ 352\\ 98\\ 352\\ 98\\ 352\\ 98\\ 352\\ 98\\ 352\\ 98\\ 352\\ 98\\ 352\\ 98\\ 352\\ 352\\ 352\\ 352\\ 352\\ 352\\ 352\\ 352$
Morse, D Morsi, K Mortarino, G Mortanino, G Mosher, D. Mosher, D. Moskovich, N. Moskovitch, N. Moskovitch, N. Moskovitch, S. Mostafa, S Mostafa, S Mothé, A. Motta, A. Moura, R. Moura, R. Moura, M. Moura, R. Moura, M. Mourer, D. Mourer, D. Mourer, D. Mourer, D. Mourer, D. Mourer, D. Mourer, D. Mourer, D. Mourer, D. Moura, R. Mourao, M. Mourer, D. Mourer, D. Mourer, D. Mourer, D. Mourer, D. Muser, B. Muser, B. Muser, C. Muci Kuchler, K. Mucino, V. Mucino, V. Mucino, V. Mucino, V. Mucino, V. Mucino, V. Mucino, V. Mucino, V. Mucher, E. Mughrabi, H. Muhktar, A. Mukherjee, A. Mukherjee, A.	$\begin{array}{c} 22\\ 149\\ 149\\ 149\\ 237\\ 224\\ 309\\ 224\\ 309\\ 219\\ 219\\ 219\\ 219\\ 219\\ 219\\ 219\\ 21$
Morse, D Morsi, K Mortarino, G Mortensen, D Mosher, D Moskovich, N Moskovich, N Moskovitch, N Moskovitch, S Mostafa, S Mothé, A Motta, A Moura, R Moura, R Moura, R Moura, M Moura, B Moura, M Mourer, D Mourer, D Mourer, D Mourer, D Mourer, D Mourer, C Muciner, C Mubarok, Z Muci Kuchler, K Mucino, V Mucino, V Mucino, V Mucino, V Mucino, V Muchal, G Mughrabi, H Mukai, T	$\begin{array}{c} 22\\ 149\\ 149\\ 149\\ 149\\ 224\\ 309\\ 224\\ 309\\ 224\\ 309\\ 219\\ 219\\ 219\\ 219\\ 219\\ 229\\ 229\\ 320\\ 124\\ 35\\ 229\\ 320\\ 124\\ 35\\ 229\\ 320\\ 124\\ 35\\ 229\\ 320\\ 119\\ 35\\ 229\\ 320\\ 124\\ 35\\ 229\\ 320\\ 124\\ 140\\ 141\\ 254\\ 148\\ 187\\ 298\\ 298\\ 566\\ 76\\ 351\\ 197\\ 966\\ 272\\ 2184\\ 196\\ 308\\ 352\\ 98\\ 272\\ 2184\\ 196\\ 308\\ 352\\ 98\\ 272\\ 2184\\ 196\\ 352\\ 98\\ 272\\ 2184\\ 196\\ 352\\ 98\\ 272\\ 326\\ 358\\ 360\\ 166\\ 352\\ 98\\ 272\\ 326\\ 358\\ 360\\ 166\\ 352\\ 360\\ 360\\ 360\\ 360\\ 360\\ 360\\ 360\\ 360$

Mullis, A	
Mumcu, G	
Munroe, P	
Muppidi, T	
Muraguchi, M	
Murakami, H	
Murakami, M	
Murakumo, T	
Murashkin, M	
Murch, G	
Murphy, J	
Murphy, K	
Murphy, T	
Murr, L	117, 132, 176, 183, 185
Murty, G	
Murty, K	
Murugan, R	
Murugesan, S	64
Muschinski, A	
Musz, E	
Muthubandara, N	
Myrvold, E	

Ν

Nabarro, F272
Nabiev, I161
Nadella, R237
Nadtochy, A71
Naeth, O
Nafisi, S179
Nag, A
Nag, S
Nagai, T
Nagaraj, B209
Nagasako, N52
Nagem, N
Nagy, P179
Nahshon, K
Naik, R
Nair, A
Naixiang, F233, 296, 341
Nakai, M
Nakajima, H63
Nakamura, R63
Nakanishi, T43
Nakano, Y
,
Nakano, Y
Nakayama, T43, 361 Nalamasu, O64
Nakayama, T43, 361 Nalamasu, O64 Namboothiri, S173
Nakayama, T
Nakayama, T
Nakayama, T
Nakayama, T 43, 361 Nalamasu, O 64 Namboothiri, S 173 Namilae, S 223, 251 Nan, H 350 Nancollas, G 23 Nandiraju, D 249
Nakayama, T 43, 361 Nalamasu, O 64 Namboothiri, S 173 Namilae, S 223, 251 Nan, H 350 Nancollas, G 23 Nandiraju, D 249 Nandy, T 156
Nakayama, T
Nakayama, T 43, 361 Nalamasu, O 64 Namboothiri, S 173 Namilae, S 223, 251 Nan, H 350 Nancollas, G 23 Nandiraju, D 249 Nandy, T 156 Nanstad, R 190, 317 Napolitano, R 37, 85, 188, 249,
Nakayama, T 43, 361 Nalamasu, O 64 Namboothiri, S 173 Namilae, S 223, 251 Nan, H 350 Nancollas, G 23 Nandiraju, D 249 Nandy, T 156 Nanstad, R 190, 317 Napolitano, R 37, 85, 188, 249,
Nakayama, T 43, 361 Nalamasu, O 64 Namboothiri, S 173 Namilae, S 223, 251 Nan, H 350 Nancollas, G 23 Nandiraju, D 249 Nandy, T 156 Nanstad, R 190, 317 Napolitano, R 37, 85, 188, 249,
Nakayama, T 43, 361 Nalamasu, O 64 Namboothiri, S 173 Namilae, S 223, 251 Nan, H 350 Nancollas, G 23 Nandiraju, D 249 Nandy, T 156 Nanstad, R 190, 317 Napolitano, R 37, 85, 188, 249,
Nakayama, T 43, 361 Nalamasu, O 64 Namboothiri, S 173 Namilae, S 223, 251 Nan, H 350 Nancollas, G 23 Nandiraju, D 249 Nandy, T 156 Nanstad, R 190, 317 Napolitano, R 37, 85, 188, 249, 290, 300, 345, 346 Narayan, J Narayan, R 163, 222, 271 Narayan, R 163, 284, 285 Narayan, G 123
Nakayama, T 43, 361 Nalamasu, O 64 Namboothiri, S 173 Namilae, S 223, 251 Nan, H 350 Nancollas, G 23 Nandiraju, D 249 Nandy, T 156 Nanstad, R 190, 317 Napolitano, R 37, 85, 188, 249, 290, 300, 345, 346 Narayan, J Narayan, R 163, 222, 271 Narayan, R 163, 284, 285 Narayana, G 123 Narayanan, R 78
Nakayama, T 43, 361 Nalamasu, O 64 Namboothiri, S 173 Namilae, S 223, 251 Nan, H 350 Nancollas, G 23 Nandiraju, D 249 Nandy, T 156 Nanstad, R 190, 317 Napolitano, R 37, 85, 188, 249, 290, 300, 345, 346 290, 300, 345, 346 Narayan, J 55, 62, 109, 116, 163, 222, 271 Narayan, R 163, 284, 285 Narayana, G 123 Narayanan, R 78 Narita, H 87
Nakayama, T 43, 361 Nalamasu, O 64 Namboothiri, S 173 Namilae, S 223, 251 Nan, H 350 Nancollas, G 23 Nandiraju, D 249 Nandy, T 156 Nanstad, R 190, 317 Napolitano, R 37, 85, 188, 249, 290, 300, 345, 346 200, 3045, 346 Narayan, J 55, 62, 109, 116, 163, 222, 271 Narayan, R 163, 284, 285 Narayana, G 123 Narayanan, R 78 Narita, H 87 Naritsuka, S 55
Nakayama, T 43, 361 Nalamasu, O 64 Namboothiri, S 173 Namilae, S 223, 251 Nan, H 350 Nancollas, G 23 Nandiraju, D 249 Nandy, T 156 Nanstad, R 190, 317 Napolitano, R 37, 85, 188, 249, 290, 300, 345, 346 300, 345, 346 Narayan, J 55, 62, 109, 116, 163, 222, 271 Narayan, R 163, 284, 285 Narayana, R 78 Narita, H 87 Naritsuka, S 55 Narukawa, Y 162
Nakayama, T 43, 361 Nalamasu, O 64 Namboothiri, S 173 Namilae, S 223, 251 Nan, H 350 Nancollas, G 23 Nandiraju, D 249 Nandy, T 156 Nanstad, R 190, 317 Napolitano, R 37, 85, 188, 249, 290, 300, 345, 346 200, 3045, 346 Narayan, J 55, 62, 109, 116, 163, 222, 271 Narayan, R 163, 284, 285 Narayana, G 123 Narayanan, R 78 Narita, H 87 Naritsuka, S 55



Nashat, A193
Natesan, K110
Nath, A
Nathenson, D
Naumov, 1
Navdenkin, E
Nayuta, M
Nazarbooland, A
Nazon, J180, 182
Neale, K92
Neelameggham, N
Neeraj, T207
Neil, C
Nelson, B248
Nelson, T134, 186, 247, 248, 341
Nenseter, B
Neri, M
Ness, D
Ness, D
Neu, C
Neu, R147
Neubauer, E18
Neuber, D25
Neuefeind, J
Neumann, D
Newberry, P214
Newbery, A
Newey, M
Neyrey, K
Ng, B
Ng, G
Nguven, D
Nguyen, K125
Nguyen, K
Nguyen, K
Nguyen, K
Nguyen, K. 125 Nguyen, T. 283 Nguyen-Manh, D. 27, 52 Nguyen-Thi, H. 85, 188 Nicholson, D. 47, 192, 286 Nie, J. 352 Nie, Z. 189, 198
Nguyen, K
Nguyen, K. 125 Nguyen, T. 283 Nguyen-Manh, D. 27, 52 Nguyen-Thi, H. 85, 188 Nicholson, D. 47, 192, 286 Nie, J. 352 Nie, Z. 189, 198 Niederberger, C. 32 Niedling, J. 333
Nguyen, K. 125 Nguyen, T. 283 Nguyen-Manh, D. 27, 52 Nguyen-Thi, H. 85, 188 Nicholson, D. 47, 192, 286 Nie, J. 352 Nie, Z. 189, 198 Niederberger, C. 32 Niedling, J. 333 Nieh, T. 73
Nguyen, K. 125 Nguyen, T. 283 Nguyen-Manh, D. 27, 52 Nguyen-Thi, H. 85, 188 Nicholson, D. 47, 192, 286 Nie, J. 352 Nie, Z. 189, 198 Niederberger, C. 32 Niedling, J. 333 Nieh, T. 73 Nigam, A. 164 Niihara, K. 361
Nguyen, K. 125 Nguyen, T. 283 Nguyen-Manh, D. 27, 52 Nguyen-Thi, H 85, 188 Nicholson, D. 47, 192, 286 Nie, J 352 Nie, Z 189, 198 Niederberger, C 32 Niedling, J. 333 Nieh, T 73 Nigam, A 164 Niinomi, M. 306
Nguyen, K. 125 Nguyen, T. 283 Nguyen-Manh, D 27, 52 Nguyen-Thi, H 85, 188 Nicholson, D 47, 192, 286 Nie, J 352 Nie, Z 189, 198 Niederberger, C 32 Niediling, J 333 Nieh, T 73 Nigam, A 164 Niinomi, M. 306 Nikles, D 164
Nguyen, K. 125 Nguyen, T. 283 Nguyen-Manh, D. 27, 52 Nguyen-Thi, H. 85, 188 Nicholson, D. 47, 192, 286 Nie, J. 352 Nie, Z. 189, 198 Niederberger, C. 32 Niedling, J. 333 Nieh, T. 73 Nigam, A. 164 Niinomi, M. 306 Nikles, D. 164 Ning, B. 208
Nguyen, K. 125 Nguyen, T. 283 Nguyen-Manh, D. 27, 52 Nguyen-Thi, H. 85, 188 Nicholson, D. 47, 192, 286 Nie, J. 352 Nie, Z. 189, 198 Niederberger, C. 32 Niedling, J. 333 Nieh, T. 73 Nigam, A. 164 Niing, B. 208 Ningileri, S. 69, 172, 230, 269
Nguyen, K. 125 Nguyen, T. 283 Nguyen-Manh, D. 27, 52 Nguyen-Thi, H. 85, 188 Nicholson, D. 47, 192, 286 Nie, J. 352 Nie, Z. 189, 198 Niederberger, C. 32 Niedling, J. 333 Nieh, T. 73 Nigam, A. 164 Niihara, K. 306 Nikles, D. 164 Ning, B. 208 Ningileri, S. 69, 172, 230, 269 Ningthoujam, R. 164, 222
Nguyen, K. 125 Nguyen, T. 283 Nguyen-Manh, D. 27, 52 Nguyen-Thi, H. 85, 188 Nicholson, D. 47, 192, 286 Nie, J. 352 Nie, Z. 189, 198 Niederberger, C. 32 Niedling, J. 333 Nieh, T. 73 Nigam, A. 164 Niing, B. 208 Ningileri, S. 69, 172, 230, 269
Nguyen, K. 125 Nguyen, T. 283 Nguyen-Manh, D. 27, 52 Nguyen-Thi, H. 85, 188 Nicholson, D. 47, 192, 286 Nie, J 352 Nie, Z 189, 198 Niederberger, C 32 Niedling, J. 333 Nieh, T 73 Nigam, A. 164 Niinomi, M. 306 Nikles, D 164 Ning, B 208 Ningileri, S 69, 172, 230, 269 Ningthoujam, R. 164, 222 Nino, J 100 Nishimiya, Y 167 Nishimura, T 265
Nguyen, K. 125 Nguyen, T. 283 Nguyen-Manh, D. 27, 52 Nguyen-Thi, H. 85, 188 Nicholson, D. 47, 192, 286 Nie, J 352 Nie, Z 189, 198 Niederberger, C. 32 Niedling, J. 333 Nieh, T 73 Nigam, A. 164 Niinomi, M. 306 Nikles, D 164 Ning, B 208 Ningthoujam, R. 164, 222 Nino, J 100 Nishimiya, Y. 167 Nishimura, T. 265 Nishizuka, K. 162
Nguyen, K. 125 Nguyen, T. 283 Nguyen-Manh, D. 27, 52 Nguyen-Thi, H. 85, 188 Nicholson, D. 47, 192, 286 Nie, J 352 Nie, Z 189, 198 Niederberger, C 32 Niedling, J. 333 Nieh, T 73 Nigam, A. 164 Niinomi, M. 306 Nikles, D. 164 Ning, B 208 Ningileri, S 69, 172, 230, 269 Ningileri, S 69, 172, 230, 269 Ninshimura, T 167 Nishimura, T 265 Nishizuka, K 162 Nix, W 159
Nguyen, K. 125 Nguyen, T. 283 Nguyen-Manh, D. 27, 52 Nguyen-Thi, H. 85, 188 Nicholson, D. 47, 192, 286 Nie, J 352 Nie, Z 189, 198 Niederberger, C 32 Niedling, J. 333 Nieh, T 73 Nigam, A. 164 Niinomi, M. 306 Nikles, D. 164 Ning, B. 208 Ningileri, S. 69, 172, 230, 269 Ningthoujam, R. 164, 222 Ninshimura, T 205 Nishizuka, K. 162 Nix, W. 159 Nixon, M. 243
Nguyen, K. 125 Nguyen, T. 283 Nguyen-Manh, D. 27, 52 Nguyen-Thi, H. 85, 188 Nicholson, D. 47, 192, 286 Nie, J 352 Nie, Z 189, 198 Niederberger, C 32 Niedling, J. 333 Nieh, T 73 Nigam, A. 164 Niinomi, M. 306 Nikles, D. 164 Ning, B. 208 Ningileri, S. 69, 172, 230, 269 Ningthoujam, R. 164, 222 Nins, J. 100 Nishimura, T 265 Nishizuka, K. 162 Nix, W. 159 Nixon, M. 243 Niyomwas, S. 200
Nguyen, K. 125 Nguyen, T. 283 Nguyen-Manh, D. 27, 52 Nguyen-Thi, H. 85, 188 Nicholson, D. 47, 192, 286 Nie, J. 352 Nie, Z. 189, 198 Niederberger, C. 32 Niedling, J. 333 Nieh, T. 73 Nigam, A. 164 Niinomi, M. 306 Nikles, D. 164 Ning, B. 208 Ningileri, S. 69, 172, 230, 269 Ningthoujam, R. 164, 222 Nino, J. 100 Nishimiya, Y. 167 Nishimura, T. 265 Nishizuka, K. 162 Nix, W. 159 Nixon, M. 243 Niyomwas, S. 200 Nobuhiro, I. 148
Nguyen, K. 125 Nguyen, T. 283 Nguyen-Manh, D. 27, 52 Nguyen-Thi, H. 85, 188 Nicholson, D. 47, 192, 286 Nie, J 352 Nie, Z 189, 198 Niederberger, C 32 Niedling, J. 333 Nieh, T 73 Nigam, A. 164 Niinomi, M. 306 Nikles, D. 164 Ning, B. 208 Ningileri, S. 69, 172, 230, 269 Ningthoujam, R. 164, 222 Nins, J. 100 Nishimura, T 265 Nishizuka, K. 162 Nix, W. 159 Nixon, M. 243 Niyomwas, S. 200
Nguyen, K. 125 Nguyen, T. 283 Nguyen-Manh, D 27, 52 Nguyen-Thi, H 85, 188 Nicholson, D 47, 192, 286 Nie, J 352 Nie, Z 189, 198 Niederberger, C 32 Niediling, J. 333 Nieh, T 73 Nigam, A 164 Ning, B 208 Ningileri, S 69, 172, 230, 269 Ningthoujam, R 164, 222 Nino, J 100 Nishimura, T 265 Nishizuka, K 162 Nix, W 159 Nixon, M 243 Niyomwas, S 200 Nobuhiro, I 148 Noda, T 255 Noebe, R 189 Nogaret, T 48
Nguyen, K. 125 Nguyen, T. 283 Nguyen-Manh, D 27, 52 Nguyen-Thi, H 85, 188 Nicholson, D 47, 192, 286 Nie, J 352 Nie, Z 189, 198 Niederberger, C 32 Niedling, J. 333 Nieh, T 73 Nigam, A 164 Niinomi, M 306 Nikles, D 164 Ning, B 208 Ningileri, S 69, 172, 230, 269 Ningthoujam, R 164, 222 Nino, J 100 Nishimura, T 265 Nishimura, T 265 Nishizuka, K 162 Nix, W 159 Nixon, M 243 Niyomwas, S 200 Nobuhiro, I 148 Noda, T 255 Noegaret, T 48 Nogita, K 112, 179, 264, 265
Nguyen, K. 125 Nguyen, T. 283 Nguyen-Manh, D 27, 52 Nguyen-Thi, H 85, 188 Nicholson, D 47, 192, 286 Nie, J 352 Nie, Z 189, 198 Niederberger, C 32 Niedling, J. 333 Nieh, T 73 Nigam, A 164 Nihara, K 361 Ninomi, M 306 Nikles, D 164 Ning, B 208 Ningileri, S 69, 172, 230, 269 Ningthoujam, R 164, 222 Nino, J 100 Nishimura, T 265 Nishimura, T 265 Nishiruka, K 162 Nix, W 159 Nixon, M 243 Niyomwas, S 200 Nobuhiro, I 148 Noda, T 255 Noebe, R 189 Nogaret, T 48 Nogita, K 112, 179, 264, 265 Nogueira, A 35
Nguyen, K. 125 Nguyen, T. 283 Nguyen-Manh, D 27, 52 Nguyen-Thi, H 85, 188 Nicholson, D 47, 192, 286 Nie, J 352 Nie, Z 189, 198 Niederberger, C 32 Niedling, J. 333 Nieh, T 73 Nigam, A 164 Niinomi, M 306 Nikles, D 164 Ning, B 208 Ningileri, S 69, 172, 230, 269 Ningthoujam, R 164, 222 Nino, J 100 Nishimura, T 265 Nishimura, T 265 Nishizuka, K 162 Nix, W 159 Nixon, M 243 Niyomwas, S 200 Nobuhiro, I 148 Noda, T 255 Noegaret, T 48 Nogita, K 112, 179, 264, 265

Noldin, J	
Noori, A	
Nordlund, K	
Norfleet, D	
Northwood, D	
Norton, D	33, 62, 344, 359
Norton, M	
Noskova, N	
Nossa, J	
Notten, P	
Novichkov, S	55
Nowell, M	
Noy, A	
Nuhfer, N	
Nunna, R	
Nutt, S	
Nyberg, E	
Nychka, J	
Nyilas, K	
•	

0

O'Brien, C24	0
O'Brien, K	
O'Brien, S	
O'Connell, S	
Obata, T	
Obbard, R7	
Oberebt, C	
Oberembt, C29	
Oberson, P34	
Ochsner, A7	
Ode, M20)9
Odeshi, A	80
Odette, G263, 264, 314, 31	6
Odunuga, S20	
Oehring, M21	2
Ogale, S14	
Ogata, S178, 28	
Ogata, Y	
Ogawa, M25	
Oginuma, H	
Oh, B	
Oh, C	
Oh, K150, 154, 186, 205, 31	
Oh, Y	
Oh-ishi, K	
Ohishi, K	
Ohkubo, T	
Ohnaka, K	
Ohnuma, I104, 204, 26	
Ohriner, E	
Ohshima, K25	
Ohtsuka, H4	
Oja, M	33
Okabe, T25, 75, 90, 128, 14	
Okamoto, K92, 186, 247, 29	
Oki, S	
Oktay, G17	
Okuniewski, M31	6
Oleinikov, V16	51
Oliver, E	0
Oliver, W12	
Olmsted, D	
Olsen, E	
Olson, D	
Olson, G	
Omotunde, A	
Omran, A	
Оппш, л	,0

Omura, N	25, 143
Onishi, T	246
Onodera, H	209
Opalka, S	
Opeil, C	136
Oppedal, A	20
Orchard, H	205
Ordaz, G	42
Oren, E	
Orme, C	23
Oro, D	
Ortega, U	
Ortiz, C	
Ortiz, M	155, 227
Osborn, W	197
Osborne, M	
Osborne, R	91
Osetskiy, Y	
Osetsky, Y	201, 203, 355
Oshida, Y	233
Osman, T	40
Osvaldo, F	86
Otaki, M	
Ott, R	236, 357
Ou, K	234, 330
Ouellet, B	124
Ouimet, L	91
Ou Yang, F	206
Ovcharenko, A	
Ovid'ko, I	160
Ovrelid, E	166
Owens, A	
Owolabi, G	
Øye, H	81, 340
Ozawa, T	
Ozkan, C	
Ozolins, V	
Ozsoy, I	299

Р

D 1 0 041
Packer, S
Paclawski, K209
Padgett, C216, 219
Padilla, H29
Padilla, R148
Padture, N
Pal, S
Palacio, H
Palandage, K274
Palanisamy, P
Palit, D
Palkowski, H45, 66
Palmer, M40
Pan, F
Pan, J60
Pan, T
Pan, X
Pan, Y28, 42, 43, 94, 234, 330
Panat, R
Pandey, A17, 65, 81, 118, 167, 225, 277, 285
Pandey, R
Pangan, A
Panico, M
Pantleon, W20, 267
Pao. C
Pao, P
Papadimitrakopoulos, F16
Papillon, F49
Papis, K
т цръз, тх00, 88



Pappas, N47
Pareige, C
Pareige, P
Parga, J
Parida, S
Parisi, A
Park, C40, 51, 190, 361
Park, D
Park, E73, 177, 319
Park, G102
Park, H22
Park, J
Park, K
Park, M50, 62, 115, 116, 162, 221
Park, N
Park, S19, 70, 138, 145, 186, 204, 247, 345
Park, W16, 144, 145, 346
Park, Y
Parker, D112
Parkison, A42
Parmar, B
Parra, M
Parra Garcia, M95, 340
Parsa, M
Parsey, J54, 108
Parthasarathy, T
Pashkovski, E125
Pate, T
Patel, J
Patel, M
Patil, S268, 286, 287
Patnaik, A
Patterson, B
Patwardhan, D
Patz, T
Paul, J
D 1 D 170
Paul. R
Paul, R
Paulino, L

	26, 94, 121, 229, 255, 312
· · · · · · · · · · · · · · · · · · ·	
Phillpot, S	
Pietrzyk, M	
Ping, L	
Pingin, V	
Pinkerton, A	
Pinto, E	
Pinzhin, Y	
Pitek, F	
11/	31, 83, 84, 86, 135, 188
· · · · · · · · · · · · · · · · · · ·	
Pollcok, T	
	156, 294, 307, 310, 312, 352 214
Pomykala Jr., J	
Pontin, M	

Porto, S124
Posada, M247
Potesser, M138
Potirniche, G
Pouchon, M95
Poulsen, H267
Pouly, P
Powell, A40, 97, 303, 307, 349
Powell, B91, 310
Pownceby, M185
Pozuelo, M65
Pradhan, D90
Prado, F110
Prado, J
Prajapati, B109
Prakash, V
Prasad, J
Prasad, R
Prasad, S
Prasanna Kumar, T
Prask, H
Prater, J
Pratt, L
Preble, E
Preston, D
Presuel-Moreno, F
Preuss, M
Price, D
Price, N
Pritchard, P
Proffen, T
Prorok, B
Proshkin, A
Proudhon, H
Proulx, G124
Proust, G
Provatas, N
Puech, S
Puga, C
Pulikollu, R
Pun, G
Purohit, Y
Purushotham, S
Pusateri, J
Pushparaj, V64
Pusiparaj, v
Pusztai, 1
Puthucode, A
Puzyrev, 1
Fysiikiii, S

Q

Qi, F	
Qi, L	
Qian, L	
Qian, M	[143
Qiao, B	
Qiao, L	
Qing, L	
Qingcai	, L
Qiu, G	
Qiu, K	
Qiu, R	
Qiu, S	
Qiu, T	
Qiu, Z	
Qu, X	



Quach, D	99, 182, 359
Quast, J	
Querin, J	
Quick, N	
Quinta da Fonseca, J	20
Quintino, L	134

R

R-Raissi, A93
Raab, G215, 216
Raabe, D45, 228
Raber, T197
Rablbauer, R
Rachmat, R
Rack, P
Radhakrishnan, B68, 223, 251, 312
Radiguet, B
Radosavljevic, S
Radosavljevic-Mihajlovic, A
Rae, C
Rae, P183, 251
Raetzke, K293
Raghunathan, S
Rahbar, N
Rais-Rohani, M256
Raissi, A276
Raiszadeh, R
Raj, S
Raja, K
Rajan, K40, 256
Rajeev, K
Rajendran, A
Rajulapati, K
Rakovich, Y220
Ramachandran, S109, 116
Ramakrishna, S
Rama Murty, G277
Ramanujan, R114, 284
Ramar, A
Ramasamy, K94
Ramaswami, J
Ramaswami, J
Ramaswami, J
Ramaswami, J
Ramaswami, J 232 Ramesh, K 79, 113, 140, 183, 216, 243 Ramirez, A 143 Ramirez, J 86 Ramírez, J 328
Ramaswami, J 232 Ramesh, K 79, 113, 140, 183, 216, 243 Ramirez, A 143 Ramirez, J 86 Ramírez, J 328 Rammohan, A 73
Ramaswami, J 232 Ramesh, K 79, 113, 140, 183, 216, 243 Ramirez, A 143 Ramirez, J 86 Ramírez, J 328 Rammohan, A 73 Rämö, J 80
Ramaswami, J 232 Ramesh, K 79, 113, 140, 183, 216, 243 Ramirez, A 143 Ramirez, J 86 Ramírez, J 328 Rammohan, A 73 Rämö, J 80 Ramusat, C 208
Ramaswami, J 232 Ramesh, K 79, 113, 140, 183, 216, 243 Ramirez, A 143 Ramirez, J 86 Ramírez, J 328 Rammohan, A 73 Rämö, J 80
Ramaswami, J 232 Ramesh, K 79, 113, 140, 183, 216, 243 Ramirez, A 143 Ramirez, J 86 Ramírez, J 328 Rammohan, A 73 Rämö, J 80 Ramusat, C 208 Ranganathan, S 23
Ramaswami, J 232 Ramesh, K 79, 113, 140, 183, 216, 243 Ramirez, A 143 Ramirez, J 86 Ramírez, J 328 Rammohan, A 73 Rämö, J 80 Ramusat, C 208 Ranganathan, S 23 Rangel, J 129, 290
Ramaswami, J 232 Ramesh, K 79, 113, 140, 183, 216, 243 Ramirez, A 143 Ramirez, J 86 Ramírez, J 328 Rammohan, A 73 Rämö, J 80 Ramusat, C 208 Ranganathan, S 23 Rangel, J 129, 290 Rao, K 90, 257
Ramaswami, J 232 Ramesh, K 79, 113, 140, 183, 216, 243 Ramirez, A 143 Ramirez, J 86 Ramírez, J 328 Rammohan, A 73 Rämö, J 80 Ramusat, C 208 Rangel, J 129, 290 Rao, K 90, 257 Rao, S 105, 266
Ramaswami, J 232 Ramesh, K 79, 113, 140, 183, 216, 243 Ramirez, A 143 Ramirez, J 86 Ramírez, J 328 Rammohan, A 73 Rämö, J 80 Ranusat, C 208 Ranganathan, S 23 Rangel, J 129, 290 Rao, K 90, 257 Rao, S 105, 266 Rao, W 239
Ramaswami, J 232 Ramesh, K 79, 113, 140, 183, 216, 243 Ramirez, A 143 Ramirez, J 86 Ramírez, J 328 Rammohan, A 73 Rämö, J 80 Ranganathan, S 23 Rangel, J 129, 290 Rao, K 90, 257 Rao, S 105, 266 Rao, W 239 Rasch, B 127
Ramaswami, J 232 Ramesh, K 79, 113, 140, 183, 216, 243 Ramirez, A 143 Ramirez, J 86 Ramírez, J 328 Rammohan, A 73 Rämö, J 80 Ranusat, C 208 Ranganathan, S 23 Rangel, J 129, 290 Rao, K 90, 257 Rao, S 105, 266 Rao, W 239
Ramaswami, J 232 Ramesh, K 79, 113, 140, 183, 216, 243 Ramirez, A 143 Ramirez, J 86 Ramírez, J 328 Rammohan, A 73 Rämö, J 80 Ranganathan, S 23 Rangel, J 129, 290 Rao, K 90, 257 Rao, S 105, 266 Rao, W 239 Rasch, B 127
Ramaswami, J 232 Ramesh, K. 79, 113, 140, 183, 216, 243 Ramirez, A. 143 Ramirez, J 86 Ramfrez, J 328 Rammohan, A. 73 Rämö, J 80 Ramusat, C 208 Ranganathan, S 23 Rangel, J 129, 290 Rao, S 105, 266 Rao, W 239 Rasch, B 127 Rasty, J 312 Rathz, T 235, 302
Ramaswami, J 232 Ramesh, K. 79, 113, 140, 183, 216, 243 Ramirez, A. 143 Ramirez, J 86 Ramfrez, J 328 Rammohan, A. 73 Rämö, J 80 Ramganathan, S 23 Rangel, J 129, 290 Rao, S 105, 266 Rao, S 105, 266 Rao, W 239 Rasch, B 127 Rasty, J 312 Rathz, T 235, 302 Ratvik, A 30
Ramaswami, J 232 Ramesh, K. 79, 113, 140, 183, 216, 243 Ramirez, A. 143 Ramirez, J 86 Ramfrez, J 328 Rammohan, A. 73 Rämö, J 80 Ranganathan, S 23 Rangel, J 129, 290 Rao, K 90, 257 Rao, S 105, 266 Rao, W 239 Rasch, B 127 Rasty, J 312 Rathz, T 235, 302 Ratvik, A 30 Rauscher, M 162, 362
Ramaswami, J 232 Ramesh, K. 79, 113, 140, 183, 216, 243 Ramirez, A. 143 Ramirez, J 86 Ramfrez, J 328 Rammohan, A. 73 Rämö, J 80 Ranganathan, S 23 Rangel, J 129, 290 Rao, K 90, 257 Rao, S 105, 266 Rao, W 239 Rasch, B 127 Rasty, J 312 Rathz, T 235, 302 Ratvik, A 30 Rauscher, M 162, 362 Ravi, C 77
Ramaswami, J 232 Ramesh, K 79, 113, 140, 183, 216, 243 Ramirez, A 143 Ramirez, J 86 Ramfrez, J 328 Ramohan, A 73 Rämö, J 80 Ranusat, C 208 Ranganathan, S 23 Rangel, J 129, 290 Rao, K 90, 257 Rao, S 105, 266 Rao, W 239 Rasch, B 127 Rasty, J 312 Ratvik, A 30 Ratvik, A 30 Ravicher, M 162, 362 Ravi, C 77 Ravichandran, G 184
Ramaswami, J 232 Ramesh, K. 79, 113, 140, 183, 216, 243 Ramirez, A. 143 Ramirez, J 86 Ramfrez, J 328 Rammohan, A. 73 Rämö, J 80 Ranusat, C 208 Ranganathan, S 23 Rangel, J 129, 290 Rao, K 90, 257 Rao, S 105, 266 Rao, W 239 Rasch, B 127 Rasty, J 312 Ratvik, A 30 Rauscher, M 162, 362 Ravi, C 77 Ravichandran, G 184 Ravindra, N 54, 55, 108, 109, 149, 150
Ramaswami, J 232 Ramesh, K 79, 113, 140, 183, 216, 243 Ramirez, A 143 Ramirez, J 86 Ramfrez, J 328 Ramohan, A 73 Rämö, J 80 Ranusat, C 208 Ranganathan, S 23 Rangel, J 129, 290 Rao, K 90, 257 Rao, S 105, 266 Rao, W 239 Rasch, B 127 Rasty, J 312 Ratvik, A 30 Ratvik, A 30 Ravicher, M 162, 362 Ravi, C 77 Ravichandran, G 184
Ramaswami, J 232 Ramesh, K. 79, 113, 140, 183, 216, 243 Ramirez, A. 143 Ramirez, J 86 Ramfrez, J 328 Rammohan, A. 73 Rämö, J 80 Ranusat, C 208 Ranganathan, S 23 Rangel, J 129, 290 Rao, K 90, 257 Rao, S 105, 266 Rao, W 239 Rasch, B 127 Rasty, J 312 Ratvik, A 30 Rauscher, M 162, 362 Ravi, C 77 Ravichandran, G 184 Ravindra, N 54, 55, 108, 109, 149, 150
Ramaswami, J 232 Ramesh, K 79, 113, 140, 183, 216, 243 Ramirez, A 143 Ramirez, J 86 Ramfrez, J 328 Rammohan, A 73 Rämö, J 80 Ranusat, C 208 Ranganathan, S 23 Rangel, J 129, 290 Rao, K 90, 257 Rao, S 105, 266 Rao, W 239 Rasch, B 127 Rasty, J 312 Rathz, T 235, 302 Ratvik, A 30 Ravicher, M 162, 362 Ravi, C 77 Ravichandran, G 184 Ravindra, N 54, 55, 108, 109, 149, 150 Rawal, S 33 Rawlins, H. 148
Ramaswami, J 232 Ramesh, K. 79, 113, 140, 183, 216, 243 Ramirez, A. 143 Ramirez, J 86 Ramfrez, J 328 Rammohan, A. 73 Rämö, J 80 Ranganathan, S 23 Rangel, J. 129, 290 Rao, K 90, 257 Rao, S 105, 266 Rao, W 239 Rasch, B 127 Rasty, J 312 Ratik, A 30 Rauscher, M 162, 362 Ravi, C 77 Ravichandran, G 184 Ravindra, N 54, 55, 108, 109, 149, 150 Rawal, S 33 Rawlins, H. 148 Ray, R 45
Ramaswami, J 232 Ramesh, K. 79, 113, 140, 183, 216, 243 Ramirez, A. 143 Ramirez, J 86 Ramfrez, J 328 Ramohan, A. 73 Rämö, J 80 Ranusat, C 208 Ranganathan, S 23 Rangel, J. 129, 290 Rao, K 90, 257 Rao, S 105, 266 Rao, W 239 Rasch, B 127 Rasty, J 312 Rathz, T 235, 302 Ratvik, A 30 Rauscher, M 162, 362 Ravi, C 77 Ravichandran, G 184 Ravindra, N 54, 55, 108, 109, 149, 150 Rawal, S 33 Rawlins, H. 148 Ray, R 45 Ray, T 291
Ramaswami, J 232 Ramesh, K. 79, 113, 140, 183, 216, 243 Ramirez, A. 143 Ramirez, J 86 Ramfrez, J 328 Rammohan, A. 73 Rämö, J 80 Ramusat, C. 208 Rangel, J 129, 290 Rao, K 90, 257 Rao, S 105, 266 Rao, W 239 Rasch, B 127 Rasty, J 312 Rathz, T. 235, 302 Ratvik, A 30 Rauscher, M 162, 362 Ravindra, N 54, 55, 108, 109, 149, 150 Rawal, S 33 Rawins, H. 148 Ray, R 45 Ray, T 291 Razavi, F 252
Ramaswami, J 232 Ramesh, K. 79, 113, 140, 183, 216, 243 Ramirez, A. 143 Ramirez, J 86 Ramfrez, J 328 Rammohan, A. 73 Rämö, J 80 Ramusat, C. 208 Ranganathan, S 23 Raog, J 129, 290 Rao, K 90, 257 Rao, S 105, 266 Rao, W 239 Rasch, B 127 Rasty, J 312 Rathz, T. 235, 302 Ratvik, A 30 Rauscher, M 162, 362 Ravi, C 77 Ravichandran, G 184 Ravindra, N 54, 55, 108, 109, 149, 150 Rawal, S 33 Rawins, H 148 Ray, R 45 Ray, T 291 Razavi, F 252 Read, C 42, 341
Ramaswami, J 232 Ramesh, K. 79, 113, 140, 183, 216, 243 Ramirez, A. 143 Ramirez, J 86 Ramfrez, J 328 Rammohan, A. 73 Rämö, J 80 Ramusat, C. 208 Rangel, J 129, 290 Rao, K 90, 257 Rao, S 105, 266 Rao, W 239 Rasch, B 127 Rasty, J 312 Rathz, T. 235, 302 Ratvik, A 30 Rauscher, M 162, 362 Ravindra, N 54, 55, 108, 109, 149, 150 Rawal, S 33 Rawins, H. 148 Ray, R 45 Ray, T 291 Razavi, F 252
Ramaswami, J 232 Ramesh, K. 79, 113, 140, 183, 216, 243 Ramirez, A. 143 Ramirez, J 86 Ramfrez, J 328 Rammohan, A. 73 Rämö, J 80 Ramusat, C. 208 Ranganathan, S 23 Raog, J 129, 290 Rao, K 90, 257 Rao, S 105, 266 Rao, W 239 Rasch, B 127 Rasty, J 312 Rathz, T. 235, 302 Ratvik, A 30 Rauscher, M 162, 362 Ravi, C 77 Ravichandran, G 184 Ravindra, N 54, 55, 108, 109, 149, 150 Rawal, S 33 Rawins, H 148 Ray, R 45 Ray, T 291 Razavi, F 252 Read, C 42, 341

Rebak, R	
Reddy, A	
Reddy, M	
Reddy, N4	
Reddy, R	90, 94, 174, 350
Reddy, S	
Redkin, A	
Reed, B	
Reed, R52, 53, 106, 15	
Reiche, P	
Reichelson, J Reid, D	
Reimanis, I	
Reinhart, G	
Reinhart, W	
Reinovsky, R	
Reis, A	
Reis, S	
Reisgen, U	
Reiso, O	
Reizine, F	
Remington, B	
Remmel, J	145
Ren, B	
Ren, F54,	55, 62, 108, 344
Ren, J	
Ren, R	
Ren, W	
Ren, X	
Ren, Y	
Reno, R	
Rest, J	
Reuter, M	
Reutzel, S	
Rex, S	
Reynolds, A	
Reynolds, B	
Reynolds, B Reynolds, W	
Reynolds, B Reynolds, W Rezvanian, O	
Reynolds, B Reynolds, W Rezvanian, O Rhee, H	
Reynolds, B Reynolds, W Rezvanian, O Rhee, H Rhim, W	
Reynolds, B Reynolds, W Rezvanian, O Rhee, H	
Reynolds, B Reynolds, W Rezvanian, O Rhee, H Rhim, W Riani, J. Rice, J.	
Reynolds, B Reynolds, W Rezvanian, O Rhee, H Rhim, W Riani, J	
Reynolds, B Reynolds, W Rezvanian, O Rhee, H Rhim, W Riani, J. Rice, J.	
Reynolds, B Reynolds, W Rezvanian, O Rhee, H Rhim, W Riani, J Rice, J Richard, C	
Reynolds, B Reynolds, W Rezvanian, O Rhee, H Rhim, W Riani, J. Rice, J. Richard, C. Richards, V. Richardson, H.	297 179 146 169 312 24 34 135 71 148, 324 161
Reynolds, B Reynolds, W Rezvanian, O Rhee, H Rhim, W Riani, J. Rice, J. Richard, C. Richards, V. Richardson, H. Richardson, I.	
Reynolds, B Reynolds, W Rezvanian, O Rhee, H Rhim, W Riani, J Rice, J Richard, C Richards, V Richardson, H Richardson, I Richardson, J	297 179 146 169 312 24 34 135 71 148, 324 161 346 236, 332
Reynolds, B Reynolds, W Rezvanian, O Rhee, H. Rhim, W. Riani, J. Rice, J. Richard, C. Richards, V. Richardson, H. Richardson, I. Richardson, J. Richardson, J. Richard, A.	$\begin{array}{c} & & & & & & \\ & & & & & & \\ & & & & & $
Reynolds, B Reynolds, W Rezvanian, O Rhee, H. Rhim, W. Riani, J. Rice, J. Richard, C. Richards, V. Richardson, H. Richardson, I. Richardson, J. Richardson, J. Richter, A. Richter, M.	$\begin{array}{c} & & & 297 \\ & & & 179 \\ & & & 146 \\ & & & 169 \\ & & & 312 \\ & & & & 24 \\ & & & & & 34 \\ & & & & & 135 \\ & & & & & & 71 \\ & & & & & 148, 324 \\ & & & & & & 161 \\ & & & & & & 346 \\ & & & & & & & & 326 \\ & & & & & & & & & & 100 \\ & & & & & & & & & & & 235 \end{array}$
Reynolds, B Reynolds, W Rezvanian, O Rhee, H Rhim, W Richard, J Richard, C Richards, V Richardson, H Richardson, I Richardson, J Richter, A Richter, M Richter, R	$\begin{array}{c} & & & & & & \\ & & & & & & \\ & & & & & $
Reynolds, B Reynolds, W Rezvanian, O Rhee, H Rhim, W Richard, J Richard, C Richards, V Richardson, H Richardson, I Richardson, J Richter, A Richter, R Richter, R	$\begin{array}{c} & & & & & & & \\ & & & & & & & \\ & & & & & & & \\ & & & & & & & \\ & & & & & & & \\ & & & & & & & \\ & & & & & & & \\ & & & & & & & \\ & & & & & & & \\ & & & & & & & \\ & & & & & & & \\ & & & & & & & \\ & & & & & & & \\ & & & & & & & \\ & & & & & & & \\ & & & & & & & \\ & & & & & & & \\ & & & & & & & \\ & & & & & & & \\ & & & & & \\ &$
Reynolds, B Reynolds, W Rezvanian, O Rhee, H Rhim, W Riani, J Richard, C Richards, V Richardson, H Richardson, I Richardson, J Richter, A Richter, R Richter, R Ricker, R Rickman, J	$\begin{array}{c} & & & & & & & \\ & & & & & & \\ &$
Reynolds, B Reynolds, W Rezvanian, O Rhee, H Rhim, W Riani, J Rice, J Richard, C Richards, V Richardson, H Richardson, I Richardson, J Richter, A Richter, A Richter, R Richter, R Rickman, J Rideout, C	$\begin{array}{c}$
Reynolds, B Reynolds, W Rezvanian, O Rhee, H Rhim, W Riani, J Rice, J Richard, C Richards, V Richardson, H Richardson, I Richardson, J Richter, A Richter, A Richter, R Richter, R Ricker, R Rickman, J Rideout, C Ried, P	$\begin{array}{c}$
Reynolds, B Reynolds, W Rezvanian, O Rhee, H Rhim, W Riani, J Rice, J Richard, C Richards, V Richardson, H Richardson, I Richardson, J Richter, A Richter, A Richter, R Richter, R Ricker, R Rickman, J Rideout, C Rieken, J	$\begin{array}{c}$
Reynolds, B Reynolds, W Rezvanian, O Rhee, H Rhim, W Riani, J Richard, C Richards, V Richardson, H Richardson, I Richardson, J Richter, A Richter, A Richter, R Richter, R Ricker, R Ricker, R Ricken, J Rideout, C Rieken, J Rigsbee, M	$\begin{array}{c}$
Reynolds, B Reynolds, W Rezvanian, O Rhee, H Rhim, W Riani, J. Rice, J. Richard, C. Richards, V Richardson, H. Richardson, I. Richardson, J. Richter, A. Richter, A. Richter, R. Richter, R. Ricker, R. Rickman, J. Rideout, C. Rieken, J. Rigsbee, M	$\begin{array}{c} & & & & & & & & & & & & & & & & & & &$
Reynolds, B Reynolds, W Rezvanian, O Rhee, H Rhim, W. Riani, J. Rice, J. Richard, C. Richards, V. Richardson, H. Richardson, I. Richardson, J. Richardson, J. Richter, A. Richter, R. Richter, R. Rickter, R. Ricker, R. Rickman, J. Ricken, J. Rigsbee, M. 21 Rijkeboer, A.	$\begin{array}{c} & & & & & & & & & & & & & & & & & & &$
Reynolds, B Reynolds, W Rezvanian, O Rhee, H Rhim, W. Riani, J. Rice, J. Richard, C. Richards, V. Richardson, H. Richardson, I. Richardson, J. Richardson, J. Richter, A. Richter, R. Richter, R. Rickter, R. Ricker, R. Ricker, R. Ricken, J. Rigsbee, M. 21 Rijkeboer, A. Rijssenbeek, J.	$\begin{array}{c} & & & & & & & & & & & & & & & & & & &$
Reynolds, B Reynolds, W Rezvanian, O Rhee, H. Rhim, W. Riani, J. Rice, J. Richard, C. Richardson, H. Richardson, H. Richardson, I. Richardson, J. Richardson, J. Richter, A. Richter, R. Richter, R. Rickter, R. Ricker, R. Ricker, R. Ricken, J. Rideout, C. Rieken, J. Rigsbee, M. Sigsbee, M. Rijkeboer, A. Rijssenbeek, J. Rimoli, J.	$\begin{array}{c} & & & & & & & & & & & & & & & & & & &$
Reynolds, B Reynolds, W Rezvanian, O Rhee, H. Rhim, W. Riani, J. Rice, J. Richard, C. Richards, V. Richardson, H. Richardson, I. Richardson, J. Richardson, J. Richter, A. Richter, R. Richter, R. Rickter, R. Ricker, R. Ricker, R. Ricker, R. Ricken, J. Rideout, C. Ried, P. Rieken, J. Rigsbee, M. Sigsbee, M. Rijssenbeek, J. Rimoli, J. Rinaldi, A.	$\begin{array}{c} & & & & & & & & & & & & & & & & & & &$
Reynolds, B Reynolds, W Rezvanian, O Rhee, H. Rhim, W. Riani, J. Rice, J. Richards, V. Richardson, H. Richardson, I. Richardson, J. Richardson, J. Richter, A. Richter, R. Richter, R. Rickter, R. Ricker, R. Ricker, R. Ricker, R. Ricken, J. Rideout, C. Ried, P. Rieken, J. Rigsbee, M. Sigsbee, M. Rijssenbeek, J. Rimoli, J. Rinaldi, A. Rinck, M.	$\begin{array}{c} & & & & & & & & & & & & & & & & & & &$
Reynolds, B Reynolds, W Rezvanian, O Rhee, H. Rhim, W. Riani, J. Rice, J. Richard, C. Richards, V. Richardson, H. Richardson, I. Richardson, J. Richter, A. Richter, A. Richter, R. Richter, R. Ricker, R. Ricker, R. Ricker, R. Ricken, J. Rideout, C. Ried, P. Rieken, J. Rigsbee, M. Rigsbee, M. Rijksenbeek, J. Rimoli, J. Rinaldi, A. Rinck, M. Rinderer, B.	$\begin{array}{c} & & & & & & & & & & & & & & & & & & &$
Reynolds, B Reynolds, W Rezvanian, O Rhee, H. Rhim, W. Riani, J. Rice, J. Richard, C. Richards, V. Richardson, H. Richardson, I. Richardson, J. Richardson, J. Richter, A. Richter, A. Richter, R. Rickter, R. Ricker, R. Ricker, R. Ricker, R. Ricken, J. Rideout, C. Ried, P. Rieken, J. Rigsbee, M. Rijssenbeek, J. Rimoli, J. Rinaldi, A. Rinderer, B. Rios, P.	$\begin{array}{c} & & & & & & & & & & & & & & & & & & &$
Reynolds, B Reynolds, W Rezvanian, O Rhee, H. Rhim, W. Riani, J. Rice, J. Richard, C. Richards, V Richardson, H. Richardson, I. Richardson, J. Richardson, J. Richter, A. Richter, A. Richter, R. Rickter, R. Ricker, R. Ricker, R. Ricker, R. Ricken, J. Rideout, C. Ried, P. Rieken, J. Rigsbee, M. Rijssenbeek, J. Rijssenbeek, J. Rimoli, J. Rinaldi, A. Rinck, M. Rinderer, B. Riout, F	$\begin{array}{c} & & & & & & & & & & & & & & & & & & &$
Reynolds, B Reynolds, W Rezvanian, O Rhee, H. Rhim, W. Riani, J. Rice, J. Richard, C. Richards, V. Richardson, H. Richardson, I. Richardson, I. Richardson, J. Richter, A. Richter, A. Richter, R. Richter, R. Ricker, R. Ricker, R. Ricken, J. Rideout, C. Ried, P. Rieken, J. Rigsbee, M. Rijssenbeek, J. Rimoli, J. Rimoli, J. Rinaldi, A. Rinck, M. Rinderer, B. Riout, F. Ripley, E.	$\begin{array}{c} & & & & & & & & & & & & & & & & & & &$
Reynolds, B Reynolds, W Rezvanian, O Rhee, H Rhim, W. Riani, J. Rice, J. Richard, C. Richards, V. Richardson, H. Richardson, I. Richardson, I. Richardson, J. Richter, A. Richter, A. Richter, R. Richter, R. Ricker, R. Ricker, R. Ricker, R. Ricker, R. Ricken, J. Rideout, C. Ried, P. Rieken, J. Rigsbee, M. 21 Rijkeboer, A. Rijkeboer, A. Rijkeboer, A. Rijkeboer, A. Rimoli, J. Rimoli, J. Rimoli, J. Rimoli, J. Rinaldi, A. Rinck, M. Rinderer, B. Rioult, F. Ripley, E. Riseborough, P.	$\begin{array}{c} & & & & & & & & & & & & & & & & & & &$
Reynolds, B Reynolds, W Rezvanian, O Rhee, H Rhim, W. Riani, J. Rice, J. Richard, C. Richards, V. Richardson, H. Richardson, I. Richardson, J. Richter, A. Richter, A. Richter, R. Richter, R. Rickter, R. Ricker, R. Ricker, R. Ricker, R. Ricker, J. Rigsbee, M. 21 Rijkeboer, A. Rijssenbeek, J. Rijssenbeek, J. Rimoli, J. Rimoli, J. Rimoli, J. Rinaldi, A. Rinck, M. Rinderer, B. Rios, P. Rioult, F. Riseborough, P. Ritchie, R.	$\begin{array}{c} & & & & & & & & & & & & & & & & & & &$
Reynolds, B Reynolds, W Rezvanian, O Rhee, H Rhim, W. Riani, J. Rice, J. Richard, C. Richards, V. Richardson, H. Richardson, I. Richardson, I. Richardson, J. Richter, A. Richter, A. Richter, R. Richter, R. Ricker, R. Ricker, R. Ricker, R. Ricker, R. Ricken, J. Rideout, C. Ried, P. Rieken, J. Rigsbee, M. 21 Rijkeboer, A. Rijkeboer, A. Rijkeboer, A. Rijkeboer, A. Rimoli, J. Rimoli, J. Rimoli, J. Rimoli, J. Rinaldi, A. Rinck, M. Rinderer, B. Rioult, F. Ripley, E. Riseborough, P.	$\begin{array}{c} & & & & & & & & & & & & & & & & & & &$

Rittel, D	
Ritter, C	124, 231
Ritter, G	
Rivard, J	
Riverin, J	
Rivero, R	
Riveros, G	
Rivière, C	
Rivolta, B	
Rizzi, G	
Rizzo, F	
Roalstad, J	
Robelin, C	
Roberts, S	
Robertson, C	48
Robertson, I29, 4	8, 203, 216, 355
Robertson, J	
Robertson, S	
Robinson, A	
Robles-Hernandez, F	
Robson, A	
Rocha, L	
Rockett, C	
Rodchanarowan, A	
Rodney, D	
Rodriguez, G	
Rodriguez, J	89
Rodriguez, R	
Rodriguez-Baracaldo, R	
Roe, C	
Roeder, R	
Roesler, J	
Rogach, A60, 11	
Rogers, J	
Rohatgi, P	
Rohrer, C	40
Rohrer, CRohrer, G44,	40 45, 49, 176, 349
Rohrer, C Rohrer, G44, Roldan Cuenya, B	40 45, 49, 176, 349 311
Rohrer, CRohrer, G44,	40 45, 49, 176, 349 311
Rohrer, CRohrer, G44, Roldan Cuenya, BRollett, A19	
Rohrer, C Rohrer, G	
Rohrer, C Rohrer, G	40 45, 49, 176, 349 311 9, 27, 69, 96, 97, 6, 227, 349, 354 30
Rohrer, C Rohrer, G	
Rohrer, CRohrer, G44, Roldan Cuenya, B Rollett, A19 	
Rohrer, CRohrer, G	
Rohrer, CRohrer, C	
Rohrer, CRohrer, G	
Rohrer, CRohrer, C	
Rohrer, C Rohrer, G	
Rohrer, C	40 45, 49, 176, 349 311 9, 27, 69, 96, 97, 6, 227, 349, 354 30 160, 217 35 311 256 85 309 246 97, 107, 350 90
Rohrer, C	40 45, 49, 176, 349 311 9, 27, 69, 96, 97, 6, 227, 349, 354 30 160, 217 35 311 256 85 30
Rohrer, C	40 45, 49, 176, 349 311 9, 27, 69, 96, 97, 6, 227, 349, 354 30 160, 217 35 311 256 85 309 246 97, 107, 350 90 309 245 245 245 245 245 244 244
Rohrer, C	40 45, 49, 176, 349 311 9, 27, 69, 96, 97, 6, 227, 349, 354 160, 217 128 35 311 35 311 35 311 35 311 35 311 35 311 35 31 35 31 35 31 35 31 35 31 35 31 35 31 35 31 35 31 35 31 35 31 35 31 35 31 35 31 35 31 35 31 35 35 31 35 31 35 31 35 31 35 31 35 31 35 35 31 35 31 35 31 35 31 35 31 35 31 35 30
Rohrer, C	40 45, 49, 176, 349 311 9, 27, 69, 96, 97, 6, 227, 349, 354 160, 217 128 35 311 35 311 35 311 35 311 35 311 35 311 35 31 35 31 35 31 35 31 35 31 35 31 35 31 35 31 35 31 35 31 35 31 35 31 35 31 35 31 35 31 35 31 35 35 31 35 31 35 31 35 31 35 31 35 31 35 35 31 35 31 35 31 35 31 35 31 35 31 35 30
Rohrer, C	40 45, 49, 176, 349 311 9, 27, 69, 96, 97, 6, 227, 349, 354 160, 217 128 35 31 35 31 35 31 35 31 35 31 35 31 35 31 35 35 31 35 35 31 35 31 35 35 31 35 35 31 35 35 35 31 35 35 31 35 35 31 35 35 31 35 35 35 35 31 35 31 35 35 35 31 35 35 35 35 31 35 35 35 31 35 35 31 35 35 31 35 35 31 35 35 30 30 30 30 30 30 30 30 30 30 30 30 30 30 30
Rohrer, C	40 45, 49, 176, 349 311 9, 27, 69, 96, 97, 6, 227, 349, 354 160, 217 128 31
Rohrer, C	40 45, 49, 176, 349 311 9, 27, 69, 96, 97, 6, 227, 349, 354 160, 217 128 31
Rohrer, C	
Rohrer, C	
Rohrer, C	
Rohrer, C	$\begin{array}{c}$
Rohrer, C	



Rozak, G57, 110 Ru, G246 Ruano, O215, 273 Rubinsztajn, M.....197 Ruiz, M148 Rupnowski, P108, 150 Russell, K......263, 316 Russo Spena, P.....180 Ryu, H132 Ryu, J51

S

Saal, J	
Sabau, A	
Saboohi, Y	175
Saboungi, M	303
Sacerdote-Peronnet, M182, 226,	277
Sachdev, A91, 92, 195,	
Sadayappan, K	210
Saddock, N	352
Sadik, P62,	
Sadler, B	
Sadoway, D	
Saeed, U	
Saegusa, K	
Saengdeejing, A	
Safarik, D	
Saha Podder, A	
Sahin, D	
Sahin, F	
Saigal, A	
Saito, K	
Sakai, N	
Sakanoto, K	
Sakashita, S	
Sakidja, R	
Sakidja, K	
Salaho, G	
Salazar, J	
Salazar, M	
Salee, D	
Saleh, T	
Salem, A170,	
Salman, U	
Samanta, A52, 58, 106,	
Samaras, M	
Samuel, S	
Sanchez-Araiza, M	
Sanderson, S	
Sandhu, R	
Sandoval, D	
Sangiorgi, G	
Sankaran, S	
Sansoz, F155,	
Santella, M259,	
Santhaweesuk, C	
Santisteban, J	
Santodonato, L	
Santos, A	
Sanville, E	202
Sanyal, S	
Sanyai, S	197
Sanyai, S Sarasmak, K Sarihan, V	197 337

Sarikaya, M125, 175
Sarma, G68, 223, 251, 312
Sarosi, P107, 312, 320
Sarradin, J180, 182
Sasaki, H210
Sasaki, J344
Sasaki, T352
Sastikumar, D98
Sato, A54, 131, 156, 157, 208
Sato, E
Sato, H252
Sato, K
Sato, M22, 71, 124, 175, 176, 233, 284, 330
Sato, N138
Sato, S138
Sato, T
Sato, Y
Satyapal, S42
Saucedo Muñoz, M
Saunders, N205
Sawafta, R165
Saxe, P
Saxena, A137, 189
Saylor, D
Scattergood, R
Scavino, G
Schaedler, T
Schaeublin, R
Schafler, E
Schafrik, R
Scharrer, M194
Schäublin, R
Schelling, P291
Schenk, T
Scherello, A
Scheriau, S
Schestakova, L
Schiffl, A
Schildknecht, A
Schille, J
Schlesinger, M
Schlom, D
Schmetterer, C104, 105
Schmid-Fetzer, R
Schmuki, P
Schneibel, J
Schneider, H
Schneider, J
Schoenung, J
Schönfeld, B
Schott, A
Schoers, J
Schub, C
Schuldenzucker, P
Schuldenzücker, F
Schultz, J
Schuster, B
Schweizer, P
Schwaiger, R
Schwandt, C
Schwartz, L
Schwartz, W
Schwarz, M
Schwarz, R
Schwendiman, K226
Schwendiman, K
Schwendiman, K 226 Scorey, C 39 Scott, A 101
Schwendiman, K 226 Scorey, C 39 Scott, A 101 Scott, J 236
Schwendiman, K 226 Scorey, C 39 Scott, A 101 Scott, J 236 Scott, M 226
Schwendiman, K 226 Scorey, C 39 Scott, A 101 Scott, J 236

Scrivani, A
Scully, J43, 236 Seal, S16, 64, 149, 221,
Seale, G92
Sears, J
Section A
Sediako, D
Seelaboyina, R
Segal, V
Segatz, M
Seick, C
Seidman, D27, 138, 139, 282 Sekhar, J142
Seki, Y
Sekido, N
Sekimoto, H
Sekine, 1
Semenova, I
Semenova, O
Semiatin, S170, 212 Senkov, O24, 25, 128, 167, 235, 236, 332
Senkov, S
Senn, J92
Seo, J
Seo, S103, 104, 345 Seok, H
Seong, B
Seong Yong, P191
Sepehrband, P230 Serebrinsky, S227
Serefoglu, M
Sergueeva, A
Serna-Vasquez, A55, 110, 157, 209, 269, 323 Sertel, K
Setter, K
Setyawan, A24
Severo, D124, 174 Sezer, S
Sezer, S
Shade, P
Shaghiev, M
Shahbazian Yassar, R19, 20, 68, 120, 121, 169, 228, 279
Shaikh, A
Shamsuzzoha, M164, 231
Shan, A
Shan, Z
Shang, S
Shangguan, F
Shangguan, Z
Shankar, S
Shannon, C116
Shao, H
Shao-Horn, Y
Shapiro, S
Sharma, B
Sharma, S
Sharma, V
Shaw, L197, 271
Shazly, M
She, H71
Sheikh-Ali, A106



Shen, C		189.312
		. ,
Shen, J		353
Shen P		55
Shell, I		112, 203
	, S	
Sheng, Y	ζ	
	V	
	•	
,		
Shi, J		
Shi, S		137, 355
Shi, W	·	41
Shi, Y		
· ·		
Shi, Z	31, 186, 233, 238, 283, 284,	340, 351
Shibata,	N	32, 33
Shifler I	D	240 292
	G24,	
Shih, T		102, 266
Sinjie, G	ł	
Shim, J		203, 216
Shimada	, K	60
	, F	
Shimizu	, T	
	R	
Shin, C		
Shin, S		191
Shinoha	ra, G	
	ankar, S	
Shollock	с, В	85
~		
Shorokh	ov. E	
Shorokh	ov, E	
Shtanov,	V	
Shtanov, Shubaye	V v, V	
Shtanov, Shubaye	V	
Shtanov, Shubaye Shuiping	Vv, V	
Shtanov, Shubaye Shuiping Shukla,	V v, V g, Z A	
Shtanov, Shubaye Shuiping Shukla, J Shukla, J	V v, V g, Z P	
Shtanov, Shubaye Shuiping Shukla, I Shukla, I Shurov, I	V v, V z, Z A P N	
Shtanov, Shubaye Shuiping Shukla, I Shukla, I Shurov, I	V v, V g, Z P	
Shtanov, Shubaye Shuiping Shukla, J Shukla, J Shurov, J Shutthar	V v, V g, Z A P N vandan, S	
Shtanov, Shubaye Shuiping Shukla, I Shukla, I Shurov, T Shutthar	V v, V g, Z A P N nandan, S nandan, V.	
Shtanov, Shubaye Shuiping Shukla, J Shukla, J Shuthar Shutthar Shutthar	Vy, V y, Z A P N Nandan, S andan, V a, M	
Shtanov, Shubaye Shuiping Shukla, J Shukla, J Shukla, J Shurov, Shuthar Shutthar Shyamal Shyang, Y	Vy, V	
Shtanov, Shubaye Shuiping Shukla, J Shukla, J Shukla, J Shurov, J Shutthar Shutthar Shyamal Shyng, Y Sickafus	Vy, V	
Shtanov, Shubaye Shuiping Shukla, J Shukla, J Shukla, J Shurov, J Shutthar Shutthar Shyamal Shyng, Y Sickafus	Vy, V	
Shtanov, Shubaye Shuiping Shukla, I Shukla, I Shurov, Shutthar Shutthar Shyamal Shyng, Y Sickafus Siegel, I	V v, V g, Z A P Nandan, S nandan, S andan, V a, M Z S D	
Shtanov, Shubaye Shuiping Shukla, J Shukla, I Shurov, Shutthar Shutthar Shyamal Shyng, M Sickafus Siegel, I Siegmur	Vv, V	
Shtanov, Shubaye Shuiping Shukla, J Shukla, J Shuthar Shuthar Shutthar Shyamal Shyamal Sickafus Sickafus Sickafus Sickafus Sickafus	V v, V g, Z A P N andan, S andan, S a, M Z , K D d, A	
Shtanov, Shubaye Shuiping Shukla, J Shukla, J Shurov, Shutthar Shutthar Shyamal Shyamal Sickafus Sickafus Sickafus Sickafus Sickafus Sigemur Siewert, Sigworth	V v, V g, Z A P N Mandan, S andan, S a, M <i>X</i> <i>X</i> <i>X</i> <i>X</i> <i>X</i> <i>X</i> <i>X</i> <i>X</i> <i>X</i> <i>X</i> <i>X</i> <i>X</i> <i>X</i> <i>X</i> <i>X</i> <i>X</i> <i>X</i> <i>X</i> <i>X</i> <i>X</i> <i>X</i> <i>X</i> <i>X</i> <i>X</i> <i>X</i> <i>X</i> <i>X</i> <i>X</i> <i>X</i> <i>X</i> <i>X</i> <i>X</i> <i>X</i> <i>X</i> <i>X</i> <i>X</i> <i>X</i> <i>X</i> <i>X</i> <i>X</i> <i>X</i> <i>X</i> <i>X</i> <i>X</i> <i>X</i> <i>X</i> <i>X</i> <i>X</i> <i>X</i> <i>X</i> <i>X</i> <i>X</i> <i>X</i> <i>X</i> <i>X</i> <i>X</i> <i>X</i> <i>X</i> <i>X</i> <i>X</i> <i>X</i> <i>X</i> <i>X</i> <i>X</i> <i>X</i> <i>X</i> <i>X</i> <i>X</i> <i>X</i> <i>X</i> <i>X</i> <i>X</i> <i>X</i> <i>X</i> <i>X</i> <i>X</i> <i>X</i> <i>X</i> <i>X</i> <i>X</i> <i>X</i> <i>X</i> <i>X</i> <i>X</i> <i>X</i> <i>X</i> <i>X</i> <i>X</i> <i>X</i> <i>X</i> <i>X</i> <i>X</i> <i>X</i> <i>X</i> <i>X</i> <i>X</i> <i>X</i> <i>X</i> <i>X</i> <i>X</i> <i>X</i> <i>X</i> <i>X</i> <i>X</i> <i>X</i> <i>X</i> <i>X</i> <i>X</i> <i>X</i> <i>X</i> <i>X</i> <i>X</i> <i>X</i> <i>X</i> <i>X</i> <i>X</i> <i>X</i> <i>X</i> <i>X</i> <i>X</i> <i>X</i> <i>X</i> <i>X</i> <i>X</i> <i>X</i> <i>X</i> <i>X</i> <i>X</i> <i>X</i> <i>X</i> <i>X</i> <i>X</i> <i>X</i> <i>X</i> <i>X</i> <i>X</i> <i>X</i> <i>X</i> <i>X</i> <i>X</i> <i>X</i> <i>X</i> <i>X</i> <i>X</i> <i>X</i> <i>X</i> <i>X</i> <i>X</i> <i>X</i> <i>X</i> <i>X</i> <i>X</i> <i>X</i> <i>X</i> <i>X</i> <i>X</i> <i>X</i> <i>X</i> <i>X</i> <i>X</i> <i>X</i> <i>X</i> <i>X</i> <i>X</i> <i>X</i> <i>X</i> <i>X</i> <i>X</i> <i>X</i> <i>X</i> <i>X</i> <i>X</i> <i>X</i> <i>X</i> <i>X</i> <i>X</i> <i>X</i> <i>X</i> <i>X</i> <i>X</i> <i>X</i> <i>X</i> <i>X</i> <i>X</i> <i>X</i> <i>X</i> <i>X</i> <i>X</i> <i>X</i> <i>X</i> <i>X</i> <i>X</i> <i>X</i> <i>X</i> <i>X</i> <i>X</i> <i>X</i> <i>X</i> <i>X</i> <i>X</i> <i>X</i> <i>X</i> <i>X</i> <i>X</i> <i>X</i> <i>X</i> <i>X</i> <i>X</i> <i>X</i> <i>X</i> <i>X</i> <i>X</i> <i>X</i> <i>X</i> <i>X</i> <i>X</i> <i>X</i> <i>X</i> <i>X</i> <i>X</i> <i>X</i> <i>X</i> <i>X</i> <i>X</i> <i>X</i> <i>X</i> <i>X</i> <i>X</i> <i>X</i> <i>X</i> <i>X</i> <i>X</i> <i>X</i> <i>X</i> <i>X</i> <i>X</i> <i>X</i> <i>X</i> <i>X</i> <i>X</i> <i>X</i> <i>X</i> <i>X</i> <i>X</i> <i>X</i> <i>X</i> <i>X</i> <i>X</i> <i>X</i> <i>X</i> <i>X</i> <i>X</i> <i>X</i> <i>X</i> <i>X</i> <i>X</i> <i>X</i> <i>X</i> <i>X</i> <i>X</i> <i>X</i> <i>X</i> <i>X</i> <i>X</i> <i>X</i> <i>X</i> <i>X</i> <i>X</i> <i>X</i> <i>X</i> <i>X</i> <i>X</i> <i>X</i> <i>X</i> <i>X</i> <i>X</i> <i>X</i> <i>X</i> <i>X</i> <i>X</i> <i>X</i> <i>X</i> <i></i>	283 177 329 83 43, 100 .173, 329 151 100 .232 .234 .100, 203 27 269, 323 140 179
Shtanov, Shubaye Shuiping Shukla, J Shukla, J Shuthar Shuthar Shutthar Shyamal Shyamal Sickafus Sickafus Sickafus Sickafus Sickafus	Vv, V	283 177 329 83 43, 100 .173, 329 151 100 .232 .234 .100, 203 27 269, 323 140 179
Shtanov, Shubaye Shuiping Shukla, J Shukla, J Shurov, Shutthar Shythar Shythar Sickafus Siegel, I Siegerur Siegwert Sigworth Sigworth	V v, V g, Z A P N Nandan, S andan, S andan, V a, M (, K) d, A	283
Shtanov, Shubaye Shukla, J Shukla, J Shukla, J Shurov, Shutthar Shytman Shyamal Shyamal Shyamal Shyamal Sickafus Sicegnur Siegenur Siegenur Siegenur Siegenur Siegenur Siegenur Siegenur Siegenur Siegenur Siegenur Siegenur	V v, V g, Z A P N Nandan, S andan, S andan, V a, M , K D d, A 55, 110, 157, 209, T n, G s, W	283 177 329 83 43, 100 .173, 329 151 100 .232 .234 .100, 203 27 269, 323 140 179 56 195
Shtanov, Shubaye Shuiping Shukla, J Shukla, J Shurov, Shutthar Shyamal Shyng, Y Sickafus Siegel, I Siegerur Siegerur Siewert, Siewert, Siewert Sik, C	V v, V g, Z A P N Nandan, S andan, S andan, S andan, V a, M (, K D d, A	283 177 329 83 43, 100 .173, 329 151 00 234 .100, 203 27 269, 323 140
Shtanov, Shubaye Shuiping Shukla, J Shukla, J Shurov, Shutthar Shyamal Shyng, Y Sickafus Siegenur Siewert, Sigworth Sigk, C Silleken: Silva, A Silva, G	V v, V g, Z A P N Nandan, S andan, S andan, V a, M Z , K D d, A	
Shtanov, Shubaye Shuiping Shukla, J Shukla, J Shurov, Shutthar Shyamal Shyng, Y Sickafus Siegenur Siewert, Sigworth Sigk, C Silleken: Silva, A Silva, G	V v, V g, Z A P N Nandan, S andan, S andan, S andan, V a, M (, K D d, A	
Shtanov, Shubaye Shuiping Shukla, J Shurov, Shutthar Shutthar Shyamal Shyng, Y Sickafus Siegen, I Siegmur Siewert, Sigworth Sik, C Silleken: Silva, A Silva, A Silva, A	V v, V g, Z A P N Nandan, S andan, S andan, V a, M C b, K D d, A	
Shtanov, Shubaye Shuiping Shukla, J Shurov, Shutthar Shutthar Shyamal Shyng, Y Sickafus Siegen, I Siegmur Siewert, Sigworth Sik, C Silleken: Silva, A Silva, A Silva, A Silva, A Silva, A	V v, V g, Z A P N Nandan, S andan, S andan, V a, M C , K D d, A	
Shtanov, Shubaye Shuiping Shukla, J Shurov, Shutthar Shutthar Shyamal Shyng, Y Sickafus Siegen, I Siegmur Siewert, Sigworth Sík, C Sillekem: Sillekar Sillva, A Silva, A Silva	V v, V g, Z A P N Nandan, S andan, S andan, V a, M C b, K D d, A	
Shtanov, Shubaye Shuiping Shukla, J Shukla, J Shurov, Shutthar Shutthar Shyamal Shyamal Shyamal Shyamal Sickafus Siegel, I Siegenur Siewert, Sigworth Sik, C Sillekan: Sillekan,	V v, V g, Z A P. Naandan, S. aandan, S. aandan, V. a, M. Z. , K. D. d, A	
Shtanov, Shubaye Shuiping Shukla, J Shukla, J Shurov, Shutthar Shutthar Shyamal Shyamal Shyamal Shyamal Sickafus Siegel, I Siegenur Siewert, Sigworth Sik, C Sillekan: Sillekan: Silleka, A Silleka, A Silva, A Si	V v, V g, Z A P N nandan, S andan, S andan, V a, M , K D d, A	
Shtanov, Shubaye Shuiping Shukla, J Shukla, J Shurov, Shutthar Shutthar Shyamal Shyamal Shyamal Shyamal Sickafus Siegel, I Siegenur Siewert, Sigworth Sik, C Sillekan: Sillekan: Silleka, A Silleka, A Silva, A Si	V v, V g, Z A P. Naandan, S. aandan, S. aandan, V. a, M. Z. , K. D. d, A	
Shtanov, Shubaye Shuiping Shukla, J Shurov, Shutthar Shutthar Shutthar Shyng, Y Sickafus Siegel, I Siegenur Siewert, Sigworth Sik, C Silleken: Silva, A Silva, A Silv	V v, V g, Z A p. N nandan, S andan, S andan, V a, M , K D d, A	
Shtanov, Shubaye Shuiping Shukla, J Shukla, J Shuthar Shutthar Shutthar Shyamal Shyamal Sickafus Siegel, I Siegenur Siewert, Sigworth Sik, C Silleken: Silva, A Silva, M Silva, M Silva, P Silvestri Simakov Simmel, Simmon Simoes,	V v, V g, Z A P N Nandan, S andan, S andan, V a, M (A , K D d, A h, G , A , D F s, J S	
Shtanov, Shubaye Shuiping Shukla, J Shukla, J Shukla, J Shurov, Shutthar Shutthar Shyang, Y Sickafus Siegen, I Sickafus Siegen, I Siegenur Siegentur Siewert, Sigworth Sik, C Silleken: Silva, A Silva, G Silva, M Silva, P Silvestri Simaon Simos, Simsek,	V v, V g, Z A P N Mandan, S andan, S andan, S andan, V a, M c.	
Shtanov, Shubaye Shuiping Shukla, J Shukla, J Shurov, Shutthar Shutthar Shyang, Y Sickafus Siegen, I Siegenur Simoto Simoto Simoto Simoto Simoto Singenus Singenus Singenur Si	V	
Shtanov, Shubaye Shuiping Shukla, J Shukla, J Shurov, Shutthar Shutthar Shyang, Y Sickafus Siegen, I Siegenur Simoto Simoto Simoto Simoto Simoto Singenus Singenus Singenur Si	V v, V g, Z A P N Mandan, S andan, S andan, S andan, V a, M c.	
Shtanov, Shubaye Shuiping Shukla, J Shukla, J Shurov, Shutthar Shutthar Shyamal Shyamal Shyamal Shyamal Sickafus Siegent Siege	V v, V g, Z A P N mandan, S a, M a, M b, K D c, K. D c, K. c, K. c, K. c, K. c, K. 	
Shtanov, Shubaye Shuiping Shukla, J Shukla, J Shukla, J Shurov, Shutthar Shutthar Shyang, Y Sickafus Siegenur Siekafus Siegenur Siewert, Sigwortl Sik, C Silleken Silva, A Silva, G Silva, M Silva, P Silvestri Simakov Simmel, Simos, Simsek, Sinaga, J Sinsek, Sinaga, J Sinsek, Sinaga, J	V v, V g, Z A P N nandan, S andan, S andan, S andan, V a, M c	
Shtanov, Shubaye Shuiping Shukla, J Shukla, J Shukla, J Shurov, Shutthar Shutthar Shyang, Y Sickafus Siegenur Siekafus Siegenur Siewert, Sigworth Sik, C Silleken Silva, A Silva, G Silva, M Silva, P Silvestri Simakov Simmel, Simosa, J Sindelar Sinag, J Sindelar Singer, H	V v, V g, Z A P N nandan, S andan, S andan, S andan, V a, M y, K D d, A 55, 110, 157, 209, T h, G s, W s, W F s, J S. E D. R. H.	
Shtanov, Shubaye Shuiping Shukla, J Shukla, J Shurov, Shutthar Shyng, Y Sickafus Siegeot, I Siegeot, I Siegeot, I Siegeot, Siegeot, Siegeot, Siegeot, Sigwortt Sik, C Silleken Silva, A Silva, A Silva, A Silva, A Silva, M Silva, P Silvestri Simadov Simmel, Simos, Simsek, Sinaga, J Sindelar Singer, F Singer, F	V	
Shtanov, Shubaye Shuiping Shukla, J Shukla, J Shurov, Shutthar Shyng, Y Sickafus Siegeot, I Siegeot, I Siegeot, I Siegeot, Siegeot, Siegeot, Siegeot, Sigwortt Sik, C Silleken Silva, A Silva, A Silva, A Silva, A Silva, M Silva, P Silvestri Simadov Simmel, Simos, Simsek, Sinaga, J Sindelar Singer, F Singer, F	V v, V g, Z A P N nandan, S andan, S andan, S andan, V a, M y, K D d, A 55, 110, 157, 209, T h, G s, W s, W F s, J S. E D. R. H.	
Shtanov, Shubaye Shuiping Shukla, J Shukla, J Shukla, J Shukla, J Shukla, J Shukla, J Shukla, J Shukla, J Sickafus Sickafus Sickafus Sickafus Siegen, I Sickafus Siegen, I Siegen, I Sigworth Sik, C Silleken Silva, A Silva, A Silva, A Silva, A Silva, A Silva, A Silva, A Silva, A Silva, A Silva, S Simel, I Simmon Simoes, Simsek, Sinaga, J Sindelar, Singer, I Singer, I Singer, F Singer, F Singer, A	V	

Singh, M80
Singh, N54, 108, 319
Singh, P145, 260, 269, 311
Singh, U
Singh, V
Singjai, P17
Singleton, N123
Sinha, S252, 303
Sinha, V226
Sinn, H
Sinnott, S356
Sintay, S97
Sirivolu, S238
Sisson, R
Sitdikov, V
Sivaraj, D
Siwecki, T
Sklad, P
Sklenicka, V
Skornyakov, V71
Skrotzki, B
Skury, A
Skybakmoen, E
Slattery, D
Slocik, J
Slooff, F
Slutsker, J
Smialek, J
Smid, I
Smith, A
Smith, C
Smith, G76
Smith, J136, 137, 264, 316
Smith, L220
Smith, R19, 100, 150, 198, 202, 315
Smitherman, M82
Smitherman, M
Smitherman, M
Smitherman, M
Smitherman, M 82 Smolyakov, A 214, 216 Smugeresky, J 64, 65, 166, 214 Snead, L 57, 100, 101, 315 Snure, M 62, 116
Smitherman, M 82 Smolyakov, A 214, 216 Smugeresky, J 64, 65, 166, 214 Snead, L 57, 100, 101, 315 Snure, M 62, 116 Snyder, R 175
Smitherman, M 82 Smolyakov, A 214, 216 Smugeresky, J 64, 65, 166, 214 Snead, L 57, 100, 101, 315 Snure, M 62, 116 Snyder, R 175 Soare, I 63
Smitherman, M 82 Smolyakov, A 214, 216 Smugeresky, J 64, 65, 166, 214 Snead, L 57, 100, 101, 315 Snure, M 62, 116 Snyder, R 175 Soare, I 63 Sobey, T 61
Smitherman, M 82 Smolyakov, A 214, 216 Smugeresky, J 64, 65, 166, 214 Snead, L 57, 100, 101, 315 Snure, M 62, 116 Snyder, R 175 Soare, I 63 Sobey, T 61 Sobyejo, W 22, 288
Smitherman, M 82 Smolyakov, A 214, 216 Smugeresky, J 64, 65, 166, 214 Snead, L 57, 100, 101, 315 Snure, M 62, 116 Snyder, R 175 Soare, I 63 Sobey, T 61 Sobjey, Soffe, S 198
Smitherman, M 82 Smolyakov, A 214, 216 Smugeresky, J 64, 65, 166, 214 Snead, L 57, 100, 101, 315 Snure, M 62, 116 Snyder, R 175 Soare, I 63 Sobey, T 61 Sobie, S 198 Sohn, H 118, 224, 225
Smitherman, M 82 Smolyakov, A 214, 216 Smugeresky, J 64, 65, 166, 214 Snead, L 57, 100, 101, 315 Snure, M 62, 116 Snyder, R 175 Soare, I 63 Sobey, T 61 Sobyejo, W 22, 288 Sofie, S 198 Sohn, H 118, 224, 225 Sohn, Y 28, 41, 78, 93, 131,
Smitherman, M 82 Smolyakov, A 214, 216 Smugeresky, J 64, 65, 166, 214 Snead, L 57, 100, 101, 315 Snure, M 62, 116 Snyder, R 175 Soare, I 63 Sobey, T 61 Sobyejo, W 22, 288 Sofie, S 198 Sohn, H 118, 224, 225 Sohn, Y 28, 41, 78, 93, 131,
Smitherman, M 82 Smolyakov, A 214, 216 Smugeresky, J 64, 65, 166, 214 Snead, L 57, 100, 101, 315 Snure, M 62, 116 Snyder, R 175 Soare, I 63 Sobey, T 61 Soboyejo, W 22, 288 Sofie, S 198 Sohn, H 118, 224, 225 Sohn, Y 28, 41, 78, 93, 131,
Smitherman, M 82 Smolyakov, A 214, 216 Smugeresky, J 64, 65, 166, 214 Snead, L 57, 100, 101, 315 Snure, M 62, 116 Snyder, R 175 Soare, I 63 Soboyejo, W 22, 288 Sofie, S 198 Sohn, H 118, 224, 225 Sohn, Y 28, 41, 78, 93, 131,
Smitherman, M 82 Smolyakov, A 214, 216 Smugeresky, J 64, 65, 166, 214 Snead, L 57, 100, 101, 315 Snure, M 62, 116 Snyder, R 175 Soare, I 63 Soboyejo, W 22, 288 Sofie, S 198 Sohn, H 118, 224, 225 Sohn, Y 28, 41, 78, 93, 131,
Smitherman, M 82 Smolyakov, A 214, 216 Smugeresky, J 64, 65, 166, 214 Snead, L 57, 100, 101, 315 Snure, M 62, 116 Snyder, R 175 Soare, I 63 Sobey, T 61 Soboyejo, W 22, 288 Sofie, S 198 Sohn, H 118, 224, 225 Sohn, Y 28, 41, 78, 93, 131,
Smitherman, M 82 Smolyakov, A 214, 216 Smugeresky, J 64, 65, 166, 214 Snead, L 57, 100, 101, 315 Snure, M 62, 116 Snyder, R 175 Soare, I 63 Sobey, T 61 Soboyejo, W 22, 288 Sofie, S 118, 224, 225 Sohn, H 118, 224, 225 Sohn, Y 28, 41, 78, 93, 131,
Smitherman, M 82 Smolyakov, A 214, 216 Smugeresky, J 64, 65, 166, 214 Snead, L 57, 100, 101, 315 Snure, M 62, 116 Snyder, R 175 Soare, I 63 Sobey, T 61 Soboyejo, W 22, 288 Sofie, S 198 Sohn, H 118, 224, 225 Sohn, Y 28, 41, 78, 93, 131,
Smitherman, M 82 Smolyakov, A 214, 216 Smugeresky, J 64, 65, 166, 214 Snead, L 57, 100, 101, 315 Snure, M 62, 116 Snyder, R 175 Soare, I 63 Sobey, T 61 Soboyejo, W 22, 288 Sofie, S 118, 224, 225 Sohn, H 118, 224, 225 Sohn, Y 28, 41, 78, 93, 131,
Smitherman, M 82 Smolyakov, A 214, 216 Smugeresky, J 64, 65, 166, 214 Snead, L 57, 100, 101, 315 Snure, M 62, 116 Snyder, R 175 Soare, I 63 Sobey, T 61 Soboyejo, W 22, 288 Sofie, S 118, 224, 225 Sohn, H 118, 224, 225 Sohn, Y 28, 41, 78, 93, 131,
Smitherman, M 82 Smolyakov, A 214, 216 Smugeresky, J 64, 65, 166, 214 Snead, L 57, 100, 101, 315 Snure, M 62, 116 Snyder, R 175 Soare, I 63 Sobey, T 61 Soboyejo, W 22, 288 Sofie, S 198 Sohn, H 118, 224, 225 Sohn, Y 28, 41, 78, 93, 131,
Smitherman, M 82 Smolyakov, A 214, 216 Smugeresky, J 64, 65, 166, 214 Snead, L 57, 100, 101, 315 Snure, M 62, 116 Snyder, R 175 Soare, I 63 Sobey, T 61 Soboyejo, W 22, 288 Sofie, S 198 Sohn, H 118, 224, 225 Sohn, Y 28, 41, 78, 93, 131,
Smitherman, M 82 Smolyakov, A 214, 216 Smugeresky, J 64, 65, 166, 214 Snead, L 57, 100, 101, 315 Snure, M 62, 116 Snyder, R 175 Soare, I 63 Sobey, T 61 Soboyejo, W 22, 288 Sofie, S 198 Sohn, H 118, 224, 225 Sohn, Y 28, 41, 78, 93, 131,
Smitherman, M 82 Smolyakov, A 214, 216 Smugeresky, J
Smitherman, M 82 Smolyakov, A 214, 216 Smugeresky, J
Smitherman, M 82 Smolyakov, A 214, 216 Smugeresky, J
Smitherman, M 82 Smolyakov, A 214, 216 Smugeresky, J 64, 65, 166, 214 Snead, L 57, 100, 101, 315 Snure, M 62, 116 Snyder, R 175 Soare, I 63 Sobey, T 61 Soboyejo, W 22, 288 Sofie, S 198 Sohn, H 118, 224, 225 Sohn, Y 28, 41, 78, 93, 131,
Smitherman, M 82 Smolyakov, A 214, 216 Smugeresky, J
Smitherman, M 82 Smolyakov, A 214, 216 Smugeresky, J 64, 65, 166, 214 Snead, L 57, 100, 101, 315 Snure, M 62, 116 Snyder, R 175 Soare, I 63 Sobey, T 61 Soboyejo, W 22, 288 Sofn, S 198 Sohn, H 118, 224, 225 Sohn, Y 28, 41, 78, 93, 131,
Smitherman, M 82 Smolyakov, A 214, 216 Smugeresky, J 64, 65, 166, 214 Snead, L 57, 100, 101, 315 Snure, M 62, 116 Snyder, R 175 Soare, I 63 Sobey, T 61 Soboyejo, W 22, 288 Sofie, S 118, 224, 225 Sohn, H 118, 224, 225 Sohn, Y 28, 41, 78, 93, 131,
Smitherman, M 82 Smolyakov, A 214, 216 Smugeresky, J 64, 65, 166, 214 Snead, L 57, 100, 101, 315 Snure, M 62, 116 Snyder, R 175 Soare, I 63 Sobey, T 61 Soboyejo, W 22, 288 Sofn, S 198 Sohn, H 118, 224, 225 Sohn, Y 28, 41, 78, 93, 131,

Song, K	
Song, M	
Song, X	
Song, Y	
Song, Z	
Sonnleitner, R	
Sopori, B	
Sordelet, D	
Sorensen, C	
Sorlie, M21, 30, 31, 70, 74, 81, 123, 127, 171, 173, 174,	
Soto, K	
Soubeyroux, J	
Soucy, G	
Souidi, A	
Southworth, A151, 153	
Spaepen, F	
Spangenberger, J	
Spanos, G17	
Spätig, P	
Speakman, S	209
Specht, E	, 253
Specker, A	37
Speer, J	190
Spencer, K	144
Spigarelli, S	352
Spoljaric, D	
Spowart, J168	, 225
Sreekala, S	
Sreekumar, K	
Sreeranganathan, A44, 254, 277	, 309
Srinivasan, R254, 255, 312, 320	
Srinivasan, S132, 189	
Srisukhumbowornchai, N166	
Srisukhumbowornchai, N166 Srivastava, A	114
Srisukhumbowornchai, N166 Srivastava, A Srivastava, R	114 285
Srisukhumbowornchai, N166 Srivastava, A Srivastava, R Srivastava, S	114 285 322
Srisukhumbowornchai, N	114 285 322 , 356
Srisukhumbowornchai, N	114 285 322 , 356 , 338
Srisukhumbowornchai, N	114 285 322 , 356 , 338 134
Srisukhumbowornchai, N	114 285 322 , 356 , 338 134 324
Srisukhumbowornchai, N	114 285 322 , 356 , 338 134 324 , 357
Srisukhumbowornchai, N	114 285 322 , 356 , 338 134 324 , 357 209
Srisukhumbowornchai, N	114 285 322 , 356 , 338 134 324 , 357 209 22
Srisukhumbowornchai, N	114 285 322 , 356 , 338 134 324 , 357 209 22 146
Srisukhumbowornchai, N	114 285 322 , 356 , 338 134 324 , 357 209 22 146 , 339
Srisukhumbowornchai, N	114 285 322 , 356 , 338 134 324 , 357 209 22 146 , 339 210
Srisukhumbowornchai, N	114 285 322 , 356 , 338 134 324 , 357 209 22 146 , 339 210 70
Srisukhumbowornchai, N	114 285 322 , 356 , 338 134 324 , 357 209 220 146 , 339 210 70 , 356
Srisukhumbowornchai, N	114 285 322 356 338 134 324 324 209 220 466 339 210 70 70 70 705
Srisukhumbowornchai, N 166 Srivastava, A Srivastava, R Srivastava, S Srivilliputhur, S Srivilliputhur, S 67, 151, 316 Srolovitz, D 130, 291, 330 St-Georges, L St St John, D Stach, E Stack, E 325 Stacy, J Stadermann, M Staller, S Stalley, J Staley, J Stan, M Stan, M 65 Standen, C Standen, C	114 285 322 356 338 134 209 22 146 339 210 70 70 70 71
Srisukhumbowornchai, N 166 Srivastava, A Srivastava, R Srivastava, S Srivastava, S Srivilliputhur, S 67, 151, 316 Srolovitz, D 130, 291, 330 St-Georges, L St St John, D Stach, E Stacy, J Stadermann, M Stadler, S Staley, J Staley, J Stan, M Stan, M 65 Standen, C Stanescu, C	114 285 322 356 338 134 324 324 209 210 70 70 70 70 70 71 709 71 709 710 709 710 709 710 709 710 709 710 709 710 709 7000 7000 7000 7000 7000 7000 7000 7000 7000 7000 7000
Srisukhumbowornchai, N	114 285 322 356 338 134 324 324 209 220 46 339 210 700 71 299 71 238 71
Srisukhumbowornchai, N	114 285 322 356 338 134 324 324 209 210 70 299 71 238 210 70 299 71 238 356
Srisukhumbowornchai, N 166 Srivastava, A Srivastava, R Srivastava, S Srivastava, S Sriviliputhur, S 67, 151, 316 Srolovitz, D 130, 291, 330 St-Georges, L St St, John, D Stach, E Stader, S 325 Stady, J Staller, S Stagno, E 180 Staley, J Stan, M Stan, M 65 Standen, C Stanescu, C Stanca, C 327 Stavehaug, F 327	114 285 322 356 338 134 324 327 209 210 70 238 210 70 299 71 238 356 299 71
Srisukhumbowornchai, N 166 Srivastava, A Srivastava, R Srivastava, S Srivastava, S Srivilliputhur, S .67, 151, 316 Srolovitz, D .130, 291, 330 St-Georges, L	114 285 322 , 356 , 338 134 , 357 209 210 70 , 356 299 71 238 , 328 354 354 354 354
Srisukhumbowornchai, N	114 285 322 , 356 , 338 134 324 , 357 209 210 71 238 , 328 314 317 247 244 31
Srisukhumbowornchai, N	114 285 322 , 356 , 338 134 324 , 357 209 210 71 238 , 328 314 299 71 238 , 328 354 31 247 247 224 84 84
Srisukhumbowornchai, N	114 285 322 , 356 , 338 134 324 , 357 209 210 70 , 356 299 71 238 354 354 324 31 247 247 224 247 247 247 247 247 247 247 247 247 247 247 247 247 247 247 247 299 314 247 247 299 316 299 318 247 299 318 328 328 348 348 348 348 348 348 348 348 348 348 348 348 349 348 349 349 349 349 349 349 349 349 349 349 349 349 349 349 349 349 349 348 344 347 349 344 348 344 348 344 347 348 344 344 344 344 344 344 344 344 344 344
Srisukhumbowornchai, N	114 285 322 , 356 , 338 134 324 , 357 209 210 70 , 356 299 71 238 354 354 354 31 247 224
Srisukhumbowornchai, N	114 285 322 , 356 , 338 134 324 , 357 209 210 70 , 356 299 71 238 354 354 354 31 247 224 81 93 , 240 72
Srisukhumbowornchai, N	114 285 322 , 356 , 338 134 324 , 357 209 210 70 , 356 299 71 238 354 35555555555
Srisukhumbowornchai, N	114 285 322 , 356 , 338 134 324 , 357 209 71 238 , 329 70 , 356 299 71 238 , 328 354 354 31 247 240 93 , 240 93 93
Srisukhumbowornchai, N	114 285 322 , 356 , 338 134 324 , 357 209 71 238 , 328 354 354 354 31 247 224 31 93 , 240 72 37 328
Srisukhumbowornchai, N	114 285 322 , 356 , 338 134 324 , 357 209 71 238 , 329 70 , 356 299 71 238 354 354 31 247 247 72 72 72 73 72 72 73 72 72 74 77
Srisukhumbowornchai, N	114 285 322 , 356 , 338 134 324 , 357 209 70 , 356 299 71 238 , 328 354 31 247 247 247 247 247 247 218 354 70 72



Stevenson, J145, 198, 260
Stewart, D55, 110, 157, 209, 269, 323
Stiles, D240
Stipcich, M137
StJohn, D112, 237
Stocks, G192
Stocks, M252
Stoica, A126, 332
Stoica, G219
Stojakovic, D121, 280
Stojanovic, J
Stokes, D140
Stoldt, C
Stölken, J133
Stoller, R48, 201, 267, 316, 317
Stolting, K
Stolz, D
Stone, D
Storm, R
Störmer, M
Story, C146
Stoudt, M
Street, R215
Streiffer, S
Streitz, F
Strickler, J
Stroeder, M171
Strothers, S114
Strouse, G162
Stubbins, J95, 151, 316
Stupp, S175
Su, J16
Su, M
Subhash, G74, 79, 184, 339
Subramanian K 50 102 151
Subramanian, K
153, 204, 264, 317 Subramanian, S194 Suda, H
153, 204, 264, 317 Subramanian, S194 Suda, H
153, 204, 264, 317 Subramanian, S194 Suda, H
$\begin{tabular}{lllllllllllllllllllllllllllllllllll$
$\begin{tabular}{lllllllllllllllllllllllllllllllllll$

Suryanarayana, C	
Suszuki, R	
Suzuki, A	
Suzuki, M	.55, 110, 157, 209, 269, 323
Suzuki, T	
Svoboda, M	
Swadener, J	
Swadner, J	
Swaminathan, S	
Swan-Wood, T	
Sweeney, D	
Swift, D	
Syed Asif, S	
Szczepanski, C	
Szczygiel, P	

Т

T-Raissi, A	
Tabereaux, A	
Tack, W	
Tadisina, Z	33
Tagantsev, A	64
Takahashi, H	
Takahashi, K	
Takahashi, T	83
Takaku, Y	204, 265
Takano, C	35
Takashi, I	148
Takashi, K	148
Takeda, O	90
Takeda, Y	
Takeguchi, M	
Takemoto, T	152
Takenaka, T	
Takeshi, A	
Takeuchi, T	
Takigawa, Y	
Talamantes, J	
Taleff, E	
Talekar, A	
Talia, J	
Tallapragada, R	
Tamerler, C	
Lamerier (
Tamirisa, S	226, 254
Tamirisa, S Tamirisakandala, S44, 226, 254	226, 254 4, 255, 277
Tamirisa, S Tamirisakandala, S44, 226, 254 Tamura, K	226, 254 4, 255, 277 87
Tamirisa, S Tamirisakandala, S	226, 254 4, 255, 277 87 25, 143
Tamirisa, S Tamirisakandala, S	226, 254 4, 255, 277 87 25, 143 273
Tamirisa, S Tamirisakandala, S44, 226, 256 Tamura, K Tamura, T Tan, H Tan, L	226, 254 4, 255, 277 87 25, 143 273 119
Tamirisa, S Tamirisakandala, S Tamura, K Tamura, T Tan, H Tan, L Tan, T	226, 254 4, 255, 277 25, 143 25, 143 273 119 77
Tamirisa, S Tamirisakandala, S Tamura, K Tamura, T Tan, H Tan, L Tan, T Tanaka, M	226, 254 4, 255, 277 25, 143 25, 143 273 119 77 7, 100, 349
Tamirisa, S Tamirisakandala, S Tamura, K Tamura, T Tan, H Tan, L Tan, T Tanka, M S Tang, F	226, 254 4, 255, 277 25, 143 25, 143 119 77 7, 100, 349 5, 200, 215
Tamirisa, S Tamirisakandala, S Tamura, K Tamura, T Tan, H Tan, L Tan, T Tanka, M S Tang, F 40	226, 254 4, 255, 277 25, 143 25, 143 273 119 77 7, 100, 349 5, 200, 215 285
Tamirisa, S Tamirisakandala, S Tamura, K Tamura, T Tan, H Tan, L Tanaka, M Tang, F Tang, M 58, 59	226, 254 4, 255, 277 25, 143 25, 143 273 119 77 7, 100, 349 5, 200, 215 285 9, 203, 266
Tamirisa, S Tamirisakandala, S Tamura, K Tamura, T Tan, H Tan, L Tanaka, M Tang, F Tang, M Tang, W	226, 254 4, 255, 277 25, 143 25, 143 273 119 77 7, 100, 349 5, 200, 215 285 9, 203, 266 166
Tamirisa, S Tamirisakandala, S Tamura, K Tamura, T Tan, H Tan, L Tan, T Tang, F Tang, L Tang, M Tang, M Tang, M Tang, M Tang, X	226, 254 4, 255, 277 87 25, 143 25, 143 119 77 7, 100, 349 5, 200, 215 285 9, 203, 266 166 221, 224
Tamirisa, S Tamirisakandala, S Tamura, K Tamura, T Tan, H Tan, L Tan, T Tang, F Tang, L Tang, M Tang, M Tang, M Tang, X Tang, Z	226, 254 4, 255, 277 87 25, 143 25, 143 119 77 7, 100, 349 5, 200, 215 285 285
Tamirisa, S Tamirisakandala, S Tamura, K Tamura, T Tan, H Tan, L Tanaka, M Tang, F Tang, M Tang, W Tang, Z Tangi, K	226, 254 4, 255, 277 87 25, 143 25, 143 77 7, 100, 349 5, 200, 215 285 9, 203, 266 166 221, 224 321 124, 125
Tamirisa, S Tamirisakandala, S Tamura, K Tamura, T Tan, H Tan, L Tan, T Tanaka, M Tang, F Tang, M Tang, X Tang, Z Tansita, K	226, 254 4, 255, 277 87 25, 143 25, 143 273 119 77 7, 100, 349 5, 200, 215 285 9, 203, 266 221, 224 124, 125
Tamirisa, S Tamirisakandala, S Tamura, K Tamura, T Tan, H Tan, L Tanaka, M Tang, F Tang, M Tang, W Tang, Z Tangi, K	226, 254 4, 255, 277 87 25, 143 25, 143 273 119 77 7, 100, 349 5, 200, 215 285 9, 203, 266 221, 224 124, 125
Tamirisa, S Tamirisakandala, S Tamura, K Tamura, T Tan, H Tan, L Tan, T Tanaka, M Tang, F Tang, M Tang, X Tang, Z Tansita, K	226, 254 4, 255, 277 87 25, 143 25, 143 273 119 77 7, 100, 349 5, 200, 215 285 9, 203, 266 221, 224 124, 125
Tamirisa, S Tamirisakandala, S Tamura, K Tamura, T Tan, H Tan, L Tan, T Tanaka, M Tang, F Tang, M Tang, X Tanshita, K Tanniru, M Tan, J	226, 254 4, 255, 277 87 25, 143 25, 143 273 119 77 7, 100, 349 5, 200, 215 285 9, 203, 266 221, 224 166 221, 224 124, 125
Tamirisa, S Tamirisakandala, S Tamura, K Tamura, T Tan, H Tan, L Tan, T Tanaka, M Tang, F Tang, M Tang, X Taniru, M Tano, Z Taniru, M Tano, J Tano, J	226, 254 4, 255, 277 87 25, 143 25, 143 273 119 77 7, 100, 349 5, 200, 215 285 9, 203, 266 166 221, 224 124, 125 225 142 165 272
Tamirisa, S Tamirisakandala, S Tamura, K Tamura, T Tan, H Tan, L Tan, T Tanaka, M Tang, F Tang, M Tang, M Tang, X Tanshita, K Taniru, M Tan, Z Tang, Z Tano, J Tao, N	$\begin{array}{c}226, 254 \\ 4, 255, 277 \\87 \\25, 143 \\273 \\119 \\77 \\ 7, 100, 349 \\ 5, 200, 215 \\285 \\203, 266 \\221, 224 \\124, 125 \\225 \\142 \\165 \\272 \\203 \\ \end{array}$
Tamirisa, S Tamirisakandala, S Tamura, K Tamura, T Tan, H Tan, L Tan, T Tanaka, M Tang, F Tang, M Tang, X Taniru, M Tang, J Tang, Z Tano, L Tang, X Tan, N Tan, K Tan, N Tan, K Tan, K Tan, K Tan, K Tan, K Tan, K Tao, N	$\begin{array}{c}226, 254 \\ 4, 255, 277 \\87 \\25, 143 \\273 \\119 \\77 \\ 7, 100, 349 \\ 5, 200, 215 \\285 \\203, 266 \\21, 224 \\124, 125 \\225 \\142 \\165 \\272 \\203 \\203 \\29 \\29 \\203 \\29 \\203 \\29 \\$
Tamirisa, S Tamirisakandala, S Tamura, K Tamura, T Tan, H Tan, L Tan, T Tanaka, M 8 Tang, F Tang, M Tang, X Tanishita, K Taniru, M Tao, J Tang, A Tang, Z Tang, A Tang, Z Tang, A Tang, Z Tang, A Tang, Z Tang, Z Tang, Z Tang, Z Tanishita, K Tano, J Tao, L Tao, C Tao, N Tapasa, K Tarakanov, A Tarcy, G	226, 254 4, 255, 277 87 25, 143 25, 143 273 119 77 7, 100, 349 5, 200, 215 285 9, 203, 266 21, 224 124, 125 225 142 225 142 203
Tamirisa, S Tamirisakandala, S Tamura, K Tamura, T Tan, H Tan, L Tan, T Tanaka, M Tang, F Tang, M Tang, X Taniru, M Tang, J Tang, Z Tano, L Tang, X Tan, S Tan, S	226, 254 4, 255, 277 87 25, 143 25, 143 273 119 77 7, 100, 349 5, 200, 215 285 9, 203, 266 21, 224 124, 125 225 142 272 124, 125 203

Tata, M 339 Tatyacti, A 128 Tavasci, A 180 Taylor, J 210 Taylor, M 70, 173, 174, 232 Taylor, P 200 Tedenac, J 17, 180, 182, 335 Tedstrom, R 207 Teinze, S 198 Telang, A 228 Temur, D 67 Teo, K 161, 17 Teros, J 137, 361 Tenório, J 317, 361 Tenório, J 92, 310, 352 Terentyev, D 203 Terpstra, R 66 Terrones, L 181 Ter Weer, P 171 Tessandori, J 243, 244, 294, 295, 312, 338 Thanneeru, R 243, 244, 294, 295, 312, 338 Thanneeru, R 243 243, 244, 294, 295, 312, 338 Thaneeru, R 243 244 Thevuthasan, S Thibault, M 127, 341 Thibeaut, C 328 Thibraugarajan, K 36 Thomas, D 171, 229 Thomas, G 167 </th <th></th>	
Tavasci, A. 180 Taylor, J. 210 Taylor, J. 210 Taylor, P. 200 Tedenac, J. 17, 180, 182, 335 Tedstrom, R. 207 Teintze, S. 198 Telang, A. 228 Temur, D. 67 Teng, J. 86, 135 Teorio, J. 137, 361 Tendrio, J. 34 Teo, K. 16, 117 TerBush, J. .92, 310, 352 Terentyev, D. 203 Terpstra, R. 66 Terrones, L 181 Ter Weer, P. 171 Tessandori, J. 56 Teter, D. 243 Tewary, V. 40 Tewksbury, G. 37 Thadhani, N. 29, 79, 132, 175, 183, 218, Thaueur, K. 244 Thevuthasan, S. 100, 151, 275 Thibault, M. 127, 341 Thirumalai, N. 52 Thirumalai, N. 52 Thiory, B. 171 Tomomas, A. 161	Tata, M
Taylor, J. 210 Taylor, M. 70, 173, 174, 232 Taylor, P. 200 Tedenac, J. 17, 180, 182, 335 Tedstrom, R. 207 Teintze, S. 198 Telang, A. 228 Temur, D. 67 Teng, J. 86, 135 Tenorio, J. 137, 361 Terbrino, J. 34 Teo, K. 16, 117 TerBush, J. .92, 310, 352 Terentyev, D. 203 Terpstra, R. 66 Terrones, L. 181 Ter Weer, P. 171 Tessandori, J. 56 Teter, D. 243 Tewary, V. 40 Tewksbury, G. 37 Thadhani, N. 29, 79, 132, 175, 183, 218,	Tatiparti, S225
Taylor, J. 210 Taylor, M. 70, 173, 174, 232 Taylor, P. 200 Tedenac, J. 17, 180, 182, 335 Tedstrom, R. 207 Teintze, S. 198 Telang, A. 228 Temur, D. 67 Teng, J. 86, 135 Tenorio, J. 137, 361 Terbrino, J. 34 Teo, K. 16, 117 TerBush, J. .92, 310, 352 Terentyev, D. 203 Terpstra, R. 66 Terrones, L. 181 Ter Weer, P. 171 Tessandori, J. 56 Teter, D. 243 Tewary, V. 40 Tewksbury, G. 37 Thadhani, N. 29, 79, 132, 175, 183, 218,	Tavasci, A
Taylor, M. 70, 173, 174, 232 Taylor, P. 200 Tedenac, J. 17, 180, 182, 335 Tedstrom, R. 207 Teintze, S. 198 Telang, A. 228 Temur, D. 67 Teng, J. 86, 135 Tenorio, J. 137, 361 Tenório, J. 34 Teo, K. 16, 117 TerBush, J. .92, 310, 352 Terentyev, D. 203 Terpstra, R. 66 Terrones, L 181 Tew Weer, P. 171 Tessandori, J. 56 Teter, D. 243 Tewary, V. 40 Tewksbury, G. 337 Thadhani, N. 29, 79, 132, 175, 183, 218,	
Taylor, P. 200 Tedenac, J. 17, 180, 182, 335 Tedstrom, R. 207 Teinze, S. 198 Telang, A. 228 Temur, D. 67 Teng, J. .86, 135 Tenorio, J. .137, 361 Tenorio, J. .137, 361 Tenorio, J. .137, 361 Tenorio, J. .203 Terentyev, D. .203 Terpstra, R. .66 Terrones, L .181 Ter Weer, P. .171 Tessandori, J. .56 Teter, D. .243 Tewary, V. .40 Tewksbury, G. .37 Thadhani, N. .29, 79, 132, 175, 183, 218,	
Tedenac, J. 17, 180, 182, 335 Tedstrom, R. 207 Teintze, S. 198 Telang, A. 228 Temur, D. 67 Teng, J. 86, 135 Tenorio, J. 137, 361 Tenfey, J. 92, 310, 352 Terentyev, D. 203 Terpstra, R. 66 Terrones, L. 181 Ter Weer, P. 171 Tessandori, J. 56 Tetrer, D. 243 Tewary, V. 40 Tewsbury, G. 37 Thadhani, N. 29, 79, 132, 175, 183, 218,	
Tedstrom, R. 207 Teintze, S. 198 Telang, A. 228 Temur, D. 67 Teng, J. 36, 135 Tenorio, J. 137, 361 Tenório, J. 92, 310, 352 Terentyev, D. 203 Terpstra, R. 66 Terrones, L 181 Ter Weer, P. 71 Tessandori, J. 56 Teter, D. 243 Tewary, V. 40 Tewksbury, G. 37 Thadhani, N. 29, 79, 132, 175, 183, 218,	
Teintze, S. 198 Telang, A 228 Temur, D 67 Teng, J 86, 135 Tenorio, J. 137, 361 Tenório, J. 34 Teo, K 16, 117 TerBush, J 92, 310, 352 Terrotrey, D 203 Terpstra, R 66 Terrones, L 181 Ter Weer, P 171 Tessandori, J 56 Teter, D 243 Tewary, V 40 Tewksbury, G 37 Thadhani, N 29, 79, 132, 175, 183, 218,	
Telang, A 228 Temur, D 67 Teng, J 86, 135 Tenorio, J 34 Teo, K 16, 117 TerBush, J 92, 310, 352 Terentyev, D 203 Terpstra, R 66 Terrones, L 181 Ter Weer, P 171 Tessandori, J 56 Teter, D 243 Tewary, V 40 Tewksbury, G 37 Thadhani, N 29, 79, 132, 175, 183, 218, 243, 244, 294, 295, 312, 338 Thanneeru, R 268 Theuer, K 244 Thevuthasan, S 100, 151, 275 Thibault, M 127, 341 Thiebaut, C 328 Thinry, B 17 Thirumalai, N 52 Thiyagarajan, K 36 Thomas, D 171, 229 Thomas, G 42 Thompson, D 60 Thompson, S 166, 276 Thompson, S 166, 276 Thunuguntla, R 33 Thuanboon, S	
Temur, D	
Teng, J 86, 135 Tenorio, J. 137, 361 Tenório, J. 34 Teo, K 16, 117 TerBush, J 92, 310, 352 Terntyev, D 203 Terpstra, R 66 Terrones, L 181 Ter Weer, P. 171 Tessandori, J 56 Teter, D 243 Tewary, V 40 Tewksbury, G 37 Thadhani, N 29, 79, 132, 175, 183, 218, 243, 244, 294, 295, 312, 338 Thanneeru, R 268 Theuer, K 244 Thevuthasan, S 100, 151, 275 Thibault, M 127, 341 Thiebaut, C 328 Thierry, B 171 Thirumalai, N 52 Thiyagarajan, K 36 Thomas, D 171, 229 Thomas, G 42 Thompson, D 69 Thompson, C 33, 282 Thompson, C 33, 282 Thomson, K 272 Thonstad, J 171 Thuaboon, S	
Tenorio, J	
Tenório, J	
Tenório, J	Tenorio, J137, 361
Teo, K 16, 117 TerBush, J 92, 310, 352 Terentyev, D 203 Terpstra, R 66 Terrones, L 181 Ter Weer, P 171 Tessandori, J 56 Teter, D 243 Tewary, V 40 Tewksbury, G 37 Thadhani, N 29, 79, 132, 175, 183, 218, 243, 244, 294, 295, 312, 338 Thanneeru, R 268 Theuer, K 244 Thevuthasan, S 100, 151, 275 Thibault, M 127, 341 Thiebaut, C 328 Thierry, B 171 Thirumalai, N 52 Thiyagarajan, K 36 Thoma, D 49, 101, 137, 249 Thomas, G 42 Thomas, G 42 Thomson, K 272 Thomson, G 33, 282 Thompson, M 167 Thomson, K 272 Thomson, K 272 Thonstad, J 173 Thorton, K 168, 336 Thorton, K<	
TerBush, J	
Terentyev, D. 203 Terpstra, R.	
Terpstra, R.	
Terrones, L 181 Ter Weer, P 171 Tessandori, J 56 Teter, D 243 Tewary, V 40 Tewksbury, G 37 Thadhani, N 29, 79, 132, 175, 183, 218,	
Ter Weer, P. 171 Tessandori, J.	
Tessandori, J	
Teter, D 243 Tewary, V 40 Tewksbury, G 37 Thadhani, N 29, 79, 132, 175, 183, 218,	
Tewary, V 40 Tewksbury, G 37 Thadhani, N 29, 79, 132, 175, 183, 218,	
Tewksbury, G	Teter, D
Thadhani, N. 29, 79, 132, 175, 183, 218,	Tewary, V
	Tewksbury, G
	Thadhani, N
Thanneeru, R. 268 Theuer, K. 244 Thevuthasan, S. 100, 151, 275 Thibault, M. 127, 341 Thiebaut, C. 328 Thirry, B. 17 Thirumalai, N. 52 Thiyagarajan, K. 36 Thoma, D. 49, 101, 137, 249 Thomas, A. 161 Thomas, G. 42 Thompson, D. 69 Thompson, G. 33, 282 Thompson, M. 167 Thomson, K. 272 Thonson, K. 271 Thanson, K. 272 Thonson, K. 272 Thonson, S. 166, 276 Thuinet, L. 53, 270 Thunuguntla, R. 33 Thar, Z. 230, 281 Tian, W. 230, 281 Tian, W. 230, 281 Tian,	
Theuer, K	
Thevuthasan, S. 100, 151, 275 Thibault, M. 127, 341 Thiebaut, C. 328 Thierry, B. 17 Thirumalai, N. 52 Thiyagarajan, K. 36 Thoma, D. 49, 101, 137, 249 Thomas, A. 161 Thomas, D. 171, 229 Thomas, G. 42 Thompson, D. 69 Thompson, W. 167 Thomson, K. 272 Thonson, K. 271 Thornton, K. 168, 336 Thornton, T. 60 Thorpe, C. 171 Thuaboon, S. 166, 276 Thuinet, L. 53, 270 Thunuguntla, R. 33 Thuret, J. 108 Tian, Z. 230, 281 Tian, Z. 231, 284 Tien, S. 266 Tikare, V. 18, 67, 119, 168, 227, 278, 327 Tilak, R. 127, 237 </td <td></td>	
Thibault, M 127, 341 Thiebaut, C 328 Thierry, B 17 Thirumalai, N 52 Thiyagarajan, K 36 Thoma, D 49, 101, 137, 249 Thomas, A 161 Thomas, D 171, 229 Thomas, G 42 Thompson, D 69 Thompson, M 167 Thomson, K 272 Thonson, K 272 Thonson, K 272 Thonson, K 272 Thononson, K 167 Thomson, K 272 Thonson, K 167 Thupson, N 167 Thumpson, N 166 Thure, L 53, 270 Thunuguntla, R 33 Thuret, J 108 Tian, Z 230, 281 Tian, Z 231, 284	
Thiebaut, C.	
Thierry, B 17 Thirumalai, N 52 Thiyagarajan, K 36 Thoma, D 49, 101, 137, 249 Thomas, A 161 Thomas, D 171, 229 Thomas, G 42 Thompson, D 66 Thompson, G 33, 282 Thompson, G 33, 282 Thompson, K 272 Thonson, K 272 Thonstad, J 167 Thornson, K 272 Thonstad, J 173 Thornton, K 168, 336 Thornton, T 60 Thorpe, C 171 Thuaboon, S 166, 276 Thuinet, L 53, 270 Thunuguntla, R 33 Thuret, J 108 Tian, Z 230, 281 Tian, Z 231, 284 Tien, S 266 Tikare, V 18, 67, 119, 168, 227, 278, 327 Tilak, R 127, 237 Tiley, J 226, 348 Till, R 150 Tin, C 62, 221 Tin, S	
Thirumalai, N 52 Thiyagarajan, K 36 Thoma, D 49, 101, 137, 249 Thomas, A 161 Thomas, D 171, 229 Thomson, D 69 Thompson, D 69 Thompson, K 272 Thomson, K 272 Thonson, K 272 Thonson, K 272 Thonson, K 167 Thomson, K 173 Thornton, K 168, 336 Thornton, T 60 Thorpe, C 171 Thuaboon, S 166, 276 Thuinet, L 53, 270 Thunuguntla, R 33 Thuret, J 108 Tian, J 271 Tian, W 230, 281 Tian, Z 231, 284 Tien, S 266 Tikare, V 18, 67, 119, 168, 227, 278, 327 Tilak, R 127, 237 Tiley, J 226, 348 Till, R 150 Tin, C 62, 221 Tin, S 52, 53, 106, 155, 208, 268, 321 Tippu	
Thiyagarajan, K.	
Thoma, D	Thirumalai, N52
Thomas, A. 161 Thomas, D. 171, 229 Thoms, G. 42 Thompson, D. 69 Thompson, W. 167 Thomson, K. 272 Thonstad, J. 173 Thornton, K. 272 Thonstad, J. 173 Thornton, K. 272 Thonstad, J. 173 Thornton, K. 168, 336 Thornton, T. 60 Thore, C. 171 Thuanboon, S. 166, 276 Thuinet, L. 53, 270 Thunuguntla, R. 33 Tian, J. 271 Tian, W. 230, 281 Tian, Z. 231, 284 Tien, L. 62 Tien, S. 266 Tikare, V. 18, 67, 119, 168, 227, 278, 327 Tilak, R. 127, 237 Tiley, J. 226, 348 Till, R. 150 Tin, C. 62, 221 Tin, S. 52, 53, 106, 155, 208, 268, 321 Tippur, H. 295 Tiryakioglu, M. 111, 158, 210, 270, 324	Thiyagarajan, K
Thomas, D	
Thomas, D	
Thomas, G. 42 Thompson, D. 69 Thompson, G. 33, 282 Thompson, W. 167 Thomson, K. 272 Thonstad, J. 173 Thornton, K. 168, 336 Thornton, T. 60 Thorpe, C. 171 Thuaboon, S. 166, 276 Thuinet, L. 53, 270 Thunuguntla, R. 33 Thar, J. 210 Tian, J. 271 Tian, J. 271 Tian, Z. 230, 281 Tian, Z. 231, 284 Tien, S. 266 Tikare, V. 18, 67, 119, 168, 227, 278, 327 Tilak, R. 127, 237 Tiley, J. 226, 348 Till, R. 150 Tin, C. 62, 221 Tin, S. 52, 53, 106, 155, 208, 268, 321 Tippur, H. 295 Tiryakioglu, M. 111, 158, 210, 270, 324 Tischler, J. 304 Tissington, C. 40 Tiwari, A. 16, 62, 63, 115, 116,	
Thompson, D. .69 Thompson, G. .33, 282 Thompson, W. .167 Thomson, K. .272 Thonstad, J. .173 Thornton, K. .168, 336 Thornton, T. .60 Thorpe, C. .171 Thuaboon, S. .166, 276 Thuinet, L. .53, 270 Thunuguntla, R. .33 Thare, J. .108 Tian, J. .2711 Tian, W. .230, 281 Tian, Z. .231, 284 Tien, L. .62 Tien, S. .266 Tikare, V. .18, 67, 119, 168, 227, 278, 327 Tilak, R. .127, 237 Tiley, J. .226, 348 Till, R. .150 Tin, C. .62, 221 Tin, S. .52, 53, 106, 155, 208, 268, 321 Tippur, H. .295 Tiryakioglu, M. .111, 158, 210, 270, 324 Tischler, J. .304 Tissington, C. .40 Tiwari, A. .16, 62, 63, 115, 116,	
Thompson, G. 33, 282 Thompson, W. 167 Thomson, K. 272 Thonstad, J. 173 Thornton, K. 168, 336 Thornton, T. 60 Thorpe, C. 171 Thuanboon, S. 166, 276 Thuinet, L. 53, 270 Thunuguntla, R. 33 Thiret, J. 108 Tian, J. 2711 Tian, W. 230, 281 Tian, Z. 231, 284 Tien, L. 62 Tien, S. 266 Tikare, V. 18, 67, 119, 168, 227, 278, 327 Tilak, R. 127, 237 Tiley, J. 226, 348 Till, R. 150 Tin, C. 62, 221 Tin, S. 52, 53, 106, 155, 208, 268, 321 Tippur, H. 295 Tiryakioglu, M. 111, 158, 210, 270, 324 Tischler, J. 304 Tissington, C. 40 Tiwari, A. 16, 62, 63, 115, 116,	
$\begin{array}{cccccccccccccccccccccccccccccccccccc$	Thompson, D
Thomson, K. 272 Thonstad, J. 173 Thornton, K. 168, 336 Thornton, T. 60 Thorpe, C. 171 Thuaboon, S. 166, 276 Thuinet, L. 53, 270 Thunuguntla, R. 33 Thuret, J. 108 Tian, J. 271 Tian, W. 230, 281 Tian, Z. 231, 284 Tien, L. 62 Tien, S. 266 Tikare, V. 18, 67, 119, 168, 227, 278, 327 Tilak, R. 127, 237 Tiley, J. 226, 348 Till, R. 150 Tin, C. 62, 221 Tin, S. 52, 53, 106, 155, 208, 268, 321 Tippur, H. 295 Tiryakioglu, M. 111, 158, 210, 270, 324 Tischler, J. 304 Tissington, C. 40 Tiwari, A. 16, 62, 63, 115, 116,	
Thonstad, J	
Thornton, K. 168, 336 Thornton, T.	
Thornton, T	
Thorpe, C 171 Thuanboon, S 166, 276 Thuinet, L 53, 270 Thunuguntla, R 33 Thuret, J 108 Tian, J 271 Tian, W 230, 281 Tian, Z 231, 284 Tien, L 62 Tien, S 266 Tikare, V 18, 67, 119, 168, 227, 278, 327 Tilak, R 127, 237 Tiley, J 226, 348 Till, R 150 Tin, C 62, 221 Tin, S 52, 53, 106, 155, 208, 268, 321 Tippur, H 295 Tiryakioglu, M 111, 158, 210, 270, 324 Tischler, J 304 Tissington, C 40 Tiwari, A 16, 62, 63, 115, 116,	Thornton, K168, 336
Thuanboon, S 166, 276 Thuinet, L 53, 270 Thunuguntla, R 33 Thuret, J 108 Tian, J 271 Tian, W 230, 281 Tian, Z 231, 284 Tien, L 62 Tien, S 266 Tikare, V 18, 67, 119, 168, 227, 278, 327 Tilak, R 127, 237 Tiley, J 226, 348 Till, R 150 Tin, C 62, 221 Tin, S 52, 53, 106, 155, 208, 268, 321 Tippur, H 295 Tiryakioglu, M 111, 158, 210, 270, 324 Tischler, J 304 Tissington, C 40 Tiwari, A 16, 62, 63, 115, 116,	Thornton, T60
Thuanboon, S 166, 276 Thuinet, L 53, 270 Thunuguntla, R 33 Thuret, J 108 Tian, J 271 Tian, W 230, 281 Tian, Z 231, 284 Tien, L 62 Tien, S 266 Tikare, V 18, 67, 119, 168, 227, 278, 327 Tilak, R 127, 237 Tiley, J 226, 348 Till, R 150 Tin, C 62, 221 Tin, S 52, 53, 106, 155, 208, 268, 321 Tippur, H 295 Tiryakioglu, M 111, 158, 210, 270, 324 Tischler, J 304 Tissington, C 40 Tiwari, A 16, 62, 63, 115, 116,	Thorpe, C171
Thuinet, L	Thuanboon, S166, 276
Thunuguntla, R	
Thuret, J 108 Tian, J 271 Tian, W 230, 281 Tian, Z 231, 284 Tien, L 62 Tien, S 266 Tikare, V 18, 67, 119, 168, 227, 278, 327 Tilak, R 127, 237 Tiley, J 226, 348 Till, R 150 Tin, C 62, 221 Tin, S 52, 53, 106, 155, 208, 268, 321 Tippur, H 295 Tiryakioglu, M 111, 158, 210, 270, 324 Tischler, J 304 Tissington, C 40 Tiwari, A 16, 62, 63, 115, 116,	
Tian, J	
Tian, W 230, 281 Tian, Z 231, 284 Tien, L .62 Tien, S .266 Tikare, V .18, 67, 119, 168, 227, 278, 327 Tilak, R .127, 237 Tiley, J .226, 348 Till, R .150 Tin, C .62, 221 Tin, S .52, 53, 106, 155, 208, 268, 321 Tippur, H .295 Tiryakioglu, M .111, 158, 210, 270, 324 Tischler, J .304 Tissington, C .40 Tiwari, A .16, 62, 63, 115, 116,	
Tian, Z 231, 284 Tien, L	
Tien, L	
Tien, S 266 Tikare, V. 18, 67, 119, 168, 227, 278, 327 Tilak, R 127, 237 Tiley, J 226, 348 Till, R 150 Tin, C 62, 221 Tin, S 52, 53, 106, 155, 208, 268, 321 Tippur, H 295 Tiryakioglu, M 111, 158, 210, 270, 324 Tischler, J 304 Tissington, C .40 Tiwari, A 16, 62, 63, 115, 116,	· · · · · · · · · · · · · · · · · · ·
Tikare, V	
Tilak, R 127, 237 Tiley, J 226, 348 Till, R 150 Tin, C 62, 221 Tin, S 52, 53, 106, 155, 208, 268, 321 Tippur, H 295 Tiryakioglu, M 111, 158, 210, 270, 324 Tischler, J 304 Tissington, C 40 Tiwari, A 16, 62, 63, 115, 116,	
Tiley, J	Tikare, V18, 67, 119, 168, 227, 278, 327
Till, R 150 Tin, C 62, 221 Tin, S 52, 53, 106, 155, 208, 268, 321 Tippur, H 295 Tiryakioglu, M 111, 158, 210, 270, 324 Tischler, J 304 Tissington, C 40 Tiwari, A 16, 62, 63, 115, 116,	Tilak, R127, 237
Till, R 150 Tin, C 62, 221 Tin, S 52, 53, 106, 155, 208, 268, 321 Tippur, H 295 Tiryakioglu, M 111, 158, 210, 270, 324 Tischler, J 304 Tissington, C 40 Tiwari, A 16, 62, 63, 115, 116,	Tiley, J226, 348
Tin, C	
Tin, S	
Tippur, H	
Tiryakioglu, M	
Tischler, J	Tirvaliadu M 111 159 210 270 224
Tissington, C40 Tiwari, A16, 62, 63, 115, 116, 117, 162, 164, 221, 223, 274 Tiwari, V168 Tkac, M81	
Tiwari, A16, 62, 63, 115, 116, 117, 162, 164, 221, 223, 274 Tiwari, V168 Tkac, M	Tischler, J
117, 162, 164, 221, 223, 274 Tiwari, V168 Tkac, M81	
Tiwari, V	
Tkac, M81	117, 162, 164, 221, 223, 274
Tkacheva, O	
	Tkacheva, O



Tkatcheva, O
Tochiyama, O138
Todaka, Y
Todd, M102
Toguyeni, G
Toji, A
Tokozakura, D
Tomas, B
Tomasino, T71
Tomchik, C151
Tome, C30, 68, 169, 170, 228
Tomesani, L271
Toneguzzo, F193
Tonisch, K115
Tonnayopas, D56
Topping, T
Torbet, C
Tortorelli, P259
Tosta, R
Totemeier, A
Tran, T
Trapani, M
1
Treadway, J
Treadwell, C262
Treglio, R
Trelewicz, J
Tretyakov, Y174
Trichy, G116, 222
Trigwell, S94
Trinkle, D52, 77, 105, 136, 189
Trivedi, P244
Trivedi, R
Trolier-McKinstry, S64
Trott, W
Truci, H
Trujillo, C
Trujillo, C30, 133, 183 Trumble, K37, 113, 272
Trujilo, C30, 133, 183 Trumble, K37, 113, 272 Tryon, B66, 156
Trujilo, C
Trujilo, C
Trujillo, C
Trujilo, C
Trujillo, C
Trujillo, C
Trujillo, C
Trujillo, C
Trujillo, C
Trujillo, C
Trujilo, C
Trujillo, C
Trujilo, C
Trujilo, C
Trujilo, C
Trujilo, C
Trujilo, C
Trujilo, C
Trujilo, C
Trujilo, C
Trujilo, C
Trujilo, C
Trujilo, C
Trujilo, C
Trujilo, C
Trujilo, C
Trujilo, C
Trujilo, C

U

Ubertalli, G						.180,	339
Uberuaga, B.							.356
Uchic, M	25, 26	, 44, 1	130,	160,	177,	266,	320

Uchida, Y32, 33
Ucok, I
Ucuncuoglu, S
Uda, T
Udaykumar, H136
Ude, A
Uecker, R64
Ueda, M162
Uehara, T
Ugarte-Domínguez, V
Uggowitzer, P
Ugurlu, O
Uhlenwinkel, V
Ukai, S
Ulbricht, N
Um, N
Umemoto, M
Umeno, Y
Ungar, T
Ungureanu, A70
8
Unitt, M
Unlu, N
Unocic, R
Urban, A
Urgen, M
Uttarwar, M
Uz, M110
Uzer, G97

V

Vaidyanathan, R248, 249, 299, 300, 332
Vaillant, M286
Vainik, R179
Valdes, A
Valdez, J100, 203
Valiev, R113, 215, 217, 218, 358
Valone, S
van Dellen, S70
Vanderspurt, T
Van der Ven, A
van der Walt, T81
van de Walle, A
van Duin, A227
van Heerden, C81
Vanheule, B
Van Hoof, T165
Van Linden, J
van Linden, J55, 110, 157, 209, 269, 323
Vanmeensel, K
Van Petegem, S154
VanSchoiack, L177
Van Swygenhoven, H106, 154, 160
Van Tyne, C190
van Veldhuizen, M157
Vargas Orihuela, J
Varma, S110
Vasantha Kumar, R
Vasarni, V
Vasekar, P33
Vasshaug, K
Vassiliev, S
Vasudevan, V
Vauzelle, T
Vaynman, S
Vecchio, K23, 29, 79, 132, 133,
Vedala, H
Vedani, M217
Vedernikova, I
vodernikova, 1

Vekas, L	
Vendette, H	
Venkatachalapathy, V	
VenkataSuryaPrakash, S	
Venkatesan, T	146
Venkatesh, A	
Venkatesh, T	
Venkateswaran, S	
Ventelon, L	51
Ventura, T	
Verbeken, K	
Verbrugge, M	
Verhaege, M	
Vérité, G	356
Verma, R68, 92,	144, 195, 258, 342
Vermeulen, B	
Vermeulen, P	
Verweij, H	
Veselkov, V	71
Vespa, G	
Veyssiere, P	
Viala, J	
Viano, D	210
Vickery, C	
Vidal, E	
Vidrich, G	
Viehland, D	
Vieira, C	
Vieira, M	275
Vigliante, A	
Vilaça, P	
Vild, C	60
Vildanova, N	010
VIIUaliova. IN	
Vilela, A	174
Vilela, A Vilela, H	
Vilela, A Vilela, H Villegas, J	174
Vilela, A Vilela, H Villegas, J	174
Vilela, A Vilela, H Villegas, J Vincent, A	
Vilela, A Vilela, H Villegas, J Vincent, A Vincent, E	
Vilela, A Vilela, H Villegas, J Vincent, A Vincent, E Vincent, H	
Vilela, A Vilela, H Villegas, J Vincent, A Vincent, E Vincent, H Viswanath, R	
Vilela, A Vilela, H Villegas, J Vincent, A Vincent, E Vincent, H Viswanath, R Viswanathan, A	
Vilela, A Vilela, H Villegas, J Vincent, A Vincent, E Vincent, H Viswanath, R Viswanathan, A	
Vilela, A Vilela, H Villegas, J Vincent, A Vincent, E Vincent, H Viswanath, R Viswanathan, A Viswanathan, G26, 121,	
Vilela, A Vilela, H Villegas, J Vincent, A Vincent, E Vincent, H Viswanath, R Viswanathan, A Viswanathan, G26, 121, Vitchus, B	
Vilela, A Vilela, H Villegas, J Vincent, A Vincent, E Vincent, H Viswanath, R Viswanathan, A Viswanathan, G26, 121, Vitchus, B Vitek, V	
Vilela, A Vilela, H Villegas, J Vincent, A Vincent, E Vincent, H Viswanath, R Viswanathan, A Viswanathan, G26, 121, Vitchus, B Vitek, V Vittala Pai, D	
Vilela, A Vilela, H Villegas, J Vincent, A Vincent, E Vincent, H Viswanath, R Viswanathan, A Viswanathan, G26, 121, Vitchus, B Vitek, V	
Vilela, A Vilela, H Villegas, J Vincent, A Vincent, E Vincent, H Viswanath, R Viswanathan, A Viswanathan, G26, 121, Vitchus, B Vitchus, B Vittala Pai, D Viviers, K	
Vilela, A Vilela, H Villegas, J Vincent, A Vincent, E Vincent, H Viswanath, R Viswanathan, A Viswanathan, G26, 121, Vitchus, B Vitchus, B Vittala Pai, D Viviers, K Vízdal, J.	
Vilela, A Vilela, H Villegas, J Vincent, A. Vincent, E. Vincent, H. Viswanathan, R. Viswanathan, A. Viswanathan, G26, 121, Vitchus, B. Vitchus, B. Vitka, V. Vittala Pai, D. Viviers, K. Vízdal, J. Vlcek, J.	
Vilela, A Vilela, H Villegas, J Vincent, A Vincent, E. Vincent, H. Viswanathan, R. Viswanathan, A. Viswanathan, G26, 121, Vitchus, B. Vitchus, B. Vittala Pai, D. Vittala Pai, D. Viviers, K. Vízdal, J. Vlcek, J Vleugels, J	
Vilela, A Vilela, H Villegas, J Vincent, A. Vincent, E. Vincent, H. Viswanathan, R. Viswanathan, A. Viswanathan, G26, 121, Vitchus, B. Vitchus, B. Vitk, V. Vittala Pai, D. Viviers, K. Vízdal, J. Vlcek, J.	
Vilela, A Vilela, H Villegas, J Vincent, A Vincent, E. Vincent, H. Viswanath, R. Viswanathan, A. Viswanathan, G26, 121, Vitchus, B. Vitchus, B. Vittala Pai, D. Vittala Pai, D. Viviers, K. Vízdal, J. Vlcek, J. Vleugels, J Vlieg, E.	
Vilela, A Vilela, H Villegas, J Vincent, A Vincent, E. Vincent, H. Viswanathan, A. Viswanathan, A. Viswanathan, G26, 121, Vitchus, B. Vitek, V. Vittala Pai, D. Vitek, V. Viviers, K. Vízdal, J. Vlcek, J. Vleugels, J. Vleugel, S	
Vilela, A Vilela, H Villegas, J Vincent, A Vincent, E Vincent, H. Viswanath, R. Viswanathan, A. Viswanathan, G26, 121, Vitchus, B. Vitek, V Vitek, V. Vitek, V. Vitek, J. Vlcek, J. Vlcek, J. Vleugels, J. Vleugels, J. Vleugel, S. Vogel, S Vogler, T	
Vilela, A Vilela, H Villegas, J Vincent, A Vincent, E Vincent, H. Viswanath, R. Viswanathan, A. Viswanathan, G26, 121, Vitchus, B. Vitek, V. Vittala Pai, D. Vitek, V. Vittala Pai, D. Viviers, K. Vízdal, J. Vlcek, J. Vleugels, J. Vleugels, J. Vlieg, E. Vogel, S Vogle, R.	
Vilela, A Vilela, H Villegas, J Vincent, A Vincent, E Vincent, H Viswanathan, A. Viswanathan, A. Viswanathan, G26, 121, Vitchus, B. Vitek, V. Vittala Pai, D Vittek, V. Vittala Pai, D Vitek, J. Viviers, K. Vízdal, J. Vlcek, J. Vleugels, J. Vleugels, S. Vogel, S. Vogler, T Vogt, R. Vohra, Y.	
Vilela, A Vilela, H Villegas, J Vincent, A Vincent, E Vincent, H Viswanathan, A. Viswanathan, A. Viswanathan, G26, 121, Vitchus, B. Vitek, V. Vittala Pai, D Vittek, V. Vittala Pai, D Vitek, J. Viviers, K. Vízdal, J. Vlcek, J. Vleugels, J. Vleugels, S. Vogel, S. Vogler, T Vogt, R. Vohra, Y.	
Vilela, A	
Vilela, A	
Vilela, A	$\begin{array}{c} 174\\ 334\\ 271\\ 344\\ 271\\ 149, 292\\ 263\\ 341\\ 337\\ 98\\ 130, 217, 229, 312\\ 341\\ 51, 206\\ 232\\ 341\\ 104\\ 89\\ 234\\ 89\\ 30\\ 183, 338\\ 214\\ 176\\ 63\\ 343\\ 358, 160, 266\\ \end{array}$
Vilela, A	$\begin{array}{c} 174\\ 334\\ 271\\ 344\\ 271\\ 246\\ 263\\ 341\\ 337\\ 98\\ 130, 217, 229, 312\\ 341\\ 51, 206\\ 232\\ 341\\ 51, 206\\ 232\\ 81\\ 104\\ 89\\ 300\\ 183, 338\\ 214\\ 176\\ 63\\ 343\\ 343\\ 58, 160, 266\\ 220\\ \end{array}$
Vilela, A	
Vilela, A Vilela, H Villegas, J Vincent, A Vincent, E. Vincent, H. Viswanathan, A. Viswanathan, A. Viswanathan, G26, 121, Viswanathan, G26, 121, Vitwan, B. Vitwan, B. Vitek, V. Vittala Pai, D. Vitek, V. Vittala Pai, D. Vitek, V. Vittala Pai, D. Vitek, J. Vitek, J. Vleugels, J. Vleugels, J. Vleugels, J. Vleugels, J. Vleugel, S. Vogler, T. Vogl, R. Vogl, R. Vogler, T. Vogl, R. Volkra, Y. Volkatis, J. Volkert, C. Volkov, Y. Volland, A. Volokhov, I. Von Kaenel, R.	
Vilela, A Vilela, H Villegas, J Vincent, A Vincent, E. Vincent, H. Viswanathan, A. Viswanathan, A. Viswanathan, G26, 121, Viswanathan, G26, 121, Vitswanathan, G26, 121, Vitswanathan, G. Viswanathan, G. Vitak, J. Vitek, J. Vitek, V. Vitala Pai, D. Vitek, V. Vitala Pai, D. Vitek, J. Vitek, J. Vicek, J. Vleek, J. Vleek, J. Vleek, J. Vleek, J. Vleek, J. Vleek, J. Vleek, J. Vleek, J. Vogel, S. Vogel, S. Vogel, S. Vogel, S. Vogel, R. Vogel, R. Vofra, Y. Volakis, J. Volkert, C. Volkov, Y. Volland, A. Volokhov, I. Vondra, F. Von Kaenel, R.	$\begin{array}{c}$
Vilela, A Vilela, H Villegas, J Vincent, A Vincent, E. Vincent, H. Viswanathan, A. Viswanathan, A. Viswanathan, G26, 121, Viswanathan, G26, 121, Vitwan, B. Vitwan, B. Vitek, V. Vittala Pai, D. Vitek, V. Vittala Pai, D. Vitek, V. Vittala Pai, D. Vitek, J. Vitek, J. Vleugels, J. Vleugels, J. Vleugels, J. Vleugels, J. Vleugel, S. Vogler, T. Vogl, R. Vogl, R. Vogler, T. Vogl, R. Volkra, Y. Volkatis, J. Volkert, C. Volkov, Y. Volland, A. Volokhov, I. Von Kaenel, R.	$\begin{array}{c} 174\\ 334\\ 271\\ 344\\ 271\\ 149, 292\\ 263\\ 341\\ 337\\ 98\\ 130, 217, 229, 312\\ 341\\ 51, 206\\ 232\\ 81\\ 104\\ 232\\ 81\\ 104\\ 89\\ 234\\ 89\\ 300\\ 183, 338\\ 214\\ 176\\ 63\\ 343\\ 214\\ 176\\ 63\\ 343\\ 214\\ 176\\ 63\\ 343\\ 214\\ 176\\ 63\\ 343\\ 214\\ 176\\ 343\\ 283\\ 3189, 335, 336\\ 143\\ 283\\ 283\\ 3189, 335, 336\\ 314\\ 326\\ 326\\ 326\\ 326\\ 336\\ 346\\ 343\\ 343\\ 343\\ 343\\ 343\\ 34$
Vilela, A	
Vilela, A	
Vilela, A	$\begin{array}{c}$
Vilela, A	
Vilela, A	



W

Wadsworth, J64	
Wagermaier, W72	
Wagner, B54	
Wagner, G132	
Wagner, L195	
Wagoner, R146, 147, 148, 186, 188, 247	
Wagstaff, R237, 238	
Wahl, J53	
Walden, W141	
Waldner, G63	
Walford, G143	
Walker, D179	
Wall, J	
Wallace, R232	
Wallenius, J150	
Walleser, J103, 264	
Walley, S132, 183	
Walter, S72	
Wan, Z	
Wang, B	
Wang, C	
Wang, D58, 62, 116, 221, 331	
Wang, E	
Wang, G73, 178, 189, 212, 239, 332, 335, 360	
Wang, H58, 60, 62, 108, 112, 115, 159,	
162, 211, 213, 221, 271, 276, 325, 357	
Wang, J196, 212, 213, 215,	
Wang, K182, 313, 327	
Wang, L	
wang, L	
Wang, M18, 51, 206, 214, 318	
Wang, N	
Wang, P20, 121, 133, 250, 279, 280, 312	
Wang, Q41, 210, 281	
, vang, Q	
Wang, S102, 143, 345	
Wang, S102, 143, 345	
Wang, S	
Wang, S102, 143, 345 Wang, T	
Wang, S102, 143, 345 Wang, T	
Wang, S102, 143, 345 Wang, T	
Wang, S 102, 143, 345 Wang, T 77, 274, 337 Wang, W 24, 73, 338 Wang, X 24, 74, 337 Wang, Y 24, 73, 338 Wang, X 24, 126, 127, 134, 215, 228, 332 Wang, Y 22, 25, 28, 32, 44, 50, 74, 77, 99,	
Wang, S 102, 143, 345 Wang, T 77, 274, 337 Wang, W 24, 73, 338 Wang, X 24, 74, 337 Wang, Y 24, 73, 338 Wang, X 24, 126, 127, 134, 215, 228, 332 Wang, Y 22, 25, 28, 32, 44, 50, 74, 77, 99,	
Wang, S	
 Wang, S	
 Wang, S Wang, T T7, 274, 337 Wang, W T7, 274, 337 Wang, W Yang, W Yang, Y Yang	
 Wang, S Wang, T T7, 274, 337 Wang, W 24, 73, 338 Wang, X 46, 124, 126, 127, 134, 215, 228, 332 Wang, Y 22, 25, 28, 32, 44, 50, 74, 77, 99, 106, 107, 121, 168, 169, 174, 189, 195, 203, 212, 213, 229, 235, 236, 239, 241, 242, 265, 312, 326, 343, 356 Wang, Z 31, 60, 80, 114, 161, 186, 220, 233, 238, 273, 284, 340 Wanko, E 145 Wanner, A 258 Wanczok, A 35 Ward, W 	
 Wang, S Wang, T T7, 274, 337 Wang, W T7, 274, 337 Wang, W Yang, W Yang, Y Yang	
 Wang, S Wang, T Wang, T T77, 274, 337 Wang, W Yang, W Yang, Y Yang, Y<	
 Wang, S Wang, T Wang, T T77, 274, 337 Wang, W 24, 73, 338 Wang, X 46, 124, 126, 127, 134, 215, 228, 332 Wang, Y 22, 25, 28, 32, 44, 50, 74, 77, 99, 106, 107, 121, 168, 169, 174, 189, 195, 203, 212, 213, 229, 235, 236, 239, 241, 242, 265, 312, 326, 343, 356 Wang, Z 220, 233, 238, 273, 284, 340 Wanko, E 220, 233, 238, 273, 284, 340 Wanko, E 145 Wanner, A 258 Wanner, T 278 Warczok, A 35 Ward, W 116 Warnken, N 31, 32, 40, 181, 199 	
 Wang, S Wang, T Wang, T T77, 274, 337 Wang, W Yang, W Yang, Y Yang, Y<	
 Wang, S	
Wang, S 102, 143, 345 Wang, T 77, 274, 337 Wang, W 24, 73, 338 Wang, X 46, 124, 126, 127, 134, 215, 228, 332 Wang, Y 22, 25, 28, 32, 44, 50, 74, 77, 99,	
 Wang, S	
Wang, S 102, 143, 345 Wang, T 77, 274, 337 Wang, W 24, 73, 338 Wang, X 46, 124, 126, 127, 134, 215, 228, 332 Wang, Y 22, 25, 28, 32, 44, 50, 74, 77, 99,	
Wang, S 102, 143, 345 Wang, T 77, 274, 337 Wang, W 24, 73, 338 Wang, X 46, 124, 126, 127, 134, 215, 228, 332 Wang, Y 22, 25, 28, 32, 44, 50, 74, 77, 99,	
Wang, S 102, 143, 345 Wang, T 77, 274, 337 Wang, W 24, 73, 338 Wang, X 46, 124, 126, 127, 134, 215, 228, 332 Wang, Y 22, 25, 28, 32, 44, 50, 74, 77, 99,	
Wang, S 102, 143, 345 Wang, T 77, 274, 337 Wang, W 24, 73, 338 Wang, X 46, 124, 126, 127, 134, 215, 228, 332 Wang, Y 22, 25, 28, 32, 44, 50, 74, 77, 99,	
Wang, S 102, 143, 345 Wang, T 77, 274, 337 Wang, W 24, 73, 338 Wang, X 46, 124, 126, 127, 134, 215, 228, 332 Wang, Y 22, 25, 28, 32, 44, 50, 74, 77, 99,	
Wang, S 102, 143, 345 Wang, T 77, 274, 337 Wang, W 24, 73, 338 Wang, X 46, 124, 126, 127, 134, 215, 228, 332 Wang, Y 22, 25, 28, 32, 44, 50, 74, 77, 99,	
Wang, S 102, 143, 345 Wang, T 77, 274, 337 Wang, W 24, 73, 338 Wang, X 46, 124, 126, 127, 134, 215, 228, 332 Wang, Y 22, 25, 28, 32, 44, 50, 74, 77, 99,	
Wang, S 102, 143, 345 Wang, T 77, 274, 337 Wang, W 24, 73, 338 Wang, X 46, 124, 126, 127, 134, 215, 228, 332 Wang, Y 22, 25, 28, 32, 44, 50, 74, 77, 99,	
Wang, S 102, 143, 345 Wang, T 77, 274, 337 Wang, W 24, 73, 338 Wang, X 46, 124, 126, 127, 134, 215, 228, 332 Wang, Y 22, 25, 28, 32, 44, 50, 74, 77, 99,	

Wedde, G36	
W ₂₂ A 60	
Wee, A60	
Weerasooriya, T38, 140, 141, 253, 304, 305	
Weertman, J	
Wegener, J42	
Wei, C	
Wei, D256, 320	
Wei, H	
Wei, J	
Wei, L	
Wei, Q113	
Wei, W55, 109, 163	
Wei, Y	
Wei, Z	
Weidenmann, K258	
Weigend, F	
Weil, K	
Weiland, H20, 68, 282, 349	
Weinberger, C161	
Weiss, B	
Weissmüller, J275, 326, 337	
Welch, B231	
W II D 100 000 000	
Welk, B130, 229, 312	
Wells, J158, 338	
Wen, C	
Wen, Y	
Weng, L	
Wenner, M	
Wensley, C	
Werner, F	
Wesolowski, R49	
Westbrooke, E156	
Westerholt, K	
Weygand, D	
Wheeler, K	
Wheeler, R160	
Whelan, S	
w neian, S124	
White, D	
White, D74, 75, 348	
White, D74, 75, 348 White, H183	
White, D74, 75, 348 White, H183 White, P198	
White, D74, 75, 348 White, H183 White, P198	
White, D74, 75, 348 White, H183 White, P198 White, P	
White, D	

Willms, R251
Wilson, T178, 236
Wimmer, E
Win, Z
Windl, W
Winter, R
Winterton, J165
Winther, G121
Wirth, B48, 100, 101, 150, 201, 202,
Withers, J
Withers, P
Witt, P
Witte, F
Witusiewicz, V135
Wng, Y195
Wochner, P
Wögerer, C60, 63, 88
Wolf, A
Wolf, B100
Wolf, D
Wolf, W
Wolverton, C27, 28, 77
Wong, C
Wong, K
Wong, N
Wong, S
Wong, W
Woo, C
Woo, W
Wood, W
Woodard, S
Woodward, C51, 105, 154, 181,
Wright, I209, 259, 311
Wright, S75, 121, 169
Wright, T79, 243
Wu, A
Wu, C
Wu, D
Wu, E
Wu, J
Wu, K125
Wu, L
Wu, M76
Wu, R
Wu, S
Wu, T
Wu, W
Wu, X56, 95, 113, 155, 216, 357
Wu, Y166, 209
Wu, Z
Wuelker, C25
Wunderlich, R
Wunsch, C
,

X

Xi, J	185
Xia, G94, 1	98, 260
Xia, K	216, 294
Xia, S	215
Xia, Z98, 102, 103, 1	10, 264
Xiang, L	186
Xiang, Q	330
Xiangdong, Y	232
Xiao, Y	259
Xiao, Z	276
Xichang, S	99



ALC: NO. OF THE OWNER.

Xie, C
Xie, J
Xie, M273
Xie, X110
Xie, Y185
Xie, Z121
Xin, Y
Xinzheng, L185
Xiong, J125, 184, 313
Xiong, S
Xiong, X76
Xiong, Y214, 260
Xiquan, Q296
XiYun, Y99
Xu, C112
Xu, D103, 262, 313, 316
Xu, F120
Xu, H247, 251, 262
Xu, J31, 126, 231, 260, 283
Xu, M236
Xu, S151
Xu, W21, 113, 216
Xu, X59, 70, 73, 214, 217, 295, 350
Xu, Y
Xu, Z238, 274, 289
Xuanhui, Q224
Xue, J
Xueliang, D
Xueping, Z224
Xueyi, G
Xuguang, G

Y

Yablinsky, C156
Yadava, M187
Yajima, M154
Yalisove, S
Yamaguchi, A209
Yamaji, K
Yamamoto, T263, 264, 314
Yamamoto, Y55, 260, 323
Yamazaki, A
Yan, X
Yan, Y
Yan, Z
Yanada, I153
Yang, B
Yang, C
Yang, D
Yang, F204, 239, 287
Yang, G46
Yang, H
Yang, J27, 158, 188, 284, 296, 297
Yang, K
Yang, L
Yang, Q61, 165
Yang, R
Yang, S50, 105, 258, 297, 304
Yang, W172, 232, 283, 304, 322
Yang, Y136, 169, 213, 288, 322, 336, 343
Yang, Z41, 93, 94, 145, 197,
Yanli, J
Yannas, I72
Yanqing, L
Yao, G17, 46, 70, 118, 123, 129,
Yao, Z
100, 2

Yaowu, W
Yapici, G119, 193, 228
Yarrapareddy, E
Yashiki, T43 Yasuda, K220, 304
Yavari, A
Yavorsky, M
Yavuz, M
Ye, F
Ye, J207
Ye, W61
Ye, Y190, 236
Yeh, A156
Yen, Y
YeXiang, L61
Yexiang, L
Yi, J156, 292 Yihan, L119, 345
Yilmaz, S
Yim, C
Yin, D
Yin, F
Yin, J
Yin, W69, 282
Yin, Z276, 281
Yokokawa, H42, 260
Yokokawa, T
Yokoyama, Y74, 178, 286, 332
Yolton, C
Yong, W
Yong, Z
Yonggang, Z
Yoo, C
Yoo, J204
Yoo, K
Yoon, E273
Yoon, J50, 253, 319, 359
Yoon, K
Yoon, S
Yoon, Y196, 328, 359, 360 Yorikado, Y
Yo Sep, Y
Yoshikawa, T
You, B143
You, K
Young, D131, 360
Young, H345
Young, P217
Youssef, Y
Yu, C
Yu, D
Yu, H46, 123, 184, 207, 328
Yu, J50, 85, 102, 151, 204, 223, 264, 317
Yu, K
Yu, L
Yu, S
Yu, Y103
Yu, Z
Yuan, B
Yuan, F
Yuan, Q
Yuan, W
Yucel, O
Yue, S
Yue, W
Yuefeng, G107
Yuezhong, D233, 296

Yufeng, G	142
Yujin, C	
Yun, Y	
Yunaz, H	70
Yurkov, V	

Z

Zabaras, N19, 77, 99, 119, 120, 146,	199
Zabel, H	252
Zabinski. Jr. J	
Zagrebelnyy, D	
Zaidi, T	.345
Zaikov, Y173, 283,	
Zaluzny, M	274
Zangiacomi, C	232
Zarandi, F92,	144
Zarkevich, N	
Zarouni, A	
Zartoshtimanesh, S	
Zayak, A	
Zehetbauer, M113,	
Zeifert, B	
Zeller, S	18
Zemanová, A	104
Zeng, K	
Zeng, Q117,	
Zeng, X47, 92, 154, 195, 196, 211, 309,	252
Zerilli, F	
Zestrea, V	
Zettler, R134,	
Zhai, Q46, 98, 99, 261, 262, 313,	354
Zhai, X	166
Zhan, J	
Zhang, C	
Zhang, D213, 255,	
Zhang, F	228
Zhang, H54, 74, 77, 79, 126, 130, 289,	309
Zhang, J71, 115, 131, 212, 285, 295,	304
Zhang, K	
Zhang, L	
Zhang, M17, 42,	
Zhang, R	
Zhang, S	
Zhang, T236,	
Zhang, W	
Zhang, X	213,
	357
Zhang, Y37, 59, 100, 127, 209, 212, 295,	
Zhang, Z	
Zhao, J	
Zhao, J	
Zhao, M	
Zhao, P	
Zhao, W	232
Zhao, Y225, 271,	274
Zheleva, T	163
Zheng, G	
Zheng, H	
Zheng, K	
Zheng, L	
Zheng, W240,	
Zheng, X	280
Zheng-Johansson, J	220
Zhgilev, I	
Zhi, Z	
Zhilyaev, A113, 216, 219, 273,	
Zhimeng, G Zhipeng, C	
Intend (41



Zholnin, A
Zhong, H230, 281
Zhong, J
Zhongliang, T185
Zhou, H222, 310
Zhou, J71, 72
Zhou, L
Zhou, M96, 337
Zhou, N
Zhou, O63, 117
Zhou, Y56, 62, 218, 221
Zhu, A
Zhu, C76, 331
Zhu, F
Zhu, H
Zhu, J
Zhu, L
Zhu, T58, 106, 161, 327
Zhu, W
Zhu, X100, 261, 292
Zhu, Y58, 112, 159, 211,
Zhu, Z126
Zhurkin, E165
Zikry, M169
Zimmerman, L
Zimmerman, M
Zimprich, P318
Zindel, J
Zinkle, S100, 316
Zok, F
Zöllmer, V
Zrnik, J95, 112
Zu, G17, 194, 230
Zúberová, Z178
Zuniga, D
Zuo, L
Zuo, R
Zuo, X

Plan to join us in America's most authentic and culturally rich city - rejuvenated!

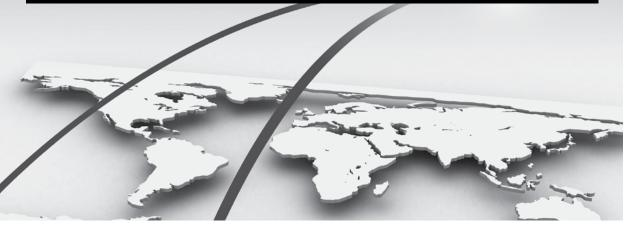


137th Annual Meeting & Exhibition



March 9-13, 2008 Ernest Morial Convention Center New Orleans, Louisiana

Details to come at www.tms.org/annualmeeting.html



Linking Science and Technology for Global Solutions